NASA
CP
2036-
pt.1
c.1

NASA Conference Publication 2036

Part I

LOAN COPY: RE
AFWL TECHNIC
KIRTLAND AFB
0067287
TECH LIBRARY KAFB, NM

CTOL Transport Technology - 1978

Proceedings of
a conference held at
Langley Research Center
Hampton, Virginia
February 28 - March 3, 1978

NASA

5 JUL 1978
Technical Library
Air Force Weapons
Laboratory

TECH LIBRARY KAFB, NM
0067287

NASA Conference Publication 2036

Part I

CTOL Transport Technology - 1978

Proceedings of
a conference held at
Langley Research Center
Hampton, Virginia
February 28 - March 3, 1978

NASA
National Aeronautics
and Space Administration

**Scientific and Technical
Information Office**

1978

PREFACE

The proceedings of the NASA CTOL Transport Technology Conference held at Langley Research Center on February 28 — March 3, 1978, are reported in this NASA Conference Proceedings.

The purpose of the Conference was to provide early dissemination of new technology generated by NASA and specifically associated with advanced conventional take-off and landing (CTOL) transport aircraft. The last such NASA conference in this general area was held in 1971 and was reported in NASA SP-292, entitled "Vehicle Technology for Civil Aviation — The Seventies and Beyond."

The technology reported in this conference resulted from both in-house and contract efforts, including those of the ongoing Aircraft Energy Efficiency (ACEE) Program. The topics covered by session were

I. Propulsion
II. Structures and Materials
III. Laminar Flow Control
IV. Advanced Aerodynamics and Active Controls
V. Operations and Safety
VI. Advanced Systems

The efforts of the members of the Steering Committee, who developed the structure of the Conference and selected and reviewed the papers, are particularly appreciated.

Certain commercial equipment and materials are identified in this paper in order to specify the procedures and configurations adequately. In no case does such identification imply recommendation or endorsement of the product by NASA, nor does it imply that the equipment or materials are necessarily the only ones or the best ones available for the purpose. In many cases equivalent equipment and materials are available and would probably produce equivalent results.

D. William Conner
Conference Chairman

STEERING COMMITTEE

D. William Conner, Chairman
Langley Research Center

Paul G. Johnson
NASA Headquarters

John M. Klineberg
NASA Headquarters

Robert W. Leonard
Langley Research Center

Donald L. Nored
Lewis Research Center

Ronald H. Smith
NASA Headquarters

CONTENTS

Part I

PREFACE iii

STEERING COMMITTEE iv

1. OVERVIEW OF NASA CTOL PROGRAM 1
James J. Kramer

SESSION I - PROPULSION
Chairman: Donald L. Nored

2. ACEE PROPULSION OVERVIEW 9
Donald L. Nored

3. CF6 JET ENGINE PERFORMANCE DETERIORATION RESULTS 25
R. J. Lewis, C. E. Humerickhouse, and J. E. Paas

4. JT9D JET ENGINE PERFORMANCE DETERIORATION 45
A. Jay, E. S. Todd, and G. P. Sallee

5. CF6 PERFORMANCE IMPROVEMENT 59
Dean J. Lennard

6. ENGINE COMPONENT IMPROVEMENT - JT8D AND JT9D PERFORMANCE IMPROVEMENTS 79
W. O. Gaffin

7. ENERGY EFFICIENT ENGINE PRELIMINARY DESIGN AND INTEGRATION STUDIES 89
David E. Gray

8. ENERGY EFFICIENT ENGINE PRELIMINARY DESIGN AND INTEGRATION STUDIES 111
R. P. Johnston and M. C. Hemsworth

9. STATUS OF ADVANCED TURBOPROP TECHNOLOGY 139
J. F. Dugan, B. A. Miller, and D. A. Sagerser

10. PROPULSION SYSTEMS NOISE TECHNOLOGY 167
C. E. Feiler

11. ADVANCED MATERIALS RESEARCH FOR LONG-HAUL AIRCRAFT TURBINE ENGINES 187
R. A. Signorelli and C. P. Blankenship

12. GAS TURBINE ENGINE EMISSION REDUCTION TECHNOLOGY PROGRAM 205
Donald A. Petrash and Larry A. Diehl

13. IMPACT OF BROAD-SPECIFICATION FUELS ON FUTURE JET AIRCRAFT 217
Jack Grobman

SESSION II - STRUCTURES AND MATERIALS
Chairman: Louis F. Vosteen

14. INTRODUCTION TO SESSION ON MATERIALS AND STRUCTURES 235
Louis F. Vosteen

15. ENVIRONMENTAL EFFECTS ON COMPOSITES FOR AIRCRAFT 239
Richard A. Pride

16. DEVELOPMENT OF ADVANCED COMPOSITE STRUCTURES FOR LOCKHEED AIRCRAFT 259
Warren A. Stauffer and Arthur M. James

17. KEY ISSUES IN APPLICATION OF COMPOSITES TO TRANSPORT AIRCRAFT 281
M. Stone

18. ADVANCED STRUCTURAL SIZING METHODOLOGY 311
W. Jefferson Stroud and Jaroslaw Sobieszczanski-Sobieski

19. TRANSITION FROM GLASS TO GRAPHITE IN MANUFACTURE OF COMPOSITE AIRCRAFT STRUCTURE 331
Harvey E. Buffum and Vere S. Thompson

SESSION III - LAMINAR FLOW CONTROL
Chairman: Ralph J. Muraca

20. LAMINAR FLOW CONTROL OVERVIEW 349
Ralph J. Muraca

21. FLIGHT INVESTIGATION OF INSECT CONTAMINATION AND ITS ALLEVIATION 357
John B. Peterson, Jr., and David F. Fisher

22. DEVELOPMENT OF ADVANCED STABILITY THEORY SUCTION PREDICTION TECHNIQUES FOR LAMINAR FLOW CONTROL 375
Andrew J. Srokowski

23. DESIGN OF A LAMINAR-FLOW-CONTROL SUPERCRITICAL AIRFOIL FOR A SWEPT WING 395
Dennis O. Allison and John R. Dagenhart

24. APPLICATION OF LAMINAR FLOW CONTROL TECHNOLOGY TO LONG-RANGE TRANSPORT DESIGN 409
L. B. Gratzer and D. George-Falvy

25. TOWARD A LAMINAR-FLOW-CONTROL TRANSPORT FOR THE 1990's 449
R. F. Sturgeon

26. APPLICATION OF POROUS MATERIALS FOR LAMINAR FLOW CONTROL 497
Wilfred E. Pearce

Part II*

SESSION IV - ADVANCED AERODYNAMICS AND ACTIVE CONTROLS TECHNOLOGY
Chairman: William J. Alford, Jr.

27. ADVANCED AERODYNAMICS AND ACTIVE CONTROLS TECHNOLOGY SESSION INTRODUCTION 523
William J. Alford, Jr.

28. NASA SUPERCRITICAL-WING TECHNOLOGY . . . . . DELETED 533
Dennis W. Bartlett and James C. Patterson, Jr.

29. EXPERIMENTAL RESULTS OF WINGLETS ON FIRST, SECOND, AND THIRD GENERATION JET TRANSPORTS 553
Stuart G. Flechner and Peter F. Jacobs

30. RECENT EXPERIENCES WITH THREE-DIMENSIONAL TRANSONIC POTENTIAL FLOW CALCULATIONS . . . . . DELETED 571
David A. Caughey, Perry A. Newman, and Antony Jameson

31. TOWARDS COMPLETE CONFIGURATIONS USING AN EMBEDDED GRID APPROACH . . . . . DELETED 593
Charles W. Boppe

32. WINGLET AND LONG-DUCT NACELLE AERODYNAMIC DEVELOPMENT FOR DC-10 DERIVATIVES 609
A. Brian Taylor

33. APPLICATION OF WINGLETS AND/OR WING TIP EXTENSIONS WITH ACTIVE LOAD CONTROL ON THE BOEING 747 625
Robert L. Allison, Brian R. Perkin, and Richard L. Schoenman

34. DEVELOPMENT AND FLIGHT EVALUATION OF ACTIVE CONTROLS IN THE L-1011 647
J. F. Johnston and D. M. Urie

35. ADVANCED AERODYNAMICS AND ACTIVE CONTROLS FOR A NEXT GENERATION TRANSPORT 687
A. Brian Taylor

36. ACTIVE CONTROLS TECHNOLOGY TO MAXIMIZE STRUCTURAL EFFICIENCY . . . 709
James M. Hoy and James M. Arnold

*Papers 27 to 49 are presented under separate cover.

SESSION V - OPERATIONS AND SAFETY
Chairman: John H. Enders

37. OPERATIONS AND SAFETY INTRODUCTION 733
John H. Enders

38. OVERVIEW OF SAFETY RESEARCH 735
John H. Enders

39. WAKE VORTEX TECHNOLOGY 757
R. Earl Dunham, Jr., Marvin R. Barber, and Delwin R. Croom

40. SUMMARY OF NASA LANDING-GEAR RESEARCH 773
Bruce D. Fisher, Robert K. Sleeper, and Sandy M. Stubbs

41. NOISE PREDICTION TECHNOLOGY FOR CTOL AIRCRAFT 805
John P. Raney

42. FLIGHT EXPERIMENTS TO IMPROVE TERMINAL AREA OPERATIONS 819
Seymour Salmirs and Samuel A. Morello

43. ESTIMATING AIRLINE OPERATING COSTS 849
Dal V. Maddalon

44. A METHOD FOR THE ANALYSIS OF THE BENEFITS AND COSTS FOR AERONAUTICAL RESEARCH AND TECHNOLOGY 871
Louis J. Williams, Herbert H. Hoy, and Joseph L. Anderson

SESSION VI - ADVANCED SYSTEMS
Chairman: William S. Aiken, Jr.

45. ADVANCED SYSTEMS OVERVIEW 885
William S. Aiken, Jr.

46. SHORT-HAUL CTOL AIRCRAFT RESEARCH 891
Louis J. Williams

47. PROGRESS IN SUPERSONIC CRUISE AIRCRAFT TECHNOLOGY 909
Cornelius Driver

48. PROGRESS ON COAL-DERIVED FUELS FOR AVIATION SYSTEMS 927
Robert D. Witcofski

49. STUDIES OF ADVANCED TRANSPORT AIRCRAFT 951
A. L. Nagel

OVERVIEW OF NASA CTOL PROGRAM

James J. Kramer
NASA Headquarters

It is a pleasure to be here today to help kick off this Conference on CTOL Transport Technology. I commissioned this activity to provide a forum for early dissemination of the new technologies being generated by NASA, both in-house and under contract to industry, specifically oriented toward advanced commercial air transports. The program has been laid out to bring you the latest results in our Aircraft Energy Efficiency (ACEE) program and in related disciplinary areas.

Before getting on with the technical papers and discussions, I would like to put our CTOL efforts into perspective relative to the total NASA aeronautics program. The prismlike chart shown in figure 1 breaks the aeronautics program by our budget categories on the left and by vehicle specific categories on the right. Our R&T Base activities are designed to maintain a strong research base in the technology disciplines. These activities are basic and exploratory in nature and, in CTOL, are characterized by the disciplinary papers which will be presented at the end of each of the sessions of this conference.

When ideas and concepts in the R&T Base reach a state of maturity and are ready for more focused activity, Systems Technology and Experimental Programs are employed to bring the technologies to a state of readiness where they can be applied in the commercial sector. In CTOL, the Aircraft Energy Efficiency programs are in these categories.

Although the R&T Base, Systems Technology, and Experimental Programs categories are useful for budget purposes, we find it more effective to think of the aeronautics program along eight vehicle-specific lines with a backdrop of generic research and technology activity. There are some obvious difficulties in categorizing some technology efforts along rigid vehicle types. In some efforts there is substantial fallout from one category to another, particularly from CTOL to General Aviation. However, we try very conscientiously to identify which of the vehicle types benefit primarily from our various technology efforts.

Looking at the aeronautics budget as a whole in figure 2, the pie charts show how our total R&T program of $228 million in FY 1978 is divided — on the left by budget category and on the right by the various vehicle-specific types. The R&T Base represents about 40 percent of our total aeronautics program; Systems Technology programs about 30 percent; and Experimental Programs 25 percent, with a small continuing effort devoted to Systems Studies. By vehicle-specific categories, CTOL efforts represent nearly 50 percent of our total aeronautics dollar investment. The balance is split, as shown, among the other categories from General Aviation to Supersonic Cruise Aircraft Research

(SCA), with Generic R&T being the second largest category. The CTOL share will remain a significant part of our budget for the foreseeable future as the ACEE program reaches its funding peak and as we continue to identify new technology advancements for this major segment of the air transportation system.

Figure 3 delineates the CTOL FY 1978 funding by the budget categories. Whereas the overall aeronautics program contains 40 percent R&T Base activities, CTOL contains only about 15 percent R&T Base. This is not because of a lesser interest in CTOL-related basic activities but because of the large funding requirements of most of the ACEE focused elements, which are all in the Systems Technology and Experimental Programs categories. The ACEE programs currently represent nearly 70 percent of the CTOL budget.

The CTOL program disciplines around which this conference has been structured are

Propulsion
Materials and Structures
Aerodynamics and Active Controls
Safety and Operating Systems

Figure 4 splits the FY 1978 CTOL activities by these discipline areas in terms of funding and personnel. To support the expenditure of over $100 million in CTOL, NASA has over 1000 in-house direct personnel assigned. Nearly half of these people are working on aerodynamics and controls, so that when the salaries and overhead associated with the in-house staff are included in the total resource expenditures, there is a fairly even balance among the three largest disciplinary areas.

Since a large part of this conference is devoted to the ACEE program, I would like to spend a few minutes describing the process which was used to initiate this major program. Three years ago, the Senate Committee on Aeronautical and Space Sciences requested NASA to establish a special program to develop technology for more energy-efficient aircraft. The Senate letter stressed the importance of a program which would facilitate the technology transfer process and recommended that the plan be developed in consultation with industry. The objective was to make technically possible a new generation of fuel-efficient aircraft which could be flying in the 1980's.

NASA spent the next 7 months working closely with the major engine and airframe manufacturers, the airlines, other Government agencies, and universities to develop a comprehensive technical program plan for improved aircraft energy efficiency. Involvement of the industry both in the development of the plan and in the conduct of major portions of the research is necessary for assurance that the technology is reasonably likely to be implemented. It is also an important first step in the implementation process itself.

The plan was submitted to the Senate in September 1975. It called for the expenditure of additional resources of more than $600 million over 10 years for the aggressive development of aeronautical technology in the areas of propulsion, aerodynamics, and structures. The schedule and phasing of the six technology programs underway is shown in figure 5. Funding for FY 1976 was provided by reprogramming ongoing activities, and additional resource authority

was provided in NASA's FY 1977 and 1978 budgets for the first phases of the program.

The ACEE program is directed at modest but significant improvements in the near term, considerably greater gains for the mid- to late 1980's, and still more ambitious advances for the 1990's.

In propulsion, the near-term concentration is on engine component improvement, both to reduce the fuel consumption of current engines and to identify methods to minimize the performance deterioration of current and future turbofan engines. The work is being carried out largely under contract by Pratt & Whitney and General Electric, with support by the transport aircraft manufacturers and the airlines.

For the mid- to late 1980's, the Energy Efficient Engine (E^3) program is under way with the two major U.S. manufacturers of commercial aircraft engines. The goal of this program is to provide the technology advancements which will permit a reduction in fuel consumption of 10 to 15 percent over current high-bypass engines, while simultaneously improving direct operating costs, emissions, and noise levels.

A program on advanced turboprop technology is included to establish a basis for potential 1990's aircraft powered by advanced turboprops which can operate at speeds and altitudes comparable with today's turbofan aircraft. An advanced turboprop propulsion system offers a minimum of 15 percent additional fuel savings over advanced turbofan engines with equivalent core technology. The efficiency goal appears to be achievable, but considerable research is still required to assure reliability and acceptably low external and internal noise levels and to develop a data base for optimized propeller design.

Advanced aerodynamic and active controls technology is being pursued in the Energy Efficient Transport program for application to both derivative and new aircraft, with technology readiness in the early to mid-1980's. The goal is up to 20 percent improvement in aerodynamic efficiency for new transport designs. The commercial air transport manufacturers are heavily involved in this activity, in efforts aimed to both derivative and next-generation transport aircraft.

Laminar Flow Control, which promises fuel savings of from 20 to 40 percent, is potentially the most productive of the fuel-conservative technologies. It is also the most future-oriented and highest-risk element of the ACEE program. We have a long way to go, but the potential payoff appears well worth it.

The remaining element is the Composite Primary Aircraft Structures program. Here too the approach is a step-by-step progression in size, weight, and complexity with time, with the technology expected to be proven for the smaller components in the early 1980's. The present emphasis is on the design, development, and extensive structural testing of three composite secondary structural components and three moderate-sized primary structures. Each of the three commercial transport companies is responsible for one of the secondary and one of the moderate-sized components, to ensure that a wide diversity of

structural concepts is investigated and to facilitate subsequent implementation.

We have very recently modified the composites program to deal with the problem of the high electrical conductivity of free carbon/graphite fibers which might be released accidentally. The research is being expanded to assess fiber effects and protective techniques and to reduce the risk of fiber release. The structural evaluation, fabrication technology, and ground testing of full-scale components and large subcomponents will continue as planned. Flight-service testing of the new components is not contemplated at this time, and the development of a composite wing is being deferred until we understand better the potential electrical problem and its solution. Composite materials are considered to hold great promise for major weight, fuel, and cost savings in future transport aircraft, and we intend to pursue the research vigorously to successful completion.

It is clear that the ACEE technology advances will be maturing over a span of years, as is typical of research results in any high-technology field. In fact, we can expect continuing advances in aircraft energy efficiency even after the ACEE program itself is completed.

In closing I would like to stress that, in addition to providing a good mechanism for disseminating our technology results to the aviation community early, a Conference such as this, even possibly more importantly, provides an opportunity for the kind of dialogue with industry that we need to assure that our efforts are relevant. I hope the discussions here have produced a significant amount of such dialogue.

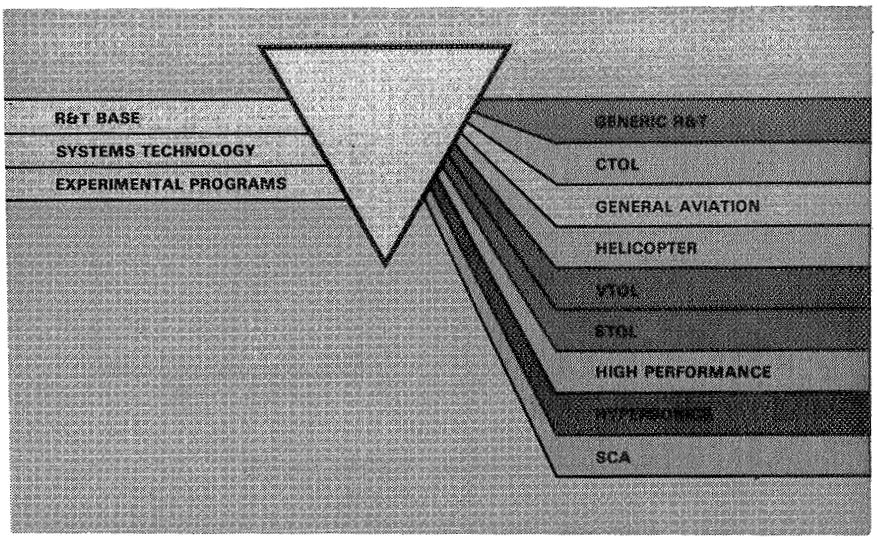

Figure 1.- Aeronautics program.

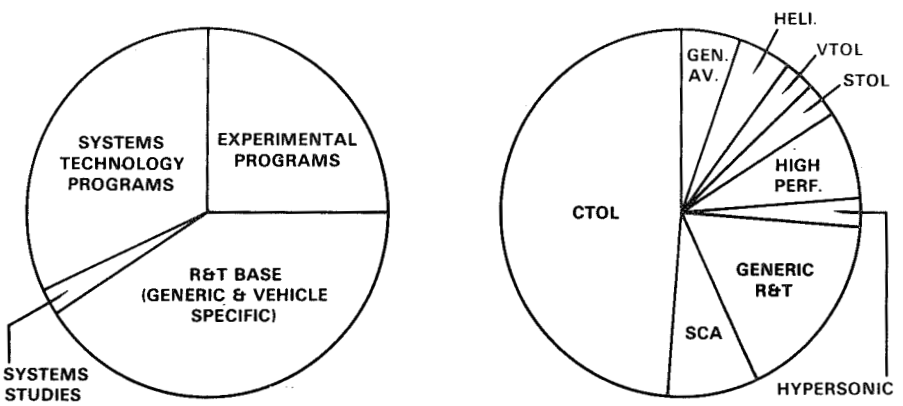

Figure 2.- Aeronautics R&T — 1978. Total R&T: $228 million.

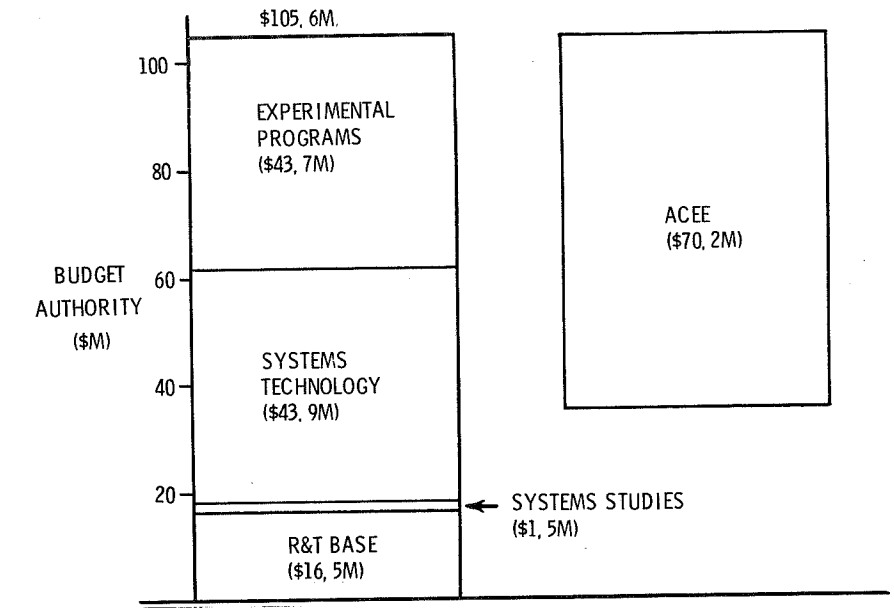

Figure 3.- CTOL budget — FY 1978.

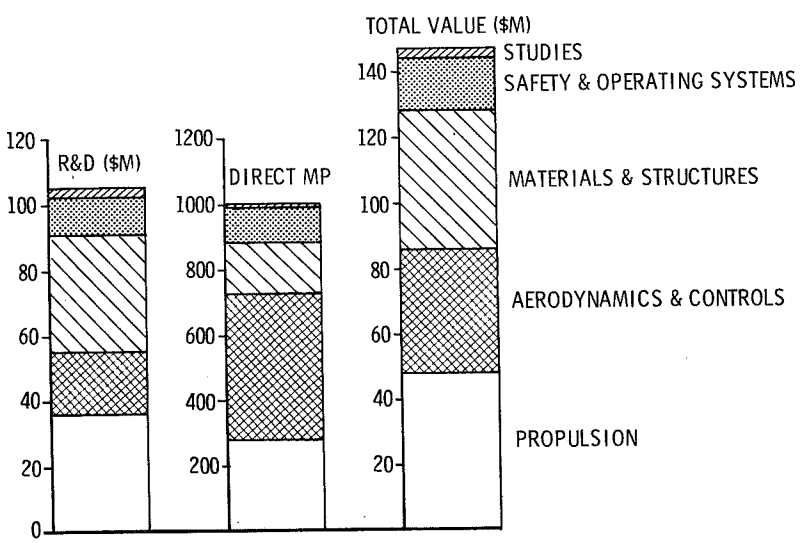

Figure 4.- FY 78 CTOL program by discipline.

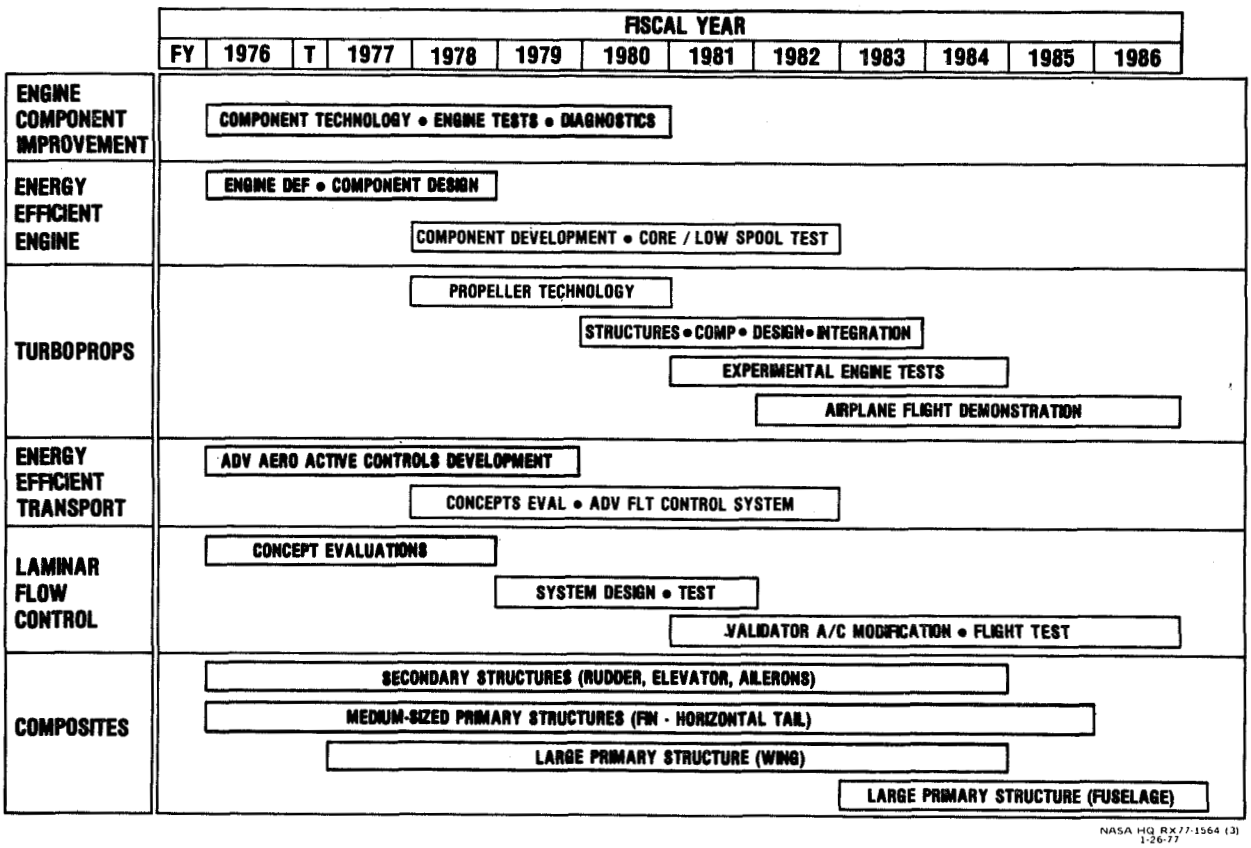

Figure 5.- Aircraft Energy Efficiency program.

ACEE PROPULSION OVERVIEW

Donald L. Nored
National Aeronautics and Space Administration
Lewis Research Center

SUMMARY

The Aircraft Energy Efficiency (ACEE) program, a major aeronautical research program within NASA, involves a wide range of efforts directed toward developing technology for fuel-efficient subsonic CTOL transport aircraft. The propulsion part of this program comprises three efforts: (1) the Engine Component Improvement (ECI) project, (2) the Energy Efficient Engine (E^3) project, and (3) the Advanced Turboprop project. This paper reviews the overall goals and objectives of each project, and then gives the approach and schedule for accomplishing these project goals and objectives.

INTRODUCTION

Minimizing fuel consumption has become a prime design parameter for aircraft propulsion systems. It is expected to remain so in the future. This situation has occurred because of (1) the recent and projected increases in the price of fuel and (2) a general recognition of our dwindling petroleum supply and its possible effect on future airline growth. In response to this growing importance of fuel efficiency, from the standpoint of fuel conservation as well as the impact on commercial aircraft operating economics, the Aircraft Energy Efficiency (ACEE) program was formulated and implemented by NASA. This program is to develop technology that will make possible a substantial improvement in the efficiency of transport aircraft fuel utilization. Three of the six major technology projects in the ACEE program involve propulsion (ref. 1). These three projects -- Engine Component Improvement, Energy Efficient Engine, and Advanced Turboprops -- are managed by the Lewis Research Center and represent an aggressive, focused approach to developing technology for energy-conservative propulsion systems.

The remainder of this paper discusses the programmatic aspects and technical requirements of each propulsion project to provide a better understanding for the papers that follow.

ENGINE COMPONENT IMPROVEMENT

This project is concerned with improving the fuel efficiency of current aircraft engines -- specifically the CF6 engine manufactured by the General Electric Company and the JT8D and JT9D engines manufactured by the Pratt & Whitney Aircraft Group (fig. 1). These engines power most of the commercial jet fleet and will continue to do so throughout the 1980's.

The goal of this project is to achieve up to a 5-percent reduction in fuel consumption over the life of the engine. Both improved engine performance and improved performance retention will contribute to achieving this goal. Accordingly, the Engine Component Improvement (ECI) project is divided into two parts: (1) Performance Improvement and (2) Engine Diagnostics. The Performance Improvement part is to develop technology for fuel-saving components for these three currently used engines with a time goal permitting introduction by 1980-1982. The Engine Diagnostics part is to identify, isolate, and quantify the sources of performance deterioration of the two high-bypass turbofan engines, the JT9D and the CF6, and to establish design or other criteria to minimize performance deterioration. The total anticipated ECI project funding by the government is approximately $37 million with the Performance Improvement effort being cost-shared by the contractors.

The primary approach to the Performance Improvement part consists of feasibility analyses of promising component or component modification concepts followed by the development and evaluation of selected concepts through rig or engine tests, including flight tests if necessary. The feasibility analyses are to identify component concepts, assess their fuel-savings potential over the life of the engine, and assess their economic merits, airline acceptability, and overall potential for implementation through either new production or retrofit. The feasibility analyses are accomplished by a team effort involving two teams. Assisting General Electric are Boeing and Douglas, representing the airframe users of the CF6 engine, and United and American Airlines, representing two major domestic airline operators of this engine. Associated with Pratt & Whitney are also Boeing, Douglas, United, and American. In addition, TWA is a Pratt & Whitney team member and performs the analysis of fleet modeling, route structure, and airline economic effects. (In the case of the GE team, these analyses are performed by Boeing and Douglas.) Specific details and current results of the feasibility analyses are presented in references 2 and 3. In addition, NASA is using Eastern and Pan American World Airlines as consultants to provide independent comments on the merits of the improvement concepts, particularly in areas relating to maintenance and possible retrofit potential, prior to NASA selection of concepts for development.

The Engine Diagnostics activity is directed toward investigating the reasons for performance degradation of operational engines; the deterioration trends are illustrated in figure 2. During the initial operation of the engine, rapid performance degradation of the order of several percent has been noticed. This has been labeled "short term performance deterioration." This degradation is believed to occur during the first flight or flights of the aircraft as the engine structure responds to the flight environment. In the longer term deterioration continues, but at a slower rate. Partial restoration is achieved as the engine is periodically repaired. In general, however, there is increasing deterioration in performance; this trend is termed "long term performance deterioration."

The general approach to the Engine Diagnostics part of the ECI project is to

(1) Gather existing flight data, ground test data, and used parts information to establish historical trends

(2) Augment available data with new data taken from in-service engines, both from in-flight trending and from ground tests

(3) Assess causes of short-term performance degradation through systematic, specialized testing of new or low-time engines

(4) Assess causes of long-term performance degradation by collecting in-service trend data on high-time engines and through specialized ground tests on the same engines

(5) Determine sensitivity and effects of deteriorated parts on performance of specific components

(6) Establish statistical trends, analytical models, and design criteria, with associated correlations of the impact of maintenance practices or operations on SFC losses, and provide recommendations for both current and future engines.

Results of specific aspects of the Engine Diagnostics effort accomplished to date are given in references 4 and 5.

The schedule for the ECI project is shown in figure 3. Feasibility analyses have been completed, and concept selection by NASA is essentially finished. The development and evaluation of two concepts, JT8D outer air seal and CF6 improved fan, were initiated in the latter part of 1977. The development of the remaining concepts will start in 1978. Overall, the final testing phase of many of the concepts are expected to run well into 1980. Engine diagnostics will also continue through 1980 with some activities, such as the component sensitivity effort, being started only after early data are evaluated.

ENERGY EFFICIENT ENGINE

The second ACEE propulsion effort, the Energy Efficient Engine (E^3) project, involves developing and demonstrating the technology base for achieving higher thermodynamic and propulsive efficiencies in future turbofan engines. The intent is to advance fuel-conservative technology sufficiently up the "learning curve" so that an engine manufacturer, as early as 1983, could select such technology for incorporation into a new or derivative commercial engine development with an acceptable degree of risk. Thus, after completing a normal commercial development cycle, these advanced technologies could appear in new turbofan engines in the late 1980's or early 1990's. Also, such technologies could appear in derivative engines as early as the mid-1980's. The E^3 core technology could also be used in future advanced turboprop propulsion systems.

Design goals for a new engine have been established to guide the development of E^3 technology. These goals are as follows:

(1) There should be a significant performance improvement over current high-bypass-ratio engines: Specifically, there should be (a) at least a 12-percent improvement in specific fuel consumption (SFC) accompanied by (b) at least a 5-percent improvement in direct operating costs (DOC) along with (c) im-

proved performance retention over the life of the engine.

(2) There should be no degradation in environmental quality. Any new engine must meet noise and emission standards that might be in force at the time of introduction. Currently, these standards are the FAR-36 noise requirements (as amended March 1977) and the EPA emission standards for engines certified after January 1981.

(3) There should be a thrust growth capability in the E^3 technology that reflects both the uncertainty as to thrust size of any future engine based on E^3 technology and the realization that commercial engine models must undergo a wide range of thrust upratings and downratings. In addition, such thrust growth capability should be accomplished without compromising the other goals.

To meet these goals there must be major engine cycle improvements, and these must be accompanied by improved efficiencies in every component of the engine. To explore and optimize the many variables and design parameters involved, NASA awarded engine definition study contracts to both manufacturers of large commercial engines, Pratt & Whitney Aircraft Group and the General Electric Company. Several different engine cycles and types were studied. Assistance was provided by Boeing, Douglas, and Lockheed in evaluating the impact of different potential 1990 aircraft designs on factors such as thrust level, cycle, and overall engine configuration as influenced by integration with the aircraft. Again, as in the ECI project, NASA also had Pan American World Airways and Eastern Airlines under separate contract to provide independent evaluations of the study assumptions and designs.

Results of the engine definition studies and trade-offs are given in references 6 and 7 and are summarized in figure 4. Current and advanced engines are compared; the increases in cycle conditions (overall pressure ratio, bypass ratio, and rotor inlet temperature) required at cruise to achieve a significant reduction in SFC are illustrated. As can be seen, the studies indicate the 12-percent SFC reduction goal can be achieved. In addition, the studies also indicate the DOC goals are achievable. Associated with the improved cycle conditions are various component advancements. Better materials, better use of cooling air, increased aerodynamic efficiencies, tighter clearances (including active clearance controls), and exhaust gas mixing are examples of the advanced technologies required for a future energy efficient engine.

These engine definition studies established the basic design parameters around which the E^3 technology program was planned. Schedules for the resulting program are shown in figures 5 and 6. The E^3 project is basically a component development and integration effort that is directed toward large high-bypass-ratio commercial engines. Thus, to enhance the probability of successfully meeting the nationally important fuel efficiency goal, both Pratt & Whitney Aircraft and General Electric are participating in the project. Anticipated total government funding is about $170 million with a significant level of contractor cost sharing. The engine designs of the two companies, while superficially similar (both are two-spool, direct-drive engines), reflect different levels and types of component technology. As such, their schedules and critical paths are somewhat different. Technology advances will first be pursued in all the engine components related to the turbomachinery, combustor, and mixer.

When component characteristics are sufficiently known, the high-pressure core components will be assembled and tested to evaluate component interactions, core performance, and design integrity. Parallel to the core effort, some activity may continue on the individual components to improve their performance beyond that demonstrated in the core. Upon satisfactory core demonstration, the low-spool components (fan, low-pressure turbine, and mixer) will be assembled with the core and a metal boilerplate nacelle, and then the integrated package will be tested to evaluate uninstalled performance.

Supporting this entire technology development effort will be the continuing engine analysis activity to update and refine the previous engine definition studies. "Traceable" technology (i.e., any technology (1) as demonstrated and residing in the E^3 components, core, or integrated core/low-spool, or (2) from any other technology efforts ongoing within the company, such as materials development, noise technology, or emissions reduction efforts) will be factored back into the basic E^3 design for evaluation purposes.

It should be noted that the E^3 project is not developing a prototype engine. Components are integrated only to the extent necessary to assess overall performance, component interactions, and system-related technologies. Thus, the project does not include any experimental efforts related to items such as a composite long-duct nacelle. Preliminary designs, weight estimates, and possible aircraft integration penalties for such items will, however, be factored into the flight propulsion system performance. In this manner a comparison to the design goals will be performed.

ADVANCED TURBOPROPS

The third ACEE propulsion effort is the Advanced Turboprop project. NASA-funded studies (refs. 8 to 18) indicate that the propulsion system with the greatest potential for reducing fuel consumption is the advanced turboprop. (A model of such a propeller installed in the NASA Lewis Research Center 8×6 Foot Supersonic Wind Tunnel is shown in fig. 7.) Many different airplane configurations were examined in these studies; two examples are shown in figure 8.

Results from three of these design studies (as summarized in ref. 19) indicate a potential 10- to 20-percent fuel savings for an advanced technology turboprop-powered aircraft relative to a comparable technology turbofan-powered aircraft at Mach 0.8 and a 20- to 40-percent fuel savings relative to a current technology turbofan aircraft. Exact values for the fuel savings depend on the selected aircraft configuration, operational and design stage length, and other study ground rules and assumptions (such as propeller efficiency). These fuel savings translate into potential direct operating cost savings of 3 to 6 percent with 7.9¢/liter (30¢/gal) fuel to 5 to 10 percent with 15.85¢/liter (60¢/gal) fuel relative to a turbofan-powered aircraft.

Results of a passenger survey (ref. 20) by United Airlines indicate a passenger would fly an advanced turboprop-powered aircraft if seating comfort, speeds, and cabin environment (noise, smoothness) were equivalent to today's jet-powered aircraft. Indeed, results show a passenger would accept measurably longer trip times if a fare advantage was associated with the advanced turbo-

prop while maintaining jet-equivalent cabin comfort levels.

Finally, all the studies recommend that research and technology efforts be conducted in four major areas -- propeller efficiency, propeller noise and fuselage attenuation, airframe and engine integration, and propeller and gear-gox maintenance. Indeed, because of the uncertainty in these areas, in particular the feasibility of achieving high propeller efficiencies at high speeds (above Mach 0.7), NASA did not immediately start the Advanced Turboprop project as part of the overall ACEE program. Instead, under the NASA R&T program, efforts were directed to achieving high propeller efficiencies and to further evaluating the maintenance question. Results are given in reference 21.

Based on 1976 wind tunnel tests conducted under the NASA R&T Base program for models such as shown in figure 7, installed propulsive efficiencies are now projected to be about 20 percent better at Mach 0.8 than a high-bypass-ratio turbofan. This efficiency advantage is even greater at lower speeds, as illustrated in figure 9, and is a considerable improvement over the early turboprops. Such an improvement and extension in operating range is due to improved airfoil shapes, multiple blades, and higher power loadings. Based on these results, NASA implemented Phase I of the ACEE Advanced Turboprop project in fiscal 1978 with an anticipated total funding of approximately $7 million.

The basic objective of the Advanced Turboprop project is to demonstrate technology readiness for efficient, economic, reliable, and acceptable operation of turboprop-powered commercial transports at cruise speeds to Mach 0.8 and at altitudes above 9.144 kilometers (30,000 ft). This technology would also apply to possible new military aircraft requiring long-range or long-endurance capability. A major goal is to achieve at least a 15-percent fuel savings relative to a turbofan engine with an equivalent level of core technology. This goal must, of course, be achieved with a cabin environment which is acceptable (i.e., as comfortable and quiet as today's jet-powered commercial transports).

Phase I of the Advanced Turboprop project is an enabling technology effort estimated to require approximately 3 years to accomplish. The effort is divided into six major areas. Current plans in each area are as follows:

(1) The propeller aerodynamic-acoustic design area involves optimizing the propeller design from both the efficiency and generated noise standpoint. Wind tunnel performance and noise tests will be conducted on subscale models (diam. = 62.2 cm, 24.5 in.). Flight tests of the same models, using a Lockheed JetStar Aircraft, will provide in-flight verification of propeller noise. Analytical programs will be developed to enable accurate predictions of propeller efficiency and noise.

(2) Propeller blade structural development will be conducted to establish basic structural designs for future scale-up efforts. Blade preliminary design, materials development, blade segment model tests, aeroelastic model tests, and aerodynamic excitation tests are activities to be conducted under this effort.

(3) Propeller, nacelle, and airframe interactions will be evaluated to develop a data base for propeller slipstream swirl recovery and the avoidance of excessive installation drag.

(4) The cabin acoustics area involves studies of lightweight fuselage-wall acoustic attenuation concepts and model tests of the most promising concepts.

(5) Aircraft studies, similar to previous studies, will be continued to provide program guidance.

(6) Design concepts for advanced gearboxes and pitch change mechanisms will be evaluated in order to select concepts for possible large-scale technology efforts. Engine drives for possible large-scale future propeller tests will also be screened.

Lewis Research Center has total program responsibility, but overall accomplishment will be through a multicenter effort involving Lewis, Ames, Langley, and Dryden Flight Research Centers. Each center will conduct in-house/contractual efforts in those work areas where there is center expertise.

Current planning indicates a need for subsequent phases, as shown in figure 10. Initiation of such phases would be based, of course, on the success of the Phase I effort and budgetary approvals. A Phase II activity, directed toward advanced component development, would involve larger components than those tested in Phase I. Propellers with diameters of the order of 2.4 to 4.3 meters (8 to 14 ft) would be tested in a wind tunnel or with a test-bed aircraft to verify that the aerodynamic, acoustic, and aeroelastic results of Phase I could indeed be scaled. A variety of other tests involving full-scale fuselage segments would also be conducted to verify the merits of an acoustic design concept and the scalability of the design techniques. The development of an advanced gearbox and pitch change mechanisms would also be started.

The next phase, System Integration, could involve flight testing a complete turboprop engine (or engines) on a test-bed or research aircraft. If possible, this engine would be composed of the large-scale components developed under Phase II. The aircraft could have a modified fuselage to incorporate the acoustic design concept developed under Phase II. Flight tests using this aircraft would be conducted to evaluate and verify acceptable cabin environment, fuel savings potential, and system interactions under a full range of realistic operational conditions such as icing, FOD, cross flow, and thrust reversing. Results forthcoming from this last phase would be critical in providing technology readiness for future commercial applications.

CONCLUDING REMARKS

Potential benefits of the three ACEE propulsion efforts for commercial CTOL air transports are shown in figure 11. ECI benefits can be realized in current engines by the early 1980's. The E^3 benefits could be realized by the late 1980's in new engines. Advanced turboprop benefits -- requiring a major change in propulsion systems from those in current use -- might be realized by

the late 1980's or early 1990's, assuming successful completion of the phased program outlined previously. As mentioned before, these three projects represent an aggressive and focused approach to developing fuel-conservative propulsion technology. Such an approach is required, however, if the large potential benefits are to be realized, and the impact of fuel consumption on commercial aircraft operating economics is to be minimized.

The papers to be presented in the remainder of this session will cover current results for each of the three ACEE propulsion projects. In addition, papers will also be presented on several key propulsion technology areas. These key areas have been selected because of their possible future impact on CTOL aircraft requirements and because they are typical of those NASA R&T efforts which provided the basic technology needed to initiate the ACEE propulsion program.

REFERENCES

1. Povinelli, Frederick P.; Klineberg, John M.; and Kramer, James J.: Improving Aircraft Energy Efficiency. Astronaut. Aeronaut., vol. 14, Feb. 1976, pp. 18-31.

2. Lennard, D. J.: CF6 Performance Improvements. CTOL Transport Technology Conference.

3. Gaffin, W. O.: JT9D/JT8D Performance Improvements. CTOL Transport Technology Conference.

4. Lewis, R. J.; Humerickhouse, C. E.; and Paas, J. E.: CF6 Jet Engine Performance Deterioration. CTOL Transport Technology Conference.

5. Salee, G. P.: JT9D Short Term Performance Deterioration. CTOL Transport Technology Conference.

6. Johnston, R. P.; and Hemsworth, M.C.: Energy Efficient Engine -- Preliminary Design and Integration Studies. CTOL Transport Technology Conference.

7. Gray, D. E.: Energy Efficient Engine -- Preliminary Design and Integration Studies. CTOL Transport Technology Conference.

8. Gray, D. E.: Study of Unconventional Aircraft Engines Designed for Low Energy Consumption. (PWA-5434, Pratt and Whitney Aircraft; NASA Contract NAS3-19465.) NASA CR-135065, 1976.

9. Neitzel, R. E.; Hirschkron, R.; and Johnston, R. P.: Study of Unconventional Aircraft Engines Designed for Low Energy Consumption. (R76AEG597, General Electric Co.; NASA Contract NAS3-19519.) NASA CR-135136, 1976.

10. Foss, R. L.; and Hopkins, J. P.: Fuel Conservation Potential for the Use of Turboprop Powerplants. SAE Paper 760537, May 1976.

11. Hopkins, J. P.; and Wharton, H. E.: Study of the Cost/Benefit Tradeoffs for Reducing the Energy Consumption of the Commercial Air Transportation System. (LR-27769-1, Lockheed-California Co.; NASA Contract NAS2-8612.) NASA CR-137927, 1976.

12. Hopkins, J. P.: Study of Cost/Benefit Tradeoffs for Reducing the Energy Consumption of the Commercial Air Transportation System. (LR-27769-2, Lockheed-California Co.; NASA Contract NAS2-8612.) NASA CR-137926, 1976.

13. Stern, J. A.: Aircraft Propulsion - A Key to Fuel Conservation: An Aircraft Manufacturer's View. SAE Paper 760538, May 1976.

14. Kraus, E. F.: Cost/Benefit Tradeoffs for Reducing the Energy Consumption of Commercial Air Transportation System. Vol. 1 - Technical Analysis. (MDC-J7340-Vol. 1, Douglas Aircraft Co., Inc.; NASA Contract NAS2-8618.) NASA CR-137923, 1976.

15. VanAbkoude, J. C.: Cost/Benefit Tradeoffs for Reducing the Energy Consumption of Commercial Air Transportation System. Vol. 2 - Market and Economic Analysis. (MDC-J7340-Vol. 2, Douglas Aircraft Co., Inc.; NASA Contract NAS2-8618.) NASA CR-137924, 1976.

16. Kraus, E. F.; and VanAbkoude, J. C.: Cost/Benefit Tradeoffs for Reducing the Energy Consumption of Commercial Air Transportation System. (MDC-J7340, Douglas Aircraft Co., Inc.; NASA Contract NAS2-8618.) NASA CR-137925, 1976.

17. Energy Consumption Characteristics of Transports Using the Prop-Fan Concept: Summary. (D6-75780, Boeing Commercial Airplane Co.; NASA Contract NAS2-9104.) NASA CR-137938, 1976.

18. Energy Consumption Characteristics of Transports Using the Prop-Fan Concept: Final Report. (D6-75780, Boeing Commercial Airplane Co.; NASA Contract NAS2-9104.) NASA CR-137937, 1976.

19. Dugan, J. F.; Bencze, D. P ; and Williams, L. J.: Advanced Torboprop Technology Development. AIAA Paper 77-1223, Aug. 1977.

20. Coykendall, R. E.; et al.: Study of Cost/Benefit Tradeoffs for Reducing the Energy Consumption of the Commercial Air Transportation System. (United Airlines Inc.; NASA Contract NAS2-8625.) NASA CR-137891, 1976.

21. Dugan, J. F.; Miller, B. A.; and Sagerser, D. A.: Status of Advanced Turboprop Technology. CTOL Transport Technology Conference.

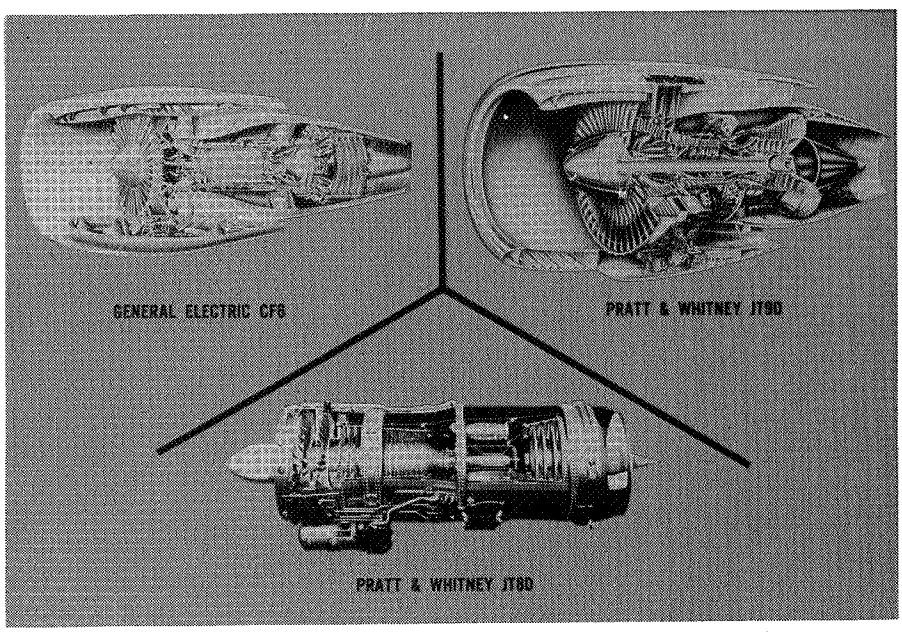

Figure 1.- Engine component improvement.

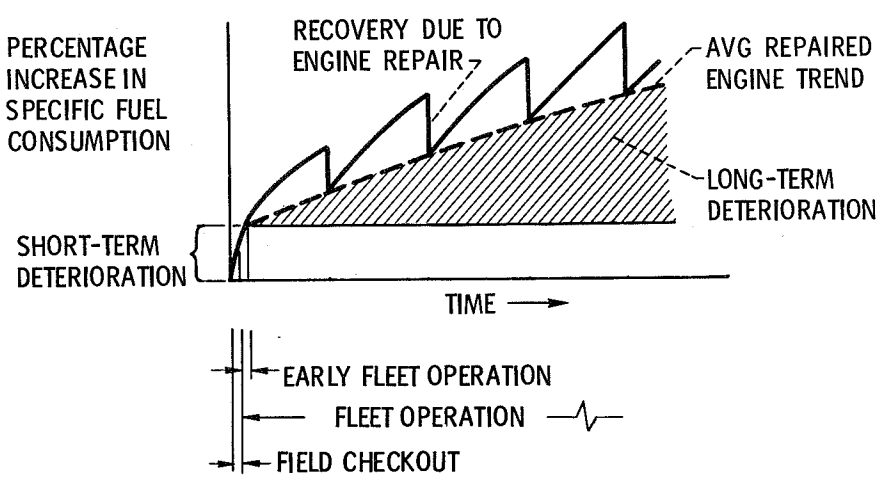

Figure 2.- Engine component improvement - engine diagnostics. SFC performance deterioration trends for typical engine.

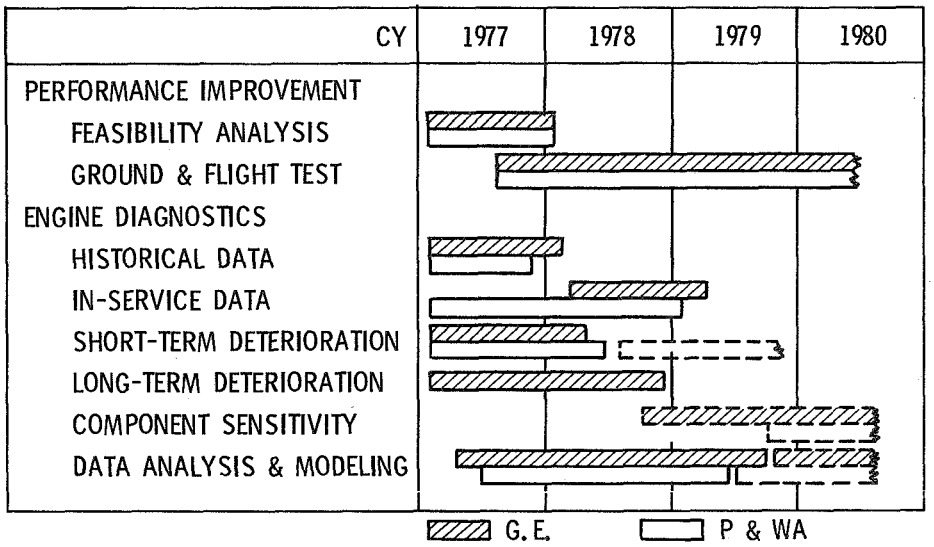

Figure 3.- Engine component improvement schedule.

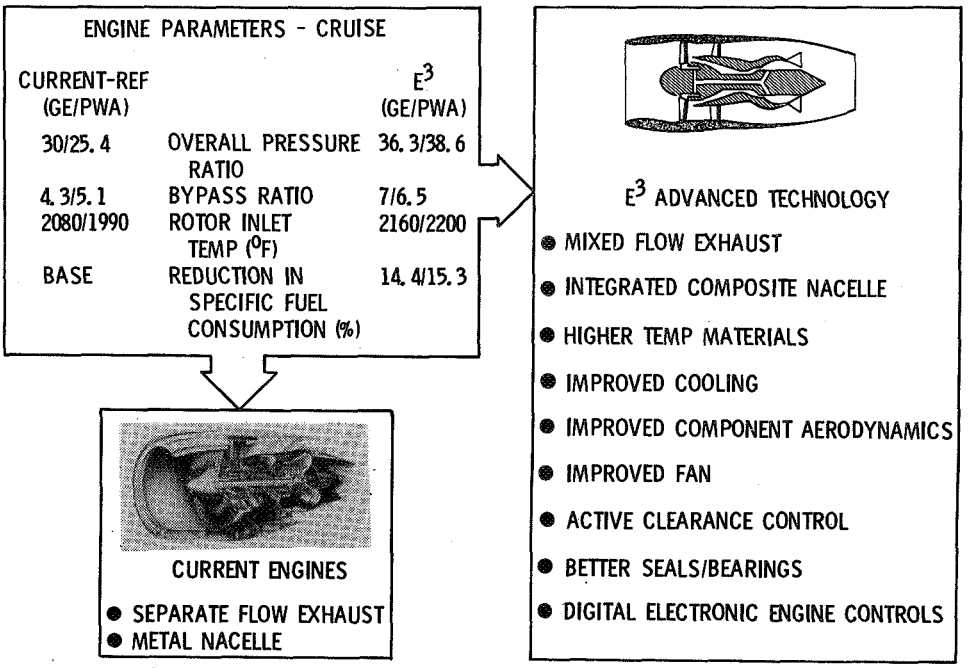

Figure 4.- Definition study results of energy efficient engine.

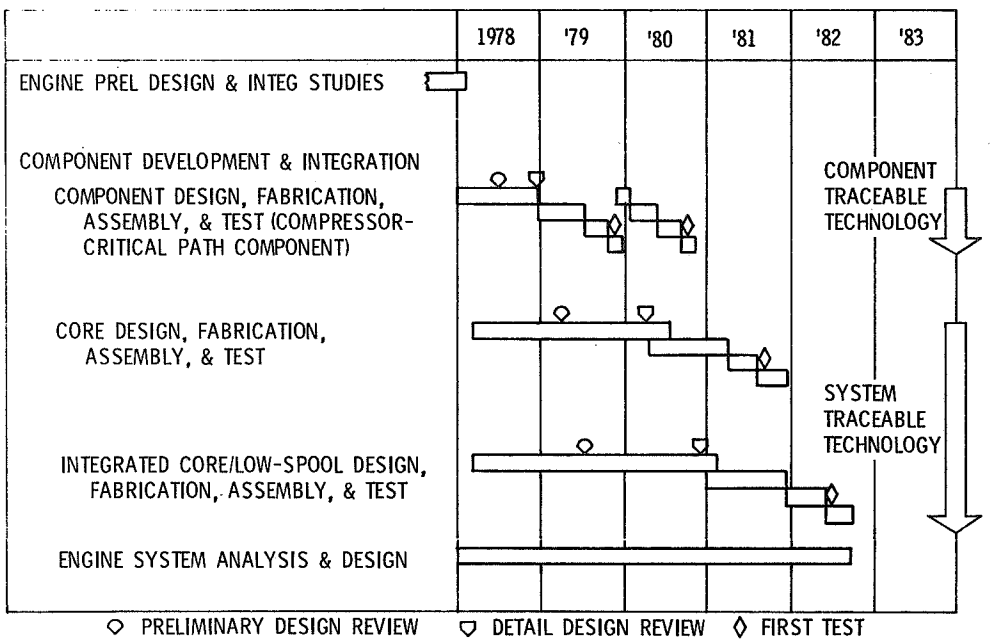

Figure 5.- Energy efficient engine schedule - General Electric Company.

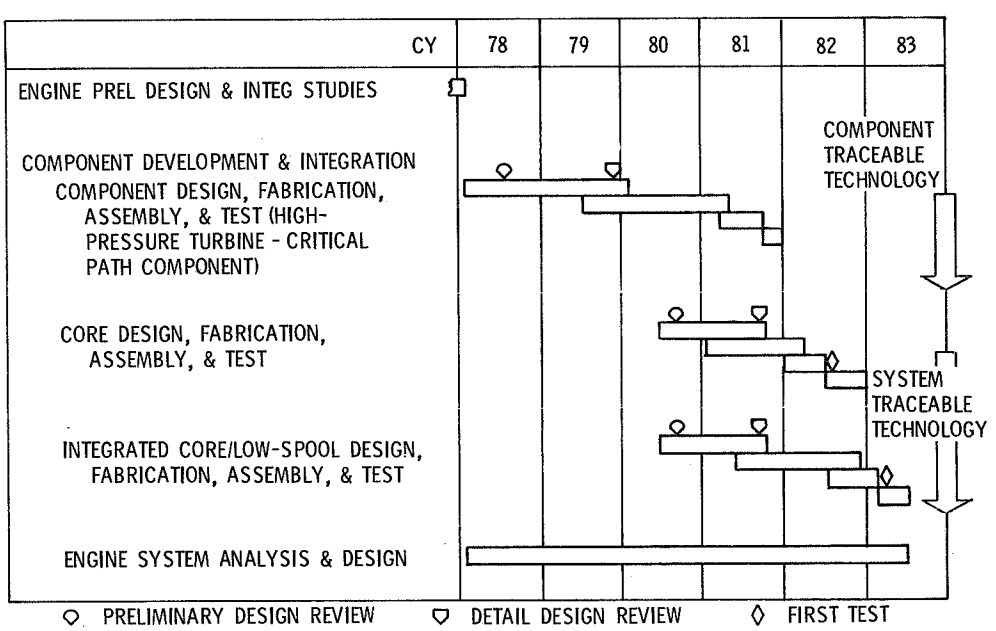

Figure 6.- Energy efficient engine schedule - Pratt & Whitney Aircraft Group.

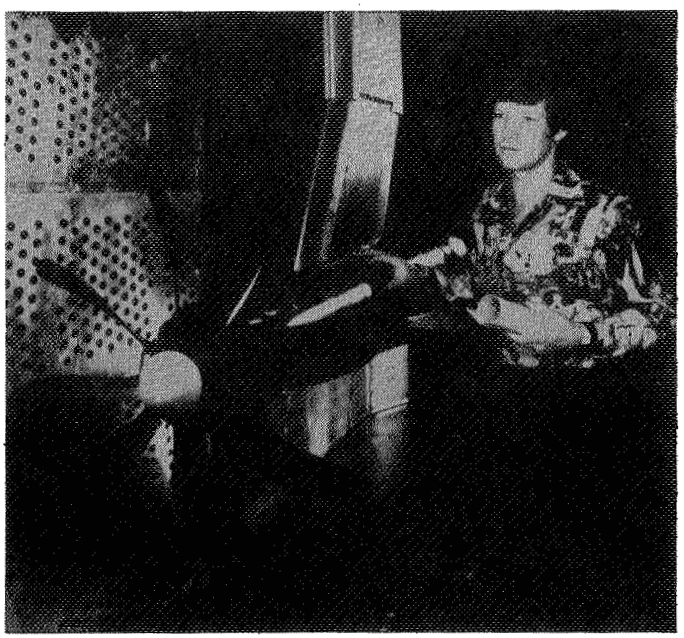

Figure 7.- Advanced propeller model.

Figure 8.- RECAT turboprop airplane concepts.

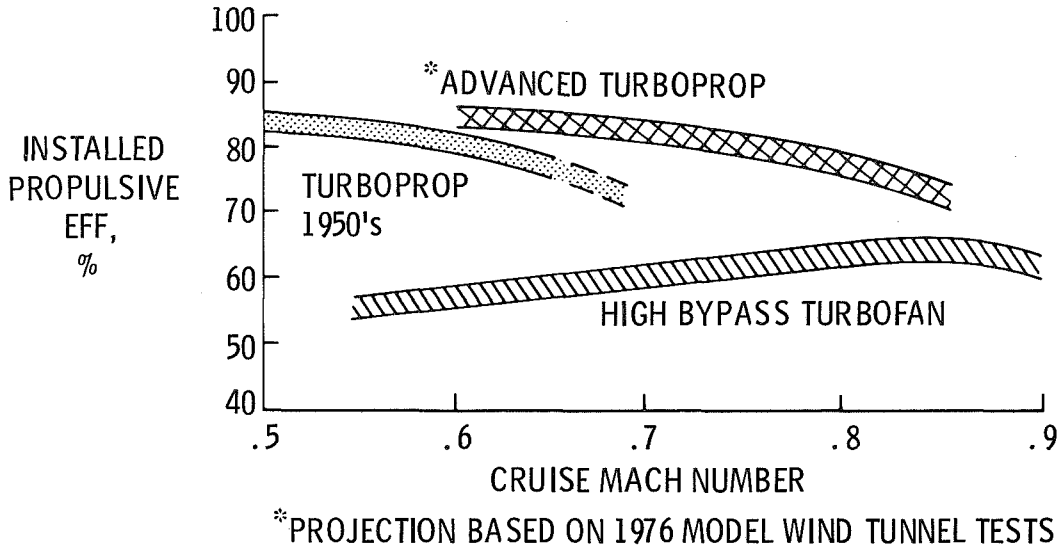

Figure 9.- Influence of cruise Mach number and engine type on propulsive efficiency.

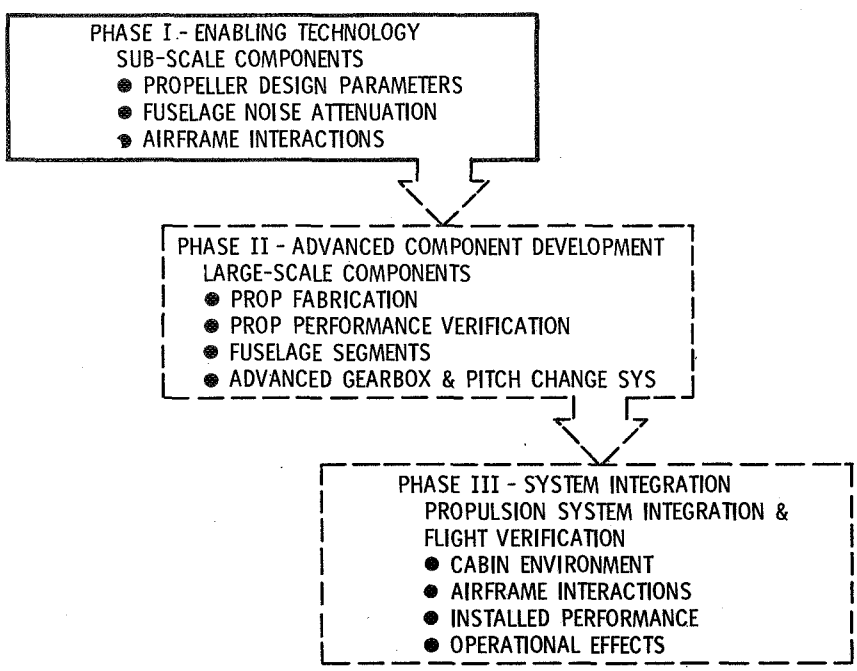

Figure 10.- Phases of advanced turboprop project.

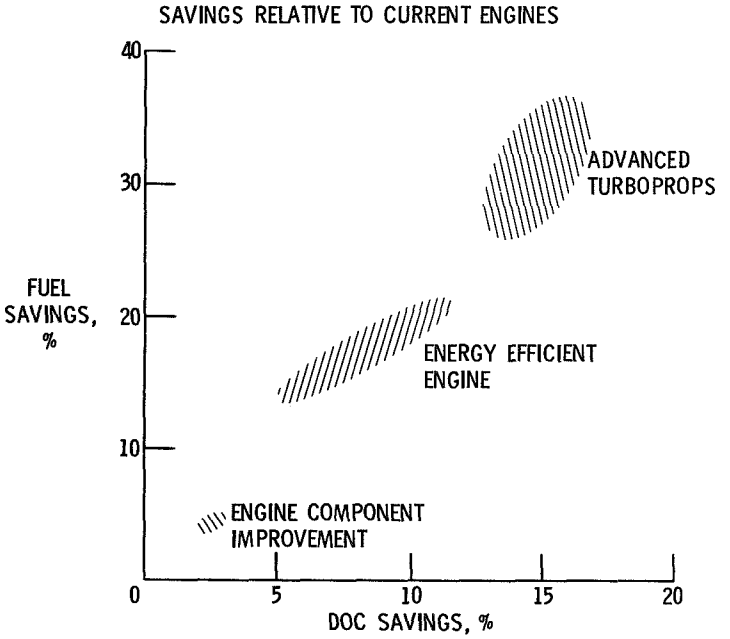

Figure 11.- Potential benefits of ACEE propulsion programs.

CF6 JET ENGINE PERFORMANCE DETERIORATION RESULTS *

R.J. Lewis, C.E. Humerickhouse and J.E. Paas
General Electric Company

SUMMARY

There are many factors which contribute to the performance/deterioration trends of a high bypass-ratio jet engine over a typical life span. In order to identify and effectively introduce fuel conservation measures for such engines, it is necessary to expand information and technology related to these trends. Representative results to-date from an investigation of the General Electric CF6 engines under the NASA Lewis Research Center sponsored "CF6 Jet Engine Diagnostics Program" are reported herein with particular emphasis on the CF6-6D engine model.

Gross measurements of engine performance, such as airline fleet averages, are typically presented as changes relative to a reference baseline. These delta performance levels are the results of not only engine deterioration, but also of design change effects and of performance restoration during airline maintenance.

The revenue service deterioration trends for recent vintage CF6-6D engines have been established for the first installation. The average cruise losses after 4000 flight hours of service are a 2.5% increase in WFM (fuel flow), a 2.0% increase in SFC (specific fuel consumption) and a 17°C increase in EGT (exhaust gas temperature). The rate of deterioration declines with time; for example, the WFM rate is 1.0%/1000 hours for the first 1000 hour period while this rate decreases to 0.5%/1000 hours for the third 1000 hour period.

Modular assessments of deteriorated engines typically indicate that more than 50% of total SFC losses occur in the core hot section. Most of these losses are recovered during normal airline refurbishment. Further, average fleet outbound performance of refurbished engines appears to be stable after the initial (approximately two) shop visits. Moreover, it appears that increased performance restoration can be achieved by added maintenance effort on the low pressure system.

Pre-delivery performance losses occurring during new airplane checkout flights, but before airplane delivery, have also been quantified as a 0.9% increase in SFC. These losses are incurred during the first several flights and have been incorporated in the flight planning manual. Further, the magnitude of these losses has been observed to be less than half when the engines

* This investigation is supported by NASA Lewis Research Center under Contract No. NAS3-20631.

enter revenue service as airline spares rather than by normal aircraft delivery.

A number of studies, both experimental and analytical, are currently underway to further define typical CF6 performance and hardware characteristics through an engine life cycle. The information and technology produced from these NASA/General Electric Company studies will be used to reduce fleet fuel usage by minimizing performance deterioration and improving performance restoration for current and future engines.

INTRODUCTION

By 1990, high bypass-ratio engines such as the CF6 are expected to account for about 75 percent of the total fuel consumed by the U.S. commercial aviation fleet. This aviation fuel, however, is no longer as plentiful and inexpensive as it once seemed to be. Efforts have thus been initiated to determine how to conserve this important resource, especially in relation to its use by these high bypass-ratio engines.

As part of the NASA Aircraft Energy Efficiency (ACEE) program, the Lewis Research Center is conducting an engine diagnostic program on the CF6 engine, with the General Electric Company as the prime contractor. This "CF6 Jet Engine Diagnostics Program" will continue through the end of 1979. The primary objective of this program is to provide additional information and technology which can be used, beginning within the next few years, to minimize the performance deterioration and improve performance restoration of current CF6 engines and their derivatives, thereby realizing significant fuel savings. Emphasis is being placed on the identification and quantification of specific components within the engine which contribute to performance deterioration.

Since this program addresses fuel conservation, the primary interest will be on SFC (specific fuel consumption) performance. This differs from the historical emphasis placed on EGT (exhaust gas temperature) by the airlines and engine companies. EGT, the temperature of the core airstream entering the low pressure turbine of the CF6 engine, is an useful parameter to indicate engine performance in that it can be directly measured by the airlines. On the other hand, SFC must be computed from test cell measurements of thrust and fuel flow or derived from correlations of cruise fuel flow. As such deterioration, impending overhaul requirements and minimum outbound performance have been primarily keyed to EGT prior to this program with little regard for SFC. The emphasis of this investigation on SFC trends should produce advances in the field of fuel conservation.

The CF6 engines provide a good base for this program. These engines are currently installed in large subsonic transports with twin, tri, and quad airplane configurations. Further, these airplanes are produced by various airframe companies and are being used by numerous airlines over a wide variety of route structures.

Engine performance, and changes therein, are complex phenomena involving many diverse factors. This is especially so when considering more than just overall changes in performance. At this time, aspects which are not correlated well include: the sources and causes of deterioration, the relative performance losses of the individual engine modules, and the relation of engine parts condition to performance. Likewise, the effects of variables in the airline utilization of engines, such as length of service versus number of cycles, route structure, usage of derated takeoff power, aircraft type, or engine location are not well understood.

This program addresses the broad scope of engine performance deterioration and restoration through the many facets of a typical engine life cycle. This life cycle includes (for both the CF6-6D & CF6-50 engines) production acceptance testing, flight checkout by the airplane manufacturer, the first installation and refurbishment during airline revenue service, as well as successive revenue service installations and refurbishments. The sources of existing or historical information include: 1) for installed cruise - airline in-service trend data and airplane manufacturer flight checkout data; 2) for test cell data - production acceptance tests, inbound tests prior to maintenance, and outbound tests after refurbishment; and 3) for parts condition - teardown inspection results for special engines and overhaul facility records/experience. In addition, a number of controlled back-to-back tests and hardware inspections are being conducted to provide new information. The combination of refined analyses of existing data with new experimental results will be used to define typical engine performance/hardware characteristics through an engine life cycle.

The initial findings from these studies are presented in this paper. A number of engine performance and restoration aspects are addressed. Statistical trends of CF6-6D performance are shown. Brief discussions of CF6-50 performance trends and of some on-going diagnostic studies are also included. Further, examples of methods to improve overall performance by reducing performance deterioration and improving performance restoration are discussed.

INSTALLED PERFORMANCE

Typical Airline Trends

Airlines are very conscientious about tracking the installed performance of the engines powering their airplane fleet. Cruise trend information is recorded regularly for individual engines as a normal operational procedure during revenue service. This information is used to monitor the relative health of each engine, to anticipate normal maintenance requirements of the engines, and to help assess the profitability of the fleet operation.

These cruise data consist of cockpit measurements of significant engine parameters, most notably WFM (fuel flow), EGT and N1 (fan rotational speed), during stabilized operation at altitude. For the CF6 family of engines, fuel

flow measurements are compared to values from the Flight Planning & Cruise Control Manual for the same flight condition and N1. This manual (FPM) is a tabulation of baseline reference curves for installed engine performance under various operating conditions. The baseline is representative of the installed performance of early CF6 production engines used in a flight test program to define reference engine performance.

These cruise data, delta WFM and delta EGT from FPM at constant N1, are trended versus operating time for individual engines and versus calendar time for the fleet. The individual engine trends are useful for indicating significant internal engine changes/damage warranting hardware inspections or indicating impending requirements for maintenance. On the other hand (due to inherent large scatter in individual engine trending), fleet average trending is typically used to define engine performance deterioration. Thus, improved engine performance and fuel savings resulting from technology developed during the deterioration studies will be reflected in airline fleet average trends.

Trend Levels - Basic Factors

A typical airline monthly DC10-10 fleet trend of cruise fuel flow (deltas relative to the airline FPM, ΔWFM) is presented in Figure 1. The average fleet monthly ΔWFM, as well as the data range, are shown for 1973 through 1977. It can be seen that the fuel flow trends increased during the early years of the fleet operation before stabilizing in 1975. These early fleet fuel flow increases of the CF6-6D engines in the DC10-10 fleet resulted from two factors: 1) the deterioration of engines (a majority which had less than 3000 hours of operation in mid-1973), and 2) the introduction of engine design changes into the fleet which resulted in increased average fuel flow levels as well as, in many cases, increased thrust at N1. The fleet installed fuel flow has stabilized in recent years as the effects of these two factors spread through the airline fleets. The hardware improvement item which had the major impact on fuel flow and thrust at N1, namely modified fan blades, had been incorporated into the DC10-10 airline fleets by 1975. Also, the performance level averages stabilized as the fleet matured.

Performance deterioration and engine design changes, plus limited performance restoration, have produced the present fleet fuel flow level relative to the FPM baseline. The effects of these factors on engine performance, such as fuel flow, are shown schematically in Figure 2. Note that, as indicated in the sketch, additional maintenance beyond normal refurbishment would improve the installed performance. The cost effectiveness of this additional maintenance has not, at this time, been determined.

Design Changes - Effect On Cruise Performance

Design changes were incorporated into the DC10-10 fleet in order to improve CF6-6D performance retention and/or durability after the FPM baseline had been defined by the CF6-6D flight test program. This flight planning

manual to which all installed performance is referenced is not normally updated to reflect such engine design changes for an engine model. Since these hardware changes affect the gross measurement of performance, it is thus necessary to identify the magnitude of the associated installed performance changes in order to separate and define the engine operational deterioration.

Both specific design changes and associated changes in performance are presented in Figure 3. (These design changes and the effects are discussed in greater detail in Reference 1.) All of these items have been incorporated in recent vintage engines (i.e. ESN 451-406 & above) during production, while earlier engines had the changes incorporated through factory changes and/or service bulletins. The net effect on cruise performance, relative to the FPM, of all these changes has been to increase net thrust at N1 by 2.5% while producing higher fuel flow at N1 (3.2% increase), EGT at N1 (7.0°C increase), and SFC at Fn (0.79% increase), while still meeting SFC requirements.

To illustrate the installed performance effects of the design changes on measured fuel flow, initial airline revenue service cruise data have been trended on new engines that had been shipped with these changes. Presented in Figure 4 are these data for the DC10-10 installation of the CF6-6D engine. It can be seen that fuel flow is 3.2% higher than the reference baseline as the engines started revenue service. Again, note that these engines were shipped with acceptable SFC margins.

Typical Deterioration Trends

Typical installed deterioration trends are established from these cruise data which were recorded for engines prior to any maintenance by three DC10-10 operators during normal revenue service. A curve fit representative of the average CF6-6D cruise fuel flow of post -406 engines is shown in Figure 4. It can be observed that the rate of deterioration was greater early in the life of these engines. During the first 1000 hours of operation, the average cruise deterioration rate was about 1%/1000 hours, while during the third 1000 hours of operation the deterioration rate had decreased to less than half of that rate, being about 0.5%/1000 hours.

The cruise EGT and SFC deterioration trends (not shown) of these same installed engines were similar. About 40% to 45% of the average cruise performance deterioration after 4000 hours of operation was lost during the first 1000 hours of service for these CF6-6D engines. The average change in performance at cruise power during these engines' first 1000 hours was a 7 1/2°C increase in EGT at N1, and an equivalent 0.8% increase in SFC at Fn based on ΔWFM. It is suspected that the higher early deterioration rate was related to the average rate at which engine clearances (rotating and stationary) opened up. For instance, during initial installation the engine clearances are tighter, thus the likelihood of a rub which will cause a performance loss is higher. The events which result in increased clearances and losses in performance are distributed more heavily in the early operational time.

Installed Performance Trend Summary

The average installed engine performance levels, relative to the FPM baseline, are thus the sum of the effects of deterioration and of hardware design changes. The delta fuel flow and SFC variations with time of CF6-6D, post ESN 451-406, engines are shown in Figure 5 for a typical first installation of these engines. After 4000 hours of operation, the average level of fuel flow at N1 was 5.7% above the baseline of which 2.5% was due to deterioration and 3.2% was due to engine design changes. Likewise, after 4000 hours of operation, the average cruise SFC at Fn increased 2.0% above the initial service level where the aircraft had acceptable specific range (i.e. measure of airplane specific fuel consumption).

METHODS TO IMPROVE PERFORMANCE & REDUCE FUEL CONSUMPTION

Two approaches toward improving the performance and reducing fuel consumption of the airline fleets are: 1) reduce performance deterioration, 2) attain additional performance restoration during maintenance. The intent of the current diagnostic studies is to develop a better understanding of engine performance, as well as improve technology. This will be accomplished in order to identify specific and viable actions for both approaches, thereby yielding performance improvements and fuel savings for current and future engines. As part of on-going investigations, not only will overall engine performance (losses and restoration) be considered, but modular performance, as well as the hardware conditions relative to performance changes, will also be examined.

Reduce Deterioration

There are a number of avenues open when exploring the approach to improved performance by means of reducing deterioration. Design changes can be incorporated in engines to reduce deterioration rates. Operational procedures can be modified, within certain constraints, to reduce the severity of the conditions under which the engines operate. Examples of these avenues will be given. Further, the sources and causes of pre-delivery deterioration (losses occurring during initial flights, particularly during airplane checkout flights) are being investigated to determine what actions might be taken to reduce this loss.

Design Changes To Reduce Deterioration

Consider first the effect of engine design changes on deterioration rates. As part of engine diagnostic studies, the effect of hardware changes on deterioration, such as the CF6-6D improvements introduced in production with ESN 451-406, will be examined. Such a study will involve accounting for the fleet mix of engines with and without these improvements. At this date a comparison more readily made would be between two CF6 engine models,

the -6D and the -50A. The CF6-50, being a derivative of the CF6-6D, incorporated many basic design philosophy changes that were based on mechanical and aerodynamic experience with the CF6-6D. Moreover, typical cruise deterioration histories prior to refurbishment have been established for these engines.

This comparison of the cruise deterioration rates of CF6-6D and CF6-50A engines installed in DC10 airplanes is presented in Figure 6. Losses in performance of these non-refurbished engines relative to their respective FPM baselines are shown at 1000 flight hour intervals. It can be observed that the rate of deterioration is lower for the CF6-50A. In particular, the fuel flow was consistently lower for the CF6-50A through 3000 hours, as were the average SFC and EGT rates of deterioration. In other words, the design changes incorporated in the CF6-50A model resulted in better average performance retention prior to the first refurbishment of the engines. Nevertheless, the deterioration characteristics are similar for both engine models. This similarity generally allows performance improvements designed for one engine model to be applied to the other model.

Operational Procedures To Reduce Deterioration

Another avenue to achieve deterioration rate reductions is through flight operation procedures, certainly within the constraints of safety. One procedure employed by airlines to reduce deterioration is to operate their engines derated when conditions permit (load factors, airport temperature and altitude considerations). An example is presented in Figure 7 showing for the CF6-50 the average EGT deterioration rate per 1000 hours as a function of the percent of rated CF6-50C thrust. Curves of the average deterioration rate are shown for the first 1000, 2000, and 3000 hours of revenue service operation. As noted, airlines typically operate CF6-50 engines at 7% derated thrust. Based on this preliminary analysis, it can be observed that the effect of derate is to substantially reduce the average performance losses (in this case, EGT) for a CF6-50 engine. For instance, after 1000 hours of operation, the average EGT relative to initial flight levels would be about 9 °C higher without derate. CF6-50 engines operating at derated thrust have better average EGT performance throughout a typical installation. The improved EGT performance is also indicative of improved SFC and fuel flow performance.

Pre-Delivery Losses

Another aspect of engine performance deterioration must be considered; namely pre-delivery losses, the performance losses prior to initial revenue service. This deterioration becomes evident as a loss in performance after the initial flights, but prior to revenue service of the engine, when compared to predicted performance levels of production test cell calibrations. These losses have been shown for both the CF6-6D and CF6-50 to be real and not reversible when low time engines were recalibrated in test cells after

undergoing airplane checkout procedures. These losses are included in the airline reference datum point as defined by initial revenue service and are incorporated in the FPM baseline. Since these losses were also incurred during the flight test program prior to defining the flight planning manual, all of the baseline data to which the engines are now being compared are, therefore, consistent.

Another characteristic of pre-delivery loss which has been observed is that installed performance losses are larger for engines undergoing airplane checkout procedures conducted by the aircraft manufacturer than for those engines entering revenue service as airline spares. As yet, no General Electric engines have been torn down to develop an analytical assessment of the causes of this deterioration. However, an investigation is currently underway to identify and quantify the sources and causes of this deterioration.

During the checkout of a new airplane prior to delivery to an airline, ground run-ups of the engines are made in order to trim the throttle levers and linkages plus several flights are flown to checkout the systems through their full range of operations. Engine cockpit parameters are typically recorded by the airframer during the first flight. The average cruise losses after the airplane checkout for these CF6-6D engines were 1.3% increase of WFM at N1, 0.9% increase of SFC at Fn, and 16°C increase in EGT at N1. As previously noted, these are incorporated in the FPM. Modular assessments of the losses are not complete as part of the diagnostic studies, but it is estimated that the losses were primarily in the HP turbine. The causes of these losses will be investigated as part of the diagnostic studies.

As mentioned earlier, engines going through airplane checkout procedures characteristically experience greater losses than engines entering revenue service as airline spares. A comparison indicating this difference is presented in Figure 8. Average revenue service deterioration of WFM and EGT are shown for the first installation of CF6-6D post ESN 451-406 engines. Even though the data are sketchy, it can be observed that the spare engines entered service with better performance and remained consistently better through the first installation (typically less than 5000 hours). The average difference was about 0.4% WFM at N1, and 9°C EGT at N1. These differences seemingly are the result of the rigorous airplane/engine flight checkout procedures required for aircraft checkout, prior to delivery and entry into revenue service.

Additional Performance Restoration

Another approach to improve fleet performance and reduce fuel usage is to attain additional performance restoration during maintenance. The key to success for this approach is to identify specific hardware refurbishment with the potential of restoring significant performance losses and to determine the cost effectiveness of such work. An important element in this is the assessment of modular performance losses and the relation of these losses to the hardware condition.

The refurbishment of CF6 engines is generally accomplished on a modular replacement basis; non-serviceable modules are replaced with restored, serviceable modules. The workscope for a particular engine during a particular shop visit is suited to the condition of that engine at that time. The basic objectives of the refurbishment efforts in the overhaul facilities have been to replace damaged or non-serviceable parts and to restore EGT temperature margin (the basic shop measure of overall performance) so that the engine can be returned to revenue service for a reasonably long period of time.

The largest causes of CF6 engine removals are related to the hot section core items; e.g. the HP turbine, the HP turbine nozzle, and the combustor. The refurbishment emphasis, as a result, has been on the hot section to restore core performance as discussed in Reference 2. As outlined in this reference, numerous studies have been conducted to identify cost effective refurbishment activities.

With the normal workscope aimed at the core, the largest potential for additional performance restoration during engine maintenance in the overhaul shop probably lies in the low pressure system. Typically, little work is done on the LP system during a shop visit. The amount of performance that is restorable through cost effective LP refurbishment is being examined as part of the CF6 diagnostics studies.

Modular Performance Assessment

As part of these studies, two CF6-6D engines have been run inbound in a test cell prior to any maintenance in order to assess the modular contributions to the overall deterioration. The apportionments of the overall SFC losses measured in the test cell for these two engines, ESN 451-380 & 451-479, as well as for two other engines, are presented in Figure 9. This assessment is shown as a percentage of the total SFC loss relative to production acceptance test levels and is divided between the HP compressor, the HP turbine, and the LP system. The losses in the HP turbine are further divided between efficiency changes and cooling flow changes, while the LP system assessment represents the combined losses in the LP turbine and the fan or LP compressor.

For the first three engines, it can be observed that the largest SFC losses, about 65% of the total, have been assessed to be the result of HP turbine deterioration. This assessment illustrates why the typical airline refurbishment emphasis has been directed at the core hot section. HP compressor deterioration has been assessed at 16% to 28% of the total SFC deterioration, while the remaining 7% to 21% have been assigned to deterioration of the LP System. The fourth engine, ESN 451-479, appeared to have an untypically low percentage of SFC deterioration in the HP compressor and LP system.

As part of the CF6 diagnostic studies, ESN 451-380 & 451-479 underwent teardown inspections, after inbound tests, to assess the hardware condition and to determine the major hardware contributors to modular performance deteriora-

tion. The major items influencing as-recieved engine performance for each section of the engine were as follows.

TWO SPECIAL DIAGNOSTIC CF6-6D ENGINES

MAJOR HARDWARE CONDITIONS AFFECTING PERFORMANCE

HP Compressor	- Airfoil Surface Finish
Core Hot Section	- HP Turbine Tip Clearances
	- Forward Shaft Seals
Low Pressure System	- Stage 1 Fan Blade Cleanliness & LE Contour
	- LP Turbine Clearances

This list notes only the major hardware conditions which result in modular performance deterioration. Numerous dimensions, surface finishes, and general part conditions were recorded throughout these two engines prior to any refurbishment activity. The above items were determined to have the most significant impact on performance based on a combination of the observed wear of these parts and previously developed hardware/performance influence factors. These influence factors relate measured changes in hardware condition to overall performance.

As previously indicated, airline maintenance of deteriorated engines is typically directed toward refurbishment of the core hot section, where the largest performance deterioration usually occurs. This emphasis on core refurbishment can be observed in all overhaul facilities; the workscope for most engine visits includes replacement and/or refurbishment of hot section parts, while only occasionally including work on the low pressure system. The resulting performance restoration of the core can be derived from analysis of test cell measured, overall performance improvements. Since core components have a somewhat larger influence on EGT than LP system components, a percent of core efficiency improvement produces more EGT reduction than a similar improvement in LP system efficiency.

Typical Outbound Performance

Although the amount of restoration attained for individual engines/visits varies substantially, the average outbound performance appears to be stable for a given set of engines. To illustrate this point, histories of outbound SFC and EGT deltas relative to a 10,000 hour average are shown in Figure 10 for twelve refurbished CF6-6D engines through three or more shop visits per engine (74 total outbound tests). While there is a wide data spread, the outbound levels measured in this airline test cell were observed to be steady-to-improving over 10,000 hours of revenue service for this twelve-engine sample. This trend has resulted from an increased maintenance scope to restore EGT margin

and performance of older engines.

Further, average sea level SFC and EGT margins (about 2 1/2% below new engine specs and 8°C EGT margin) imply that the average refurbished engine has performance losses remaining in LP efficiency when returning to revenue service. When these outbound margins are compared to average production engine acceptance test cell levels, the performance deltas indicate that the new engines were typically 3% to 3 1/2% better in SFC and 20°C better in EGT. This ΔSFC/ΔEGT combination suggests that the average LP system efficiency of these refurbished engines was on the order of 3% lower than typical production CF6-6D engines (worth 2% in SFC). This observation coincides with typical overhaul facility workscopes which emphasizes core hot section work.

LP System Restoration Potential

Previous investigations were properly directed toward identifying cost effective refurbishment procedures and techniques for the core because the greatest return on maintenance efforts required to restore EGT within acceptable margins relative to certified limits should be in the core. With escalating fuel prices and dwindling fuel resources, however, efforts must be directed toward obtaining additional performance restoration for the engines during normal maintenance. Since there is typically little refurbishment effort for the LP system and since outbound performance after maintenance suggests significant residual SFC losses in the LP system, it appears that studies are needed to define the amount of performance restoration that might be expected with expanded LP refurbishment activities and the projected cost effectiveness of such activities. As part of the NASA Lewis Research Center sponsored "CF6 Jet Engine Diagnostic Program", a major investigation into LP system performance deterioration is currently underway.

A series of back-to-back engine tests is planned in 1978 to compare the performance of new production low pressure turbine modules to that of typical airline serviceable LP turbine modules which are installed on refurbished outbound engines. These tests should provide results which indicate the degree of LP turbine efficiency which is not regained during normal maintenance. In addition, tests are also planned to measure the amount of performance restoration which can be obtained by refurbishment or replacement of selected LP turbine parts. This investigation should provide deeper insight into the possibilities of additional performance restoration through expanded maintenance procedures.

Improvement of the typical outbound SFC performance margins of refurbished engines, such as shown in Figure 10, will lead directly to fleet fuel savings. If expanded refurbishment efforts can be demonstrated to be cost effective, such practices can be introduced rapidly in the field. As such, fuel savings can be realized for all engines currently in service, as well as for new engines. The important factor in identifying added or revised refurbishment activities which will yield improved performance and lower fuel consumption is understanding the contributions of modular deterioration to overall performance losses,

as well as understanding the relation of parts condition on performance. Diagnostic studies are currently proceeding to broaden this understanding, not only for the LP turbine, but for all the major engine modules.

CONCLUDING REMARKS

The study of jet engine performance over a typical life span is a broad and complex topic. The gross measurements, such as fleet fuel flow levels, of engine performance are impacted by many factors. Factors which produce these levels consist not only of engine deterioration, but also of design change items and the performance restoration of engines during airline maintenance. In order to improve performance and reduce fleet fuel usage, it is necessary to identify the contribution of each of these factors.

The use of the performance baseline from the flight planning manual as a reference to measure changes in cruise fuel flow rates has been discussed. For the CF6-6D engine, the introduction of design changes for performance and durability reasons was seen to introduce an average increment relative to this baseline of 3.2% WFM increase at N1, 2.5% Fn increase at N1, 0.8% SFC increase at Fn, and 7°C EGT increase at N1, while maintaining sufficient SFC margin of the delivered airplane. The effect of revenue service deterioration and performance restoration relative to the reference was shown to be an adder on top of these design effects.

A schematic of typical CF6-6D performance through revenue service and airline maintenance is presented in Figure 11, in terms of percent cruise SFC relative to an airline datum point (average level upon entering revenue service). The typical changes in SFC margin are shown for airline revenue service through four installations and refurbishments. The relative magnitudes of the changes and frequency of shop visits are representative of post ESN 451-406 engines.

The overall installed performance trends for these engines are well understood through the first installation. These deterioration losses are summarized below relative to the airplane datum point.

AVERAGE CRUISE LOSSES FOR FIRST INSTALLATION

	ΔWFM @ N1	ΔSFC @ Fn	ΔEGT @ N1
4000 Hour Deterioration	2.5%	2.0%	17°C

Further, during the typical airline restoration of the CF6-6D engine more than 50% of the modular losses of a typical inbound deteriorated engine are in the core hot section. Most of these losses are recovered during normal refurbishment. The resulting average outbound performance of these refurbished engines appears to be stable with operational time. Losses typically remain in the LP system after refurbishment, but the amount that is recoverable through additional maintenance has yet to be defined.

Pre-delivery losses occurring before airplane delivery have also been defined in terms of overall performance changes. These average cruise losses after airplane checkout are 1.3% WFM increase at N1, 0.9% SFC increase at Fn, and 16°C EGT increase at N1. It has also been observed that engines entering revenue service as spare engines display less than half the losses incurred during aircraft checkout flights and the performance of these spare engines remain consistently better through the first installation. The causes of these losses are not fully defined at this point, but they are being carefully investigated in an attempt to improve delivered airplane/engine performance.

The current "CF6 Jet Engine Diagnostic" studies will continue through the end of 1979. To date, test cell and cruise performance data have been examined for both the CF6-6D and CF6-50 engines to establish or confirm statistics and trends of engine performance. As part of the continuing diagnostics program both experimental and analytical studies are currently underway during which 1) overall performance trending and deterioration models will be extended and refined over the complete engine life cycle; 2) modular deterioration rates will be further assessed; and 3) typical hardware conditions will be related to performance losses. The information and technology produced from these studies will be used to reduce fleet fuel usage by minimizing performance deterioration and improving performance restoration for current and future engines.

REFERENCES

1. Epstein, N. and Hess, P.J.; "Improving Performance Retention of High Bypass Engines", SAE Paper No. 750620, May 1975.

2. Wulf, R.H.; "Recent Development In Engine Performance Refurbishment", AIAA Paper No. 76-646, July 1976.

NOMENCLATURE

Values are given in SI units or as percentages. The measurements and calculations were generally made in U.S. Customary Units.

Airline Datum Point	aircraft performance reference level as determined during initial revenue service
As-Shipped	production acceptance test cell data
EGT	exhaust gas temperature, in °C
EGT Margin	test cell EGT margin (zero margin in test cell equivalent to 17 °C margin on wing)
ESN	engine serial number
FPM	"Flight Planning & Cruise Control Manual", tabulation of baseline reference curves for installed engine performance under various operating conditions
Fn	net thrust, rated CF6-6D takeoff installed thrust = 173 kN (38,900 lbf)
HP	high pressure
HPT	high pressure turbine
LP	low pressure
LPT	low pressure turbine
N1	fan rotational speed, rated CF6-6D takeoff fan speed = 3443 rpm
SFC	specific fuel consumption, CF6-6D takeoff guarantee level (0.357)
SFC Margin	difference between SFC level & guarantee SFC, %
SPEC	airplane delivery specification
TSO	time since overhaul, in hours
TSN	time since new, in hours
WFM	fuel weight flow
ΔWFM, ΔWf	change in fuel weight flow relative to the FPM reference, in %

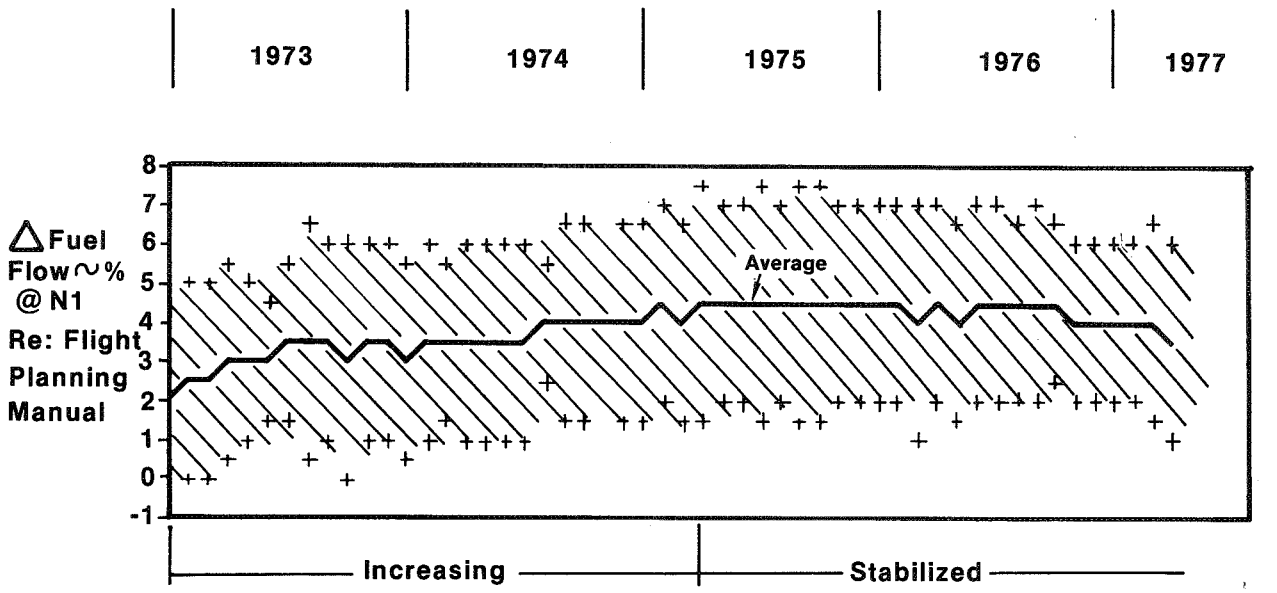

Figure 1.- Typical airline fuel flow trends.

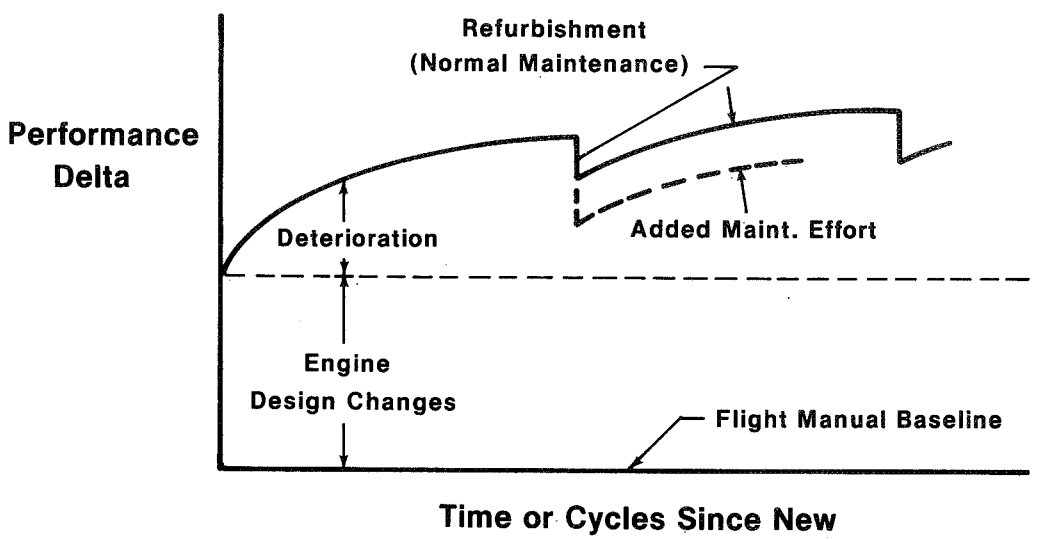

Figure 2.- Schematic of typical engine revenue service history.

Performance Items	ΔWf%@N1	ΔFn@N1	ΔEGT°C@N1	ΔSFC%@Fn
• Fan Blades LE Recontour (P16)	+2.02	+2.17	+7.2	-0.31
• Increase LP Nozzle Flow Function	+0.29	+0.43	-8.9	+0.06
Durability Items				
• Frame Revent	+0.22	-0.13	+2.0	+0.35
Fan Clearance Increase	+0.44	-0.02	+1.3	+0.49
• Miscellaneous				
— Solid Fan Blades (P04)				
— Honeycomb Shrouds				
— G44 Combustor				
— HPT Improvements				
Total	+0.21 +3.18%	+0.01 +2.46%	+5.4 +7.0°C	+0.20 +.79%

Figure 3.- Effect of CF6-6D design changes on cruise performance.

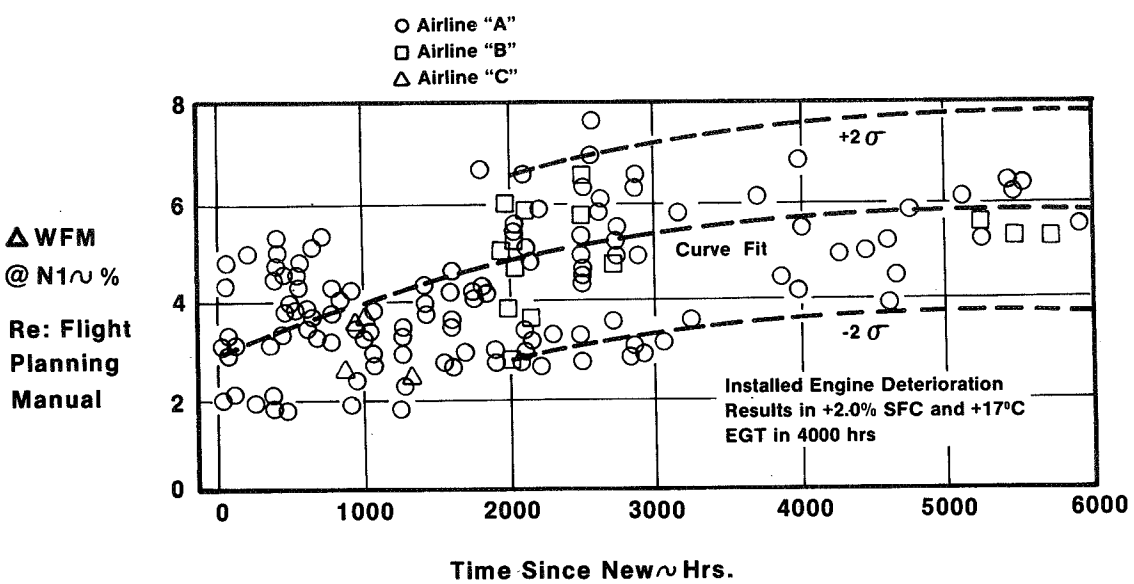

Figure 4.- CF6-6D installed cruise deterioration trends - first DC10-10 installation.

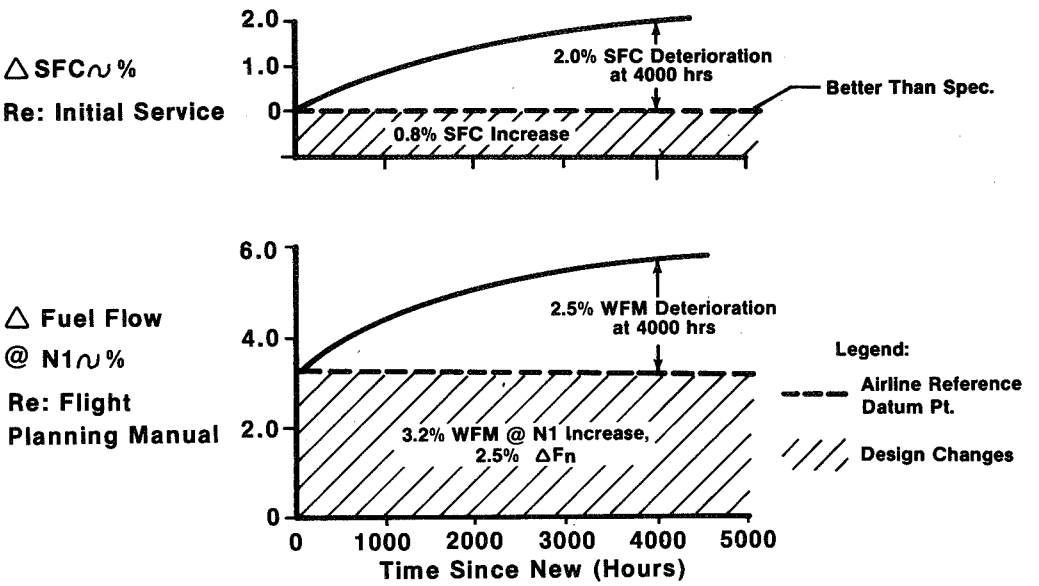

Figure 5.- First installation cruise characteristics - design changes plus deterioration effects.

Comparison of CF6-6D and CF6-50A Prior to Refurbishment

- **Cruise Deterioration Rates**

	△Fuel Flow @ N1		△SFC @ Fn		△EGT @ N1	
	-6D	-50A	-6D	-50A	-6D	-50A
First 1000 Hours	1.0%	0.6%	0.8%	0.6%	8°C	5°C
@ 2000 Hours	1.7%	1.2%	1.4%	1.1%	13°C	10°C
@ 3000 Hours	2.2%	1.7%	1.7%	1.5%	15°C	14°C
@ 4000 Hours	2.5%	2.1%	2.0%	1.9%	17°C	17°C

Figure 6.- Effects of engine model design changes on deterioration rates.

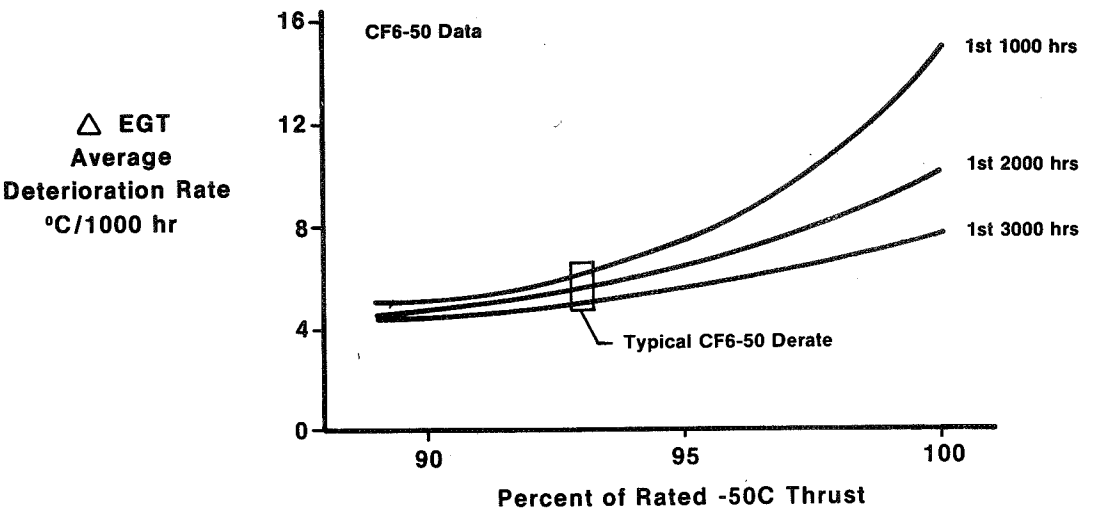

Figure 7.- Operational procedure which reduces deterioration rates - effect of derate.

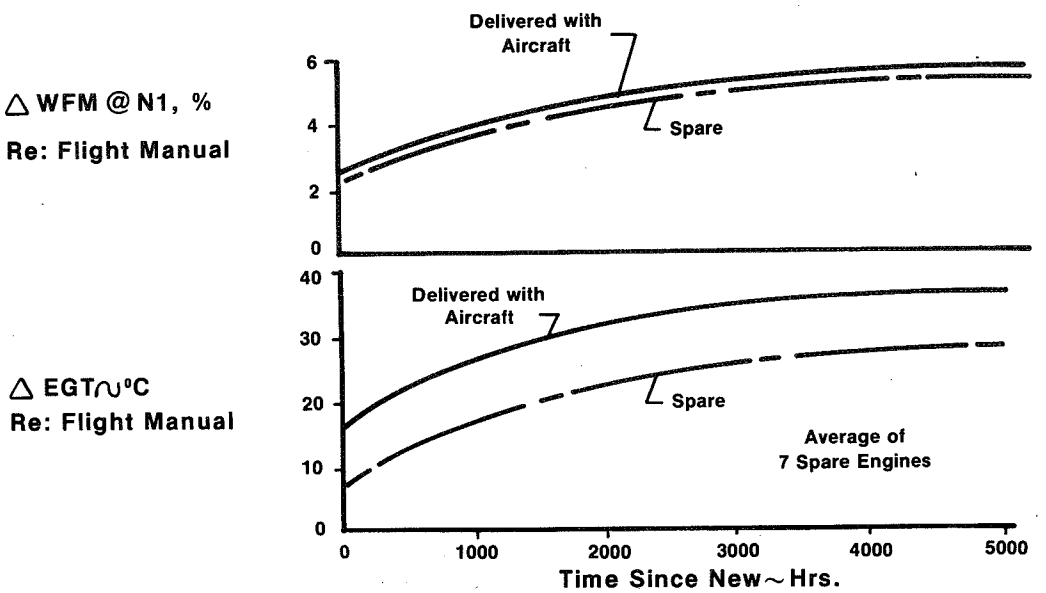

Figure 8.- Deterioration of CF6-6D's delivered as airline spares.

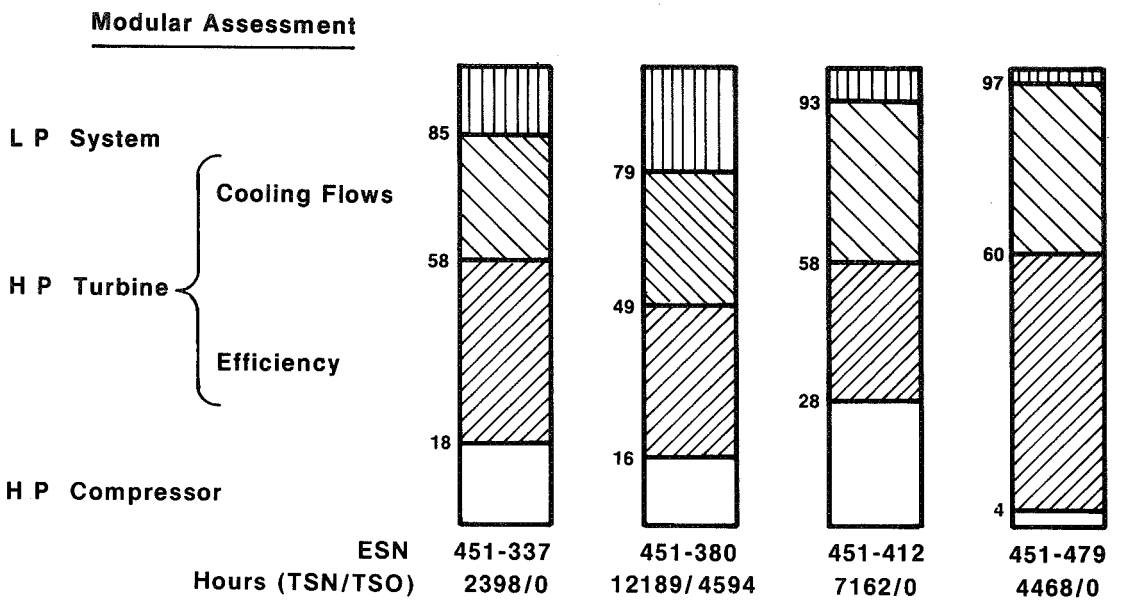

Figure 9.- Examples of CF6-6D modular contribution to SFC deterioration.

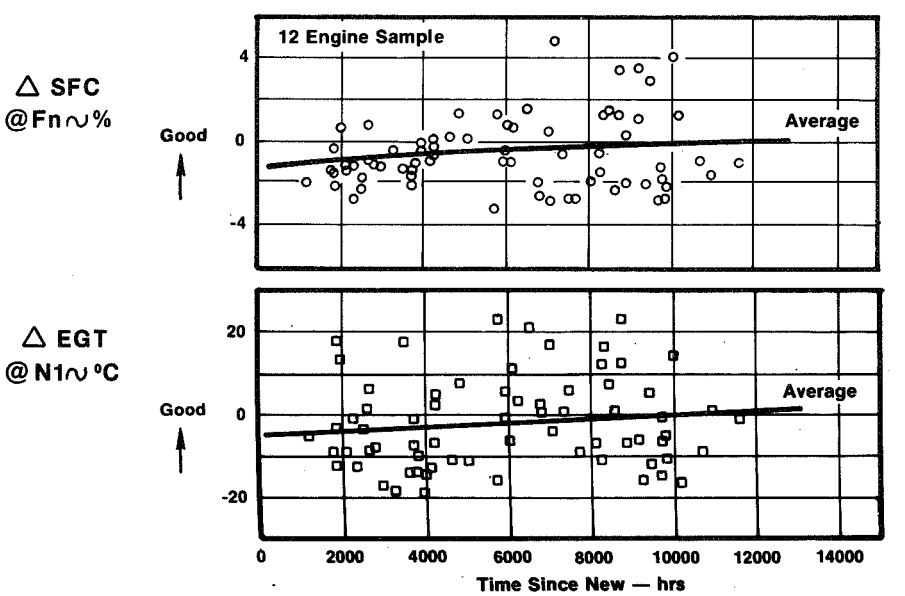

Figure 10.- CF6-6D outbound performance history.

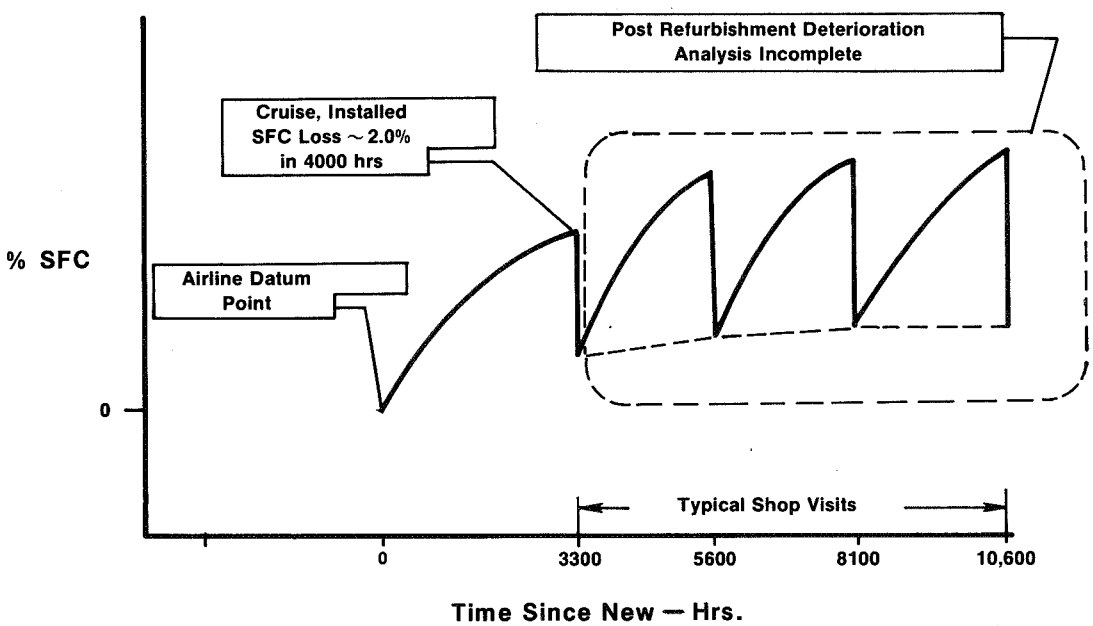

Figure 11.- Summary of CF6-6D SFC performance trend.

JT9D JET ENGINE PERFORMANCE DETERIORATION*

A. Jay, E. S. Todd and G. P. Sallee
Commercial Products Division
PRATT & WHITNEY AIRCRAFT GROUP

SUMMARY

Escalating fuel costs and the need to meet national energy conservation goals have led to a new industry awareness of the importance of maintaining good fuel consumption throughout the life-cycle of an engine. However, higher fuel consumption is only part of the overall engine deterioration picture which consists of reduced surge margin, higher exit gas temperature, and other hot section distress. Engine deterioration characteristics can, in general, be divided into two time periods. The first, called short-term deterioration, occurs in less than 250 flights on a new engine and in the first few flights following engine repair. Engine deterioration in the second time period, characterized as long-term, involves primarily hot section distress and compression system losses which occur at a somewhat slower rate than short-term deterioration.

It is generally accepted that the causes for short-term deterioration are associated with clearance changes which occur in the flight environment. In this paper, the analytical techniques utilized to examine the effects of flight loads and engine operating conditions on performance deterioration are presented. The role of gyroscopic, gravitational and aerodynamic loads are shown along with the effect of variations in engine build clearances. These analytical results are compared to engine test data along with the correlation between analytically predicted and measured clearances and rub patterns. Conclusions are drawn and important issues are discussed.

INTRODUCTION

The current and projected high cost of fuel for gas turbine engines places a premium on incorporation of design features which increase the operating efficiency of aircraft propulsion systems. One such feature, universally recognized to be of major importance, is the maintenance of tight operating clearances between static and rotating components of flowpath seals. In practice, this is rather difficult to accomplish since the individual seal components and their supporting structures experience wide excursions in temperatures, rotational speeds, and other loadings at different points in the flight cycle which give rise to relative deflections that can lead to contact, wear, and increased clearances between seal parts. Early gas turbine designs (turbojets and low bypass ratio turbofans) accounted for these time varying loads and associated deflections as part of the standard process and attempted to tune rotor and case growths such that tight clearances (maximum efficiency) would occur during steady-state operation (climb, cruise) without introducing damaging rubs during transient conditions (takeoff, landing). In view of the ready availability of inexpensive fuel and other

* Work performed under NASA contract NAS3-20632

factors, designs which dropped a few percent in efficiency after a year or two in service were considered adequate at that time.

Today's situation is quite different as a consequence of two factors. First, fuel costs have more than doubled in the past few years and are expected to continue to rise, and second, higher bypass ratio engines are more susceptible to structural deformations which can cause tight seal clearances to be degraded by rubs. The second factor follows from the larger size (increased thrust and air loads) and increased thrust-to-weight ratio (lightweight, flexible structures) characteristics of the turbofan engines which power current commercial transports. In order to define powerplant configurations which will meet the more stringent performance retention requirements of tomorrow's marketplace, today's designer must have at his disposal a more advanced set of analytical tools with which to anticipate the response (deflections) of an engine to its flight environment (loads) than was previously necessary.

This paper describes progress that has been made toward development of a comprehensive analytical procedure for predicting the effects of flight loads on short-term gas turbine performance deterioration (fig. 1). The damage mechanism considered is wear of flowpath outer airseals due to interference of rotating (blade tip) and stationary (rubstrip) seal components. Wear behavior of inner airseals is more complex and has been omitted from the current study. Other mechanisms such as erosion and contamination which decrease engine efficiency more gradually than seal rubs are deemed to be of secondary importance in short-term deterioration and have been excluded.

SYMBOLS

Values are given in SI units. The measurements and calculations were made in U.S. Customary Units.

M_n	Engine inlet Mach number
% Δ TSFC	Percent change in engine thrust specific fuel consumption
V_S	Airplane stall velocity
ζ_{ij}	Performance influence coefficient for stage j, condition i
$\bar{c}_j$	Average clearance change for stage j

ANALYTICAL MODEL

This section provides a general description of the analytical procedure employed to assess the effects of steady flight loads on short-term performance deterioration of the JT9D-7/747 propulsion system. In essence, the model provides a vehicle for predicting blade tip rub damage caused by structural deformations which occur during flight operation and relates the corresponding enlarged seal clearances to increases in engine thrust specific fuel consumption (TSFC).

Flight Profile Definition

The starting point for all deterioration predictions to be discussed in this paper is a description of the sequence of operating conditions or events which comprise an engine mission or flight profile. The cycle may be relatively simple in terms of power level changes and exposure to external loads, as is the case for standard "green runs" and engine acceptance tests on the ground, or may encompass load spectra from runway roughness to clear air turbulence which are commonly encountered by commercial airlines. Each such cycle is constructed from a series of time segments (start-up, taxi, takeoff, climb, cruise, descent, approach, landing, shutdown), the end points of which can be characterized by unique combinations of aircraft and engine operating parameters (gross weight, altitude, attitude, Mach number (Mn), rotor speeds, temperatures, pressures, flows) that serve to define boundary conditions for subsequent aerodynamic, thermodynamic and structural analyses. For this paper, attention has been primarily focused on the airplane acceptance test flight (figs. 2, 3) chiefly because the profile is well defined and secondly, test data defining the magnitude of the change in TSFC is available for a number of engines covering the flight cycle range of interest. Ground tests and fleet service which precede and follow the flight acceptance test, respectively, have also been included but in somewhat less rigorous fashion. Quantitative information on idealization of these cycles for the JT9D-7 engine is discussed later.

Loads and Structural Deflections

Temperature, pressure and centrifugal force fields play an important role in determining internal seal clearances. These are always present during engine operation. Perhaps, the most convenient feature of this set is the common assumption that circumferential variations in these fields are small and, for the purposes of deflection analysis, can be neglected. The second important characteristic is that each field varies appreciably in response to changes in power level and requires a transient analysis for proper representation. Specialized computational procedures have evolved to perform the secondary flow, heat transfer, and other analyses that define temperature, pressure, and rotor speed time histories for desired flight profiles. These loads are input to axisymmetric structural analysis programs which generate histories of relative deflections (gap closures) between static and rotating components. Combination of the axisymmetric closures with values for the initial build clearances (cold gaps, also assumed to be uniform) then provides the sought after hot clearances as functions of time. Since they essentially indicate the gaps available for accommodation of additional deflections due to external flight loads, plots of these data will hereafter be referred to as baseline clearance curves.

A second set of structural deformations is related to loads which are not uniformly distributed with respect to the engine centerline. Generally, this set arises from external motions or restraints imposed by the flight environment and is composed of airloads (inlet lift), maneuver loads (g's, gyros), and thrust (including thrust reverse). As would be expected, consideration of these loads and their contribution to the performance deterioration problem presents a greater challenge than was the case for the previous group. A NASTRAN finite element model of the JT9D-7/747 was required to simulate the engine's response to external loads (figs. 4, 5.).

The burden of defining cowl pressure distributions (airloads) and maneuver load factors for candidate flight missions has traditionally been borne by the airframe manufacturers. Since these data are usually supplied to Pratt & Whitney Aircraft (P&WA) only in gross form (force/moment resultants, design limits/envelopes), provision was made for Boeing Commercial Airplane Company (BCAC) to generate detailed pressure load descriptions. Conversion of internal and external pressure distributions into appropriate descriptions of thrust and thrust reverse loads was also performed by P&WA and BCAC, respectively. Nodal forces consistent with inlet cowl pressure distributions, internal thrust build-up, maneuvers, and thrust reverse loadings were applied to the NASTRAN model and corresponding rotor/case displacement solutions obtained.

Blade-Tip/Rub-Strip Damage Calculation and Performance Deterioration

The process whereby structural deflections are translated into blade-tip/rubstrip damage involves calculations for a sequence of time points selected from a given flight profile. For each time point, the effects of axisymmetric loads (baseline clearances), engine offset grinds, and rub damage from previous time points are combined to establish the circumferential variation of clearance that is available for accommodation of non-axisymmetric structural deformations. Asymmetric rotor/case deflections are then introduced and when the relative closures exceed the available gap, the extent of local interference is recorded. Finally, wear characteristics of the contacting materials are considered to determine the trade-off between blade-tip/rub-strip damage due to the interference. Gap changes caused by shortened blades and the worn rubstrip are in turn carried forward to appear as increased initial clearances for the next time point. At the end of the cycle, the accumulated damage for each rub-strip is circumferentially integrated and added to blade-tip wear to provide the average clearance change for the stage.

The final step to be taken involves conversion of permanent clearance changes for the total cycle to increases in TSFC under standard performance conditions. This is accomplished by simply summing the contributions from each stage, or,

$$(\%\,\Delta\,\mathrm{TSFC})_i = \sum_{\substack{\text{all}\\ \text{stages}}} \zeta_{ij}\,\bar{c}_j$$

The influence coefficients (ζ) are unique to a particular engine model.

ENGINE DETERIORATION SIMULATION

Airplane Flight Acceptance Test

The production flight acceptance test was selected for simulation because every 747 off the assembly line is tested this way, according to a routine that is kept as standard as possible. The purpose of the flight acceptance test is to check out airplane internal systems. Airplane takeoff gross weight, airspeed, and throttle setting vary somewhat from one test to another because pilot instructions are given in terms of obtaining a signal from a warning or control instrument rather than in terms of achieving a specified flight condition.

Operating conditions to be considered as part of the flight test are defined in terms of rotor speeds, pressures, and temperatures from engine performance tables along with flight-related parameters such as attitude, altitude, inlet Mach number, airplane weight, and fuel distribution in the wing. Airloads present on the inlet are described for the flight acceptance profile. Thermal, pressure and centrifugal loadings are accounted for by the use of baseline clearance curves. These curves describe axisymmetric clearances between rotating and stationary seal components as functions of time for the flight acceptance profile. Inertia (g's) and gyroscopic effects as a function of time are also characterized for the acceptance profile.

The computer simulation of the flight acceptance test incorporates the proper combination of nacelle loadings, engine thrust, inertia and gyroscopic effects, baseline clearances, and engine airseal/blade abradability factors. Exposure to thrust and maneuver loads results in deformation of propulsion system structural members and leads to relative motion between static and rotating components of flowpath seals. If the motions are larger than can be accommodated by the available clearances, rubs and wear will occur and hence a loss in performance. This simulation covers 16 conditions along the mission profile as shown in figure 2. A summary of relevant flight parameters is given in figure 3.

JT9D-7/747 Service Experience

In the simulation of the 747 service experience, the previously defined flight acceptance test was refined to include only those maneuvers which are typical of a revenue flight. For the simulation, relative values of the loads remain unchanged, but the absolute values are increased to account for the probability of encountering larger loads during the life of the airplane.

The simulation of 747 service experience, as well as airplane acceptance, has been accomplished at several discrete times (after 500, 1000, etc., flights) in the lifetime of the airplane. In the lifetime of the airplane an ever-increasing chance of exposure to increasing load levels causes engine deterioration. Results from the model strongly reinforce the conclusion that flight induced seal rubs are the primary cause of short-term (250 flights or less) engine performance deterioration and they are a significant contributor to the additional deterioration accumulated over the long term. As part of this simulation, it has been shown that certain engine components are particularly sensitive to certain types of loads. In figure 6, it can be seen that the fan stage is very sensitive to gyroscopic loadings and relatively insensitive to varying gravitational (g) loading levels. It can also be seen that the high pressure turbine (HPT) stages are relatively insensitive to gyros but sensitive to g loadings.

Effects of Engine Build Clearance Tolerances

Ultimately an engine's rate of deterioration is a function of its design. An engine built with open clearances deteriorates at a slower rate than an engine with tight clearances. An engine with loose clearances has a high initial fuel consumption, but shows little deterioration from load effects with time. An engine with tight clearances has a low initial fuel consumption, but exhibits a much greater initial short-term deterioration rate. Modeling studies

have shown that although an engine built with tight clearances deteriorates at a greater rate, it still exhibits better fuel consumption than a nominally built engine over its life cycle. This is true, in part, because rubs are local and the stage is still tighter on the average.

The effects of build clearance tolerances were investigated by using company standard engine build tolerance values in conjunction with the previously mentioned baseline clearance curves. Figure 7 depicts the results obtained from this investigation. From the figure, it is obvious that an engine built with open clearances shows less deterioration with time than an engine built with tight clearances. In this figure, however, no attempt has been made to bias the curves due to initially higher fuel consumption or initially lower fuel consumption. Correlation of predicted % Δ TSFC ranges with short-term engine deterioration data is shown in figure 8. The predicted values bracket the engine data quite well.

The trend in predicted changes in % Δ TSFC of the JT9D-7 from loads versus time was found to be in good agreement with 747 fleet experience trends as shown in figure 9. Figure 10 suggests that beneficial effects of module reoperation or replacement (where only build clearances are restored) are only temporary and, as the engine re-enters service and encounters flight loadings, the airseals in the restored module (HPT or LPT) once again experience rub damage and deterioration within a short-term time frame.

Analysis of the results from the simulation reveals that calculated average clearance changes for the individual stages also correlate well with the JT9D-7 experience. Except for the fan stage (fig. 11), however, predicted and observed circumferential rub damage distributions do not compare satisfactorily. Figure 12 depicts 1st-stage HPT outer airseal damage as a function of angular location for both a NASTRAN prediction and measured data on an engine that was torn down and measured in-house. A significant point to make with respect to this correlation is that the rub pattern exhibited by this engine is not typical of data measured on several other engines. In each case, the NASTRAN predicted values of average damage are in agreement with measured engine data. Figure 13 reinforces the conclusion that the trend in change of turbine tip clearance is increasing with time.

CONCLUSIONS

An analytical procedure for assessing the effects of flight loads on engine performance deterioration has been developed and applied to predict short- and intermediate-term changes in TSFC for the JT9D-7/747 installation. Good correlation between predicted and observed values for Δ TSFC serves to confirm the basic assumption that load-induced seal rubs have a significant effect on short-term performance deterioration.

The correlation between analytical prediction and measured clearance change is acceptable, but further refinements are desirable to explain specific rub pattern variations.

The analytical procedure provides for the detailed description of loads and deflections as they vary with time for arbitrary flight profiles and thereby permits the effects of individual loads to be isolated for evaluation. For the JT9D-7, studies of this kind indicate that airloads (inlet lift) are the dominant factor, maneuver loads (g's, gyros) are of secondary importance, and thrust loads do not contribute to performance losses after the engine acceptance test.

Usefulness of this procedure as a diagnostics tool for understanding the major causes of early performance deterioration (rub-induced clearance changes) has been demonstrated. At the same time, potential usefulness of the procedure as a design tool which can be used to minimize these effects in the future through use of load-sharing nacelles, active clearance control, optimum bearing placement, etc., has also been inferred. Better in-flight load predictions will be needed for future engine design clearance optimization for active clearance control systems.

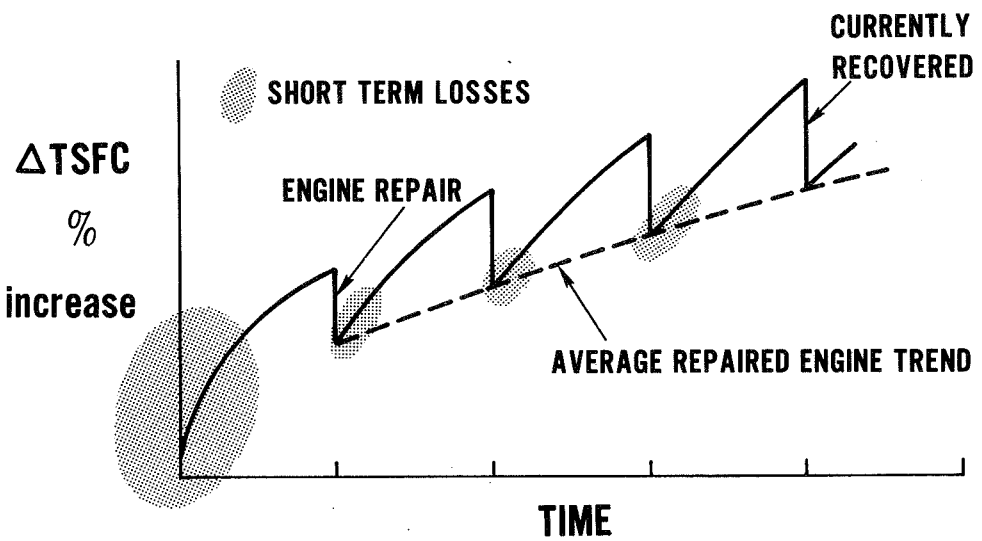

Figure 1.- General characteristic of TSFC performance deterioration trends.

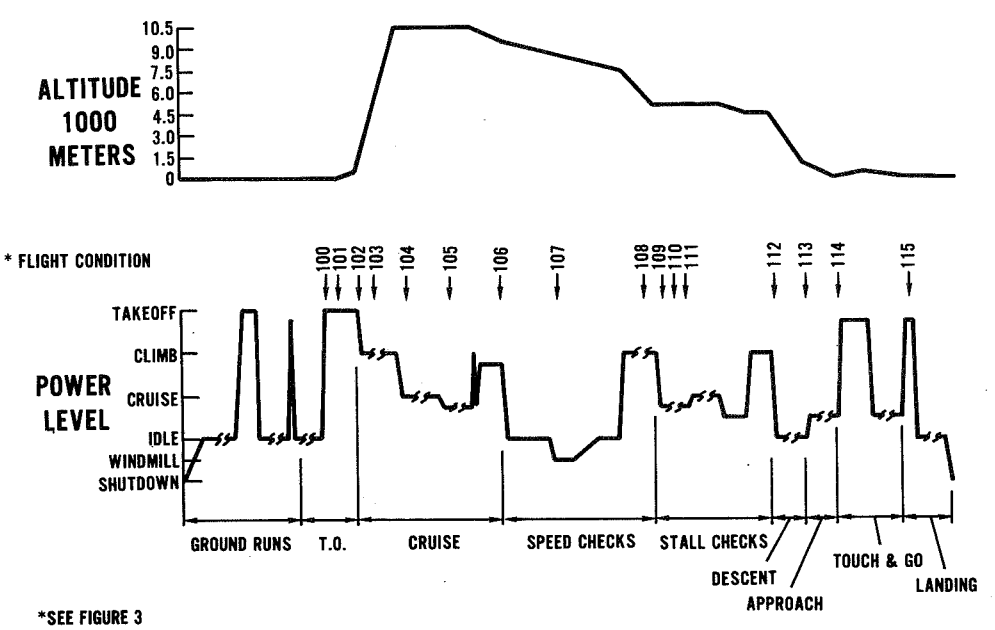

Figure 2.- Airplane acceptance test flight profile.

FLIGHT CONDITION	DESCRIPTION	ALTITUDE (M)	AIRSPEED M_N
100	TAKEOFF ROLL	0	0.186
101	TAKEOFF ROTATION	0	0.214
102	EARLY CLIMB	914	0.401
103	MID CLIMB	5,330	0.617
104	HIGH MACH CRUISE	10,670	0.860
105	LOW MACH CRUISE	10,670	0.770
106	MAXIMUM MACH	9,750	0.920
107	IN-FLIGHT SHUTDOWN	8,380	0.720
108	MAXIMUM SPEED	6,100	0.830
109	1.3 VS. 0° FLAPS	5,180	0.340
110	1.3 VS. 10° FLAPS	5,180	0.340
111	1.3 VS. 30° FLAPS	5,180	0.340
112	EARLY DESCENT	5,180	0.440
113	APPROACH, 20°FLAPS	914	0.240
114	TOUCHDOWN	0	0.271
115	THRUST REVERSE	0	-

Figure 3.- Airplane acceptance test flight profile parameters.

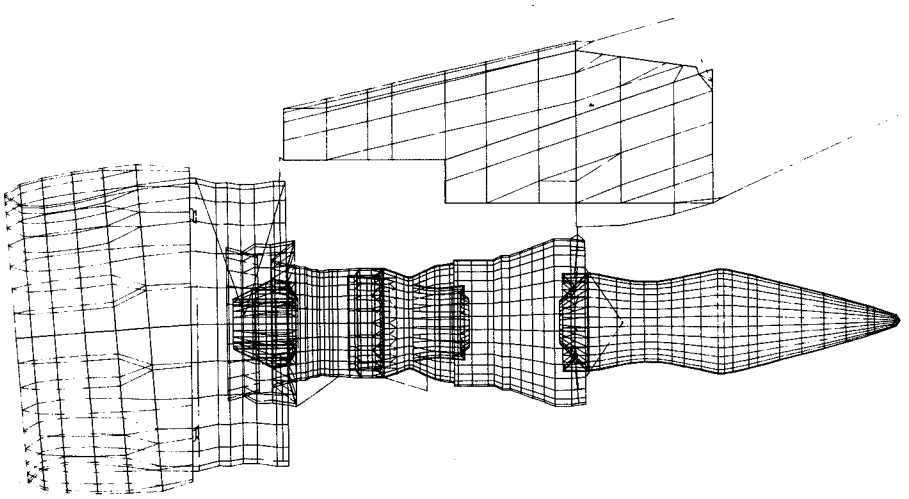

Figure 4.- JT9D-7/747 integrated NASTRAN structural model.

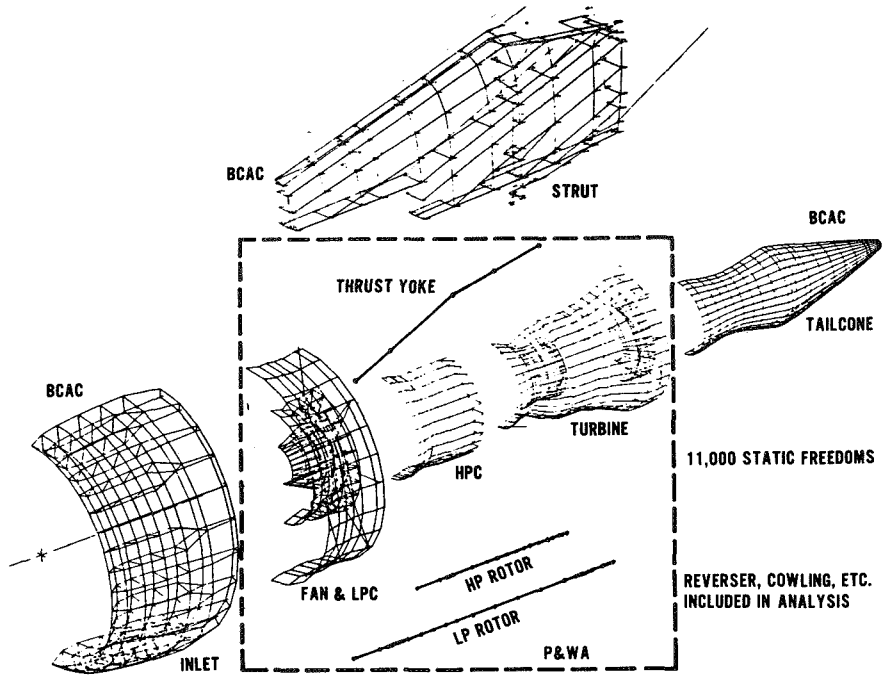

Figure 5.- JT9D-7/747 propulsion system substructures.

	AVERAGE DAMAGE (MM)		
STAGE	1/150 FLIGHTS THRUST AND AIR LOADS	1/150 FLIGHTS THRUST, AIR AND G LOADS	1/150 FLIGHTS THRUST, AIR, G AND GYRO LOADS
FAN	0.508	0.508	0.787
2 LPC	0.025	0.051	0.102
3 LPC	0.381	0.381	0.381
4 LPC	0.584	0.584	0.584
3 LPT	0.025	0.025	0.025
4 LPT	0.076	0.076	0.076
5 LPT	0.127	0.127	0.127
6 LPT	0.254	0.254	0.254
ALL HPC	—	—	—
1 HPT	0.127	0.178	0.178
2 HPT	0.305	0.356	0.356
%ΔTSFC (SSLTO)	1.5	1.61	1.65

Figure 6.- JT9D engine average damage.

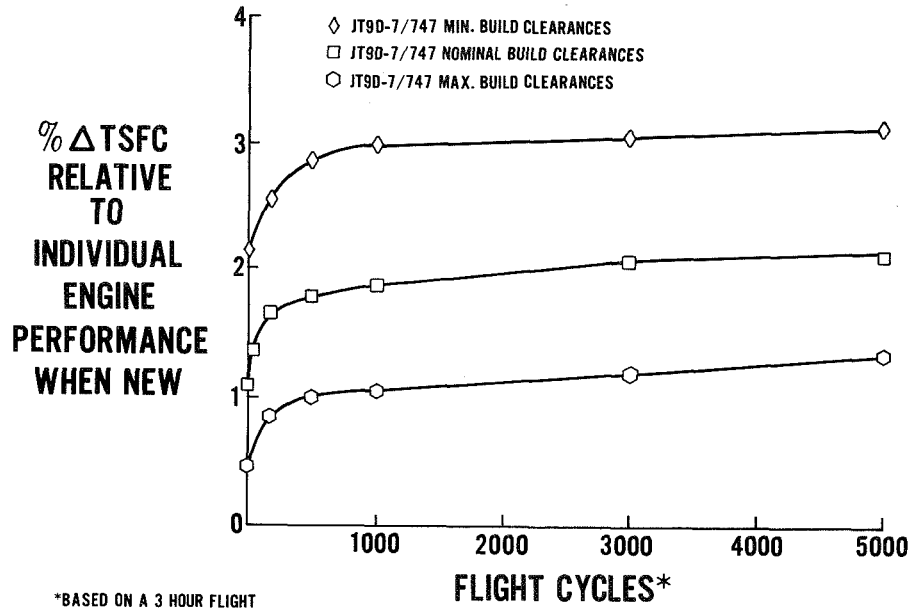

Figure 7.- Predicted effect of build clearance on short and long term deterioration.

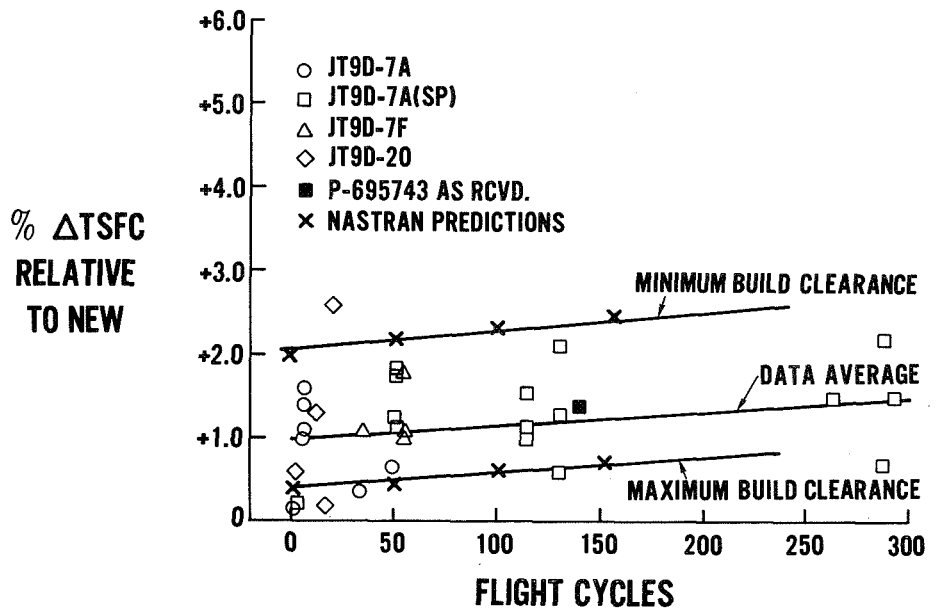

Figure 8.- Short term deterioration predictions bracket engine data.

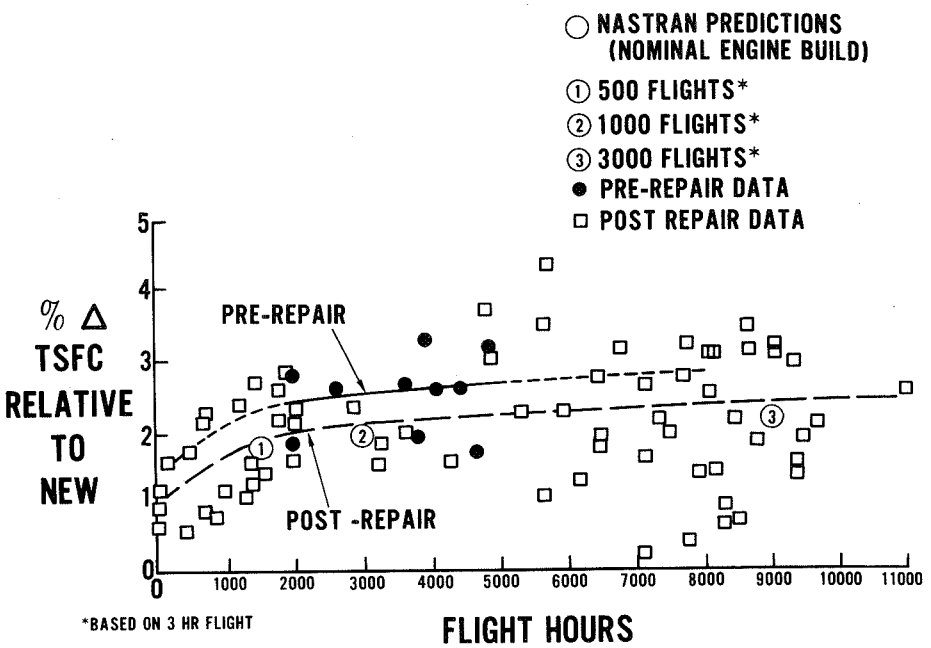

Figure 9.- Long term deterioration predictions are in good agreement with fleet experience.

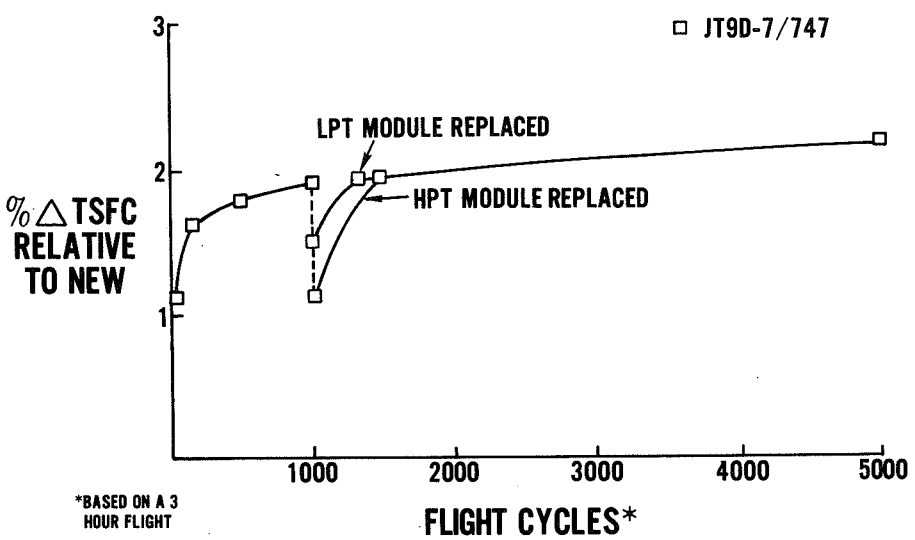

Figure 10.- Effects of turbine module replacement and subsequent deterioration.

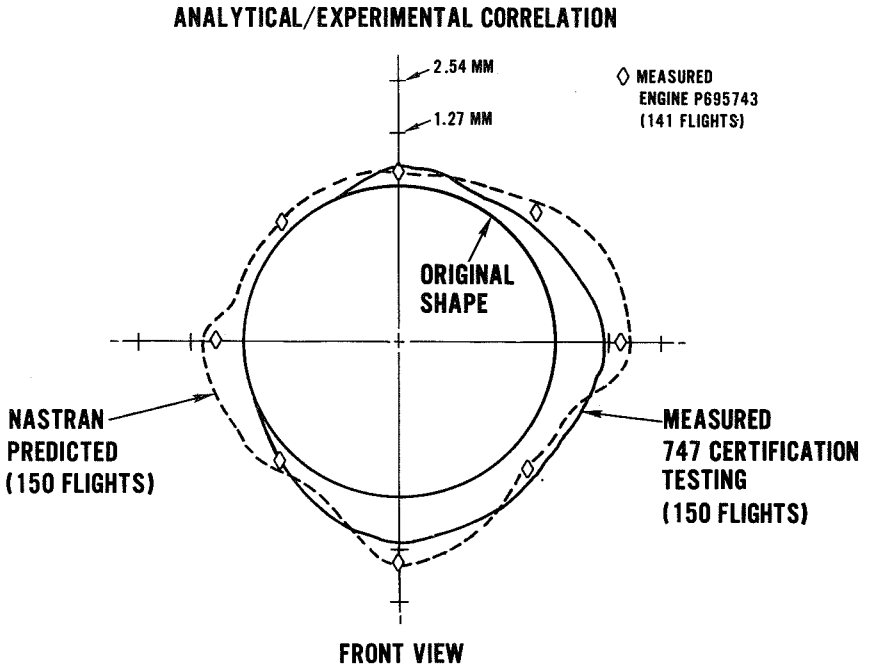

Figure 11.- Predicted fan rub patterns compared to measured data.

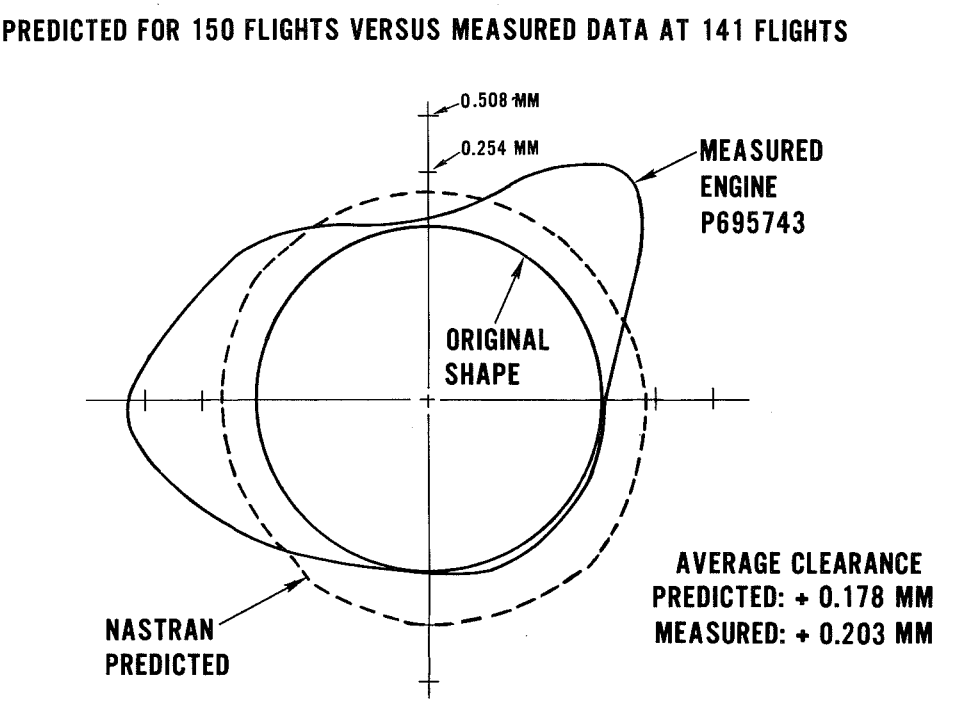

Figure 12.- Predicted first HPT outer airseal rub damage compared to measured data.

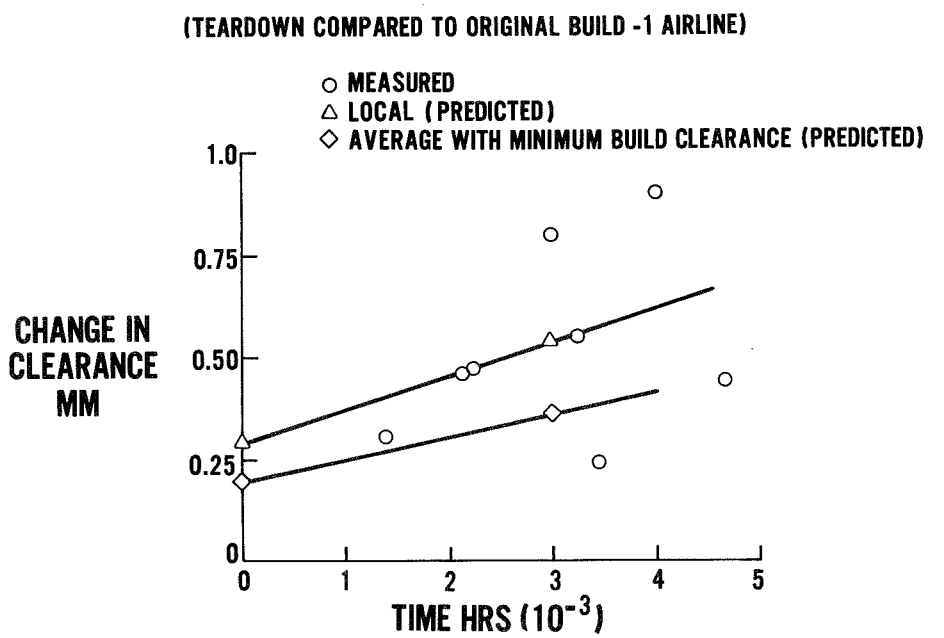

Figure 13.- JT9D-7 high pressure turbine tip clearance change with time.

CF6 PERFORMANCE IMPROVEMENT

Dean J. Lennard
Aircraft Engine Group
General Electric Company

SUMMARY

Potential CF6 engine performance improvements directed at reduced fuel consumption have been identified and screened relative to airline acceptability. The screening process was developed to provide evaluations of fuel savings and economic factors including return on investment and direct operating cost. In addition, assessments of development risk and production potential were made. Based on a ranking involving these factors, several promising concepts have been selected for full-scale development.

INTRODUCTION

The expanding national energy demand is outpacing domestic supply and is causing an increased U.S. dependence on foreign oil plus rising fuel prices. These events are significantly impacting the U.S. economy including both public and private sectors. A major user of petroleum products is the U.S. transportation system; the U.S. Government, with the support of private industry, has initiated programs directed at both the supply and demand aspects of the transportation problem for both the long and short range. With regard to the aviation industry, a promising short range approach to reduced fuel usage is improvement in the fuel efficiency of current aircraft engines. An evaluation of this approach has indicated that up to five percent reduction in fuel consumption, through both improved engine performance plus improved performance retention, may be possible starting in the early 1980's. To this end, the National Aeronautics and Space Administration is sponsoring programs directed at achieving the above goal.

The CF6 series of engines, developed by General Electric, includes the CF6-6 engine which powers the Douglas DC-10-10 aircraft and the CF6-50 engine (Figure 1) that powers the Boeing 747-200, Douglas DC-10-30, and Airbus Industrie A300 aircraft. These high bypass turbofan engines, at the time of their initial development, offered significant fuel savings over preceding engines. Subsequently, airline operational experience and technology advancements have indicated that further reductions in fuel consumption are possible. This paper presents the results to date of the NASA-sponsored CF6 Performance Improvement Program that is directed at these further reductions.

PROGRAM STRUCTURE

The CF6 Performance Improvement Program consists of the following three technical efforts:

- Feasibility analysis
- Development and evaluation - ground test
- In-service and flight testing

The Feasibility Analysis involves the identification of performance improvement and retention concepts, the development of an analytical screening procedure, evaluation and ranking of the concepts, and preparation of technology development plans and proposals for subsequent development. The second and third efforts are to provide for this subsequent development of the selected concepts prior to introduction into commercial airline service. Figure 2 traces the flow of a concept through this process.

Implementation of this program involves a complex series of interfaces as illustrated in Figure 3. General Electric placed subcontracts with Boeing and Douglas to provide for aircraft system evaluation and the economic analyses. They, in turn, have American and United Airlines as consultants to provide support for the economic evaluation as well as to comment on airline acceptance of the improvement concepts. In addition, Eastern and Pan American Airlines are functioning as NASA technical consultants under contract to NASA. This arrangement provides participation by all elements from the

producer through the user and gives high assurance relative to the overall concept acceptability and the ultimate production introduction of selected concepts.

ANALYTICAL SCREENING PROCEDURE

An analytical screening procedure was developed to provide an evaluation and ranking of each concept relative to four criteria:

- Fuel savings
- Economic impact/airline acceptability
- Development risk
- Production potential

This analytical procedure is shown schematically in Figure 4. The first step in the process was the preliminary design of promising concepts by General Electric. The preliminary design proceeded to the point where the required engine impact data could be estimated. These data consisted of manufacturing costs and subsequent prices, weight changes, performance (thrust and SFC) at seven key aircraft mission points, maintenance data including material and labor, retrofit capability, and other impacts including noise and aircraft system power management. These data were submitted to Boeing and Douglas for evaluation in their respective aircraft. This evaluation included the determination of reduction in fuel consumption for three mission profiles which were based on data supplied by American and United Airlines. Figure 5 shows a typical mission profile. In lieu of a complete route analysis, three representative missions were selected for each aircraft to determine potential airline fuel savings achieved with each engine improvement. Current airline usage for the study aircraft was determined from the August 1976 Official Airline Guide. Departures for each airplane were distributed by stage length. Then this distribution of total departures was divided into three equally weighted groups, and the average stage lengths of each group were selected as the three representative missions (Figure 6). Preliminary aircraft design studies to assess any required aircraft changes were performed, and the resulting data were combined with the General Electric inputs

and "flown" in the standard missions to determine improvements in aircraft system impacts for each stage length. Data from this effort included airplane performance changes (range, payload, block fuel, field length, and climb performance), operating empty weight, maintenance cost changes, prices, and other impacts. These data plus engine maintenance costs then were used to determine incremental direct operating costs (DOC), return on investment (ROI), and payback periods. The economic data for each concept were determined for the three stage lengths, three fuel prices, and all applicable aircraft and retrofit options as appropriate. These data then were submitted to United and American for evaluation. The final step consisted of evaluation of the foregoing data in terms of total impact and ranking of concepts considering airline comments plus technical and other risks, production potential, and other factors provided by General Electric and the other contributors as appropriate.

ECONOMIC ANALYSIS

The first step in the determination of the economic impact involved the calculation of the incremental net yearly savings which included aircraft fuel, insurance and maintenance costs, and the cash outlay which included the engine and aircraft modification costs, additional spares inventory, and installation costs. The payback period is simply the initial cash outlay divided by the net yearly savings.

The return on investment (ROI) is the discount rate at which the net present value of future cash inflows equals the initial cash outlay. This is depicted in the following equation:

$$\sum_{N=1}^{\text{Useful Life}} \frac{\text{Cash In}}{(1 + \text{ROI})^{N}} = \text{Cash Out} \qquad (1)$$

Significant features of this approach include the following:

- Based on cash flow of engine modification and annual savings
- Recognizes time value of money

- Relatable to any airlines cost of capital to show how much such a modification is above or below the "hurdle rate"
- Cash flow is in constant dollars to assure consistent comparison of different modifications
- Effect of inflation is contained in airline ROI "hurdle rate"

All ROI data were determined on a before-tax basis; however, before- and after-tax relationships were calculated for basic assumptions of depreciation and tax rate to permit evaluation on an after-tax basis.

HIGH POTENTIAL CONCEPTS

In the intial concept identification phase, 62 improvement ideas were identified. Initial screening based on qualitative engineering judgement reduced this list to 23 items which then were subjected to the screening process defined above. Some of the more promising concepts, that illustrate the extent and type of improvements studied, are presented below.

Improved Fan

This improvement concept involves the aerodynamic redesign of the current CF6 fan blade principally in the area of the midspan shroud. This shroud, which is dictated by vibratory stress requirements, results in performance losses. The redesign involves repositioning the shroud (see Figure 7) in such a manner as to minimize the aerodynamic losses. Coupled with this change is a change in the fan operating line to shift the fan cruise operating point to a region of higher efficiency. This is accomplished through a modest increase in fan exhaust nozzle area. Another item also included in this overall improvement concept is the reduction in fan-blade-to-casing clearance. The addition of a stiffener ring (see Figure 8) to the case was found to change system vibratory response such that the clearances could be reduced without undesirable vibratory interaction between the rotor and the stator.

The net result of the above items is a predicted 1.8% reduction in specific fuel consumption (SFC) for the CF6-50 and a 1.6% reduction for the

CF6-6 engines. A modest engine weight increase of 13 kilograms is required. One other favorable effect is a maintenance cost reduction (lower DOC) resulting from the lower turbine gas temperatures that accompany the improved engine performance. The thrust setting parameter of the CF6 engines is fan speed. Because the speed-airflow characteristics of the new fan are different from the current fan, changes to aircraft power management procedures are required.

The predicted aircraft fuel savings and economic data for this and the following concepts are presented in a later section.

New Front Mount

The CF6 engine thrust loads are transferred to the aircraft pylon through a mount located at the junction of the fan frame and the top front end of the high pressure compressor case. Because of the displacement of this mount, relative to the centerline of the engine, a bending moment is induced in the engine and is reacted through radial force vectors at the front and rear mounts. This bending moment results in local inward deflections of the compressor case at the top 12-o'clock position. This deflection then establishes the maximum rotor blade tip diameter for each rotor stage that can be produced without rotor-casing rubs. Analysis and static load tests indicated that the modification of the front mount through the addition of tangential links (Figure 9) would better distribute the loads and reduce the local deflection to levels more closely approaching the deflection produced from simple beam bending without the local 12-o'clock distortion (see Figure 10). This reduction in deflection then permits increases in rotor blade diameters with a net reduction in clearance and a commensurate improvement in compressor efficiency and engine sfc reduction of approximately 0.3%.

Improved High Pressure Turbine

The core of the CF6-6 engine was initially developed over ten years ago for the USAF TF39 engine which powers the C5. There have been subsequent technology advancements especially in the high pressure turbine. Figure 11

presents a proposed new turbine for the CF6-6 engine that is predicted to provide a sfc reduction of up to 1.3%, improved performance retention and reliability, and a significant reduction in maintenance cost.

The key features of this turbine include single-shank HPT blades that have optimized cooling both initially and after long-time operation, revised exit swirl to better match the orientation of the frame located downstream of the turbine, improved rotor/stator casing clearance match, and other aerodynamic and cooling system refinements. Because of the reduction in direct operating cost, this concept is predicted to be very attractive even for an attrition retrofit into current in-service engines.

Short Core Exhaust

There currently are two core exhaust systems in operational service on the CF6: (1) a combination core engine reverser/nozzle system and (2) a simple nozzle having the same flow path contour but no reverser capability. Parametric nacelle model testing, conducted by General Electric and Douglas, indicates that installed CF6-50 engine performance could be improved through a recontour of the core nacelle aft of the fan exhaust and a shortening of the core engine exhaust system. The flow path contours for the proposed new exhaust are compared to the current system in Figure 12. Improved nozzle performance is accrued through reduced internal and external skin friction drag and reduced wing/nacelle interference drag. This is predicted to result in a sfc reduction of one to three percent depending on the final reduction in interference drag.

High Pressure Turbine Roundness and Clearance Control

Clearance control in all the turbomachinery components is required for minimum fuel consumption, the high pressure turbine being the most critical component. The problem of clearance control/retention is compounded because of the significant thermal growths that accompany the high temperature of the turbine components. The improvement concept described herein (See Figure 13) is directed at achieving an improved thermal response of the stator system such that reduced rotor/stator clearances can be maintained during engine

steady-state cruise operation while still permitting full engine transient operability. Also included in this item are improvements in the turbine mid-frame located aft of the turbine. This strutted frame serves as the aft engine mount as well as being the aft bearing support for the high pressure rotor. Mount loads plus nonuniform start temperatures cause asymmetric radial deflections that are transmitted to the turbine stator. These deflections result in the increased turbine clearances relative to the ideal case of a perfectly round stator system. The proposed improvements would further isolate the stator shrouds from the local frame deflections and would also produce a better radial growth match between the frame struts to improve roundness. The net result would permit an overall decrease in turbine clearance with an increase in efficiency and a decrease in engine sfc of approximately 0.3% for new engines and a retention improvement of an additional 0.3%.

Active Turbine Thermal Response

This improvement concept is intended to achieve further high pressure turbine clearance reduction at cruise power settings. Generally, the minimum clearance between the rotor blades and stator occurs at the high engine power settings; however, the clearance increases for the lower cruise power condition because of reduced disk centrifugal growth and rotor/stator thermal growth differences. Passive techniques involving improved rotor/stator growth matching can provide clearance reduction, but there are limitations.

One potential solution is to provide variable source/temperature cooling air to the turbine stator that is controlled as a function of engine power setting. Thus lower temperature air can be supplied at cruise to reduce the stator temperature effecting a clearance reduction. This concept (Figure 14) is predicted to produce a cruise sfc reduction of approximately 0.4%.

Cabin Air Recirculation

One means of reducing engine fuel consumption is the lowering of the power or bleed air extractions required for operation of the aircraft. Currently, the cabin air environmental system on the DC-10 provides air direct

to the cabin area. By adding a recirculation system involving filters and fans (Figure 15), the fresh air required from the refrigeration packs can be reduced by about 40% while still maintaining adequate passenger comfort. This results in a potential engine sfc reduction of approximately 0.7%.

ECONOMIC ANALYSIS RESULTS

An example of the economic analysis is provided by Table 1, which shows the improved fan annual savings, ROI, and payback period for each aircraft at the three stage lengths and median fuel price. ROI and payback data also are included for both attrition and campaign retrofit replacement as well as new engines. It readily can be observed that the fan improvement concept is very attractive for both new engine and attrition replacement introduction. Retrofit with full scrappage of replaced parts only appears attractive for the longer stage lengths. Table 2 presents a summary of the sfc savings, and Table 3 presents the economic analyses for the concepts described above under the median conditions of stage length and fuel price.

CONCEPT COMPARISON

Figure 16 shows one of the comparisons used in concept ranking, in addition to tabulations similar to Table 2. In this comparison, yearly aircraft fuel savings versus payback period for the median range and fuel price was depicted. The improved fan, which has been identified, has the highest yearly fuel savings. Also identified are the other concepts described earlier. The shaded region shows the range of savings for the Douglas DC-10-10 and the longer-range Boeing 747-200. In addition to the quantitative economic and fuel saving comparisons, the concepts also were ranked on the basis of development risk. Finally (using General Electric market forecasts, service introduction, and retrofit estimates), total fuel savings for the 1980-1990 time period were predicted.

TECHNOLOGY DEVELOPMENT

The foregoing constitutes the Feasibility Analysis. The next step in the Performance Improvement Program is that of development and evaluation of

the most promising concepts. The improved fan has been selected by NASA for development. The fan development program, which is typical of other concepts, includes engineering, component tests, and full-scale engine noise, performance endurance, and crosswind stress testing. These programs are designed to provide the technical confidence needed prior to the certification and production introduction phases.

CONCLUDING REMARKS

The Feasibility Analysis program has been very effective in the identification and evaluation of high potential improvement concepts. Further, the Feasibility Analysis has suggested additional improvements beyond those evaluated under this program.

NASA participation in the development of performance improvement concepts has served as a catalyst for the initiation of General Electric performance improvement programs and is resulting in the accelerated development of concepts with a higher probability of ultimate airline service introduction. The concepts scheduled for development programs initiated to date plus those being evaluated are expected to produce a very measurable and worthwhile fuel savings in the 1980's and beyond.

TABLE 1
Fan Economic Analysis Data
Median Fuel Price

Aircraft	Stage Length km	Stage Length St. Mi.	ΔDOC * Dollars	ROI/Payback %/Years New	ROI/Payback %/Years Attrition	ROI/Payback %/Years Campaign
B747-200	772	480	-14,800	74/1.4	36/2.4	—
	3459	2150	-24,800	123/0.8	67/1.5	0/7.0
	6194	3850	-49,100	244/0.4	136/0.7	21/3.5
DC-10-10	634	400	-16,200	46/2.2	25/3.2	—
	1689	1050	-23,400	67/1.5	42/2.2	—
	3701	2300	-26,400	75/1.3	48/1.9	—
DC-10-30	805	500	-16,900	48/2.1	27/3.0	—
	2735	1700	-29,600	85/1.2	55/1.7	1/6.7
	6275	3900	-57,400	164/0.6	112/0.9	23/3.4

* 1977 Dollars

* Fuel Price DC-10-10, B747-200 — $.12/liter ($.45/Gallon); DC-10-30 — $.15/liter ($.55/Gallon)

TABLE 2
High Potential Concepts
SFC Improvements

Item	Potential ΔSFC @ Cruise — % CF6-6	Potential ΔSFC @ Cruise — % CF6-50
Improved Fan	-1.6	-1.8
Short Core Exhaust	—	-1.0 to -3.0
Improved HPT	-1.3	—
New Front Mount	-0.3	-0.3
HPT Roundness/ Clearance Control	—	-0.3
Active HPT Thermal Response	-0.4	-0.4
Cabin Air Recirculation	-0.7	-0.7

TABLE 3
Economic Analysis Comparison
High Potential Concepts
Median Stage Length and Fuel Price

	ROI % *	Payback Years *
Improved Fan	67/85/123	1.5/1.2/0.8
Short core Exhaust	-/-/-	-/-/-
Improved HPT	600/-/-	0.2/-/-
New Front Mount	165/201/166	0.6/0.5/0/6
HPT Roundness/ Clearance Control	-/145/111	-/0.7/0.9
Active HPT Thermal Response	10/21/-	7.7/4.4/-
Cabin Air Recirculation	64/87/-	1.6/1.2/-

*DC-10-10/DC - 10-30/747-200

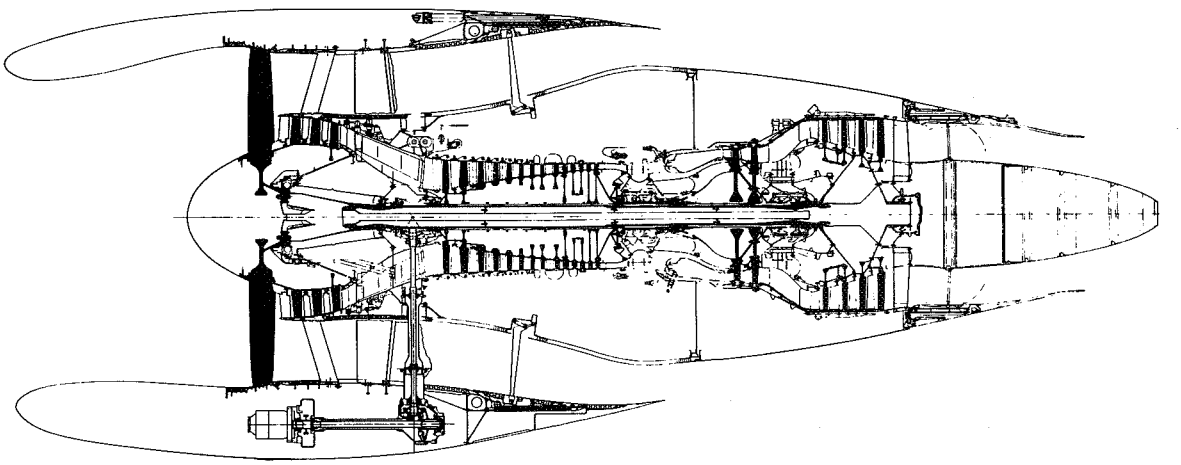

Figure 1.- CF6-50 engine cross section.

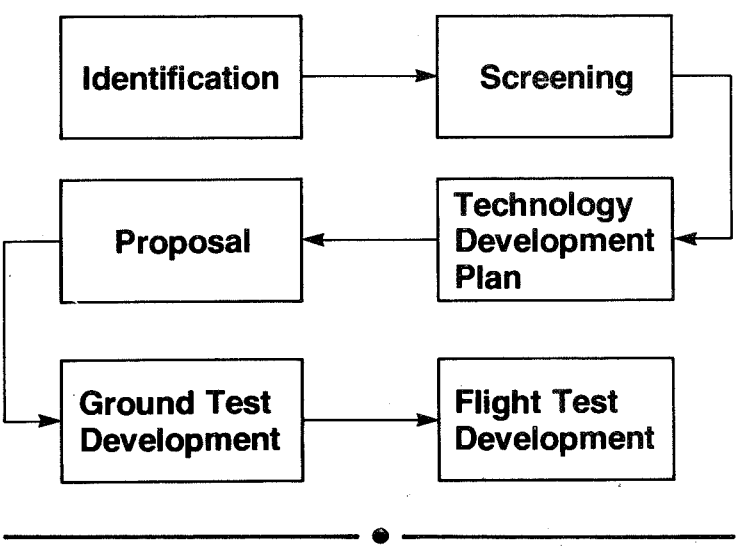

Figure 2.- Concept flow chart.

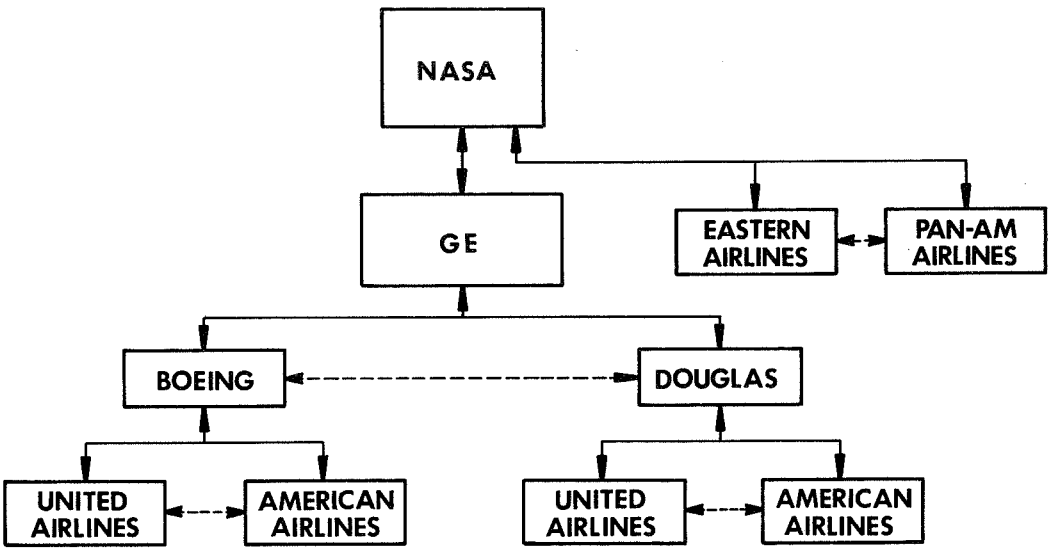

Figure 3.- CF6 jet engine performance improvement program channels of interface.

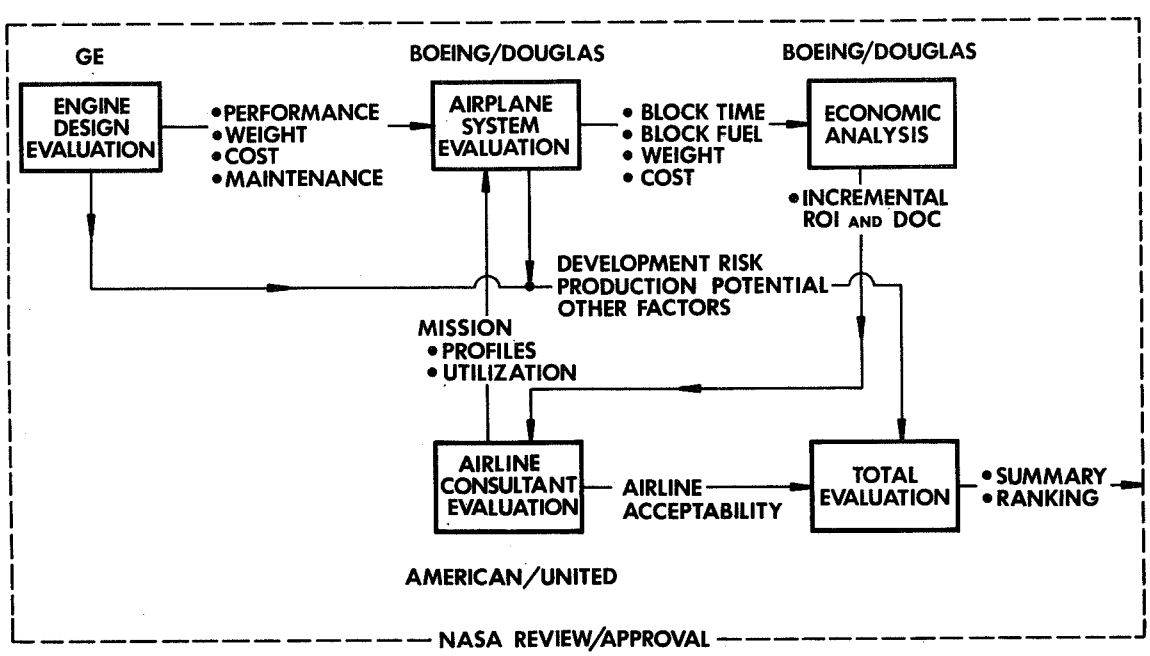

Figure 4.- Analytical procedure.

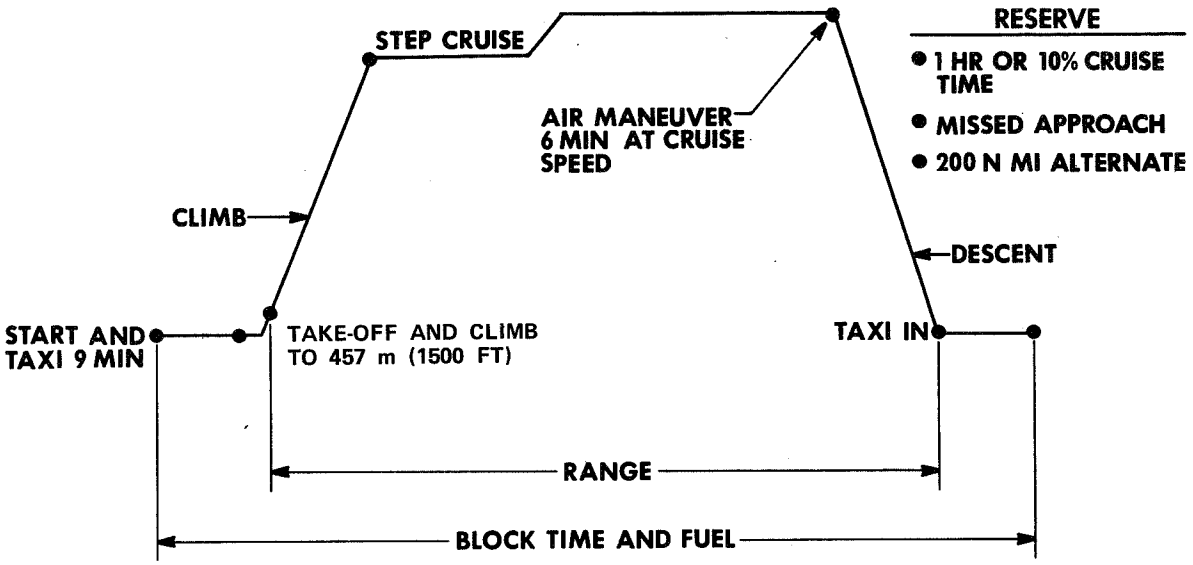

Figure 5.- Mission profile.

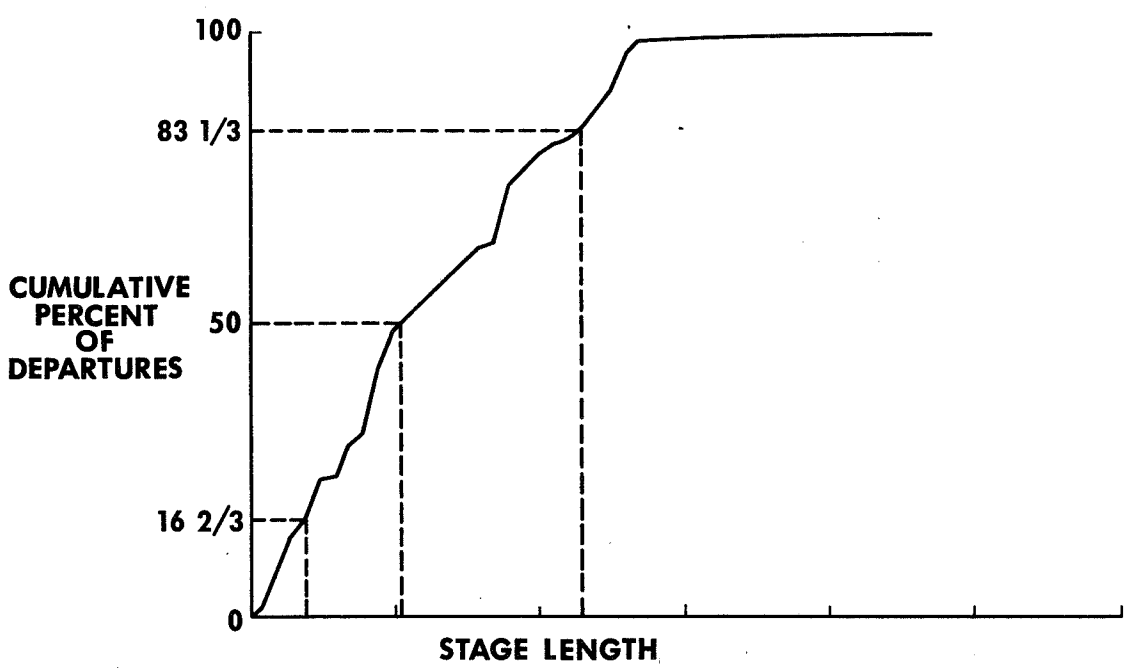

Figure 6.- Aircraft departures.

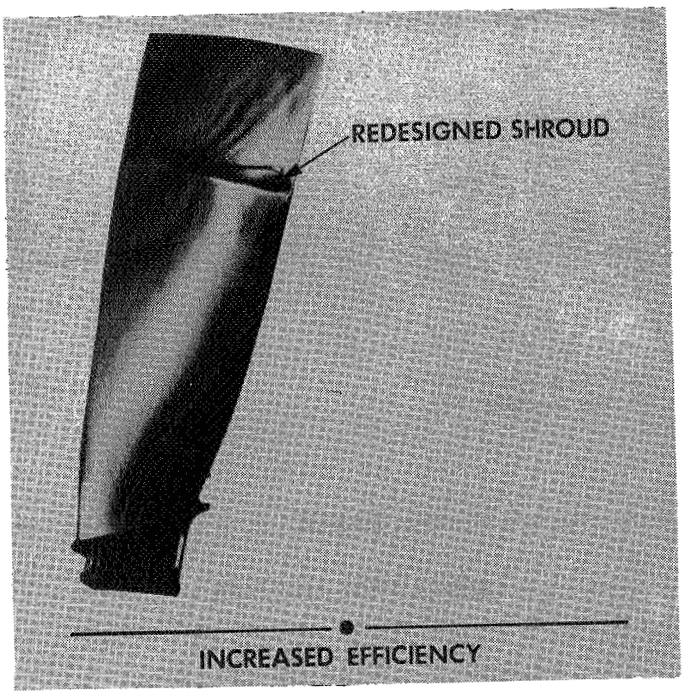

Figure 7.- New fan blade.

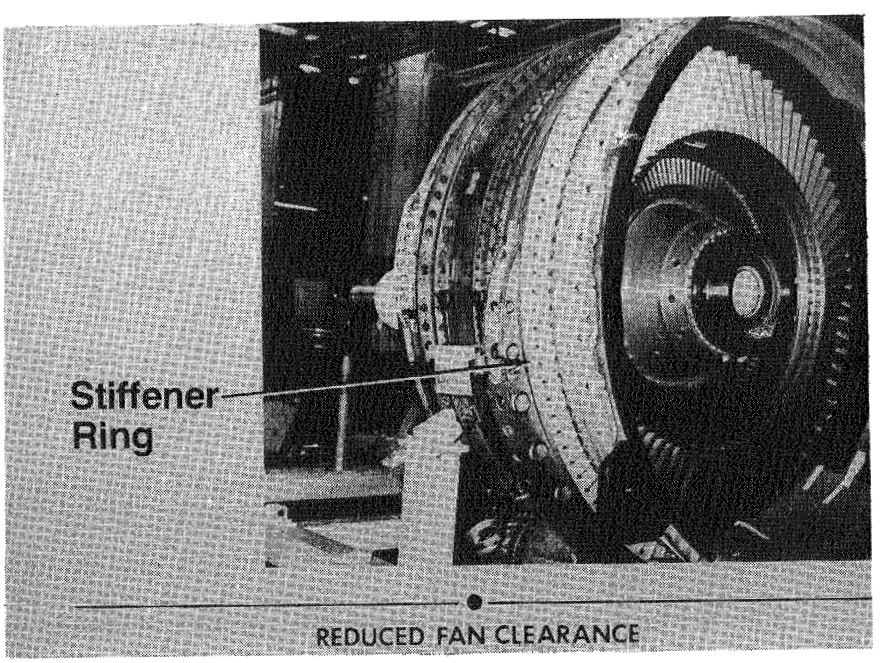

Figure 8.- Fan case stiffener.

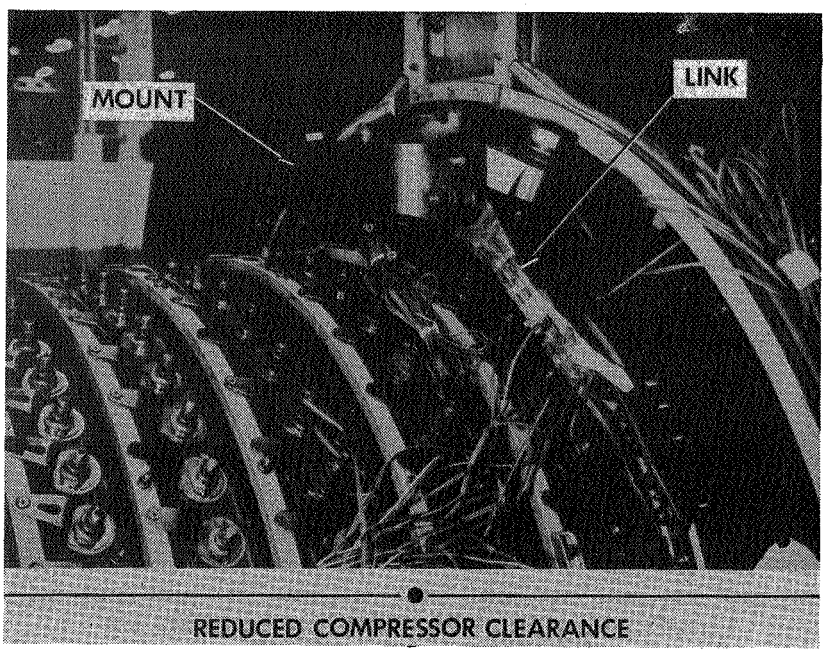

Figure 9.- New front mount.

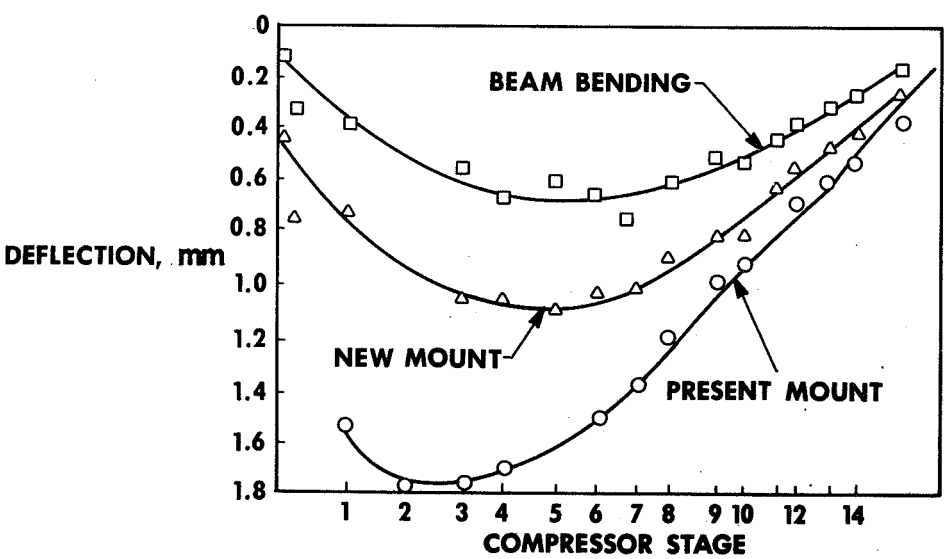

Figure 10.- Mount radial deflection comparison.
12 o'clock position; take-off/rotation.

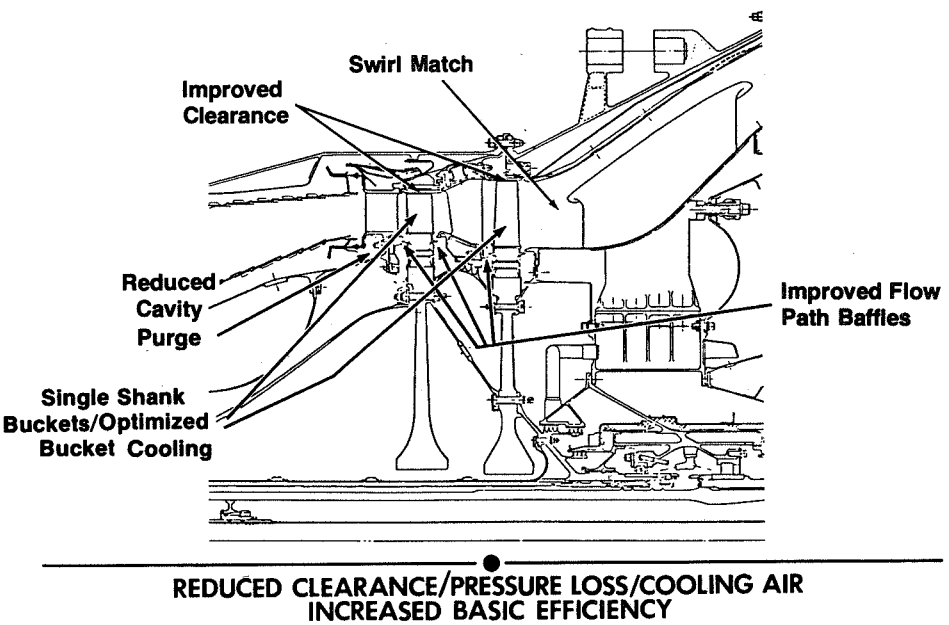

Figure 11.- Improved high pressure turbine design.

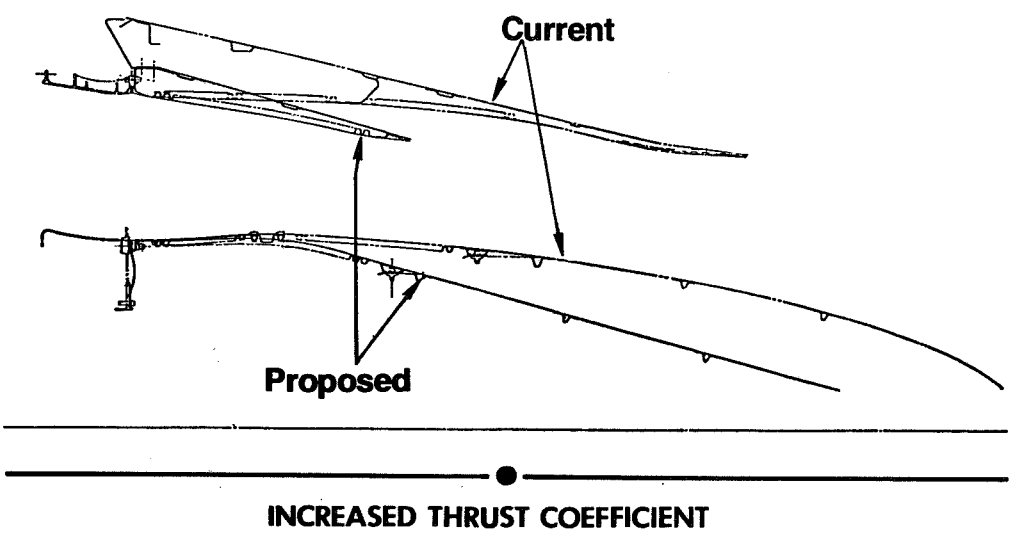

Figure 12.- Flow path contours for short core nozzle.

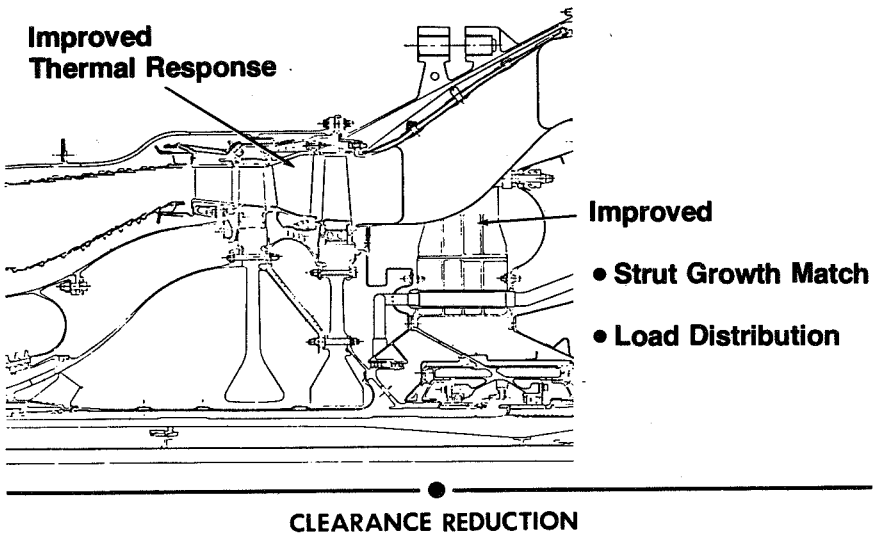

Figure 13.- High pressure turbine roundness and clearance control.

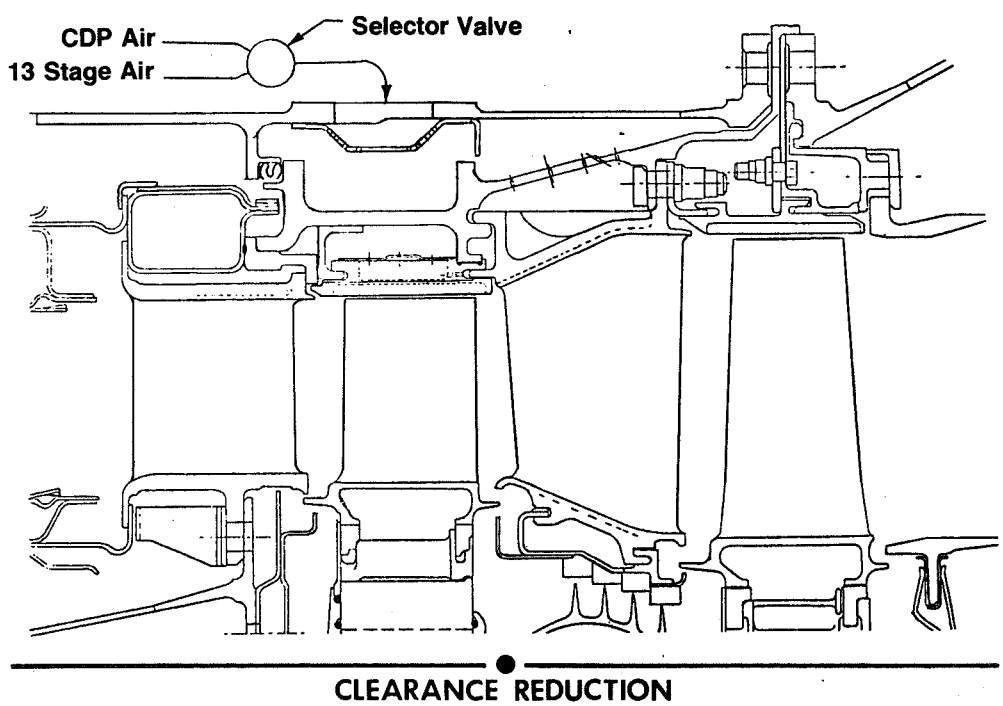

Figure 14.- Active thermal response variable cooling air.

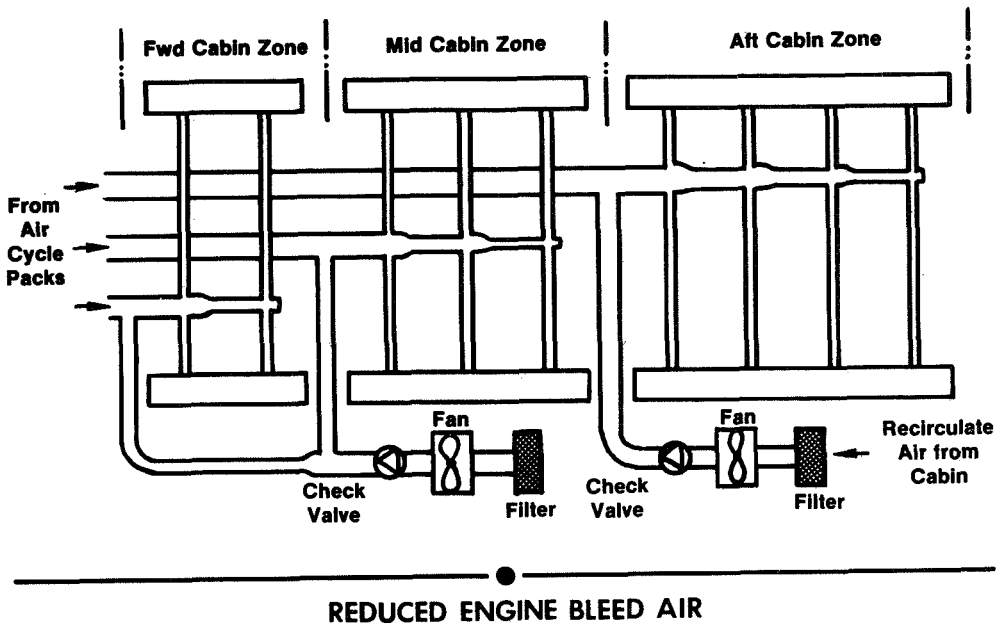

Figure 15.- Cabin air recirculation system.

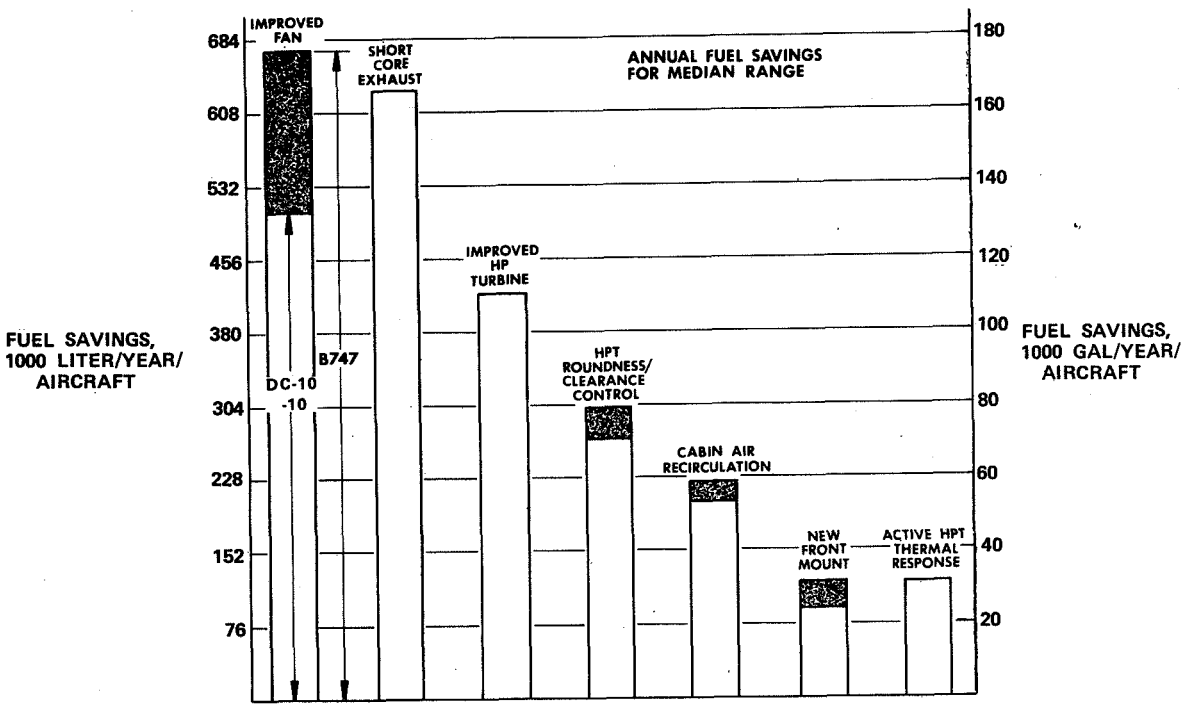

Figure 16.- Concept comparison.

ENGINE COMPONENT IMPROVEMENT – JT8D AND JT9D PERFORMANCE IMPROVEMENTS

W. O. Gaffin
Pratt & Whitney Aircraft Group

SUMMARY

A new feasibility analysis screening method for predicting the airline acceptance of a proposed engine performance improvement modification has been developed for NASA by Pratt & Whitney Aircraft, Trans World Airlines, Boeing, and Douglas Aircraft with consultation by American, United, Eastern and Pan American Airlines. This method uses technical information derived from available test data and analytical models along with conceptual/preliminary designs to establish the predicted performance improvement, weight and installation characteristics, the cost for new production and retrofit, maintenance cost and qualitative characteristics of the performance improvement concepts being evaluated. These results are used to arrive at the payback period, which is the time required for an airline to recover the investment cost of concept implementation, and to predict the amount of fuel saved by a performance improvement concept. The assumptions used to calculate the payback period and fuel saved are discussed.

A summary of the results when the screening method is applied is presented for several representative JT8D and JT9D performance improvement concepts. An example of the input information used to develop the summary results is shown.

Based on the results of the screening method, NASA has selected several performance improvement concepts for development and evaluation.

INTRODUCTION

The general objective of the NASA-sponsored Engine Component Improvement - Performance Improvement (ECI-PI) effort at Pratt & Whitney Aircraft is to demonstrate the specific fuel consumption benefits of JT8D and JT9D component improvements which have a good probability of production incorporation. A goal of 5% fuel saving over the engine lifetime has been established for each engine model. As the first step in accomplishing this general objective, a feasibility analysis with the following specific objectives has been completed:

- perform conceptual design studies of candidate component improvements;
- assess the performance improvement concepts in terms of economics, airline acceptability, and probability of incorporation into existing engines (retrofit) and into future production of current engines; and
- develop plans for the introduction of promising performance improvement concepts.

The second step in accomplishing the general objective consists of rig testing, engine ground testing, and engine flight testing to develop the technology and demonstrate the performance improvement of selected concepts. This effort has begun on three concepts.

DISCUSSION

In arriving at desirable performance improvement concepts for development under the ECI-PI program, a long list of potential candidates was compiled. The more promising concepts from reference 1, the newer ideas being explored in the development groups at P&WA, and ideas suggested by NASA and the airplane and airline companies involved in the program were all included on this early "shopping list". The general areas of performance improvements represented by this list are summarized on figure 1.

The long list of concepts was reduced early in the evaluation effort to 28 candidates (11 for JT8D engines and 17 for JT9D engines), which were subjected to a detailed evaluation process. The reduction was accomplished by eliminating concepts with small fuel saving potential, high development risk, or other practical limitations. This preliminary screening effort was based mostly on qualitative judgements, supplemented by quantitative evaluations of critical parameters.

The detailed evaluation procedure, which was applied to the 28 remaining concepts, was developed under the contract specifically for the purpose of identifying the most promising fuel saving concepts for development under the ECI-PI program. In developing the procedure, Pratt & Whitney Aircraft and its subcontractors were striving to duplicate or simulate as closely as possible the decision making process that normally occurs when the engine and airplane manufacturers offer equipment modifications (improvements) to the airline operators. The procedure is summarized in flow chart form on figure 2. The "bottom-line" results of this procedure are payback period, percent change in fuel burned, cumulative fuel saved and contractor ranking. Payback period is the economic acceptability parameter. The change in fuel burned indicates the day-to-day effect on energy conservation to be expected from each engine or airplane equipped with a performance improvement concept. The cumulative fuel saving shows the effect of incorporating the concept in any situation where it is economically acceptable, and continuing to use it for the life of the engine. The contractor ranking represents the combined recommendations of Pratt & Whitney Aircraft and its subcontractors based on the other "bottom-line" results modified by any qualitative considerations, such as development risk and hardware commonality, which were judged to be significant.

The effect of each concept on the operational and economic characteristics of a typical fleet of airplanes on a typical route structure was evaluated using a computerized simulation. The spare engines and parts provisioning requirements were estimated by airline maintenance experts. The results of the economic evaluation of each application of a concept was compared to an acceptability standard (required payback period) which was established earlier on the basis of airline requirements. Only those applications which met or bettered this standard were considered for the cumulative fuel saving estimate step of the evaluation. The evaluation procedure was developed and applied by a team which includes the manufacturers of the JT8D and JT9D engines and the airplanes in which they are used, plus several major airlines which operate this equipment. Pratt & Whitney Aircraft defined the effects of each component improvement concept on the en-

gine characteristics using standard design, evaluation, and pricing procedures, and also provided overall coordination of the evaluation process. The Boeing Commercial Airplane Company defined the effects on the 727, 737, and 747 airplanes and the Douglas Aircraft Company defined the effects on the DC9 and DC10 airplanes, using their standard design evaluation and pricing procedures. Trans World Airlines estimated the operational and economic effects in typical fleets and typical route structures using a previously developed computer simulation. American Airlines and United Airlines, serving as consultants to P&WA, BCAC, DACO and TWA, completed the evaluation team. Their function was to insure that the overall evaluations, and the TWA evaluation in particular, are typical of a major portion of the U.S. airline business. Eastern Airlines and Pan American Airlines served as consultants to NASA on this and other programs. Their efforts in the ECI-PI program served to insure that the evaluation results have even broader applicability.

The general input assumptions to the evaluation procedure are summarized on figure 3. The fuel prices and maintenance labor rates were selected by NASA based on the recommendations of the evaluation team to be consistent with the values used in related studies. Projections of the future sales of JT8D and JT9D engines were established for the evaluation by averaging the individual projections made by the Pratt & Whitney Aircraft team members. The required payback period, which will be discussed later, represents a consensus of the airline members of the team. The fleet size and route structure used with each airplane/engine model combination were defined by the airline members of the team to be typical of the use of this equipment in U.S. airline service. The annual fuel usage for each engine model represents an average of the entire U.S. airline industry, as reported to the Civil Aeronautics Board.

Perhaps the best way to explain the evaluation procedure is by an example. The evaluation of a modification to the JT8D high pressure turbine, applied at the time of engine production and as a retrofit to engines already in service, is summarized on figures 4 and 5. This modification requires additional steps and processes in the manufacture of the cooled turbine blades and the associated outer air seal ring, which will increase the price of these parts and of the complete engine. These increases combine with spare engine and spare parts requirements to increase the total investment cost associated with each airplane that an airline buys. The higher parts prices also result in an increase in the cost of materials used in maintaining the engines. However, the improved performance provided by the modification reduces the turbine temperature required to achieve a given thrust level, extending the time between engine removal for maintenance, and reducing the maintenance labor required per engine operating hour. The performance improvement is indicated by the thrust specific fuel consumption (TSFC) reductions shown on the figures. The TSFC reductions combine with any engine or installation weight changes (there were none in this case) to determine the fuel savings that will result if the concept is used in the typical fleet on the typical route structure. The fuel cost saving follows directly from the fuel saving, and combines with the maintenance cost change to produce the change in annual operating cost per airplane. Dividing the incremental investment cost per airplane by the incremental annual cost saving yields the payback period. This estimated payback period must be compared to the standard defined on figure 6 to determine the acceptability of the concept in each situation being evaluated.

The maximum acceptable payback period was calculated based on investment criteria and tax rule interpretations defined by the airline members of the team. While the airlines did not agree exactly in detail, the net result of their respective criteria and interpretations was remark-

ably close agreement on the desired capitol recovery rate and resulting maximum acceptable payback period. For this evaluation, the economic life of a new engine was assumed to be 15 years. It follows that the remaining economic life of a used engine being retrofit is 15 years minus the age of the engine at the time of retrofit. The maximum acceptable payback period then becomes a function of engine age as shown on figure 6, with the high value of 6 years for a new engine decreasing to zero (instantaneous payback) for a 15 year old engine. Applying this payback period standard to the estimated payback periods shown on figures 4 and 5, it may be concluded that the concept being evaluated should be acceptable to the airlines in new purchases of the 727, 737, and DC9, and for retrofit in 727 engines which are 4 years old or newer. The estimated payback period for retrofit in the DC9 and 737 (7.3 years) falls outside the acceptable limits, which means the airlines would probably choose to operate these airplane/engine combinations without incorporating the modifications. A practical consideration may arise which could reverse this latter conclusion and it is described here to illustrate the limitations of the evaluation procedure, and to underscore the need for direct airline participation in such an evaluation. An airline which operates 727 airplanes and either DC9 or 737 airplanes might choose to retrofit all of its JT8D engines to maintain commonality, with the accompanying benefits of parts and engine interchangeability, reduced spares inventory, and simplified maintenance procedures.

Figure 7 illustrates graphically the procedure used to estimate the cumulative fuel saving that will result from incorporating the concept in every situation where it is economically acceptable. The "engine entering service" curve is based on actual airplane sales through the year 1976, and represents the team consensus projection from that time onward. The "engines being retired" curve is the "engines entering service" curve displaced 15 years to represent the assumed 15 year economic life of each engine. Only the JT8D-15 and -17 models are considered here since the concept being evaluated applies only to these models, which have cooled high pressure turbine blades. The start of service date for the concept was estimated to be January 1980, based on a review of the development effort required. The "engines entering service" curve of figure 7 projects about 800 engines to enter service between 1980 and 1990 (the cut-off date chosen by NASA for the evaluation). Since the concept is economically acceptable for all of these new engines, and will reduce their fuel consumption until they are retired 15 years later, the shaded area between the curves represents the number of new engine-years that are affected. The concept is also available for retrofit starting in 1980, and will be applied to Boeing 727 engines that entered service in the 4 years before 1980. For convenience, the airlines would probably choose to install the modified parts when the engines come into the maintenance shop for other reasons. This will spread the introduction of the concept over the time it takes for all engines to return to the shop, approximately 3 years. This analysis assumes all of these engines will be retired when they are 15 years old regardless of when the concept was incorporated. The retrofit engine-years affected would be represented by the shaded area marked on figure 7 if all three airplane models were to be retrofitted. Since only the 727 airplane engines were found to be economically feasible for retrofit, the engine-years were reduced proportionally.

The engine-years affected are combined with the average annual fuel usage of the JT8D and the percent fuel saving estimated for the concept to produce the cumulative fuel savings shown on figures 4 and 5, which combine for a total of 340×10^6 liters (90×10^6 gallons) of fuel saved.

The evaluation procedure was applied to all 28 candidate concepts, and the team then ranked the concepts. As shown by the flow chart in figure 8, NASA combined the results of the

evaluation with development program schedule and cost information supplied by the manufacturers and NASA's own technical and funding considerations to make the final decision to include a concept in the ECI-PI development and demonstration effort. The concepts thus selected are listed in figure 9 along with a summary of the evaluation of each selected concept. NASA has funded development of the three concepts included in the boxes in figure 9 and work has begun on the programs. The others are expected to be funded and started during the next several months.

CONCLUDING REMARKS

Under the NASA sponsored Engine Component Improvement - Performance Improvement Program, an effective evaluation process was developed and successfully demonstrated. Using this process, a team formed by Pratt & Whitney Aircraft and including representatives from airframe manufacturers and the airlines evaluated 28 performance improvement concepts and identified 9 that were judged to have a high probability of meeting the economic and performance requirements for implementation. NASA has funded development and demonstration efforts for three of the nine concepts and these programs are currently in progress.

REFERENCE

1. Gray, D. E.,: Study of Turbofan Engines Designed for Low Energy Consumption - Final Report. NASA CR-135002, April 1976.

Considered well over 100 candidate concepts derived from:

- Improved component aerodynamics
- Improved flowpath sealing
- Blade tip clearance control
- Improved turbine cooling effectiveness
- Improved turbine materials and coatings
- Duct and nozzle aerodynamic refinements
- Nacelle aerodynamic refinements
- Forced exhaust mixers
- Advanced nacelle materials
- Advanced fuel control

J18506-1
783001

Figure 1.- General areas of performance improvement considered.

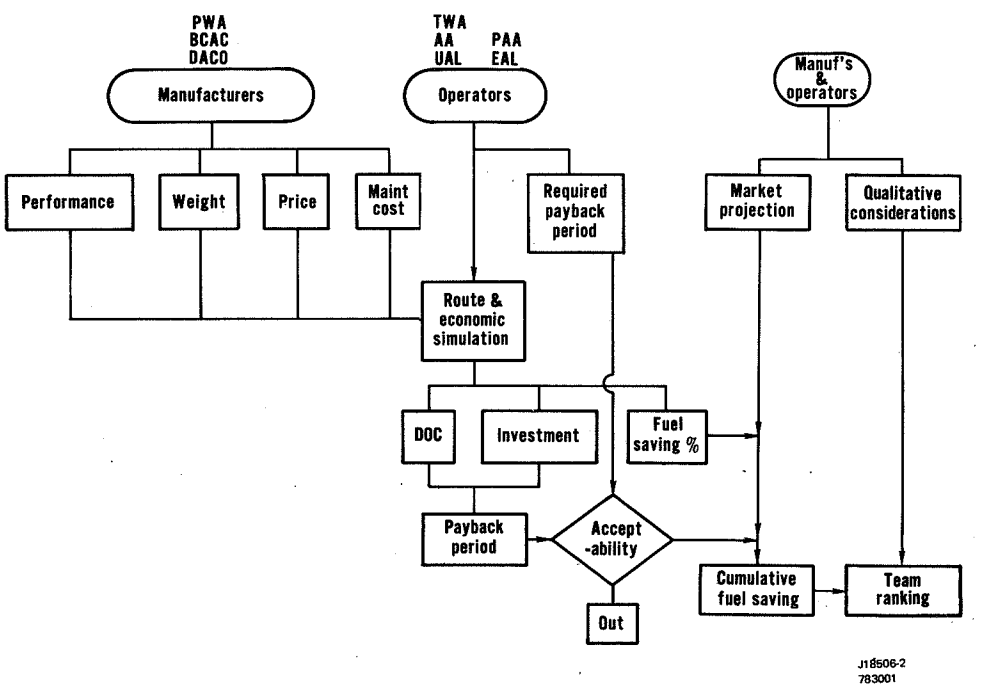

Figure 2.- Detailed evaluation procedure flow chart.

Fuel price	9.2¢/liter (35¢/gal) domestic, 11.9¢/liter (45¢/gal) international			
Maint. labor rate	30$/hr. (fully allocated)			
Spares requirements	Variable			
Market projection	Team consensus			
Max. acceptable payback period	Function of engine age			
Airplane model	DC-9-50	727-200	DC10-40	747-200
Engine model	JT8D-17	JT8D-15	JT9D-59	JT9D-7 or -70
Fleet size	18	39	28	11
City pairs	62	129	45	24
Flights per week	714	1416	397	136
Avg. stage length, km (N.Mi)	669(361)	1093(590)	2967(1602)	5545(2994)

	JT8D	JT9D
Avg. annual fuel usage, 10^6 liters(gal) per eng-yr	3.8(1)	11.3(3)

J18506-10
R781602

Figure 3.- Summary of evaluation input assumptions.

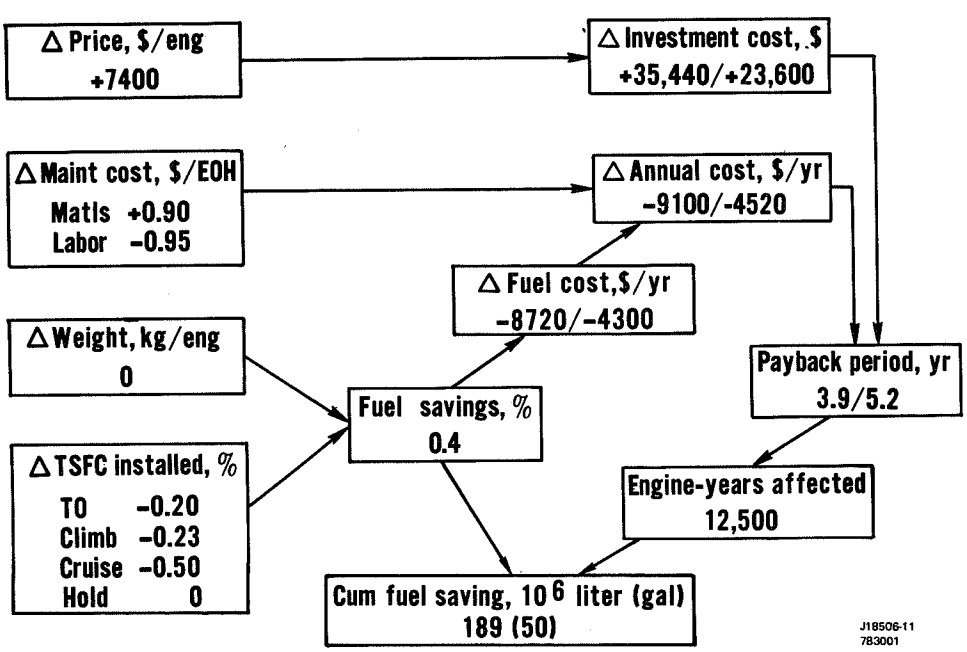

Figure 4.- Evaluation of JT8D revised HPT outer air seal for new buy 727-200/DC9-50.

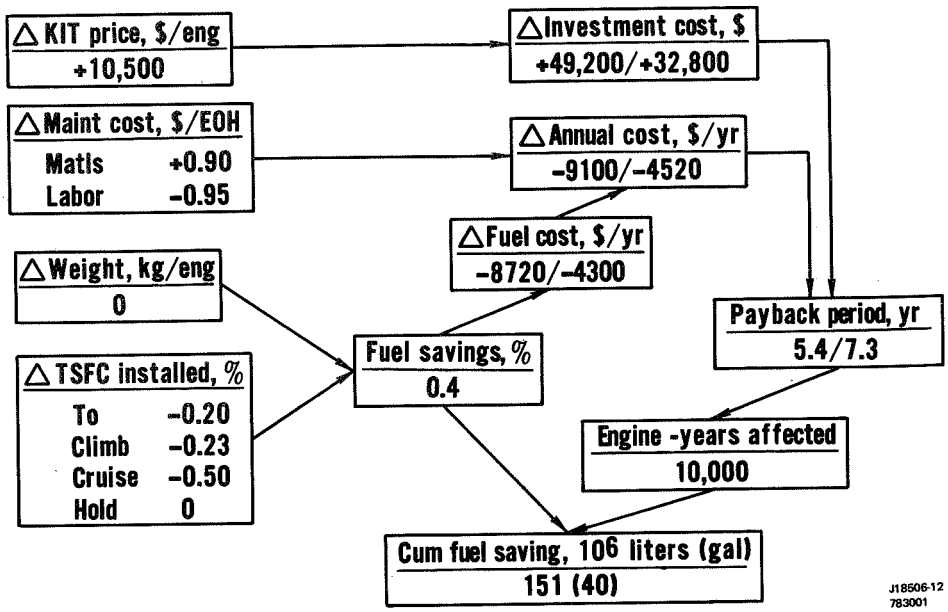

Figure 5.- Evaluation of JT8D revised HPT outer air seal for retrofit 727-200/DC9-50.

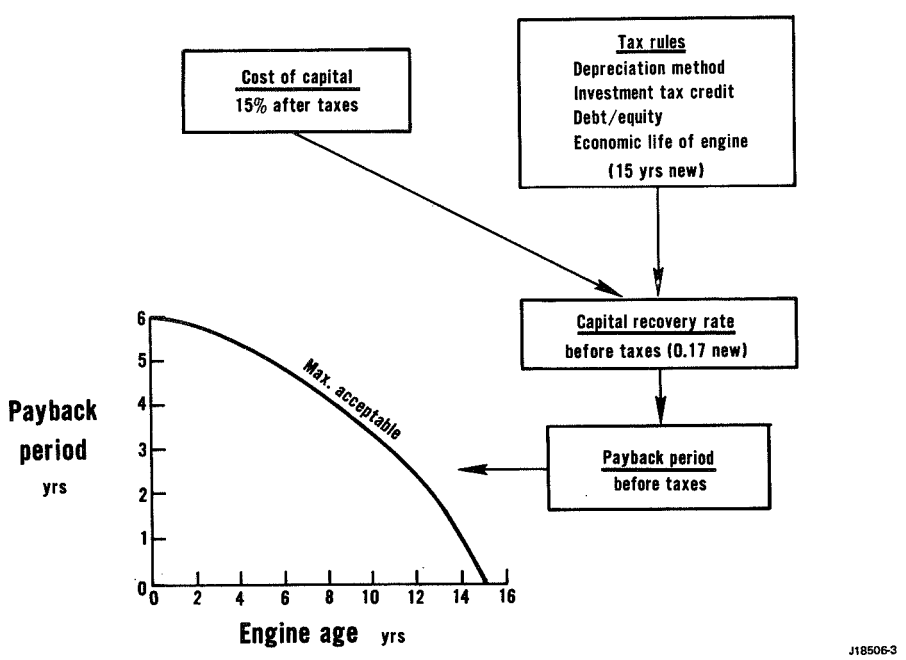

Figure 6.- Maximum acceptable payback period determination.

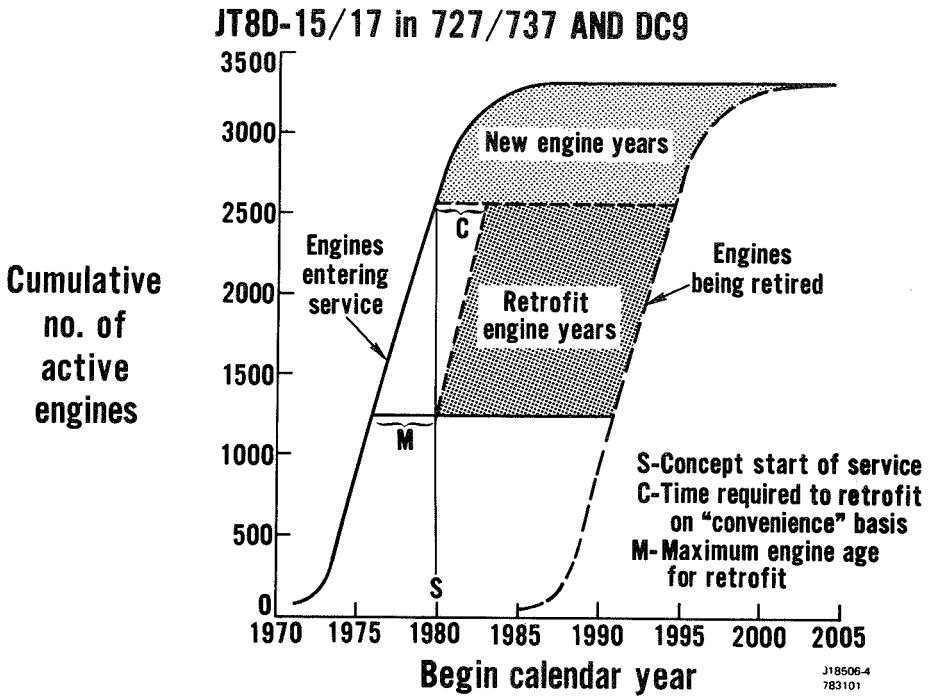

Figure 7.- Cumulative fuel savings estimate procedure.

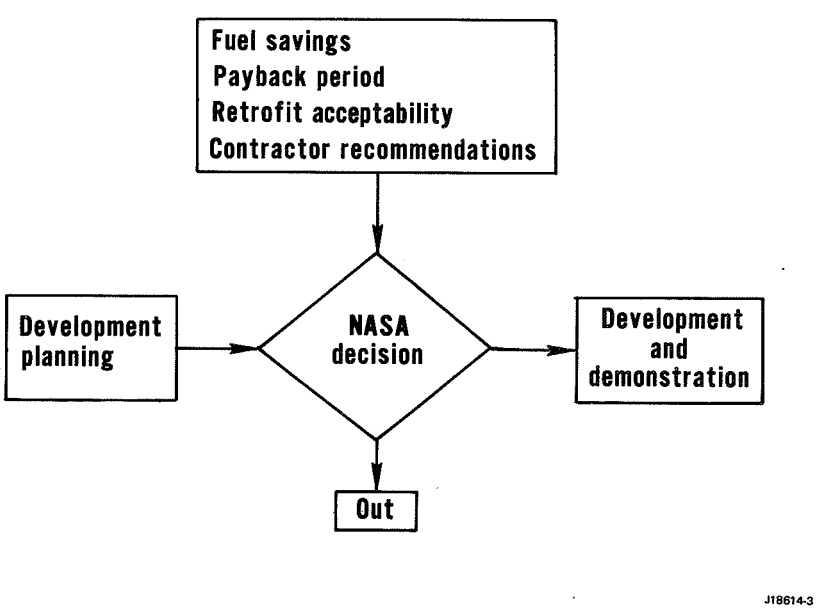

Figure 8.- NASA concept selection procedure.

	Start of service date	Payback period*		Fuel saving		
		New	Retrofit	%	Cum, 10^6 liters	(gal)
Total JT8D				**2.7**	**3860**	**(1023)**
Revised HPT outer air seal (-15/17)	1/80	3.9/5.2	5.4/7	0.4	340	(90)
Root discharge of HPT blade cooling air (-15/17)	6/81	0/0	0/0	0.8	980	(259)
Abradable, trenched HPC blade tips	3/81	1.2/1.4	5.0/6	1.0	2220	(589)
DC9 reverser stang fairing	1/79	-/0.7	-/0.7	0.5	320	(85)
Total JT9D				**3.4**	**9280**	**(2456)**
Improved HPT active clearance control (-70/59)	6/79	1.0/2.1	6 /12	0.9	1770	(468)
3.8 aspect ratio fan (single shroud) (-7)	1/80	1.8/ -	10/ -	1.5	2720	(720)
Trenched HPC blade tips	3/81	0.1/0.1	0.7/0.3	0.4	1860	(493)
Ceramic HPT blade tip seals	1/82	0.3/0.5	0.5/0.7	0.4	1950	(516)
Thermal barrier coating on HPT vane platform	1/82	0/0	0/0	0.2	980	(259)

*727/DC9 or 747/DC10

J18506-5
R781602

Figure 9.- Evaluation results for recommended concepts.

ENERGY EFFICIENT ENGINE

PRELIMINARY DESIGN AND INTEGRATION STUDIES

David E. Gray
Pratt & Whitney Aircraft Group

SUMMARY

This paper summarizes the results of the NASA sponsored Energy Efficient Engine Preliminary Design and Integration Studies conducted by Pratt & Whitney Aircraft, with the assistance of Boeing, Douglas and Lockheed. A mixed exhaust, direct drive fan turbofan configuration was selected from the four candidates considered. This choice was based on its ability to exceed study goals of 12% lower TSFC and 5% lower direct operating cost by the 1990's with commercially acceptable technical risk and relative mechanical simplicity. The evaluation leading to configuration selection is discussed. Necessary technology advancements are identified and related to the goals.

INTRODUCTION

A NASA sponsored fuel conservative turbofan analytical effort conducted in 1974 and 1975 - The Study of Turbofan Engines Designed for Low Energy Consumption - indicated that over a 15% fuel savings was possible by utilizing projected 1985 technology. The estimation of this potential assumed major improvements in component efficiencies, availability of advanced materials, and structural innovation.

Four turbofan design configurations - direct drive and geared fan engines with separate or mixed exhausts - were each found to provide, within 2%, the same fuel savings potential. This closeness made it impossible to clearly segregate a preferred configuration and to ascertain the necessary unique technology advancements.

More detailed study of the four candidate configurations, including detailed airframe-engine system evaluation, was needed before a choice could be made. The Energy Efficient Engine Preliminary Design and Integration Studies were initiated by NASA in 1977 to provide the additional information necessary for engine configuration selection and to firmly establish vital technology development requirements prior to starting technology demonstration and proof testing.

DEFINITIONS

TSFC	–	thrust specific fuel consumption
DOC	–	direct operating cost
EPA	–	Environmental Protection Agency
EEE	–	Energy Efficient Engine

FAR 36 – Federal Aviation Regulations - Part 36

EPNdB – Effective Perceived Noise ~ dB

CANDIDATE CONFIGURATION DESCRIPTIONS

Conceptual designs of the four candidate engine configurations which combined a common high spool with various low pressure spool components and exhaust systems for parametric study were defined. General engine arrangements are illustrated in figure 1. Engine components were defined through regression analysis of many different configurations followed by more refined analysis of several attractive approaches. The following paragraphs describe the selected components at the 10,700 m (35,000 ft), Mach 0.8 cruise design point.

High Pressure Spool Components

A 10 stage high pressure compressor was selected to produce an 18:1 pressure ratio at a 445 m/sec (1460 ft/sec) inlet corrected tip speed. The combustor was conceptually designed with two combustion zones for low emissions. A two stage, high pressure turbine, with a loading coefficient [1] of only 1.2, was selected for high efficiency.

Low Pressure Spool Components

Low pressure spool configurations differed considerably depending on the fan drive mechanism - direct or gear.

Parametrically defined direct drive fans ranged from 6 to 9 bypass ratio with corresponding pressure ratios from 1.8 to 1.6. The pressure rise per stage of a three stage low pressure compressor was adjusted as necessary to hold overall compressor pressure ratio constant at 39:1. High loading coefficient, low pressure turbines had 4 or 5 stages dependent on the fan bypass ratio. A typical 7 bypass ratio engine with separate exhausts had a 1.74 pressure ratio fan, rotating at 470 m/sec (1550 ft/sec) tip speed. The fan and low pressure compressor were driven by a 2.5 loading coefficient, low speed, 5 stage low pressure turbine. With the 7 bypass ratio mixed exhaust configuration, the fan pressure was reduced to 1.66 to equalize turbine exhaust and fan exhaust total pressures for efficient mixing.

The range of bypass ratios studied for the geared drive fan configurations were 7 to 11 with fan pressure ratios from 1.75 to 1.45. The low pressure compressor rotated at 2½ times fan speed resulting in one less stage than required in the direct drive configurations to produce the same overall pressure ratio. A typical 9 bypass ratio engine with separate exhausts had a gear driven fan with a 1.58 pressure ratio and a 380 m/sec (1250 ft/sec) corrected tip speed. A high speed, 3 stage low pressure turbine with a loading coefficient of only 1.5 was utilized. A star reduction gear was positioned behind the fan. Gear generated heat was rejected in a fuel/oil cooler and a supplemental air/oil cooler located in the fan duct. The fan for the mixed exhaust configuration had a tip speed of 360 m/sec (1175 ft/sec) with a pressure ratio of 1.52.

[1] Loading coefficient relates turbine work output to available kinetic energy. Low values imply light aerodynamic loading for increased efficiency.

Exhaust Systems

The separate exhaust configurations included three-quarter length fan cowls with full acoustic lining for low noise. The mixed exhaust configurations included a forced mixer with a predicted mixing efficiency of 85% on a gross thrust basis. The efficiency prediction is based on JT8D and high bypass ratio mixer model test programs.

CONFIGURATION EVALUATION

Configurational capabilities were measured against the study goals of figure 2. The JT9D-7A, the most widely used current operational high bypass ratio engine, was used as the baseline. The TSFC goal includes the effects of isolated nacelle drag at a 10,700 m (35,000 ft), Mach 0.8 cruise condition. The direct operating cost reduction goal encompasses, in addition to fuel costs, the effects of propulsion system weight, price, and maintenance costs. The DOC goal penalizes weight and cost increases which could otherwise negate the operating economy attendant with TSFC. Stringent environmental goals were established which required incorporation of technological concepts aimed at substantial exhaust emissions and noise reductions. Goals for performance deterioration with operating time and for thrust growth allowance were set to assure continued fuel savings over the lifetime of the engine family. In combination, the study goals directed attention to expected requirements of future commercial transport engines of the 1990's.

Boeing, Douglas and Lockheed assisted in an engine-aircraft system evaluation of the four configurations. They first projected the spectrum of new commercial transport aircraft possible in the 1990's. Forecasts are obviously imprecise; however, many new aircraft are expected to be introduced in that time period. Each selected two representative aircraft - a domestic and an international service design. Advanced technology wide body aircraft, illustrated in figure 3, ranged from a Boeing 86,300 kg (250,000 pound) domestic twin-jet to a Douglas 210,000 kg (600,000 pound) international tri-jet.

For each of the study aircraft, the airplane companies conducted integration studies to size engines, determine installation effects, and define aircraft performance characteristics. A most important integration consideration was the potential for high interference drag with long, acoustically treated nacelles. This problem was addressed in under-the-wing installations by applying minimum drag nacelle-to-wing positioning criteria based on the aerodynamic development and testing of current high bypass ratio engine installations. Tail engine installations were positioned to maintain present high bypass ratio engine installation interference drag levels and to provide necessary nacelle-to-ground clearance during takeoff rotation. The airplane companies also estimated airframe noise, fuel burned, and aircraft weight as inputs into Pratt & Whitney Aircraft's direct operating cost, noise, performance deterioration, and thrust growth comparisons.

Results of the evaluation against goals are summarized in figures 4 through 6 for 7 bypass ratio, direct-drive configurations and 9 bypass ratio, geared configurations. TSFC and typical mission fuel burned reductions relative to scaled JT9D-7A powered equivalent aircraft are shown in figure 4. All four configurations exceeded the study TSFC goal as shown on the figure. Although a fuel burned study goal was left unspecified, fuel savings is a more important parameter than TSFC reduction. Fuel burned reductions varied substantially in response to differences in the ranges and payloads of the six aircraft types. The Boeing shorter range, domestic twin-jet exhibited the least fuel burned reduction amounting to approximately 60 percent of that for the very long

range Lockheed international quadjet. A comparison of the capabilities of the four engine configurations was obtained by averaging the results obtained with each engine configuration in the domestic and international aircraft as illustrated on figure 4. On this basis, mixing of the engine exhausts and reduction gearing each increased the fuel savings potential by an additional 2-½%.

DOC and fuel burned trends were similar as can be seen by comparing figures 4 and 5. Using the average values of the results, mixing of the engine exhausts reduced DOC by 1.1%. Gearing, including the effects of gear set maintenance costs, reduced DOC by an average of 0.7 percent. It was additionally noted that, for many of the domestic aricraft, the DOC reduction potential was small. Bypass ratio of the direct-drive engine configurations was reduced from 7 to 6.5 for a small DOC improvement of about 0.2 percent based on parametric analysis.

The overall evaluation against goals results are summarized in figure 6. As previously noted, all configurations exceeded the TSFC goal and approached, or exceeded, the DOC goal. By incorporating an advanced two stage, low emissions combustor, all of the configurations were calculated to meet 1981 EPA carbon monoxide and unburned hydrocarbons emissions goals. However, all configurations were assessed to be incapable of meeting the oxides of nitrogen goal with known emissions technology. Noise goals could be met by the four configurations with projected advancements in fan source noise and acoustic absorption technologies. The effects of opened-up blading tip clearances, erosion, turbine airfoil creep and distortion, leakage, and foreign object damage were examined to assess performance deterioration. The engines were estimated to have a 4000 operating hour TSFC deterioration rate approximately one-half that of the JT9D-7A. Equal thrust growth potential of over 20% from the initial rating was predicted for all four configurations by compressor supercharging and higher turbine temperature.

Based on this evaluation, only mixed exhaust configurations were considered further. The mixed exhaust configurations embodied all of the propulsion technology advances requiring further development in engines with separate exhausts. The additional fuel savings and DOC benefits associated with mixing were judged to outweigh the added development risk of the exhaust mixer.

Preliminary designs were executed for direct-drive and geared, mixed-exhaust engine configurations. High spools with one and two-stage turbines were considered for each engine configuration. The probability of success for achieving each individual propulsion system technology advancement included in the preliminary designs was estimated. The individual technology probabilities were statistically summed to arrive at an overall engine configuration probability curve for improving TSFC. Similar analyses were made for weight, price and maintenance costs. Sensitivity factors were applied to these results to arrive at fuel savings and DOC reduction for each configuration on an equal probability of success basis.

Figure 7 lists the relative advantages identified in this evaluation for one and two-stage high pressure turbine engines. The overall comparison resulted in 0.7% less fuel savings, but over a 1% DOC advantage for the one-stage turbine approach. By the use of advanced, high strength blade and disk alloys expected to be available by 1985, the one-stage turbine could be designed with only 60% of the two-stage turbine airfoils without exceeding allowable stresses in the blade-disk attachment region. A corresponding 6% engine acquisition cost reduction and a 10% lower engine maintenance cost were estimated. The one-stage turbine blades would operate transonically for a 3% loss in efficiency, however. After considerable deliberation, the one-stage turbine approach was chosen for cost reduction.

Relative advantages of the geared fan and direct drive fan configurations are compared in figure 8. Additional fuel savings of 1-½% for the geared fan configuration derive from the higher propulsive efficiency of the larger diameter fan. The 10% lighter direct drive fan engine installation was estimated to have an equally lower cost and a 4% lower maintenance cost. A net DOC advantage of 0.5 to 1.0% resulted for the direct drive fan configuration. Degradation of the geared fan advantages relative to the conceptual study reflected the low probabilities of achieving both the originally assumed gear efficiency of 98.8% and the very low gear system bearing and gear replacement rate.

Preliminary design analyses identified several unique requirements of the geared engine high speed low rotor system which increased engine complexity. Last stage low pressure turbine blade pull stresses were estimated at 4.48×10^8 N/m^2 (65 ksi) requiring use of blade and disk materials usually reserved for the high pressure turbine. An additional mid-engine bearing compartment with intershaft and high rotor bearings was found necessary to avoid low rotor critical speeds within the engine running range. An additional fan rotor roller bearing was also required to uncouple fan and low pressure turbine induced rotor vibration. Failure analysis indicated that sophisticated containment and fast acting low pressure turbine gas blow-off devices would very likely be required to avoid nacelle penetration by high kinetic energy engine parts in the event of the 1.49×10^4 to 3.73×10^4 kW (20,000 to 50,000 hp) gear system internal failure. Based on the preliminary design analyses and the results shown in figures 4 through 7, the mixed exhaust, direct drive turbofan with a one-stage high pressure turbine was selected as the Pratt & Whitney Aircraft proposed configuration for the Energy Efficient Engine.

DESCRIPTION OF P&WA'S ENERGY EFFICIENT ENGINE PRELIMINARY DESIGN

The Energy Efficient Engine cycle parameters are listed in figure 9. The engine has a 38.6:1 overall pressure ratio at the cruise design point for a 3 to 4 percent fuel consumption improvement relative to present engines. A bypass ratio of 6.5:1 and fan pressure ratio of 1.74:1 were selected from the parametric study to minimize direct operating cost. The design turbine rotor inlet temperature at cruise was set at 1205°C (2200°F) to minimize fuel consumption. There is margin for over 20% thrust growth by supercharging to 45:1 overall pressure ratio while increasing turbine rotor inlet temperature by 110°C (200°F).

The propulsion system cross-section is shown in figure 10. The main design features of the propulsion system are an integrated engine/nacelle structure to improve engine performance retention, advanced clearance control concepts to achieve high component efficiencies, and a low maintenance, one-stage high pressure turbine.

The fan is a shroudless, single-stage, hollow titanium design with a pressure ratio of 1.74:1 and a corrected tip speed of 470 m/sec (1550 ft/sec). The four-stage low pressure compressor incorporates controlled endwall loss concepts, low loss airfoils, and increased aerodynamic loading. The high pressure compressor is a high inlet corrected tip speed (405 m/sec, 1325 ft/sec), 10-stage design with 1.7:1 average aspect ratio airfoils. Compressor pressure ratio is 14:1 driven by the one-stage high pressure turbine. High strength titanium and an advanced high strength nickel base alloy (MERL 76) disk materials are used in the rear section to permit the higher rotor speeds and increased temperatures associated with high overall pressure ratio. The compressor has active clearance control, controlled loss endwalls and reduced loss airfoil concepts to raise efficiency levels.

A staged vortex burning and mixing (vorbix) combustor is used for low emissions. This combustor is conceptually derived from the NASA Experimental Clean Combustor. Design changes were conceived relative to the experimental burner to make it commercially practical without sacrificing low emissions characteristics. An oxide-dispersion strengthened, film-cooled, louvered combustion zone liner is incorporated to provide commercial durability at the elevated compressor exit temperatures encountered in the engine.

The one-stage high pressure turbine is designed with a low 1.6 loading coefficient, which requires a high disk rim red-line speed of 530 m/sec (1730 ft/sec). The disk is of high strength MERL 76. Single crystal alloy blades with up to a 56°C (100°F) higher metal temperature capability than present are used to minimize compressor coolant bleed air. The four-stage low pressure turbine counterrotates relative to the high pressure turbine to minimize interturbine gas turning and pressure loss, and is designed for a 2.4 loading coefficient. The turbine uses titanium-aluminide airfoils in the cooler rear stages to save weight. Active clearance control is incorporated in the turbine section to increase efficiency.

The exhaust mixer is a scalloped design with low pressure loss and high mixing efficiency. High temperature titanium is the preferred mixer material. Its lightweight, one-piece superplastic forming capability allows engine weight savings and reduced fabrication costs relative to conventional welded-up steel units. A full authority digital electronic control is used to reduce operating cost and to provide efficient engine operation. The nacelle features an integrated engine/nacelle structure to restrain engine deflections caused by thrust and cowl loads.

Pratt & Whitney Aircraft has established flight engine design goals from this study of 15.3 percent TSFC improvement and a 6% DOC reduction relative to the JT9D-7A. Fuel savings of over 15% are also made possible with the selected engine configuration. Boeing, Douglas, and Lockheed evaluations of this engine resulted in fuel savings ranging from 11 to 26% and DOC reductions of from 3 to 15% compared with JT9D powered equivalent aircraft.

The realization of the Energy Efficient Engine potential is keyed to successful development of the many state-of-the-art advancements in fuel saving concepts included in the preliminary design. Technology must be balanced with practicality to ensure airlines acceptance of future energy efficient turbofan engines. Based on preliminary design analysis, critical propulsion technology areas have been identified which need to be translated into commercially acceptable hardware before the fuel savings promise can be realized (fig. 11). The remainder of the paper describes these technologies and the related benefits.

Active Clearance Control & Nacelle Load Sharing

Rotor blades and the engine cases have different rates of thermal expansion which can create large rotor tip-to-case clearances during cruise operation where up to 90% of the fuel is consumed. Cruise efficiency can be improved if these clearances, and the resultant leakage, are reduced. The thermal active clearance control system bathes the compressor and turbine cases with hot or cool air to precisely match the case diameter to the rotor tip diameter during cruise while providing sufficient tip clearance to avoid rubs during take-off roll, rotation and climb-out. The result is up to 55% reduced blade tip clearance during cruise with the benefit of over a 1.5% improvement in compressor and turbine efficiencies (fig. 12).

Active clearance control is already being introduced into the turbine sections of operational high bypass ratio turbofan engines as knowledge of case thermal response increases with operational experience. Computerized, finite element thermal and structural modeling techniques are being developed for the engine rotor system, engine static structure, and nacelle. These models permit the full use of active clearance control in the compressor and turbine sections for a 3% fuel savings.

The energy efficient engine is being designed with short, stiff rotors to minimize rotor deflections under thrust, gravitational or gryoscopic loads. A load sharing nacelle is included to minimize engine backbone bending which has been identified as a major cause of engine performance deterioration from rub induced blade tip wear.

Load sharing is achieved by structurally attaching the fan duct walls to the engine cases. These ducts act as structural "beams" in parallel with the engine case beam. The larger diameter fan ducts are inherently stiffer than the engine cases and will carry the majority of the load. This reduced load on the engine cases will keep deflections low. In conjunction with active clearance control, the rigid rotor systems and load sharing are projected to reduce the long term 4000 hour TSFC deterioration to approximately half that of current high bypass (fig. 13) ratio engines.

Advanced Internal Aerodynamics

Many new aerodynamic concepts have recently been analytically or empirically identified which, in total, can produce major component efficiency improvements. The improvements involve both better airfoil performance and lower losses in the endwall regions of the gaspath.

Titanium fan blades on operational high bypass ratio turbofan engines require inter-blade shrouds to limit blade vibration stress to an acceptable level. Shrouds reduce fan efficiency by upsetting the airflow through the fan. Fan efficiency can be increased over 2% by eliminating shroud induced aerodynamic losses shown in figure 14.

Vibration can be controlled in shroudless blades by elongating blade chord 50% but this increases the fan assembly weight. One way to reduce weight is to hollow-out the titanium blades. The problem becomes how to make hollow titanium fan blades inexpensively.

Superplastic forming manufacturing techniques have recently been developed to mold titanium into complex shapes, at low cost. Superplastic forming is especially suitable to titanium, which has the capability of being elongated 300% without local thinning under controlled temperature and strain rate. Superplastic forming can be combined with diffusion bonding techniques so that two titanium pieces can be mated along their edges in a die, heated to 925°C (1700°F) and pressurized to 2.07×10^6 N/m^2 (300 psi). The pieces simultaneously bond along their edges and expand into the die to complete the fabrication process.

Through recent developments in computer analysis techniques, increased freedom in compressor airfoil shape selection is also being exploited. Multiple-arc and supercritical compressor airfoil contours have been identified which operate transonically at 15% higher relative air Mach numbers than the JT9D-7A with the same efficiency. The airfoils are also capable of carrying higher aerodynamic loads at peak efficiency. This ability is being used to reduce compressor and turbine airfoil count and to reduce the through-flow gas velocity to improve efficiency.

Compressor and turbine research tests have identified a significant efficiency loss caused by flowpath air recirculating into and out of inner engine cavities beneath blade and vane root shrouds. In the turbine, vane inner shroud forward projections overlapped by blade shrouds were tested to isolate these cavities from the flowpath. Efficiency capability increased 1.0%. Compressor rig testing has shown both cavity size and shape to significantly impact compressor efficiency. As a result of the tests, small, smooth, low leak cavity designs with the potential for improving compressor efficiency by 0.5% are becoming possible.

These aerodynamic improvements, taken together, were estimated to reduce the amount of fuel burned by 5%.

Forced Exhaust Mixer

It has long been realized that engine thrust output could theoretically be increased without burning more fuel by forcefully mixing the fan discharge air with the turbine exhaust gases prior to discharge through a common nozzle. This approach could provide substantial fuel savings but has not been used in the past because the theoretical gains were offset by parasitic losses and weight associated with forced mixing.

Mixing now appears more attractive for conserving fuel as a result of recent tests of forced mixers that successfully combining high mixing efficiency, low parasitic loss, and short length. These tests include model and full scale tests of JT8D mixers and model tests of high bypass ratio (5 to 7) mixers. The results of these tests were used to arrive at the EEE mixer predictions.

Much remains to be accomplished before deciding on the exact mixer geometry and its ultimate performance potential. Model tests of various candidate geometries are required as an important step before finalizing a design approach and deciding on the mixer application to future powerplants. Integration of the long nacelle with the aircraft without incurring increased interference drag is also a big step in realizing the 3% fuel savings potential identified in this study program (fig. 15).

High Pressure Ratio

In order to take a full 15% advantage of fuel savings technology, a compressor system pressure ratio which is 50 percent higher than the JT9D-7A will be required (fig. 16). Higher pressure ratio was shown to provide significant fuel savings potential in the low energy consumption turbofan study. The question became how to produce the additional pressure with the same number of stages as the JT9D-7A to hold down cost. The straight forward solution was to use 25% higher compressor average diffusion factor combined with 28% higher compressor blade speeds than the JT9D-7A.

The higher airfoil loading capability derives from increased understanding of compressor design variables. Higher rotor speeds permit higher airfoil loadings. With a given compressor geometry, the peak pressure ratio increases with wheel speed. However, if the number of compressor blades are reduced, the achievable pressure ratio is also reduced. Thus higher speed can be traded for increased stage pressure ratio, or alternatively, for reduced airfoil count. The EEE high pressure compressor compared with the JT9D-7A in figure 17 represents a balance between increased stage pressure ratio, and lower airfoil count. The lower compressor blade count can give a 12% reduction in compressor module maintenance cost.

Advanced Hot-Section Materials

The high pressure ratio and high speed, high spool rotor system dictated the use of advanced, higher strength titanium and nickel base alloy compressor and turbine disks, single crystal HP turbine airfoils and a higher temperature combustor liner. High-strength blade and disk alloys are presently being developed to permit safe operation at higher speeds and temperatures of the EEE. A single crystal alloy for blades and a nickel superalloy (MERL 76) for the disk allow a 55% higher turbine wheel rim speed and an attendent 80% total blade and vane count reduction in relation to the 2-stage JT9D-7A turbine (fig. 18). High temperature titanium mid-stage disks and MERL 76 aft stage disks can also operate at the higher speeds and increased pressure levels in the compressor.

Current burner liners presently operate at about a 870°C (1600°F) maximum metal temperature. The energy efficient engine burner liner was calculated to require a metal temperature capability of 1040°C (1900°F) to permit 65% of the inlet air to be used for emissions and exit temperature profile control leaving a maximum of 35% for liner cooling. An advanced oxide dispersion strengthened material, which has the required operating temperature capability, is being considered as the primary design approach for the energy efficient engine.

Electronic Fuel Control

Current hydromechanical engine fuel controls are bulky - the JT9D-7A requires five control components to manage engine operation. Advances in digital electronic technology now make electronic fuel controls a practical alternative. An advanced, full authority digital electronic control, consisting of only two major components, the computer and a flow metering unit, will perform all of the necessary functions (fig. 19). This control will perform 60% more functions than the current hydromechanical controls. This additional capability can be used to have the unit continuously monitor the condition of the engine and give early warning of problems or situations which require maintenance action.

The payoff is a 33% reduction in control system weight and a 44% reduction in control maintenance cost. In-flight shut-downs due to control problems can be reduced by 80%. This control approach may also save fuel by eliminating the need for periodic ground run trimming of the engine and control.

Acoustically Treated Lightweight Nacelle

The nacelle of the future will require the latest light weight composite materials and lightweight structures to reduce weight by 15 percent relative to current configurations (fig. 20). Materials for the various applications within the nacelle will be selected from filament materials (boron, graphite, Kevlar and glass), matrix materials (epoxy, polyimide and aluminum) and composite honeycomb.

Stricter noise rules can be expected in future years. A noise goal of FAR 36 (1969) minus 10 EPNdB was established by NASA for this study. A fully treated nacelle, fan noise 3 EPNdB lower than present, and advanced acoustical treatment to attenuate fan noise by an additional 2 EPNdB are needed to meet this goal. The required noise reduction could be achieved by 1990 by directing research towards the definition of improved, low noise fan blading shapes, and

by developing segmented liners with improved tone and broadband noise attenuation capabilities. FAR 36 (amended 1977) rules can be fully met with currently available acoustic technology.

Vorbix Combustor

The low emissions design concept is based on a combustor developed in the NASA-sponsored Experimental Clean Combustor Program (ECCP) which demonstrated significant reductions in exhaust emissions. It represents a major departure from conventional combustors in commercial engines. Two in-line burning zones are used. The front, or primary zone, is designed to the specific requirements of reduced carbon monoxide and unburned hydrocarbon emissions at very low power settings near idle. The aft, secondary zone is designed to control NOx. Swirlers are used to thoroughly mix the fuel and air leading to the acronym vorbix for vortex burning and mixing. The short length of the secondary zone minimizes the residence time at high temperature to cut NOx generation in half.

The vorbix concept has been tested in the JT9D as experimental hardware. The EEE emissions predictions were derived from the results of these tests by using emissions indices which correct for the different burner thermodynamic conditions with the higher pressure ratio cycle. Development margin and production tolerances were included in the estimates. The estimated EPA parameters are compared with the current JT9D-7A production combustor and the 1981 regulations in figure 21. Low power emissions were estimated to meet the regulations. NOx generation, estimated to be 43% lower than the JT9D-7A, needs to be reduced by an additional 30% to meet 1981 regulations. A technique to provide the additional reduction has not yet been identified.

The EEE combustor design concept is simplified substantially from the ECCP configurations. The throat between the two zones was removed and replaced with less costly and more maintainable straight inner and outer wall sections. The number of fuel nozzles were reduced 20 percent and clustered in groups of three to limit fuel supply tube case penetrations to 24 circumferential locations. Substantial additional development work is needed to verify the emissions characteristics of this more practical burner before it can be considered for commercial service.

ENGINE BENEFITS

Improvements in component efficiencies, achieved by advancing technology and fully exploiting active clearance control, use of a high pressure ratio cycle and a mixed flow exhaust system can provide an engine cruise TSFC reduction of 15% relative to the JT9D-7A.

The lower TSFC can produce large fuel savings and reduced DOC. Improved performance retention can be achieved by advanced technology application of a rigid rotor support system in combination with a load sharing nacelle. With full application of key technologies identified in this study, over a 15% fuel savings, a 6 to 10% DOC reduction, and one-half of the present JT9D-7A performance deterioration rate are all possible.

A long nacelle, fully lined with low pressure loss acoustic treatment, has the potential of fully meeting future requirements. The staged vorbix combustor concept, a major departure from conventional configurations, shows promise for reducing exhaust emissions by 43 to 96%.

FUTURE PLANS

Pratt & Whitney Aircraft is presently embarking on an analytical and experimental program, the NASA sponsored Energy Efficient Engine Component Development and Integration Program, to complete the flight propulsion system preliminary design and to empirically verify the pertinent turbomachinery and mixer related technology benefits. Nacelle related benefits are also being pursued by NASA in other on-going technology programs such as the Energy Efficient Transport Project. The overall objective of this intensive effort is to provide needed technology by the mid 1980's to produce significant fuel savings in future commercial turbofan engines of the 1990's.

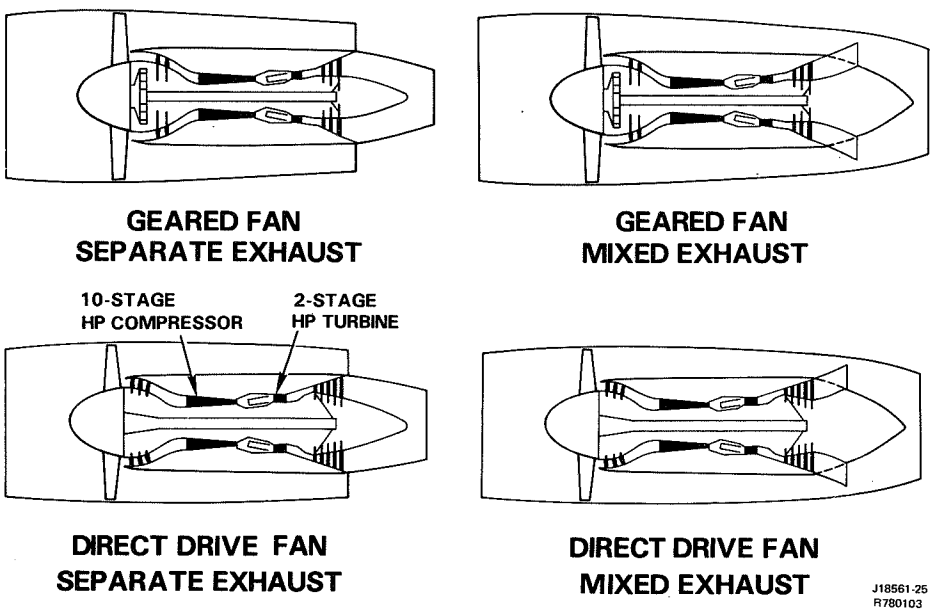

Figure 1.- Four study turbofan design configurations — different low spools and exhaust types were combined with a common high spool.

CRUISE TSFC	−12% MIN. (JT9D-7A REF)
DOC	−5% MIN. (JT9D-7A REF)
EXHAUST EMISSIONS	1981 EPA STANDARDS
NOISE	FAR 36 (1969) MINUS 10 EPNdB
PERFORMANCE DETERIORATION	IMPROVED (JT9D-7A REF)
THRUST GROWTH	W/O COMPROMISING OTHER GOALS

Figure 2.- Study goals — goals balance fuel savings technology with practicality.

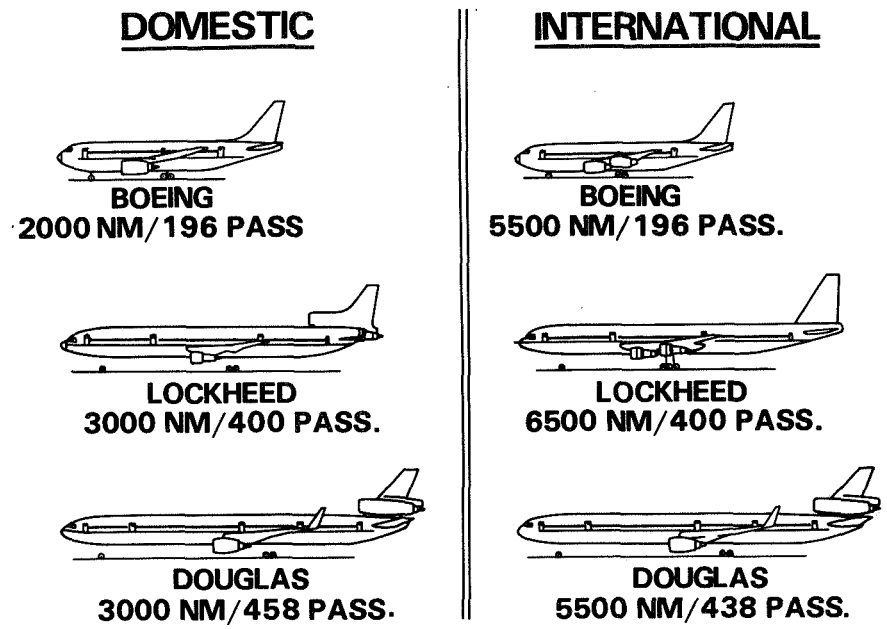

Figure 3.- Advanced study aircraft — wide spectrum selected for engine configuration evaluation.

2-STAGE HIGH PRESSURE TURBINE

AVERAGE MIXING ADVANTAGE = 2.5% FUEL BURNED
AVERAGE GEARING ADVANTAGE = 2.7% FUEL BURNED

FAN DRIVE	DIRECT		GEARED	
EXHAUST	SEPARATE	MIXED	SEPARATE	MIXED
BYPASS RATIO	7	7	9	9
REL TSFC (JT9D-7A REF)	-15%	-18%	-19%	-21%

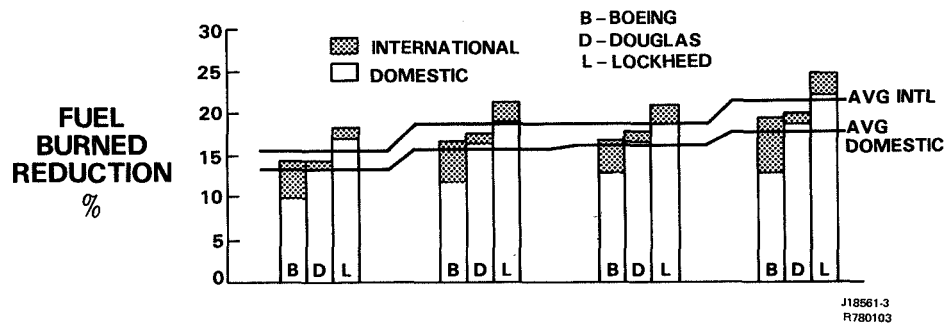

Figure 4.- Conceptual study fuel savings — exhaust mixing and low rotor gearing each improve fuel consumption by 2-½%.

2-STAGE HIGH PRESSURE TURBINE

AVERAGE MIXING ADVANTAGE = 1.1% DOC
AVERAGE GEARING ADVANTAGE = 0.7% DOC

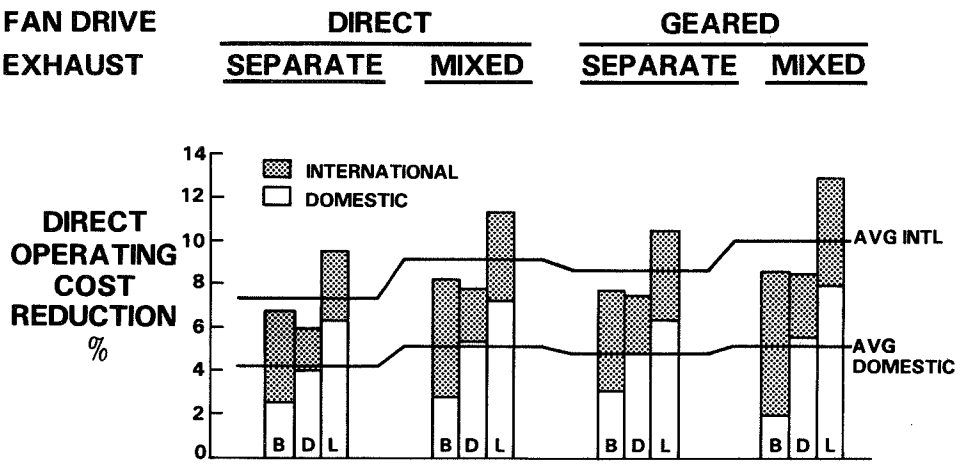

Figure 5.- Conceptual study DOC reductions — exhaust mixing and low rotor gearing each reduce DOC by 1%.

2-STAGE HIGH PRESSURE TURBINES

	STUDY GOAL	DIRECT DRIVE SEPARATE	DIRECT DRIVE MIXED	GEARED SEPARATE	GEARED MIXED
INSTALLED CRUISE TSFC	-12% MIN.(REL TO JT9D-7A)	-15%	-18%	-19%	-21%
DIRECT OPERATING COST (DOC)	-5% MIN. (REL TO JT9D-7A)				
DOMESTIC AIRCRAFT (AVG)		-4.3%	-5.2%	-4.9%	-5.3%
INTERNATIONAL AIRCRAFT (AVG)		-7.4%	-9.2%	-8.7%	-10.1%
EMISSIONS	1981 EPA	MEETS 1981 THC AND CO, EXCEEDS NO_X			
TOTAL NOISE					
(W/CURR TECH)	FAR 36 (1969) MINUS 10 EPNdB	MEETS FAR 36 (1977)			
(W/ADV TECH)		MEETS FAR 36 (1969) MINUS 10 EPNdB			
TSFC DETERIORATION at 4000 HRS	BETTER THAN JT9D-7A (2.8%)	1.5%	1.5%	1.2%	1.2%
THRUST GROWTH	NO COMPROMISING OTHER GOALS	PRESSURE RATIO AND TURBINE INLET TEMPERATURE SELECTED WITH THRUST GROWTH ALLOWANCE			

J18561-5
780902

Figure 6.- Conceptual study results against goals — relative capabilities led to selection of mixed exhaust type.

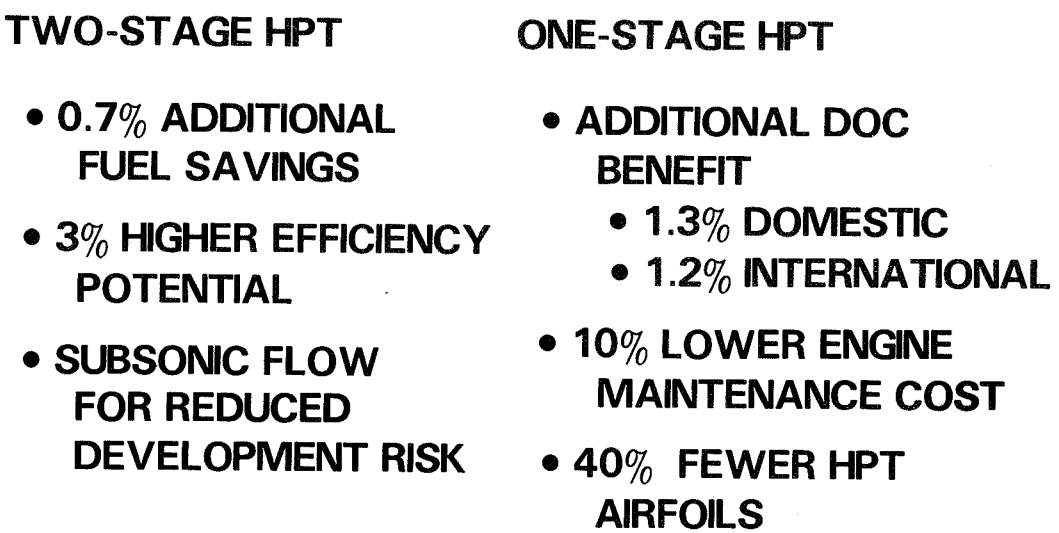

Figure 7.- Relative advantages of one- and two-stage high pressure turbines - economic advantages led to the choice of the one-stage approach.

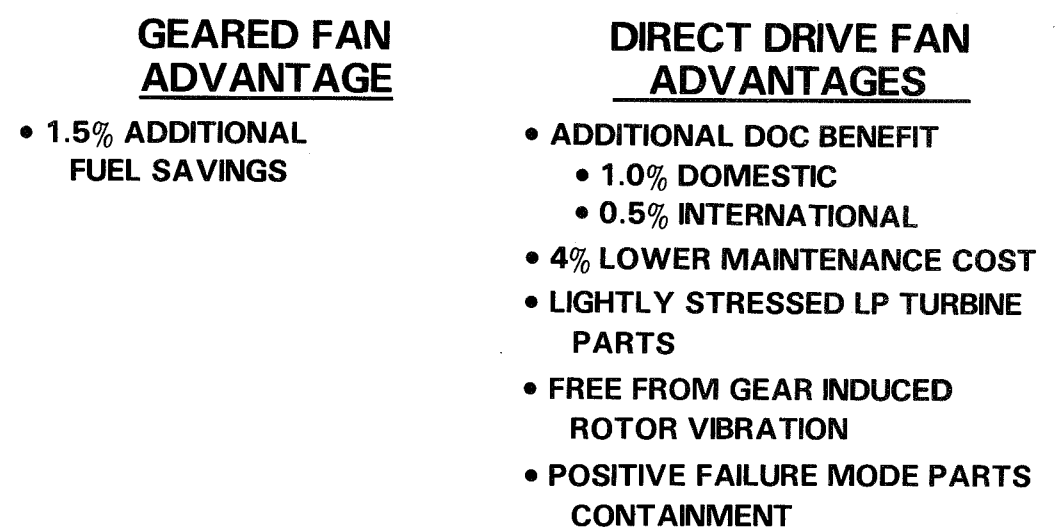

Figure 8.- Relative advantages of direct drive and geared fans — economic and operational advantages led to the choice of the direct drive fan approach.

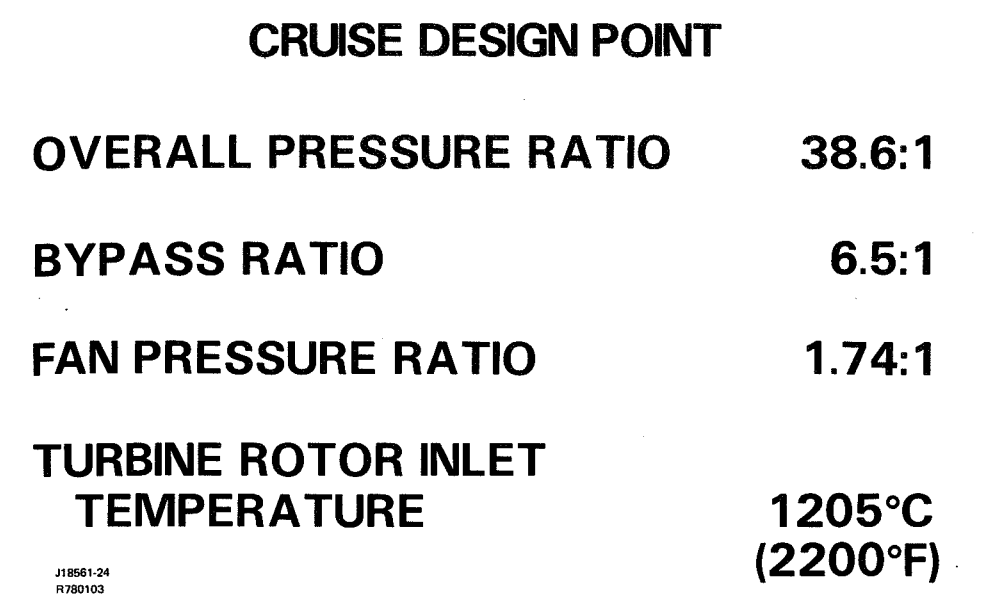

Figure 9.- Energy efficient engine cycle parameters — advanced cycle parameters provide fuel savings and reduced DOC.

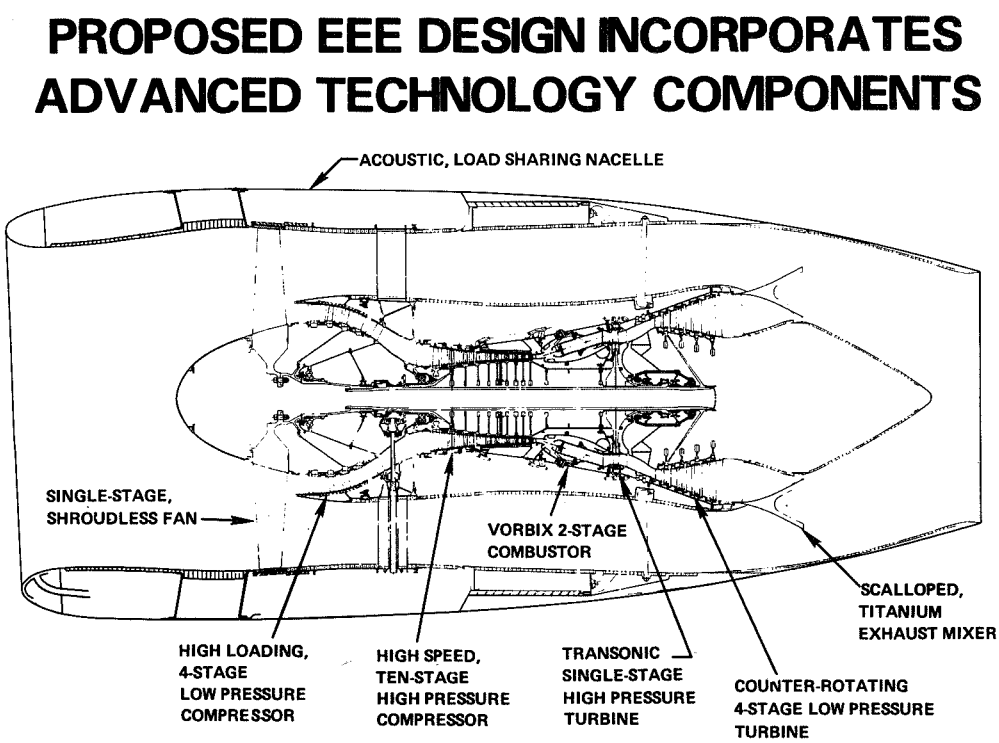

Figure 10.- Energy efficient engine preliminary design —high efficiency and low cost components provide fuel savings and reduced DOC.

- ACTIVE CLEARANCE CONTROL & NACELLE LOAD SHARING
- ADVANCED MATERIALS
- ADVANCED INTERNAL AERODYNAMICS
- ELECTRONIC FUEL CONTROL
- FORCED EXHAUST MIXER
- ACOUSTICALLY LINED LIGHTWEIGHT NACELLE
- HIGH PRESSURE RATIO
- VORBIX COMBUSTOR

Figure 11.- Critical propulsion technologies — successful development of key technologies is needed to realize projected fuel savings.

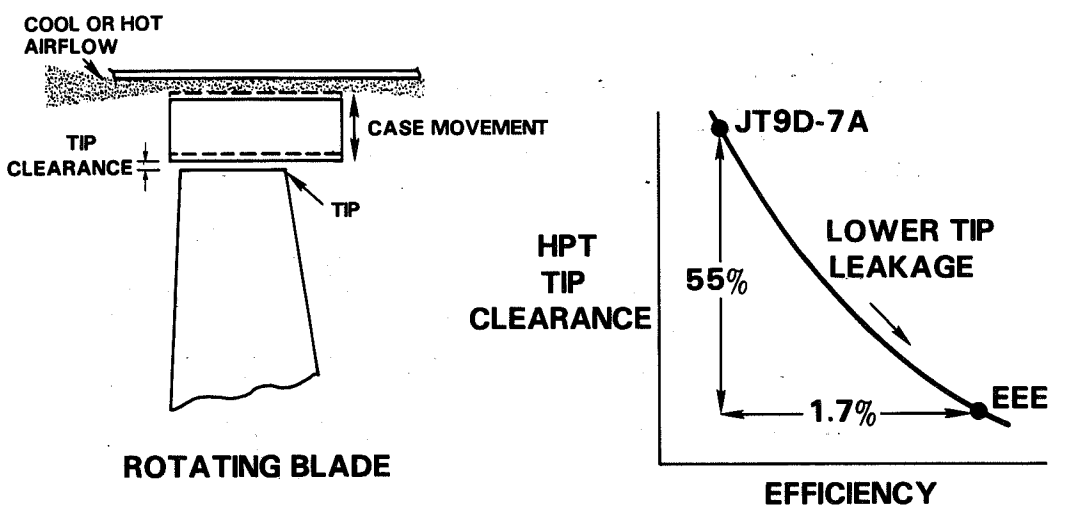

Figure 12.- Active clearance control — reduced blade tip clearances in compressor and turbine can provide a 3% fuel savings.

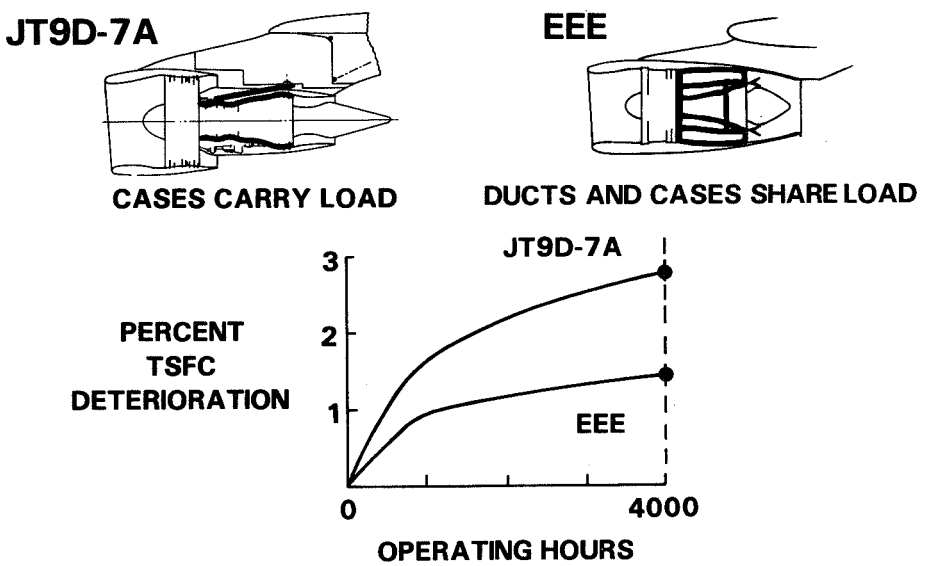

Figure 13.- Load sharing nacelle — nacelle load sharing design retains fuel savings over long-term operation.

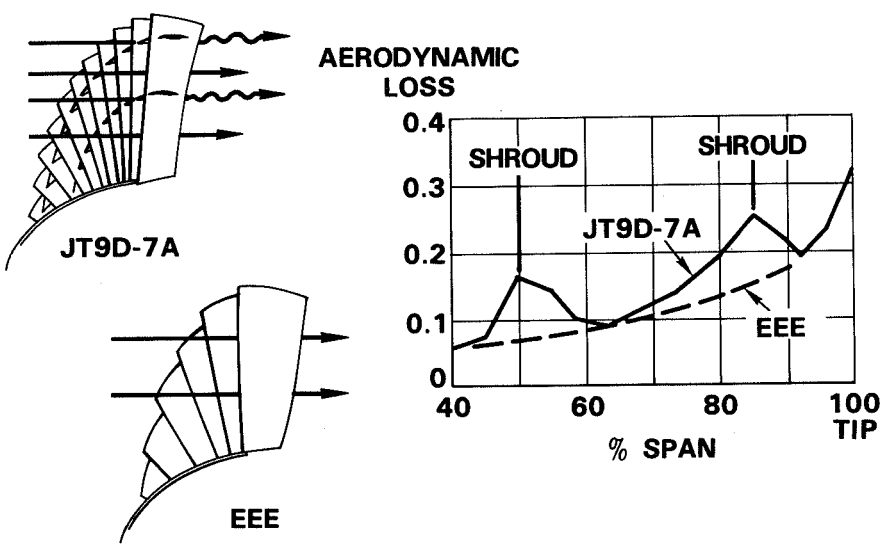

Figure 14.- Shroudless fan blades — shroudless fan blades have the potential for 2% efficiency improvement.

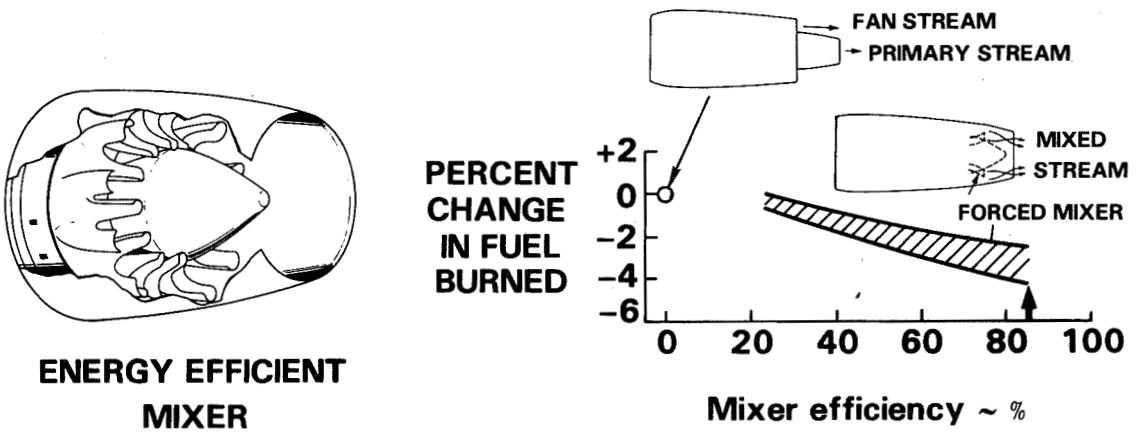

Figure 15.- Advanced exhaust mixer — shorter mixer, possible with advanced technology, reduces losses and weight for a 3% fuel savings potential.

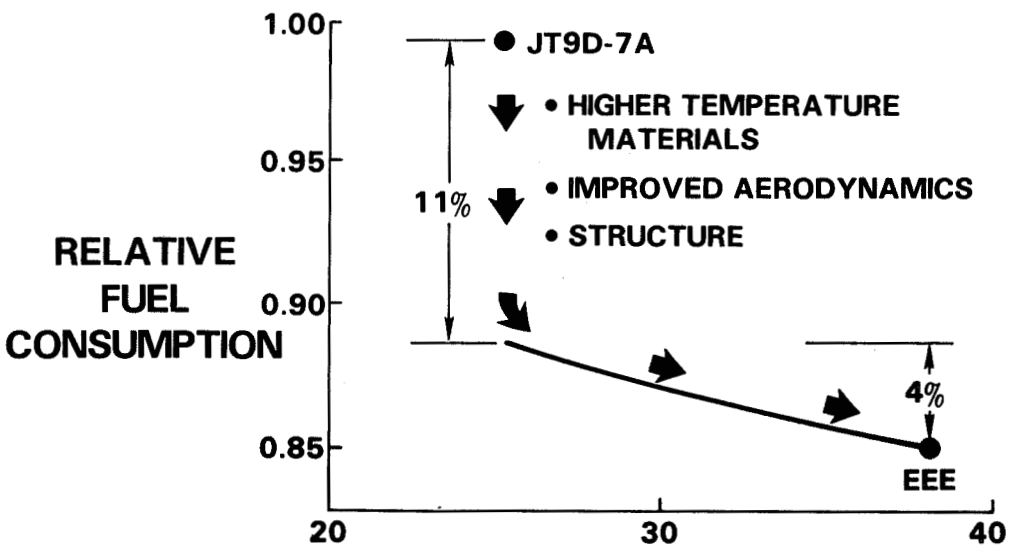

Figure 16.- High overall pressure ratio — high pressure ratio made possible by advanced technology provides an additional 4% fuel savings potential.

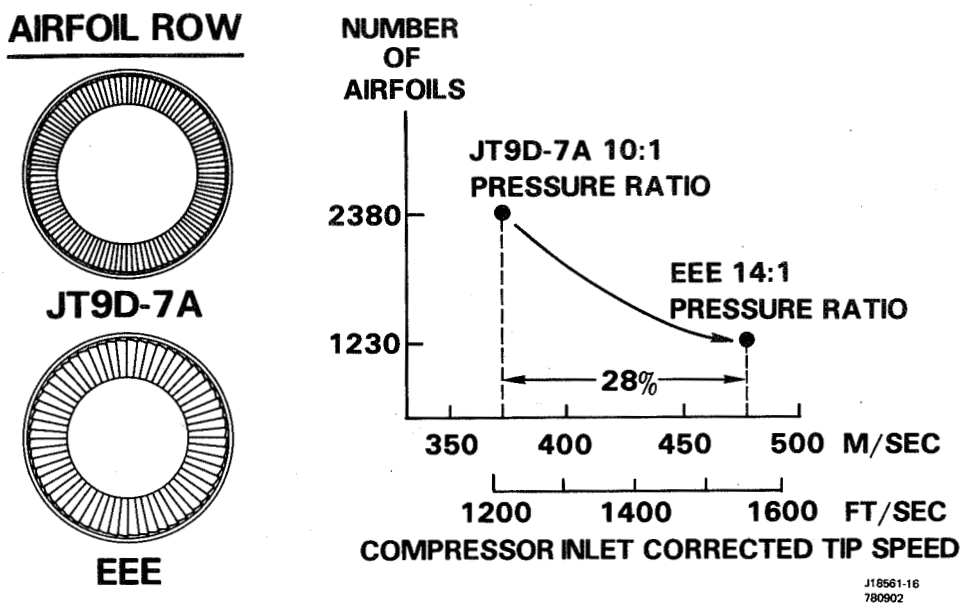

Figure 17.- High speed compressor — 48% fewer airfoils result in a 12% lower compressor maintenance cost.

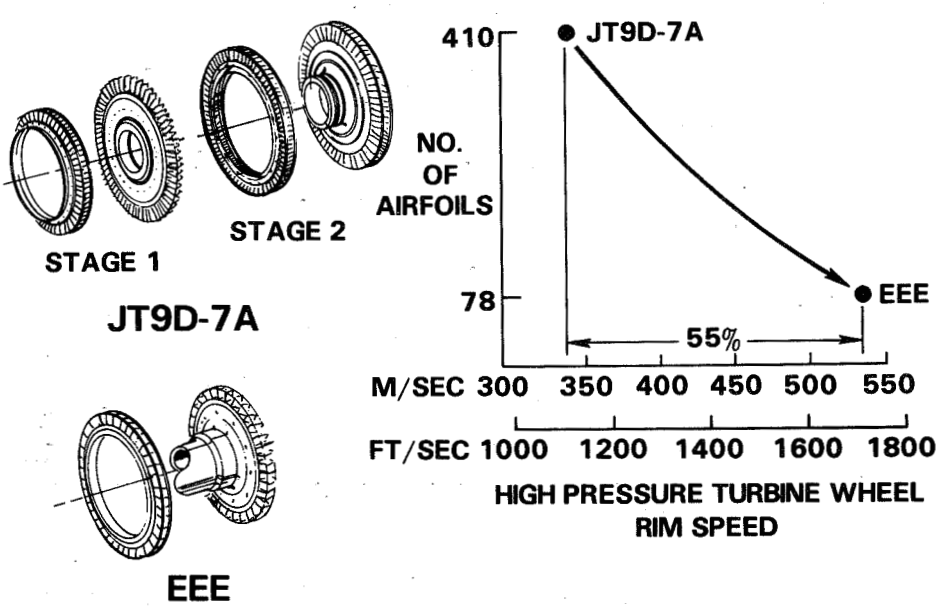

Figure 18.- High work turbine — high speed, single-stage high pressure turbine, with 80% fewer blades and vanes, has potential for a 30% lower module maintenance cost.

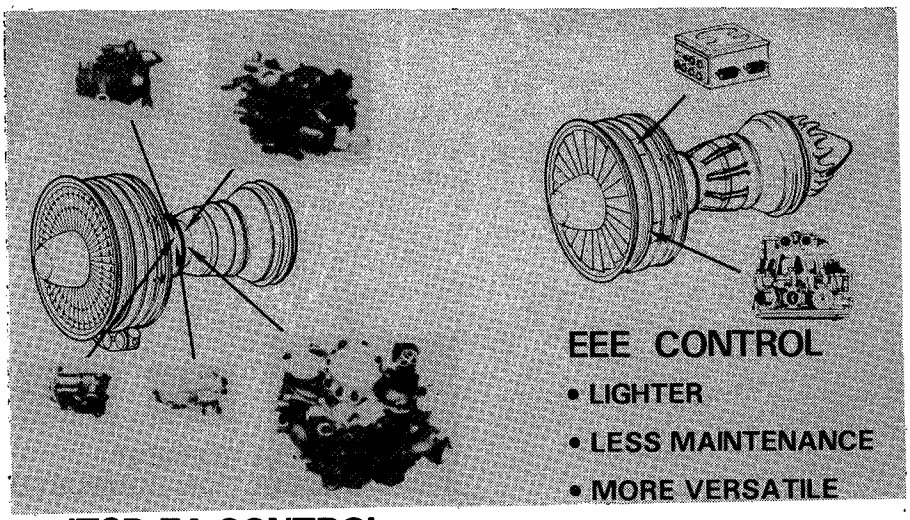

Figure 19.- Electronic fuel control — 2 major electronic control units are equivalent to 5 hydro-mechanical components.

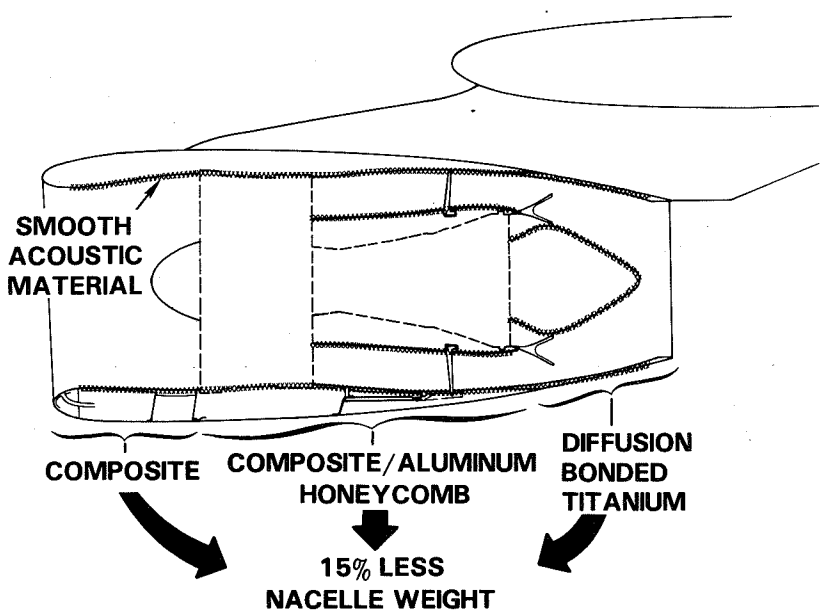

Figure 20.- Acoustically treated lightweight nacelle — 15% less weight and FAR36-10 EPNdB noise are possible through use of composites and improved acoustical technology.

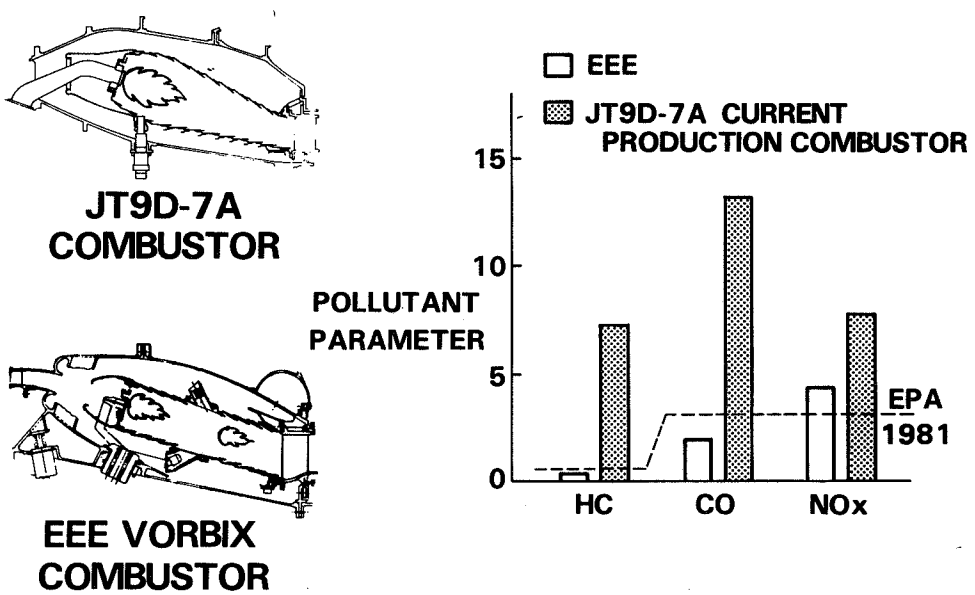

Figure 21.- Vorbix combustor — emissions reductions from 43 to 96% are projected with the two-stage vorbix combustor concept.

ENERGY EFFICIENT ENGINE PRELIMINARY DESIGN AND INTEGRATION STUDIES

R. P. Johnston and M. C. Hemsworth
General Electric

SUMMARY

A NASA sponsored study to determine the characteristics and system benefits of an Energy Efficient Engine (E^3) suitable for use on advanced subsonic transport aircraft has been completed. Relative to a current CF6-50C engine, the following benefits were estimated.

- 14.4% reduction in installed cruise Specific Fuel Consumption
- A reduction in Direct Operating Cost of more than 5%

The advanced technology E^3 system would also permit:

- Compliance with FAR 36 (1977) noise limits
- Compliance with 1981 EPA Emission Standards

The above was accomplished with an engine design that meets all anticipated commercial standards.

INTRODUCTION

With the advent of fuel shortages in the fall of 1973 and a general public realization that fossil fuel sources for our economy are not only limited but subject to disruption came pressure to find ways to conserve and extend our fuel supplies. One response to the problem has been an effort to plan and develop new transport aircraft that would provide the level of fuel economics over current aircraft that wide bodied high bypass turbofan aircraft provided over the earlier narrow body pure jet aircraft.

To provide impetus and technology base, NASA began to sponsor studies of advanced engines that would conserve fuel yet be economically attractive to airline users. Several of these studies performed by General

Electric are summarized in References 1 and 2. Out of these studies came general configuration and cycle choices for an advanced technology direct drive turbofan engine that showed promise of an approximate 10% reduction in SFC (Specific Fuel Consumption) compared to a current CF6-50C engine.

In conjunction with the above studies, NASA also funded studies to determine the potential value of various advanced material technologies such as ceramics, directionally solidified turbine blade alloys and high temperature, high strength turbine disk alloys. To provide a basis of comparison the studies (Reference 3 and 4) employed benefit analyses based on an advanced airframe-engine system with SFC, DOC (Direct Operating Cost), ROI (Return on Investment) and other merit factors derived. From these materials studies came the recognition of the importance of the newer turbine blade materials, lightweight composites and ceramics in fuel efficient engines.

The Energy Efficient Engine (E^3) studies sponsored by NASA under contract NAS3-20627 and beginning in December of 1976 were the culmination of these advanced engine studies to define and study advanced technology engines suitable for advanced subsonic transport aircraft that could be certified in the late 1980's and early 1990's.

E^3 STUDY GOALS

NASA defined some important goals for this study. They were as follows:

- A 12% reduction in installed SFC relative to a current high bypass engine installed on an advanced subsonic transport plane at maximum cruise power.
- A 5% reduction in DOC.
- Ability to meet FAR 36 (1969) - 10 EPNdB (Effective Perceived Noise Decibels) level.
- Ability to meet 1981 EPA emissions standards.
- Engine growth should not compromise the above goals.

ABBREVIATIONS

App	Approach
DOC	Direct Operating Cost
E^3	Energy Efficient Engine
ECCP	Experimental Clean Combustor Program
EGV	Exit Guide Vane
F_n	Thrust
FOD	Foreign Object Damage
FPS	Flight Propulsion System
GE	General Electric
LCC	Lockheed Company of California
M	Mach Number
MCD	McDonnell/Douglas Company
NA	Not available
PAX	Number of Passengers
P/P	Pressure Ratio
ROI	Return on Investment
SFC	Specific Fuel Consumption
SL	Side Line
SLS	Sea Level Static
SLTO	Sea Level Take-Off
TBC	The Boeing Company
T/O	Take-Off
TOGW	Take-Off Gross Weight
W_f	Fuel Burned

STUDY METHODS

It was necessary to select a reference engine for comparison purposes for the study. General Electric selected the CF6-50C as the comparison engine since it was the most advanced General Electric high bypass ratio turbofan in current wide spread commercial service. In addition, its performance, cost, and excellent thrust to weight ratio provided a challenging goal.

The study was conducted by performing a mission system benefit analysis of candidate engines installed on projected advanced aircraft systems thought to be typical of the late 1980's and early 1990's. Sub-contracts were let to The Boeing Company, the Lockheed Company of California and the McDonnell/Douglas Company to provide aircraft/engine mission evaluations. There were also internal aircraft-engine evaluations of the candidate engines. Both a domestic and intercontinental mission were evaluated.

The studies were performed with rubberized engines and aircraft with each company defining its own advanced aircraft-engine systems. For all the studies, the mission and payloads were fixed while airframe characteristics and engine sizes were altered to reflect differences in engine performance. Properly scaled CF6-50C engines were used on comparable advanced technology aircraft to provide a comparison with the advanced aircraft engine system.

From these studies, direct comparisons of DOC, TOGW (Take-Off Gross Weight), W_f (fuel burned) and other important merit factors were carried out. Noise estimates were also made and other aspects of aircraft engine integration were investigated, especially by the sub-contractors.

STUDY RESULTS

The early portions of the study were concerned with evaluating direct and geared engines with both separate and mixed flow exhaust configurations to determine what advanced engines and installations could best meet the NASA goals. Earlier studies had used a cruise condition of .8 M at 10,668 m (35,000 feet) as the reference performance point and this was continued for the internal General Electric studies. From this reference performance point, selection of fan pressure ratio had been in a range of

1.65 to 1.75 and an overall engine pressure ratio of 38 to 1 was retained from the STEDLEC and USTEDLEC studies (Reference 1 and 2).

Four advanced engines were defined for this portion of the study and their descriptions are given in Table 1 along with that of the reference CF6-50C engine. The engine sizing point was the maximum climb thrust condition at 10,668 m (35,000 feet) altitude and .8 M since this was the probable limiting power condition for the advanced aircraft/engine systems studied.

In making the comparison, each engine was configured to its best advantage while maintaining overall performance parameters constant such as fan and overall engine pressure ratio and turbine inlet rating temperatures. For instance, work extraction from the core stream was different for the separate and mixed flow engines to produce the best overall cycle performance. Evaluation of each engine on a General Electric advanced study aircraft produced the performance evaluation shown in Table 2. Higher bypass ratio and lower fan pressure ratios were employed on the geared engines to take better advantage of the benefits of gearing.

The separate flow configuration was 2 to 3% worse in SFC relative to the mixed flow exhaust engine on a consistent basis. Most of that difference was due to the mixer performance outweighing the advantage gained by a more highly extracted separate flow engine cycle. As a result, effort in the E^3 study was directed to further evaluation and definition of a geared and direct drive mixed flow engine. A summary of the engine comparisons including estimates of DOC, emissions, and growth potential and fuel usage is given in Table 3 for the mixed and separate flow engines.

For the second part of the E^3 study, General Electric and the airframe sub-contractors both evaluated a refined direct and geared engine (shown in Figure 1) installed on an advanced subsonic transport aircraft. From this part of the E^3 study was to come the recommendation of one engine cycle and configuration for a more intensive preliminary design definition.

For the mission evaluation, General Electric and each sub-contractor defined both a domestic and intercontinental advanced aircraft. A partial description of these aircraft and engines is provided in Table 4.

The two advanced technology engines were studied and compared with the current technology CF6-50C. As before, all engines were scaled to produce the same installed maximum climb thrust as the base line advanced technology direct drive engine.

Studies were performed to determine expected engine performance weight, costs and maintenance. From these, scaling information on thrust was provided to the sub-contractors to enable them to adjust the characteristics of the reference CF6-50C and advanced engines to the needs of their advanced aircraft. Performance characteristics of the advanced engines were calculated on a consistent installed cruise thrust basis for both the direct and geared engine with results given in Table 5. At the maximum cruise point, the direct and geared engine showed a 12.1% and 14.6% reduction in installed SFC, respectively, over the base CF6-50C engine. Figure 2 presents the economic benefits estimated for the direct drive advanced engine on a domestic and intercontinental aircraft by the sub-contractors and General Electric. For these evaluations, differences in engine cost and maintenance were not included due to the preliminary state of such estimates. It can be seen that both the Δ(Delta) DOC and ΔW_f estimates indicate that the advanced direct drive study engine would be a significant improvement over the reference CF6-50C.

Emission estimates were made for the direct and geared drive engine and their growth versions. When compared to the 1981 EPA Standards, only the NO_x emissions exceed the limit for all engines, except the design geared engine.

The benefits of the geared versus direct drive engine were determined using internal General Electric merit factor derivatives. For the domestic mission, uninstalled SFC of the geared engine was 2.5% better than the direct drive engine (relative to the CF6-50C), but the weight, cost and drag effects predominate such that the DOC was 1.3% higher and the fuel saving was only .9%.

A short summary of the results of this portion of the E^3 study is given in Table 6. Since the geared engine was estimated to only reduce fuel consumption by .9% while incurring a DOC penalty of 1.3%, the direct drive engine was recommended to NASA as the engine for further efforts in the preliminary design portion of the E^3 study.

NASA indicated that more SFC margin would be required for a direct drive engine to assure that the original 12% SFC reduction goal would be met. Therefore, further engine cycle and configuration optimization effort began to determine what changes could be made to improve the fuel consumption of the direct drive engine. Three additional engines were studied in some detail with small changes in fan pressure ratio and LP spool configuration only. Prior studies had indicated that the engine overall pressure ratio and turbine inlet temperatures were already well matched so these parameters were not varied (except for growth).

The three additional engines studied had the following characteristics. The first was a modification of the direct drive engine studied already but with the fan tip speed reduced and a short LP turbine transition duct to improve LP turbine efficiency. The other two engines were altered in configuration to permit a lower fan pressure ratio (and tip speed) but core supercharge was held constant with the use of a quarter stage booster. As with the improved engine, a short transition duct was employed to permit a higher LP turbine tip speed with a corresponding increase in efficiency.

Table 7 presents a comparison of the final advanced geared and direct drive study engines. On a comparable installed net thrust basis, the geared engine weighed over 480 kilograms more, burned 1.9% more fuel even with a small SFC advantage and was 2.1% higher in DOC than the advanced direct drive engine. For these reasons, the final direct drive configuration was retained for the remainder of the E^3 study.

As designed, the advanced technology study engine incorporated many advanced technology features in terms of configuration, component performance, material systems, performance retention, design features and environmental protection. Figures 3 through 8 show and illustrate many of these features and some of the reasons behind the choice of the very advanced 10 stage high compressor.

An estimate of the emissions performance of the advanced double annular combustor (see Figure 6) is presented in Table 8. It is believed that this combustor design can be developed to permit compliance with the 1981 EPA emission standards.

A comparison of several operating parameters for the final direct drive study engine and the reference CF6-50C is shown in Figure 9 for equivalent installed maximum climb thrust. At the maximum cruise measuring point, it is estimated that the advanced study engine would permit a 14.4% reduction in SFC compared to the reference CF6-50C. Table 9 shows an estimate of the source of SFC reduction. The largest improvements come from component improvements, cycle effects and the mixed exhaust system.

An updated benefit analysis was performed as previously described using a rubberized engine and aircraft with only the mission and payload fixed. Aircraft technology assumptions for the General Electric study aircraft are given in Table 10 while the merit factor derivatives that go with these advanced study aircraft are given in Table 11.

The revised airframe sub-contractor study results using the final study engine characteristics are shown in Table 12. Since price or

maintenance effects were not included in these results, an estimate of these effects (as derived from the General Electric study aircraft) is included in Table 13. Even though some of the advanced technology and performance retention features resulted in an estimate of a higher relative initial engine cost (than a CF6-50C) many of these higher initial cost features permit a lower mature engine maintenance cost estimate. This estimated savings offset the first price penalty and resulted in a further 2% DOC reduction over those DOC estimates done without price and maintenance effects. Table 14 shows the large estimated potential fuel burned savings at the maximum cruise condition for the advanced engine on General Electric study aircraft. For the domestic mission, a 21% reduction is shown and for the intercontinental mission a nearly 28% reduction is possible. Integrated mission fuel savings tend to be somewhat lower, however.

Noise estimates were also developed for the final E^3 study engine installed on advanced General Electric study aircraft. Acoustic design features, shown schematically in Figure 10, were used for the estimates.

Estimated noise levels relative to FAR 36 (1969) and FAR 36 (1977) are shown in Table 15 for both the domestic and intercontinental GE study aircraft.

CONCLUSION

Under NASA Study Contract NAS3-20627 (Energy Efficient Engine) General Electric identified an advanced direct drive turbofan engine capable of meeting (or exceeding) all fuel, economic and emission goals and the FAR 36 (1977) noise standards. The final advanced study engine is estimated to provide an installed SFC reduction (relative to the CF6-50C) of 14.4%. The final advanced study engine would provide significant savings in fuel and DOC over a comparable CF6-50C powered aircraft.

REFERENCES

1. Neitzel, R.E., Hirschkron, R. and Johnston, R.P.: Study of Turbofan Engines Designed for Low Energy Consumption. Prepared for NASA under Contract NAS3-19201, NASA CR-135053 August, 1976.

2. Hirschkron, R., Johnston, R.P., and Neitzel, R.E.: Study of Unconventional Aircraft Engines Designed for Low Energy Consumption. Prepared for NASA under Contract NAS3-19519, NASA CR-135136, December, 1976.

3. Ross, E.W., Johnston, R.P., and Neitzel, R.E.: Cost Benefit Study of Advanced Materials Technology for Aircraft Turbine Engines. Prepared for NASA under Contract NAS3-17805, NASA CR-134702, November, 1974.

4. Hillery, R.V., and Johnston, R.P.: Cost Benefit Study of Advanced Materials Technology for Aircraft Turbine Engines. Prepared for NASA under Contract NAS3-20074, NASA CR-135235, September, 1977.

TABLE 1.- EARLY E^3 STUDY ENGINES

	Reference Engine CF6-50C	Study Engine 1	Study Engine 2	Study Engine 3	Study Engine 4
Fan drive	Direct	Direct →		Geared →	
Exhaust configuration	Separate	Separate	Mixed	Separate	Mixed
SLS take off F_n, kN	224	157	155	176	177
— (lb)	(50250)	(35300)	(34800)	(39600)	(39800)
Engine bypass ratio, mx.cr.	4.3	7.1	6.3	9.6	8.6
No. of stages Fan/LPC/HPC/HPT/LPT	1/3/14/2/4	1/0/10/2/5	1/0/10/2/4	1/1/10/2/3	1/1/10/2/3

TABLE 2.- EARLY E^3 STUDY RESULTS

	Reference Engine CF6-50C (scaled)	Study Engine 1	Study Engine 2	Study Engine 3	Study Engine 4
Fan drive	Direct	Direct →		Geared →	
Exhaust configuration	Separate	Separate	Mixed	Separate	Mixed
Δ SFC-bare engine, mx. cr.—%	Base	-9.4	-10.6	-13.4	-15.7
Δ SFC installed, mx.cr.—%	Base	-10.0	-12.0	-13.2	-16.0

TABLE 3.- SUMMARY OF COMPARISONS BETWEEN EXHAUST SYSTEMS

	Separate vs Mixed
Fuel Usage	3-6% Disadvantage
DOC	2½ to 3½% Disadvantage
Emissions	No Difference
Growth Potential	No Difference

TABLE 4.- DOMESTIC AND INTERCONTINENTAL MISSION AIRCRAFT DEFINITION

Study Mission	General Electric		Boeing		McDonnell/ Douglas		Lockheed	
	Domestic	Inter.	Domestic	Inter.	Domestic	Inter.	Domestic	Inter.
Des. range — km (n. miles)	5556 (3000)	10190 (5500)	3704 (2000)	10190 (5500)	5556 (3000)	10190 (5500)	5556 (3000)	12040 (6500)
Des. payload — PAX	225	225	196	196	458	438	400	400
Cruise Mach no.	.8	→	→	→	→	→	→	→
Initial cruise — m —(feet)	10668 (35000)	10668 (35000)	10668 (35000)	10058 (33000)	10058 (33000)	9449 (31000)	10668 (35000)	10668 (35000)
No. engines	3	3	2	4	3	3	3	4
Thrust/engine—SLTO, kN —(lb)	113 (25300)	165 (37100)	152 (34200)	100 (22500)	189 (42400)	225 (50500)	158 (35500)	147 (33100)

TABLE 5.- ADVANCED ENGINE COMPARISON

	Reference SF6-50C (scaled)	Advanced Direct Drive	Advanced Gear Drive
Exhaust configuration	Separate	Mixed	Mixed
Overall nacelle length - m —(inches)	6.55 (258)	5.66 (223)	5.92 (233)
Δ Installed weight—kg —(lb)	Base	-476 (-1050)	+191 (+420)
Max. climb fan pressure ratio	1.76	1.71	1.55
Δ SFC installed, mx. cr.—%	Base	-12.1	-14.6

TABLE 6.- E^3 STUDY (ENGINE-AIRFRAME) INTEGRATION — RESULTS SUMMARY OF COMPARISON BETWEEN ADVANCED GEARED AND DIRECT DRIVE ENGINE AND CF6-50C INSTALLED ON DOMESTIC TRANSPORT

	CF6-50C	Direct	Geared
Δ SFC — %	Base	-12.1	-14.6
Δ W_f — %	Base	-17.8	-18.7
Δ DOC — %*	Base	- 8.2	- 6.9
Emissions	—	Meets 1981 std. except NO_x	Meets 1981 stds.
Noise	—	Meets FAR 36 (1977)	Meets FAR 36 (1977)
Growth potential	—	Meets reqmts.	Meets reqmts.

* No price or maintenance effects

TABLE 7.- IMPROVED ADVANCED ENGINE STUDY RESULTS

(EQUIVALENT INSTALLED MAXIMUM CLIMB THRUST)

	Final Geared Drive	Final Direct Drive
Bypass ratio — mx. cr.	8.6	6.98
Fan pressure ratio mx. cl.	1.55	1.65
Installed weight — kg —(lb)	+482 (+1065)	Base
Δ SFC installed — % (Rel. base line)	-.7	Base
Δ DOC — % (domestic mission)	+2.1	Base
Δ W_f (fuel burned) — %	+1.9	Base

TABLE 8.- FPS EMISSIONS ESTIMATE INTEGRATED MISSION EVALUATION

	FPS Base line	1981 EPA Standards
CO	2.0	3.0
HC	.1	.4
NO_x	3.0	3.0
Smoke no.	15	20

TABLE 9.- CONTRIBUTIONS TO IMPROVED INSTALLED SFC

(Relative to CF6-50C)

Contributor	ΔSFC — %
Engine component improvements	—4.0
Pressure drop improvements	— .6
Reduced cooling flows	— .4
Cycle effects — T_{41}, P/P, bypass ratio	—6.0
Mixed exhaust	—2.7
Reduced installation drag	- .7
Total Improvement	—14.4

TABLE 10.- GENERAL ELECTRIC ADVANCED AIRCRAFT ASSUMPTIONS

Wing characteristics	— 30^{o} sweep ¼C, ar = 10, supercritical design
Aircraft structure	— Partial composite, advanced materials 5% lighter wing, fuselage, gear and pylons than 1976 10% lighter tail than 1976 15% lighter surface controls than 1976
Active controls	— .95 factor applied to tail area and wing weight
Aerodynamics	— 1% reduction in interference drag vs 1976 levels
Engine configuration	— Trijet

TABLE 11.- BENEFIT ANALYSIS DERIVATIVES

	Domestic Trijet	International Trijet
Design range — km —(n. mile)	5556 (3000)	10190 (5500)
Avg. mission range — km —(n. mile)	1296 (700)	3704 (2000)
Passenger capacity	225	225
Load Factor — %	55	55
Fuel costs $/m^3 (¢/gal)	92.50 (35)	118.90 (45)

	Δ's — %				Δ's — %			
	DOC	ROI	TOGW	W_f	DOC	ROI	TOGW	W_f
1% SFC	.53	-.17	.57	1.31	.93	-.36	1.12	1.69
45.4 kg engine/nacelle wt. (100 lb)	.19	-.08	.31	.26	.19	-.09	.28	.26
$1/flt. hr. - maint. cost	.16	-.03	—	—	.14	-.03	—	—
$10000 engine/nacelle price	.05	-.04	—	—	.03	-.03	—	—

TABLE 12.- SUB-CONTRACTOR EVALUATION OF ADVANCED TECHNOLOGY ENGINE ON ADVANCED AIRCRAFT (RELATIVE TO REFERENCE CF6-50C)

	Boeing		McDonnell/Douglas		Lockheed	
Mission	Domestic	Intercont.	Domestic	Intercont.	Domestic	Intercont.
Range, km (n. miles)	3704 (2000)	10190 (5500)	5556 (3000)	10190 (5500)	5556 (3000)	12040 (6500)
PAX	196	196	458	438	400	400
ΔW_f—% (fuel burned)	-14.8	-20.3	-17.1	-16.6	-17.5	-22.2
Δ DOC—%*	N/A	N/A	- 8.1	- 9.3	- 5.5	-10.2

*No price or maintenance cost effects

TABLE 13.- E^3 FPS PRICE AND MAINTENANCE

vs

SCALED CF6-50C DOC EFFECTS

	Mission Sized			
	Domestic		International	
	Design Value	Δ DOC—%	Design Value	Δ DOC—%
Installed cost — K$	+107.3	+.5	+124.5	+.4
Maint. cost — $/flt. hr. (Parts + labor + o.h.)	-14.51	-2.3	-17.90	-2.5
		-1.8		-2.1

Fuel cost 35¢/gal. domestic
45¢/gal. international

TABLE 14.- FPS ENGINE ΔW_f BREAKDOWN

vs

CF6-50C REFERENCE (SCALED)

	Mission Sized (Mx. Cr. Condition Only)			
	Domestic		International	
	Design Value Δ	Δ W_f—%	Design Value Δ	Δ W_f—%
Installed wt. — kg (lb)	-412 (-909)	-2.4	-643 (-1398)	-3.6
Installed SFC — % (Mx. cr. — std day)	-14.4	-18.9	-14.4	-24.3
Total %		-21.3		-27.9

TABLE 15.- ESTIMATED ENGINE NOISE NOMINAL SUPPRESSED NOISE LEVELS — NO MARGIN

	Domestic Mission FPS Engine			International Mission FPS Engine		
	T/O	App	SL	T/O	App	SL
Engine noise, EPN^{d}B	93.1	96.0	90.9	96.5	98.2	91.3
Relative to:						
FAR 36 (1969)	-9.4	-9.8	-14.9	-9.2	-8.8	-15.7
FAR 36 (1977)	-4.5	-5.8	-8.0	-3.6	-4.9	-9.2

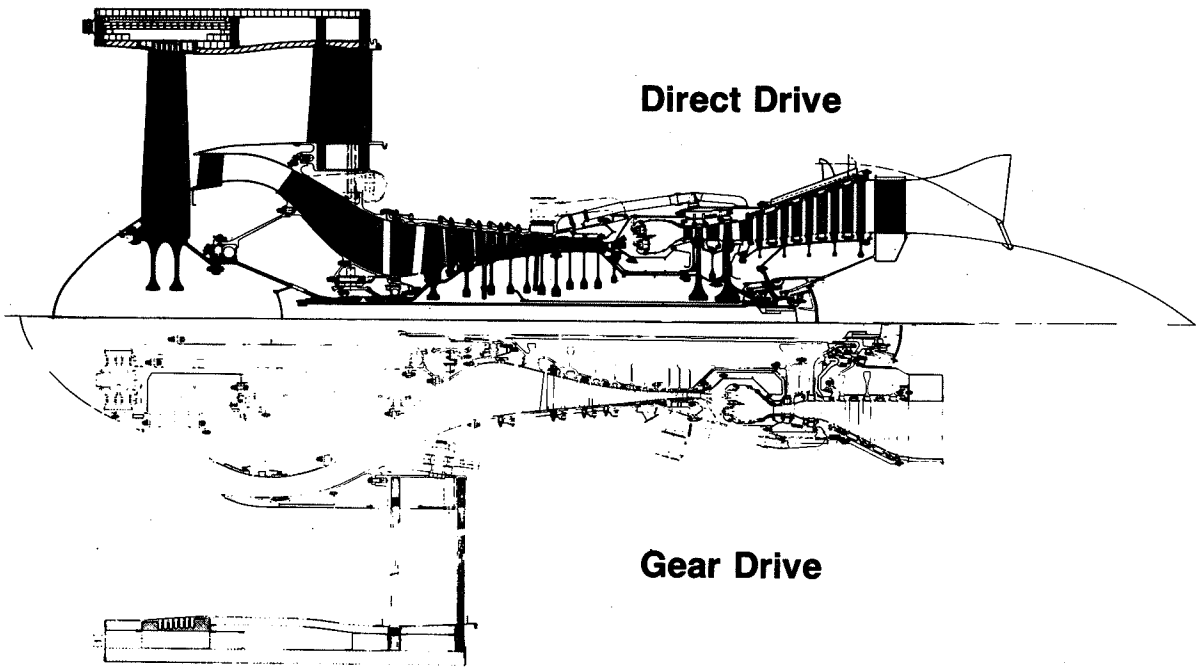

Figure 1.- E^3 study advanced engines.

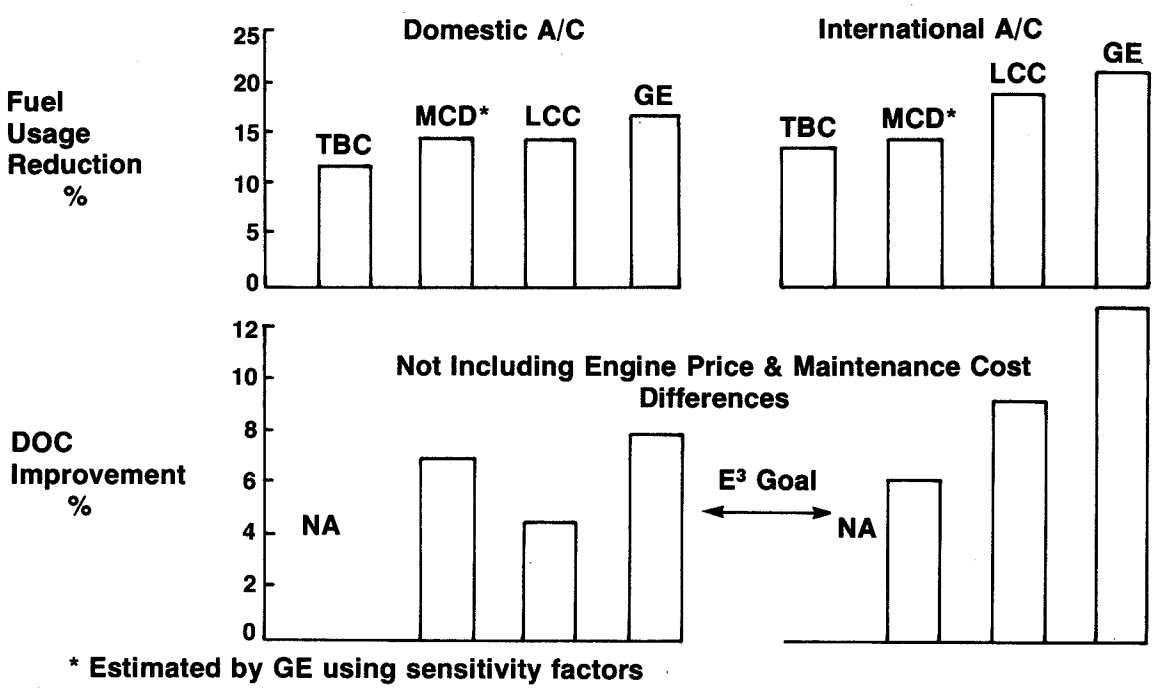

Figure 2.- Advanced direct drive engine benefits (CF6-50C reference).

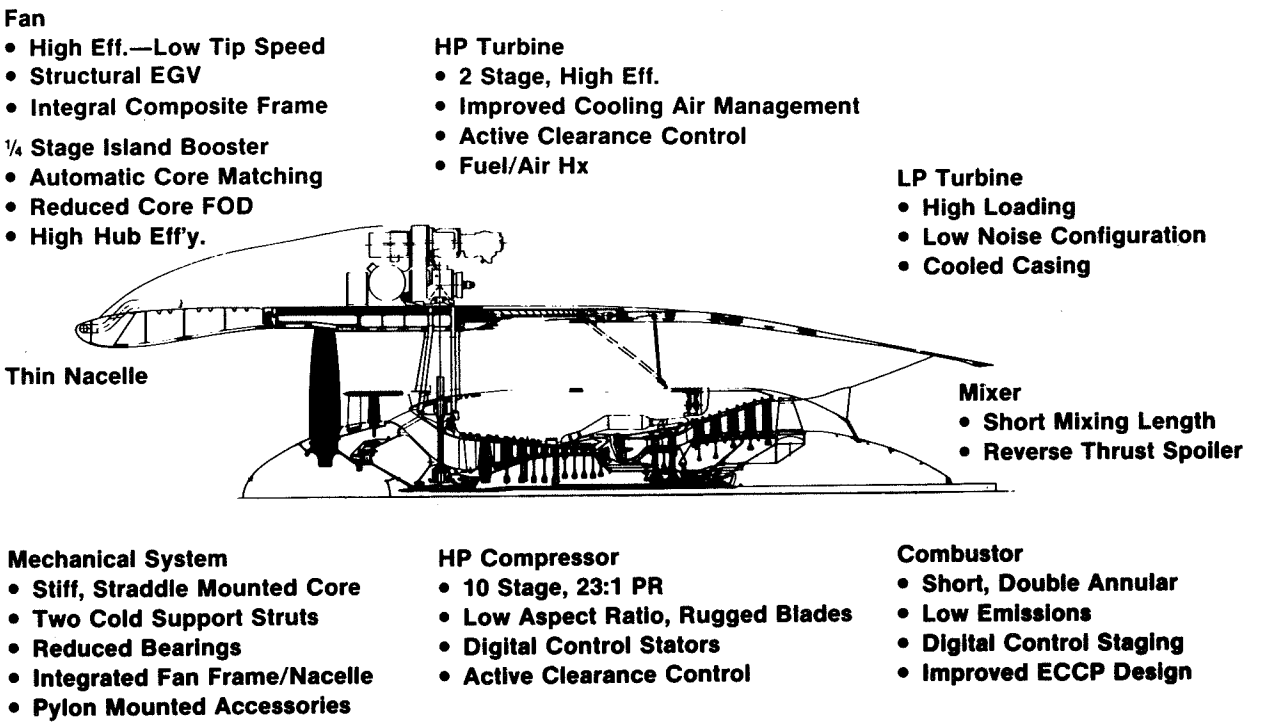

Figure 3.- Advanced technology features.

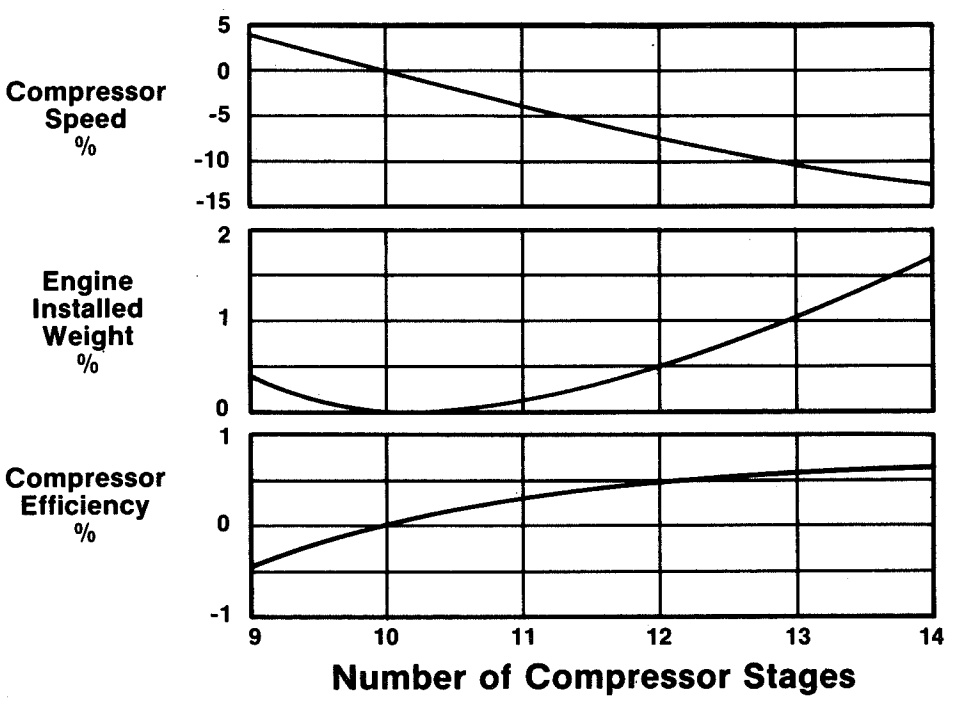

Figure 4.- Effect of compressor stage number.

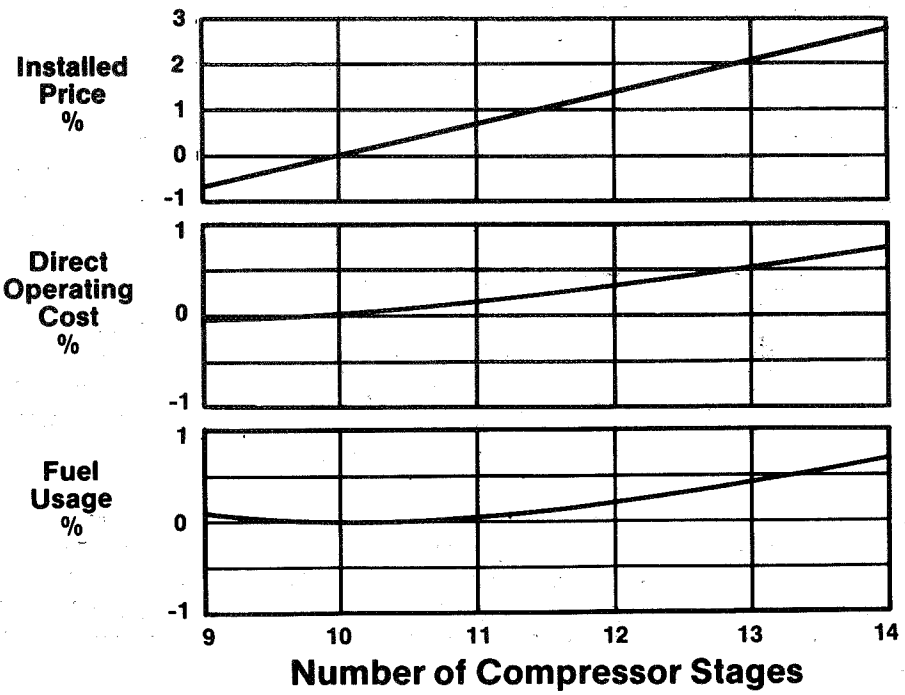

Figure 5.- Economic results.

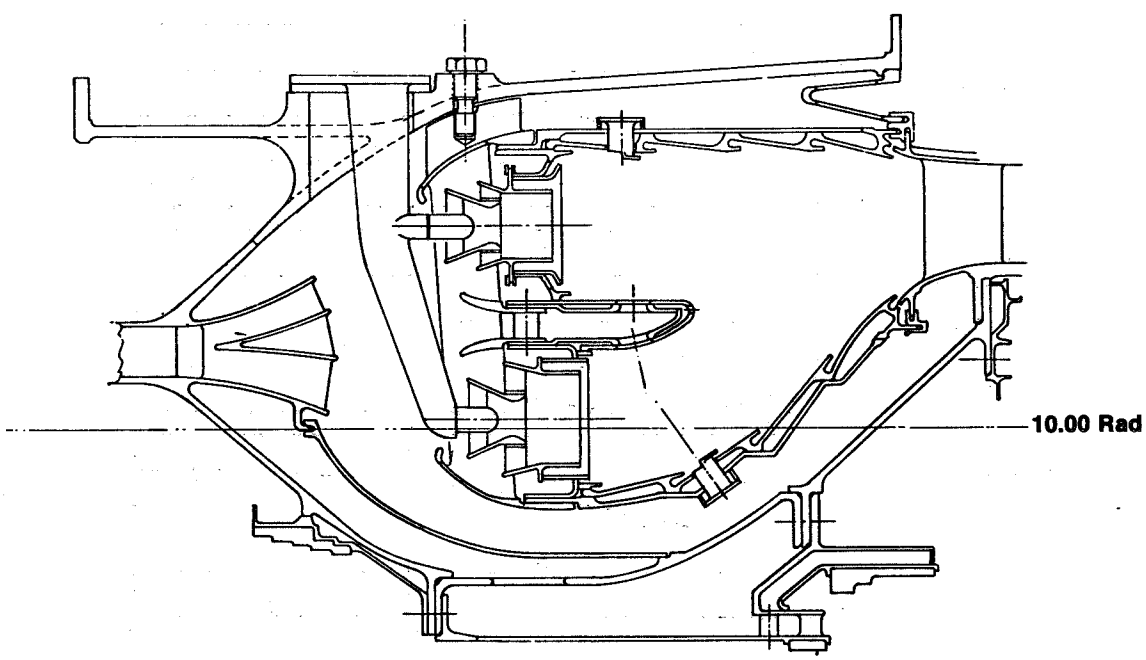

Figure 6.- Double annular combustor.

Fan
- Low Tip Speed — Reduced Erosion
- Stiff Integrated Nacelle/Frame Casing

¼-Stage Island Booster
- Separates Debris From Core Air

HP Turbine
- Abradable Erosion Resistant Ceramic Shrouds
- Active Clearance Control
- Increased Cooling Air Levels

LP Turbine
- Casing Cooling
- 360° Circumferential Casing

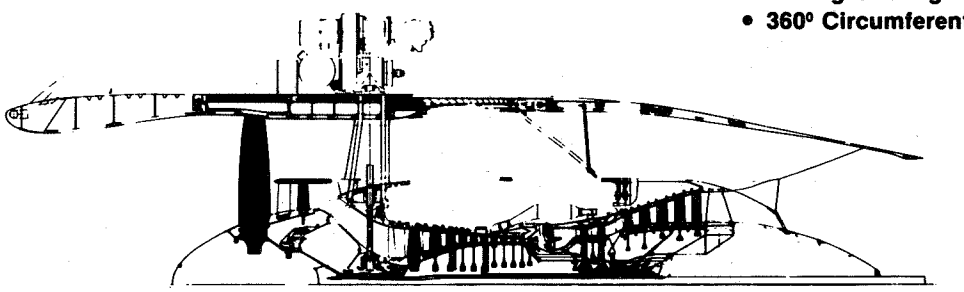

Mechanical System
- Short, Rigid, Two-Bearing Core Engine
- Two-Bearing Core Support
- Two Cold Frame Bearing Supports
- Designed for Heavy Unbalance
- Load Isolating Aft Mount
- Thrust Links Reduce Engine Bending

HP Compressor
- Wide-Chord Erosion-Resistant Blading
- Abradable Casing Liners
- Aft Casing Isolation Mount
- Active Clearance Control
- Cooled Rotor

Combustor
- Short, Rugged Design
- Film/Impingement Cooling

Figure 7.- Performance retention features.

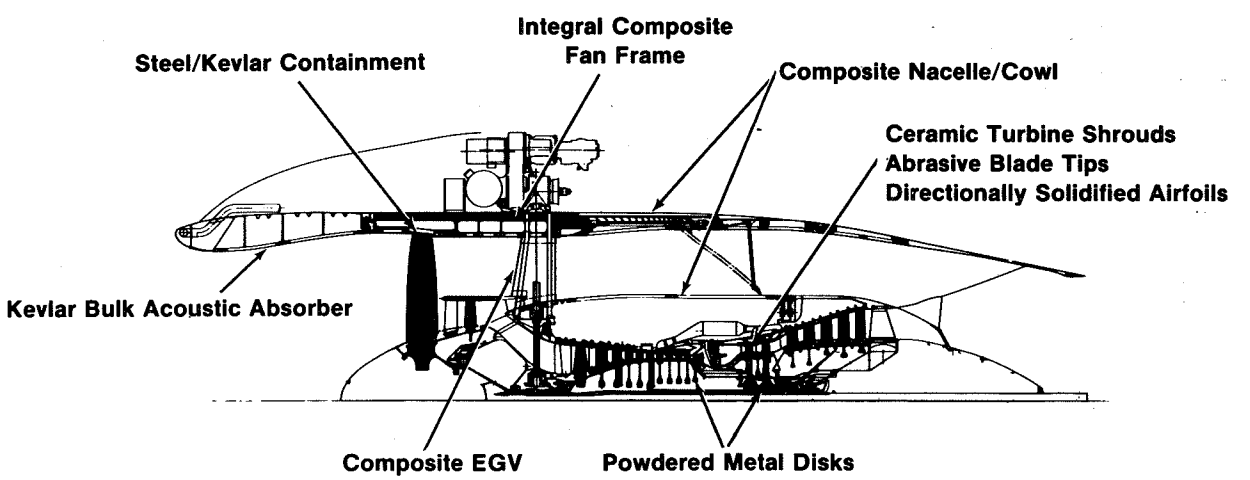

Thermal Barrier Coatings
- HPT Blade/Vane Airfoils
- HPT Blade/Vane Platforms
- Combustor Liner

Figure 8.- Advanced materials.

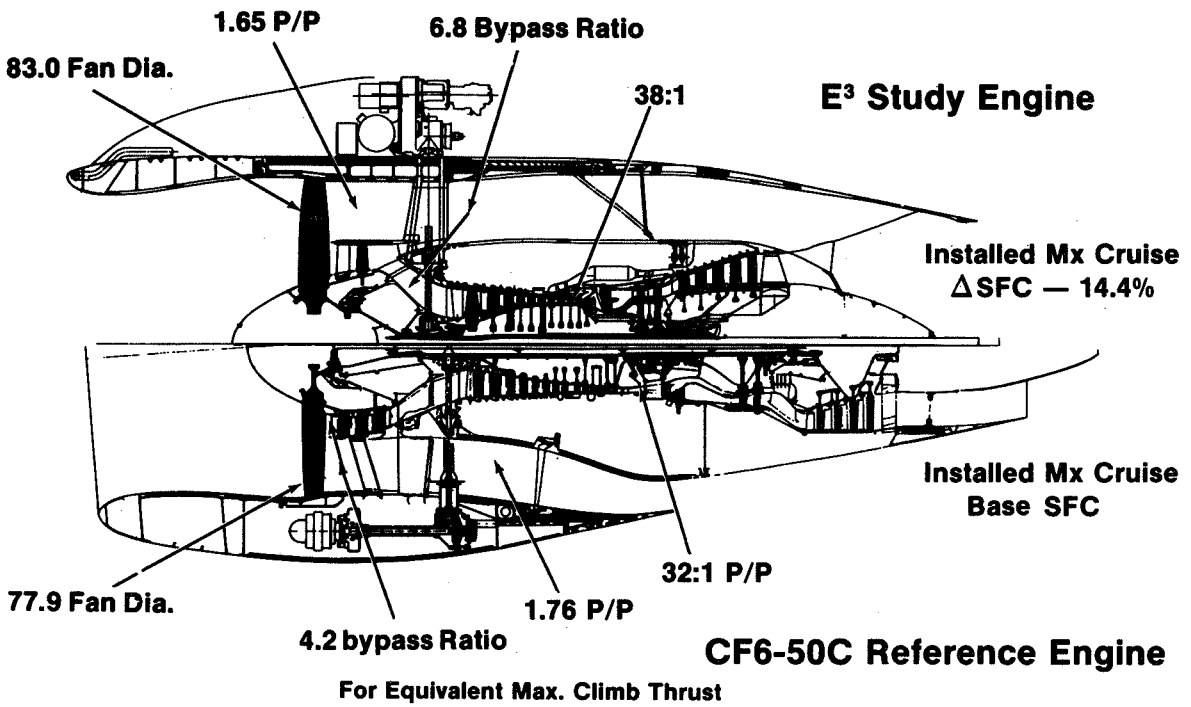

Figure 9.- Engine comparison.

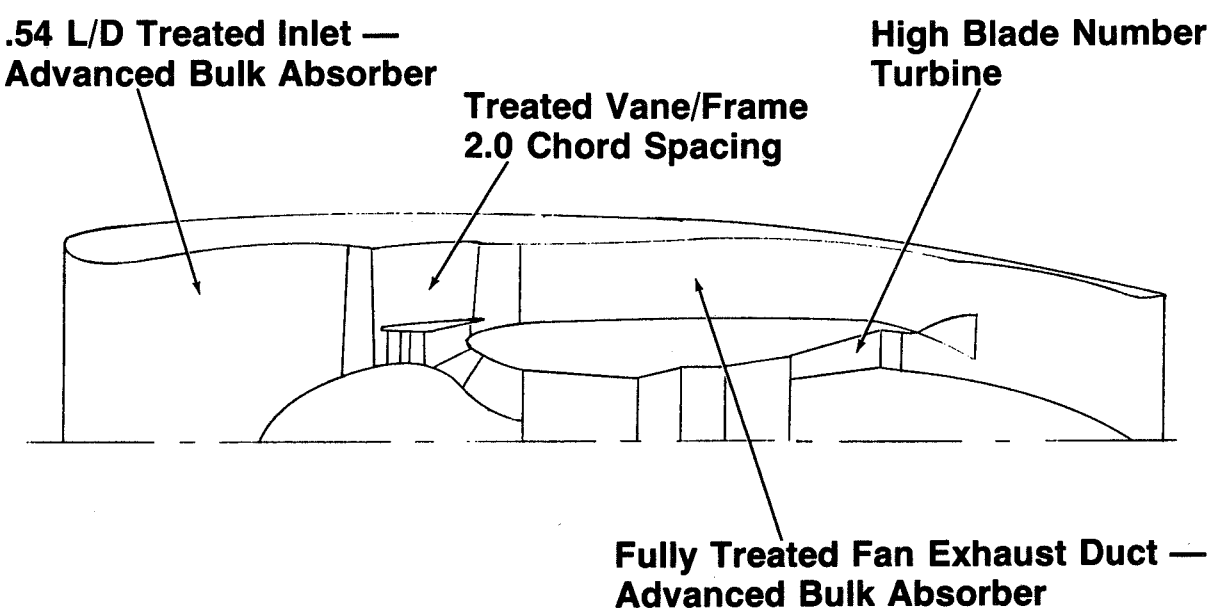

Figure 10.- Advanced engine installation low noise features.

STATUS OF ADVANCED TURBOPROP TECHNOLOGY

J. F. Dugan, B. A. Miller, and D. A. Sagerser
Lewis Research Center

SUMMARY

When used to power medium-range transport aircraft cruising at Mach 0.8, advanced turboprops offer a 10 to 20 percent fuel saving relative to advanced turbofans and a 5 to 10 percent DOC advantage with 15.8¢/liters (60¢/gallon) fuel. Because of this attractive potential, NASA began the Advanced Turboprop Program in fiscal year 1978 as the sixth major part of its Aircraft Energy Efficiency Program. In the two previous fiscal years, NASA supported, as part of its R&T base program, some turboprop-powered transport studies, some wind tunnel aerodynamic and acoustics tests of model propellers (0.62 m in diameter), a study of turboprop maintenance, and an experimental wind-tunnel program on airframe-turboprop interactions. This paper reviews each of these areas and describes plans for continued development of the technology for advanced turboprop transport aircraft.

INTRODUCTION

The Advanced Turboprop Program is one of six major technology programs that compose the NASA Aircraft Energy Efficiency Program (ref. 1). It is intended to demonstrate the technology readiness for efficient, reliable, and acceptable operation of turboprop-powered commercial transports at cruise speeds up to Mach 0.8 and at altitudes above 9.144 km (30 000 ft). This technology would also apply to possible new military aircraft requiring long-range and long-endurance subsonic capability.

The Advanced Turboprop Program grew out of studies of low-energy-consumption aircraft engines. These studies, which ran from 1974 to 1976, were conducted, under contract to Lewis, by General Electric (refs. 2 and 3) and Pratt & Whitney Aircraft (refs. 4 and 5). The objectives of these studies were to identify and evaluate ways to reduce fuel consumption in current and future subsonic transport engines. Among the conclusions was this: The most promising unconventional engine concept is an advanced turboprop, which may permit a 15- to 20-percent fuel saving compared with the projected fuel usage of an advanced turbofan engine. This conclusion prompted, in late 1975, NASA R&T studies of high-speed propellers (the High-Speed Propeller Technology program). By 1977 enough progress had been made in propeller technology to justify the start of phase I of the Advanced Turboprop Program. The planning of the Advanced Turboprop Program and the status of research in advanced turboprops as of July 1977 are discussed in reference 6.

This paper, an update of reference 6, reviews results obtained since July 1977. It includes propeller efficiency data from three sets of propeller

blades tested in the Lewis 8- by 6-foot wind tunnel, propeller-wing interaction drag obtained in the Ames Research Center 14-foot wind tunnel using a propeller slipstream simulator, final cost figures from a study of turboprop-system reliability and maintenance costs, and recent estimates of fuel savings and direct-operating-cost (DOC) savings for turboprop-powered transports compared with projected fuel usage and cost for turbofan-powered transports.

MAJOR AREAS OF ADVANCED TURBOPROP PROGRAM

The four major areas involved in the Advanced Turboprop Program - the propeller and nacelle, cabin environment, installation aerodynamics, and mechanical components - are shown in figure 1. These areas interact, and all contributed to the program goals of low fuel consumption, low operating cost, and passenger acceptance.

The propeller and its nacelle must be designed to achieve high efficiency for cruise at speeds up to Mach 0.8 above 9.144 km (30 000 ft). The propeller blades will be very thin and have swept leading edges in order to minimize compressibility losses. The spinner and nacelle will be shaped to minimize choking and compressibility losses, especially near the blade roots. The successful application of these concepts will result in higher propeller efficiencies. This, of course, will contribute to both low fuel consumption and low operating cost, since fuel accounts for such a large fraction of operating cost.

In a later section, Propeller Efficiency, the propeller data obtained from three sets of blades tested in the Lewis 8- by 6-Foot Wind Tunnel will be discussed; the plans for testing four more sets of blades before selecting the propeller design for large-scale propeller development in phase II of the Advanced Turboprop Program will also be discussed.

The sketch at the lower right of figure 1 labeled "cabin environment" reminds us that the fuselage is in the direct noise field of the propeller (whereas the inlet duct of a turbofan shields the fuselage from fan noise). The propeller tips may be slightly supersonic at the Mach 0.8 cruise condition, resulting in a relatively high noise level. The noise level must be attenuated by the cabin wall in order to provide a quiet cabin environment. Since it is likely that additional airframe weight will be needed to achieve the required attentuation, the quiet cabin environment is achieved at the expense of fuel economy and operating cost. Just how much is not known at this time.

Included in the section Propeller Noise and Fuselage Attenuation will be a discussion of early noise data obtained by simulating Mach 0.8 cruise conditions, plans to obtain more reliable noise data in flight at Mach 0.8, and a brief description of three fuselage structural concepts proposed for attenuating propeller noise.

At the lower left of figure 1 the sketch labeled "installation aerodynamics" depicts an accelerated, swirling propeller slipstream flowing over a wing. Here, there is a potential for higher drag which would adversely affect

fuel consumption and operating cost. The increased Mach number of the flow over the wing segments washed by the propeller slipstream and the flow rotation in the propeller slipstream may cause large interference drag penalties in cruise. On the other hand, there is the possibility that fuel consumption and operating cost can be improved by special tailoring of the wing segments washed by the propeller slipstream. The magnitude of swirl in the propeller slipstream results in very substantial losses in propeller efficiency which are attributed to the swirl component of slipstream momentum. A properly designed wing in the slipstream can be expected to straighten the flow and to experience a corresponding thrust force. This resulting thrust force may offset or even exceed the drag penalties due to propulsion system/airframe interference. Because of the complexity of the aerodynamic processes involved, detailed wind-tunnel testing and analysis will be required to provide reliable answers.

These planned experimental and analytical programs are discussed in the Airframe-Propulsion System Integration section; also discussed are some early experimental results obtained using a slipstream simulator.

The sketch in the upper left shows the mechanical components of an advanced turboprop propulsion system. Two of the components are singled out as being especially important in achieving a low operating cost: the advanced propeller and its gearbox. For maximum direct operating cost advantage, their maintenance costs must be lower than the costs of earlier-design commercial turboprop aircraft. The final results from a study of turboprop-system reliability and maintenance costs are discussed in the Propeller and Gearbox Maintenance section.

The most recent assessment of the fuel savings and the DOC savings of turboprop-powered transports is discussed in the section Advanced Turboprop Aircraft Studies.

Propeller Efficiency

One aspect of the advanced turboprop system performance that required early experimental verification was the propeller aerodynamic efficiency. Test results were needed to demonstrate that high efficiency at high cruise speeds could be obtained with advanced propeller designs that use thin blade sections. Three propeller models (62.23-cm (24.5-in.) in diam.) have been designed and are being tested in a wind tunnel to measure their performances. Two of the models, designated SR-1 and SR-2, were first tested by Hamilton Standard (under NASA contract) in a wind tunnel at United Technologies Research Center (UTRC; refs. 7 and 8). These two and a third model, SR-1M, are now being tested in a wind tunnel at Lewis. Propeller model SR-1 is shown installed on the propeller test rig in the Lewis 8- by 6-foot wind tunnel in figure 2.

All three models have eight blades and were designed to operate at a cruise speed of Mach 0.8, a tip speed of 244 m/sec (800 ft/sec), and a disk loading of 301 kW/m^2 (37.5 shp/ft^2) at an altitude of 10.67 km (35 000 ft). Two of the models, SR-1 and SR-1M, were designed with 30° of aerodynamic sweep at the blade tips, and the third, SR-2, has straight blades. Both the SR-1 and

SR-1M models incorporated conical spinners, and the SR-2 model incorporated an area ruled spinner that was designed to lower flow velocities in the hub region where choking could be a problem.

Model SR-1M is actually a modification to the SR-1 design and differs primarily in the blade twist and camber distribution from hub to tip. This model was created when the results of initial wind tunnel tests at the UTRC showed that the radial loading differed from the design distribution and the efficiency was somewhat lower than predicted. The changes incorporated in model SR-1M were designed to increase the loading in the outboard region of the blade to conform more closely to the initial objective.

Predicted and measured efficiencies for the three models are tabulated in table I. The values shown are at the design loading and tip speed of 301 kW/m^2 (37.5 shp/ft^2) and 244 m/sec (800 ft/sec), respectively, which results in a Cp of 1.7 and a J of 3.06. The current prediction design-point efficiency of SR-1 is over 2 percent higher than that of SR-2. This reflects the anticipated benefit of the 30° of blade sweep. However, when these models were tested, their measured efficiencies were about the same and were close to the predicted value for SR-2. Because the slightly higher than predicted performance for SR-2 may be associated with the area-ruled spinner used on this model, further tests of this spinner configuration are planned.

Tests of model SR-1M showed that the modifications made to the blade twist and camber distributions did not improve the design point efficiency even though recent radial wake survey measurements made downstream of the blades indicated that the intended radial loading distribution had been achieved and no gross flow problems occurred. At lower Mach numbers, however, model SR-1M performed significantly better than models SR-1 and SR-2. For example, at Mach 0.7 SR-1M's 81.7 percent efficiency was about 1.5 percent better than either SR-1 or SR-2. The value of 81.7 percent is within 4 percent of the ideal induced efficiency (inviscid) limit of 85.1 percent and thus is about as high as can be practicably achieved for a thin bladed propeller operating without compressibility losses.

The results obtained from the models tested so far suggest that the lower than predicted efficiencies at design conditions may have resulted from higher than anticipated compressibility losses. This, in turn, suggests that performance at the higher cruise speeds may be improved by the use of additional blade sweep.

It is appropriate at this point to compare the model test results with the efficiency goal of 80 percent, a value assumed in the inital RECAT studies references 9 to 13. This is done for model SR-1M in figure 3 - a plot showing the effect of cruise Mach number and loading on efficiency. The SR-1M test data used in this figure differ somewhat from data shown in table I in that the blade angle and tip speed were chosen for maximum efficiency at the specified value of loading rather than holding the design value for J and thus fixing tip speed. It should also be noted that the power loading (power/diameter^2 or P/D^2) varied with the cruise velocity cubed by maintaining constant values for Cp/J^3. Such a variation approximately matches the thrust levels required by a family

of similarly sized aircraft, each designed for different cruise speeds.

At the design cruise speed of Mach 0.8 and 100 percent loading, the measured efficiency for model SR-1M was less than 3 percent below the goal. By reducing the loading to somewhat less than 70 percent of design (and thus increasing the propeller tip diameter a little over 20 percent) the efficiency goal of 80 percent can be obtained. This efficiency can also be reached at 100 percent loading by lowering the cruise speed to slightly less than Mach 0.75 or by some combination of reduced loading and reduced cruise speed. Reducing cruise speed or loading also has the effect of reducing the maximum efficiency tip speed, and lower tip speeds result in lower noise levels.

Thus, while current propeller models have not demonstrated the 80 percent efficiency goal at design conditions, performance at this level has been demonstrated at reduced loading or reduced cruise speeds. Improvements continue to be made in propeller aerodynamic design methodology based on new test results and analysis. Performance improvements are expected to result from additional blade sweep, improved area ruling in the hub, and a better understanding of the propeller flow field through improved flow survey testing. These improvements are expected to result in obtaining the 80 percent efficiency goal at design loading and Mach number.

A new propeller model, designated SR-3, is currently being fabricated for wind-tunnel tests in April and May of this year. This model is the first to be designed with acoustic considerations. Its plan form and significant design characteristics are compared with models SR-1, SR-1M, and SR-2 in figure 4. The tip speed, loading, and number of blades are the same for all of these models. But the tip sweep angle was increased to 45° for model SR-3 because of the expected aerodynamic and acoustic benefits. Because of this and other refinements in the blade design procedures and spinner area ruling, the estimated design efficiency is 2 percent higher, and the estimated design cruise noise level is 6 dB lower than the SR-1 and 1M designs.

NASA's current propeller model test program is diagramed in figure 5. Four propeller design approaches, in terms of cruise Mach number, tip speed, loading, and number of blades, are included in the model program so that the trade-offs among the more important propeller design parameters may be evaluated.

The first approach assumes an 0.8 cruise Mach number, eight blades, a 244-m/sec (800-ft/sec) tip speed, and a 301-kW/m^2 (37.5-hp/ft^2) disk loading. Three models, SR-1, SR-2, and SR-1M, have been designed, built, and are being tested to determine their performance and noise characteristics. A fourth model, SR-3, has been designed, is being built, and will be tested to determine the effect of additional sweep and improvements in design methodology. A fifth model in this category, SR-4, will be used to evaluate the benefit of advanced airfoils on performance.

Because propeller noise level requirements are, at present, uncertain, two lower-tip-speeds-design approaches are planned. Both will have 10 blades and

lower disk loadings (larger tip diameters) to maintain high efficiency at the lower tip speeds. The 213-m/sec (700-ft/sec) tip-speed SR-6 model is expected to have an efficiency about the same as SR-3. And the 183-m/sec (600-ft/sec) tip speed SR-5 model is expected to have a slightly lower efficiency than SR-3, but SR-5's tip relative Mach number is just sonic and therefore much lower noise levels are expected.

A final design approach, which assumes a 0.7 cruise Mach number, is included in the plan to assess the benefits of lower cruise speeds on propeller design. The design of this model will be compared with an 0.8 cruise Mach number design to determine if there is enough difference in the resulting blade shape and predicted performance to justify fabrication and test. If not, the test results of a 0.8 Mach number design operating off-design down to Mach 0.7 will be used to assess the effect of lower cruise speed on propeller design performance.

The test results from the propeller models representing each design approach will be used with results from other tests and design studies affecting the propeller design to define a system-optimized design, designated SR-7. The other studies include the development of improved aerodynamic and acoustic design tools, studies of full-size blade structural designs, aeroelastic model tests, fuselage noise attenuation design studies, and aircraft system studies. A model of the SR-7 design will be tested to verify predicted performance. Then, a full scale model of this design, or a modification of it, will be built and flight tested as part of phase II of the program.

PROPELLER NOISE AND FUSELAGE ATTENUATION

Propeller Noise

For an advanced turboprop aircraft to be competitve with an advanced turbofan aircraft, the turboprop cabin interior during cruise should be equivalent in comfort (low levels of noise and vibration) to that of the turbofan aircraft. However, quiet cabin interior will be more difficult to achieve in the turboprop aircraft because its fuselage is in the direct noise field of the propeller (whereas the inlet duct of a turbofan shields the fuselage from fan noise).

Some preliminary noise tests of SR-1 and SR-2 were completed in 1976 in the UTRC Acoustic Research Tunnel (fig. 6). To simulate Mach 0.8 cruise operation, the tunnel was operated at its maximum through-flow Mach number (Mach 0.32), and the propeller model was oversped so that the blade tip relative Mach number was the same as for the Mach 0.8 cruise condition. The propeller model had only two blades in these tests because of the limited horsepower of the electric drive rig. Microphones were located on a line parallel to the propeller axis of rotation at three radial distances in the near field and one radial distance in the far field. Measured noise levels in the tunnel were compared with levels predicted by a theoretically based computer program. Empirical adjustments were made to the noise prediction program, which was then used to predict full-scale propeller noise at the desired altitude and cruise conditions. The overall near-field sound pressure level (SPL) of SR-1 and SR-2 at

Mach 0.8 cruise is 146±3 dB. The 6-dB uncertainty band is a result of imperfections in the testing technique and the prediction program.

With the intent of acquiring better propeller noise data at Mach 0.8 cruise conditions, two feasibility studies were conducted: one of a high-speed wind tunnel and the other of flight tests (fig. 7). For the flight tests the 0.61-m (2-ft) diameter propeller model would be mounted above the fuselage of a JetStar aircraft, and the fuselage instrumented with microphones. The flight tests would yield high quality acoustic data with respect to noise level, spectral content, and directionality. Data obtained from the high-speed wind tunnel, however, would be uncertain with respect to both level and directionality. Such an uncertainty in the tunnel data is extremely difficult to quantify without comparison with flight data. Thus a decision was made to proceed with the flight tests.

Fuselage Attenuation

The noise perceived by the passenger inside the cabin is a strong function not only of the noise generated by the propellers, but also of the noise attenuated by the fuselage and interior cabin construction. The present state of affairs is illustrated in figure 8. The desired cabin noise level is assumed to be 75 dB A. Assuming the cabin noise to be dominated by the blade passing frequency tone at 160 Hz, the sound pressure level would be 90 dB inside the cabin. An aircraft with a conventional fuselage and wing-mounted turboprops could tolerate a propeller noise level outside the cabin of about 110 dB.

Now, consider the propeller noise level estimated from the 1976 tests of SR-1 and -2; that is, 146±3 dB. By tailoring the sweep and planform of the SR-3 blades for lower noise, a sound pressure level of about 140 dB is predicted. A further reduction to about 135 dB might be achieved by using new low-noise airfoils. That is probably the lower limit of propeller noise for the design parameters noted (eight blades; tip speed, 244 m/sec (800 ft/sec); power loading, 301 kW/m^2 (37.5 hp/ft^2)).

However, a 135-dB propeller noise level is about 45 dB above the desired cabin noise level and about 25 dB above the noise level that can be attenuated with conventional fuselage construction. Four ways of bridging this 25-dB gap have been suggested: (1) Design propeller tip speed could be reduced to lower the noise generated by the propeller. (2) Fuselage design and cabin acoustic treatment can almost certainly be improved using conventional techniques to increase noise attenuation. (3) The propeller and fuselage design can be integrated, particularly in the selection of propeller blade passing frequency and fuselage acoustic modes. This is expected to produce even greater improvement in propeller noise attenuation. (4) Finally, the engine location on the aircraft can be optimized; for example, mounting the engines farther outboard on the wing or on the aft end of the fuselage behind the passenger cabin would result in less cabin noise.

Three quite different fuselage structural concepts for attenuating propeller noise are illustrated in figure 9. A conventional fuselage attenuates noise generated at different frequencies as shown in figure 9(a). The least attenuation occurs in the frequency range of several hundred hertz. Unfortunately, the blade passing frequency of many propeller designs falls in this range. Three concepts have been suggested to resolve this problem:

(1) One concept involves structural tuning and damping (fig. 9(b)) wherein the structure is designed to couple in preferred modes of vibration the acoustic energy that can then be effectively reduced by damping material. When only discrete tones are the source of excitation, the structure can be tuned to have much reduced response at those frequencies. This concept is currently in a state of analytical development, although some encouraging experimental results have been obtained. For this reason only very general trends of noise reduction and attendant weights of fuselage structure change are available.

(2) The increased stiffness approach to attenuating propeller noise is shown in figure 9(c). High stiffness is achieved by fastening aluminum skin to closely spaced aluminum and graphite-epoxy frames. This concept is more effective at lower propeller blade frequencies. Thus, lower propeller tip speed and fewer blades enhance propeller noise attenuation. (Of course, lowering propeller tip speed is also a way to reduce the noise generated by the propeller.)

(3) The double limp wall concept (fig. 9(d)) is more effective at the higher propeller blade frequencies. Attenuation improves as propeller tip speed increases, but then, so does propeller noise generation. The double limp wall concept also is in the development stage. It may, for example, be necessary to increase the number of propeller blades in order to raise the blade passage frequency to a value that will allow the fuselage wall to exhibit mass-like behavior. Also, structural damping may be required in order to approximate mass-like response.

It is quite possible that an optimized fuselage acoustic design will selectively employ portions of all three concepts to obtain maximum noise reduction with minimum weight penalty.

AIRFRAME-PROPULSION SYSTEM INTEGRATION

The initial systems studies (refs. 9 to 15) identified the integration of the turboprop propulsion system with the airframe as one of the areas of high uncertainty that requires additional research. The integration of a turboprop is more critical than that of a turbofan because of the large interaction between the slipstream and wing. As outlined in the studies, the combination of a supercritical swept wing and the highly loaded propeller can give rise to a considerable level of aerodynamic interference. Inherent in the slipstream are Mach number and swirl increments of approximately 0.05 and 6.0°, respectively. Both of these flow perturbations can significantly affect the flow over a supercritical wing which has been designed to operate at a specific Mach number. Either can cause the section of the wing within the slipstream to operate

well into drag-rise, effectively reducing the installed performance of the propeller. In addition, the propeller will be subject to a nonuniform flow field created by the airframe, thus potentially reducing its performance.

To reduce the uncertainties associated with the installation of these advanced turboprop propulsion systems, a combined experimental and analytical research program has been initiated. The primary objectives, as enumerated in figure 10, are to assess the magnitude of the aerodynamic interference, to understand the aerodynamic phenomena associated with the installation, and to develop an analytical and experimental data base. The data base will be acquired using a slipstream simulator and a powered semispan model. The determination of the aerodynamic interference between the propulsion system and airframe will significantly contribute to the technology required to establish the overall performance potential of the proposed high-speed turboprop aircraft. The design and optimization of the propulsion system installation requires a detailed understanding of the aerodynamic and flow characteristics associated with this type of installation. The development of the analytical and experimental data base will contribute to this understanding.

Experimental Program

Current experimental programs for the near future include two complementary test programs: the first uses a simulated propeller slipstream, and the second, an active propeller.

The slipstream simulator program (fig. 11) provided fundamental force and pressure data on the interaction of a representative slipstream and a supercritical wing. The slipstream was generated using an ejector-driven nacelle strut mounted in front of a transonic wing-body model. The ejector-drive nacelle was powered by 20 sets of ejector nozzles which controlled the energy and hence the velocity of the slipstream. The nacelle also included a set of swirl vanes to induce swirl into the slipstream. The wing-body model was mounted on a force balance and the wing was pressure instrumented. With this arrangement, the effects of slipstream Mach number and swirl on the wing-body forces and pressure were determined. To provide a more detailed understanding of the interaction between the slipstream and wing, a wake rake was used to measure the wake characteristics along the span of the wing. This information provided a detailed description of the local drag characteristics along the wing and identified the local drag increments resulting from the slipstream-wing interaction. The slipstream simulator test program was conducted in the latter part of fiscal year 1977 in the Ames Research Center 14-foot wind tunnel. The results are shown in figure 11. For all test points the slipstream Mach number was higher than the cruise Mach number by 0.075. With zero swirl in the simulated slipstream, aircraft drag increased about 2.5 percent. Theory predicts that, as swirl increases in the slipstream, aircraft drag will decrease. The experimental data bear this out, except for an anomaly at a 6° swirl. The reason for this is not yet known. These preliminary results show that the drag penalties associated with the interaction of a turboprop slipstream and a supercritical wing are not excessive and that the potential does exist to recover some of the propeller swirl losses with the wing.

The second, or active propeller program will provide a more accurate estimate of the interference between the propulsion system and the airframe, including the effects of the installation on the actual propeller performance. This test program, which will be conducted in the Ames 11- by 11-foot wind tunnel during the first half of fiscal year 1979, will use an active propeller mounted on a semispan wing-body model. To insure consistency between these results and those of the isolated propeller tests, the propeller blades of the two test programs are the same aerodynamic design. Furthermore, the semispan wing-body model is a scaled version of the full-span model used with the slipstream simulator. This will allow a detailed comparison with the slipstream simulator data. The propeller on the semispan model will be powered by an air turbine motor and be instrumented for propeller thrust and power measurements. The wing-nacelle combination will be mounted on a floor balance and be instrumented for pressure measurements.

The slipstream simulator tests and the active propeller tests complement each other. The slipstream simulator tests, although providing only an approximate simulation in terms of slipstream Mach number and swirl, does allow the individual interactions to be investigated separately and in combination. Because of the necessity of maintaining the alinement between the ejector nacelle and the free-stream flow direction, only measurements corresponding to the conditions around the cruise angle of attack can be obtained. However, the relative position of the slipstream and wing can be easily varied. In contrast, the active propeller program provides an accurate and complete simulation of the flow field over the full angle-of-attack range. However, it is more difficult to identify the effects of the various flow perturbations and to vary them to establish trends that can be used to optimize the installation. Jointly though, these two test programs should provide a detailed understanding of the various interference effects and establish an accurate assessment of installed performance of these high-speed turboprops.

Analytical Program

To provide an analytical base for the integration of these advanced turboprop propulsion systems, two approaches are being pursued: The first is to apply existing linear paneling techniques to the wing-nacelle-slipstream combination as described in reference 16. Although these techniques are applicable only subcritically, it is believed that many of the potential transonic flow problems can be identified by examining the local pressure distributions at subscritical conditions. Several paneling techniques are being applied to this area and include those described in references 16 to 18. The accuracy of these methods will be evaluated using the experimental results obtained from the test programs. The second, a long-range analytical effort, is to develop a transonic computational technique capable of analyzing a wing-nacelle-slipstream combination under transonic flow conditions.

PROPELLER AND GEARBOX MAINTENANCE

A study of turboprop system realiability and maintenance costs was completed in May 1977 by Detroit Diesel Allison (DDA) for Lewis. The objectives of the study were to determine the overall reliability and maintenance costs (R&MC's) of past and current turboprop systems and then to project the R&MC improvements that could be expected for new turboprop systems for the 1985-1990 IOC. Hamilton Standard (HS) was a subcontractor to DDA and provided information on past, current, and new propellers. The aircraft studied were the Lockheed L188 Electra, Convair CV580, and Lockheed L382 Hercules. These aircraft were powered by the DDA 501-D13 turboshaft engine and either the DDA 606 propeller or the HS 54H60 propeller. The data used in the study were obtained from airline records, outside repair facilities, CAB Form 41, and the DDA reliability department records.

The fully burdened turboprop maintenance cost was quite high. Using data from 1966 through 1969 for Electra L188 operations averaging 0.80 hour per flight, the turboprop (DDA 501-D13/HS 54H60) maintenance cost was $42.30 per flight hour (FH) (in CY 1976 dollars).

In figure 12 the high maintenance cost of the DDA/HS turboprop is compared with the maintenance cost of the JT8D turbofan that powered B-737 aircraft from 1971 to 1973. The higher turboprop maintenance cost ($53.18/FH) resulted from scaling the turboprop so that its thrust capability equaled that of the JT8D turbofan at Mach 0.8 and 10.67 km (35 000 ft) altitude. In this comparison, the turboprop maintenance cost exceeds the turbofan maintenance cost by $22.71 per engine flight hour or by 74.5 percent. However, most of the difference ($18.13) was due to the higher maintenance cost of the older technology turboprop core. The small remaining difference ($4.58) comes from the higher maintenance cost of the turboprop's propeller and gearbox compared with the turbofan's fan and thrust reverser. For future systems it can be assumed that the maintenance cost of the core will be no greater for a turboprop than that for a turbofan if the same level of technology is used. This leaves the cost of the propeller and gearbox, which must be reduced to the level of the fan and reverser in order for the turboprop maintenance costs to be comparable with the turbofan.

The cost drivers and design features of the propeller and gearbox from the 501-D13/54H60 system were examined in the study to project maintainability improvements that could reasonably be expected from a new design for the 1990's. The results of that analysis are summarized in figure 13. The unburdened costs for the 1960-era turboprop (501-D13/54H60) propeller and gearbox scaled to the advanced turboprop mission and size total $4.58 as shown in the left bar. These same costs could be reduced to $0.73 in the advanced design by incorporating design features that improve maintainability.

The most significant of these is the elimination of scheduled removals through improved fault isolation and diagnostics. This alone accounted for over 60 percent of the maintenance cost reduction for the propeller and gearbox. The use of modularity is another maintainability feature, common to both the

advanced propeller and gearbox, which was lacking in the 1960-era turboprop. This allows repairs to be made on small equipment packages without disturbing the rest of the engine. Using a simpler design with fewer parts and a more reliable heater accounts for the remaining maintenance cost improvements for the advanced propeller.

Other maintainability features of the advanced gearbox design include using longer life bearings and the removal or simplification of accessories. The engine accessories were removed from the gearbox and installed on the engine core, as is the case for a turbofan; and the aircraft accessories were assumed to be aircraft mounted and their multiple drives simplified to a single shaft. With this arrangement, accessory failures will not require removal of the gearbox as was the case in the 1960-era turboprops.

Since the maintenance costs determined for the advanced turboprop are only estimates, which could prove to be higher in actual practice, the effect of doubling the propeller and gearbox maintenance costs on direct operating costs was evaluated using data from the Lockheed and Boeing RECAT studies (refs. 11 and 15). As shown in figure 14, the effect is small compared with the advantage the turboprop system has over the turbofan.

ADVANCED TURBOPROP AIRCRAFT STUDIES

To evaluate the advanced turboprop's overall impact on complete aircraft configurations, a number of design studies have been completed. Results from three of these studies (refs. 9 to 15) are shown in figures 15 and 16. In figure 15, fuel savings of turboprop (or prop-fan) aircraft are shown relative to turbofan aircraft. Because of different study aircraft configuration assumptions, the prop-fan aircraft fuel savings range from 8 to 28 percent for a 1852-km (1000-n.mi.) stage length. In all cases the increased efficiency of the prop-fan at lower altitudes and speeds results in greater fuel savings at shorter stage lengths. This is one reason why advanced turboprops look particularly attractive for the short- and medium-range flight markets currently being served by the DC-9, B-737, and B-727 aircraft.

The largest fuel saving is for the prop-fan derivative DC9-30 (refs. 12 and 13). The fuel saving is larger than that obtained in the other two studies because the comparison is with the current DC9-30 low-bypass-ratio JT8D turbofan engines. The Douglas study examined two levels of prop-fan performance. One assumed an eight-bladed prop-fan with a rotational tip speed of 219.5 m/sec (720 ft/sec) (corresponding to the Lockheed Electra) and current technology turboshaft engine performance, which would result in a propeller efficiency of 0.73 and an installed cruise thrust specific fuel consumption (TFSC) of 0.0738 kg/hr/N (0.65 lb/lb/hr). The other also assumed an eight bladed prop-fan but with a 243.8 m/sec (800-ft/sec) tip speed and turboshaft engine performance corresponding to the STS-476, a Pratt & Whitney turboshaft engine based on the JT10D engine core, which would result in a propeller efficiency of 0.80 and an installed TSFC of 0.0602 kg/hr/N (0.53 lb/lb/hr). Depending on the assumed propulsion system efficiency, the derivative prop-fan uses 27 to 33 percent less fuel than the DC9-30 at its average operational stage length of 537 km (290 n.

mi.). For the same takeoff gross weight and a passenger load factor of 58 percent, this fuel saving translates into a maximum range improvement of 41 to 73 percent, depending on the propulsion system efficiency assumed.

Admittedly, the fuel saving shown for the prop-fan derivative is higher because the comparison is with an older technology, low-bypass-ratio turbofan rather than a comparable technology turbofan. However, the prop-fan derivative does not include the application of any of the other advanced aerodynamics, structures, or active controls technologies that can improve the efficiency still further. Also, the low-bypass-ratio engines are the ones that are currently being used and sold in large quantities on this airplane type.

In the Lockheed design study (refs. 9 to 11), both the prop-fan and the turbofan were developed using 1985 technology. The resulting fuel saving for the prop-fan aircraft was 20.4 percent for a typical in-service stage length of 880 km (475 n. mi.) and a 58 percent passenger load factor.

The fuel saving for the Boeing prop-fan aircraft compared with an equivalent technology turbofan (refs. 14 and 15) were more modest, amounting to 13.5 percent for the wing-mounted configuration at a 926-km (500-n. mi.) stage length and 13 percent for the aft-mounted configuration. This smaller fuel saving reflects the Boeing study assumptions of a prop-fan noise level in cruise 10 dB higher than the long-range noise goal suggested by Hamilton Standard (the higher noise level results in a larger acoustic treatment weight penalty) and an increase in drag due to the effect of the propeller slipstream on the wing aerodynamics. These two critical technology areas were discussed under Propeller Noise and Fuselage Attenuation and Airframe-Propulsion System Integration sections.

The direction operating cost (DOC) savings identified in these studies (fig. 16) reflect the differences identified in the fuel saving comparisons. The largest DOC saving was obtained for the DC9-30 prop-fan derivative, even at the lower propulsion system efficiency with a TSFC of 0.0738 kg/hr/N (0.65 lb/lb/hr). The DOC saving for this aircraft at a stage length of 537 km (290 n. mi.) was 5.5 percent for fuel at 7.92¢/liter (30¢/gal) and 9.9 percent for fuel at 15.85¢/liter (60¢/gal). The Lockheed prop-fan aircraft obtained a DOC saving for a stage length of 880 km (475 n. mi.) of 5.9 percent for fuel at 7.92¢/liter (30¢/gal) and 8.5 percent for 15.85¢/liter. (60¢/gal) fuel. For the Boeing wing-mounted prop-fan, the DOC saving for a 963-km (520-n. mi.) stage length was 4.3 percent with 7.92¢/liter (30¢/gal) fuel and 6.5 percent with 15.85¢/liter (60¢/gal) fuel. The variation with stage length in the DOC savings reflects the trade between the fuel savings percentage decreasing with increasing stage length while fuel cost, as a fraction of DOC, increases.

The results of these 1976 design studies indicated a potential fuel saving of 10 to 20 percent for a wing-mounted prop-fan-powered aircraft relative to a comparable technology turbofan for the same mission cruising at Mach 0.8. This corresponds to a fuel saving of 20 to 40 percent relative to current turbofan aircraft, depending on the current aircraft against which the comparison is made. Accounting for all the design differences between the prop-fan and turbofan-powered aircraft, these fuel savings would result in a

saving in direct operating cost ranging from 3 to 6 percent with 7.92¢/liter (30¢/gal) fuel to 5 to 10 percent with 15.85¢/liter (60¢/gal) fuel.

Lockheed has completed a follow-on study to their original RECAT study. This study was performed to further assess the advantages of a turboprop-powered aircraft for the commercial air transportation system. The advantages of the turboprop aircraft were assessed by comparing them with an equivalent turbofan aircraft. Revised prop-fan aerodynamic and acoustic characteristics were used. The revised data supplied by Hamilton Standard reflected the results of the wind-tunnel tests of an eight-bladed propeller model and included their predictions for a 10-bladed prop-fan. The revised data show an increase in propeller net efficiency of 1.7 percent and an increase in propeller noise during Mach 0.8 cruise of 8 dB for the eight-bladed propeller tip speed of 243.8 m/sec (800 ft/sec). The propeller design trade-offs considered included variations in propeller tip speed, power blading, and number of blades. Fuselage wall-treatment-design assumptions and methods were revised. The treatment now covers the entire circumference of the cabin rather than just the sidewalls. Total treatment length is divided into five segments. Segment length and weight varies with propeller diameter, tip clearance, external sound pressure level and directivity. Also, minimum inner and outer wall weight structural design constraints were imposed for each of the five treatment segments. Besides the original mission calling for Mach 0.8 cruise and a range of 2780 km (1500 n. mi.) two alternative mission were considered: Mach 0.8 cruise with a range of 3700 km (2000 n. mi.) and Mach 0.75 cruise with a range of 2780 km (1500 n. mi.). Comparisons of turboprop and turbofan aircraft were made using alternative and advanced engine technology levels.

The block fuel results are shown in figure 17. The block fuel used by a reference turbofan aircraft for the Mach 0.8 (1500 n. mi.) mission is represented by the bottom bar. Using either of two comparable technology turboprop aircraft, the block fuel savings is 18 percent. When cruise speed is lowered from Mach 0.8 to Mach 0.75, the turboprop block fuel saving becomes 21 percent, which value reflects the higher propulsive efficiency of the turboprop at Mach 0.75. The top two bars show block fuel requirements for a 1990 IOC aircraft. The aircraft are powered by turboprop and turbofan engines having 1985 technology (refs. 4 and 5). For these higher technology engines, the turboprop block fuel savings is 17 percent.

In figure 18 comparisons of turboprop and turbofan aircraft are made in terms of direct operating cost. The PWA turboprop has an 8 percent lower DOC than the turbofan, and the DDA, 10 percent. This additional 2 percent decrease in DOC is due to a significant decrease in installed propulsion system weight. The middle two bars indicate a 10 percent DOC advantage for the turboprop aircraft at Mach 0.75. The top two bars show a comparison for 1990 IOC aircraft. The turboprop DOC saving of 8 percent is the same as for the 1985 IOC aircraft.

SUMMARY OF RESULTS

Before NASA began the Advanced Turboprop Program in October 1977 as the sixth major element in its Aircraft Energy Efficiency Program, NASA supported

some wind tunnel aerodynamic and acoustic tests of propeller models, an experimental wind tunnel program on turboprop-airframe interactions, a study of turboprop maintenance and reliability, and several studies of turboprop-powered commercial transports. These efforts have yielded some encouraging results.

At this time, three highly loaded Mach 0.8 propellers have been built and tested. One of these propellers (SR-1M) was 80 percent efficient when tested at Mach 0.8 and 70 percent of design loading. When tested at Mach 0.7, propeller efficiency was 82 percent at design loading and 85 percent at 70 percent of design loading. Early experimental results on turboprop-airframe interactions indicate that installation drag need not be large. Moreover, designing the wing to accomodate swirl in the propeller slipstream has the potential of reducing installation drag. The study of turboprop system reliability and maintenance cost concluded that an advanced turboprop and an advanced turbofan, using similar cores, would have very competitive maintenance costs. A recent study to assess the potential of turboprop-powered aircraft relative to turbofan-powered aircraft confirms the earlier study results. With 15.85¢/liter (60¢/gal) fuel, the DOC advantage of the turboprop aircraft is about 10 percent. The fuel saving for medium-range turboprop-powered aircraft is 21 percent for Mach 0.75 aircraft and 17 percent for Mach 0.8 aircraft.

REFERENCES

1. Klineberg, J. M.: Technology for Aircraft Energy Efficiency. Presented at the American Society of Civil Engineers, International Air Transportation Conference, (Wash., D.C.), Apr. 4-6, 1977.

2. Neitzel, R. E.; Hirschkron, R.; and Johnston, R. P.: Study of Turbofan Engines Designed for Low Energy Consumption. (R76AEG432, General Electric Co., NASA Contract NAS3-19201.) NASA CR-135053, 1976.

3. Neitzel, R. E.; Hirschkron, R.; and Johnston, R. P.: Study of Unconventional Aircraft Engines Designed for Low Energy Consumption. (R76AEG597, General Electric Co.; NASA Contract NAS3-19519.) NASA CR-135136, 1976.

4. Gray, D. E.: Study of Turbofan Engines designed for Low Energy Consumption. (PWA-5318, Pratt & Whitney Aircraft; NASA Contract NAS3-19132.) NASA CR-135002, 1976.

5. Gray, D. E.: Study of Unconventional Aircraft Engines Designed for Low Energy Consumption. (PWA-5434, Pratt & Whitney Aircraft; NASA Contract NAS3-19465.) NASA CR-135065, 1976.

6. Dugan, J. F.; Bencze, D. P.; and Williams, L. J.: Advanced Turboprop Technology Development. AIAA Paper 77-1223, Aug. 1977.

7. Rohrbach, C.: A Report on the Aerodynamic Design and Wind Tunnel Test of a Prop-Fan Model. AIAA Paper 76-667, July 1976.

8. Mikkelson, D. C., et al.: Design and Performance of Energy Efficient Propellers for Mach 0.8 Cruise. SAE Paper No. 770458, Mar. 1977.

9. Foss, R. L.; and Hopkins, J. P.: Fuel Conservation Potential for the Use of Turboprop Powerplanes. SAE Paper 760537, May 1976.

10. Hopkins, J. P.; and Wharton, H. E.: Study of the Cost/Benefit Tradeoffs for Reducing the Energy Consumption of the Commercial Air Transportation System. (LR-27769-1, Lockheed-California Co.; NASA Contract NAS2-8612.) NASA CR-137927, 1976.

11. Hopkins, J. P.: Study of the Cost/Benefit Tradeoffs for Reducing the Energy Consumption of the Commercial Air Transportation System. (LR-27769-2, Lockheed-California Co.; NASA Contract NAS2-8612.) NASA CR-137926, 1976.

12. Stern, J. A.: Aircraft Propulsion - A Key to Fuel Conservation: An Aircraft Manufacturer's View. SAE Paper 760538, May 1976.

13. Kraus, E. F.: Cost/Benefit Tradeoffs for Reducing the Energy Consumption of Commercial Air Transportation System. Vol. I: Technical Analysis. (MDC-J7340-Vol.-1, Douglas Aircraft Co., Inc.; NASA Contract NAS2-8618.) NASA CR-137923, 1976. Van Abkoude, J. C.: Cost/Benefit Tradeoffs for Reducing the Energy Consumption of Commercial Air Transportation System. Vol. II: Market and Economic Analyses. (MDC-J7340-Vol.-2, Douglas Aircraft Co., Inc.; NASA Contract NAS2-8618.) NASA CR-137925, 1976.

14. Energy Consumption Characteristics of Transports Using the Prop-Fan Concept: Summary (D6-75780, Boeing Commercial Airplane Co.; NASA Contract NAS2-9104.) NASA CR-137938, 1976.

15. Energy Consumption Characteristics of Transports Using the Prop-Fan Concept: Final Report. (D6-75780, Boeing Commercial Airplane Co.; NASA Contract NAS2-9104.) NASA CR-137937, 1976.

16. Shollenberger, C. A.: Three-Dimensional Wing/Jet Interaction Analysis Including Jet Distortion Influences. J. Aircraft, vol. 12, no. 9, Sep. 1976, pp. 706-713.

17. Rubbert, P. E.; and Saaris, G. R.: Review and Evaluation of a Three-Dimensional Lifting Potential Flow Computational Method for Arbitrary Configurations. AIAA Paper 72-188, Jan 1972.

18. Hess, J. L.: Calculation of Potential Flow About Arbitary Three-Dimensional Lifting Bodies. MDC-J5679-01, Douglas Aircraft Co., Inc., 1972.

19. Stolp, P. C.; and Baum, J. A.: Advanced Turboprop Propulsion System Reliability and Maintenance Cost. SAE Paper-771009, Presented at the SAE Aerospace Engineering and Manufacturing Meeting, (Los Angeles, Calif.), Nov. 14-17, 1977.

TABLE I. - MEASURED MODEL PROPELLER PERFORMANCE[a]

[Advance ratio, J, 3.06; power coefficient, C_p, 1.7.]

Configuration	Blade tip sweep, deg	Design point efficiency,[b] %		Measured efficiency,[c] percent
		Current prediction	Test data	
SR-1	30	78.9	77.1	80.2
SR-1M	30	79.2	77.1	81.7
SR-2	0	76.6	77.0	80.2

[a]Data taken in the Lewis 8- by 6-foot wind tunnel.
[b]Mach 0.8; power loading, 310 kW/m^2 (37.5 hp/ft^2); tip speed, 244 m/sec (800 ft/sec).
[c]Mach 0.7.

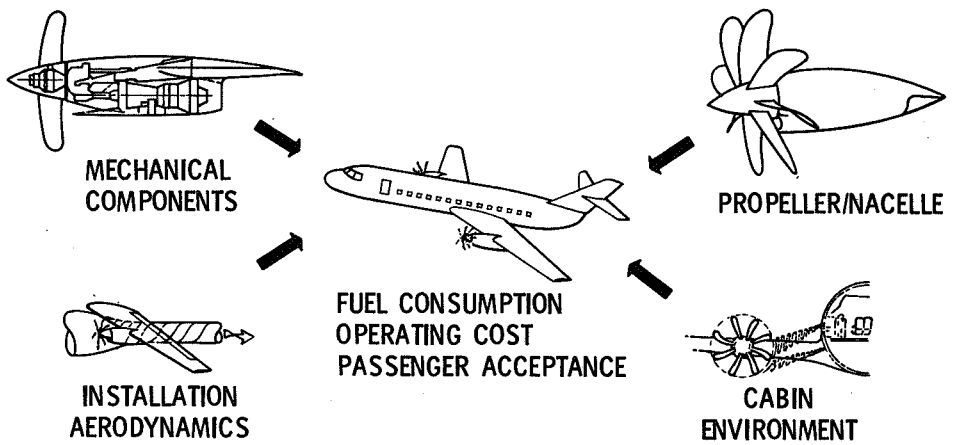

Figure 1.- Major areas of advanced turboprop program.

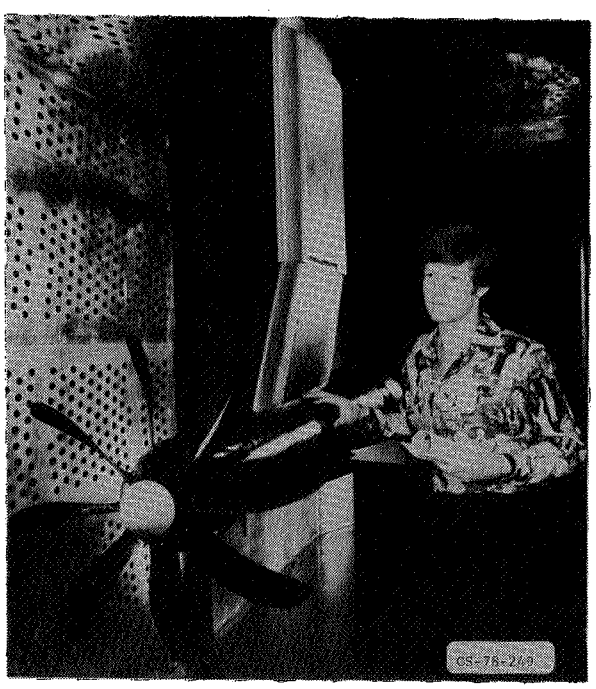

Figure 2.- Propeller model in Lewis wind tunnel.

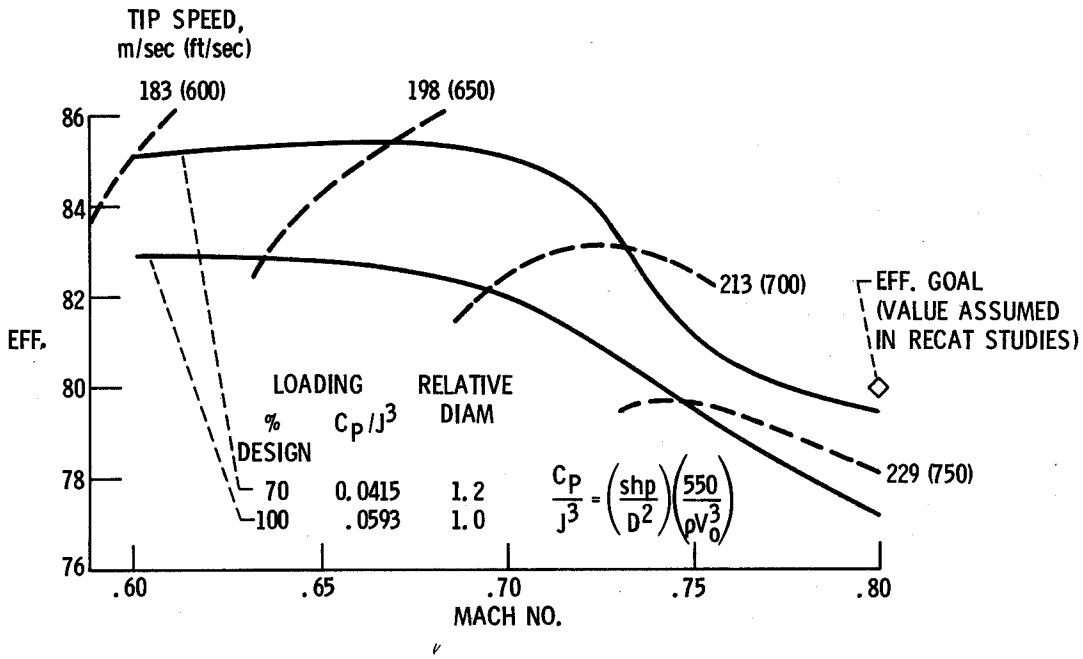

Figure 3.- Effect of cruise Mach number on efficiency. Propeller model SR-1M; data taken in Lewis 8- by 6-ft wind tunnel; blade angle and tip speed varied for maximum life.

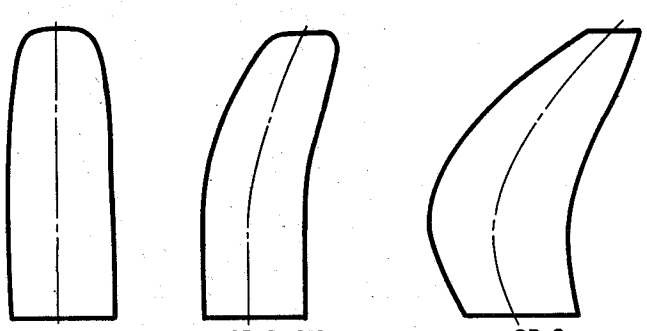

	SR-2	SR-1, 1M	SR-3
TIP SPEED, m/sec (ft/sec)	244 (800)	244 (800)	244 (800)
POWER LOADING, P/D^2, kW/m^2 (shp/ft^2)	301 (37.5)	301 (37.5)	301 (37.5)
NO. OF BLADES	8	8	8
TIP SWEEP ANGLE, deg	0	30	45
DESIGN EFF., %	77	79	81
DESIGN NOISE LEVEL, dB	143	143	137

Figure 4.- Comparison of propeller models.

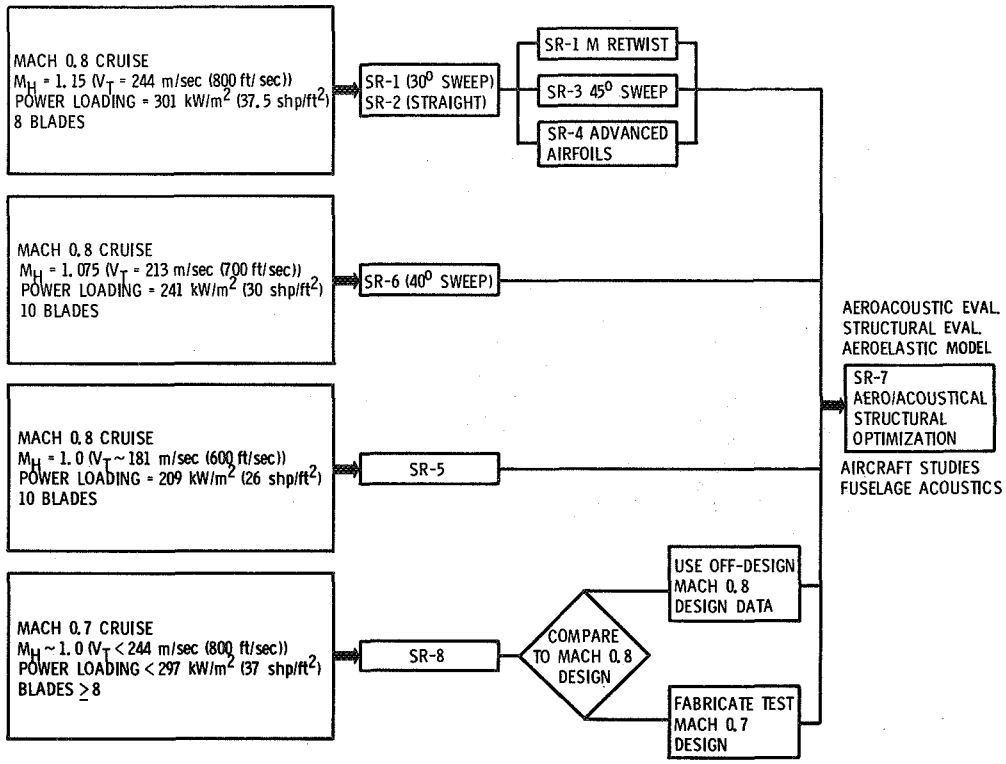

Figure 5.- Current propeller model performance test program.

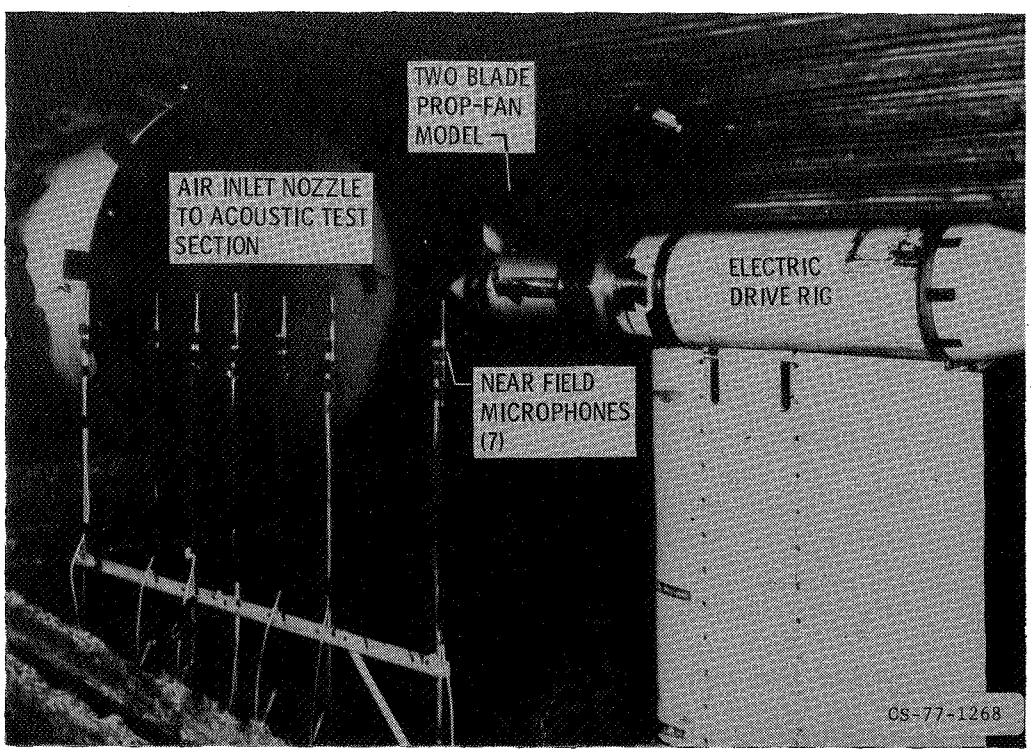

Figure 6.- Propeller model tests in UTRC acoustic research tunnel.

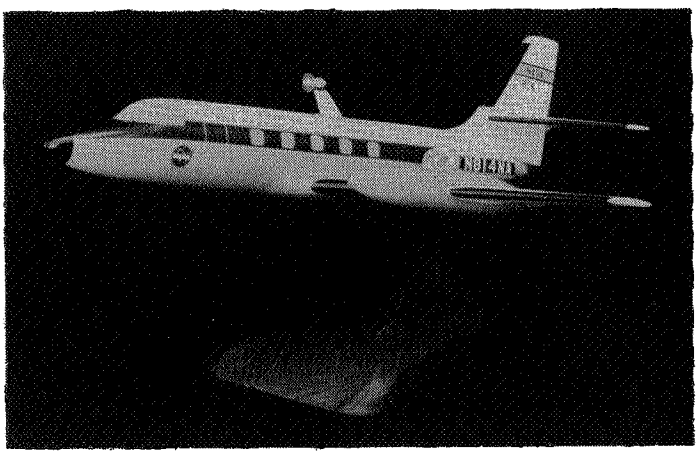

Figure 7.- Depiction of propeller model mounted on aircraft for acoustic tests.

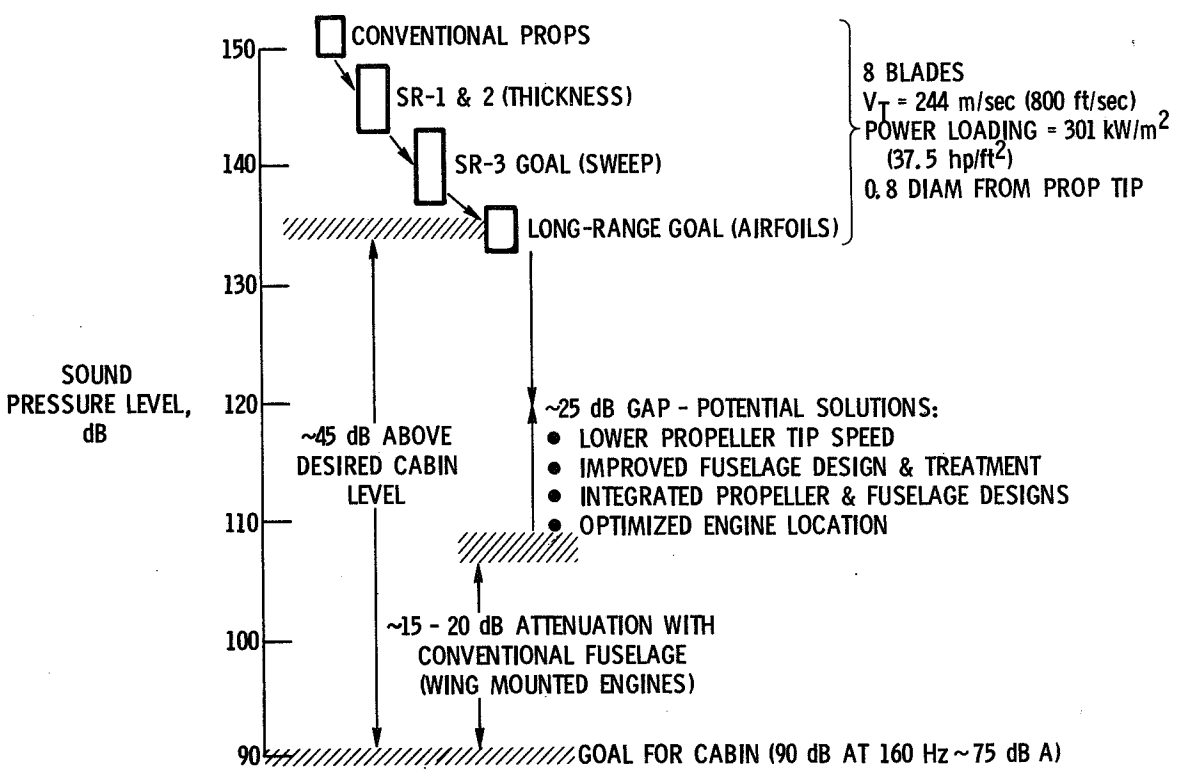

Figure 8.- Propeller and cabin noise. Cruise speed, Mach 0.8; altitude, 10.67 km (35 000 ft).

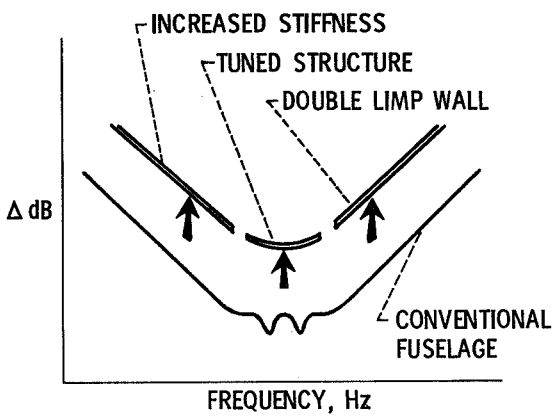

(a) Effect of frequency.

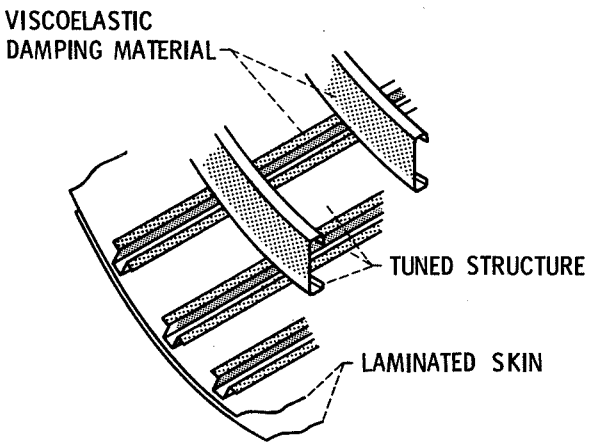

(b) Tuned structure.

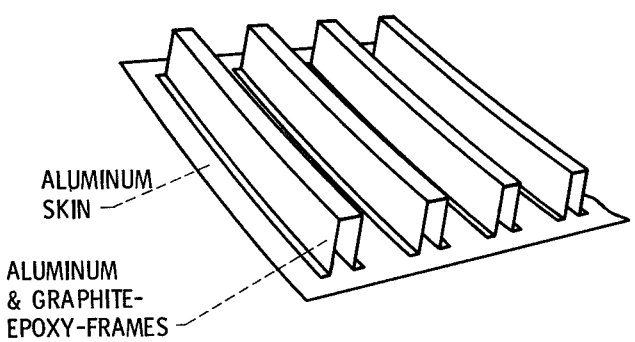

(c) Increased stiffness.

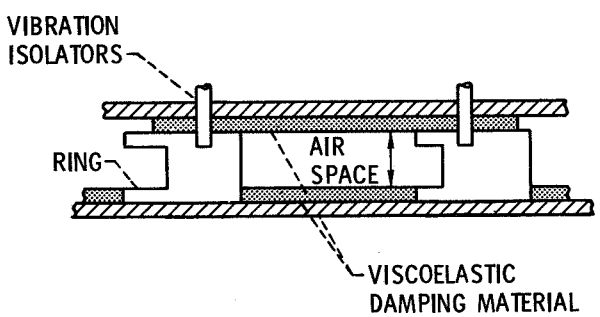

(d) Double limp wall.

Figure 9.- Fuselage structural concepts for propeller noise reduction.

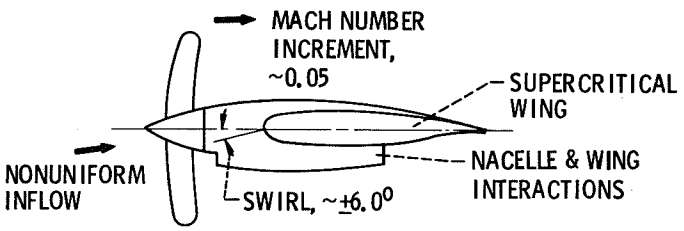

- ASSESS MAGNITUDE OF AERODYNAMIC INTERFERENCE
- UNDERSTAND AERODYNAMIC PHENOMENA
- DEVELOP ANALYTICAL & EXPERIMENTAL DATA BASE
- USE SLIPSTREAM SIMULATOR & POWERED SEMISPAN MODEL

Figure 10.- Airframe-propulsion system integration program.

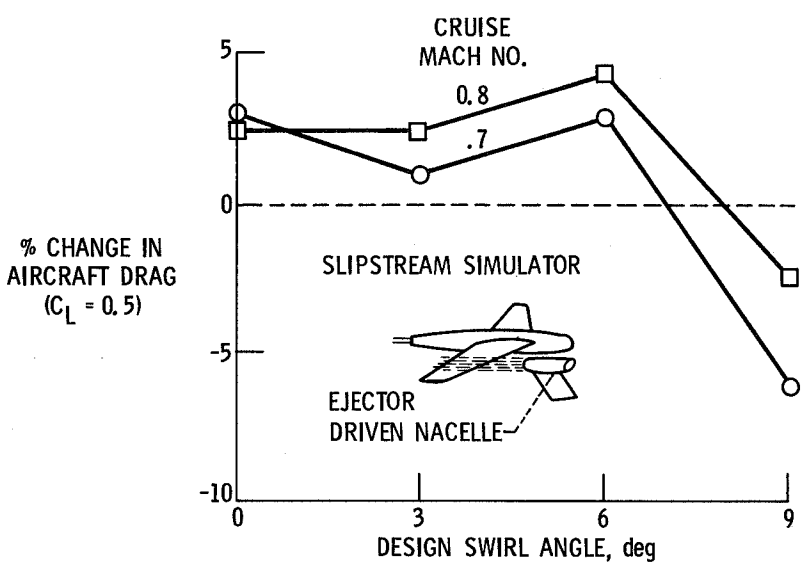

Figure 11.- Effect of simulated slipstream on aircraft cruise drag. Preliminary ARC wind tunnel data. Slipstream Mach number variation, 0.075.

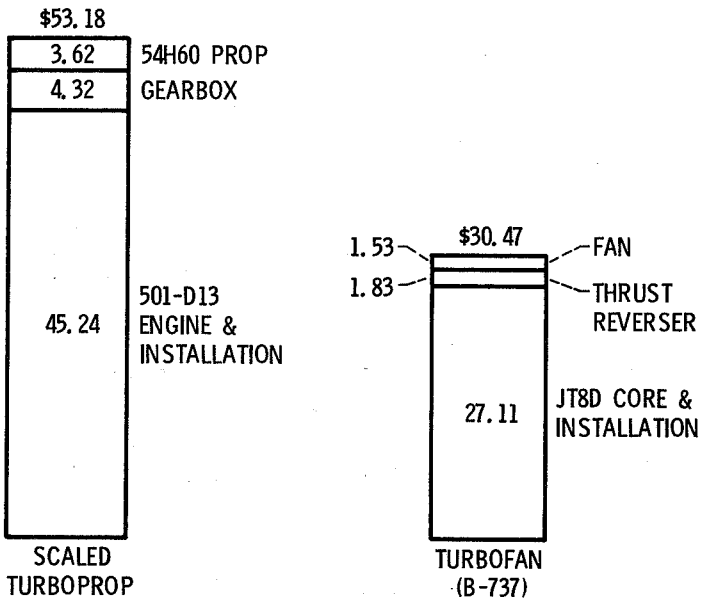

Figure 12.- Comparison of 1960-era turboprop and turbofan maintenance costs. Fully burdened cost in 1976 dollars per flight hour; duty cycle, 1.3 per engine flight hour.

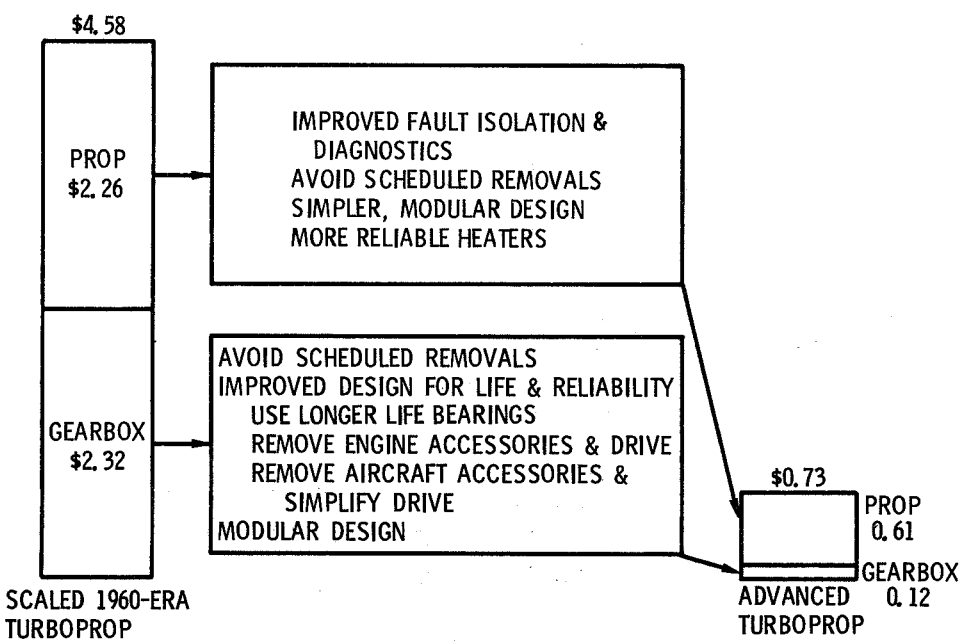

Figure 13.- Maintenance cost reduction for propeller and gearbox. Unburdened costs in 1976 dollars per flight hour; duty cycle, 1.25 per flight hour.

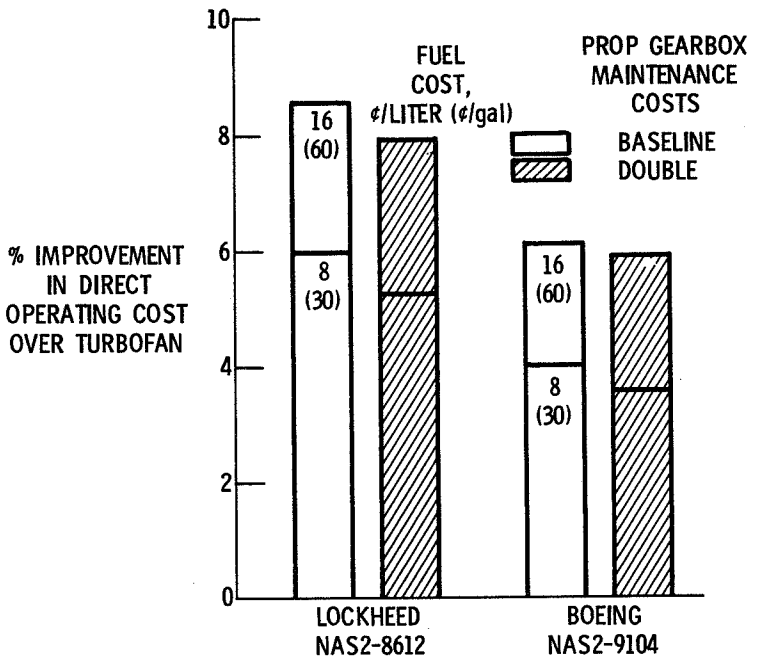

Figure 14.- Direct operating cost sensitivity to propeller and gearbox maintenance costs.

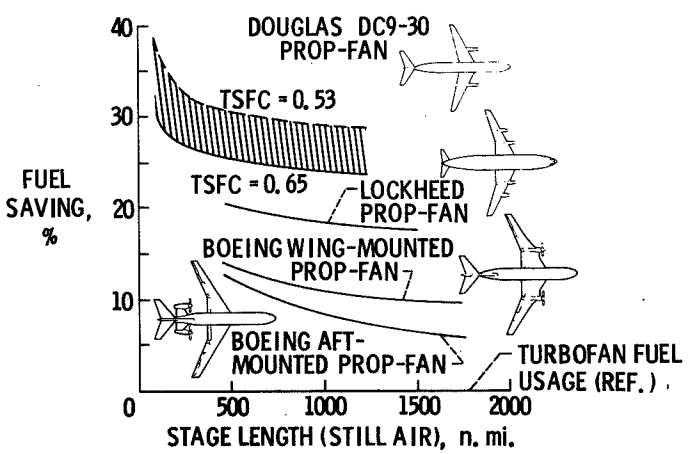

Figure 15.- Turboprop aircraft fuel savings.

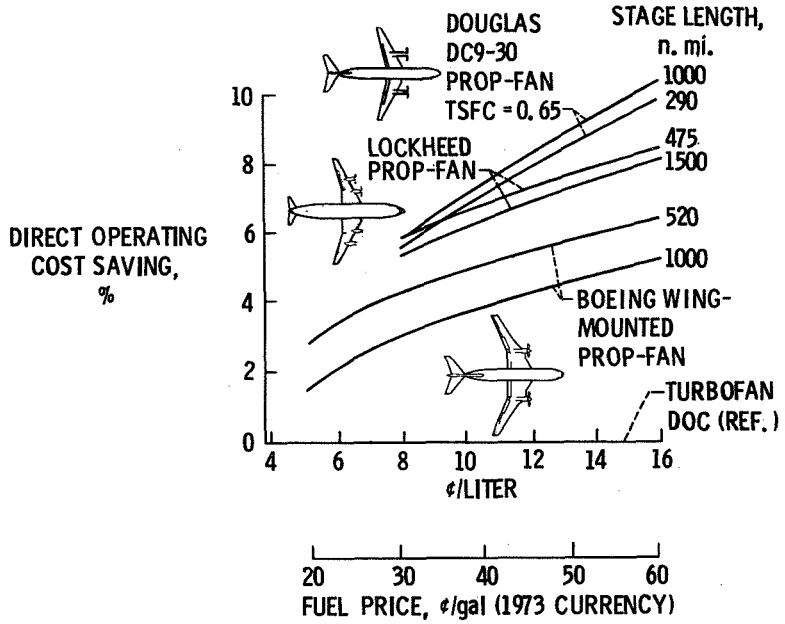

Figure 16.- Turboprop aircraft operating cost savings.

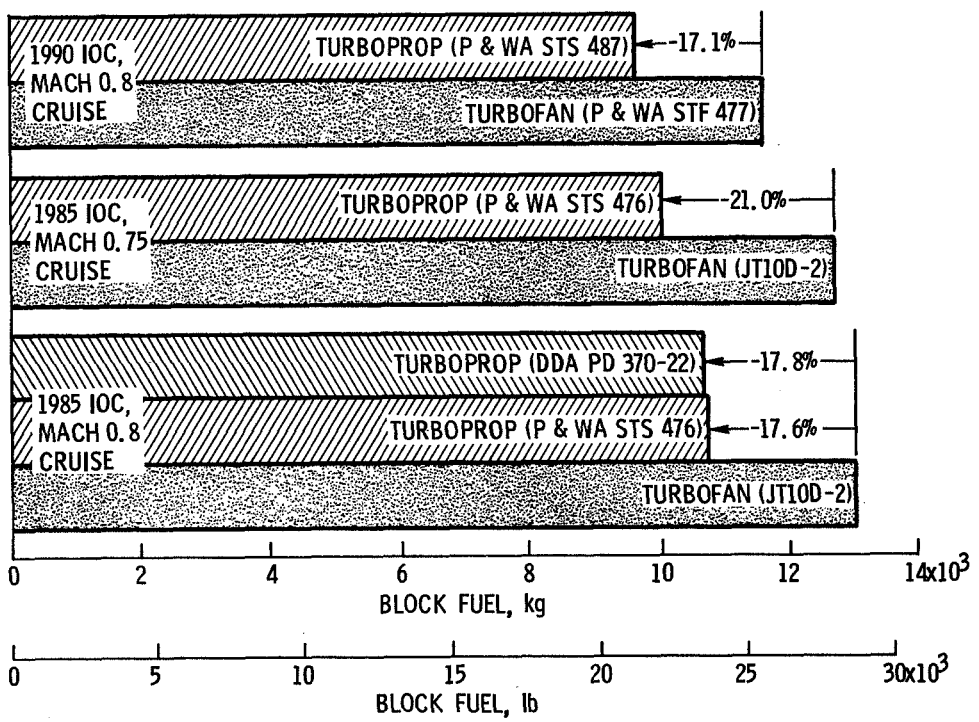

Figure 17.- Effect of aircraft design on block fuel usage. Data from Lockheed RECAT follow-on study (NAS2-8612). Mission Characteristics: Number of passengers, 200; trip distance, 2780 km (1500 n. mi.); load factor, 100 percent. Design characteristics: four wing-mounted engines; eight-bladed propellers (on turboprops).

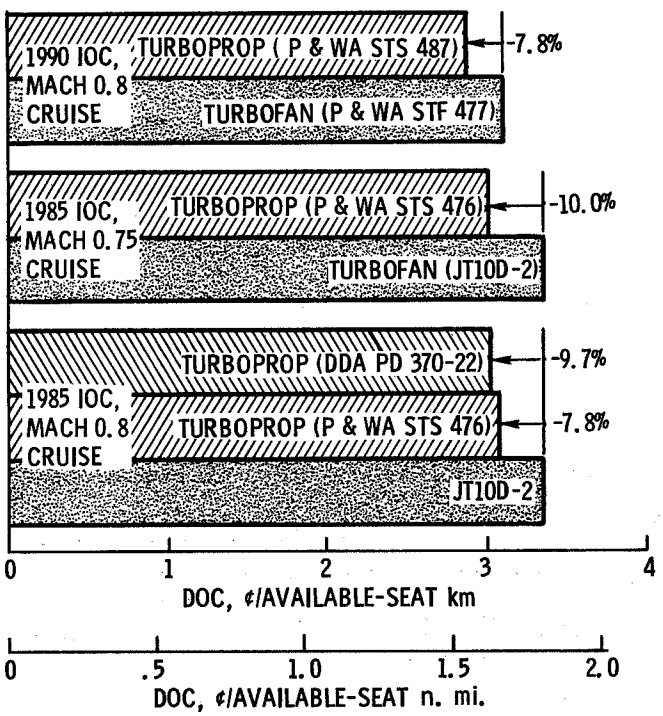

Figure 18.- Effect of aircraft design on direct operating costs. Data from Lockheed RECAT follow-on study (NAS2-8612). Mission characteristics: Number of passengers, 200; trip distance, 2780 km (1500 n. mi.); load factor, 100 percent. Design characteristics: four wing-mounted engines; eight-bladed propellers (on turboprops). Fuel cost, 15.85¢/liter (60¢/gal).

PROPULSION SYSTEMS NOISE TECHNOLOGY

C. E. Feiler
Lewis Research Center

SUMMARY

Recent turbofan engine noise research relevant to conventional aircraft is discussed. In the area of fan noise, static to flight noise differences are discussed and data are presented for two different ways of simulating flight behavior. These results show that simulation of flight behavior should be possible in ground-based facilities. Experimental results from a swept-rotor fan design are presented which show that this concept has potential for reducing the multiple-pure-tone or buzz-saw noise related to the shock waves on a fan operating at supersonic tip speeds. Acoustic suppressor research objectives have centered recently around the effect of the wave system generated by the fan stage that is the input to the treatment. A simplifying and unifying parameter, mode cutoff ratio is described. This parameter appears to correlate all aspects of the propagation and attenuation of sound in acoustically treated ducts and its radiation to the far field. Results are presented which show that suppressor performance can be improved if the input wave is more precisely described. In jet noise, calculated results showing the potential noise reduction from the use of internal mixer nozzles rather than separate-flow nozzles are presented. Finally, estimates of the noise of aircraft using E^3 engines are shown relative to the present FAR Part 36 noise regulations.

INTRODUCTION

This paper summarizes some of the recent research into turbofan engine noise at Lewis Research Center. Progress in noise abatement can be illustrated by reference to FAA Noise Certification Levels and estimated levels for commercial aircraft and to the FAR Part 36 Noise Regulations. These are displayed in figures 1(a) and (b) for the takeoff and approach measuring points (refs. 1 to 4). Flyover noise levels are shown for narrow-bodied aircraft with low-bypass engines and for the newer wide-bodied aircraft with high-bypass engines. Also shown in the figures is the first FAA Noise Regulation (the top curve in each figure), which became a certification standard in 1969. The narrow-bodied aircraft with their low-bypass engines generally exceeded the 1969 noise standard at both takeoff and approach. Their noise levels are dominated by jet noise at takeoff and fan noise at approach. The wide-bodied aircraft with their high-bypass engines generally are quieter than the 1969 noise rules at both takeoff and approach. This is a consequence of the lower jet noise of the high bypass engine, of fan noise reduction design features, and of the use of acoustic treatment. These noise reductions were obtained even though aircraft size was about doubled.

The figures also show the more stringent 1977 noise certification standards. The figures also show data from two research programs directed toward lowering the noise of the low-bypass engines used on the narrow-bodied aircraft. These programs are the Quiet Nacelle program and the Refan Engine program. The former sought to reduce engine noise through the extensive use of acoustic treatment in the engine nacelle, and the latter involved an engine modification that included a new single-stage fan with quieting features, an increase in engine bypass ratio, and extensive acoustic treatment in the nacelle. Both programs demonstrated lower noise technology for the bypass engines. Retrofit programs for existing aircraft have not emerged; however, the McDonnell Douglas DC-9 Super 80 aircraft using Pratt & Whitney JT8D-209 refanned engines has been introduced.

It is clear that substantial reductions in aircraft noise have been achieved since the introduction of the jet-powered fleet. But, as the louder component noise sources are quieted, further reductions become more difficult because the number of component sources contributing increases and measurable change in the noise level requires that all sources be reduced together. In the presence of multiple sources, little reduction in the noise an observer hears occurs if only one source is reduced or even completely eliminated. Thus, for several years, aircraft noise reduction research has proceeded along a broad front, addressing several different noise sources that involve very different technical disciplines. Some of this research will be discussed in this paper, and some estimates of the noise levels for aircraft powered with engines from the NASA Energy Efficient Engine Program will be given.

TURBOFAN NOISE SOURCES

Figure 2 shows, as a memory refresher, the often-used turbofan engine schematic outlining the major engine noise sources. For the high bypass engines being considered today for lower noise and greater fuel economy, these are the important noise sources. The present paper will discuss fan noise research and reduction concepts, acoustic suppressor research, and, briefly, jet noise and the concept of internal mixer nozzles.

JET NOISE

The most effective means of controlling jet noise is through engine cycle selection. Basically this involves keeping the jet exhaust velocities as low as possible. In practice, for turbofan engines this results in higher engine bypass ratios. The basic dependence of jet noise on bypass ratio is shown in figure 3.

The upper curve, for coaxial nozzles, was calculated by the interim prediction method for jet-noise reported in reference 5. The points are calculated for current engines and have been normalized to the same engine thrust.

The lower curve is the calculated noise, according to reference 5, for the same engines operating with an ideal mixer nozzle. This calculation assumed perfect mixing of the core and bypass fan jets without any generation

of noise due to mixing. The mixer nozzle concept has received some attention recently as a means of increasing engine fuel economy and reducing jet noise. Comparison of the coaxial and mixer nozzle curves suggests that under ideal circumstances the mixer nozzle may reduce jet noise up to 5 or 6 PNdB. In practice the reduction will be less than this because of imperfect mixing and the generation of internal mixing noise that will radiate to the farfield.

A single data point is shown from a study program sponsored by the FAA (ref. 6). This point, for an engine bypass ratio near unity, shows an experimental noise reduction relative to the coaxial nozzle of 3 to 4 PNdB. The use of mixer nozzles may be most important for growth versions of an engine whose jet noise would increase as the engine bypass ratio is reduced. The mixer nozzle might then be used to reduce the jet noise level to near that of the original engine cycle.

FAN NOISE

Forward Velocity Effects

Over the last year or two the chief emphasis in fan noise has been on the differences between static test and flight test results. (See ref. 7.) The differences are illustrated in figure 4 by the spectra from inlet-wall microphones taken during the static and flight operation of several engines. The data are shown at two fan tip speeds, one approximating takeoff speed and one approximating approach speed. Generalized behavior patterns are difficult to define, but it can be seen that the fan fundamental tone is lower for all the engines operating at the lower speed. In some cases reductions in the broadband occurred over a range of frequencies.

The reason for these results is represented in figure 5, which suggests that the differences in fan noise between static and flight operation are due to the presence and ingestion of flow disturbances into the inflow during static operation. In static testing, because of the effectively large inflow contraction, atmospheric turbulence is elongated by the contraction. The resulting long turbulence eddies, along with possible ground vortices and wakes from adjacent engine support structure and other hardware, are seen by the fan blades as variations in upwash or incidence angle. Depending on the length or time duration of such local disturbances, the fan generates tone or broadband noise.

During flight, on the other hand, the overall inflow is considerably more uniform and the effective contraction ratio is considerably lower, resulting in lower noise. The importance of this is the realization that, in many cases, the noise of a fan stage during static testing is due to a source mechanism either not present or of diminished importance during flight. Two consequences are that flight noise tends to be overpredicted by static test data and that source noise reduction concepts, generally related to the rotor-stator interaction noise source, prove to be ineffective in static experiments because they are masked by the noise due to inflow disturbances.

These considerations have led to a search for methods and techniques of static testing that simulate the flight behavior of fan noise. One successful tool is the anechoic wind tunnel. Figure 6 shows the Lewis 9- by 15-foot low-speed, anechoic wind tunnel with a 51-cm (20-in.) model fan stage in a nacelle. A description of this tunnel is given in reference 8.

Another tool is a flow-straightening, turbulence-damping structure. A schematic representation of such a device is shown in figure 7 as it has been employed in an anechoic chamber. This structure approximates a hemisphere and consists of flexible core aluminum honeycomb supported by a coarse mesh screen. The honeycomb cell's effective length to diameter ratio was about eight. The honeycomb cell walls were approximately parallel to the flow streamlines. A second smaller mesh screen is used between the honeycomb and the coarse screen to further control the turbulence. This control structure has been tested on a fan in the 9- by 15-foot anechoic wind tunnel (ref. 9) and in an anechoic chamber (ref. 10). A photograph of the structure mounted on the fan inlet in the Lewis anechoic test chamber is shown in figure 8.

A series of experiments has been performed in the anechoic wind tunnel in which fan-inlet noise was measured for a clean, unobstructed inlet both statically and with forward velocity and for two variations of the inflow control structure. These experiments are described in detail in reference 9; the fan stage and other aeroacoustic results are described in references 11 to 14. The fan stage had a design tip speed of 213 m/sec and a design pressure ratio of 1.2.

Figure 9 shows far-field narrowband sound spectra for each of the inflow conditions. Just as for the engine data of figure 4, these data show that forward velocity substantially lowered the fan fundamental tone. In fact for this particular fan stage the tone was reduced essentially to the broadband level. The use of the inflow control structure also reduced the fan fundamental tone, but not to the extent that forward velocity did. An interesting clue to part of the tone-causing disturbance is shown by the data with the inflow control structure when the aft portion was covered to prevent flow in the reverse direction over the exterior of the inlet. Preventing this flow from entering the inlet was beneficial in reducing the tone compared with the case when the aft portion was open to pass flow. This suggests that flow over the nacelle exterior, where there are probes and other obstructions that can generate flow disturbances, may be one of the tone noise sources. It may be also that the flow around the inlet highlight would be more disturbance free if the reverse flow over the nacelle, which is turned 180°, is minimized.

In any case, the results are encouraging and show that a properly designed inflow control structure can produce data more like those in flight. This area is receiving considerable attention under a joint program among the NASA Langley, Lewis, and Ames Research Centers.

Fan Noise-Reduction Concepts

The primary objective in fan noise research is to understand the sources and mechanisms of noise sufficiently well that low-noise designs can be developed. A photograph of a fan stage that uses two noise-reduction concepts is shown in figure 10. This fan design was proposed by the firm of Bolt, Beranek, and Newman in response to a Lewis request (refs. 15 and 16). One of the noise-reduction concepts is intended to reduce the shock-related multiple pure tone or buzz-saw noise that the fan will generate at its design tip speed of 488 m/sec. The concept is to sweep the rotor leading edge so that the velocity normal to the blade is subsonic, thereby eliminating the shock-wave system. This idea is the same one used in swept-wing supersonic aircraft. In the design sweep reversal midway along the span avoids the structural problems that might result from having the blades cantilevered too far forward or backward. The other noise-reduction concept, intended to reduce rotor-stator interaction noise, is to sweep the stator vanes back axially from hub to tip.

This fan stage was tested recently in the Lewis anechoic chamber. The results are shown in figure 11 where inlet sound power spectrum of the swept rotor fan stage is compared with spectra from two earlier supersonic-tip-speed fans. These fans are engine C of the NASA-GE Quiet Engine program and the ATT fan tested under the NASA-GE Advanced Transport Technology program (ref. 17). The swept-rotor fan stage produced about 10 decibels less noise than the earlier fans did in the spectral region below the blade passing frequency. The sound in this frequency range is associated with the shock-related noise and thus the swept-rotor concept did work. Some smaller benefits are also apparent at frequencies higher than the blade passing frequency. It should be noted that the swept-rotor data and ATT fan data were scaled to the engine C data. Sound power was scaled proportional to fan diameter squared and frequency inversely proportional to fan diameter. This scaling procedure may not be exact but is adequate for comparison. Fortunately the three fans do not differ greatly in tip speed and pressure ratio. The aerodynamic efficiency of the swept rotor fan stage was about 77 percent compared with a design value of about 86 percent. Although the performance was low, it is perhaps not too surprising in view of the unusual features of the fan design.

ACOUSTIC SUPPRESSION

Acoustic suppression research has been one of the more active areas recently. The elements of the acoustic suppressor problem are illustrated in figure 12. The problem is focussed on the propagation and attenuation of a sound field as it traverses through an inlet or exhaust duct whose walls have been treated acoustically. One of the needed inputs to suppressor analysis and design is a description of the sound field generated by the fan stage at the entrance to the treated duct. An exact description of this field is very difficult to obtain and has not been measured for fan stages operating in realistic engine tests. Thus, the input wave was often assumed to be a plane pressure wave or a wave consisting of only the least attenuated mode, on the ground that these would yield conservative estimates for suppressor design. Indeed, these assumptions proved to be far too conservative when used to estimate the acoustic performance of inlet-wall-only suppressors although they are adequate

for annular ducts or ducts with splitter rings (ref. 18). It is clear today that correct description of the input sound source field is necessary to design and to predict the performance of acoustic suppressors.

The spatial pattern of the sound field generated by a fan at a plane axially removed from the fan is described in terms of circumferential and radial coordinates. The pattern in the circumferential direction consists of an integral number of lobes and it has been shown that this pattern rotates or spins in the duct (ref. 19). There is a similar periodicity of the spatial pattern in the radial direction. Each of the discrete patterns consisting of an integral number of lobes both radially and circumferentially is termed a mode. It is this modal pattern, generated by the fan stage, that the sound suppressor must attenuate and that finally radiates in modified form from the duct termination to the far-field, where it determines the far-field sound pattern or directivity. Thus, all of the events relating to the sound field, including the design of the acoustic treatment and its performance, depend on the modes that are present in the pressure pattern and on the sound frequency. At any given sound frequency the duct can and does sustain many modes, which the fan generates. The number of modes increases with sound frequency.

The sound-field description, as just outlined, is a three-parameter representation determined by the sound frequency and the circumferential and radial mode numbers. A recent advance in duct acoustics theory was the observation by Rice that these three parameters could be replaced by a single simplifying and unifying parameter, called cutoff ratio (refs. 20 and 21). This parameter correlates the optimum wall impedance of suppressors, the associated sound attenuation, the effect of the duct termination, and the far-field radiation pattern (refs. 22 and 23). The cutoff ratio is not easily depicted in a circular duct, but it can be clearly shown in a two-dimensional duct (fig. 13). In figure 13 a wave front is represented by a line that, in general, propagates with some angle ψ to the duct axis. The cutoff ratio is given in this simple geometry by the reciprocal of the sine of the propagation angle. Figure 13 also illustrates the two extremes of propagation. An infinite cutoff ratio is shown for a plane wave that always propagates if present, and a cutoff ratio of one is shown for a transverse wave that does not propagate axially at all. The cutoff ratio thus describes, in this simple case, the propagation direction of the sound wave relative to the duct axis.

For simple situations where the number of modes is limited, the sound input wave can be experimentally determined directly from an array of pressure sensors located around the duct wall. In general, radial measurements are also required; however, the introduction of a radial probe into the duct will affect the sound field generated by the fan (as discussed in the preceding section). Theoretical models of fan source noise also yield the input wave; however, these depend on the adequacy of the description of the unsteady aerodynamics and the flow disturbances that are present but not usually known. A third method is to infer the input wave from the far-field directivity of a fan stage. In this case, the effects of factors such as the duct termination, atmospheric scattering, and convective flow field into the inlet should be included. Some success with this method has been reported (ref. 24).

When more accurate descriptions of the input wave are used to design suppressors, their performance can be improved. Figure 14 shows the experimental results from suppressors for multiple-pure-tone noise that were tested on the AVCO-Lycoming YF-102 engine and on the NASA GE engine C at Lewis. The data plotted are the sound-power attenuations in the one-third-octave band containing the peak multiple-pure-tone levels. A single suppressor length was tested on the YF-102 engine; it yielded a sound power suppression of about 48 dB per unit of suppressor L/D. This result is compared with an earlier result from the NASA-GE engine C suppressor tests. The suppressor on engine C was designed in accordance with the then current plane-wave sound-input theory. Clearly, the more recent theory represents a significant improvement in suppressor performance. Current experiments are further exploring the benefits of incorporating these advances in suppressor concepts and theories.

CONCLUDING REMARKS

Engine noise research has progressed in a broad range of disciplines involving all of the noise sources. Progress is reflected by improved understanding of the sources and by the demonstration of concepts that have lead to lower noise. Cycle selection remains the best control of jet noise, with the use of mixer nozzles showing some promise for further reductions. In fan noise the effects of flight are the subject of considerable attention, and promising means of simulating flight were shown. A new fan design concept, the swept rotor is effective in reducing the source levels of multiple-pure-tone or buzz-saw noise. In acoustic suppressors a more accurate discription of the input source wave allows designers to improve suppressor performance. A simple parameter unifying all aspects of duct propagation, including optimum wall impedance, attenuation, and radiation was described. The parameter, cutoff ratio, is the focal point of further exploration of suppressor behavior.

The data and noise certification standards shown in figure 1 are shown again in figure 15 with noise estimates from the NASA Energy Efficient Engine Program added as an illustration of possibilities in aircraft noise. The E^3 program is not aimed at noise, per se, and the noise goals of the program are the FAR Part 36, 1977, certification standards. Nevertheless, the estimates for three and four engine aircraft predict noise levels 3 to 4 decibels below the FAR Part 36, 1977, noise standards at both takeoff and approach. The approach estimates are nearing the levels for airframe noise (ref. 25) shown in the figure. As the title of reference 24 indicates, "airframe" noise is a barrier that may require reduction if the overall aircraft noise levels are reduced much further. The outlook for success in exceeding the FAR 36 - 1977 noise standards is good.

REFERENCES

1. Foster, Charles R.: Status Report on Aircraft Noise Certification. NOISE - CON '77 Proceedings, G. C. Maling, Jr., ed., Noise Control Foundation, 1977, pp. 11-40.

2. Certificated Airplane Noise Levels. Advisory Circular 36-1A, Federal Aviation Admin., 7/21/75.

3. Estimated (Uncertificated) Noise Levels of Aircraft. Advisory Circular 36-2, Federal Aviation Admin., 9/21/76.

4. Noise Level Limits and Acoustical Change Requirements for Subsonic Transport Category, Large Airplanes and for Subsonic Turbojet Powered Airplanes. Federal Aviation Regulations, Part 36, Amendment 7, Effective 10/1/77. Federal Register, vol. 42, no. 42, Mar. 3, 1977, p. 12360.

5. Stone, James R.: Interim Prediction Method for Jet Noise. NASA TM X-71618, 1974.

6. Packman, A. B.; and Eiler, D. C.: Internal Mixer Investigation for JT8D Jet Engine Noise Reduction. Final Report, FAA-RD-77-132, 1976.

7. Feiler, Charles E.; and Groeneweg, John F.: Summary of Forward Velocity Effects on Fan Noise. NASA TM-73722, 1977.

8. Diedrich, James H.; and Luidens, Roger W.: Measurement of Model Propulsion System Noise in a Low-Speed Wind Tunnel. NASA TM X-71845, 1976.

9. Shaw, Loretta M.; et. al.: Inlet Turbulence and Fan Noise Measured in an Anechoic Wind Tunnel and Statically with an Inlet Flow Control Device. NASA TM-73723, 1977.

10. Woodward, R. P.; et. al.: Effectiveness of an Inlet Flow Turbulence Control Device to Simulate Flight Fan Noise in an Anechoic Chamber. NASA TM-73855, 1977.

11. Heidmann, M. F.; and Dietrich, D. A.: Simulation of Flight-Type Engine Fan Noise in the NASA-Lewis 9×15 Anechoic Wind Tunnel. NASA TM X-73540, 1976.

12. Dietrich, Donald A.; Heidmann, Marcus F.; and Abbott, John M.: Acoustic Signatures of a Model Fan in the NASA-Lewis Anechoic Wind Tunnel. NASA TM X-73560, 1977.

13. Lewis, George W., Jr.; and Tysl, Edward R.: Overall and Blade-Element Performance of a 1.20-Pressure-Ratio Fan Stage at Design Blade Setting Angle. NASA TM X-3101, 1974.

14. Glaser, Fredrick W.; Woodward, Richard P.; and Lucas, James G.: Acoustic and Aerodynamic Performance of a Variable-Pitch 1.38-Meter-(6-ft-) Diameter 1.20-Pressure-Ratio Fan (QF-9). NASA TN-8402, 1977.

15. Hayden, Richard E.; et. al.: Analysis and Design of a High Speed, Low Noise Aircraft Fan Incorporating Swept Leading Edge Rotor and Stator Blades. (BBN-3332, Bolt, Beranek, and Newman, Inc.; NASA Contract NAS3-18512.) NASA CR-135092, 1977.

16. Bliss, D. B.; et al.: Design Considerations for a Novel Low Source Noise Transonic Fan Stage. AIAA Paper 76-577, July 1976.

17. Jutras, R. R.: Single Stage, Low Noise, Advanced Technology Fan. Volume V, Fan Acoustics, Sect. 1: Results and Analysis. (General Electric Co.; NASA Contract NAS3-16813.) NASA CR-134894, 1976.

18. Feiler, Charles E.; and Merriman, James E.: Effects of Forward Velocity and Acoustic Treatment on Inlet Fan Noise. NASA TM X-71591, 1974.

19. Tyler, John M.; and Sofrin, Thomas G.: Axial Flow Compressor Noise Studies. SAE Paper -345D, Apr. 1961.

20. Rice, Edward J.: Acoustic Liner Optimum Impedance for Spinning Modes with Mode Cut-Off Ratio as the Design Criterion. NASA TM X-73411, 1976.

21. Rice, Edward J.: Inlet Noise Suppressor Design Method Based Upon the Distribution of Acoustic Power with Mode Cut-Off Ratio. Advances in Engineering Science, NASA CP-2001, Vol. 3, 1976, pp. 883-894.

22. Rice, Edward J.: Multimodal Far-Field Acoustic Radiation Pattern - An Approximate Equation. NASA TM-73721, 1977.

23. Saule, Arthur V.; and Rice, Edward J.: Far-Field Multimodal Acoustic Radiation Directivity. NASA TM-73839, 1977.

24. Saule, Arthur V.: Modal Structure Inferred from Static Far-Field Noise Directivity. NASA TM X-71909, 1976.

25. Morgan, H. G.; and Hardin, J. C.: Airframe Noise - The Next Aircraft Noise Barrier. AIAA Paper 74-949, Aug. 1974.

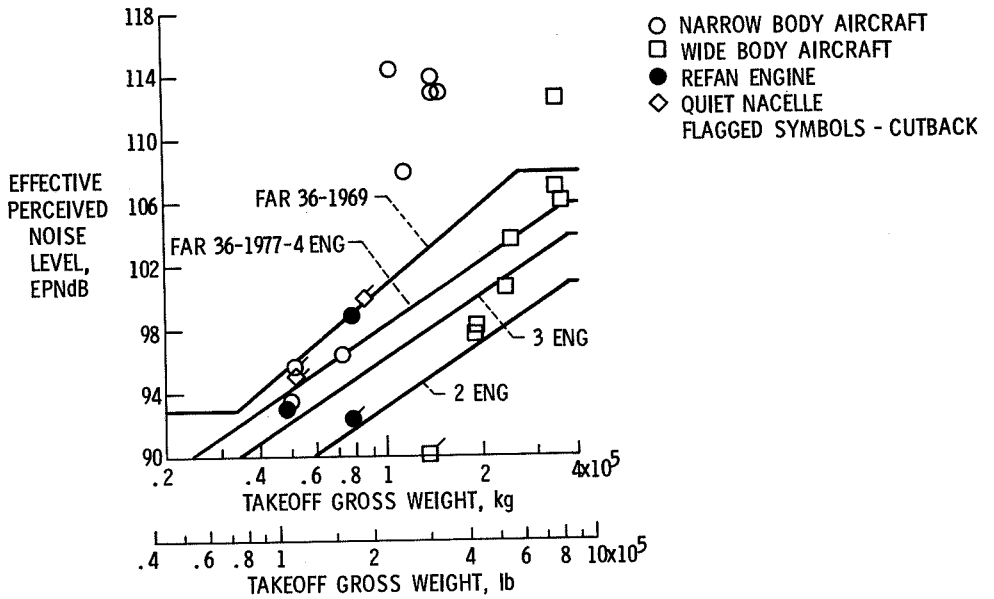

(a) Takeoff noise levels.

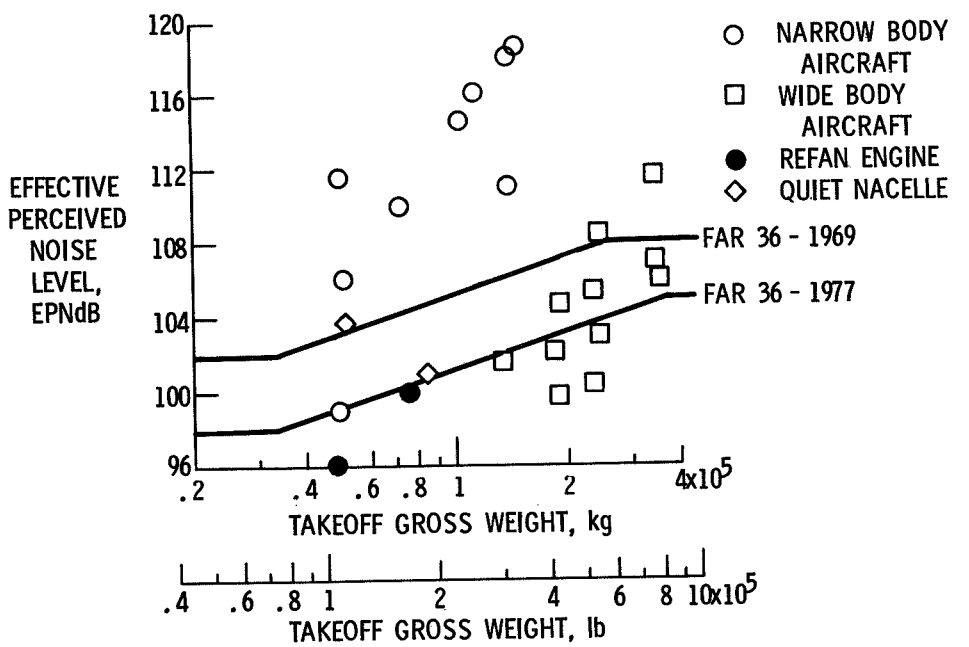

(b) Approach noise levels.

Figure 1.- Aircraft noise certification levels and regulations.

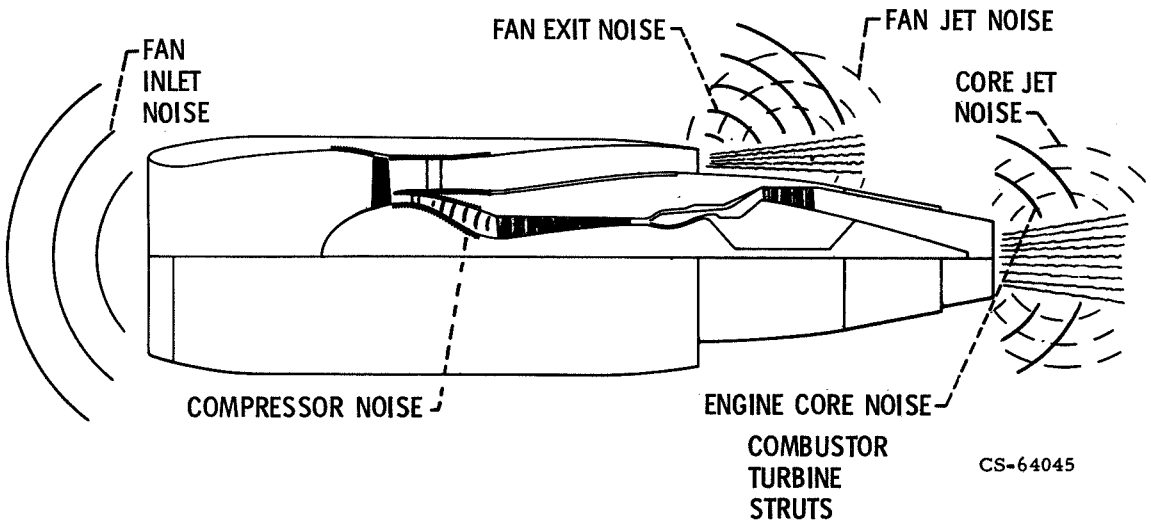

Figure 2.- Turbofan engine noise sources.

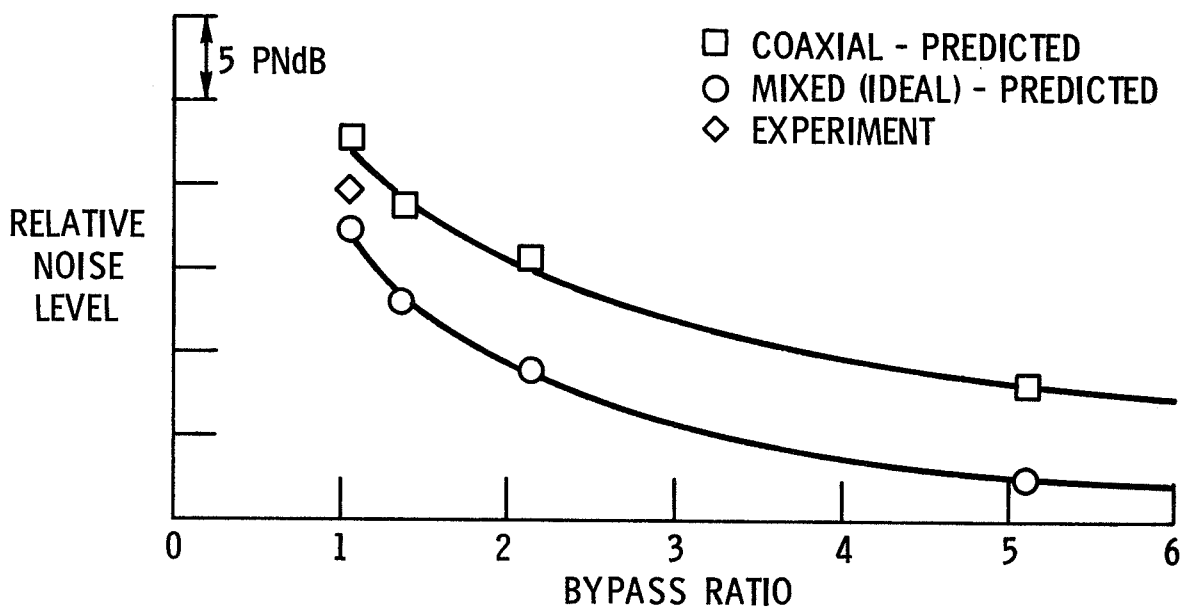

Figure 3.- Jet noise variation with engine bypass ratio for coaxial- and mixed-flow nozzles.

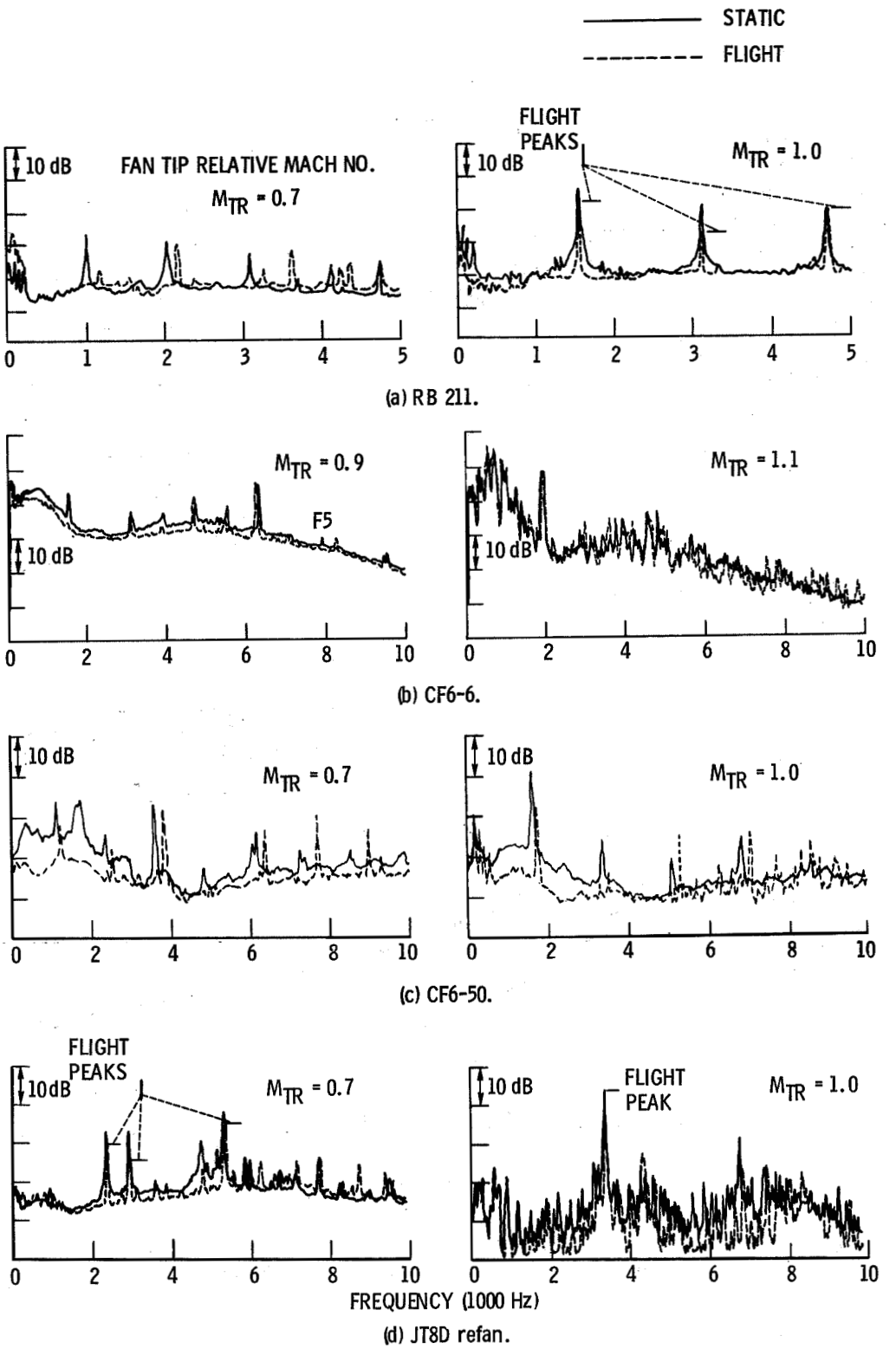

Figure 4.- Effect of flight on fan-inlet noise.

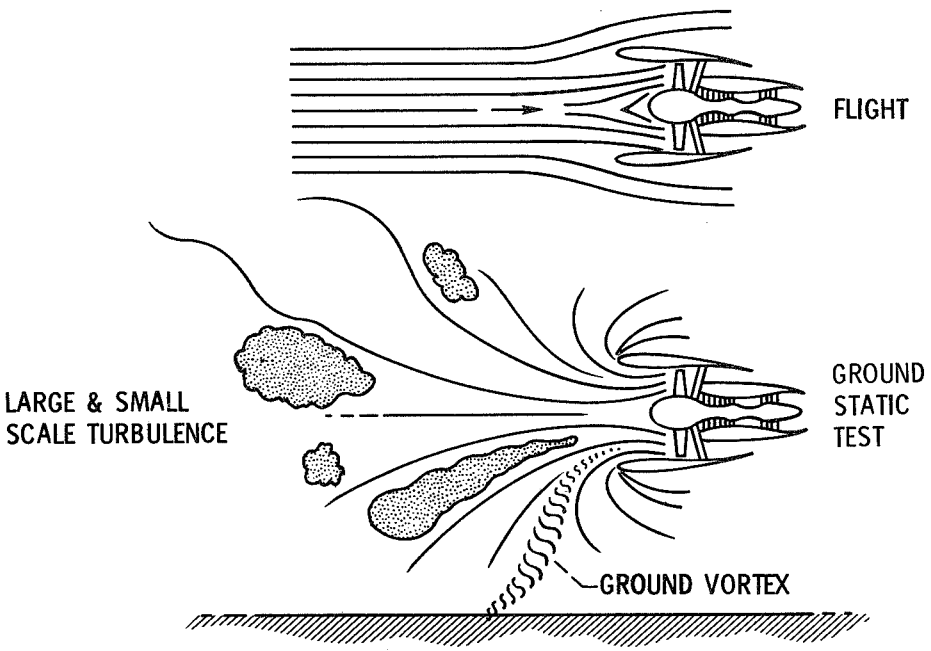

Figure 5.- Effect of flight on inlet flow.

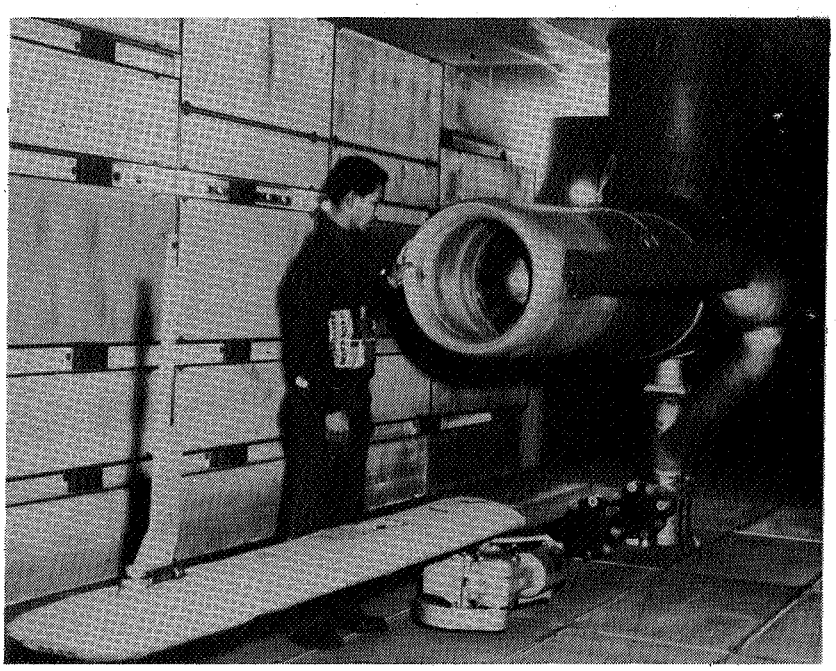

Figure 6.- Flight test simulation in an anechoic wind tunnel.

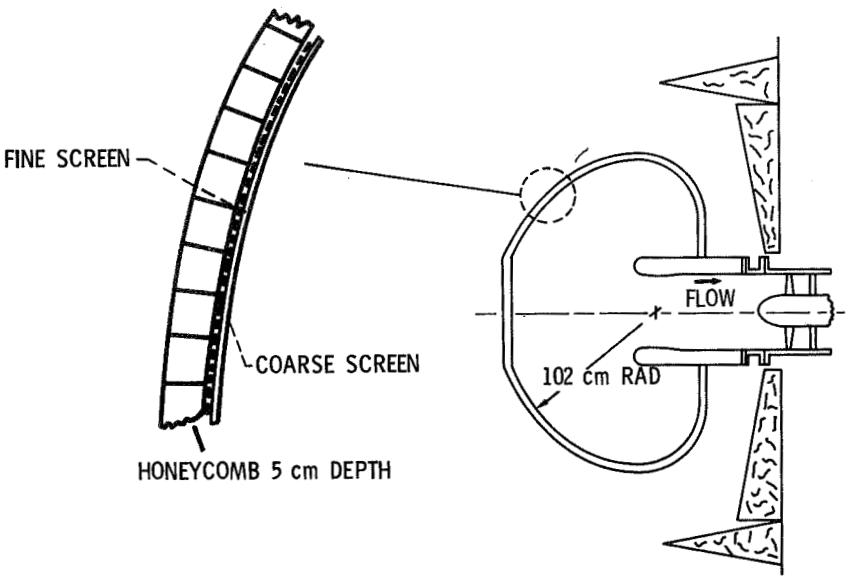

Figure 7.- Inflow-control structure schematic.

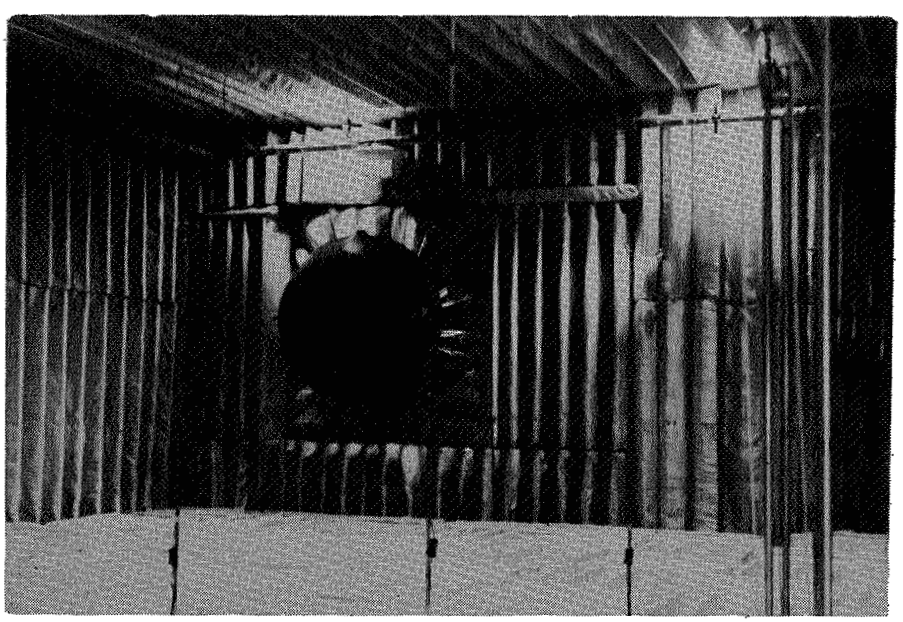

Figure 8.- Inflow-control structure mounted over fan inlet in anechoic chamber.

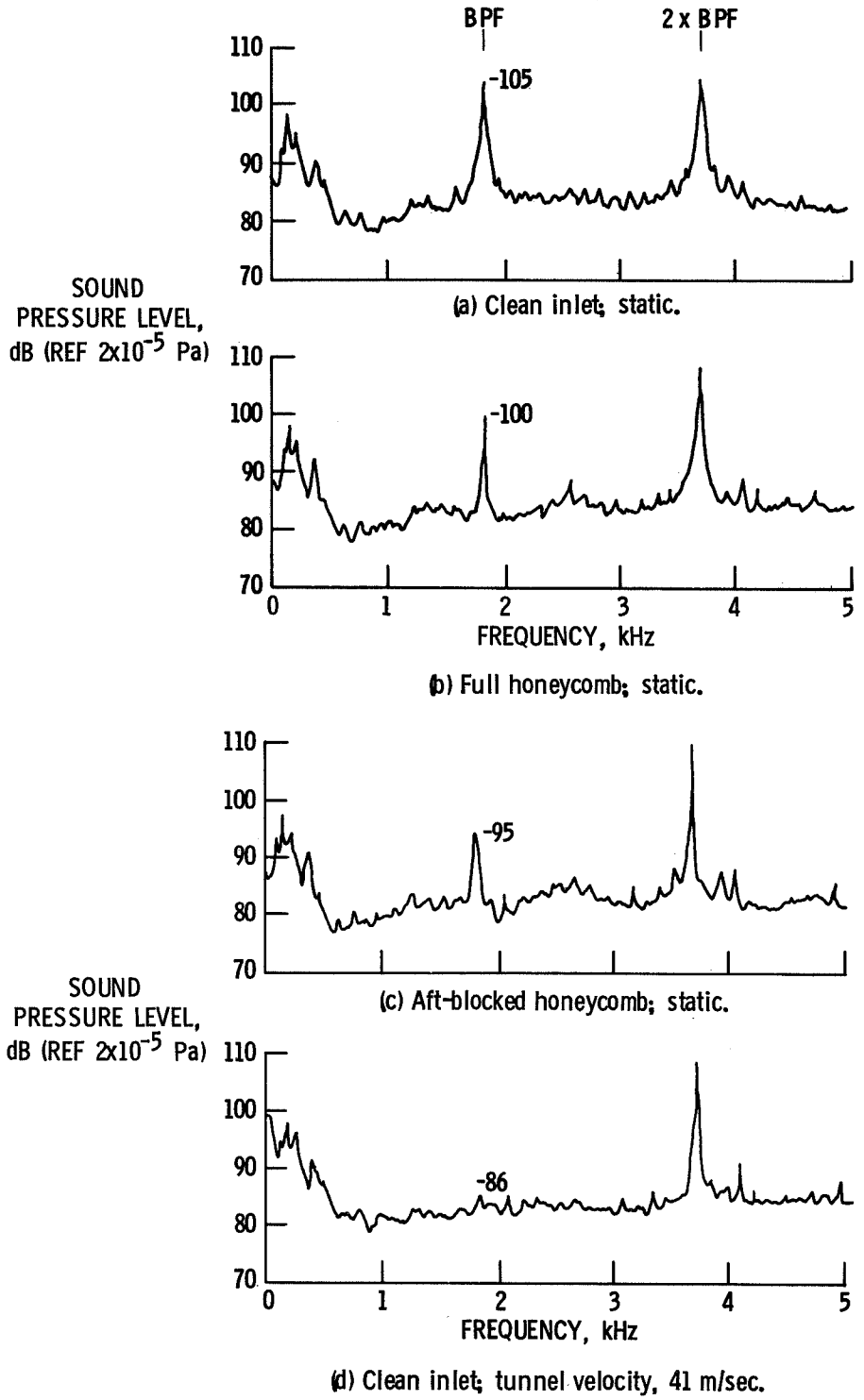

Figure 9.- Inlet fan noise variation with different approaches to inflow control.

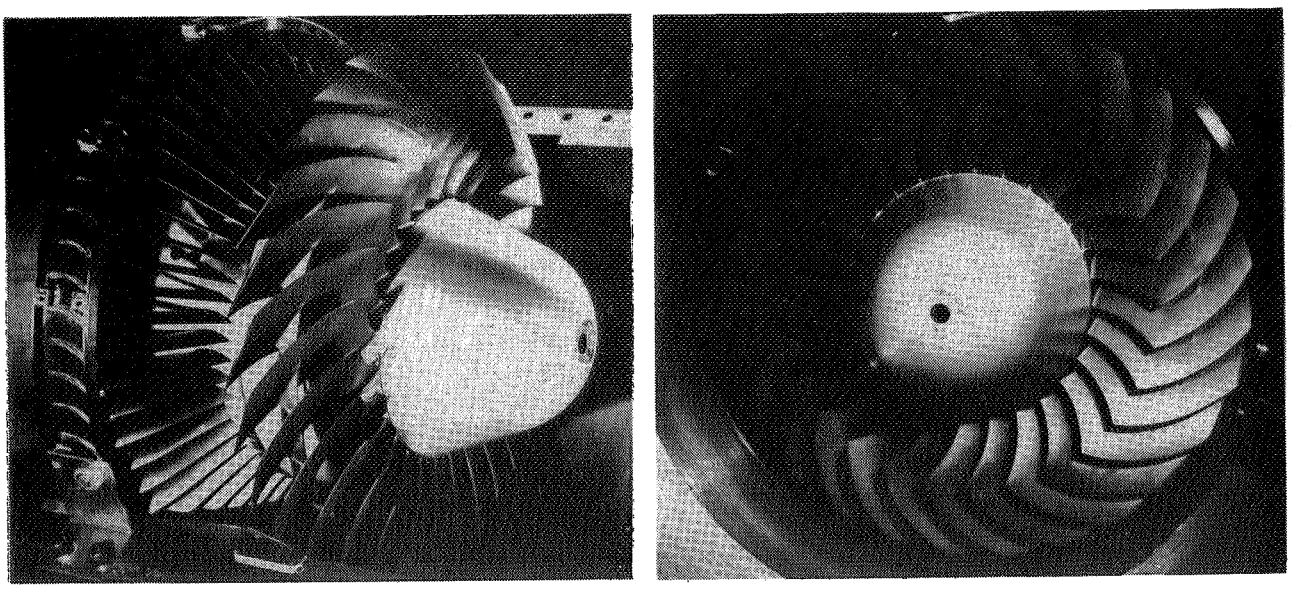

Figure 10.- Swept-rotor fan concept.

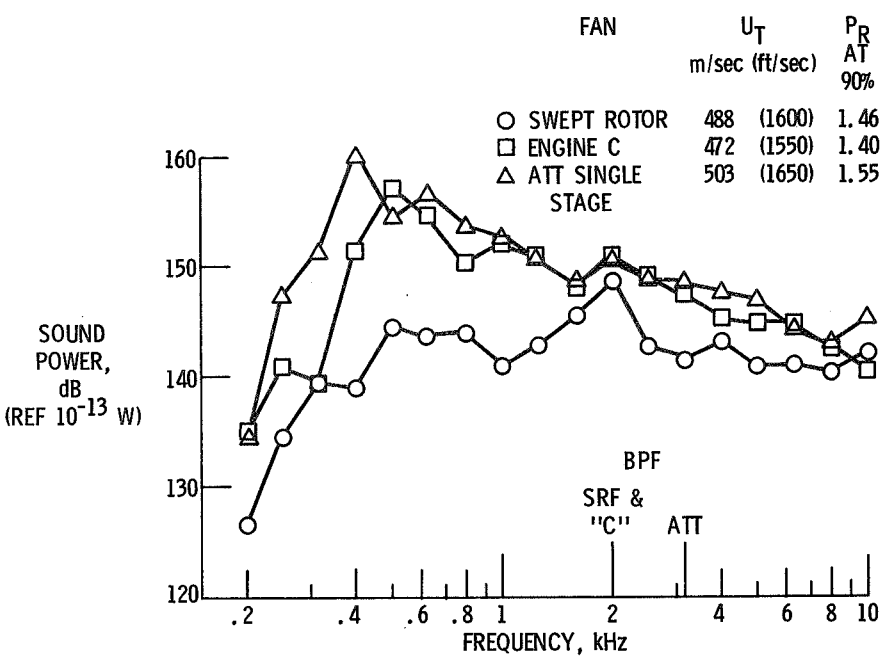

Figure 11.- Comparison of swept-rotor fan inlet noise with noise from earlier supersonic fans. Fan speed, 90% of design; full scale.

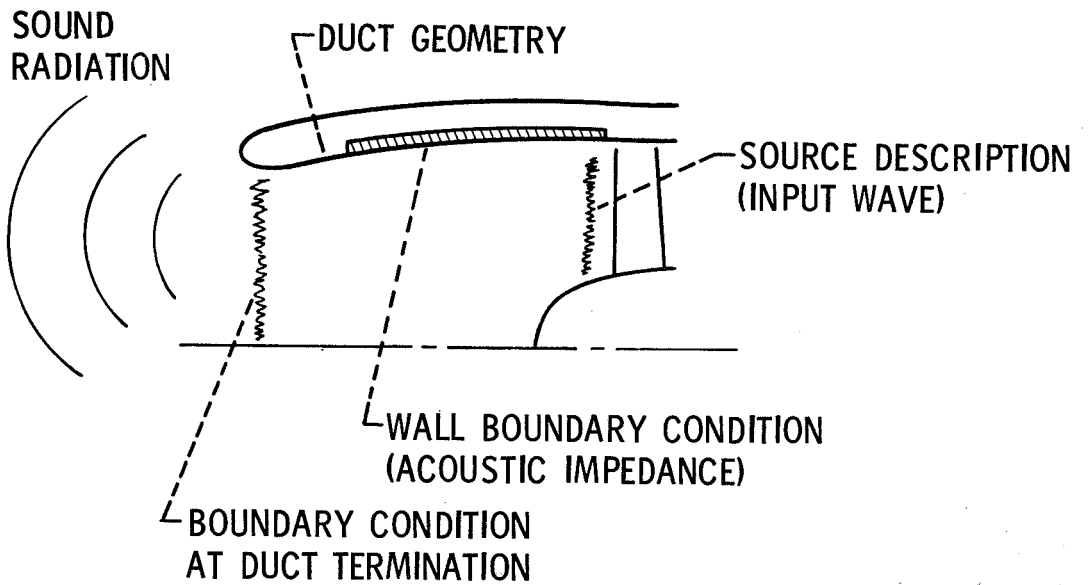

Figure 12.- Elements of the acoustic suppressor problem.

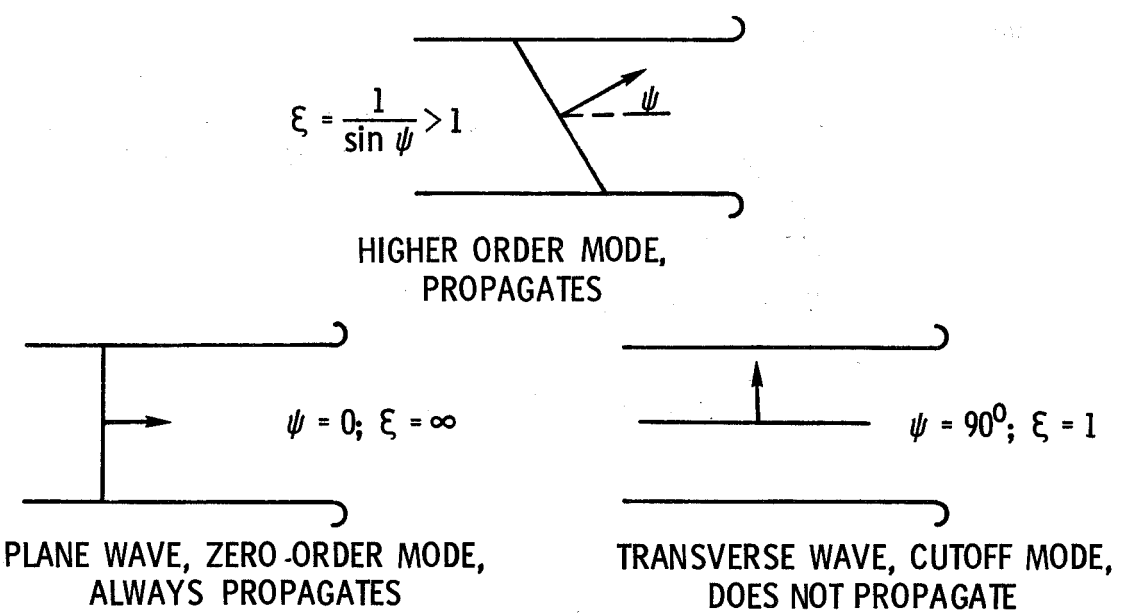

Figure 13.- Sound propagation in a two-dimensional duct illustrating mode cutoff ratio.

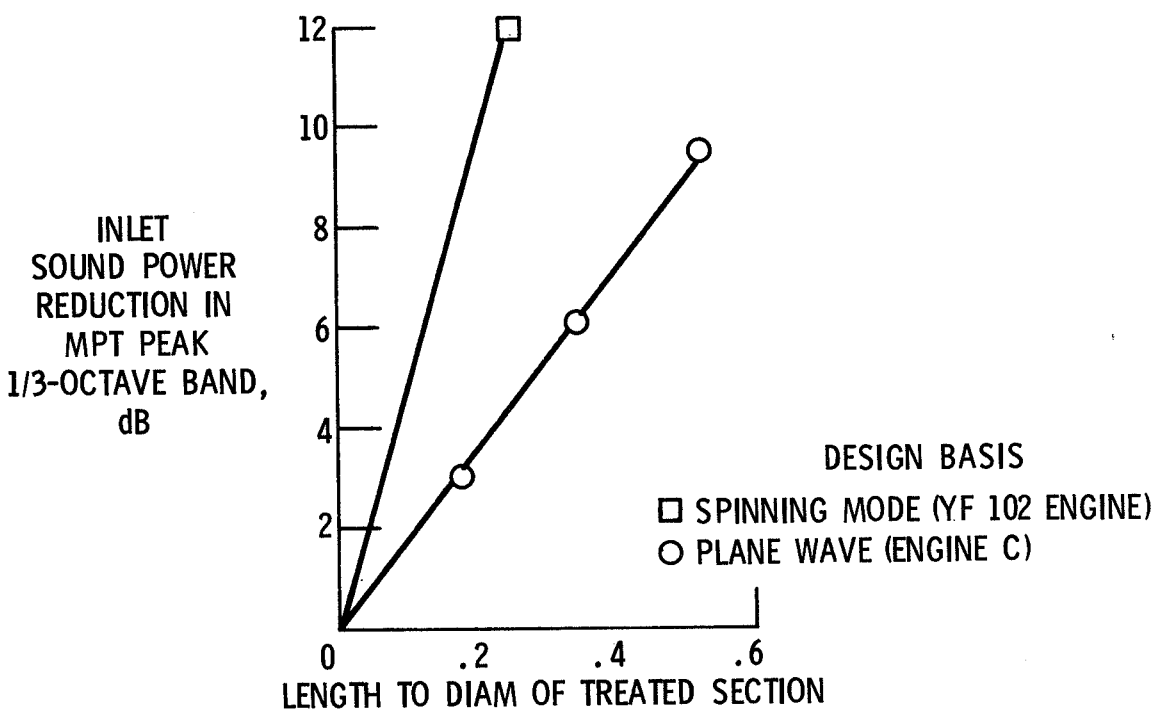

Figure 14.- Performance of suppressors based on spinning mode and plane wave designs.

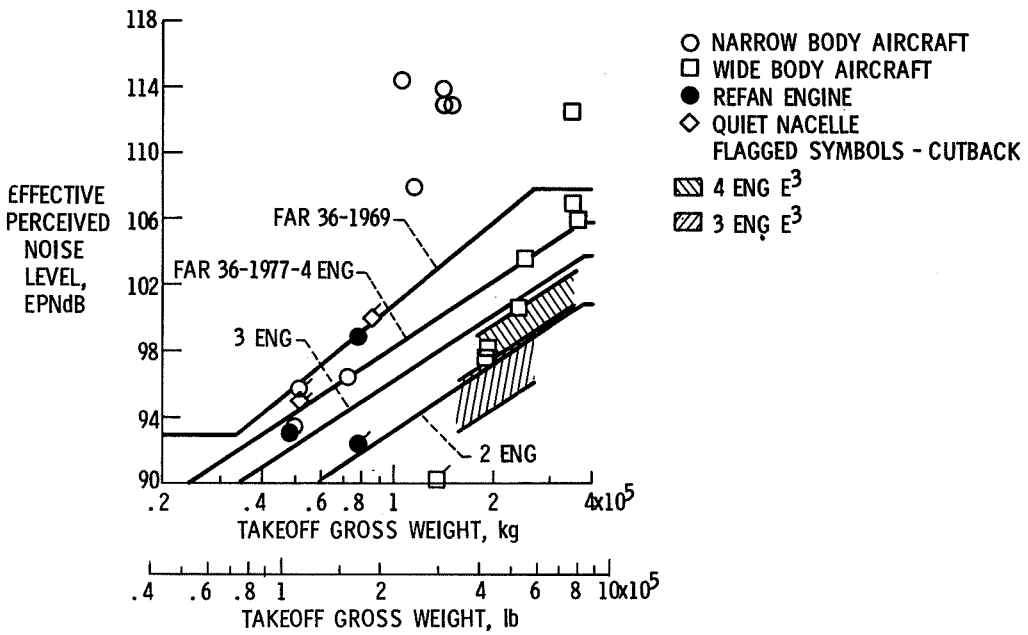

(a) Takeoff noise.

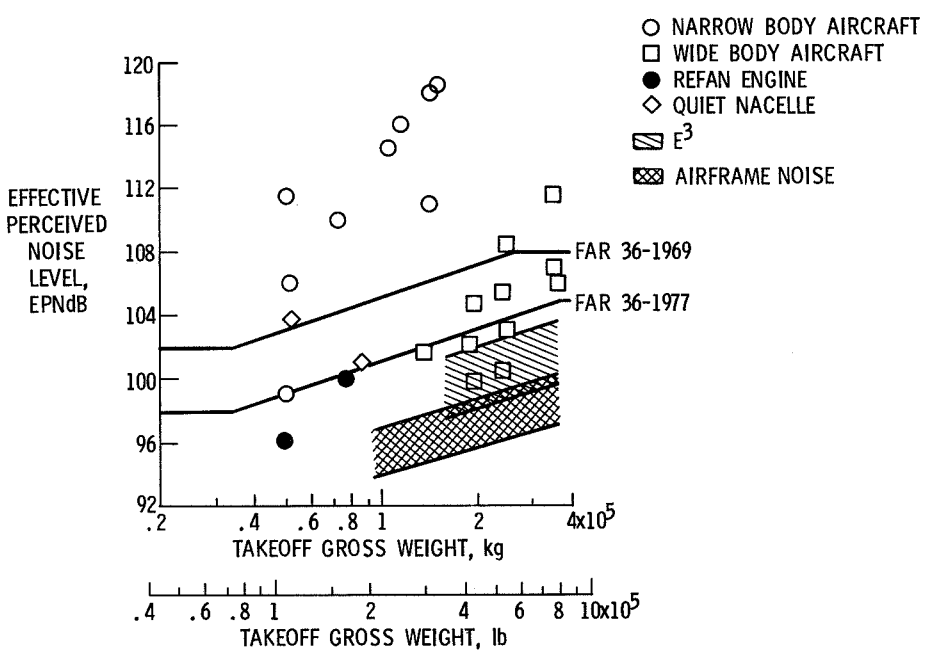

(b) Approach noise.

Figure 15.- Estimated noise levels of aircraft powered by E^3 engines.

ADVANCED MATERIALS RESEARCH FOR LONG-HAUL AIRCRAFT TURBINES ENGINES

by R. A. Signorelli and C. P. Blankenship

Lewis Research Center

SUMMARY

The use of improved materials for aircraft turbine-engine components has significantly increased performance. The components are stronger and lighter, and have higher use-temperatures and longer service lives. The improved materials may be used for components in both high- and low-temperature areas of the engines. Fiber composites and high-temperature alloys are the major advanced materials being studied for use in turbine-engine components. The engine components for which these materials are under study include fan blades, fan-exit guide vanes, fan frame and case, containment ring, nacelle, combustor, and turbine vanes, blades, and disks.

Cost-benefit analyses have shown that a significant fuel saving can be achieved by use of these materials. For example, fan blades, turbine disks, combustor, seals, and high-pressure turbine blades and vanes of these advanced materials could save a commercial fleet 600 million gallons of fuel a year.

This paper reviews the status of research efforts to apply low-to-intermediate temperature composite materials and advanced high-temperature materials and their application to the engine components. It emphasizes emerging materials technologies and their potential benefits to aircraft gas turbines. The problems are identified, and the general state of readiness of the technology for near-term use is assessed.

INTRODUCTION

Materials and processing technology continue to have a key role in the development of advanced aircraft gas-turbine engines. This paper highlights the materials technology areas that are expected to significantly affect future aircraft turbine-engine development. Approaches to the development of improved materials technology as well as its advances are included. Emphasis is placed on emerging material technologies that may be included in NASA-sponsored materials programs or aircraft-engine technology programs. These programs include the study of the components shown in figure 1: fan blades, turbine blades and vanes, turbine disks, combustors and seals.

The potential benefits of using these components are listed in table I. In recent NASA sponsored studies (refs. 1 to 6), most component-material combinations were analyzed for their potential economic benefit to commercial transport engines. These studies reflect the changing climate in materials develop-

ment from the dominance of engine performance in the past decade to that of economic benefits (ref. 7). Several factors account for this change, including the more restricted availability of development funds, a lower frequency of new engine applications, greater pressures to reduce engine maintenance costs, and greater emphasis on fuel economy.

Benefits of the advanced material technologies described herein are presented in terms of higher temperature capability, lower weight, or lower cost. It should be noted that the emphasis placed on materials with higher temperature capability does not mean that turbine-inlet temperatures in advanced engines will be higher. Most likely, this higher temperature capability would be used by the designer to reduce turbine cooling requirements or to extend component life. These types of performance improvements usually show the greatest overall economic benefit to the commercial aircraft system.

COMPOSITE FAN BLADES

Payoff studies have indicated that composite fan blades will be lighter weight, stronger, and stiffer than the current standard forged titanium. These advantages can permit improved engine performance, greater fuel economy, and reduced direct operating costs. A major obstacle to the use of composite fan blades has been their susceptibility to foreign-object damage (FOD). Foreign-object damage can be caused by rivets, ice balls, rocks, and birds. Bird ingestion is a major flight safety hazard (ref. 8). Although most bird ingestion incidents are harmless, some collisions with larger birds can cause significant damage. For example, the titanium fan blade shown in figure 2 was damaged by a 1-kg (2- to 2.5-lb) gull. Damage to composite blades in simulated service rig tests are shown in the lower figure.

Research has been directed toward improving the resistance of composite fan compressor blades (refs. 8 to 10). Progress in this research is illustrated in figure 3. A joint Air Force and NASA program is aimed at demonstrating the application of boron/aluminum (B/Al) composites to first-stage J-79 blades (ref. 11). The production J-79 blade is made of 403 stainless steel and weighs 450 g (1 lb). In impact testing of stainless-steel blades (single-blade whirling-arm tests), an 85-g (3-oz) starling caused local bending. Early B/Al blades were broken into several pieces by a similar impact. Application of NASA developed, more-impact-resistant B/Al produced improved, but inconsistent FOD results (1975-76): Some suffered only minimal damage, while others suffered extensive delamination and deformation. Later results (1977) showed no material loss and only minimal delamination. Blades in an actual engine could continue to operate normally.

The improved B/Al technology that led to these encouraging results is being included in composite FOD improvement programs aimed at large, high-bypass-engine fan blades. Several designs and materials combinations are included in the program (fig. 4). All the designs shown include the removal of the mid-span damper. The solid design is being studied with all three composite materials - the polymer matrix, metal matrix, and superhybrid combination of metal matrix and polymer matrix composites. The spar-shell design has the advantage of

a proven titanium root attachment and a titanium spar. This design is being pursued using B/Al and superhybrid composite airfoil shells. Although the hollow design can be lighter than the solid, or spar shell, it is more difficult to fabricate and, possibly, less FOD resistant. The design using hollow titanium blades is also under consideration. Further studies of this design approach using composites are expected. The patch design employs a composite inlay to stiffen a titanium blade. The composite patch increases aeromechanical stability and can permit the removal of the midspan damper, which increases aerodynamic efficiency and reduces fabrication cost. None of the design approaches have demonstrated the degree of confidence for service readiness for application to commercial engines.

A number of tests are being used to demonstrate fan blade FOD resistance (fig. 5). Single-blade rig tests are performed to demonstrate, under carefully controlled conditions, the range of severity of bird impacts that can be expected in engine service. These tests will be used to screen designs and materials combinations for the more costly full-stage rig and ground engine tests needed to qualify composite fan blades for application. All the candidate composite materials and design for large, high-bypass-engine fan blades are currently in the single-blade-rig, FOD phase of the tests. Although the outlook for composite fan blades is encouraging, a considerable amount of work has to be completed before they are ready for engine service.

TURBINE BLADES

Progress in the development of turbine-blade materials is illustrated in figure 6. As shown, conventionally cast alloys such as René 80 provide blade-metal use temperatures in the range of 900° to 950° C (1650° to 1740° F). The application of directional solidification to conventional alloys provides a modest gain in use temperature and significantly improves resistance to thermal fatigue (ref. 12). Because future engine requirements exceed the capabilities of conventional alloys, a new class of materials is being developed to meet the need for turbine blades that must operate at least 100° C (180° F) higher than present blades. These new materials are directional structures (fig. 7), which comprise single-crystal superalloys, eutectic alloys, wire-reinforced superalloys, and oxide dispersion-strengthened (ODS) alloys (refs. 13 to 19).

Single-Crystal Superalloys

Single-crystal superalloys have improved creep strength, ductility, and resistance to thermal fatigue. They are produced by a directional-solidification process similar to that used for directionally solidified, columnar-grained superalloys. In the near future development of single-crystal blade alloys is expected to emphasize modification of present high-strength superalloys. These modifications are likely to include the elimination of grain-boundary strengtheners such as boron, carbon, and zirconium; and the substitution of other elements for added γ' strengthening. Later, emphasis is likely to be placed on tailoring new alloy compositions specifically to achieve higher strength single-crystal blade alloys. Cast blade costs for single-crystal blades are likely to

be less than DS-columnar-grained alloys, since the single-crystal alloys normally contain fewer reactive elements that tend to cause blade defects during the casting process. A potential near-term application of single-crystal blades includes the use of the low-cost, exothermic DS casting process using a modified Mar-M247 blade alloy (ref. 20). This program emphasizes uncoated, single-crystal blade applications to general aviation turbine engines. Similar programs are anticipated in the near term for advanced commercial aircraft engines.

Directionally Solidified Eutectics

Directionally solidified eutectics are a relatively new class of blade materials. They have been studied extensively in the past few years under the sponsorship of NASA and DOD. Examples of eutectic alloys under evaluation include $\gamma/\gamma' - \delta$ and NiTaC-13, which have a nickel-alloy matrix reinforced with platelets and fibers, respectively. A typical microstructure of these alloys is shown in the photograph on the left of figure 8. The $\gamma/\gamma' - \delta$ and NiTaC-13 eutectics have an estimated 50° C (90° F) advantage over conventional superalloys. However, either their transverse properties or castability will probably limit their engine use. More important, the high casting cost (twice the conventional DS superalloy cast, as indicated in ref. 21), due to their slow growth requirements and mold reactivity, precludes their consideration for near-term commercial applications. Advanced eutectic-alloy development programs are focused on the required advances in technology needed to bring the DS eutectics to a state of readiness for engine application. Approaches have been identified to improve critical mechanical properties and reduce casting costs. The potential in improved engine performance offered by the eutectics certainly warrants the significant research and technology effort underway.

Wire-Reinforced Superalloy Composites

Wire-reinforced superalloy composites of interest for turbine blades combine the excellent high-temperature strength of a refractory metal, such as tungsten wire, with the oxidation resistance and toughness of a superalloy matrix. Such a composite is illustrated in the right-panel photograph of figure 8 in which tungsten wires, about 0.04 cm in diameter, are embedded in a superalloy matrix. Similar composites, using a highly oxidation-resistant iron-alloy matrix, Fe-Cr-Al-Y, have shown excellent potential for turbine-blade application. These wire-reinforced composites have the highest temperature capability of the directional structures under consideration. Although the technology for these composites is not as advanced as that of DS eutectics, sufficient studies have been conducted to demonstrate their feasibility as a turbine-blade material in terms of strength, oxidation, and fatigue resistance, and wire-matrix compatibility. Also, a potential low-cost fabrication method (fig. 9) has been demonstrated using a monolayer-tape process similar to that developed for metallic-composite fan and compressor blades (ref. 22). Concepts for selective reinforcement to achieve blade densities comparable with superalloys and concepts for blade cooling show promise for advanced turbine-blade applications. Orderly laboratory development of the excellent high-temperature potential of these composite blade materials is expected to continue.

Oxide Dispersion-Strengthened Alloys

Recent advances in the production of oxide dispersion-strengthened alloys have introduced ODS-γ' superalloys as a candidate turbine-blade material. These alloys combine both γ' and oxide-dispersion strengthening to achieve high strength at intermediate and elevated temperatures. Directional structures are achieved in these alloys by a solid-state transformation (directional recrystallization and grain growth) that alines the grains in the principal stress direction. Their potential for turbine-blade applications, other than high strength, is not yet defined because of their relatively new status. A potential problem may be low transverse ductility, which is usually characteristic of the ODS materials. Current programs are underway to better define the long-range potential of the ODS-γ' alloys for turbine blade applications.

TURBINE DISKS

Progress in the development of turbine disk alloys is illustrated in figure 10 using the 650° C (1200° F) yield strength as a reference. As indicated, improvements in conventional alloys have doubled the strength of turbine disks over the past two decades. For future disk applications, prealloyed-powder-metallurgy (PM) processing will be emphasized rather than the conventional approach of using cast ingots for later forging and machining to size. The PM approach offers two distinct advantages: First, substantial improvements in strength can be achieved (fig. 10) by specifically designing the alloys to accommodate larger quantities of strengtheners without encountering the segregation problems that occur during casting. In addition, the PM process affords improved structural homogeneity, which is expected to improve fatigue resistance even at the higher strength levels. Second, substantial reductions in disk manufacturing costs can be achieved by the PM approach (fig. 11). In the state-of-the-art practice, disks are made by vacuum melting, forging, and machining operations that result in a material utilization of about 40 percent. In the current PM approach, disks are made by forging a preform produced by hot isostatic pressing of a prealloyed powder. The material utilization for the latter approach is about 70 percent. In addition to the saving in material, about a 40-percent saving in machining costs is achieved because fewer steps are required (ref. 23).

For the longer-term, direct consolidation of disks from the prealloyed powder by hot, isostatic-compaction techniques is envisioned. The cost-reduction potential of this method is about 50 percent. Both PM disk alloy and process developments are underway to meet the anticipated requirements of advanced turbine engines (refs. 17, 24, and 25).

VANES, COMBUSTORS, AND SHROUDS

These turbine components must withstand very high temperatures, but the mechanical stresses are relatively low. For the stator vanes, ODS alloys offer a significant advantage over currently used conventionally cast alloys. (See fig. 12.) The ODS alloys have greater microstructural stability and overtemper-

ature capability (ref. 26). Their overtemperature capability is illustrated in figure 13, which compares a conventionally cast Mar-M-509 vane and an ODS alloy (TD-NiCr) vane. These vanes, contained in the same nozzle assembly, were subjected to an inadvertent overtemperature in an experimental engine test. Although cooled, the cast vanes melted, whereas the uncooled ODS alloy vanes were unaffected. In continuing studies, good engine performance has been achieved with the advanced ODS Ni-Cr alloy, Inconel MA-754 (ref. 27). Efforts are underway to develop and scale up low-cost vane fabrication technology for advanced engine applications (refs. 28 and 29).

Both the DS eutectic alloys and the wire-reinforced superalloys discussed previously for blade applications are potential vane materials for advanced turbine engines. Currently, they appear to be competitive with the advanced ODS alloys such as Inconel MA-754.

Ceramics such as SiC and Si_3N_4 also are candidates for engine vane application. (See fig. 12.) Their high-temperature capability far exceeds that of the other materials noted. However, the brittle nature of ceramics is a major deterrent to their use in aircraft engines. Progress in the use of these ceramics in related applications such as ground transportation (ref. 30) is likely to provide the technology and confidence needed to consider ceramics for aircraft engines in the future.

Combustors, including the liners and transition ducting, require sheet alloys with good forming and welding characteristics. Current combustor materials include alloys such as Hastelloy X and HS-188. ODS alloys in sheet form have both higher use temperature capability (about 100° C (180° F)) and significantly better oxidation resistance than current materials. Applying advanced ODS alloys such as Inconel MA-956 and HDS-8077 will require changes in combustor design to accommodate the relatively low ductility of the ODS alloys at elevated temperatures. Also, combustor fabrication techniques will require modification to compensate for the low high-temperature strength of fusion welds in ODS alloys. However, the temperature advantage and improved durability expected from ODS alloys appear to be sufficiently attractive to warrant their use in advanced turbine engines.

Decreasing the clearance between the blade tip and the inner wall of the turbine seal can significantly increase gas-turbine-engine performance. As shown schematically in figure 14, clearance increases during engine operation cause losses in thrust and fuel economy. A 1-percent turbine efficiency penalty has been estimated for a 0.025-cm (0.010-in.) increase in first-stage turbine blade tip clearance.

Improvements in turbine shroud materials have focused on the use of the more oxidation resistant NiCrAl alloys (ref. 31). Significant improvements in clearance control and shroud life have been achieved. Future efforts will likely emphasize both turbine-blade-tip treatments and improved shroud materials to maintain close clearance control and thereby improve engine fuel economy. Ceramics, similar to those used for vanes, are good candidates for advanced shroud applications (refs. 32 and 33). Turbine shrouds, being lower risk components, will probably be the first ceramic components used in advanced aircraft

engines. Turbine-blade-tip treatments are likely to include the use of more oxidation-resistant tip alloys, such as NiCrAl, with an abrasive tip to allow incursion into the shroud under abnormal engine operating conditions. In addition to the use of low-expansion alloys for turbine seals, support studies will yield further improvements in clearance control. Approaches such as those described are becoming increasingly important to extend blade-tip life, to control seal leakage, and, thereby, to increase fuel economy.

SUMMARY OF RESULTS

The use of advanced materials in aircraft gas-turbine engines will permit substantial economic benefits. The achievement of these benefits, with some component-material combinations, will require considerably more research, while others have a much shorter term application potential.

Composite fan blades offer the potential for a signficant advantage over titanium blades, however, their resistance to foreign object damage must be increased. A series of tests must be successfully completed to assure readiness before a commitment to application can be undertaken.

High-temperature directionally structured materials for turbine airfoils include shorter term applications using directionally solidified polycrystalline and monocrystalline alloys. To achieve the higher temperature potential of DS eutectics, ODS superalloys and tungsten fiber-reinforced superalloys will require substantially more research. These directional structures have properties that will permit 50° to 150° C (90° to 240° F) higher blade metal temperatures than conventional superalloys.

Prealloyed powder superalloy disks will be stronger and cheaper to fabricate. The use of near-net-shape, hot, isostatic pressing of powder superalloys can reduce starting material to less than half that of standard cast, forge, and machine processing. Currently, in an intermediate step, powders are hot-pressed into simple shapes, which are then forged.

More oxidation resistant, abradable turbine-seal materials are now being readied for application; for example, abradable seals that can reduce turbine tip clearances up to 70 percent. Later, the use of ceramics and low-expansion alloys may allow still smaller clearances.

REFERENCES

1. Steinhagen, C. A.; Stotler, C. L.; and Neitzel, R. E.: Study of the Costs and Benefits of Composite Materials in Advanced Turbofan Engines. (R74AE6418, General Electric Co.; NASA Contract NAS3-17775.) NASA CR-134696, 1974.

2. Ross, E. W.; Johnston, R. P.; and Neitzel, R. E.: Cost Benefit Study of Advanced Materials for Aircraft Turbine Engines. (General Electric Co.; NASA Contract NAS3-17805.) NASA CR-134702, 1974.

3. Bissett, J. W.: Cost/Benefit Study of Advanced Materials Technologies for Aircraft Turbine Engines. (PWA-5073, Pratt & Whitney Aircraft; NASA Contract NAS3-17804.) NASA CR-134701, 1974.

4. Bissett, J. W.: Cost/Benefit Analysis of Advanced Material Technologies for Future Aircraft Turbine Engines. (PWA-5453, United Technologies Corp.; NASA Contract NAS3-20072.) NASA CR-135107, 1976.

5. Faddoul, J. R.; and Signorelli, R. A.: Cost/Benefit Assessment of the Application of Composite Materials to Subsonic Commercial Transport Engines. NASA TM X-73557, 1976.

6. Hillery, R. V.; and Johnston, R. P.: Cost/Benefit Study of Advanced Material Technology for Aircraft Turbine Engines. (General Electric Co.; NASA Contract NAS3-20074.) NASA CR-135235, 1977.

7. Blankenship, C. P.: Trends In High Temperature Materials Technology for Advanced Aircraft Turbine Engines. SAE Paper 751050, Nov. 1975.

8. DeJong, A. P.: Their Airspace or Ours? Shell Aviation News, no. 290, 1970, pp. 2-7.

9. McDanels, David L.; and Signorelli, R. A.: Effect of Fiber Diameter and Matrix Alloys on Impact-Resistant Boron/Aluminum Composites, NASA TN D-8204, 1976.

10. Melnyk, P.; and Toth, I. J.: Development of Impact Resistant Boron/Aluminum Composites for Turbojet Engine Fan Blades. (ER-7806, TRW Equipment Labs.; NASA Contract NAS3-17763.) NASA CR-134770, 1975.

11. Albright, A. J.; Stabrylla, R. G.; and Stanley, M. W.: Boron/Aluminum Blade Impact Improvement. R76AEG547, General Electric Co., 1976. (AFAPL-TR-76-63, AD-B017761L.)

12. Piearcey, B. J.; and VerSnyder, F. L.: A New Development in Gas Turbine Materials - The Properties and Characteristics of PWA 664. AIAA Paper 65-742, Oct. 1966.

13. VerSnyder, Francis L.; and Shank, M. E.: The Development of Columnar Grain and Single Crystal High Temperature Materials Through Directional Solidification. Mater. Sci. Eng., vol. 6, 1970, pp. 213-247.

14. Gray, H. R.: The Promise of Eutectics for Aircraft Turbines. NASA TM-73714, 1977.

15. Signorelli, Robert A.: Metal Matrix Composites for Aircraft Propulsion Systems. NASA TM X-71685, 1975.

16. Duhl, D. N.; and Thompon, E. R.: Directional Structures for Advanced Aircraft Turbine Blades. J. Aircr., vol. 14, no. 6, June 1977, pp. 521-526.

17. Freche, J. C.; and Ault, G. M.: Progress In Advanced High-Temperature Materials Technology. NASA TM X-71901, 1976.

18. Glasgow, T. K.: An Oxide Dispersion Strengthened Ni-W-Al Alloy with Superior High Temperature Strength. NASA TM X-71888, 1976.

19. Cairns, R. L.; Curwick, L. R.; and Benjamin, J. S.: Grain Growth in Dispersion Strengthened Superalloys by Moving Zone Heat Treatments. Metall. Trans. A, vol. 6A, no. 1, Jan. 1975, pp. 179-188.

20. Materials for Advanced Turbine Engines (MATE). (Quality Report No. 21, Airesearch Manufacturing Co.; NASA Contract NAS3-20073.) Nov. 1977.

21. Barth, C. F.; Blake, D. E.; and Stelson, T. S.: Cost Analysis of Advanced Turbine Blade Manufacturing Processes. (TRW-IER-7930, TRW, Inc.; NASA Contract NAS3-20378.) NASA CR-135203, 1977.

22. Brentnall, W. D.; and Toth, I. J.: Fabrication of Tungsten Wire Reinforced Nickel-Base Alloy Composites. (ER-7757, TRW Equipment Labs.; NASA Contract NAS3-16756.) NASA CR-134664, 1974.

23. Semmel, J. W., Jr.: Opportunities in Materials and Processes for Aircraft/Ship Propulsion Gas Turbines. Materials on the Move, vol. 6. SAMPE, 1974, pp. 154-167.

24. Evans, D. J.: Materials for Advanced Turbine Engines (MATE). (Sixth Quarterly Report, Pratt and Whitney Aircraft Group; NASA Contract NAS3-20072.) 1977.

25. Bamberger, E. M.; and Mosier, J. S.: Materials for Advanced Turbine Engines (MATE). (R77AEG529, General Electric Co.; NASA Contract NAS3-20074.) 1977.

26. Bailey, P. G.: Oxide Dispersion Strengthened Alloys for Aircraft Turbine Engine Vanes. Materials on the Move, vol. 6. SAMPE, 1974, pp. 208-217.

27. Bailey, P. G.: Manufacture and Engine Test of Advanced Oxide Dispersion Strengthened Alloy Turbine Vanes - for Space Shuttle Thermal Protection. (R77AEG569, General Electric Co.; NASA Contract NAS3-18915.) NASA CR-135269, 1977.

28. Bailey, P. G.; and Perkins, R. J.: Low Cost Fabrication of Oxide Dispersion Strengthened Alloy Turbine Vanes. NASA CR-135373, Dec. 1977.

29. Perkins, R. J.; and Bailey, P. G.: Low Cost Processes for Manufacture of Oxide Dispersion Strengthened Turbine Nozzle Components. Interium Technical Report No. 5, General Electric Co., Sep. 1977.

30. Proceedings of the Workshop on Ceramics for Advanced Heat Engines. CONF-770110, Energy Research and Development Admin., 1977.

31. Bessen, I. I.; Rigney, D. V.; and Schwab, R. C.: Improved High Pressure Turbine Shroud. (R77AEG481, General Electric Co.; NASA Contract NAS3-18905.) NASA CR-135181, 1977.

32. Schwab, R. C.; and Darolia, R.: Feasibility of SiC Composite Structures for 1370° C Gas Turbine Seal Applications. (R77AEG397, General Electric Co.; NASA Contract NAS3-20082.) 1977.

33. Solomon, N. G.; Vogan, J. W.; and Stetson, A. R.: Advanced Ceramics Material for High Temperature Turbine Tip Seals. (RDR-1831-23, Solar Division of International Harvester Co.; NASA Contract NAS3-20081.) NASA CR-135319, 1977.

TABLE I. - BENEFITS OF MATERIALS FOR TURBINE ENGINES

Component	Material	Pay-offs
Fan blades	Composites	More efficient, lighter, lower cost
Combustor	Oxide dispersion-strengthened superalloys	Stronger, more oxidation resistant
Turbine airfoils	Directionally structured superalloys, ceramics	Higher temperature, reduced cooling, increased life
Turbine seals	Abradable alloys and ceramics	Reduced airflow losses, increased efficiency
Turbine disks	Prealloyed powder alloys	Increased rotor speed, reduced cost, lighter

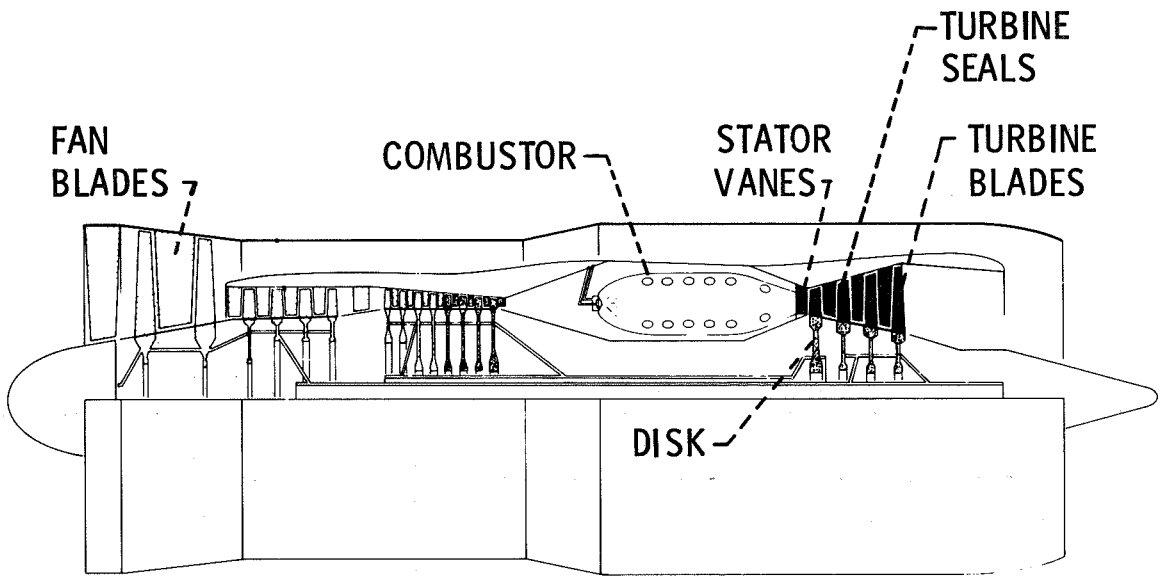

Figure 1.- Engine components studied for application of advanced materials.

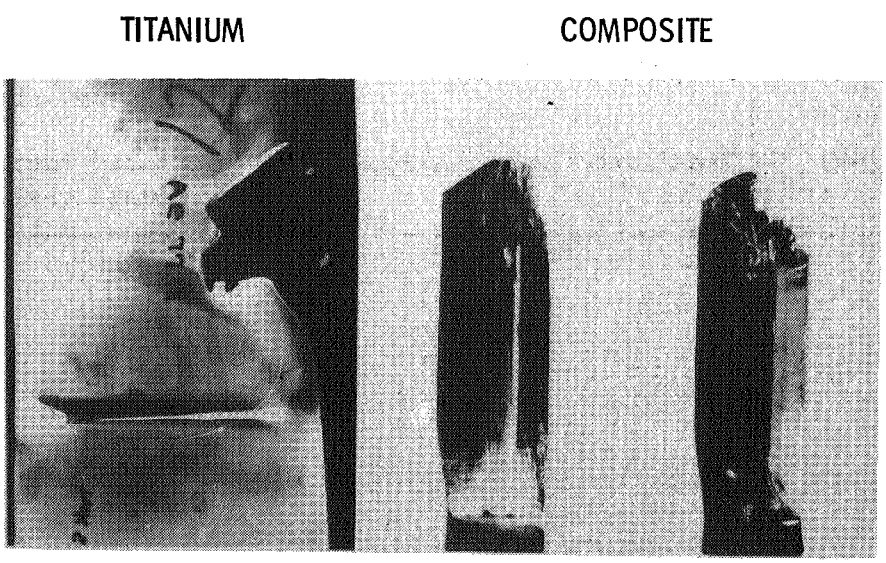

Figure 2.- Bird-ingestion damage to fan blades.

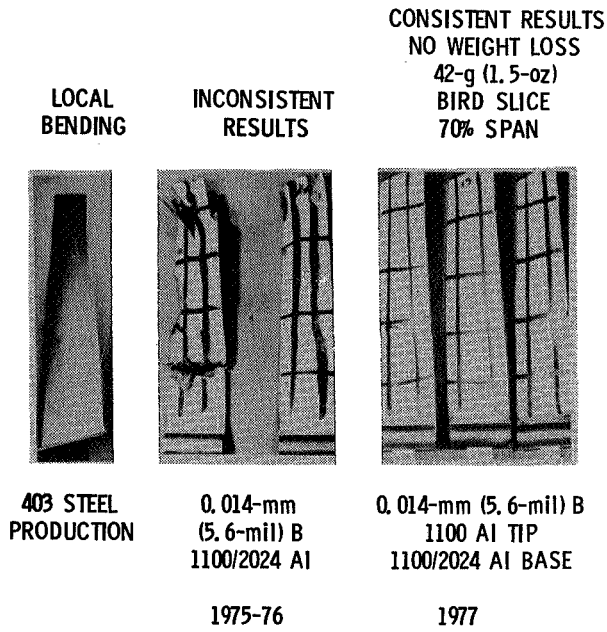

Figure 3.- J-79 stage boron/aluminum blades after starling-impact tests.

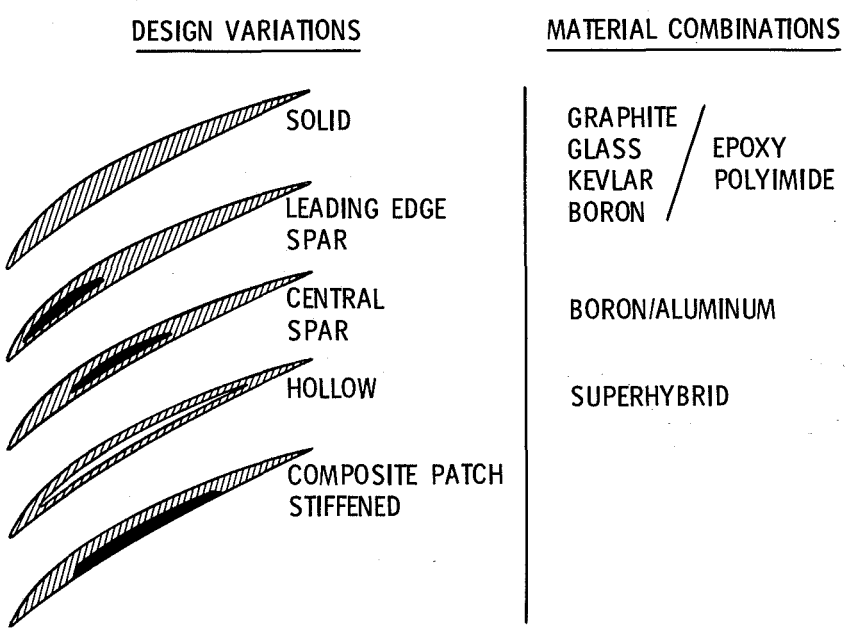

Figure 4.- Composite fan blade materials and design.

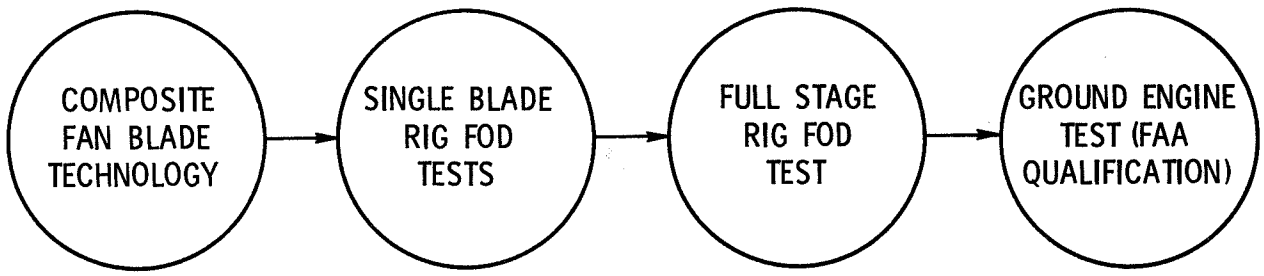

Figure 5.- Procedure for demonstrating composite-fan-blade resistance to foreign-object damage.

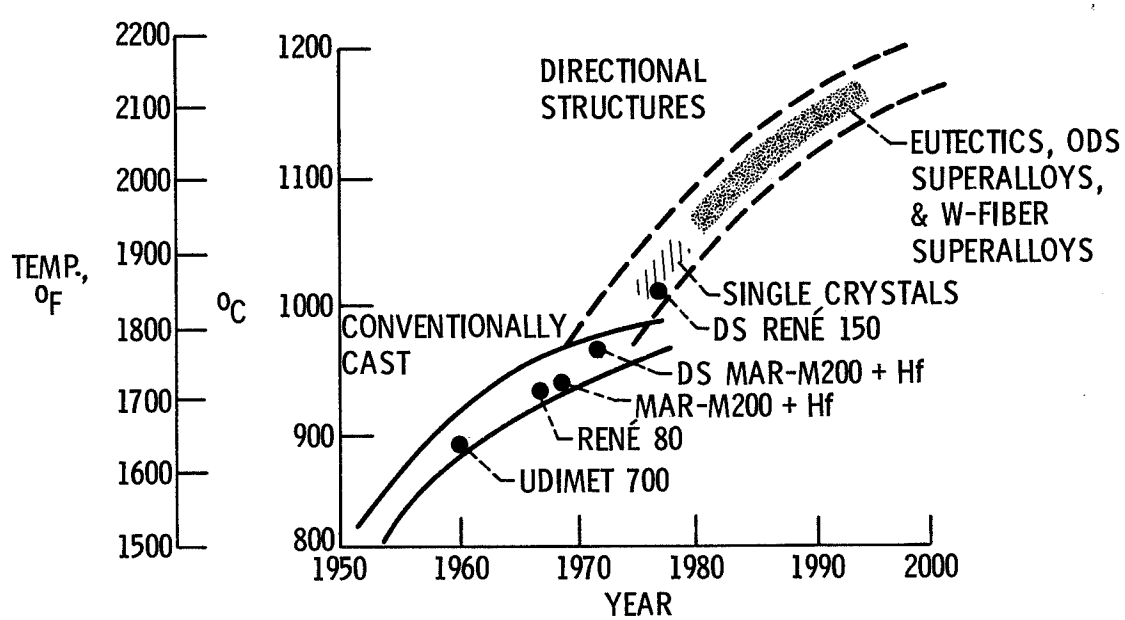

Figure 6.- Use temperatures of turbine-blade materials.

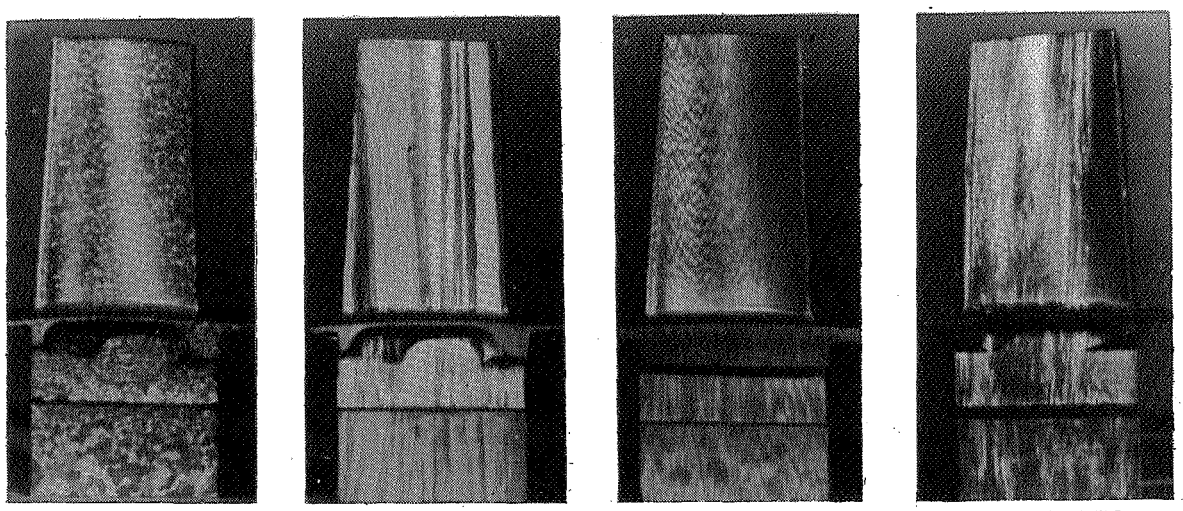

Figure 7.- Trends in turbine-blade material casting methods.

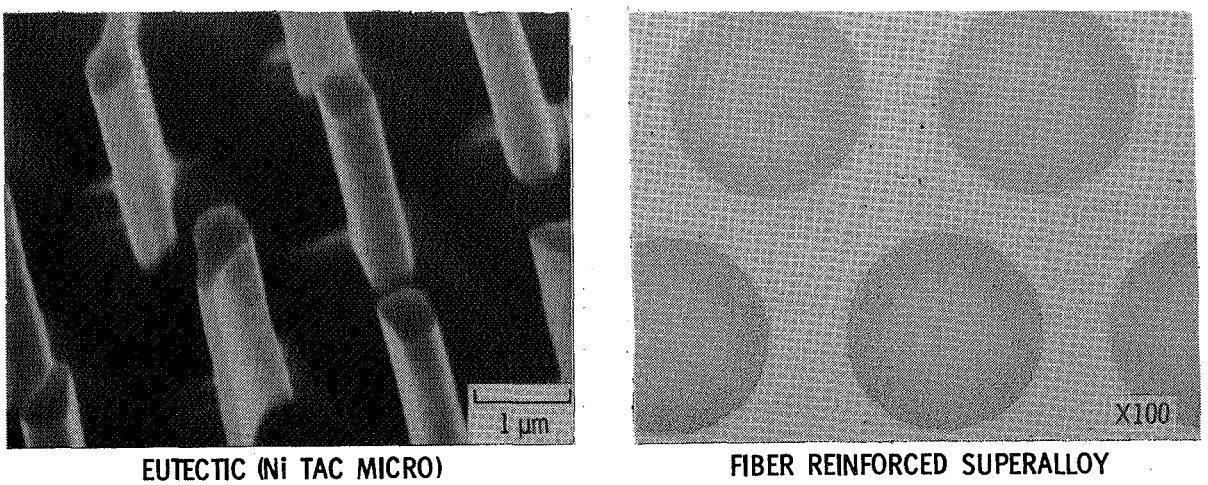

Figure 8.- Directional structures. (Print reduced 30%.)

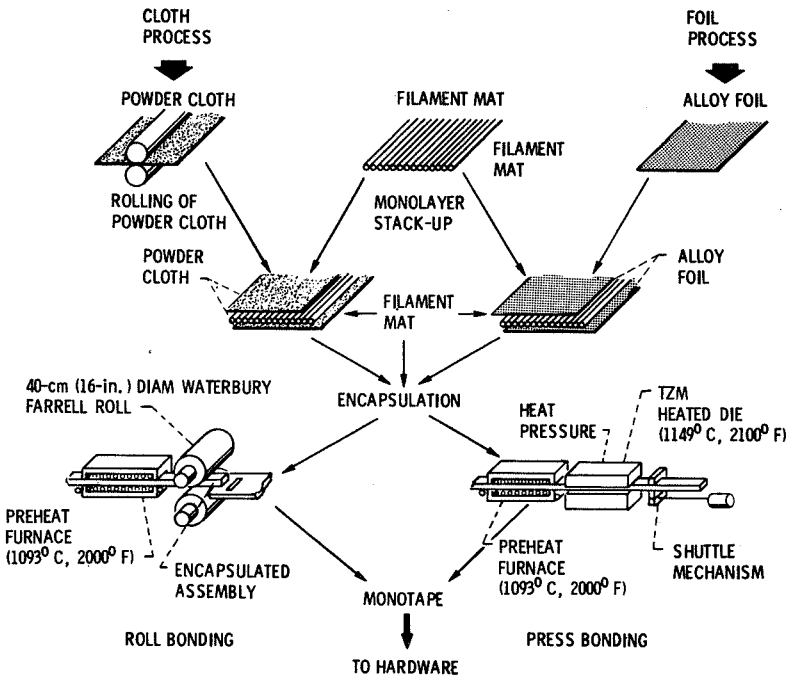

Figure 9.- Manufacture of wire-reinforced superalloy monotapes.

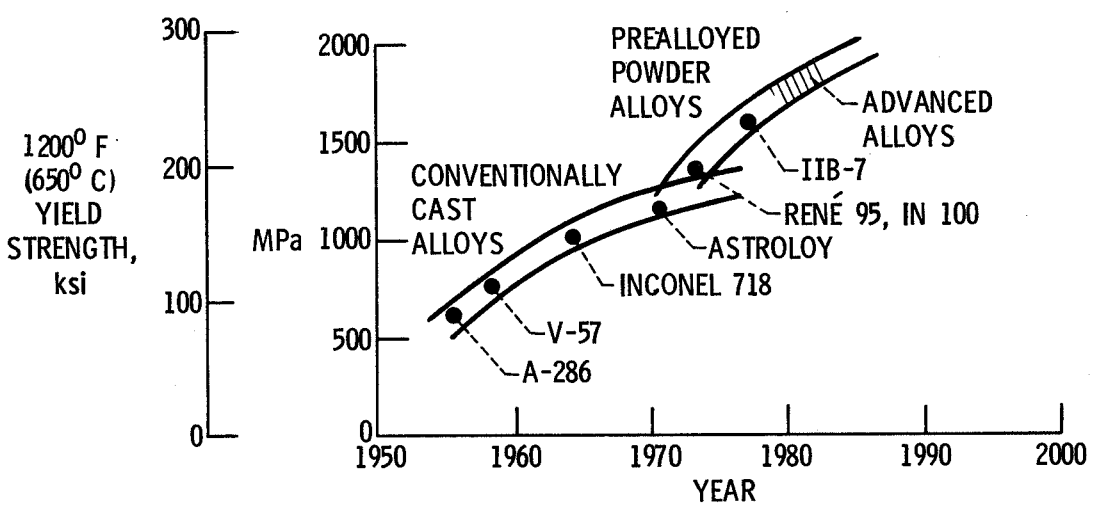

Figure 10.- Strength of turbine disk alloys.

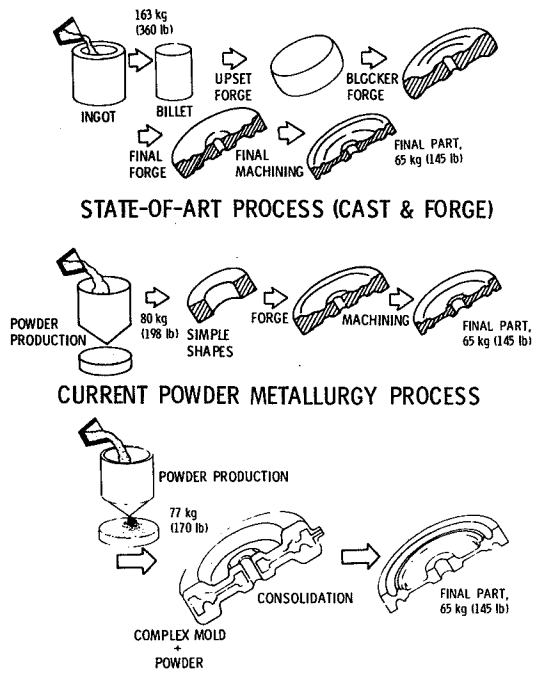

Figure 11.- Turbine disk fabrication processes.

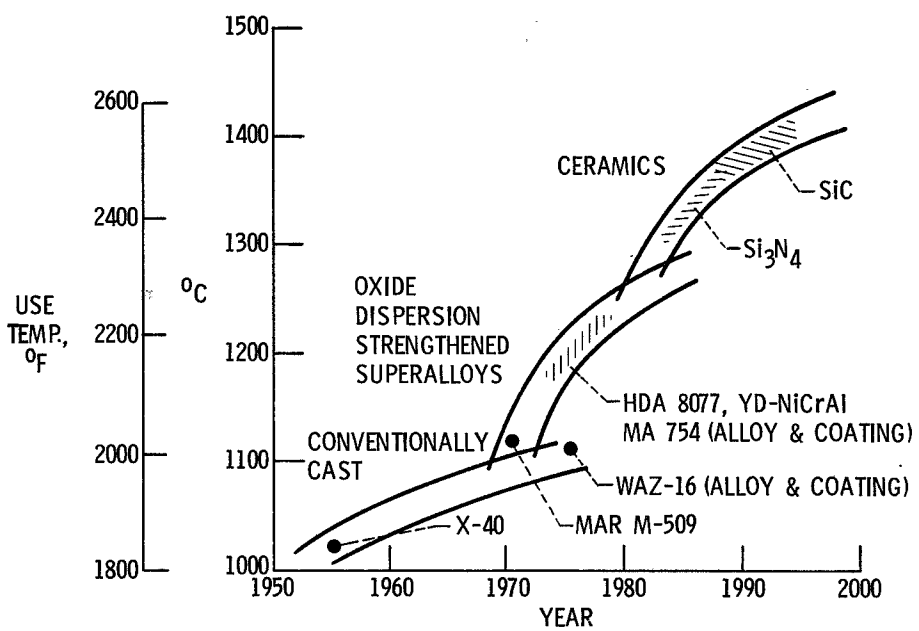

Figure 12.- Predicted higher use temperatures of ODS superalloys and ceramics for turbine vanes.

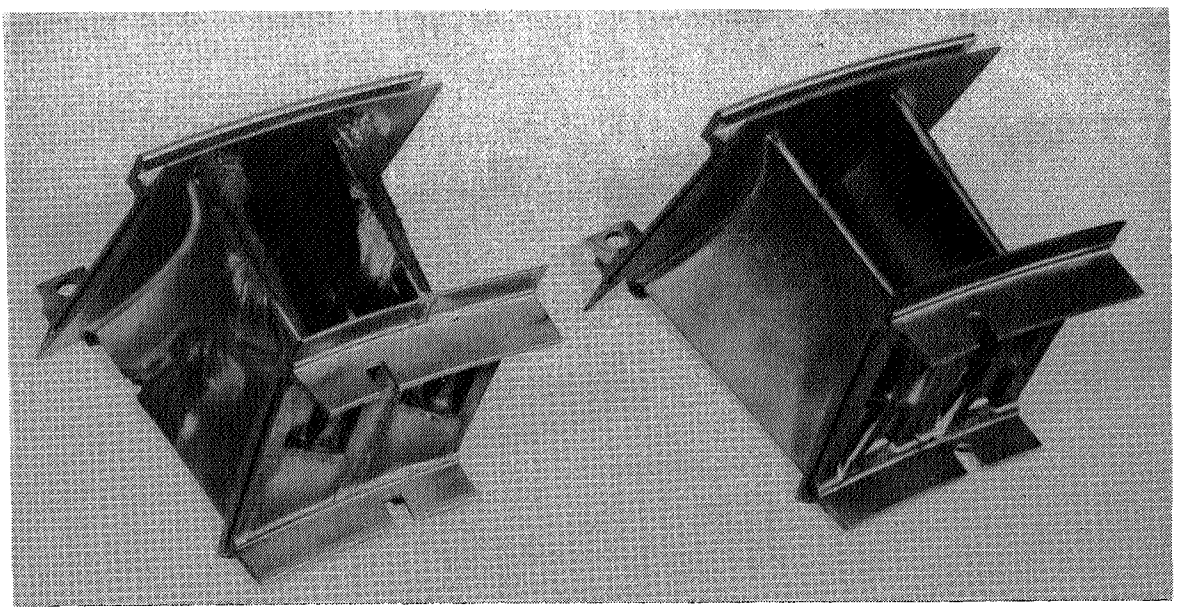

Figure 13.- Superiority of ODS vanes to conventionally cast vanes subjected to an overtemperature.

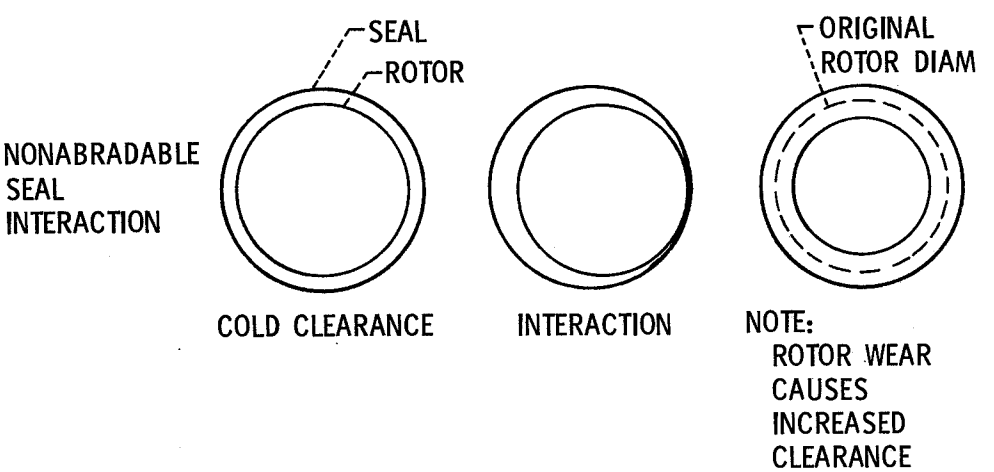

REMEDIAL APPROACHES:
- ABRADABLE ALLOYS (NiCrAl)
- NONABRADABLE CERAMICS
- LOW-EXPANSION MATLS

Figure 14.- Schematic of turbine seal and clearance degradation. (Note: Rotor wear causes clearance to increase 0.25 mm (0.010 in.).)

GAS TURBINE ENGINE EMISSION REDUCTION TECHNOLOGY PROGRAM

Donald A. Petrash and Larry A. Diehl

Lewis Research Center

SUMMARY

The Clean Air Act of 1970 empowered the Environmental Protection Agency to establish standards for the allowable pollutant emission levels of aircraft gas turbine engines. The standards, first issued in July 1973, established allowable levels for three gaseous pollutants and smoke. The gaseous pollutants were hydrocarbons, carbon monoxide, and the oxides of nitrogen. These emission standards were sufficiently stringent that combustor technology existing at the time was not sufficient to permit the design of the advanced combustors that would be needed to meet the standards. NASA therefore began a major program in emission reduction technology. The program consisted of in-house experimental research on low-emission advanced combustor concepts and a contracted research program with the major aircraft engine manufacturers. The purpose of this presentation is to review the results of the contracted research program with emphasis on the high-bypass-ratio turbofan engines which power the large commercial aircraft.

INTRODUCTION

The Clean Air Act of 1970 empowered the Environmental Protection Agency to establish standards for the allowable emission levels of aircraft gas turbine engines. The standards were first issued in July 1973. Earlier, in mid-1971, NASA began a major program in emission reduction technology, which would consist of a continuing in-house effort on low-emission combustor concepts and of contracted research programs with the major aircraft engine manufacturers. This paper gives an overview of the contracted emission reduction technology programs, which were begun with two firm objectives.

First, it was essential to investigate new combustor concepts that had the potential to significantly lower the emission levels. Considerable research with existing combustors had already shown that present concepts would not meet all of the EPA standards. The new concepts would have to be developed not only from an emissions standpoint but also from a conventional performance goals standpoint. Second, it was necessary to measure the combustor emissions in an engine test. The engine test would show whether the combustor concept could be installed in an engine and meet the engine operating requirements while producing the desired low emissions. Engine testing was also required to achieve the needed pressure levels and to avoid extrapolation of emission levels from lower pressure tests. And finally, engine testing would reveal those areas of the combustor that needed further development.

Multiphase contracts were awarded to the engine manufacturers. These phases consisted of screening, refining, and engine testing. In the first phase many combustor concepts would be screened to determine those having the most potential for low emissions. The best concepts would be further developed during the refinement phase, where combustor performance and emission reduction would be emphasized. Finally the best, or most engine ready, combustor would be installed and tested in an engine.

PROGRAM PLAN

As conceived, the emission reduction technology program would develop technology for representative engines in each of the EPA engine classes. With the exception of the T4 class, which consists solely of the JT8D family of engines, competitive contracts were awarded in each class. Table I shows the EPA classes, the engines, and the manufacturers that participated in the program. The T1 class consists of engines with thrusts less than 36 kN (8000 lb). The T2 class consists of engines with thrusts greater than 36 kN (8000 lb), and the P2 class consists of turboprop engines. Engines in the remaining two EPA gas turbine engine classes, T3 and T5, were not studied as a part of this program. The T3 class consists solely of the JT3D family of engines, and the T5 class consists of engines for supersonic aircraft, at present only the Olympus engine in the Concorde SST.

The goal of these programs was to meet the 1979 EPA Aircraft Engine Emission Standards. Table II shows the 1979 standards for the three gaseous pollutants and smoke for each of the engines in the program. The EPA standards are expressed in EPA parameter values for the specified landing-takeoff cycle. The production engine values are given as a percentage of the EPA standard values. In general, the production values exceed the standards by several hundred percent. Therefore, to meet the EPA standards, combustor technology had to be developed with the potential for significantly lower emission levels. Noteworthy are a few instances where the standards were already achieved - the oxides of nitrogen (NO_x) level for the P2 class and the smoke for the T2 class.

CHARACTERISTICS OF ENGINE EMISSIONS

Emission characteristics common to all engine classes are shown in figure 1. This figure is a plot of typical production engine emissions as a function of takeoff thrust level. The landing-takeoff cycle points are identified on the abscissa with their associated thrust levels. The ordinate values were obtained by summing the species emission index values over the landing-takeoff cycle and are shown as the percentage contribution at each cycle point. Emissions from all engine classes conform very well to this trend.

Virtually all hydrocarbon and carbon monoxide (CO) emissions are generated at low power, primarily at engine idle. These emissions are significantly reduced at approach power levels and virtually disappear at high power levels. Typical production aircraft engines have combustion inefficiencies at idle of 4 to 12 percent. This accounts for the high hydrocarbon and CO emissions at

idle. To reduce these emissions, combustor research must be directed toward increasing combustion efficient at idle. In practice, relatively large reductions in hydrocarbon and CO emissions have been achieved with relatively minor combustor modifications.

Oxides of nitrogen emissions, on the other hand, are at a minimum at engine idle and increase as engine power increases. To reduce NO_x emissions, combustor research must be directed toward the high power operating conditions. In general, NO_x reduction requires the lowering of the flame temperature and reduction of the residence time of gases at high temperatures. In practice, significant reduction in NO_x emissions require relatively major combustor modifications which are difficult to implement.

EARLY EMISSIONS REDUCTION RESEARCH

Before the contracted emission reduction technology program had even been planned, advanced combustor research at Lewis had identified several approaches to obtain low emissions. The research had indicated two promosing multiple-burning-zone combustors - specifically, the double-annular and swirl-can modular combustors. Both air-assist and air-blast fuel-injection techniques were studied to evaluate their potential for reducing emissions. Controlled combustion was also studied by varying the fuel and air schedules to the advanced combustors.

Some of the results obtained in 1972 tests are shown in figure 2, which shows the NO_x emissions for conventional combustors and the two advanced combustor concepts tested at Lewis. Note that the NO_x emissions are a strong function of combustor inlet-air temperature. This is because the inlet-air temperature is directly related to the combustion flame temperature and NO_x formation. This figure also indicates that NO_x control will be more difficult with high-pressure-ratio engines since an increase in engine compressor pressure ratio results in an associated increase in combustor inlet-air temperature. The advanced combustors did demonstrate significant reductions, and these results showed that substantial NO_x emission reductions were possible.

Improvements in fuel atomization may have a dramatic effect on pollutant emission levels. During engine idle, the fuel is sprayed from the duplex nozzle through the small-flow primary nozzle. This results in a spray that is generally coarse, consisting of large, sometimes poorly distributed drops. This combination of large drops and poor distribution results in high levels of hydrocarbon and CO emissions. An air-assist nozzle uses a small amount of air bled from the engine compressor and injects it through the unused secondary fuel nozzle. This air-assist reduces droplet size, improves the uniformity of the spray, and thereby reduces engine idle emissions. Typical results obtained from the application of this technique are shown in figure 3. The tests were conducted on a JT8D combustor and a production fuel nozzle. Emissions of hydrocarbons and CO are given on the ordinate and the injected air differential pressure on the abscissa. The use of air-assist considerably lowers the emissions: hydrocarbons were decreased by a factor of 8 and CO by nearly a factor of 4. The amount of air injected was quite small, being less than 0.5 percent of the combustor airflow at the maximum differential pressure.

RESULTS AND DISCUSSION

Because of the time required for a detailed discussion of all the programs and because of the thrust of the present conference, the T2 class engine will be emphasized in this discussion of the emission reduction technology program. The two engines studied in this part of the program were the Pratt & Whitney JT9D-7 and the General Electric CF6-50, both high-bypass-ratio turbofan engines which power current large aircraft.

The Pratt & Whitney JT9D-7 (fig. 4) engine has a maximum thrust of 205 kN (46 150 lb), a pressure ratio of 22:1, and an annular combustor. The production engine emission values (also shown in the figure) indicate that all emissions with the exception of smoke require large reductions. Figure 5 shows the production JT9D-7 combustor and the advanced low-emissions combustor that was used in the engine tests. The advanced-technology, Vorbix combustor is an axially staged design. The pilot zone has been optimized to reduce hydrocarbon and CO emissions at engine idle. And the main zone was optimized to reduce high-power NO_x emissions. In all, the pollution reduction concepts used to design the Vorbix combustor included multiple burning zones, air-blast fuel injectors, enhanced mixing, and fuel staging. Clearly, this combustor modification is more than minor and will require further development before it can be put into service.

The data obtained from the full-scale engine test of the Vorbix combustor are shown in figure 6. The CO, hydrocarbons, and NO_x emissions were 74, 25, and 90 percent of the EPA standard values, respectively; smoke levels exceeded the EPA standard value. The high smoke level appears to be result of fuel-rich zones at the main combustor inlet. It is felt that smoke levels can be reduced to acceptable levels.

The General Electric CF6-50 (fig. 7) engine has a maximum thrust of 224 kN (50 000 lb), a pressure ratio of 30:1, and an annular combustor. The production-engine emission levels shown in the figure also indicate that large reductions in all gaseous emissions are required to meet the emission standards. Figure 8 shows the production CF6-50 combustor and the advanced low-pollutant combustor used in the engine tests. This advanced-technology, double-annular combustor is a radially staged design. Again, the pilot stage was optimized to reduce hydrocarbon and CO emissions at engine idle, and the main zone was optimized to reduce the high-power NO_x emissions. As with the Vorbix, the double-annular combustor used the low-pollutant concepts of multizone burning, air-blast fuel injectors, enhanced mixing, and fuel staging.

The data that were obtained from the full-scale engine test of the double-annular combustor are shown in figure 9. Also shown are the best values obtained during the combustor refinement phase of the program conducted in the combustion test facility. Preliminary analysis of the engine-test data yields values for CO, hydrocarbons, and NO_x of 147, 38, and 187 percent of the standard value. The smoke level is also considerably above the EPA standard value. These disappointing results had not been anticipated. As can be seen, rig test values for CO and hydrocarbons were below the EPA standard values. The combustor tested in the engine had been substantially altered from the version tested in the previous phase. Most of the modifications involved "upgrading"

the combustor to an "engine ready" status. Additional rig testing, conducted in an attempt to restore the lost emissions performance, was only partially successful. However, the results of the earlier phase of the program encourage our belief that engine emission levels of CO, unburned hydrocarbons, and smoke can be reduced to acceptable levels.

Table III is a summary of all the emission results obtained in the program, with the engines ordered by increasing engine pressure-ratio. The unburned hydrocarbon standards were achieved for all engines. Carbon monoxide standards were essentially achieved for all but the JT8D and the CF6-50. The difficulty of achieving the NO_x standard increased directly with increasing engine pressure-ratio. The 501-D22A engine, with a 9.7:1 pressure ratio, easily met the NO_x standard with only a minor combustor modification. The TFE-731 engine, with a 13:1 pressure-ratio, barely met the NO_x standard and required a relatively major combustor modification. The JT8D, which has a 17:1 engine pressure-ratio, did not achieve the standard, in large part because of the high specific fuel consumption of the engine. For the T2 class engines, major modifications to the combustor of the JT9D, with an engine pressure-ratio of 22:1, did result in achievement of the NO_x standard, but the CF6-50 with an engine pressure ratio of 30:1 did not meet the standards.

The results presented have been compared with the 1970 EPA standards. More stringent gaseous emissions standards will apply to newly certified aircraft gas turbine engines in 1981. Table IV shows the levels achieved in terms of the 1981 standards for the advanced technology combustors tested in the JY9D-7 and CF6-50 engines. Although such a comparison is not completely valid, it is the EPA's intent that a newly certified engine be designed from the beginning with emissions control in mind and that design aspects such as pressure ratio, bypass ratio, allowable combustor volumes, and pressure drop and their influence on engine emission levels be considered. Such was not the case with the engines cited. The comparison does indicate where additional emission reduction technology development is required. Although emission control of unburned hydrocarbons appears well in hand, the same cannot be said of carbon monoxide. While further development of present technology may bring more CO reductions, it is not clear if it will be sufficient to satisfy all requirements. It is clear that new technology may be necessary if high-pressure-ratio engines are to achieve the required NO_x levels.

CONCLUDING REMARKS

The emission reduction technology program discussed in this report represents NASA's most recent efforts to reduce emissions for near-term applications. Continuing work is addressed to the development of emission reduction concepts that will be required to meet far-term needs. In particular, additional research is needed to further reduce emissions of carbon monoxide and oxides of nitrogen. Fundamental technology programs now underway have indicated that further reductions by as much as an order of magnitude may be possible. The extent to which this fundamental technology can be converted to practical engine hardware is yet unknown and will require several more years of research by NASA and the engine manufacturers.

TABLE I. - SCOPE OF EMISSIONS REDUCTION TECHNOLOGY PROGRAM

EPA engine class	Engine	Manufacturer
T1 - turbofans	TFE-731-2	Garrett AiResearch
T2 - turbofans	CF6-50	General Electric
	JT9D-7	Pratt & Whitney
T4 - JT8D engines	JT8D-17	Pratt & Whitney
P2 - turboprops	501-D22A	Detroit Diesel Allison

TABLE II. - EMISSION GOALS FOR 1979 EPA STANDARDS

Engine class	Engine	THC		CO		NO_x		Smoke	
		Standard	Production value, % of standard	Standard	Production value, % of standard	Standard	Production value, % of standard	Standard	Production value, % of standard
P2	501-D22A	4.9	306	26.8	118	12.9	48	29	189
T1	TFE-731	1.6	331	9.4	180	3.7	162	40	118
T4	JT8D-17	.8	500	4.3	356	3.0	260	25	120
T2	JT9D-7	.8	488	4.3	198	3.0	197	20	50
T2	CF6-50	.8	538	4.3	251	3.0	257	19	68

TABLE III. - POLLUTION SUMMARY FOR ALL ENGINE CLASSES

EPA class	Engine	Engine pressure ratio	Modification required	THC	CO	NO_x	Smoke
				Percent of 1979 EPA standard			
P2	501-D22A	9.7	Minor	6	17	57	59
T1	TFE-731-2	13	Major	25	107	100	---
T4	JT8D-17	17	↓	25	207	146	108
T2	JT9D-7	22	↓	25	74	90	150
T2	CF6-50	30	↓	38	77-147	147-187	132

TABLE IV. - POLLUTION SUMMARY FOR

T2 CLASS ENGINES

Engine	THC	CO	NO_x
	Percent of 1981 EPA standard		
JT9D-7	50	106	90
CF6-50	76	110-211	147-187

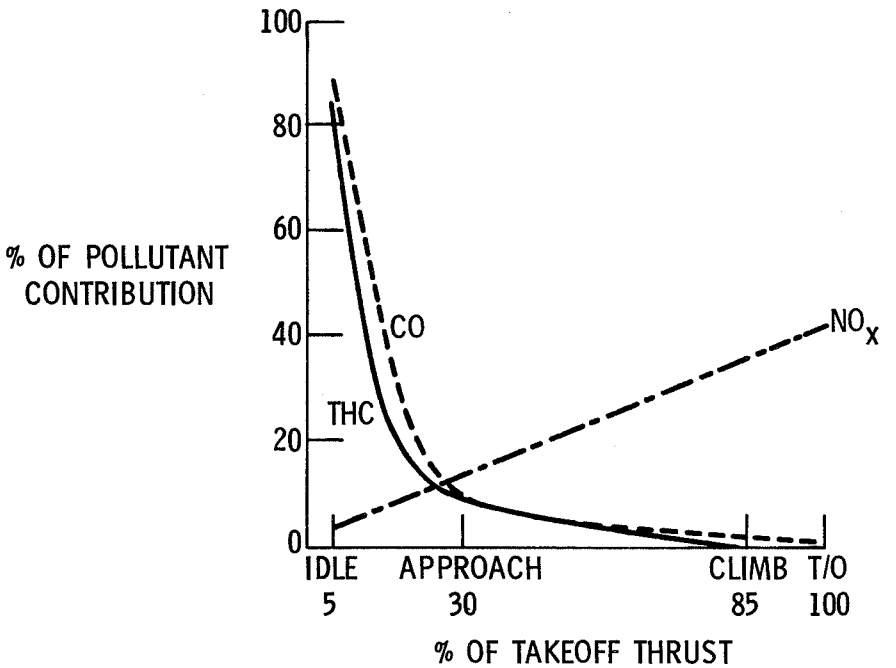

Figure 1.- Typical engine emission characteristics.

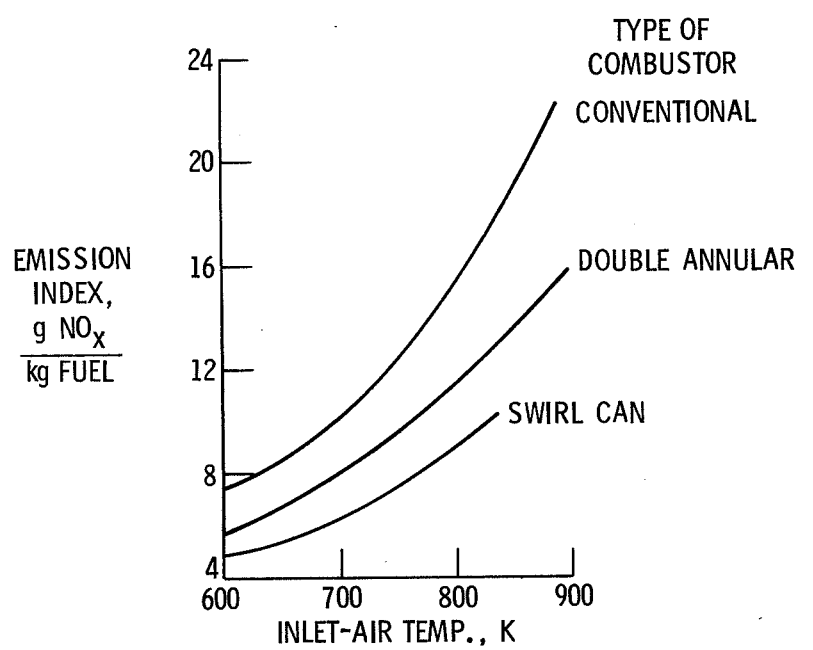

Figure 2.- Oxides of nitrogen emissions as function of combustor-inlet temperature. Combustor pressure, 6 atm.

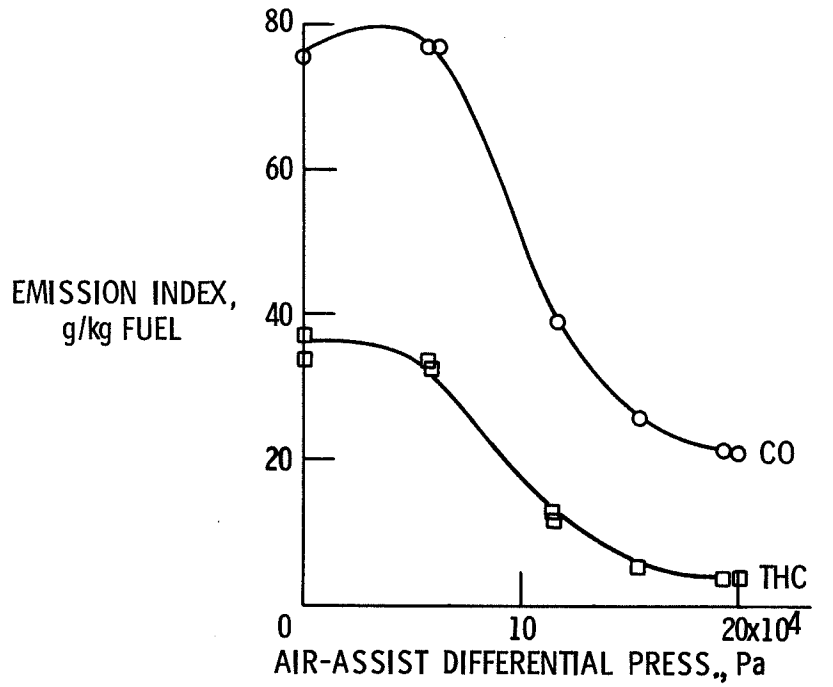

Figure 3.- Effect of improving fuel atomization on gaseous emissions.

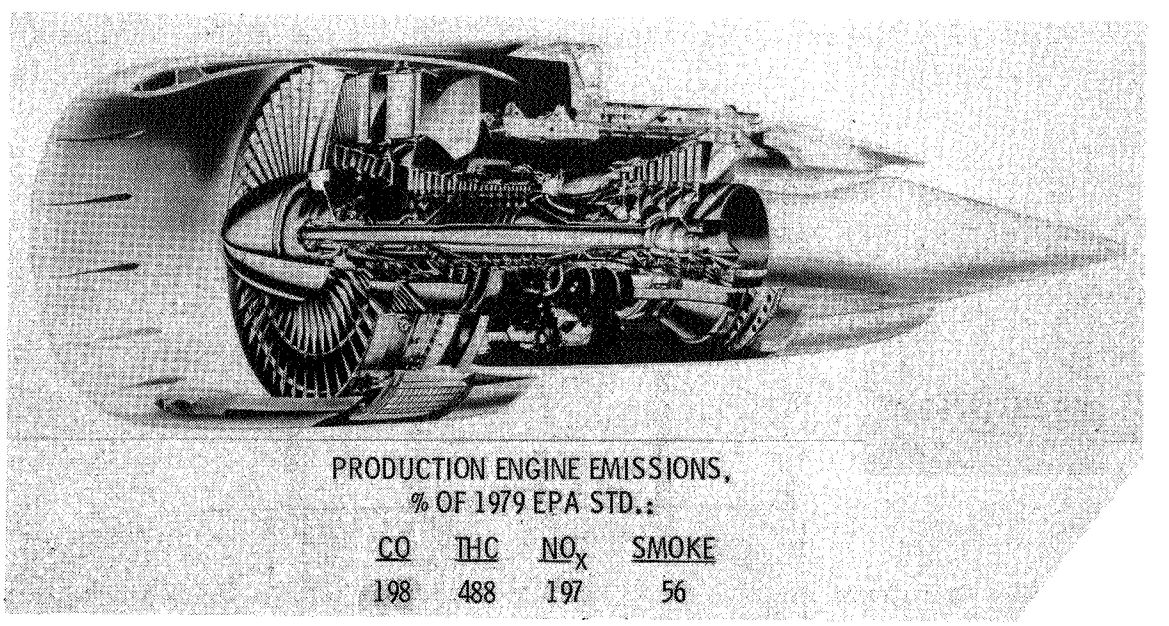

Figure 4.- EPA class T2 jet aircraft engine JT9D-7. Thrust, 205 kN; pressure, 22:1; type of combustor, annular.

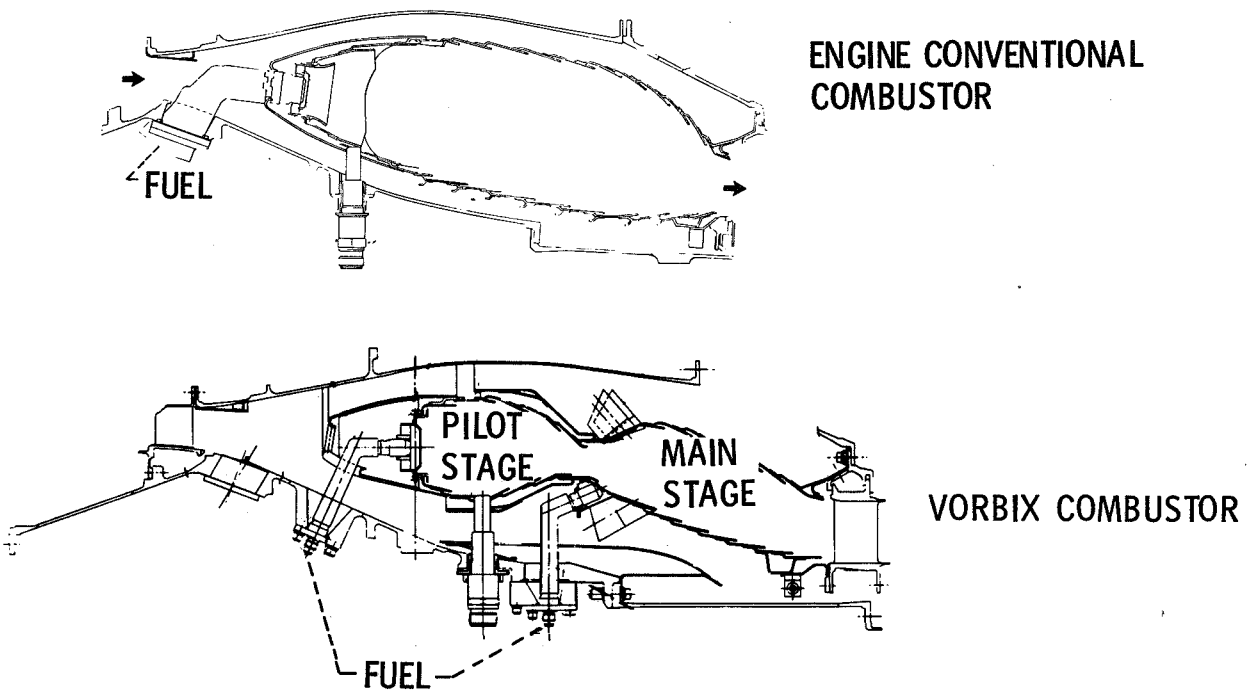

Figure 5.- Low-emission, staged combustor for the JT9D-7 engine.

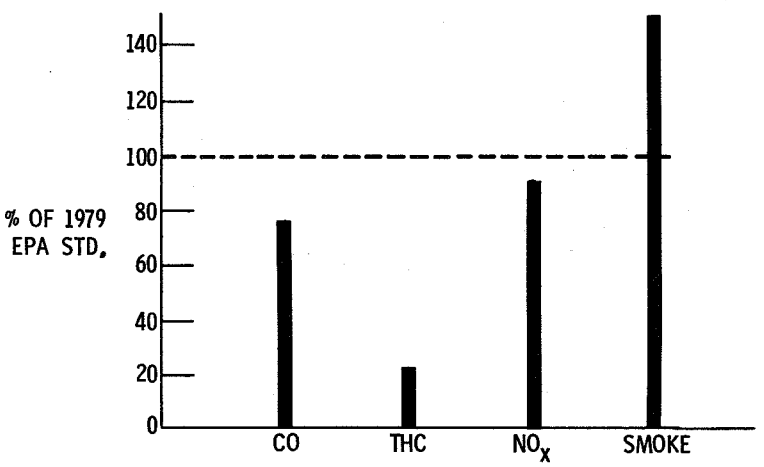

Figure 6.- Emissions results from Vorbix combustor tests in JT9D-7 engine.

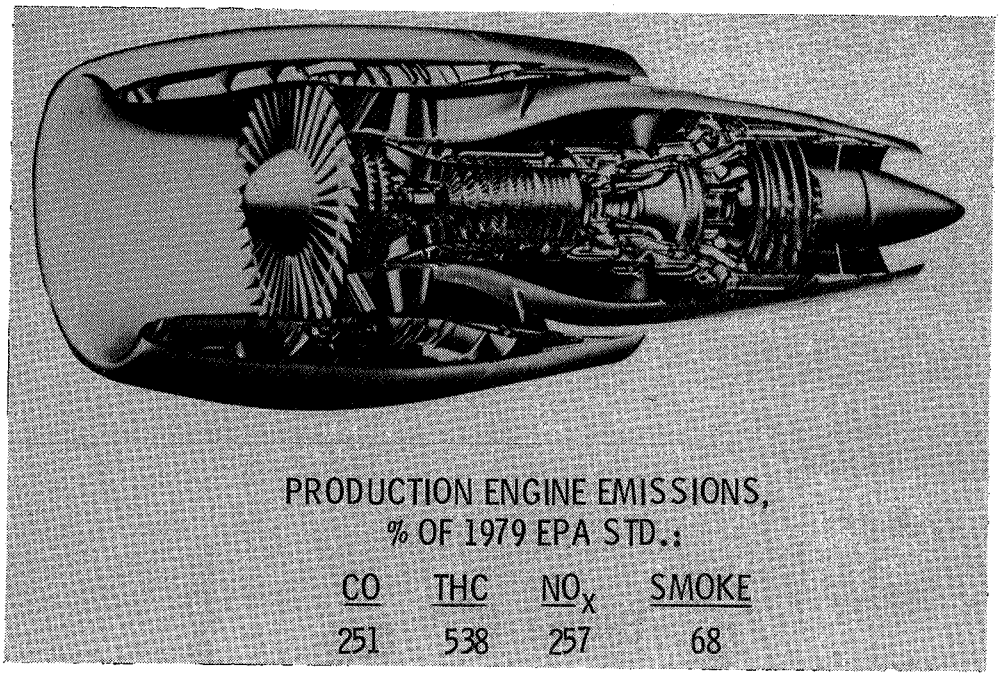

Figure 7.- EPA class T2 jet aircraft engine CF6-50. Thrust, 224 kN; pressure ratio, 30:1; type of combustor, annular.

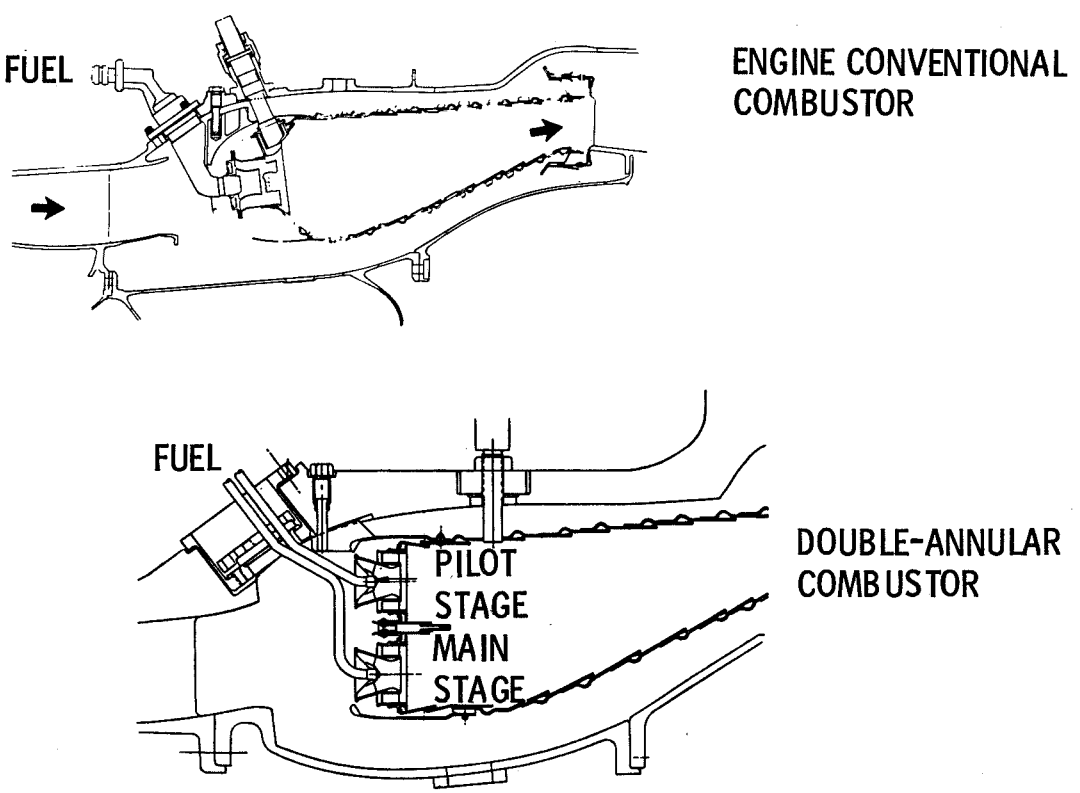

Figure 8.- Low-emission, staged combustor for the CF6-50 engine.

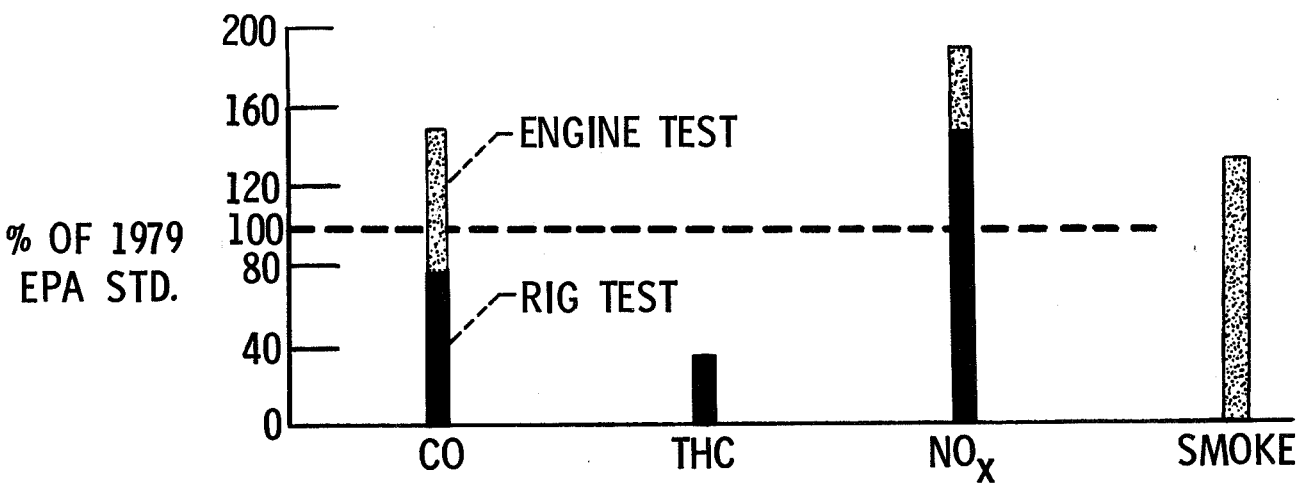

Figure 9.- Emission results from double-annular combustor tests. Full-scale tests conducted in CF6-50 engine.

IMPACT OF BROAD-SPECIFICATION FUELS ON FUTURE JET AIRCRAFT

Jack Grobman
Lewis Research Center

SUMMARY

The efficient use of fossil fuels by future jet aircraft may necessitate relaxing or broadening current aviation turbine fuel specifications. The most likely specification changes could be toward an increased aromatics content (increased carbon to hydrogen ratio) and a higher final boiling point. Permitting an increase in aromatics would minimize refinery energy consumption and costs for fuels derived from highly aromatic crudes or from nonpetroleum sources such as shale or coal. In addition, a higher aromatic content and final boiling point would allow greater jet fuel yields by simple distillation and low-cost refinery processes. A jet fuel with an increased aromatic content and higher final boiling point could cause increased gaseous pollutant emissions, increased smoke, increased carbon deposition, increased combustor liner temperatures, poorer thermal stability, poorer ignition characteristics, and potential fuel-tank pumpability problems due to increased fuel freezing point and viscosity. Broad-specification fuels could, therefore, reduce engine life and thereby increase maintenance costs. This paper discusses the effects that broad-specification fuels may have on present-day airframe and engine components, and it also describes the improvements in component technology that may be required to use broad-specification fuels without sacrificing performance, reliability, maintainability, or safety.

INTRODUCTION

Jet fuel price increases and projected jet fuel shortfalls due to shifts in future supply and demand have led to serious considerations of the actions necessary to prevent a constraint on the future growth of air transportation. These actions must be addressed to the overall conservation of energy in both the air transportation and petroleum refining industries. NASA, along with other government agencies and private industry, has been conducting a research and technology effort to establish the data base necessary to optimize future jet fuel characteristics in terms of refinery energy consumption and trade-offs in jet aircraft and engine design (ref. 1). Other research and technology efforts are being conducted by NASA to reduce jet fuel consumption by improving aircraft energy efficiency (ref. 2).

Broadening current jet fuel specifications would permit reductions in energy consumption at the refinery. A broad-specification fuel may be defined arbitrarily as a liquid hydrocarbon fuel with key properties or characteristics that substantially exceed current specification limits for aviation turbine

fuels. Significant production of synthetic crude oil from shale or coal is not expected until about the turn of the century; therefore, petroleum will remain the only source of jet fuel for the foreseeable future. Although research is being conducted to evaluate the economic feasibility of using hydrogen as a jet aircraft fuel, conventional hydrocarbon fuels will, in all probability, continue to be used commercially well into the next century. This paper, therefore, emphasizes the problems related to broadening the specifications for conventional jet aircraft fuels produced from petroleum.

The probable characteristics of broad-specification fuels and the impact that these broad-specification fuels may have on future jet aircraft are discussed herein. (The topics covered include the properties of current commercial jet aircraft fuel, the projected future changes in jet fuel properties, the potential engine and airframe component problems that result from broadening fuel specifications, and the component technology improvements that are required to use broad-specification fuels without sacrificing performance, reliability, maintainability, or safety.

JET AIRCRAFT FUEL PROPERTIES

Jet fuel has traditionally been manufactured by distillation from petroleum crude followed by a mild hydrogen treatment to control sulfur, corrosivity, or thermal stability as needed. The boiling range of the major petroleum-derived fuels is shown in figure 1. Crude petroleum normally has a boiling range that extends to about 600° C. As the demand for jet fuel, diesel oil, and heating oil increases, a point will be reached where there is an insufficient quantity of material in the proper boiling range. It will then become necessary to convert fractions boiling above 300° C to these lower boiling products. These cracked products are, in general, higher in aromatic content (increased carbon to hydrogen ratio) than are the naturally occurring fractions. The processing required to produce current specification jet fuel from the higher boiling fractions consumes considerably more energy because of the process hydrogen requirements than does the conventional production of jet fuel by crude distillation.

The commercial jet aircraft fuel, Jet A, has a relatively narrow boiling range specification (fig. 1). The initial boiling point, a minimum of about 170° C, is necessary to keep the flash point above 40° C to reduce the probability of a fire during fueling or following an emergency landing. The final boiling point for Jet A is usually below 270° C to comply with limits on the freezing point. Figure 2 shows the increase in freezing point to be expected as the final boiling point is increased. The freezing point of a fuel blend is the temperature at which wax components in the fuel solidify. The specification for Jet A limits the freezing point to a maximum of -40° C. Figure 2 indicates that the freezing point is quite sensitive to the final boiling point; however, an increased final boiling point would clearly allow increased flexibility in the production of jet aircraft fuel.

Trends in the average aromatic content of commercial Jet A fuel between 1960 and 1976 are shown in figure 3. The average aromatic content has

increased from 14 percent (by volume) in 1960 to about 17 percent in 1976. The ASTM Jet A specification for aromatic content is a maximum of 20 percent. During the emergency period of 1973-1974, the limit was temporarily raised to 25 percent; more recently, a waiver has permitted the limited use of Jet A with a maximum aromatic content of 25 percent. During the emergency period, the limited quantities of Jet A refined from heavy Arabian crude had aromatic contents as high as 22 percent. Projections indicate that Jet A refined from Alaskan crude may have aromatic contents as high as 25 percent. These increases in aromatic content may be attributed in part to the production of Jet A by distillation of crudes with relatively higher aromatic content. In addition, several other factors could cause the aromatic content of jet fuel to increase. As mentioned earlier, the cracking of higher boiling materials to produce a product within the jet fuel boiling range increases the fuel aromatic content. The aromatic content of jet fuel may also be increased by extending the distillation range to a higher final boiling point. As shown in figure 4, these increases in aromatic content result in a proportionate lowering of the hydrogen content of the fuel. Decreasing the hydrogen content can increase the soot and flame radiation levels within the combustor and thus can increase the combustion liner temperatures.

In the future, as the relative demand for jet fuel increases, it will be necessary for refineries to consume considerable quantities of hydrogen in order to meet the requirements for current specification aviation turbine fuel. Since the production of hydrogen requires significant energy consumption, and since hydrogen and the processes using it are very expensive, consideration of cost and energy conservation encourages minimizing these types of refining. Thus, there is a definite need to investigate the effects of broadening jet aircraft fuel specifications on jet engine performance and durability in order to develop a data base which will allow an optimization of future fuel characteristics that takes both refinery energy consumption and aircraft engine design trade-offs into account. In order to implement this optimization effort it is desirable to establish a target fuel for use in research programs on both fuel production and aircraft/engine design. An experimental fuel has been recommended with properties that approach those shown in table I (ref. 3). Comparing the representative values for the properties of the proposed future broad-specification fuel with those of current Jet A fuel indicates that the major changes to be expected would be (1) an increased aromatic content corresponding to a reduction in hydrogen content, (2) a higher final boiling point, (3) a higher freezing point, and (4) a lower thermal stability JFTOT (jet fuel thermal oxidation test) breakpoint temperature. The thermal stability breakpoint temperature is an empirical laboratory indication of the degree to which the fuel may be heated without incurring significant levels of fuel decomposition. The properties designated for the future broad-specification fuel tend to be similar to those of the current number 2 diesel fuels.

JET AIRCRAFT PROBLEMS RELATED TO USING BROAD-SPECIFICATION FUELS

Effect of Hydrogen Content of Fuel on Turbine Engine Combustors

Increases in aromatic content or, conversely, decreases in hydrogen content of the fuel have a pronounced effect on smoke and on liner temperatures. Combustor tests have been conducted using prepared fuel blends with varying amounts of aromatics (ref. 4). At cruise and takeoff conditions strong increases in exhaust smoke were observed as the hydrogen content of the fuel decreased (fig. 5). The effect of hydrogen content on maximum liner temperatures is shown in figure 6. As the aromatic content of the fuel increases and hydrogen content decreases, the flame becomes more sooty and more luminous; hence, radiation to the liner increases. Sharp increases in maximum liner temperatures were observed as the hydrogen content of the fuel decreased. At cruise, liner temperatures observed with fuels in the Jet A range (13.5 to 14 percent) were 800° C or less for all fuels. However, with fuels having a lower hydrogen content, severe liner durability problems could arise. At takeoff, maximum combustor liner temperatures exceeded 900° C for all fuels. However, the time spent at takeoff and, hence, the exposure time of the liner to these high temperatures are quite short.

Advanced Combustor Technology

In the NASA Experimental Clean Combustor Program, experimental combustors have been developed which promise not only lower exhaust emissions but also reduced sensitivity to relaxed fuel specifications (refs. 5 and 6). Two of these combustors, the Vorbix combustor for the P&W JT9D engine and the Double-Annular combustor for the G.E. CF6-50 engine, are shown for reference in figure 7. Both combustors feature staged combustion with a relatively rich zone for idle operation and a leaned-out main combustion zone for high-power operation.

Some of the results obtained with these combustors are shown in figure 8. Since the various data were not all obtained at the same combustor-inlet conditions, the data are plotted as the difference between maximum liner temperatures and combustor-inlet temperature. The two top curves, representing data obtained with a production-model full-annular combustor and a single-can JT8D combustor, exhibit the strong dependency of maximum liner temperature on hydrogen content of the fuel. The bottom curve, representing data obtained with the experimental Vorbix and Double-Annular combustors, shows a relative insensitivity of maximum liner temperatures to the hydrogen content of the fuel. Similarly, since soot formation is a strong function of combustor design as well as fuel composition, there is good reason to expect that the advances in combustor design illustrated here could allow satisfactory combustion of fuels containing less hydrogen.

Another method of reducing liner temperatures is to coat the inside of the combustor liner with a thermal-barrier coating (ref. 7). A JT8D combustor liner was coated with a thermal-barrier coating developed at the Lewis Research Center for application to turbine blades. The coating consists of a bond of a

nickel-chromium-aluminum-yttrium alloy covered with a ceramic layer of 12 percent (by weight) yttria-stabilized zirconia. The results obtained with Jet A fuel, for both cruise and takeoff, indicated that reductions in maximum liner temperatures were achieved.

While these findings represent limited laboratory tests and their practicality requires demonstration in a full development program, they do indicate that important advances may be feasible in the ability of aircraft gas turbine engines to use low hydrogen content fuels.

Fuel Tank Temperatures During Cruise

Fuel stored in aircraft tanks can reach very low temperatures during long flights. Figure 9 shows extreme fuel temperatures that may be encountered during long-range flight. These data were calculated to show fuel tank temperatures when the static temperature at altitude is as low as -72° C (ref. 8). This is an extreme case with a one-day-a-year probability. Two curves are shown, each with a widely different initial ground loading fuel temperature. The effect of the different initial temperatures on in-flight fuel temperatures decreases as the flight progresses. After a period of time, the in-flight fuel temperature is completely independent of the initial temperature. The fuel temperature eventually reaches a minimum of -43° C, which is approximately the stagnation temperature at a cruise Mach number of 0.84 for the ambient static temperature. The rise in temperature at the end of the flight occurs because of increased altitude ambient temperature at the latter portion of the flight.

Jet fuel is a mixture of chemical compounds and does not have a fixed freezing point. Instead, it undergoes a large increase in viscosity and a partial phase change over a range of temperatures. Even this semisolid fluid can threaten operating problems. Fuel freezing has always been avoided by in-flight monitoring of fuel tank temperatures and by using jet fuels with low, conservative freezing-point specifications.

Fuel System Technology for Use of High-Freezing-Point Fuels

Fuels with higher freezing points than those listed in current specifications might be used if the fuel is heated in flight. Figure 10 shows several curves of predicted fuel temperatures during a long-range flight. The zero-heat-input curve repeats the in-flight temperature calculations shown in figure 9, and it represents an extreme case expected one day a year with a minimum fuel temperature of -43° C. The other two curves illustrate the in-flight fuel temperatures with the fuel heated at the rates indicated. The minimum in-flight fuel temperature can be raised to -29° C by heating the fuel at a rate of 3700 kJ/min (3500 Btu/min) or can be raised to -18° C by heating the fuel at a rate of 6500 kJ/min.

The calculated heating requirements can be reduced by insulating the fuel tanks. Using insulation can result in a sizable decrease in heating requirements. For example, without insulation 6500 kJ/min are required to maintain

the fuel above -18° C. With 1.3-cm-thick insulation, the same minimum temperature can be maintained with 3000 kJ/min; with 2.5-cm-thick insulation, only 2000 kJ/min are required.

The Boeing Company under NASA Contract (ref. 8) has completed a preliminary study of practical fuel heating systems based on the 747 airplane. Figure 11 is a cutaway drawing showing several possible heat source systems mounted on the wing fuel tanks and engines of the 747. Some existing components, with minor modifications, can be used as heat sources. Three examples are shown: the cabin air conditioning heat rejection, fuel recirculation from the fuel pump, and fuel recirculation from the engine lubricating oil heat exchanger. The latter two heating systems would be based on pumping fuel at a maximum rate at all times and then recirculating or returning the excess fuel back to the wing tank. The excess fuel would be heated by the pump or the lubricating oil heat rejection to warm the bulk of the tank fuel. Three additional systems, each capable of higher heating rates, are also shown. These systems, which involve major modifications, include a tailpipe heat exchanger, an engine compressor air bleed heat exchanger, and an electric heater powered by an engine-drive generator. Most likely, these systems would heat the fuel indirectly through a second heat exchanger loop by using an inert fluid. Wing tank insulation is also shown in figure 11.

Data on these fuel heating systems are compared in table II. The first three systems are minor modifications of existing aircraft components that use heat sources with 2100 to 4500 kJ/min ranges. These rates could be increased by combining systems at the risk of control complexity. Two columns in this table show predicted penalties for the heating systems in terms of airplane weight increase and fuel consumption, expressed as percent of cruise fuel flow. These calculations for the minor modifications indicate that the penalties would be low. These systems, for the most part, use existing heat rejection in the airplane and power plants.

Table II also compares the major modifications, which involve greater weight and performance penalties but which promise future use with very high-freezing-point fuels. These systems are sized for 6500 kJ/min and can maintain fuel temperatures above -18° C for all cases. Weight increases per airplane for these systems are estimated as 250 to 450 kg. Fuel consumption penalties for energy diverted to fuel heating are least for the tailpipe heat exchanger (0.1 percent of the cruise fuel flow rate) and greatest for compressor air bleed (3.9 percent). On the other hand, the tailpipe heat exchanger is perhaps the furthest from the state of the art in development feasibility.

Table II includes two other items. Insulation, which holds great promise for reducing heating requirements, has a serious drawback in system weight and corresponding fuel consumption penalty. Reducing the heating requirements, as discussed earlier, would not be sufficient to compensate for the insulation weight. Future designs, however, with composite wing material may incorporate lightweight insulation in the basic designs. Finally, table II shows the equivalent fuel consumption representing 6500 kJ/min of combustion energy, about 40 kg/hr, or 0.4 percent of the cruise fuel flow. Systems that use the heat rejection otherwise unavailable in the engine thermodynamic cycle, such as

the tailpipe heat exchanger or some minor modifications, can have lower fuel consumption penalties than this combustion equivalent.

CRITICAL RESEARCH AND DEVELOPMENT NEEDS

Combustor Technology

The previous section discussed the potential of using either staged combustion or a thermal-barrier coating as a means of minimizing the combustion liner surface temperature when burning highly aromatic fuels. It is important to maintain acceptable liner surface temperatures without increasing the quantity of air used to cool the combustion liner. Any increase in liner cooling airflow requires an equivalent reduction in the dilution-mixing air that is used to cool the high-temperature combustion gases. The dilution mixing air controls the gas temperature distribution entering the turbine by cooling the high-temperature gases leaving the primary zone of the combustor. Reducing the dilution-mixing airflow would result in a more peaked combustor exit temperature distribution and would thereby place a lower limit on the turbine operating temperature and service life. This problem could be more critical in advanced engines with higher compressor pressure ratios and higher turbine inlet temperatures.

A staged combustor permits leaner combustion during takeoff and cruise and thus reduces flame radiation to the liner surface by reducing soot formation within the combustor. A thermal-barrier coating provides insulating and oxidation protective coverings over the surface of the liner. Another way to minimize liner cooling airflow requirements could be to use advanced cooling liners with increased cooling effectiveness. These as well as other approaches, such as advanced structural designs for combustion liners, could be investigated.

The formation of hard carbon particles or deposits within the combustion chamber must be avoided. Hard carbon particles may strike the turbine and cause erosion of the leading and trailing edges of the blades. Significant carbon deposition on either the fuel injectors or combustion liner may result in distorted fuel flows or cooling-air-hole blockages; either of these might cause local overheating or peaked temperature distributions at the turbine. Combustor testing with broad-specification fuel is needed to determine the effect of lowering fuel hydrogen content on carbon deposition. Research is needed to obtain a more fundamental understanding of the mechanisms of carbon formation within combustors.

More extensive combustor testing is needed to obtain parametric data on the effects of reduced fuel hydrogen content and reduced volatility on the exhaust emissions of different engines. The impact of broad-specification fuels on the emission levels of combustors designed to meet E.P.A. emission standards must be assessed. Smoke and nitric oxide emissions may increase during takeoff and cruise for some engines. Carbon monoxide and unburned hydrocarbons may increase during idle. Improvements in fuel atomization and fuel-air mixing may be required to cope with these problems.

Many of the aforementioned problems might be partially resolved by improvements in fuel injector design. Further research may be required to evolve more effective air atomizing fuel injection systems for handling more viscous and/or less volatile fuels. Ignition and relight of fuels with higher viscosity and/or lower volability could be another significant problem. On cold days fuel heaters may be needed at starting conditions with such fuels. In addition, special provisions such as a pilot burner may be needed to permit satisfactory ignition at altitude relight operating conditions.

Fuel System Technology

Possible approaches to fuel tank heating to enable using fuels with higher freezing points have been described herein. A more detailed analytical study has recently been initiated by Boeing under a NASA contract to design practical fuel heating systems for future jet aircraft. In addition, an experimental study has been initiated by Lockheed under another NASA contract to obtain a better understanding of the low-temperature pumpability limits of fuels with varying freezing points in a subscale fuel system simulator. These research efforts should eventually lead to the evaluation of broad-specification fuels in full-scale fuel system simulators.

Preventing fuel manifold and fuel injector fouling is another critical problem. Aircraft turbine fuels must be stable at the temperatures they will encounter in the fuel system. Practically, this means there must be no gum or deposit buildup on heated surfaces such as heat exchanger tubes or manifold piping, and there must be no cracking or particulate buildup to clog small passageways in the fuel system such as filters or fuel nozzles. Current jet aircraft fuels are marginally stable in present-day engines. The chemical changes that result in deposit formation occur at an increased rate as the fuel temperature is increased. Future engines with higher compressor pressure ratios will therefore be even more susceptible to deposition problems since the fuel manifold and fuel injectors may be exposed to higher compressor discharge air temperatures. Obviously, using broad-specification fuels with lower thermal stability will increase the severity of this problem. Modifications to the fuel system may, therefore, be required to limit the maximum temperature to which the fuel is exposed. Possible design approaches such as insulating or cooling the fuel manifold and fuel injector could be investigated. Fuel line purging during shutdown is another technique that could be evaluated. Fuel decomposition is known to be influenced by the oxygen dissolved in the fuel. Deoxygenation and fuel additives to control deposit formation rates should be investigated. In addition, more basic and applied research is needed to acquire a better understanding of the fuel system variables and fuel composition variables that affect deposit formation.

The compatibility of broad-specification fuels with sealants and elastomers used in the fuel tank and fuel system must be identified. Improved polymeric materials may be required to cope with higher aromatic contents. Finally, problems related to ground handling of broad-specification fuels must be examined. Ground heating of high-freezing point fuels might be required in northern hemisphere cities during the winter.

Obviously, the critical research and development needs emphasized herein have not covered all of the possible problems related to the use of broad-specification fuels. We are just beginning the task of determining the effects of broad-specification fuels on aircraft and engine components and of identifying the technology required to use broad-specification fuels.

CONCLUDING REMARKS

The advantages and disadvantages of several solutions to the problems associated with using broad-specification fuels are summarized in table III. The first solution is to continue developing the necessary technology at the refinery to produce specification jet fuels regardless of the feedstock that is used. By this approach, the fuel properties may be optimized or tailored to the needs of future jet aircraft. Furthermore, this would eliminate the serious cost penalty of retrofitting existing aircraft and engines. The disadvantage of this approach would be increased energy consumption at the refinery and thus increased fuel cost.

On the other hand, the second solution shown in table III is to minimize energy consumption at the refinery and keep fuel costs down by relaxing specifications. The disadvantage of this approach is that more complex component technology must be developed to cope with problems such as increased pollutant emissions, increased combustor liner temperatures, poorer thermal stability, poorer ignition characteristics, and restricted fuel pumpability. Furthermore, using broadened specification fuels may adversely affect engine life, thereby increasing aircraft maintenance costs. Ultimately, the solutions to these problems will involve determining the most energy efficient and cost effective path. The most practical solution will probably require a compromise between partially relaxing fuel specifications and a limited redesign of the aircraft and engine.

REFERENCES

1. Grobman, Jack S., et al.: Alternative Fuels. Aircraft Engine Emissions. NASA CP-2021, 1977, pp. 277-308.

2. Povinelli, Frederick P.; Klineberg, John M.; and Kramer, James J.: Improving Aircraft Energy Efficiency. Astronautics & Aeronautics, vol. 14, no. 2, Feb. 1976, p. 18-31.

3. Longwell, J. P., ed.: Jet Aircraft Hydrocarbon Fuels Technology. NASA CP-2033, 1978.

4. Butze, Helmut F.; and Ehlers, Robert C.: Effect of Fuel Properties on Performance of a Single Aircraft Turbojet Combustor. NASA TM X-71789, 1975.

5. Roberts, R.; Peduzzi, A.; and Vitti, G. E.: Experimental Clean Combustor Program, Phase II. (PWA-5370, Pratt & Whitney Aircraft, NASA Contract NAS3-18544.) NASA CR-134970, 1976.

6. Gleason, C. C.; and Bahr, D. W.: Experimental Clean Combustor Program, Alternate Fuels Addendum, Phase II. (R76AEG268, General Electric Co.; NASA Contract NAS3-18551.) NASA CR-134972, 1976.

7. Butze, Helmut F.; and Liebert, Curt H.: Effect of Ceramic Coating of JT8D Combustor Liner on Maximum Liner Temperatures and Other Combustor Performance Parameters. NASA TM X-73581, 1976.

8. Pasion, A. J.; and Thomas, I.: Preliminary Analysis of Aircraft Fuel Systems for Use with Broadened Specification Jet Fuels. (D6-44538, Boeing Commercial Airplane Co.; NASA Contract NAS3-19783.) NASA CR-135198, 1977.

TABLE I. - MAJOR PROJECTED CHANGES IN FUEL PROPERTIES

	Current Jet A fuel	Future broad-specification fuel
Aromatics, vol %	17 to 25	30 to 35
Hydrogen, wt %	14 to 13.5	13.0 to 12.5
Final boiling point, °C	260 to 280	290 to 330
Freezing point, °C	-46 to -40	-34 to -29
Thermal stability (JFTOT) breakpoint temperature, °C	≥260	≥240

TABLE II. - COMPARISON OF POSSIBLE FUEL HEAT SOURCES

	Maximum heating rate per tank, kJ/min	Weight increase, kg	Fuel penalty, %
Air conditioning system	2200	140	0
Lubrication oil heat exchanger	4500	140	~.4
Fuel boost pump recirculation	2100	140	~.4
Compressor air bleed	6500	300	3.9
Engine-drive electric heater	6500	450	.5
Tail-pipe heat exchanger	6500	250	.1
Insulation, 2.54 cm thick	----	5900	14.6
Equivalent heating by combustion	6500	----	.4

TABLE III. - ASSESSMENT OF POTENTIAL SOLUTIONS TO JET FUEL PROBLEM

Solution	Advantages	Disadvantages
Produce specification jet fuel	Optimized fuel properties Aircraft/engine retrofit not required	Increased refinery energy consumption Increased fuel cost
Relax jet fuel specification	Conservation of energy Reduced fuel cost	More complex component technology required Adverse effect on engine life

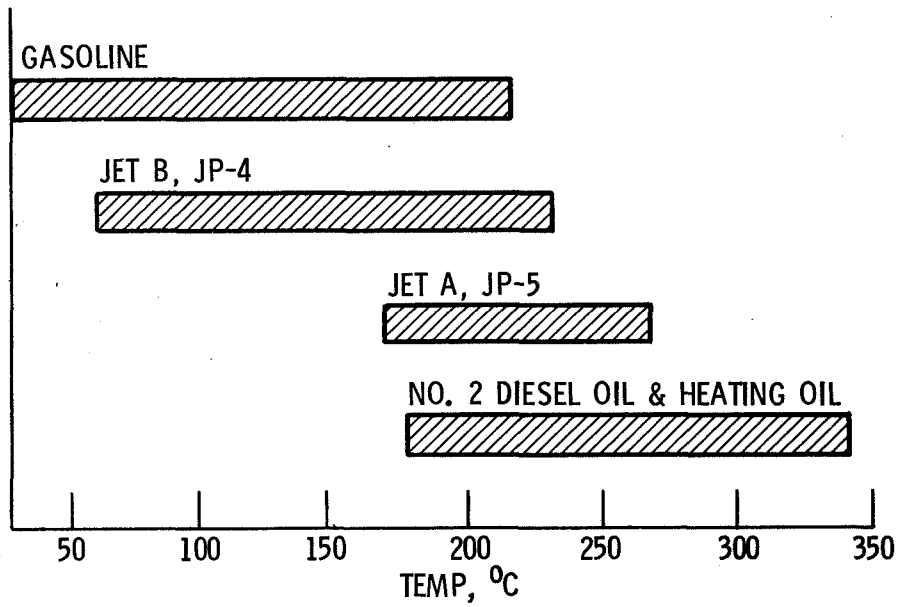

Figure 1.- Boiling range of various petroleum products.

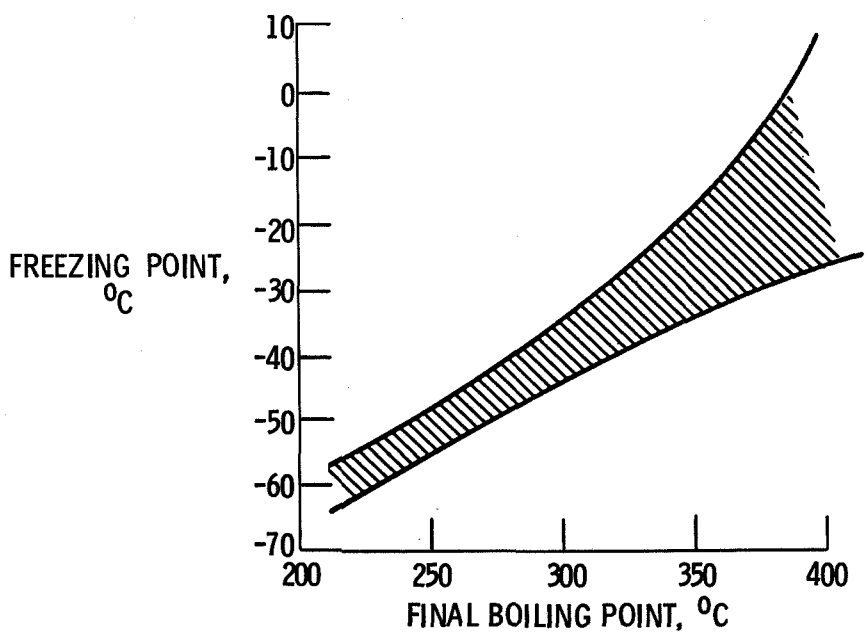

Figure 2.- Typical fuel blend freezing points.

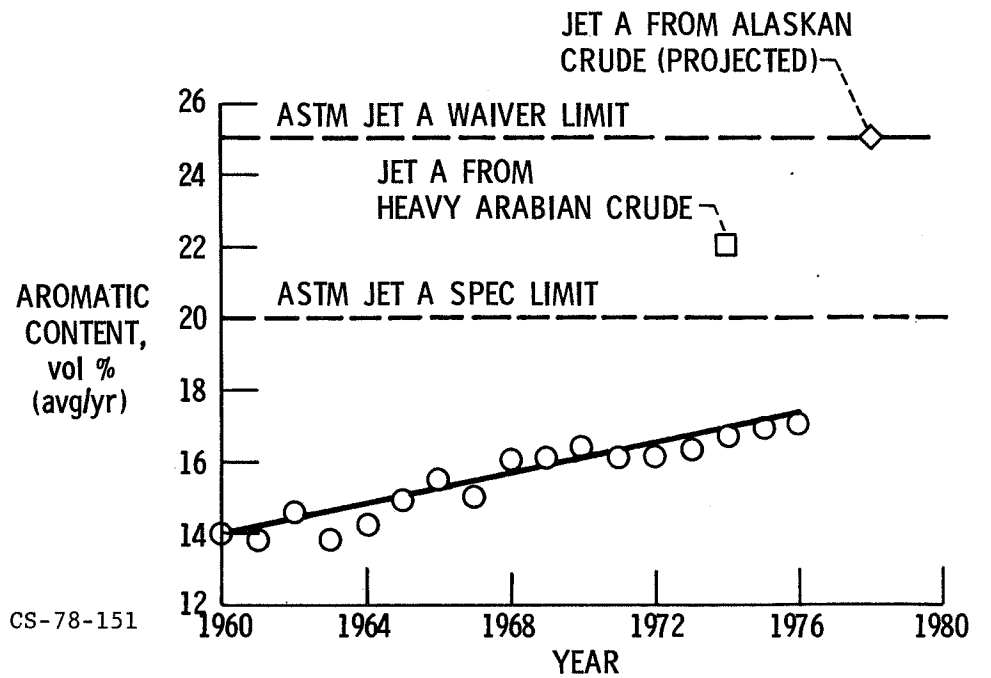

Figure 3.- Trends in aromatic content of commercial Jet A fuel.

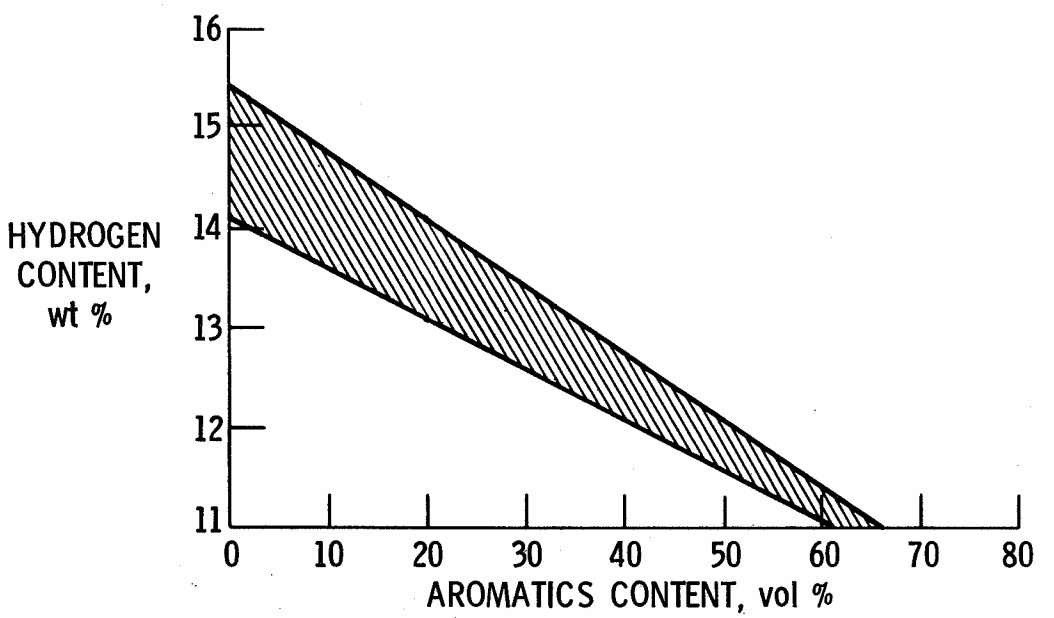

Figure 4.- Variation of hydrogen content with aromatics content.

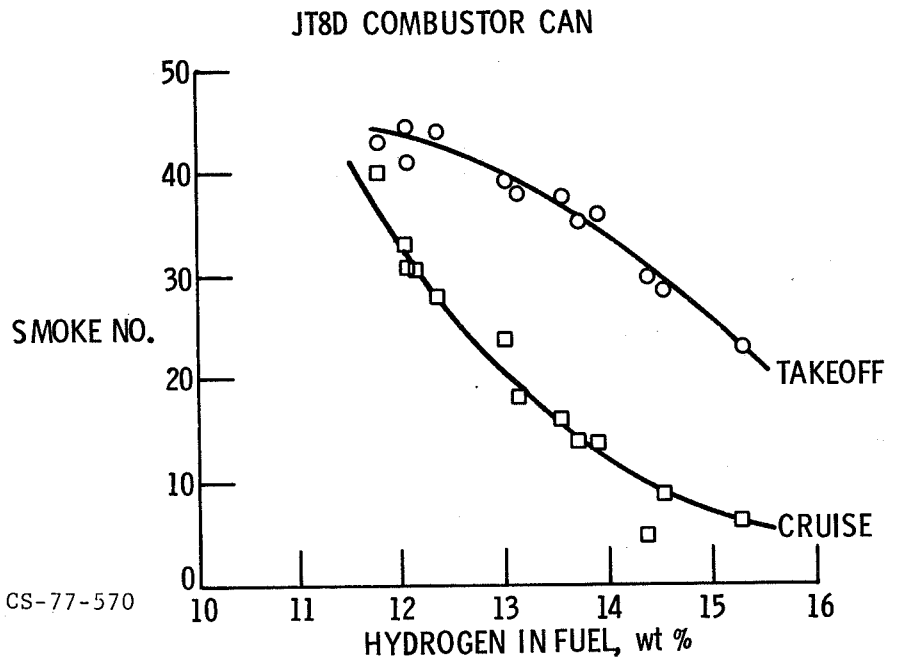

Figure 5.- Effect of hydrogen content of fuel on smoke number.

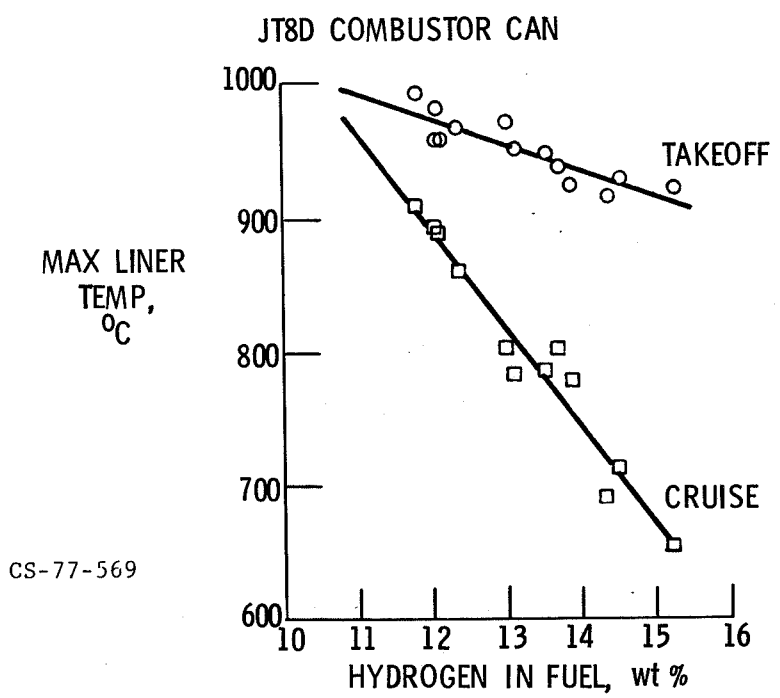

Figure 6.- Effect of hydrogen content of fuel on maximum combustor liner temperature.

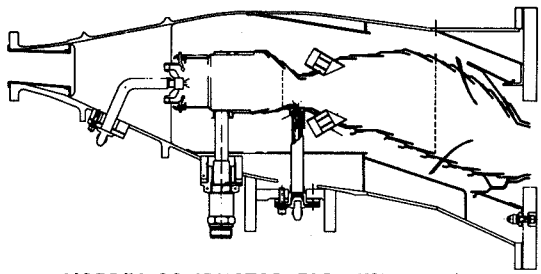

VORBIX COMBUSTOR FOR JT9D ENGINE

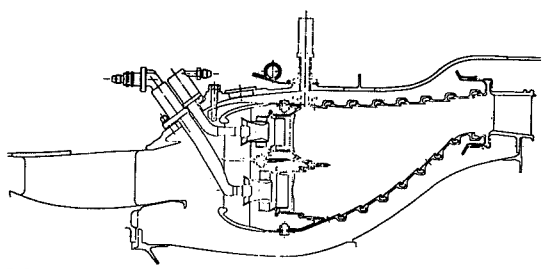

DOUBLE-ANNULAR COMBUSTOR FOR CF6-50 ENGINE

Figure 7.- Combustor designs evaluated in NASA Experimental Clean Combustor Program.

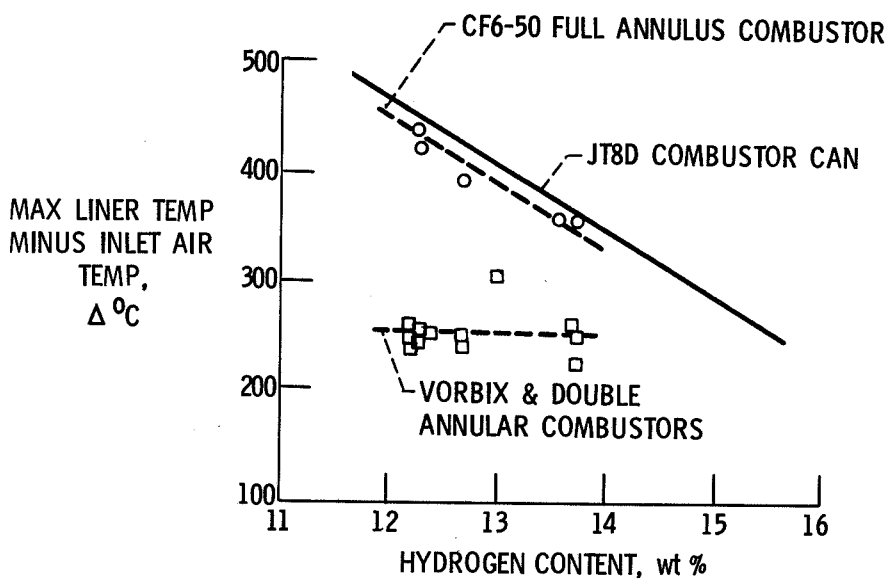

Figure 8.- Effect of hydrogen content of fuel on maximum combustor liner temperature of several different combustor designs.

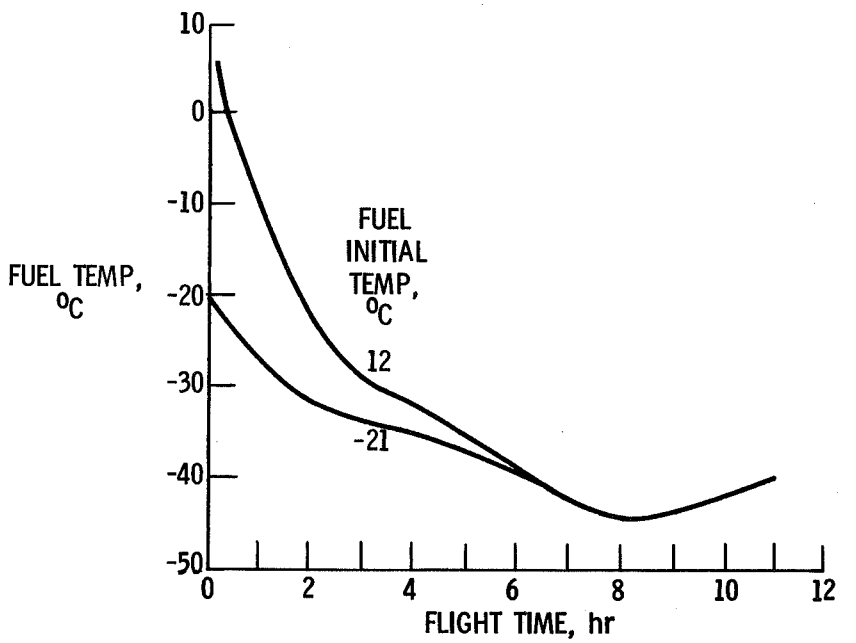

Figure 9.- Fuel tank temperatures for 5000 n. mi. flight.

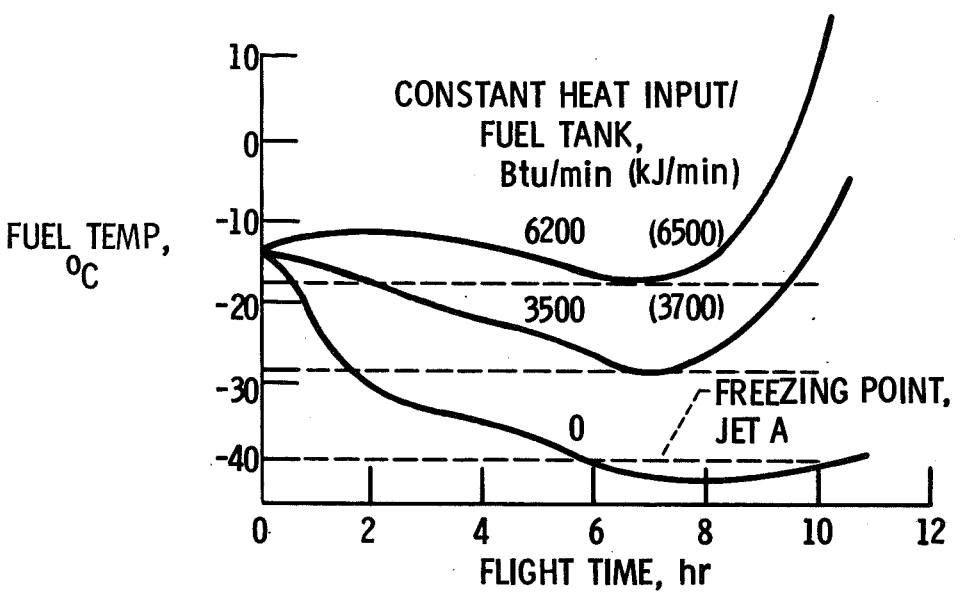

Figure 10.- Fuel tank temperatures for 5000 n. mi. flight with heating.

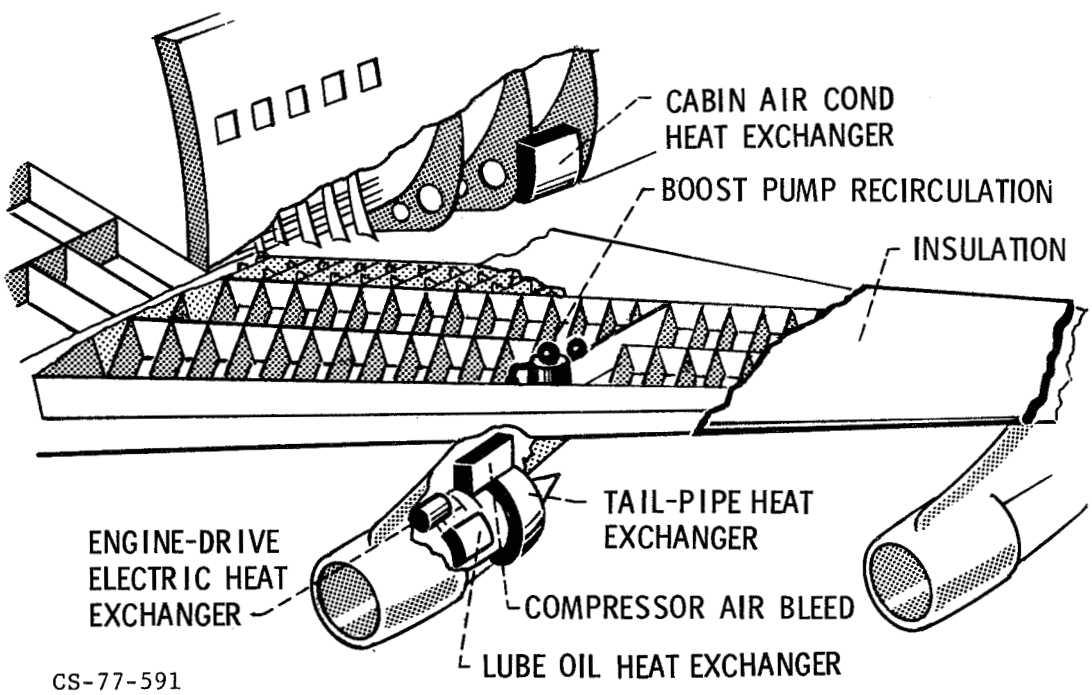

Figure 11.- Fuel tank heating sources.

INTRODUCTION TO SESSION ON MATERIALS AND STRUCTURES

Louis F. Vosteen
NASA Langley Research Center

Activities at Langley Research Center on the development of composites for aircraft can be divided into two main areas: supporting base technology and the Aircraft Energy Efficiency Composites Program. The principal elements of the supporting base technology program are

- Environmental effects on materials
- Material quality and chemical characterization
- Design and analysis methods
- Structural durability
- Impact sensitivity
- Carbon fiber electrical effects

The work on environmental effects on materials is covered in the paper by Pride. The work on material quality and chemical characterization is aimed at consistent quality and is confined at present to work with epoxy resin systems; fiber quality is not being addressed: First, the significant variables that affect quality are being determined. Second, the quality required to meet the aircraft composite needs that are expressed in terms of these variables will be established. Third, reliable methods for monitoring material quality will be developed. Special test techniques may be required. In so far as possible, techniques will be standarized so that suppliers, users, and new material developers can relate their data. The goal is to assure consistent, acceptable materials for aircraft use.

One aspect of the NASA work on design and analysis methods will be covered by Stroud and Sobieszczanski-Sobieski.

The elements of the program on structural durability are

- Design methods for fatigue
- Fracture characteristics
- Fail safe designs
- Joints
- Bonded reinforcements

The emphasis here is on the development of analytical methods although some of these methods may be based on empirical relationships.

Some composite materials, particularly graphite epoxy, are impact sensitive. Work being conducted at Langley Research Center on impact sensitivity is both analytical and experimental. Experimental efforts are used to help define the significant variables governing the sensitivity of composites to impact and

also to evaluate the analytical methods that are being developed. The impact sensitivity of composites is related to the operating strain level. Below a certain strain, impacts do not appear to cause damage that propagates readily. The crashworthiness of aircraft that use composite materials is one aspect of the impact sensitivity problem that will be discussed by Stone.

Recently, the government announced that it was initiating a program to investigate the affects of carbon fiber on electrical components. Carbon fibers are electrical conductors; free fibers in contact with an unprotected electrical circuit can cause shorts, electrical arcing, or resistive loading. It should be noted that fibers confined in a plastic matrix do not pose any electrical hazard. Several of the ways in which free carbon fibers can be released into the atmosphere, and thereby pose a potential hazard, are

Industrial operations
Scrap and waste disposal
Destructive testing
Incineration of products
Aircraft crash and fire

Of these items, all but aircraft crash and fire can be fairly well controlled at their origin. However, aircraft crash and fire could result in uncontrolled release of fibers if the binding matrix material is burned away cleanly and the fibers become airborne. Graphite fibers used in aircraft composites are extremely fine and can float long distances from their point of release. The NASA program to investigate graphite-fiber electrical problems is in two areas. The first area is to better quantify the potential problem of using composites on civil aircraft. This includes a better understanding of the way in which carbon fibers can be released in the event of an aircraft crash and subsequent fire, the propagation of fibers away from the fire site, and the vulnerability of electrical components, especially in other aircraft and in the surrounding area. The second area, in parallel with this activity to better quantify the problem, is to develop materials that will alleviate or eliminate the electrical hazard. These programs will include modifications or changes in the resin system which would prevent the release of fiber following a fire and the development of nonconductive fibers to replace graphite.

The two principal activities of the Aircraft Energy Efficiency Composites Program are the development of composite components and wing-study activity. The components being developed, by company, are

The Boeing Commercial Airplane Company:

727 elevator
737 horizontal stabilizer

Douglas Aircraft Company:

DC-10 upper aft rudder
DC-10 vertical stabilizer

Lockheed-California Company:

L-1011 inboard aileron
L-1011 vertical stabilizer

The status of the development of these components is covered in part in the papers by Stone, Stauffer and James, and Buffum and Thompson. Wing-study activity is currently nearing completion. The principal goal of the studies is to define the specific technologies that will be required in order to proceed with large primary structure such as the wing.

ENVIRONMENTAL EFFECTS ON COMPOSITES FOR AIRCRAFT

Richard A. Pride
NASA Langley Research Center

INTRODUCTION

The influence of the operational environment on the behavior of composite materials and aircraft components fabricated with these composite materials is a subject of continuing concern both for the aircraft manufacturer and the airline operator. The structural weight savings and the potential for manufacturing cost savings have been well documented in a number of composite hardware development programs in recent years. These advantages have left the question of long-term environmental durability for composites as the major undetermined issue for widespread acceptance and application.

This paper reports on the interim results from a number of ongoing, long-term, environmental effects programs. The flight service experience to date of composite components is evaluated. In addition, the influence of a number of worldwide, ground-based outdoor exposures on the physical and mechanical properties of six composite materials is discussed. In particular, the current extent of the ultraviolet surface degradation and the moisture gained by diffusion is shown. Finally, several new environmental programs which have been started recently are reported to show the type of information that can be expected to be available in the next few years.

FLIGHT SERVICE OF COMPOSITE COMPONENTS

A number of composite structural components have been designed, manufactured, tested, and placed in operational service on a variety of aircraft. This operational flight service is monitored periodically to evaluate the long-term experience with composite durability. The types of aircraft and composite components are shown in figure 1. The L-1011 application is six fuselage fairing panels involving two types of Kevlar-49 epoxy composite on each of three airplanes (ref. 1). Three graphite-epoxy material systems are used for the spoilers on 27 Boeing 737 airplanes (ref. 2). A fourth graphite-epoxy material is used in the upper, aft rudder segment on ten DC-10 airplanes (ref. 3), and boron-aluminum composite skin is used in a panel on the aft pylon adjacent to the engine on three DC-10 airplanes (ref. 4). Boron-epoxy is used as a selective reinforcement in the aluminum aft fuselage, or tail cone, of an Army CH-54B helicopter (ref. 5) and in the aluminum center wing box of two Air Force C-130 transports (ref. 6).

The status of these composite structural components in the Langley flight service program, as of January 1, 1978, is given in table I. The boron-epoxy composite in the CH-54B helicopter tail cone has been in service for the longest calendar time, six years, but it has been flown very little compared to the other types of aircraft. The Kevlar-49 epoxy in the L-1011 fairing panels has

accumulated the greatest single component flight time, 13 138 flight hours in five years of service. The graphite-epoxy in the 108 spoilers on the 737 airplanes has accumulated the greatest total component flight hours, 921 600 in four and one-half years. The graphite-epoxy in one of the DC-10 upper aft rudders has been acquiring flight service time at the greatest rate of any of the components in the table, a rate of 400 hours per month or about 13 hours per day. Overall the 142 composite components have accumulated in excess of one million component flight hours in service around the world with 17 operators. Each of these composite components has been inspected at least annually by the manufacturer, under terms of the NASA contracts. There have been no significant incidents or damage detected in any of these flight components. Maintenance has been reported as less than that required on similar standard, production parts.

COMPOSITE SPOILERS

The large number (108) of replicate spoilers with graphite-epoxy skins allows a program of planned retrievals from flight service without seriously impairing the total exposure. Six spoilers are selected at random for removal annually, two of each of the three material systems. These spoilers are shipped to The Boeing Company where they are nondestructively inspected by ultrasonic C-scan. The C-scan record is compared with similar records made at the completion of manufacturing. To date, no significant differences have been observed. Three of the six spoilers are then selected for destructive testing and the remaining three are returned to flight service.

For destructive testing the spoilers are mounted in the same static test jig as was used for the initial airworthiness certification tests (ref. 2). A distributed load is applied to the outer surface of the spoiler, simulating aerodynamic loads, and the magnitude is increased until failure occurs. Results of these residual static strength tests on the graphite-epoxy spoilers are shown in figure 2. The residual strengths for each material system have been divided by the failure strength of the initial certification test for each material, and the results are presented nondimensionally as a function of the time in service. A scatter band for strength tests of 16 new replicate spoilers manufactured with the T300-5209 graphite-epoxy material has been superimposed on the individual tests of spoilers removed from service. In four years of service, the scatter in strength for the individual spoilers generally falls within the width of the new spoiler strength scatter band; an indication of essentially no degradation in strength.

After several years of unsuccessfully attempting to determine the moisture absorbed by the graphite-epoxy spoilers in service, a technique of cutting plugs from near the trailing edge was developed (fig. 3). The eight rectangular areas shown with an arrow in the center of each represent the whiffletree loading areas for static strength tests. Since failures always have initiated near the leading edge at one of the center hinges, it has been determined that three plugs of 6.4 cm (2.5 in.) diameter could be cut from the region behind the loading areas without influencing the failure load. These plugs, which consist of aluminum honeycomb core, two graphite-epoxy face sheets, two layers of epoxy film adhesive and two exterior coats of polyurethane paint, have about

90 percent of their weight in the composite faces, including the paint and adhesive. A good determination of the moisture level in the spoiler can be made by drying the plug and noting the weight change. After three years of service with Lufthansa Airlines in Germany, plugs taken from a T300-5209 graphite-epoxy spoiler indicated a moisture content of 0.64 percent, based on the composite weight. Somewhat greater significance may be attached to this value when corrections have been determined for relative differences in equilibrium moisture levels in the paint, the composite matrix, and the adhesive.

Subsequent to the introduction into flight service of the graphite-epoxy-skinned spoilers, a development program was undertaken for an all-composite spoiler which included glass-epoxy honeycomb core, molded graphite-epoxy hinge fittings and leading edge spar, and thermoplastic graphite-polysulfone skins (ref. 7). It was recognized that the polysulfone matrix had an environmental sensitivity to phosphate-ester-based hydraulic fluids, and the laboratory testing demonstrated this in elevated temperature, stressed immersions. However, based on the room temperature experience it was believed that the material could be successfully used in flight components with only minor, intermittent exposures to hydraulic fluid leakage from the spoiler actuators. Twelve of these spoilers were fabricated and placed in service on six of the aircraft that were flying graphite-epoxy spoilers. After six months of operational flight service the two spoilers installed on Aloha Airlines were reported to have developed significant delamination of the lower surface skin directly aft of the actuator attachment fitting (fig. 4). Within a month a third spoiler was reported as starting to experience delamination, so it was decided to remove all the remaining graphite-polysulfone spoilers. A closeup view of the delaminated area is shown in the photograph in figure 5. This experience demonstrated the difficulty of performing adequate laboratory accelerated environmental testing and provided a good example of the necessity for flight service evaluation.

There have been several instances in which the graphite-epoxy spoilers have received damage in service sufficient to require repairs. Examples of these are illustrated in figure 6. On this program, damaged spoilers are removed from the aircraft and returned to The Boeing Company for repair. Repairs are made by cutting out the damaged area, replacing honeycomb core as needed, and replacing graphite-epoxy plies on a one-for-one basis with each ply lapped over the underlying one by about 6 mm (0.25 in.). One piece of adhesive film is placed under the patch assembly and the built-up patch is cured and bonded in one cycle in an autoclave with the spoiler supported in its original assembly tooling (ref. 7). The repaired spoiler is ultrasonically inspected and returned to flight service with the airline which had previously used it.

WORLDWIDE GROUND-BASED OUTDOOR EXPOSURE

As a parallel part of the flight service exposures of composite components, a number of replicate mechanical property specimens have been manufactured from the same composite material systems used in the components. These specimens have been mounted in racks which are deployed on rooftops of airline buildings at a number of airports around the world so as to receive maximum exposure to the airport ground environment. The location of six of the exposure

sites is shown on the map of the world in figure 7. Each of these locations has an exposure rack with unstressed specimens as indicated in figure 8. Each of the five panels mounted in the rack contains triplicate specimens of four graphite-epoxies, one graphite-polysulfone, and two Kevlar-49 epoxies in short beam interlaminar shear, flexure and compression configurations. After one year and three years of exposure a panel is removed from each rack and shipped to Langley Research Center for specimen testing and evaluation.

In addition to the unstressed exposures, three racks containing stressed tensile specimens (fig. 9) are also deployed, one each at San Francisco, Seattle, and Langley. Individual specimens are mounted in fixtures which apply a constant load through a compressed helical spring. Unstressed tensile specimens are also placed in these same racks for comparison.

When specimens are removed and shipped to Langley periodically, they are weighed to determine weight changes associated with moisture absorption and weathering. An example of the specimen weight changes with exposure time is shown in figure 10 for a thin graphite-epoxy specimen in the unstressed rack at Langley. The solid curve in the center of the figure drawn through the circular test points is the record of the repeated weighings. The specimen initially gained weight and then began to gradually lose weight as a result of the combined effects of moisture and solar ultraviolet exposure. The exposure of this specimen was terminated after 140 days and the specimen was then dried to a fully dry condition. The weight change associated with this drying indicated the actual measured moisture level in the specimen at 140 days. Comparing the fully dry weight to the initial fully dry weight showed the measured ultraviolet effect of a weight loss after 140 days. Since the ultraviolet effect is a loss from the exposed specimen surface, it is assumed to be linear with exposure time. Corrections can then be calculated for the measured weights at intermediate times, and an interpolated moisture curve can then be plotted as shown by the upper dashed line in figure 10. This curve appears to have reached an equilibrium level of moisture absorption between 0.6 and 0.7 percent. The small fluctuations correspond to changes in the daily levels of relative humidity.

The results of fully drying the flexure specimens from five exposure sites after three years of exposure provided a pattern of weight losses due to ultraviolet exposure as shown in figure 11. For any given material, the weight losses are greater for exposure sites closest to the equator. Variations in the epoxy matrices for the different material systems seem to provide a greater variation in weight loss than changes in exposure site latitude. In all cases the specimens were exposed in an as-laminated condition without any protective coating. The weight losses in three years time correspond to less than 25 percent of one ply thickness.

Scanning electron micrographs of two areas on one of the T300-5209 graphite-epoxy specimens exposed at the Honolulu site are shown in figure 12. The left-hand area was shielded from the solar ultraviolet by the specimen mounting clamp on the exposure rack. The magnified view is essentially the original as-laminated surface, which is entirely epoxy. The right-hand area was typical of the unshielded portion of the same specimen. In this area the epoxy matrix has been removed by the ultraviolet weathering process, exposing

a layer of individual graphite fibers. Although the effect looks bad, it really is quite superficial in three years time and it can be prevented by painting the exposed specimen surface.

The amount of moisture absorbed by the various composite material systems is shown in figure 13. These results represent the determinations made on flexure specimens after their worldwide outdoor exposures for times up to three years. The weight gains shown have been corrected for the ultraviolet weight losses as described previously for figures 10 and 11. The scatter bands indicated for the three-year exposures contain all the data for triplicate specimens and five exposure sites. In general there is no separation of individual sites by the magnitude of absorbed moisture. The largest variable appears to be the type of epoxy matrix used in the composites. Even the Kevlar-epoxy values are in the same range as one of the graphite-epoxies. Data for T300-5208 graphite-epoxy is only shown for a 1.7-year exposure because the specimens which were made as a part of the graphite-epoxy rudder flight service program were not available to be deployed in the exposure rack panels until 1.3 years after the other specimens were deployed. However, the absorbed moisture for the T300-5208 is essentially the same as for the T300-5209 material, and both appear to be at an equilibrium level of about 0.5 percent of the laminate weight.

A comparison of the measured moisture contents for both T300-5208 and T300-5209 materials with predicted moisture contents for a 12-ply laminate of T300-5208 graphite-epoxy is shown in figure 14. The predicted moisture contents are based on calculations using the Fickian diffusion equations with varying inputs for relative humidity and temperature (ref. 8). These varying inputs are taken directly from tape recordings of the weather at Langley Research Center. The predicted curve marked "No Solar" was calculated assuming that the temperature of the specimen was the same as that of the ambient air. This is a reasonable assumption for specimens exposed in shade; however, if the specimens are exposed to the Sun, they will be heated to temperatures well above the ambient air temperature on clear, sunny days. This will increase the rate of moisture diffusion and, more importantly, decrease the local relative humidity at the surface of the specimens. Inclusion of these effects in the calculations results in the lower predicted curve marked "Solar". The weather data for the year 1962 were used repetitively in the calculations, starting at the first of October to correspond with the initial deployment of the exposure racks and specimens. The experimental data points at 1, 1.7, and 3 years are taken from the overall worldwide exposure data previously discussed in figure 13 for T300-5208 and T300-5209 graphite-epoxies. The correlation between prediction and experiment is good.

The observed loss of material from ultraviolet exposure and pickup of moisture from the relative humidity leads to a concern for the effect on residual mechanical properties. Figure 15 shows the results of flexure strength tests performed after various exposure times at all of the worldwide exposure sites for six composite materials. The data are shown in nondimensional form obtained by dividing residual strengths by the initial as-laminated strengths. The width of the scatter band for strength is largely a function of the scatter in triplicate tests from various exposure sites. However, it is not sufficiently greater than the scatter in the initial replicate tests to justify any

conclusions. It is evident that for three years of outdoor ground-based unstressed exposure there has been no indication of degradation in flexure strength. Similar conclusions can be drawn from results of the short beam interlaminar shear and the compression tests also, after three years of unstressed outdoor exposure.

To consider the possible influence of constant stress during the outdoor exposure, three sets of tensile specimens have been included in the program. The first set consists of T300-5209 graphite-epoxy material laminated at $\pm 45^{\circ}$ ply orientation and stressed during exposure at 25 percent of the initial ultimate strength. Exposure and residual strength testing have been conducted in the Seattle, Washington area by The Boeing Company under NASA contract. Results shown in figure 16 indicate essentially no difference between stressed and unstressed exposure and no degradation in tensile strength for up to three years of exposure. The second and third sets of tensile specimens are T300-5208 graphite-epoxy material laminated in a $[0^{\circ}, \pm 45^{\circ}, 90^{\circ}]$ quasi-isotropic ply orientation and stressed during exposure at 40 percent of the initial ultimate strength. Exposure sites for these are located at the San Francisco airport and at Langley. Specimens have been retrieved and tested at Langley after one and three years exposure. The results shown in figure 17 indicate about the same amount of scatter as shown previously for the flexure strengths and indicate essentially no difference between stressed and unstressed exposures and no degradation in tensile strength.

Another type of environmental exposure includes the interaction of composite materials with extended exposure to aircraft fuels and hydraulic fluids. Under NASA contract The Boeing Company has conducted a series of exposures of several composite materials in JP-4 jet fuel, a commercial aviation phosphate-ester hydraulic fluid, a fuel-and-water mixture, and a fuel-and-air cyclic environment. All exposures are outdoors in an unheated shed in the Seattle area. Short beam interlaminar shear and tensile specimens are being exposed. Typical results are shown in figure 18 for T300-5209 graphite-epoxy material laminated at a $\pm 45^{\circ}$ ply orientation. The data indicate no degradation in tensile strength for up to three years exposure in any of the above environments.

NEW ENVIRONMENTAL PROGRAMS

All of the previously described environmental activities have been under way for extended times and are planned to continue for some time in the future. As data have developed from these and other composite materials technology programs, the need for additional environmental exposure data has become apparent. Several new programs have been started recently which will be producing significant data in the future and these are described in the following paragraphs to provide a more complete view of the Langley program.

Figure 19 shows two views of an outdoor environmental exposure site at Langley in which the Structural Integrity Branch is conducting flight-by-flight spectrum loading on chains of composite materials specimens. The two views provide graphic evidence that the specimens see the full extremes of summer and winter weather. Specimens with and without open-hole stress concentrations

are being exposed. Similar chains of specimens are being subjected to the same loads inside a controlled-environment laboratory for comparison.

Technology for designing primary structural discontinuities such as bolted joint wing splices in composite materials is being developed in programs like the one discussed in reference 9. Test specimens with multiple, repeating patterns of bolted fasteners (fig. 20) have been fabricated with laminate thicknesses of 1.37 cm (0.54 in.) and static strength tested successfully. With the validation of the static design, replicate specimens have been fabricated and are under long-term stressed exposure outdoors at Langley as shown in figure 21. The sustained stress level has been set at 25 percent of the static ultimate.

In order to obtain some information on the rate of moisture diffusion into composite materials in actual flight service, as well as to determine directly the equilibrium levels achieved, two programs have been initiated to fly specimens of three graphite-epoxy material systems on three 737 and three DC-10 transport airplanes which are already involved in the flight service evaluation of graphite-epoxy spoilers and rudders. Moisture pickup in flight on the exterior surface of the 737 airplane will be determined from specimens mounted on both the upper and lower surfaces of the flap track fairing tail cone as shown in figure 22. Specimens are mounted in titanium holding fixtures which are attached to the fiberglass tail cone. Periodically one upper and one lower surface fixture are removed and sent to The Boeing Company where they will be weighed and fully dried. Moisture pickup in flight on interior surfaces of parts which are vented to the atmosphere on DC-10 airplanes will be determined from specimens mounted in a holding fixture attached inside the wing leading edge as shown in figure 23. Periodically these specimens will be removed, weighed, and reinstalled by Douglas Aircraft Company personnel during normal aircraft stopovers at Los Angeles or San Francisco.

CONCLUSIONS

Interim results from a number of programs relating to the long-term environmental durability of composite materials in the commercial airline operational environment have been presented and the following conclusions can be drawn:

1. More than five years and 1 000 000 component flight hours of successful flight service evaluation have been achieved for 142 composite components.

2. Residual strength tests of graphite-epoxy spoilers removed from service annually have shown no significant effects in four years.

3. Ground-based outdoor exposures of composite material coupons after 3 years of exposure have reached equilibrium levels of moisture pickup ranging from 0.5 to 2.1 percent of the composite laminate weight, and have produced a solar ultraviolet-induced material loss for unprotected epoxy matrix specimens which is less than 25 percent of one ply. Specific levels of moisture pickup are predictable and are dependent on the particular material system.

4. No significant degradation has been observed in residual strength tests of 3-year outdoor exposures worldwide for interlaminar shear, flexure and compression specimens; for stressed and unstressed tensile specimens; and for exposures to aviation fuels and fluids.

REFERENCES

1. Wooley, John H.; Paschal, Dale R.; and Crilly, Eugene R.: Flight Service Evaluation of PRD-49/Epoxy Composite Panels in Wide-Bodied Commercial Transport Aircraft. Contract No. NAS 1-11621, Lockheed-California Co., Mar. 1973. (Available as NASA CR-112250.)

2. Stoecklin, Robert L.: Development, Manufacturing, and Test of Graphite-Epoxy Composite Spoilers for Flight Service on 737 Transport Aircraft. NASA CR-132682, 1976.

3. Lehman, George M.; et al: Advanced Composite Rudders for DC-10 Aircraft - Design, Manufacturing, and Ground Tests. NASA CR-145068, [1976].

4. Elliot, S. Y.: Boron-Aluminum Skins for the DC-10 Aft Pylon - Final Report. NASA CR-132645, 1975.

5. Welge, R. T.: Application of Boron/Epoxy Reinforced Aluminum Stringers and Boron/Epoxy Skid Gear for the CH54B Helicopter Tail Cone. Phase II: Fabrication, Inspection and Flight Tests. Contract No. NAS 1-10459, Sikorsky Aircraft, United Aircraft Corp., July 1972. (Available as NASA CR-112101.)

6. Harvill, W. E.; and Kizer, J. A.: Program for Establishing Long-Time Flight Service Performance of Composite Materials in the Center Wing Structure of C-130 Aircraft. Phase IV - Ground/Flight Acceptance Tests. NASA CR-145043, 1976.

7. Stoecklin, Robert L.: 737 Graphite Composite Flight Spoiler Flight Service Evaluation. NASA CR-145207, 1977.

8. Unnam, J.; and Tenney, D. R.: Analytical Prediction of Moisture Absorption/Desorption in Resin Matrix Composites Exposed to Aircraft Environments. Volume A - Structures and Materials, AIAA/ASME 18th Structures, Structural Dynamics & Materials Conference, Mar. 1977, pp. 227-235.

9. Johnson, R. W.; and McCarty, J. E.: Design and Fabrication of Graphite-Epoxy Bolted Wing Skin Splice Specimens. NASA CR-145216, 1977.

TABLE I
LANGLEY COMPOSITES FLIGHT SERVICE PROGRAM

AIRCRAFT, COMPONENT	TOTAL COMPONENTS	START OF FLIGHT SERVICE	CUMULATIVE FLIGHT HOURS	
			HIGH TIME AIRCRAFT	TOTAL COMPONENT
CH-54B TAIL CONE	1	MARCH 1972	924	924
L-1011 FAIRING PANELS	18	JANUARY 1973	13 138	186 600
737 SPOILER	108	JULY 1973	11, 315	921, 600
C-130 CENTER WING BOX	2	OCTOBER 1974	2 394	4 800
DC-10 AFT PYLON SKIN	3	AUGUST 1975	6, 516	19 400
DC-10 UPPER AFT RUDDER	10	APRIL 1976	6 600	27 800
GRAND TOTAL	142			1, 161, 100

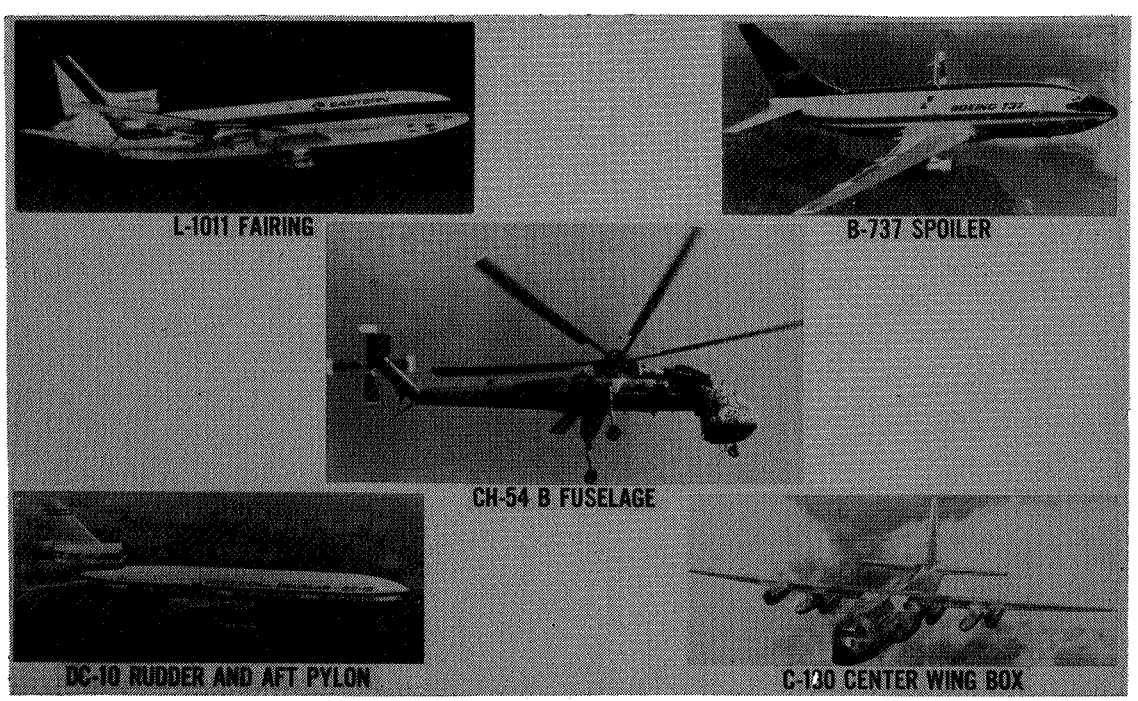

Figure 1.- Flight service evaluation of composite structural components.

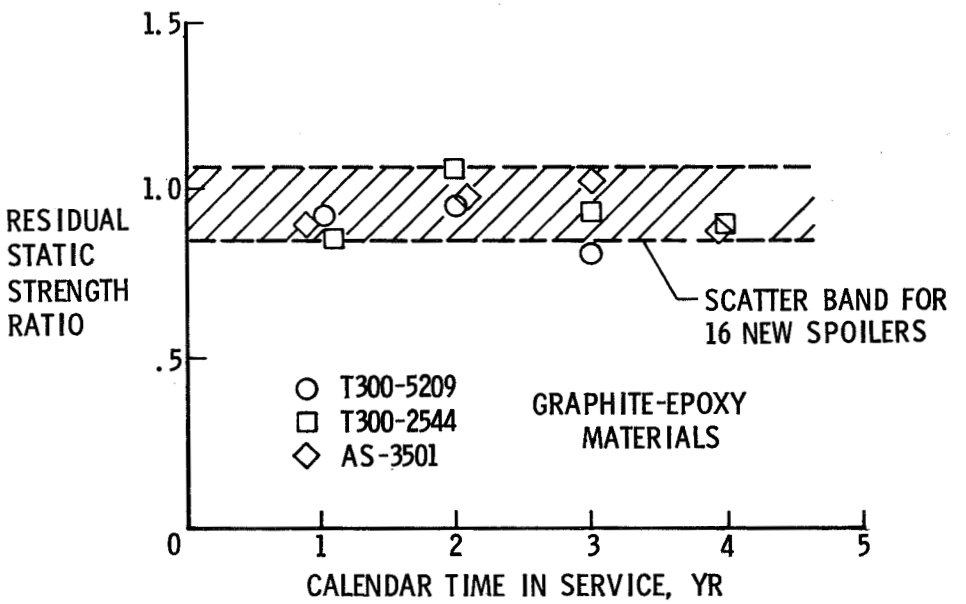

Figure 2.- Residual static strength of graphite-epoxy spoilers.

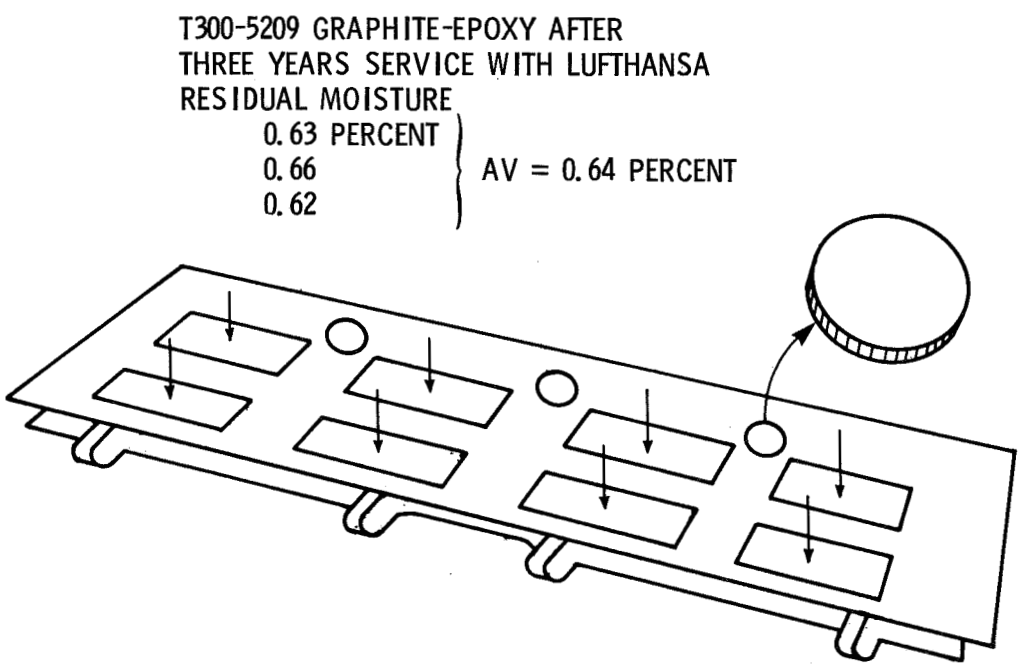

Figure 3.- Spoiler moisture levels determined from plugs.

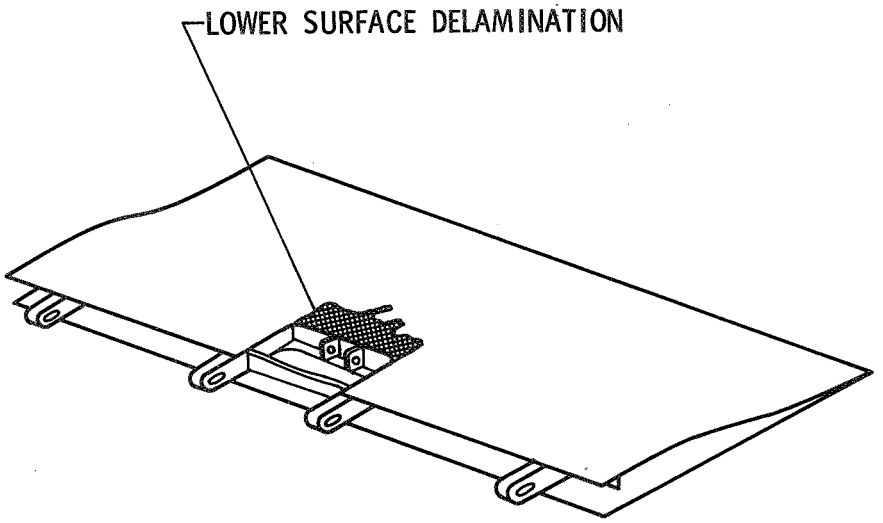

Figure 4.- General area of spoiler delamination.

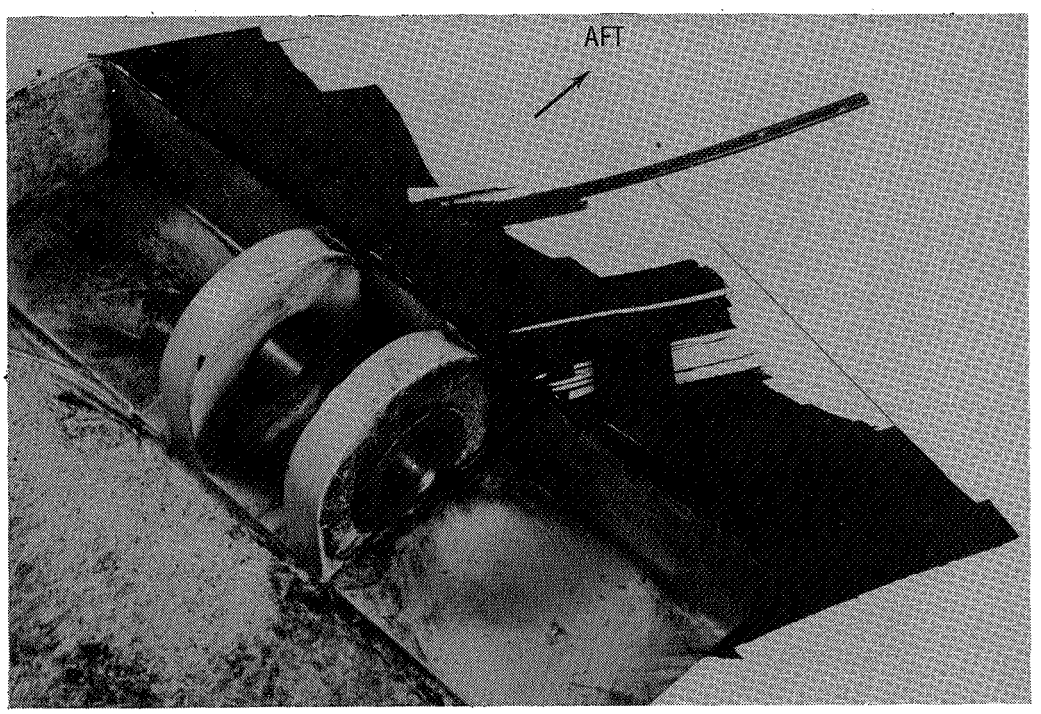

Figure 5.- Delamination of spoiler cover due to hydraulic fluid attack.

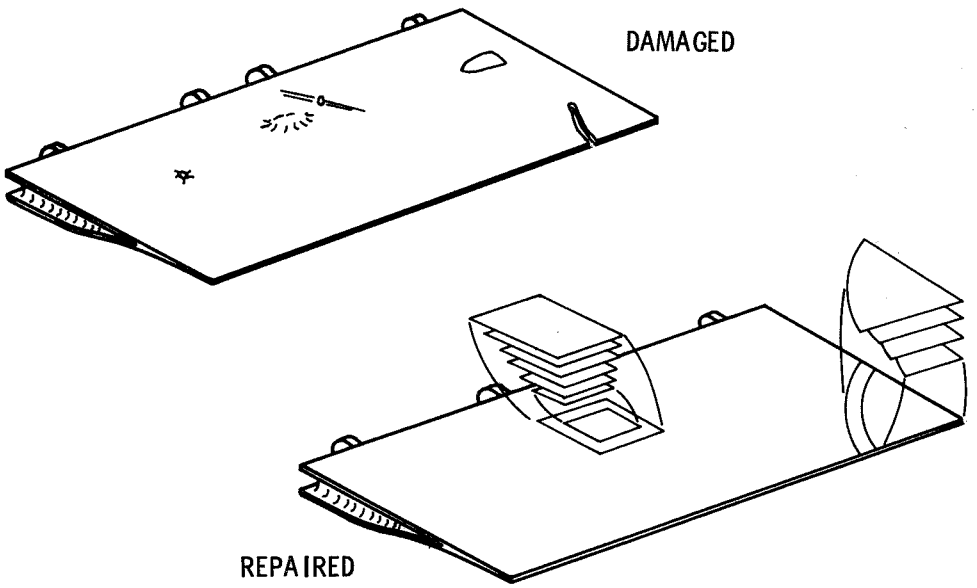

Figure 6.- Graphite-epoxy spoiler repair techniques.

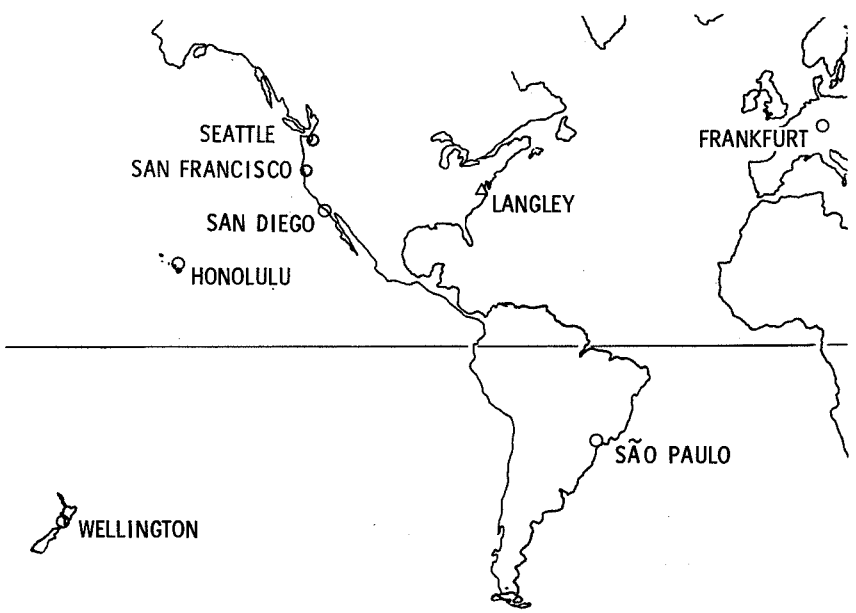

Figure 7.- Distribution of environmental exposure racks.

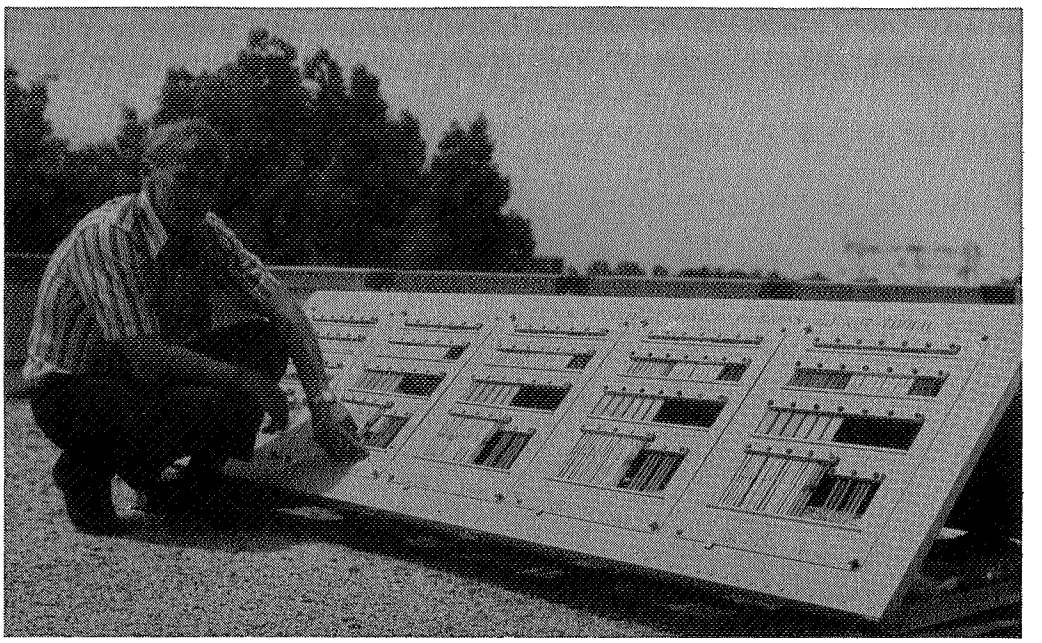

Figure 8.- Unstressed exposure rack.

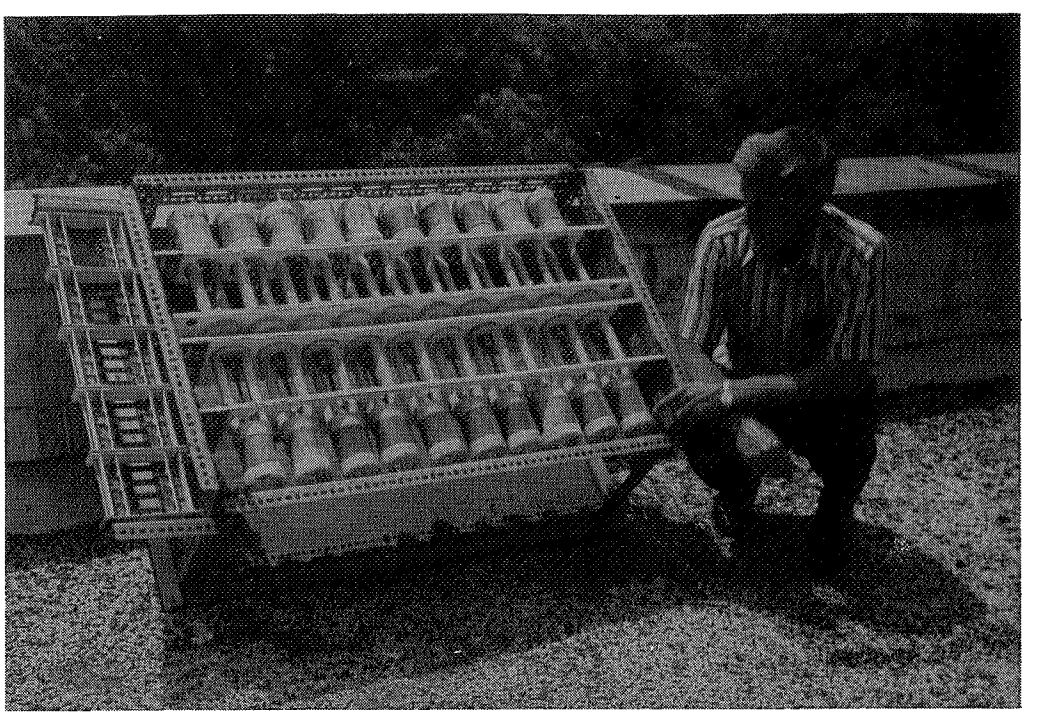

Figure 9.- Stressed exposure rack.

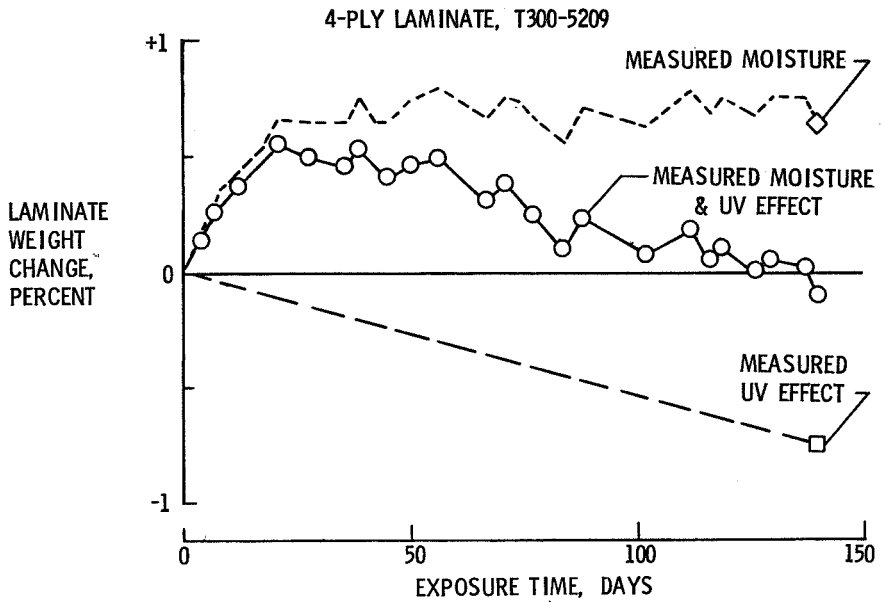

Figure 10.- Weight change in outdoor exposure; 4-ply laminate, T300-5209.

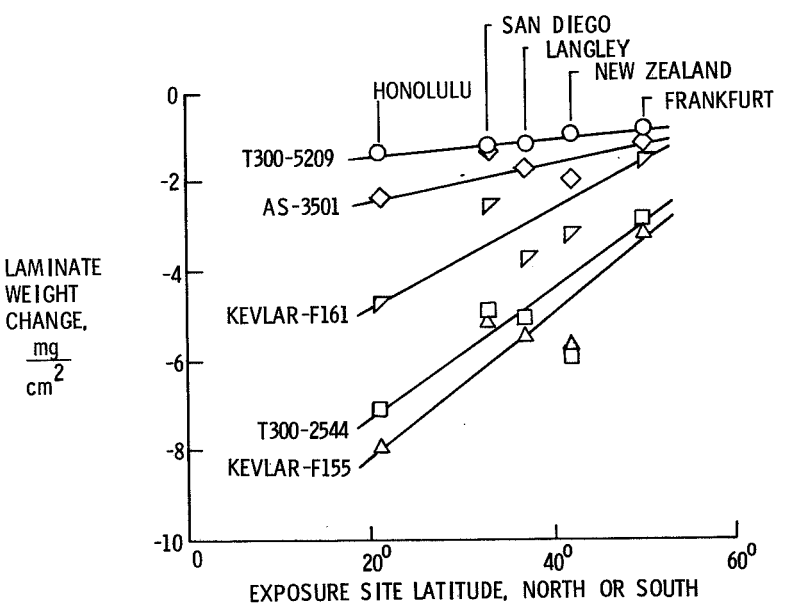

Figure 11.- Weight loss from three years outdoor ultraviolet exposure.

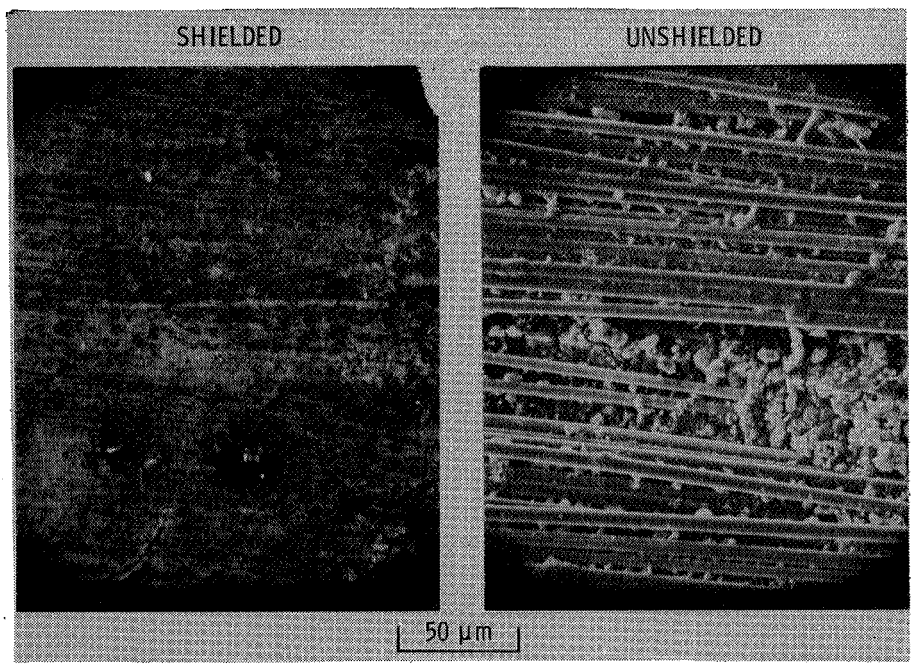

Figure 12.- Graphite-epoxy surface degradation; 3-year outdoor exposure.

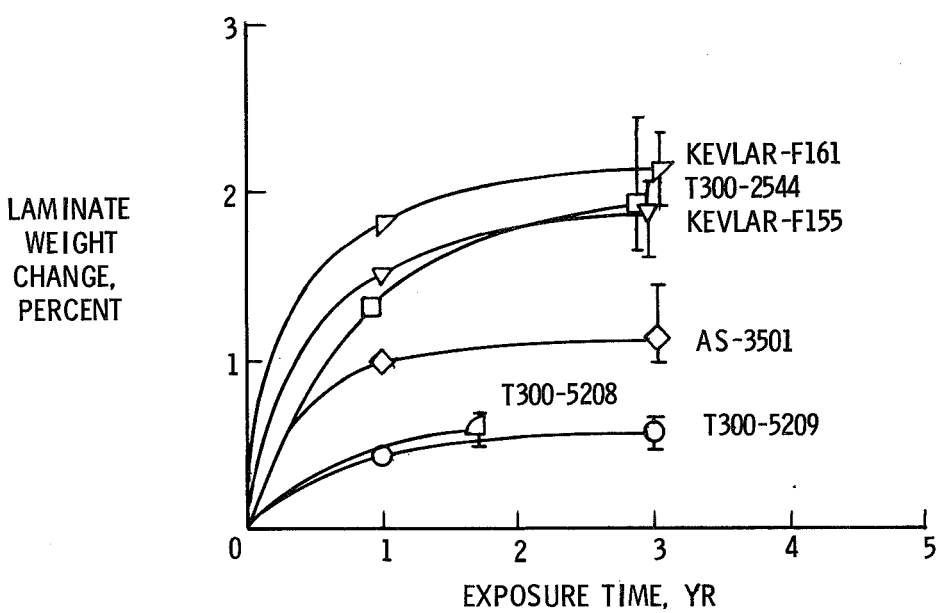

Figure 13.- Moisture pickup after worldwide exposures.

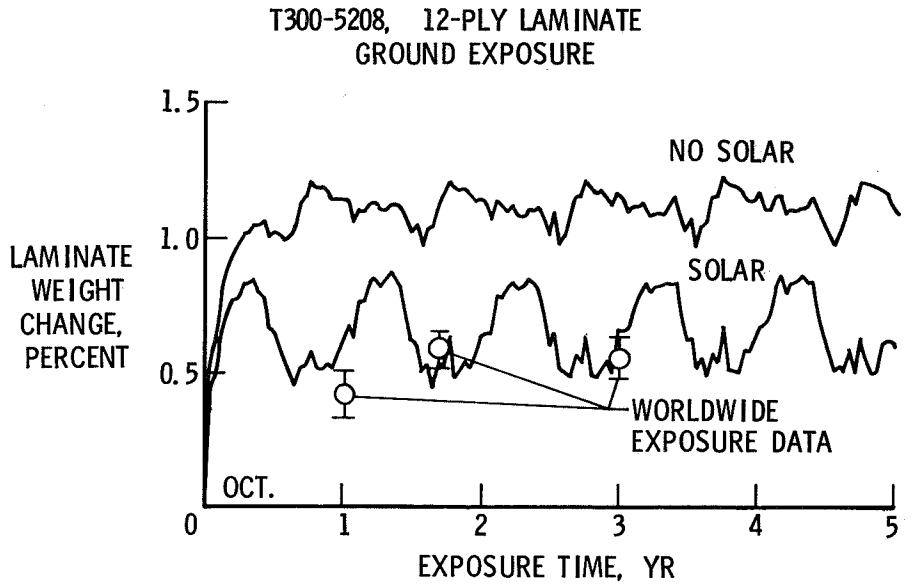

Figure 14.- Comparison of predicted and measured moisture contents; T300-5208, 12-ply laminate; ground exposure.

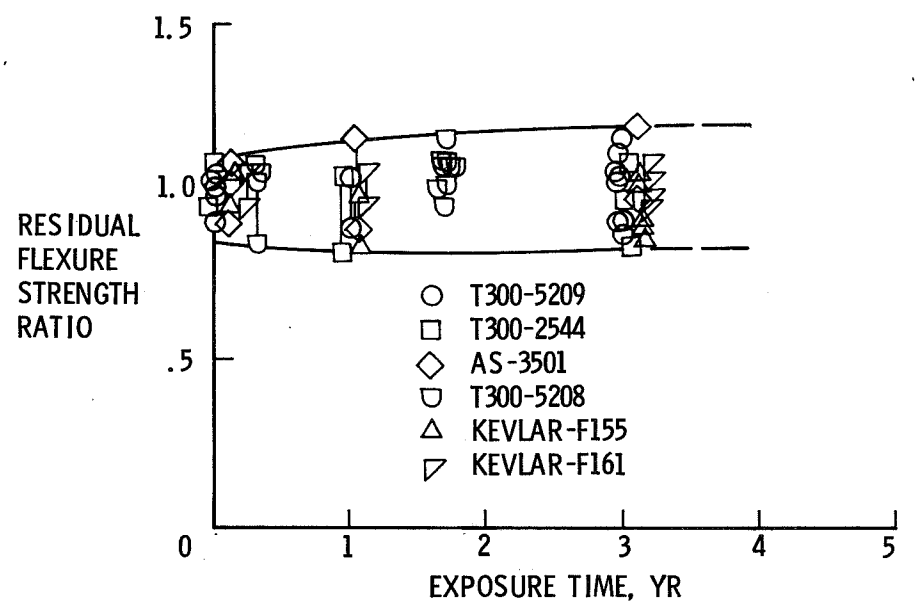

Figure 15.- Residual flexure strength after worldwide exposure.

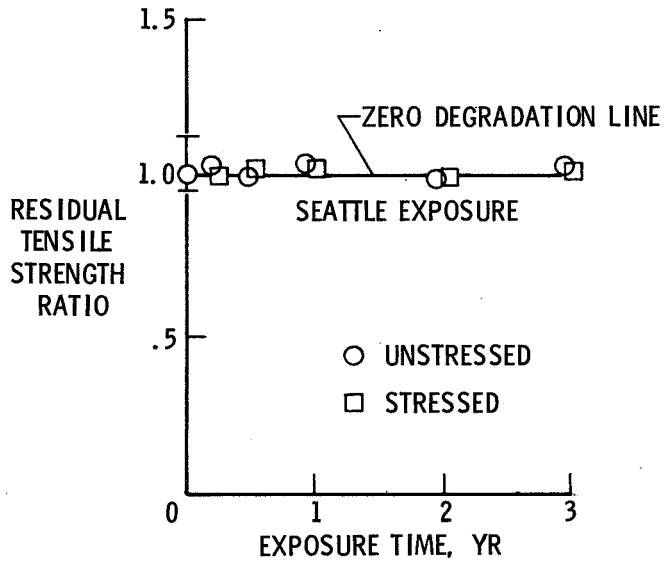

Figure 16.- Residual tensile strength after sustained stress outdoor exposures; T300-5209, ±45° laminate stressed at 25 percent ultimate.

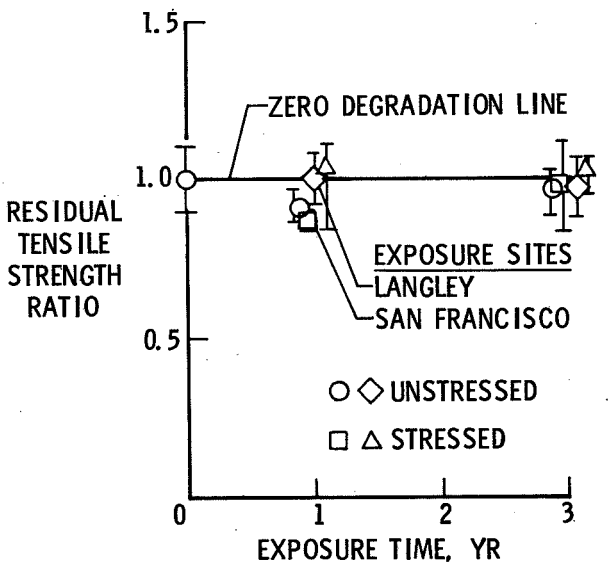

Figure 17.- Residual tensile strength after sustained stress outdoor exposures; T300-5208, [0°, ±45°, 90°] laminate stressed at 40 percent ultimate.

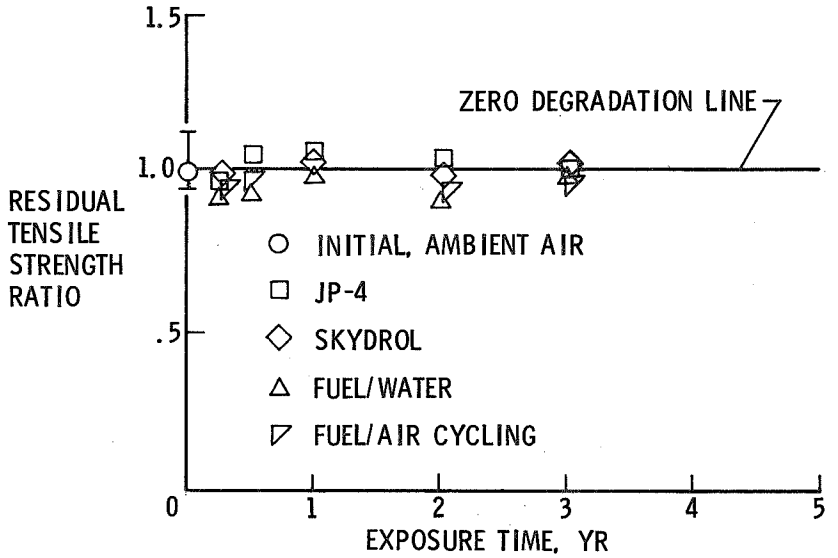

Figure 18.- Effect of fuels and fluids on strength; T300-5209, $\pm 45^{\circ}$ tensile specimens.

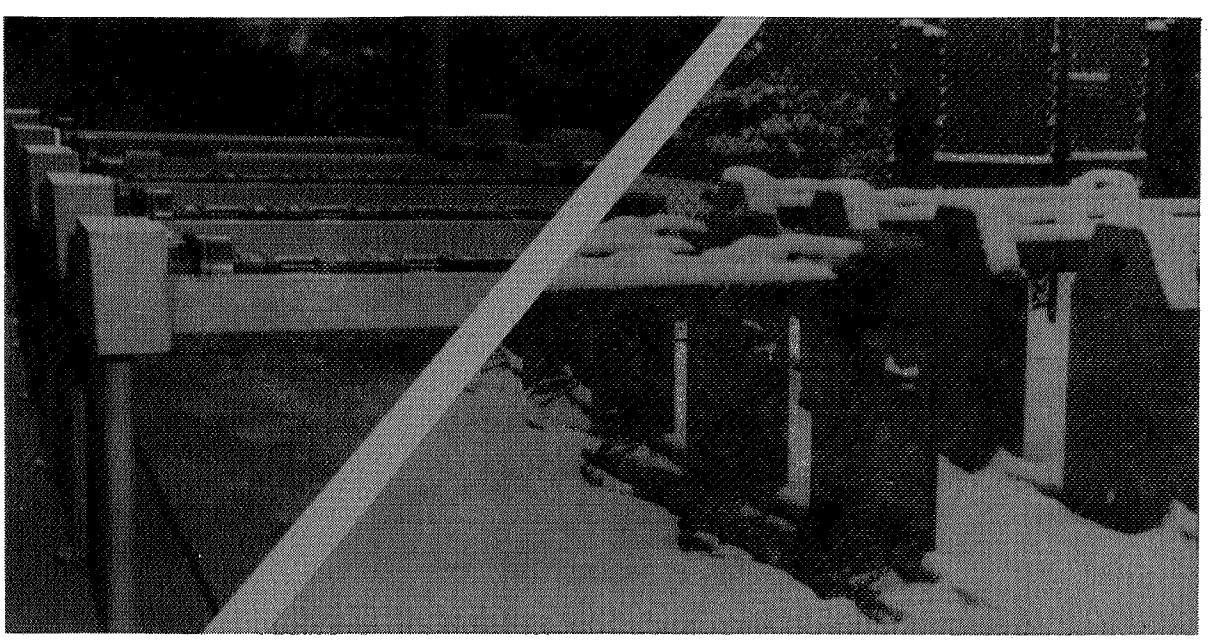

Figure 19.- Environmental fatigue tests on composites.

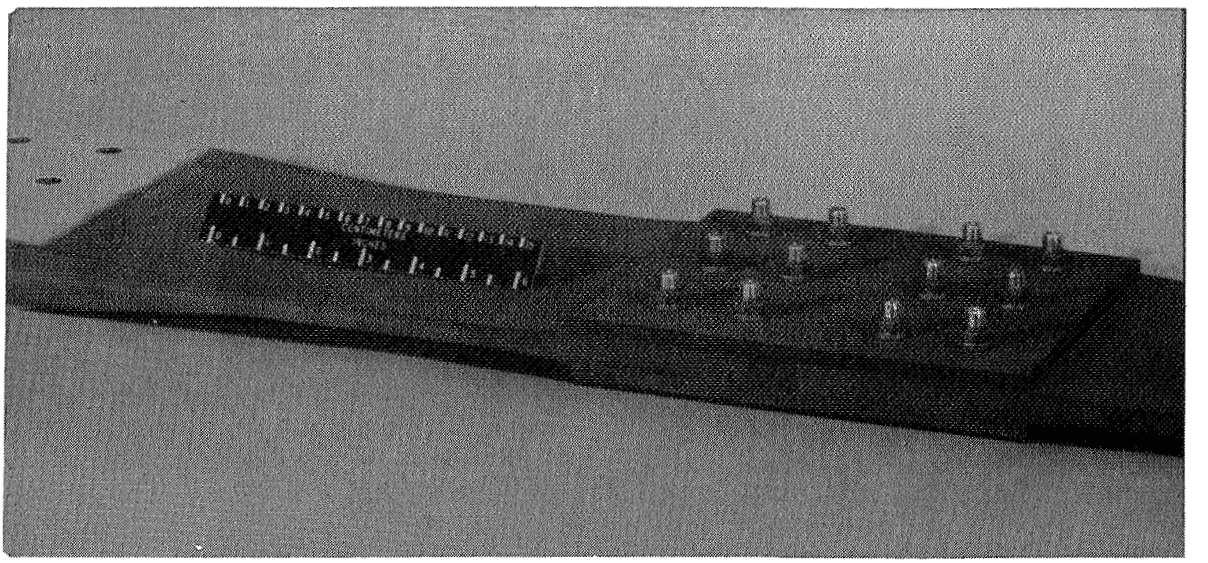

Figure 20.- Bolted joint for graphite-epoxy wing splice.

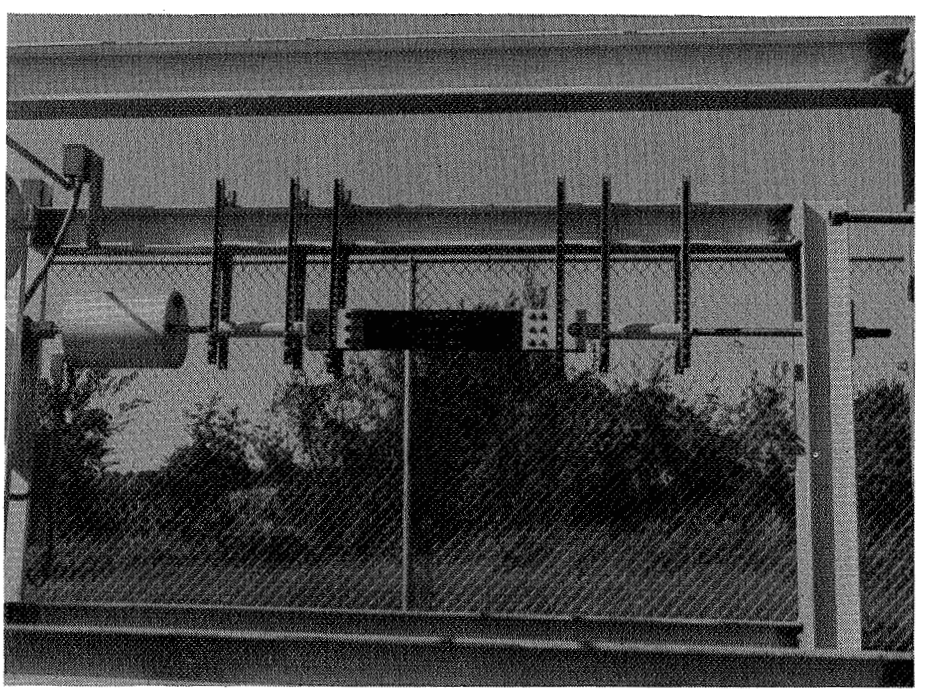

Figure 21.- Wing splice environmental exposure.

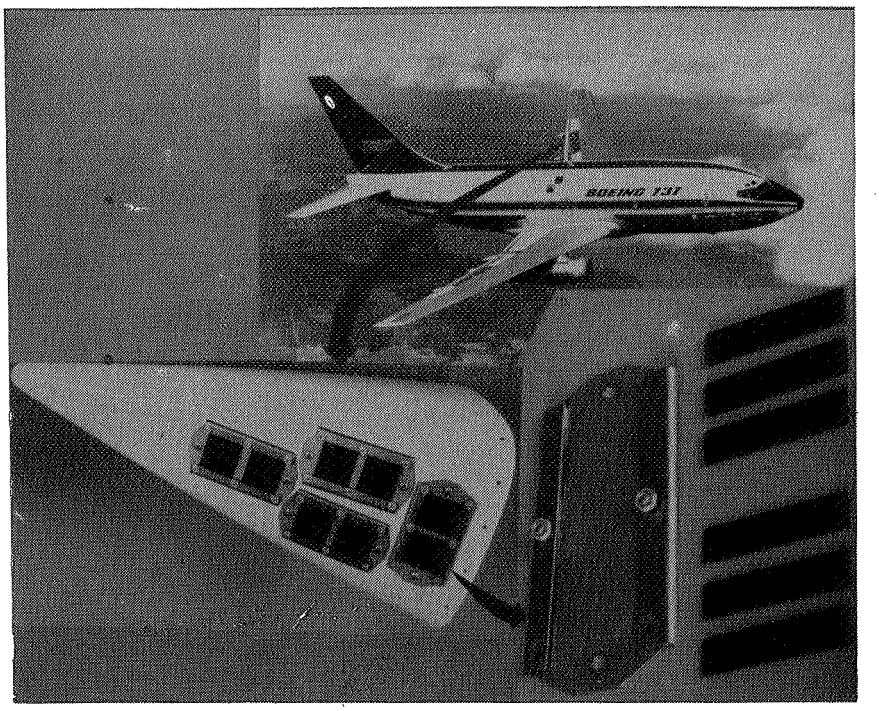

Figure 22.- Exterior moisture pickup in flight.

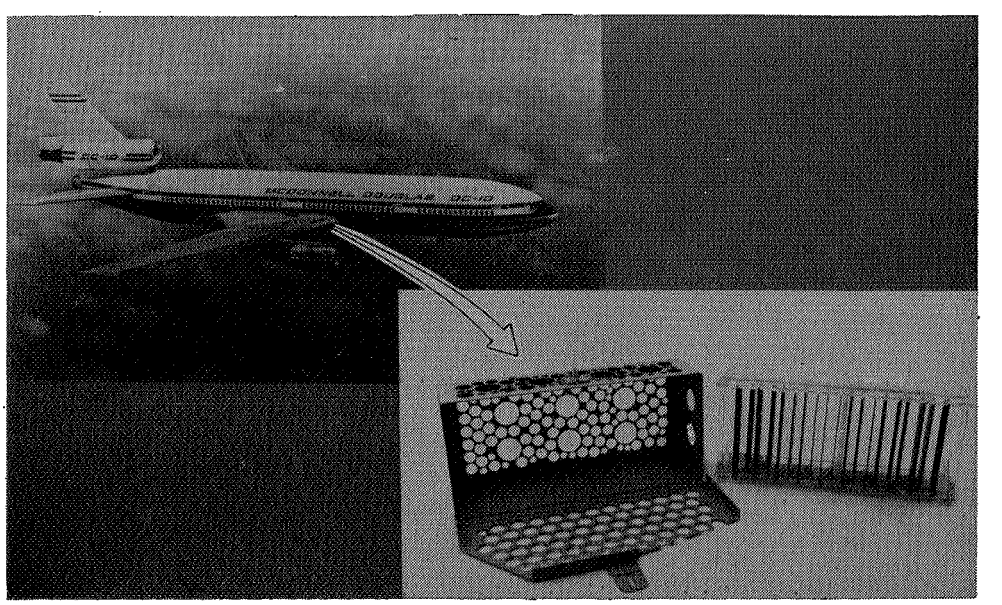

Figure 23.- Interior moisture pickup in flight.

DEVELOPMENT OF ADVANCED COMPOSITE STRUCTURES FOR LOCKHEED AIRCRAFT

Warren A. Stauffer and Arthur M. James
Lockheed-California Company

SUMMARY

Lockheed is currently engaged in three NASA-sponsored Aircraft Energy Efficiency (ACEE) composite structure programs: the L-1011 Advanced Composite Vertical Fin (ACVF), the L-1011 Advanced Composite Aileron (ACA), and a wing study program. These programs are all structured to provide the technology and confidence for a Lockheed committment to the use of advanced composite materials for both primary and secondary structures of future transport aircraft. Material tests conducted on advanced composite material indicate that the 400K (260°F) cure system tested should be limited to structural applications not exposed to high temperature and moisture, while the 450K (350°F) cure system appears adequate for the environment of transport aircraft. The FAA Advisory Circular on certification of composite structure emphasizes the need to identify and account for the effects of the environment (moisture and temperature) on mechanical properties.

INTRODUCTION

Lockheed is currently engaged in three NASA-sponsored Aircraft Energy Efficiency (ACEE) composite structure programs: the L-1011 Advanced Composite Vertical Fin (ACVF), the L-1011 Advanced Composite Aileron (ACA), and a wing study program. These programs are structured to provide the technology and confidence for a Lockheed committment to the use of advanced composite materials for primary and secondary structures of future transport aircraft.

The ACVF program encompasses the design, fabrication, and certification of an advanced composite vertical fin installed on L-1011 transport aircraft. The primary emphasis of the program is to gain a level of confidence in the structural integrity of advanced composite structures through an expanded series of ground tests. Included are tests of selected subcomponent elements for four years in loading/environment conditions which will simulate twenty years of service, and includes the fabrication of three full-scale components for test and to verify manufacturing cost projections. These tasks were preceded by extensive tests to characterize and determine the effects of airline environments on candidate graphite/epoxy material systems. The latter led to a material change from a 400K (260°F) cure graphite/epoxy system (T300/5209) to a 450K (350°F) cure graphite/epoxy system (T300/5208) to provide greater margins in structure subjected to extreme operational environments.

The current status of these tasks is discussed in this paper. The results of coupon tests for both material systems are presented as well as the ACVF environmental (moisture and temperature) requirements.

The effect of moisture and temperature on the mechanical properties of advanced composite materials as shown in this paper can be quite significant. For this reason, the FAA has recently published an Advisory Circular relating to Certification Guidelines for Civil Composite Aircraft Structure. The requirements set forth in this circular are discussed as they relate to the ACVF.

SYMBOLS

Values are given in both SI and U.S. Customary Units.

$f_{notched}$	notched laminate strength (gross area), MPa (KSI)
$f_{unnotched}$	unnotched laminate strength, MPa (KSI)
RH	relative humidity, percent
T	time, hr
T_{AMB}	ambient temperature, K (^{o}F)
T_{MAX}	maximum vertical fin box thickness, m (in.)

ADVANCED COMPOSITE VERTICAL FIN PROGRAM (ACVF)

Structural Configuration

The ACVF is defined as the main structural box of the L-1011 vertical fin; it includes the front and rear spars, left and right covers, and all ribs (see Figures 1 & 2). The tip closure rib, hinge and actuator fittings, and the auxiliary spar are metal. The covers feature a single-stage cure assembly of prebled skins and prebled hat stiffeners. At the lower end of each cover, the stiffeners are cut off at a 45^{o} angle for the cover to mate with the existing fuselage-to-cover bolted joint. The covers utilize 0^{o}, $\pm$45^{o} T300/5208 graphite/epoxy material with thicknesses and ply orientations selected to match the strength and stiffness requirements of the metal fin. The substructure consists of ten full ribs, one partial rib, and continuous front and rear spars. The spars are molded from T300/5208 graphite/epoxy tape material with integrally molded rib attach angles and stiffeners. Two different rib designs are utilized in the ACVF: solid web ribs integrally stiffened for the upper three ribs and partial rib, and truss ribs with graphite/epoxy molded caps and aluminum diagonals for the remaining seven full-size ribs.

The current indicated production cost of the ACVF (cumulative average for 100 aircraft) is 9% below the estimated cost of a metal fin, determined on the same basis. The indicated weight saving is currently 27.6% (107.3KG (236.6 lbs.)). Composite material utilization is currently predicted to be 77.1% of the redesigned fin box weight.

Environmental Considerations

Environmental considerations of particular importance to the ACVF are moisture and temperature. Available data on graphite/epoxy composites indicate mechanical property reduction when exposed to high temperature and moisture. The extent of this reduction, particularly on matrix dominated properties, is influenced by the moisture content of the material and the ratio of the operating temperatures to the glass transition temperature of the matrix material. Therefore, it is essential that moisture and temperature conditions be considered in the design of composite structures.

For the ACVF, the moisture absorption for graphite/epoxy is conservatively assumed to correspond to 1.0% weight gain. With 1.5% weight gain assumed for fully saturated graphite/epoxy (T300/5208), 1.0% represents exposure to about 67% relative humidity 100% of the time.

The temperature range applicable to the ACVF is 219K (-65^{o}F) to 355K (+180^{o}F). The 219K is based on L-1011 specifications, and the 355K was determined from a solar heating analysis conducted on the ACVF. A survey of world commercial airport weather patterns led to the selection of Las Vegas, Nevada as being representative of the most adverse temperature conditions. An ambient temperature of 319K (114^{o}F) can occur on the order of once in 10,000 hours as shown in Figure 3.

A review of airline tail logos used on L-1011 aircraft in service indicates that dark colored paints, such as dark blue, are commonly used. The significance of color on skin temperature is indicated in Figure 4. In still air (ambient air temperature of 319K), with the sun position at 45^{o} relative to the fin surface, the skin temperature with dark blue paint increases to 365K (182^{o}F); with white paint, the skin temperature is 23K (42^{o}F) less. The ground time-temperature histories due to solar heating for three structural elements (cover, rib cap, and spar cap) are shown in Figure 5. For these calculations, the horizontal stabilizer was assumed to be unpainted with a solar absorptivity of 0.5 and reflectivity of 0.5. Direct solar heating of the fin and heating due to reflection from the horizontal stabilizer are accounted for in the thermal analysis. Cooling of the sun-facing surface of the fin by external radiation and internal radiation to the shadow exposed surface is also included. The maximum temperature reached for the cover is 363K (194^{o}F). Figure 6 gives the temperature time history of the cover during taxi, takeoff, and climb after ground solar heating. It is assumed that during taxi the sun-facing fin surface continued to be exposed to the maximum solar heating intensity, and only during takeoff and climb was this surface assumed to be oriented away from the sun. It can be seen from Figure 6 that the maximum structural temperature for the skin is 355K (180^{o}F) at the begin-

ning of takeoff and the maximum structural temperature at the end of the takeoff run is 347K (165°F), which occurs in the crown of the hat stiffener. Since design loads can occur any time during the takeoff run, the temperature of 355K (180°F) has been established as the design maximum temperature for the ACVF.

Material Characterization

Characterization of the following advanced composite material systems has been completed:

- Thornel 300/5209
- Kevlar 49/5209 181 Fabric
- Thornel 300/5208

The 5209 resin is a 400K (260°F) cure material, and the 5208 resin is a 450K (350°F) cure material. The characterization program was structured to establish basic lamina property behavior as it varies with temperature for both dry and wet conditioning.

The temperature range covered in this program was 219K (-65°F) to 355K (+180°F). This temperature range was assumed to adequately cover that expected in commercial service. Coupons were wet conditioned to ensure a minimum of 1% weight gain. Conditioning was accomplished in a humidity chamber at 95 to 100 percent relative humidity at 339 $\pm$3K (150° $\pm$5°F) for times determined by coupon thickness.

The material characterization results indicate that the effect of moisture and temperature is most pronounced on the 400K (260°F) cure resin material system, particularly on the material properties which are matrix dominated. Figures 7 through 9 show the reduction in compression strength for T300/5209, T300/5208 unidirectional material and Kevlar 49/5209 181 cloth due to the combined effects of moisture and temperature. Whereas elevated temperatures alone do not cause a significant reduction in longitudinal compressive strength, the combination of temperature and moisture does result in drastically reduced compressive strengths for 400K (260°F) cure resin system. This behavior is explained by the fact that moisture conditioning reduces the glass transition temperature of the resin. Subsequently, at elevated temperatures the matrix does not provide sufficient support for the fibers, resulting in low failure stresses. Comparison of the room temperature dry compression data with the 344K (160°F) wet compression data (Figure 7) indicates a 60 percent reduction in compression strength for the T300/5209 material system, while the T300/5208 material system comparison indicates a 13 percent reduction at 355K (180°F). For Kevlar 49, the reduction in compression strength is 62 percent going from room temperature dry to 344K (160°F) wet as shown in Figure 8. It should be noted that the longitudinal modulus is not significantly influenced by either moisture or elevated temperature for the two graphite/epoxy material systems. However, Kevlar 49/5209 181 cloth material system longitudinal

moduli are significantly affected as shown in Figure 9. These data indicate that the fiber, in addition to the matrix, is adversely affected by moisture and elevated temperature.

Laminate coupon test results of both T300/5209 and T300/5208 are shown in Figures 10 and 11. The test variables include notched and unnotched coupons, room temperature dry and elevated temperature wet. The coupons are approximately 25.4 x 279.4mm (1 x 11 inches) with fiberglass tabs bonded to the ends to leave a 152.4mm (6 inch) gage length. All coupons were strain gaged. The notched specimens have centrally located 4.76mm (3/16 inch) diameter holes. The ends are clamped with bolted fixtures carefully aligned in the test machine. To prevent buckling, the gage region is clamped between two "I" shaped, Teflon-coated steel plates with cutouts for strain gage and thermocouple wires, see Figure 12. The specimen and fixtures are enclosed in a temperature-controlled box, as shown in Figure 13, and the thermocouples are monitored for coupon temperature. Most of the coupons failed in the gage length. All of the coupons with 50%, 0° plies, fabricated from T300/5209, failed at the grip, apparently due to misalignment.

The results of the laminate strength tests again indicate a significant drop in compressive strength of the T300/5209 composite material when exposed to elevated temperature and moisture. When compared to room temperature dry properties, the unnotched compressive strength drops 60 percent at 344K (160°F) with 1% moisture content for laminates with 50%, 0° plies, and a 45% drop for laminates with 14%, 0° plies, see Figure 10. For T300/5208 (Figure 11), the unnotched compressive strength drops 10 percent at 355K (180°F) with 1% moisture for laminates with 50% or 14%, 0° plies. The compression ultimate of the laminates tested can be characterized by a failure mode involving delamination of the laminate into sublaminates and crippling of the $\pm 45^{\circ}$ sublaminates. The 0° sublaminates sometimes cripple and delaminate locally and sometimes appear to simply crush and fail without further delamination on a shear plane at about 40° to the surface. This failure mode is highly sensitive to minor variations in test support such as fixture clamping, minor test eccentricities, and variations in unsupported column length. This sensitivity produces large test scatter, in spite of the special care taken to minimize testing variables. From the nature of the failure mode, one must conclude that the test results are also a strong function of the test specimen detail design, and not necessarily relevant to performance in aircraft structure.

It is quite evident from the results of both the lamina and laminate coupon tests that the application of the 5209 resin system should be limited to structure not subjected to high temperature and moisture.

The effect of notches on the tension and compression strength of T300/5208 laminates is shown on Figure 14. It is quite evident from this figure that a significant reduction in both tension and compressive strength occurs in the presence of a notch. The notch factor, $f_{notched}/f_{unnotched}$ based on gross area for tension is .49 at room temperature and .69 for compression at 219K (-65°F). The reduction in strength in tension in the presence of a notch far outshadows the reduction in strength in compression in the presence of a notch including moisture and elevated temperature effects.

Production Readiness Verification Testing

The ACVF program provides for multiple large-scale subcomponents of the structure for evaluation of variability in static strength and for assessment of durability under extended time laboratory tests involving both load and environment simulation. This production readiness verification testing (PRVT) program is supplemental to the ancillary test program. These tests are designed to provide information to answer the following questions:

1. What is the range of production qualities that can be expected for components manufactured under conditions similar to those expected in production, and how realistic and effective are proposed quality standards and quality control procedures?

2. What variability in static strength can be expected for production quality components, and are the design margins sufficient to account for this variability?

3. Will production quality components survive laboratory fatigue tests involving both load and environment simulation of sufficient duration and severity to provide confidence in long-term durability in the service environment?

The questions are not primarily directed towards basic material properties. It is believed that the combination of service experience on secondary structures and coupon tests in the ancillary test program provide confidence in durability of the basic material. The questions are directed instead to the realities of production quality as influenced by cost objectives and by scale-up and complexity effects which will cause structural quality to differ from that represented by idealized small coupons.

Twenty duplicates of each of two key structural elements of the ACVF will be fabricated for test. One element will represent the front spar to fuselage joint area, and the other element will represent the cover to fuselage joint area, see Figure 15. These elements are identical to subcomponent test specimens which will be static tested prior to the fabrication of the PRVT specimens. These specimens will be manufactured as near as practical under conditions anticipated for production hardware and then subjected to NDI procedures. Anomalies from baseline accept/reject criteria will be reviewed and a decision made on whether to accept, accept conditionally, repair, or reject. Ten specimens of each type will then be subjected to static strength tests; and the other ten of each type will be used for durability tests.

At the onset of the durability tests, accept/reject criteria will have been established for many aspects of fabrication variability. Many of these should not affect static strength but are yet unproven from the standpoint of durability for commercial aircraft which have numerous ground-air-ground thermal cycles and the requirement for long life with minimal maintenance. Typical of this category of criteria are those for voids, hole quality, fiber

volume ratios, porosity, wrinkles, acceptance of prepreg, etc. If these factors are too closely controlled, they can increase production costs. It too loosely controlled, they could impair durability. Therefore, these criteria must be evaluated carefully. To do this, it is necessary to define the quality that can in fact be achieved during production and second to substantiate that the quality that can meet economic requirements will be able to sustain the expected service loads and environments. Upon completion of the durability portion of the PRVT program, it must have been demonstrated that the potential in-service durability of the ACVF is as good as or better than that of its metal counterpart.

The test fixtures and control system for the durability tests will be designed and fabricated to minimize the need for monitoring and maintenance during the course of the test. In particular, this will include:

- Computer control of loads and environment
- Malfunction detection devices for remote monitoring
- Premium quality load jacks to reduce down time and repairs
- A central environment mixing chamber with an environment distribution system to individual test specimens

The general approach to test equipment is shown on Figures 16 and 17.

The durability of the ACVF will be demonstrated by testing ten each of the two specimens in an extended time environment/load test. The load and environment spectra will be of the type and general make-up shown on Figure 18. This figure shows anticipated upper and lower bound test temperatures, segments of the flight to be considered and other appropriate conditions to define the flight environmental and load profile. Salient features to be incorporated into the finally selected test/environment spectra will be:

- The time-at-load for at least the higher loads in the spectra will be near real time. Since the gust loadings for the tail range in duration from five to eight seconds per cycle depending on aircraft speed and altitude, there should be no difficulty in attaining this simulation.
- Temperature and moisture cycles will be approximately real time in the critical portions where gradient effects are expected to be most critical. In particular, this will include the heat up to 355K (180°F) and the cool down simulating take-off.
- Ground storage will be accelerated by adjustment of temperature and humidity so that the anticipated service moisture levels will be approximately maintained.
- Moisture/temperature control at the central environment chamber will be the same for all specimens. Chamber

design and ducting controls will differ for the cover and spars to convert the baseline environment into that for the cover and spar. For the cover it is anticipated that the heating and cooling will be accomplished from the outside surface with the reverse side permitted to seek a cycle similar to that expected of the ACVF interior. For the spar, an effort will be made to control the temperature/humidity cycle to approximate that of the near surface and interior of the ACVF by appropriate simulation of the surface structure in the design of the chamber. Thus by using the central environment chamber to approximate the external ACVF environment, along with approximations of the manner in which the structure is being heated and cooled, the gradient effects will be approximated during the course of the tests. The actual cycle development will be accomplished by a combination of analyses, small coupon tests, and trial and error simulations during the development and setup of the test facility.

The durability specimens will be tested side-by-side to load/environmental spectra of sufficient severity to assure that twenty years of service usage will be duplicated in four years of laboratory testing. Periodically each specimen will be inspected per field service inspection technique. Any damage will be monitored for growth, or will be repaired using field service repair techniques, depending on extent and location of the damage. At the completion of the long-term durability tests, each specimen will be inspected and extent of damage assessed. Five of each of the specimens will be selected for residual static strength tests. The remaining ten specimens will be held, subject to an option to continue durability testing.

ADVANCED COMPOSITE AILERON (ACA)

Structural Configuration

The ACA is defined as the main structural box of the inboard aileron on the Lockheed L-1011 aircraft. The inboard aileron is located on the wing trailing edge between the outboard and inboard trailing edge flaps and is directly behind the engine as shown on Figure 19. The existing metallic design shown in Figure 20 is a single cell box beam with added trailing edge wedge, leading edge shrouds, and end fairings. The box consists of a front spar, a rear spar, and upper and lower skins, joined by 18 ribs.

Certain subassemblies used on the aluminum aileron will also be used for the composite aileron. These include the leading edge shrouds, the end fairings, the trailing edge wedge, the shroud supports, feedback fitting and the hinge/actuator fittings. These subassemblies were not redesigned because analysis indicated it would not be cost effective and no significant weight savings could be achieved.

Engineering Development

Various combinations of structural configurations and materials have been evaluated for the major subcomponents of the aileron. For each configuration, a variety of materials and materials combination was also studied. A total of thirty-one designs were evaluated for the covers, front spar, rear spar, intermediate ribs, main ribs, and rib backup fittings.

Each design was subjected to a quantitative analysis to determine weight and recurring cost and qualitative analysis of such factors as manufacturing processes, inspectability, etc. Results of the studies for each subcomponent are displayed in a matrix format to allow selection of the most viable concept. The evaluation matrix for the covers is shown in Table 1.

Based on the evaluation of the subcomponents, two ACA assembly concepts were selected for further evaluation. The first, shown in Figure 21, is a honeycomb core sandwich cover design with no intermediate ribs. This concept was selected because it offered the greatest cost saving potential. The second, shown in Figure 22, is a multi-rib design with a graphite/syntactic sheet skin cover. This design offered the greatest weight savings potential. A detailed cost and weight analysis, and qualitative assessment of factors such as producibility, maintainability, inspectability, etc. has lead to selection of the multi-rib concept for the ACA.

CONCLUDING REMARKS

The potential weight and cost saving which will lead to more energy efficient structure have been shown in several ways. However, the needed confidence, data base, and analysis methods are only now materializing. These data are identifying the characteristics of composite materials which are vital for good design, i.e., the effects of moisture, temperature, notches, etc. on material properties. However, the long-term effects of the environment on the durability of composite aircraft structure still need to be identified. These effects will be determined through a controlled environmental load program such as the Production Readiness Verification Test (PRVT) program.

TABLE 1 - COVER EVALUATION MATRIX

Concept	Sheet Skin				Sandwich			Stiffened Skin	
Materials & Construction	Gr Tape	Gr Tape	Gr Tape Syntactic Core	Gr Tape Syntactic Core	K49 Skins Nomex Core	Gr Skins Nomex Core	Hybrid Gr-K49 Skins Nomex Core	Gr Tape 5 Hats	Gr Tape 6 Hats
No. of Intermediate Ribs	6	10	5	4	0	0	0	0	1
Weight Ratio (1) to Aluminum	68.6%	66.2%	54.0%	59.1%	81.7%	77.7%	79.7%	87.2%	83.1%
Cost Ratio (1) to Aluminum	92%	120%	88%	91%	67%	82%	72%	99%	115%
Qualitative (2) Assessment	3.0	2.7	2.8	3.0	1.8	1.7	1.5	1.8	1.8

(1) Includes covers and intermediate ribs (if required).

(2) Includes producibility, inspectability, maintainability, repairability, etc. rated on a scale from 1 to 3 with 3 being best.

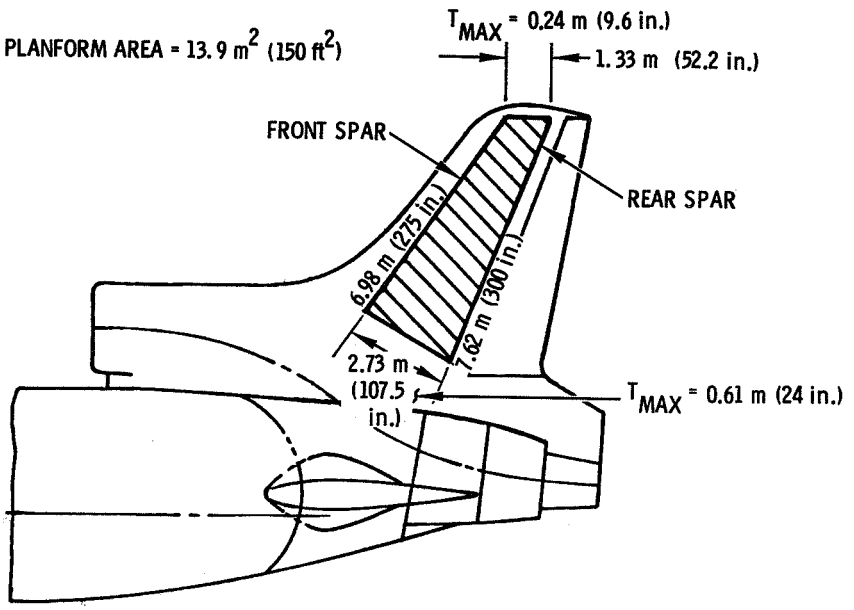

Figure 1.- L-1011 vertical fin box basic data and orientation.

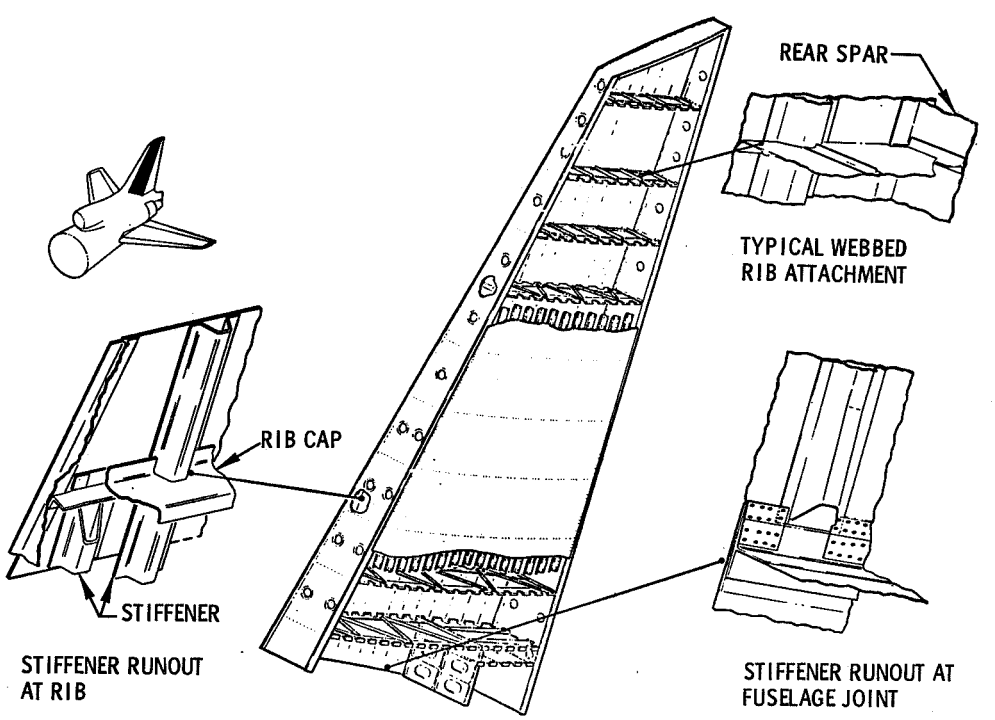

Figure 2.- ACVF configuration.

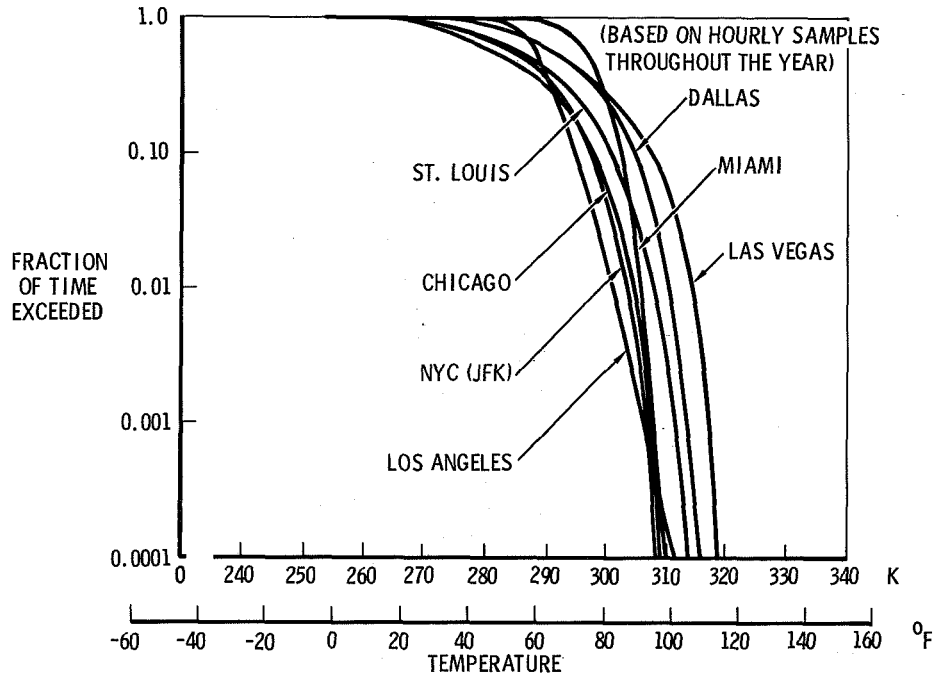

Figure 3.- Fraction of time exceeded — temperature of selected U.S. cities.

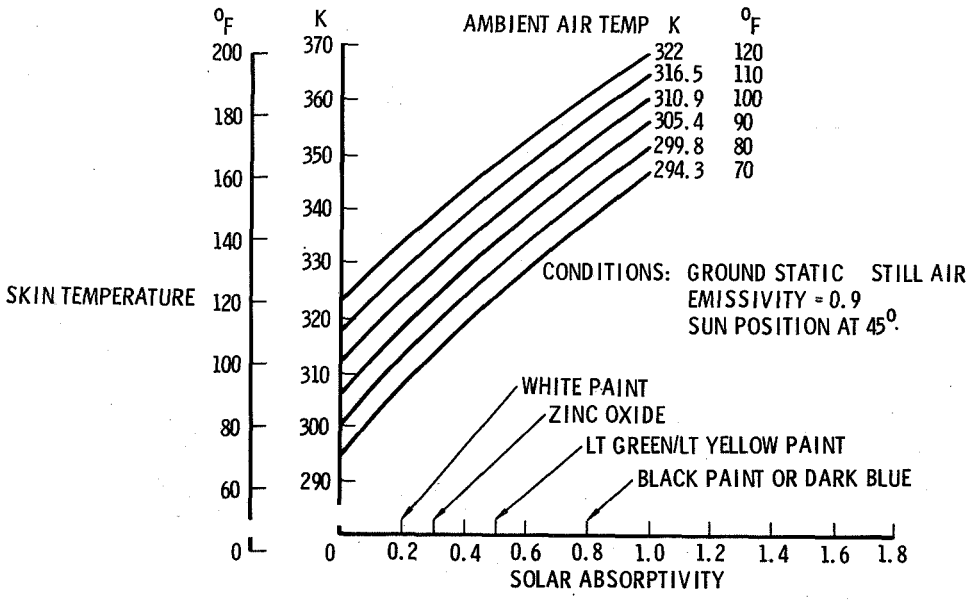

Figure 4.- Steady state — maximum vertical fin skin temperatures.

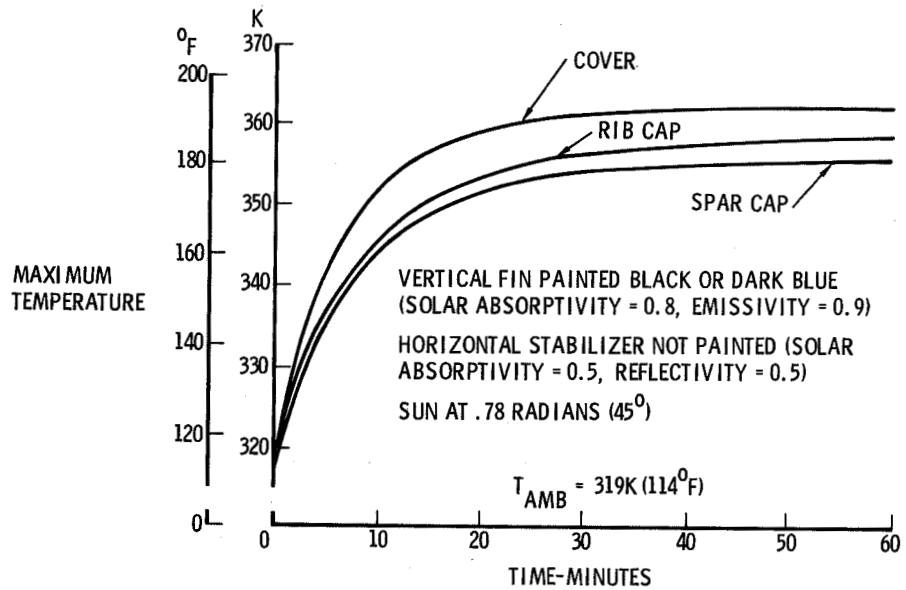

Figure 5.- Time to reach maximum skin temperatures.

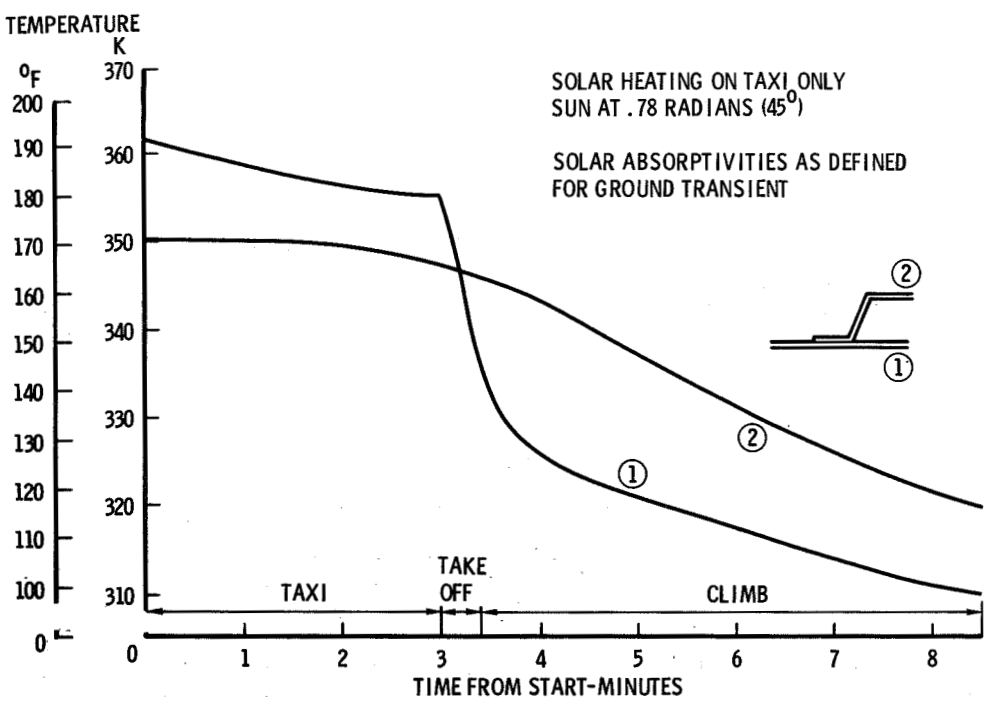

Figure 6.- Temperature-time history — cover.

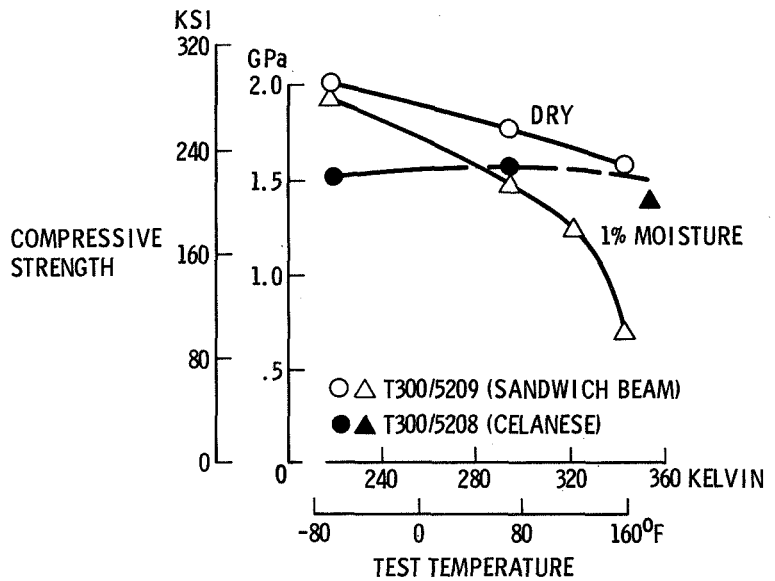

Figure 7.- Effect of moisture and temperature on compressive strength graphite/epoxy (0°).

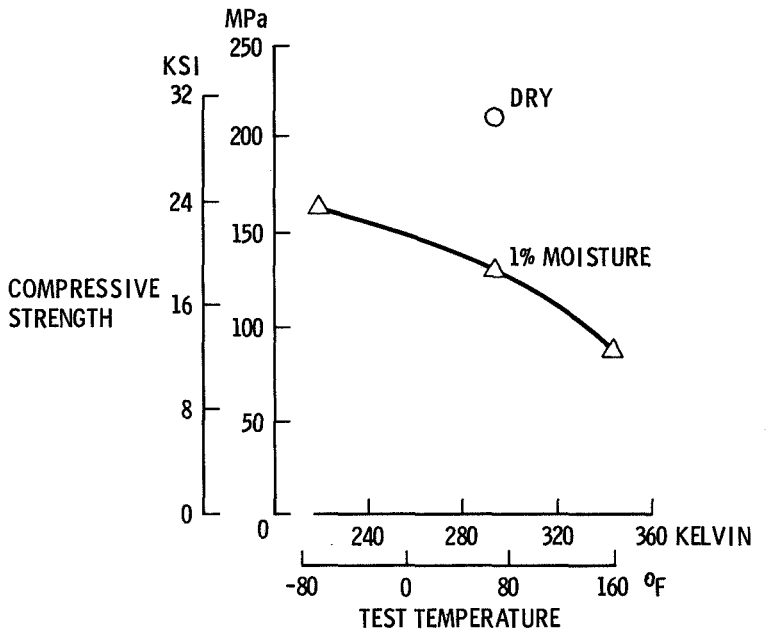

Figure 8.- Effect of moisture and temperature on compressive strength Kevlar 49-181 fabric/5209 (0°). 1.27- by 3.81-cm (0.5- by 1.5-in.) specimen.

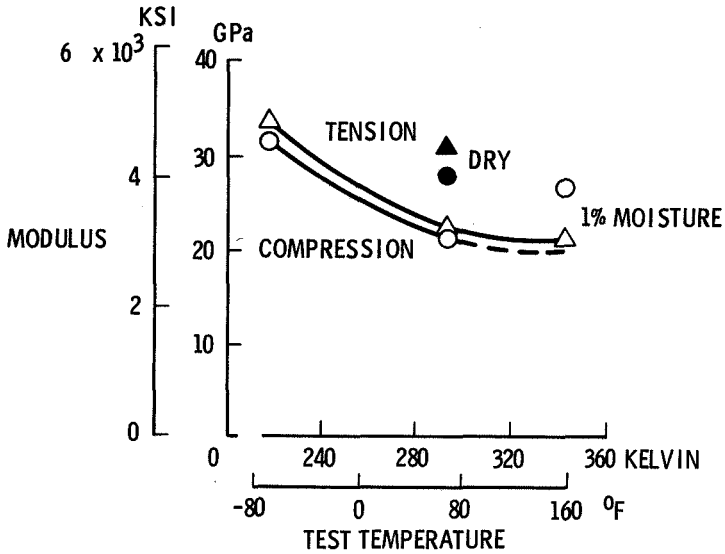

Figure 9.- Effect of moisture and temperature on modulus Kevlar 49-181 fabric/5209 (0^{o}).

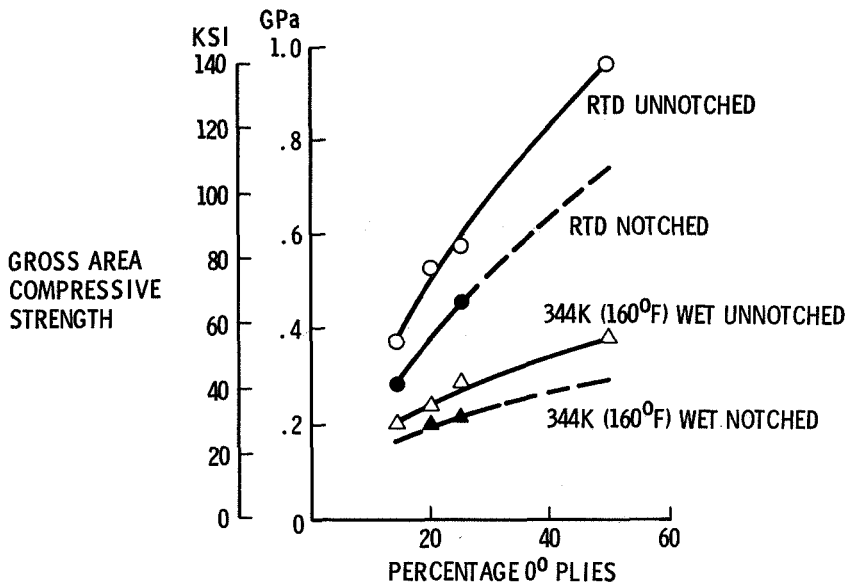

Figure 10.- Laminate compressive strength comparison T300/5209 graphite epoxy laminate ($\pm 45^{o}_{i}$, 0^{o}_{j}). Notch: 0.48-cm (3/16-in.) diameter hole; 2.54-cm (1-in.) wide specimen.

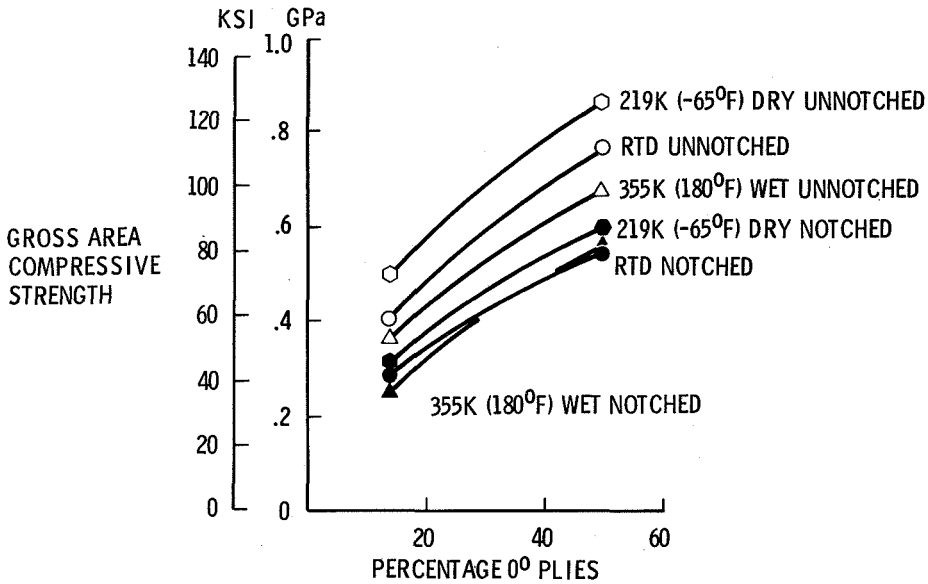

Figure 11.- Laminate compressive strength comparison T300/5208 graphite epoxy laminate ($\pm 45^{\circ}_{i}\ 0^{\circ}_{j}$). Notch: 0.48-cm (3/16-in.) diameter hole; 2.54-cm (1-in.) wide specimen.

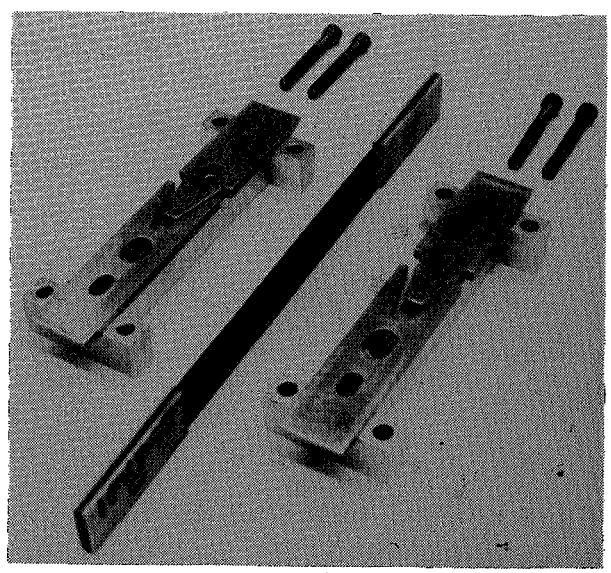

Figure 12.- Full-fixity apparatus-laminate testing.

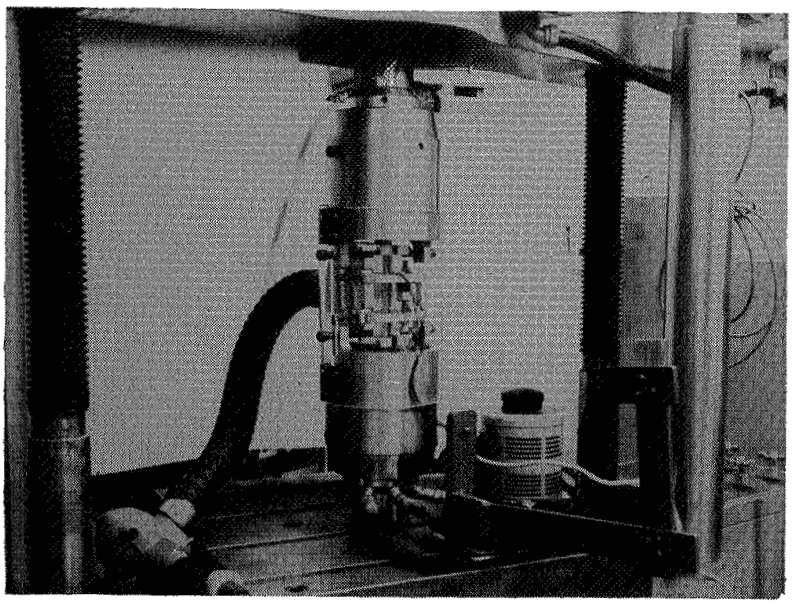

Figure 13.- Laminate compression test apparatus.

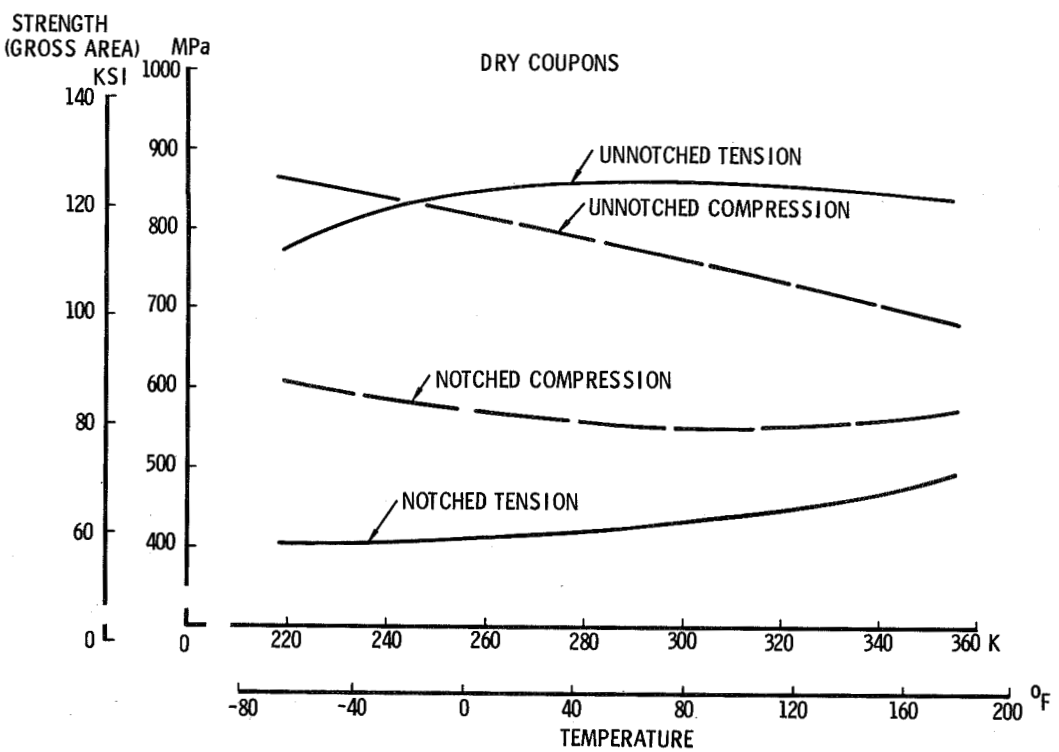

Figure 14.- Advanced composites. T300/5208 graphite/epoxy $(0^{o}_{2}/+45^{o})$ 16 ply coupons; 50 percent, 0^{o} plies.

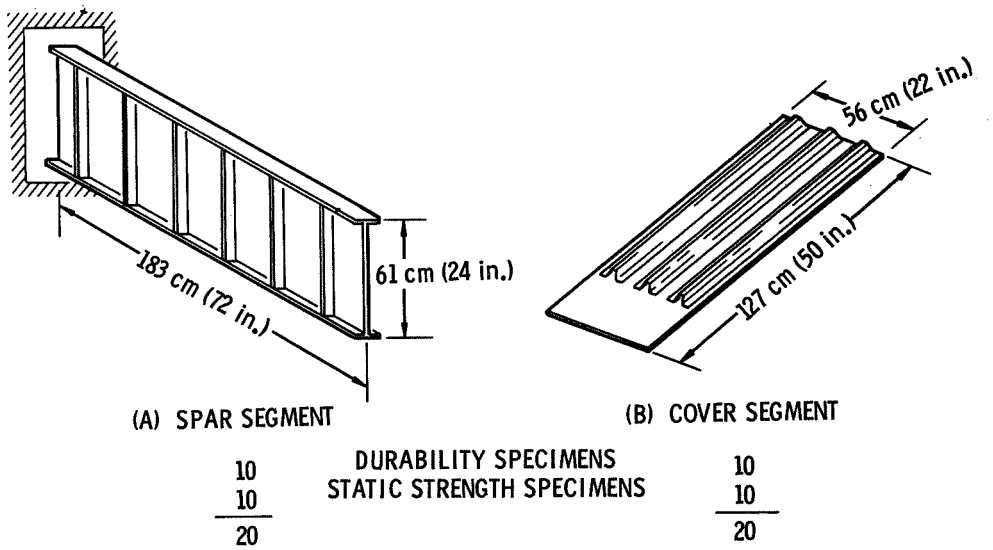

Figure 15.- Production readiness verification tests (PRVT).

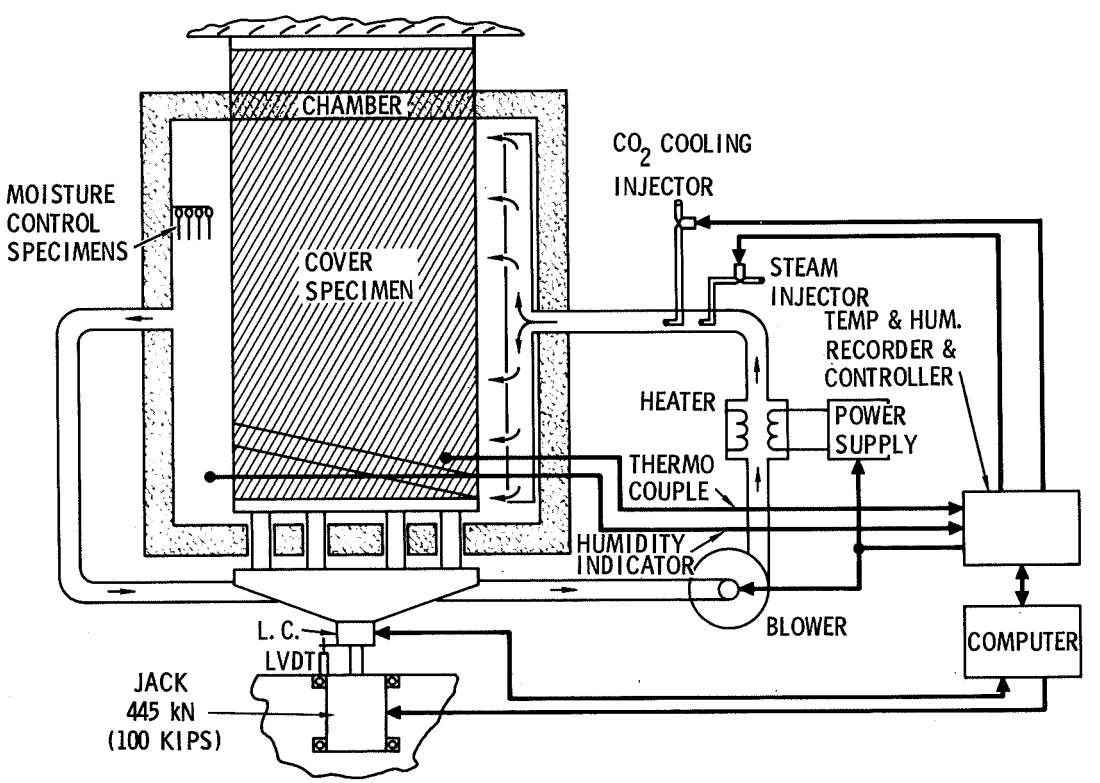

Figure 16.- PRVT schematic of cover test setup.

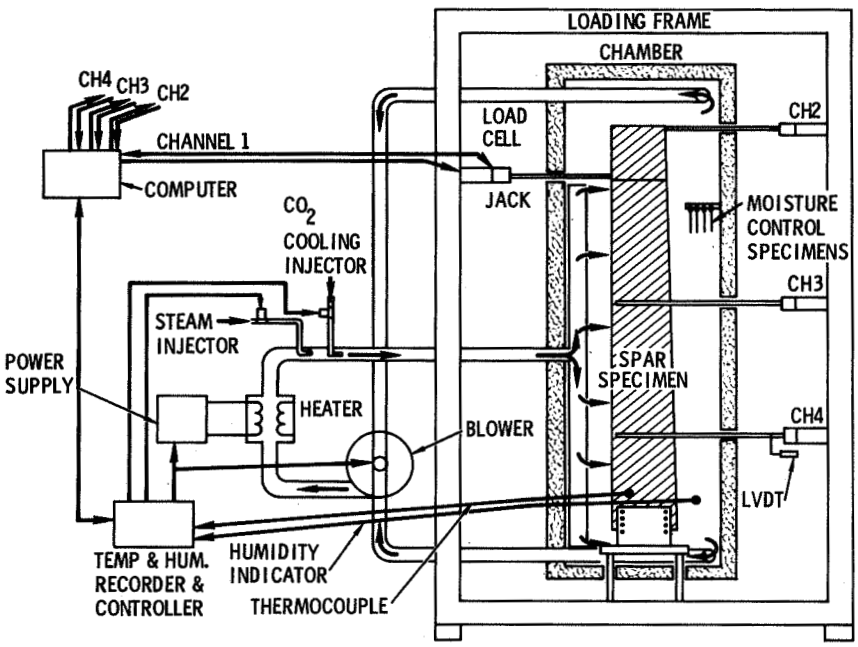

Figure 17.- PRVT schematic of spar test setup.

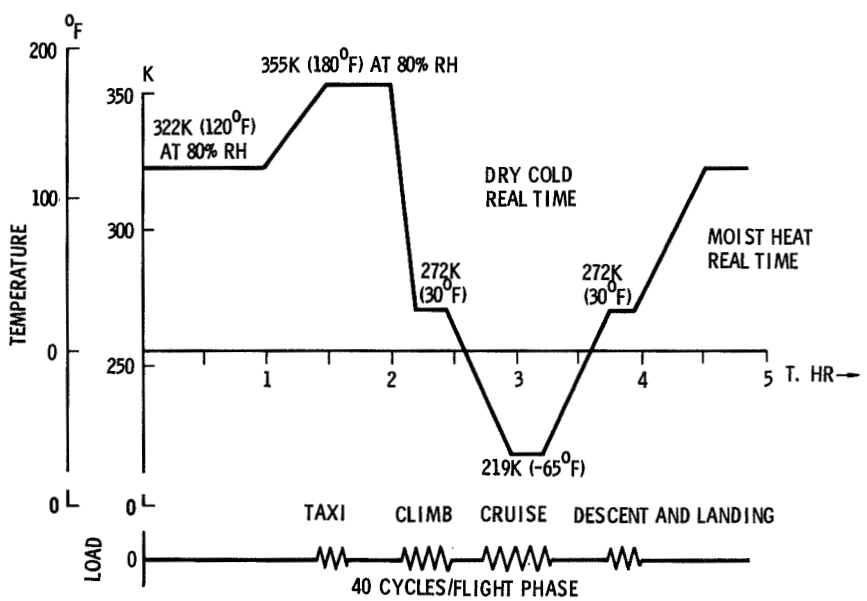

Figure 18.- Preliminary loads/environment simulation basic loading block.

Figure 19.- L-1011 inboard aileron.

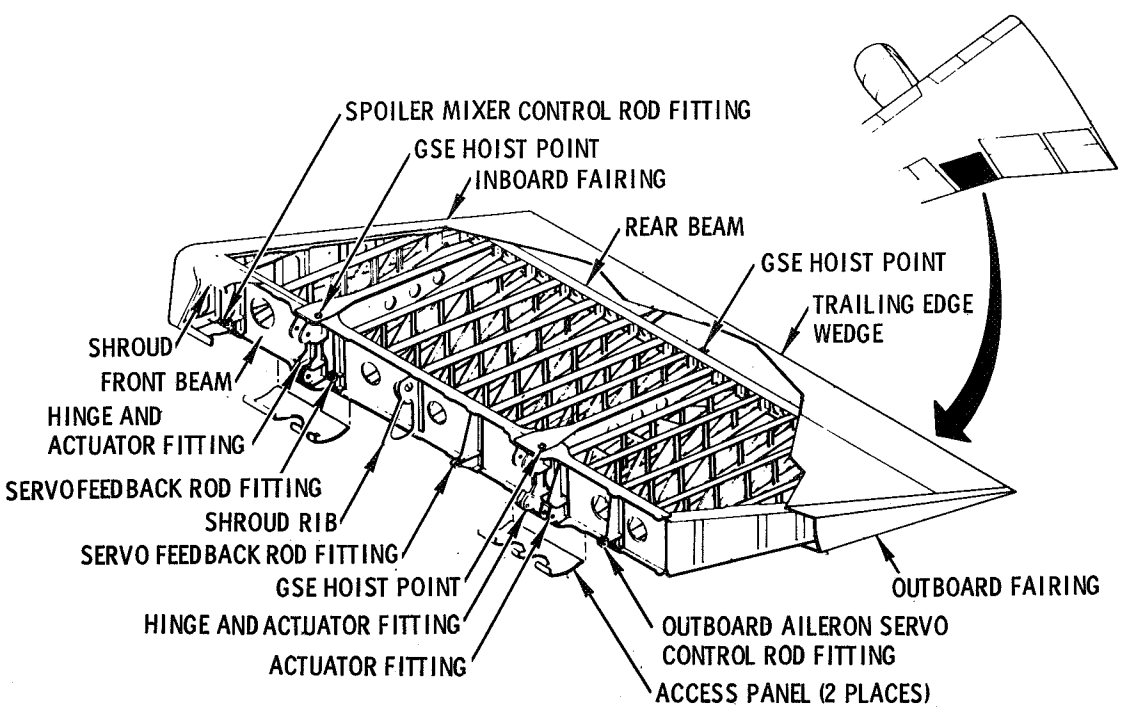

Figure 20.- Inboard aileron.

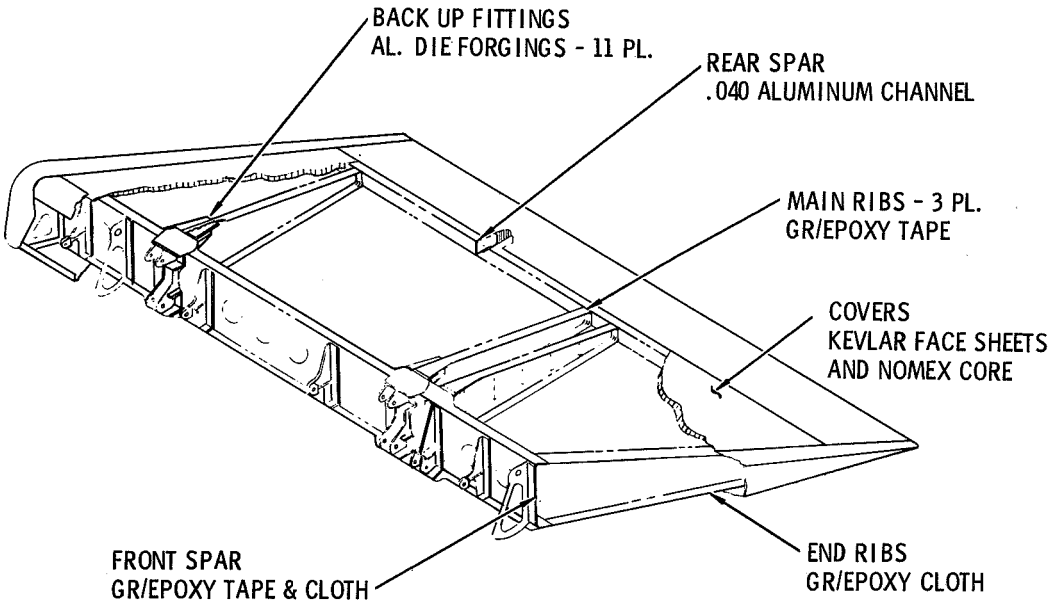

Figure 21.- Advanced composite aileron — concept no. 1.

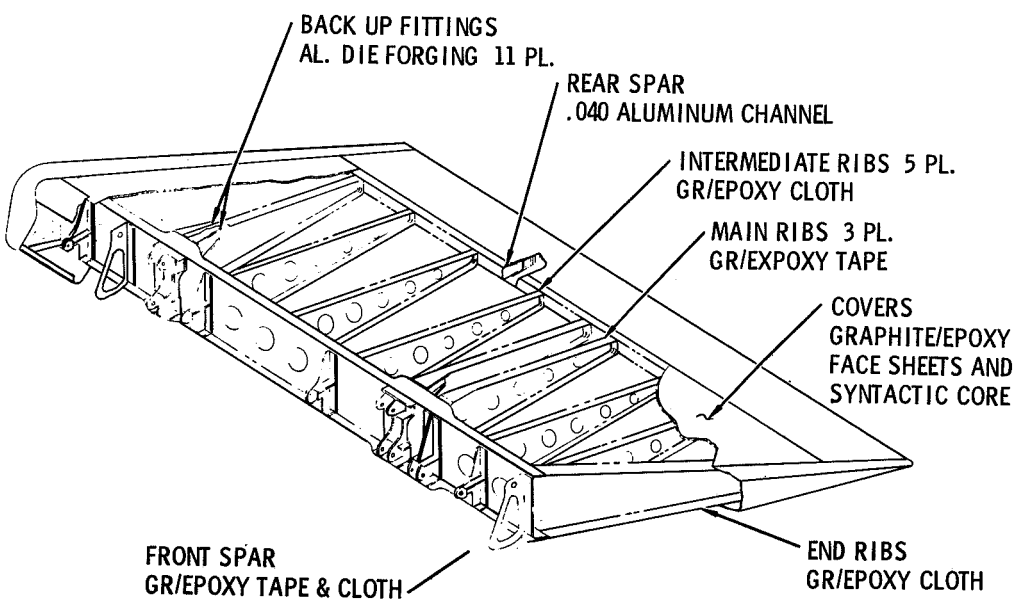

Figure 22.- Advanced composite aileron — concept no. 2.

KEY ISSUES IN APPLICATION OF COMPOSITES TO TRANSPORT AIRCRAFT

M. Stone
Douglas Aircraft Company

ABSTRACT

Key technical issues in the application of composite materials to transport aircraft are identified and reviewed. The issues involve the major contributing disciplines of design, manufacturing, and processing.

The key issues include: crashworthiness considerations (structural integrity, postcrash fires, and structural fusing), electrical/avionics subsystems integration, lightning, and P-static protection design; manufacturing development, evaluation, selection, and refining of tooling and curing procedures; and major joint design considerations.

The Douglas Aircraft Energy Efficiency (ACEE) composite structures program for which key issues are examined includes the DC-10 rudder, DC-10 vertical stabilizer, and the DC-9 wing study projects.

The Federal Aviation Administration (FAA) interface and the effect on component design of compliance with Federal Aviation Regulation 25 Composite Guidelines are discussed.

INTRODUCTION

The application of composite materials to transport aircraft structures has the potential of providing vehicle systems with significant performance improvements. The performance improvements include weight reduction, increased resistance to fatigue, and improved corrosion-resistance. In addition, reductions in acquisition and life-cycle costs can be realized in selected applications. However, the economic impact of composite components on the user airlines is central to their acceptance. The reliability and maintainability of the composite material systems when subjected to the operating environment of commercial transport aircraft is extremely important to the acceptance of the air carriers. The manufacturer must also be confident of his capability to design and produce composite structures within airplane program scheduling constraints and to meet targeted costs. In addition to acceptance requirements for the manufacturer and airlines, composite structures must conform to special guidelines established by the FAA to ensure compliance with Federal aviation regulations.

The physical, chemical, and mechanical characteristics and properties of advanced composite materials differ significantly from conventional aircraft structure, which affects all aspects of the design. Stress-strain-ductility relationships impose severe constraints on major joint design and structural repair. The material impact resistance will govern the allowable strain levels for damage-tolerant design requirements, and the response of composite materials to environments in which electrical phenomena are present is an important design consideration. Nonmetallic material processing and manufacturing procedures alter facility requirements, and a new component fabrication and assembly cost base must be developed.

A number of key technical problems have emerged during research and development efforts and flight service experience for which solutions must be found to realize the potential of advanced composite materials. To further examine this problem, selected key issues that relate to the development phases of the Douglas-NASA Aircraft Energy Efficiency (ACEE) composite structures program are discussed in detail in the following sections. The discussion includes crashworthiness, electrical/avionics requirements, manufacturing development, and major load transfer considerations.

FEDERAL AVIATION ADMINISTRATION INTERFACE

The certification of structural components for use on civil aircraft requires more extensive testing and associated documentation than for conventional metallic structures. This is in part due to the current minimum data base and lack of maturity of the technology.

An advisory circular for composite materials, released by the FAA, contains guidance information which the FAA considers acceptable for showing compliance with the certification requirements of civil composite aircraft. The advisory circular will be modified periodically to reflect technological advances. The document presently specifies the following with respect to compliance: (1) material and fabrication development, (2) proof of structure static, (3) proof of structure of fatigue/damage tolerance, (4) crashworthiness, (5) flammability, (6) lightning protection, (7) protection of structure, (8) quality control, (9) repair, and (10) fabrication methods. These requirements are indicative of the spectrum of key technology issues to be addressed.

To show compliance with the FAA advisory circular, the following tests and documentation are necessary:

1. Certification Plan – This document outlines all the tests and analyses which will demonstrate complete compliance for FAA certification.

2. Material Allowables Test Program – This document outlines all the material tests which are necessary to show compliance. It covers such allowables as tension, compression, interlaminar shear, and fatigue, and includes environmental effects such as humidity and temperature.

   The material allowables test plan must be approved by the FAA before the test program is begun, and tests must be FAA-witnessed or witnessed by an FAA-designated engineering representative (DER). Test results are submitted to the FAA for approval.

3. Static and Fatigue/Damage Tolerance Test Program – Static and fatigue/damage tolerance tests should be conducted on full scale or representative structural components to demonstrate the ultimate strength and the fatigue and damage tolerance capabilities of the structure. All test plans and test results must be approved by the FAA and all tests must be witnessed by the FAA or an FAA DER.

4. Strength Substantiation – The advanced composite material structure design must be substantiated by analytical methods to prove structural integrity for ultimate strength, fatigue and damage tolerance capability, crashworthiness, ability to withstand lightning strikes, and any other considerations specified in the advisory circular.

5. Manufacture and Repair – All manufacturing and material process specifications for composite materials require FAA approval. Composite material structural repairs which are published in the airplane service repair manuals must also be approved by the FAA.

CRASHWORTHINESS

The objective of FAA criteria for crashworthiness of the airframe is to ensure that occupants have every reasonable chance of escaping serious injury under survivable crash conditions.

Crashworthiness is considered a key issue because airframe structure which utilizes advanced composite materials must provide the same level of safety as conventional construction and because the behavior of composites in a crash situaiton has not been established. Advanced composites are generally thought of as poor materials for crashworthiness (compared to aluminum) because of their known brittle behavior. However, for many structural configurations, ductility can be shown to not be a crashworthiness factor, and comparable levels of safety can readily be achieved.

The crashworthiness of a structure is measured by its capability to perform three major functions: (1) the reduction of mechanical forces upon impact with the ground or other objects; (2) the capability of the fuselage shell to remain intact to provide the occupants with protection in the event of a postcrash fire; and (3) the maintenance of fuel tank integrity in a crash.

Crashworthiness of aircraft with conventional fuselage shells is enhanced because the aluminum construction possesses the ability to absorb considerable energy through deformation and tearing. This material behavior results principally from the inherent ductility of aluminum. If the aluminum is replaced with an advanced composite material, energy absorption would be reduced and more structural breakup would be expected to occur.

The ductility and energy absorption characteristics of a quasi-isotropic T300/5208 graphite/epoxy composite are compared to those of 2024-T3 in Figure 1 by using typical stress-strain curves for the two materials. Ductility is a direct function of the strain rate, and energy absorption capability is a direct function of the area under the stress-strain curve from zero to the strain rate at failure. Typically, the aluminum could sustain more than 24 times the deformation and has more than 64 times the energy absorption capability of the composite material. However, the total structural response to crash loads is also dependent upon the flexibilities due to the structural arrangements, and the overall performance of full-scale advanced composite structures to crash loads has not been established.

Based on limited tests to date (reference 1), there is encouraging evidence that in a fire, graphite-resin material systems would provide considerably greater burn-through protection for occupants in a nonpunctured composite fuselage shell than present aluminum structure. This protection affords reduced thermal threat, smoke, and toxicity, and extends the time for safe egress.

For wing structures, the goal is to avoid fuel spillage from the integral wing tanks by designing to maintain fuel tank integrity for a reasonable set of crash conditions or off-runway incidents. The following failure conditions must be considered:

1. The tank within the fuselage contour must be protected so that exposure to ground scraping action is unlikely for a wheels-up landing.

2. The tank within the fuselage contour must be capable of sustaining 9-g forward crash loads.

3. Airframe components supported by the main wing box integral tank structure must be designed to break away from the wing box without rupturing the wing tank.

These crashworthiness criteria have been conceptually satisfied for a DC-9 aircraft with an advanced composite wing box structure in a current NASA ACEE study.

The DC-9 center wing box is located inside the fuselage and has a fuel capacity of 3528 liters (932 gallons). The tanks are protected against scraping during a wheels-up landing by the fuselage shell and the heavy main keel member in the wheel well. The lower surface of the wing is 58.4 cm (23 inches) above the lower fuselage loft line at the front spar and 43.2 cm (17 inches) above the lower loft line at the rear spar. In addition, there are two cant panels and a heavy keel member directly under the wing which shield the wing box structure (Figure 2).

In over 15 million flight-hours accumulated by the DC-9 fleet, there has been no damage to the center wing box in survivable incidents because the wing box is protected by the structure under it. Thus, the composite wing box is afforded the same level of protection as the conventional wing box.

Inertia loads of 9 g must be sustained by the wing box structure inside the fuselage. Pressure loads are derived based on a full fuel tank with a 9-g head for this condition. The less ductile characteristics of composites can be accounted for in the detailed design by ensuring positive margins of safety for a 9-g fuel load condition and do not impose any special design problems.

Structural fusing as employed in conventional structures allows specific components to break free at predetermined load values to preclude penetration or other damage to the fuel tank. Pylons, landing gear support fittings, and some flight control fittings fall within this category.

The landing gear may be subjected to loads far in excess of design loads after contact with ditches, runway light standards, or other obstacles involved in off-runway incidents. These incidents are infrequent but must be accounted for in the design to prevent fuel tank rupture in accordance with FAR 25.721. The DC-9 main gear is designed to fail in the gear cylinder for high drag-load conditions, but other fuse points must be utilized for high resultant vertical and drag load combinations. The concept used for the DC-9 composite wing design allows for the main gear to remain intact. The failure will occur aft of the tank boundary in the following sequence:

1. The graphite/epoxy lower cover skin and titanium doubler will fail aft of the rear spar due to overload.

2. The primary restraining load path is then transferred to the two tension bolts attaching the support fitting to the lower bulkhead cap. These two bolts will fail due to overload.

3. The shear bolts attaching the support to the rear spar web will fail in the thin bolt heads as the support fitting breaks free from the rear spar.

4. The upper two bolts and upper cover skin and doubler will bend upward as the intact gear and support fitting rotate upward due to lack of a restraining moment.

A breakaway conceptual design for a composite wing box is illustrated in Figure 3. The composite lower skin and titanium doubler structural margins forward of the rear spar must be maintained at least 10 percent greater than aft of the rear spar. The in-tank aluminum support bulkhead is designed to be 5 percent stronger than the maximum strength of the two lower support fitting attach bolts.

The wing flaps in the landing flap position and wing-mounted engines will contact the runway if the landing gear collapses during landing. FAR 25.963 specifies that fuel tank integrity must be maintained for this condition.

The DC-9 wing flap is attached to the main composite wing box at three support locations. Four bolts attach the hinge fittings at each location (see Figure 4). The lower two bolts at each hinge fitting are necked down outside the tank boundary to form a fuse point for high tension loads caused when the flap structure strikes the runway. The fitting will then rotate about the two upper bolts and the wing tank will not rupture. The primary design task is to ensure that the flap bulkhead inside the tank is stronger than the fuse point of the attach bolt.

ELECTRICAL AND AVIONICS REQUIREMENTS

The use of graphite/epoxy composite structures on aircraft instead of conventional aluminum structures has necessitated the development of new design practices for electrical and avionics subsystems, especially for lightning protection designs. Electrical currents and heat are easily conducted by conventional skin panels made of aluminum. Aluminum panels are frequently used to conduct electrical elements of ground return paths and antenna elements. The metal skin also provides good electromagnetic shielding for critical electronic components and good conductive paths for lightning currents. Recent research and development programs sponsored by Government and industry have defined some of the conductive characteristics of graphite composite structures (references 2 and 3). They are far less conductive than aluminum structures, and investigations were made to determine if composite structures are satisfactory for shielding and lightning protection. Also, the low cost and lightweight aspects of the graphite composite structure design must be especially considered in integrating electrical and avionics subsystems and in incorporating lightning protection hardware.

Early test results (reference 4) indicated that certain types of graphite composite structures could be severely damaged by lightning strike attachment (Figure 5). Graphite composite structures are conductive enough to attract lightning strike current in a similar manner as aluminum structures, and yet they are not conductive enough to transfer the high energy involved in a severe lightning strike. The flow of lightning currents across structural joints also becomes a major design consideration. A composite structure joint damaged by lightning test is shown in Figure 6. Two new low cost and lightweight lightning protection design concepts have been developed (reference 5) and successfully demonstrated in several composite structure programs. They are the isolation concept and the conductive concept.

Isolation Design Concept

The isolation design concept is based on isolating the graphite composite structure from lightning current flow paths by covering the surface of graphite or boron composite skins with high dielectric strength material to prevent the swept-stroke/restrike lightning channel from attaching to the skins. The dielectric material may be in the form of a film or coating and its thickness will depend upon the dielectric strength required. The design principle is illustrated in Figure 7.

During the swept-stroke event, the lightning channel is forced to remain attached to a forward metal surface as it bends over the composite skin panel by the forward movement of aircraft. The lightning channel has an IZ impedance voltage drop V_c. There is also a breakdown voltage V_b between the lightning channel and the composite skin panel. As the channel is swept rearward, the portion of lightning channel lying over the composite panel is lengthened and V_c is increased. When V_c exceeds V_b, a new lightning attachment can occur. Therefore, by incorporating a dielectric layer over a composite skin panel, a certain span of the composite skin panel can be protected from the swept-stroke/restrike attachment.

The isolation concept for lightning protection is utilized on the DC-10 composite rudder design. Douglas is currently under contract with NASA to build several graphite composite DC-10 upper-aft rudders for flight service evaluation. The rudder component is located in the upper-aft extremity of the aircraft and requires both direct and swept-stroke/restrike lightning protection. The overall rudder lightning protection design is illustrated in Figure 8. Four P-static discharger installations are located at its trailing edge area and are electrically connected to aircraft metal structure. The rudder component does not enclose electrical/avionics components and therefore does not require electromagnetic shielding protection.

The isolation design concept proved to be the most suitable for the lightning protection of this composite structural component. Two aluminum straps were installed around the fiberglass tip and trailing edge to divert and guide direct lightning strike currents to the forward rudder metal structures through a bonding jumper installation. The four P-static discharger installations were electrically connected to these aluminum straps. A dielectric coating system was applied over the graphite skin panel surface for the swept-stroke/restrike protection. The graphite composite structures are thus completely isolated from lightning stroke currents. Laboratory-simulated lightning tests have demonstrated the successful operation of this isolation design.

Conductive Design Concept

The most practical and efficient lightning protection design for large composite structure applications is to utilize the conductive characteristics of the baseline composite structures such as skin panels and joints in the overall aircraft lightning protection design.

A metal strip protection system as illustrated in Figure 9 can be used to provide direct lightning stroke protection to graphite composite structures located in the direct lightning strike region. The graphite composite skin panel surrounding these metal strips will conduct a certain amount of lightning current since it serves as a parallel path from an electrical viewpoint. However, a careful design of the fastener installation and the composite skin panel installation can limit the amount of lightning current flowing in the composite skin panel to an acceptable level.

Proper use of the conductive properties of graphite composite structures for transferring lightning currents will eliminate the requirement for additional lightning protection material to conduct lightning currents through the lightning current transfer region. This conductive design concept is being considered for application in the DC-9 composite wing box program and other advanced program proposals.

An "all-composite" aircraft will retain many metal substructures which can be used to conduct lightning currents. An important design consideration is the proper introduction of lightning currents through metal-to-composite and composite-to-composite structural joints, so that the structural integrity of these points will not be affected by the flow of lightning currents. A proposed lightning protection concept for the DC-10 composite vertical stabilizer is illustrated in Figure 10.

MANUFACTURING DEVELOPMENT

The selection of the manufacturing method for composite fabrication is an integral part of the design process and as such is the most significant element in the cost of composite structures.

Autoclave and vacuum bag curing (reference 6), matched die pressing (reference 6), and thermal expansion cure techniques (reference 7) have all been used successfully for a variety of structural elements. Part size, geometry, complexity, and required quantity are all considerations in the selection of a fabrication process.

In the preliminary design phase of the DC-10 graphite rudder, a rib-stiffened design was selected (Figure 11) as the most advantageous concept due to minimum weight and adaptability to a thermal expansion trapped rubber curing process which permitted the molding and cocuring of the rudder structural box in one piece (skins, spars, and ribs).

A standard oven was satisfactory for curing, and repeatability of the process was possible with minimal tool refurbishment. However, there were disadvantages of the process which are covered below.

Four significant problems were encountered during fabrication of several development subcomponents (Table 1). During the first cure cycle, excessive pressures were developed in the Silastic J rubber mandrels, estimated at 6.89 to 10.3 MPa (1000 to 1500 psi), and two of the 2.54-cm- (1-inch-) diameter tooling bolts retaining the side plates failed in tension and bending. The heat-up rate was also very slow due to the mass of the mold tool. The subcomponent tool and mandrels are shown in Figure 12 (tool side plates have been removed for clarity).

The internal metal mandrels were redesigned and the rubber mandrels were recast using Dapocast 38-3 rubber for the second cure cycle. The redesigned metal mandrels allowed for the correct volume of rubber and utilized internal electrical heaters to increase the heat-up rate and thus reduce the thermal gradients through the assembled tool and laminate during the cure cycle. In addition, the redesigned mandrels were a multipiece aluminum alloy rather than the one-piece steel mandrel. The aluminum alloy promoted faster internal heat transfer and the multipiece construction facilitated mandrel removal.

To verify the revised tooling, a fiberglass subcomponent was successfully cured during the second cure cycle (Figure 13). However, considerable shrinkage of the rubber mandrels was discovered after they were removed from the three rib-bays. The mandrels shrank approximately 0.635 cm (0.25 inch) on the chordal dimension of 60.96 cm (2 feet).

The cure of a third part was attempted using the rubber mandrels which shrank during the second cycle. The cured laminates had poor fiber collimation and regions of large resin accumulation because the undersized mandrels failed to expand to the required pressure threshold until the material was well into its gel period during the cure cycle. The shrinkage problem was resolved by inserting a coarse wire-mesh screening in the pieces of cast rubber. The screening provided a mechanical restraint against shrinkage and the rubber mandrels were dimensionally stable thereafter. The wire-mesh screening, as utilized on the full-scale tool mandrels, is shown in Figure 14.

During fabrication of the first three subcomponents, rubber mandrel segments were particularly difficult to remove. Although the mandrels were liberally sprayed with a release agent prior to assembly, the temperatures and pressures sustained during the cure cycles effectively bonded the rubber segments to each other, to the metal mandrels, and to the laminate. This problem was resolved by coating the segments with a 0.08-mm (3-mil) Teflon tape at all appropriate faying surfaces.

After the metal mandrels were modified to incorporate internal heaters and the rubber mandrels were stabilized with metal screening and coated with Teflon, four additional subcomponents were fabricated for final tool and processing verification. Since no problems were encountered, construction of full-scale rudder tooling was initiated. Essential details of the full-scale rudder molding die are shown in Figure 15.

Four graphite rudder boxes were cured during the full-scale proof-of-tooling phase. Additional problems encountered during cure of the first three full-scale boxes are summarized in Table 2. After the second unit had been cured, it was concluded that the rubber mandrels had been cast slightly oversize. Although the tooling bolts were carefully torqued, the curing tool could not be fully closed. Gaps near the rear-spar flanges resulted in laminates that had high void content in that locality and poor dimensional control. These problems were remedied by recasting the rubber mandrels to the correct size.

The subsequent cure cycle was completed and resulted in a part with good laminate resin and void contents and part dimensions within engineering tolerance requirements. The fabrication of 10 graphite rudder boxes was then completed for flight service. A lineup of rudders during the final assembly process is shown in Figure 16.

A rudder modification program was conducted to develop and demonstrate manufacturing processes in order to provide a cost-competitive position between the graphite rudder and the metal unit it replaces.

Changes made to reduce the unit rudder cost included revisions in the rudder unit itself and in the fabrication and assembly tooling.

The rudder material for spars, ribs, and skin doublers was changed to a bidirectional weave fabric from 7.62 cm (3 inch) unidirectional tape. The basic skin panels will be fabricated from a unidirectional

weave fabric in lieu of the original tape material. Fabrication of rudder box details will be expedited by the use of a die trimmer tool and clicker press for preparing rudder box element flat patterns with the subsequent predensification operation accomplished simultaneously in gang fashion on a vacuum table.

Additional manufacturing revisions included the modification of the temperature monitoring and control system (Figure 17) into a computer-controlled automated cure process system and an additional assembly jig to perform some operations apart from the final assembly jig.

Cost estimates based on the above improvements resulted in the following data projections:

1. The combined unit cost (recurring only) of manufacturing the graphite/epoxy mold assemblies for the last three rudder units (i.e., 18th, 19th, and 20th) is 1110 man-hours.

2. The breakeven point of graphite/epoxy production rudders with conventional production rudders based on an economic analysis of recurring costs only is projected to occur between 50 and 70 units.

The comparison of total recurring labor hours for the first set of 10 rudders for units 11 through 20 is shown in Figure 18.

MAJOR JOINT DESIGN

In realizing the full potential of composite materials in lightweight aircraft structures, it is particularly important to ensure that the joints, either bonded or bolted, do not reduce the efficiency of the structure. The joining problem is far more severe with composites than with conventional metals such as aluminum, titanium, and steel because the high-specific-strength fibers and filaments are relatively brittle. They have little capacity to redistribute loads and none of the ductility of a yielding metal to mask a multitude of design approximations. Specifically, the graphite and boron/epoxy composites fail at a strain no greater than 1 percent whereas aluminum alloys, which yield at a strain of about 0.7 percent, typically stretch without failing more than 10 percent. While the component fibers and filaments behave linearly elastically to failure, there is a significant nonlinear behavior associated with delaminating the resin matrix in the actual composite. These delaminations can often soften stress concentrations to about half the concentrations of an equivalent homogeneous orthotropic material (reference 8), and this benefit should be accounted for in design. However, this relief falls far short of the complete ductility around stress concentrations in the metal alloys prior to failure.

This ductility of metals has come to be relied upon in design practice. An example of this is to be found in the multiple-row bolted joints used to splice wing skins at the centerline or sides of the fuselage. At ultimate load, the metal yields sufficiently for each bolt to carry its proportional share of the load. If this were done in composites, however, most of the load transfer would be confined to the outer rows of bolts, leaving the inner rows very lightly loaded, even at failure (Figure 19). This represents a severe design problem for highly loaded structures and is a key situation requiring examination and solution early in the design process. This load-sharing problem is so acute for composites that testing (reference 8) has shown that two rows of bolts can transfer no more than

about 10 percent more load than a well-proportioned single-row bolted joint. Therefore, it is unlikely that one will see many applications of more-than-two-row bolted joints in composites. This is quite a departure from standard metal practice.

Adhesive bonded joints also undergo nonuniform load transfer which comes from three basic sources. The first is adherend flexibility, which is explained in Figure 20 in terms of the adherend differential movement across the adhesive layer. The adhesive therefore develops a lightly loaded elastic trough between the effective load transfer zones at the ends of the overlap. While it may seem at first sight that the joint would be improved by redesign to raise the adhesive stress in that area, it should be considered that such an increase in joint strength is found by test (reference 9) to be associated with a reduction in service life and environmental resistance because of cumulative creep damage. A minimum expanse of elastic trough is needed to keep the stress in the middle so low that the adhesive there will never creep, so that the joint strength will not degrade in service. One should, however, then try to work each end of the joint adhesive equally to maximize the load transfer. This cannot be done if there is an adherend stiffness imbalance, as described in Figure 21. The adhesive shear strains are intensified at the ends from which the softer (less stiff) adherend extends. The same end of the joint is critical whether the joint load is tensile or compressive. This stiffness imbalance has been considered in the design of the major fittings for the DC-10 composite vertical stabilizer, in which the titanium fitting thickness at the end of the bonded overlap has been set to match the extensional stiffness of the composite at the other end. A further source of adhesive inefficiency is adherend thermal mismatch (Figure 22), which is acute for the aluminum-to-graphite/epoxy combination joints and still significant for titanium-to-boron/epoxy joints. This problem arises because high-strength adhesives are customarily cured at temperatures far above their operating temperature.

The important characteristic of the so-called thermal stress imbalance is that the critical end of the joint changes with the direction in which the load is applied. With all other variables held constant, this problem becomes progressively more severe with increasingly thick adherends to the extent that some joints are observed to break apart while cooling down in the autoclave after the adhesive is cured without the application of any external load. The only solution to this problem is to use a scarf joint with very small scarf angle, as is proposed for the major fittings on the DC-10 graphite/epoxy vertical stabilizer described later in this section.

The exact thicknesses at which each of these potential problems becomes intolerable are subject to so many variables that analysis is needed to differentiate between "thin" adherends, for which the bond is much stronger than the adherends, and "thick" adherends for which the bond is weaker. A number of suitable analyses for this task have been developed under contract to NASA Langley (references 10 to 14) using an elastic-plastic adhesive model. These are now used widely throughout the aerospace industry. These analyses rely on closed-form solutions and the associated Fortran IV digital computer programs are quick to run, requiring little input.

The remaining dominant characteristic of adhesive-bonded joints is the peel stresses developed in association with the shear stresses. Like the shear stresses, the peel stresses are maximized at the ends of the joint. The inner laminate split apart locally due to the peel stresses, thereby destroying the shear transfer capacity between the inner and outer plies. This overloads the outer filaments, which fail in tension. This problem can be alleviated by tapering the outer adherends to reduce peel stress. Thickness discontinuities should not exceed about four plies of composite.

The relative use of a variety of basic bonded joint types is summarized in Figure 23. As the load level and adherend thickness increase, progressively more complex joints are needed. On the other hand, one should never use a more complex joint type than is necessary. The scales shown vary with both material and environment but, as a general rule, stepped-lap joints become necessary at an adherend thickness of about 0.5 cm (0.20 in.), while tapered-lap joints are suitable up to 0.3 cm (0.12 in.), and double-lap or double-strap joints suffice for about 0.2 cm (0.08 in.).

A bonded joint is utilized to transfer the load between the fuselage support structure and the stabilizer box spars on the DC-10 vertical stabilizer-fuselage interface joint. The DC-10 aluminum vertical stabilizer box, shown in Figure 24, is a multispar, multirib structure in which the spar caps resist bending loads and skin panels resist both torque shear loads and local air loads. The extruded spar caps have integrally machined attach fittings at the root ends through which eight bolts attach the upper stabilizer to its support structure.

In the metal design (Figure 24), bending loads are concentrated into four pairs of extruded aluminum spar caps. These caps have integrally machined attach fittings at their root ends, through which eight bolts transfer the cap loads to the lower structure.

For interchangeability reasons, the design for the composite vertical stabilizer is constrained to attach at the existing eight bolt locations, with the same basic four spar structural configuration being retained.

Of the many configurations investigated, seven major variations are shown in Figure 25. Weight estimates for five of these are given in Table 3. From this study it was evident that the all-composite wrap-around concept promised to be the lightest and most efficient design. This configuration, together with the titanium scarf joint concept, has been carried into the test program to determine the joint concept which will form the basis for the final design.

All-composite design represents the minimum-weight solution, but also poses a considerable technical challenge. Basically, the highly unidirectional spar cap material is divided to form a loop at its end through which the tension bolt passes. The layers are not continuous around this loop, but overlap to form an end plate which is twice as thick as the adjacent cap material. In the test component, this end plate has a thickness of 4.7 cm (1.85 inches) which is greater than any previously incorporated in an aircraft component. A satisfactory cure cycle for thicknesses up to 5.08 cm (2 inches) has already been demonstrated at the laboratory level. The bulk of the layup for each fitting is achieved as a separate densified element which is subsequently cocured into the total structural assembly.

The second concept, which incorporates a titanium attach fitting cocured and spliced into the composite assembly, is regarded as a backup solution in the event that the all-composite approach is not found acceptable (Figure 26). Titanium is used in preference to aluminum because its lower thermal expansion is more compatible with the graphite/epoxy material. This allows the two materials to be spliced in a cocured operation, without inducing unacceptably high residual thermal stresses in the adherends or at the adhesive interface. The bathtub end is similar to the existing aluminum design and does not present a design problem.

The titanium fitting transfers the load into the composite structure by means of a double-sided scarf joint, both titanium and graphite being tapered in the joint region. The titanium is inserted within the

laminate layers during the primary cure cycle, with FM300 adhesive film between the material faying surfaces.

Characteristically, the scarf joint does not have the nonuniformity of adhesive shear stress, which is a feature of lap-type joints. However, perfectly uniform stress is not possible where stiffness imbalance and thermal mismatch exist between the two ends of the joint. Stiffness imbalance is avoided by matching the extensional stiffness (EA) of the titanium and composite materials throughout the length of the joint; however, the thermal expansion difference between the two materials must be accounted for. Assuming that the adhesive is initially cured at 177°C (350°F), there is a temperature differential of 138°C (280°F) at room temperature, 21°C (70°F), increasing to 213°C (415°F) each time the aircraft climbs to altitude. This represents a severe fatigue condition, occurring on every flight.

An analysis was conducted which utilized the elastic-plastic behavior of the adhesive and employed the adhesive stress-strain curve in an idealized form amenable to mathematical treatment. A sample printout from this program is given in Figure 27.

The analysis was conducted to cover a range of service temperatures from −57°C (−70°F) to 82°C (180°F) by treating the T-shaped joint as a flat element. The resulting joint configuration was designed for high margins of safety to allow for the possibility that regions of disbond might occur in the adhesive joint during the life of the component. The analysis was conservative because at temperatures approaching the cure temperature there is considerable alleviation due to the rapid creep and low modulus of the adhesive. These factors, taken in conjunction with the fail-safe design condition that the loss of any one complete spar shall be considered, ensures that the joint design will not allow catastrophic failure of the structure.

CONCLUDING REMARKS

As composite technology has matured, various problems have arisen which are unique to the material system. Many of the problems became key issues relevant to the successful application of composites to transport aircraft. Some key issues relating to the NASA ACEE composite structure program have been summarized in this paper.

The successful application of composite materials to primary structure will depend to a large extent on the ability of the material to meet or exceed the crashworthiness capability of conventional aluminum structures. This has not been demonstrated for the overall performance of full-scale-composite structures at this time but some experimental evidence to date indicates better burn-through protection for postcrash fires.

Research into composite electrical/avionics requirements has provided a data base for the successful lightning protection design of a variety of structural components. Due to the poor electrical and thermal conductivity characteristics of composite materials and the different requirements (position geometry, interfacing subsystems, etc.) which must be satisfied, generalized solutions are not available at this time. However, structural hardware has been designed and demonstrated to provide the necessary degree of successful lightning protection.

Design and manufacturing engineers have a broad selection of fabrication methods and processes available to them for composite hardware manufacture. It is the close interface between component design and fabrication that is essential for low-cost hardware fabrication. The manufacturing issue is not one of producing a workable component but of producing cost-competitive hardware that satisfies all design criteria and requirements.

Joints in aircraft structure are expensive both in weight and construction cost. Composite materials afford the designer an opportunity to minimize the number of joints in a structure but the brittleness and low interlaminar tension characteristics of the composite material impose constraints that require care and finesse in successful joint design.

REFERENCES

1. Hognat, Jacques: Flammability and Fire Resistance of Metallic and Non-Metallic Materials. National Symposium on Fire Safety Aspects of Polymeric Materials, June 1977.

2. Kung, J. T.; and Amason, M. P.: Lightning Conductive Characteristics of Graphite Composite Structures. Douglas Paper 6583, Presented to the 1977 IEEE International Symposium on Electromagnetic Compability, August 1977.

3. Composite Forward Fuselage Systems Integration Program, Second Quarterly Progress Report. AFFDL Contract F33615-76-C-5439, General Dynamics, October 1977.

4. Goodrum, G. T.: Lightning Protection for Advanced Composite Aircraft Structures. SAE Paper 700935, Presented at 1970 Lightning and Static Electricity Conference, December 1970.

5. Kung, J. T.; and Amason, M. P.: Lightning Protection Concepts for Advanced Composite Structures. Douglas Paper 6477, Presented to the 1976 IEEE International Symposium on Electromagnetic Compatibility, July 1976.

6. Plastics Engineering Handbook, Third Edition. The Society of Plastics Industry, Inc., Reinhold Publishing Co. New York, N.Y.

7. Purvis, N. B.: Advanced Composite Rudder Development and Fabrication for the DC-10. Douglas Paper 6427, Presented to American Ceramic Society, October, 1975.

8. Hart-Smith, L. J.: Bolted Joints in Graphite-Epoxy Composites. NASA CR-144899, June 1976.

9. Thrall, E. W., Jr., et al.: Primary Adhesively Bonded Structure Technology (PABST), Phase 1b: Preliminary Design. Technical Report AFFDL-TR-76-141, December 1976, pp. 149-151.

10. Hart-Smith, L. J.: Analysis and Design of Advanced Composite Bonded Joints, NASA CR-2218, January 1973.

11. Hart-Smith, L. J.: Adhesive-Bonded Double-Lap Joints. NASA CR-112235, January 1973.

12. Hart-Smith, L. J.: Adhesive-Bonded Single-Lap Joints. NASA CR-112236, January 1973.

13. Hart-Smith, L. J.: Adhesive-Bonded Scarf and Stepped-Lap Joints. NASA CR-11237, January 1973.

14. Hart-Smith, L. J.: Non-Classical Adhesive-Bonded Joints in Practical Aerospace Construction. NASA CR-112238, January 1973.

TABLE 1.- SUBCOMPONENT DEVELOPMENT PROBLEMS AND SOLUTIONS

CURE CYCLE	PROBLEMS	CAUSE	SOLUTION
1	2.5-cm (1-IN.) DIAMETER TOOLING BOLTS FAILED.	EXCESSIVE PRESSURE.	CHANGED RUBBER FORMULATION. REDUCED RUBBER VOLUME.
2	RUBBER MANDRELS SHRUNK.	CREEP BEHAVIOR UNDER CURING HEAT AND PRESSURE.	REMADE RUBBER MANDRELS WITH METAL INCLUSIONS TO STABILIZE DIMENSIONS.
3	POOR FIBER COLLIMATION AND LARGE ACCUMULATIONS OF RESIN.	LAMINATE CURED WITH INADEQUATE PRESSURE.	ADDED ELECTRICAL HEATERS WITHIN METAL MANDRELS FOR INSIDE-OUT HEATING.
4	RUBBER MANDRELS STUCK.	CURING HEAT AND PRESSURES.	ADDED TEFLON TAPE AT FAYING SURFACES.
5-8	NONE	–	–

TABLE 2.- FULL-SCALE RUDDER DEVELOPMENT PROBLEMS AND SOLUTIONS

CURE CYCLE	PROBLEM	CAUSE	SOLUTION
1-2	VOIDED REGIONS NEAR REAR SPAR. POOR LATERAL DIMENSIONAL CONTROL.	UNABLE TO CLOSE MOLD BECAUSE OF OVERSIZED RUBBER MANDRELS.	RECAST RUBBER MANDRELS.
3	REGIONS OF SKIN CURED WITH INADEQUATE PRESSURE.	EXCESSIVE DENSIFICATION STAGING OF SKINS. DEVELOPED PRESSURE TOO LATE IN CURE CYCLE.	REDUCED DENSIFICATION CONDITIONS. EXPANDED RUBBER SOONER WITH INTERNAL HEAT.
1-3	LOCALIZED CRACKS IN FRONT SPAR.	INDUCED STRESSES DURING COOL-DOWN.	ADDED LOCAL LAYERS. IMPROVED PREFORM TECHNIQUE TO REMOVE ECCENTRICITIES.
4	NONE	–	–

TABLE 3.- REAR SPAR CAP WEIGHT COMPARISONS

ATTACH FITTING CONCEPT	METAL END FITTING[1] LENGTH cm (IN.)	WEIGHT, kg (LB)		
		INBOARD 81.3 cm (32 IN.)	OUTBOARD 609.6 cm (240 IN.)	TOTAL 690.9 cm (272 IN.)
BASELINE (ALL ALUMINUM)	N/A	9.95 (19.5)	9.62 (21.2)	18.5 (40.7)
ALL COMPOSITE WRAP-AROUND SECTION	N/A	4.85 (10.7)	6.67[2] (14.7)	11.5 (25.4)
ALUMINUM END BUTT-SPLICE	44.2 (17.4)	11.88 (26.2)	6.67[2] (14.7)	18.6 (40.9)
ALUMINUM END LAP-SPLICE	52.1 (20.5)	11.39 (25.1)	6.67[2] (14.7)	18.1 (39.8)
TITANIUM TRANSITION SPLICE MEMBER	37.1 (14.6)	7.48 (16.5)	6.67[2] (14.7)	14.2 (31.2)
TITANIUM END WITH BONDED SPLICE	49.5 (19.5)	6.99 (15.4)	6.67[2] (14.7)	13.7 (30.1)

(1) MEASURED FROM STATION Z_{FR} = 292.255 TO OUTBOARD END FITTING.

(2) BASED ON AMC 7185 REAR SPAR CAP "EA"

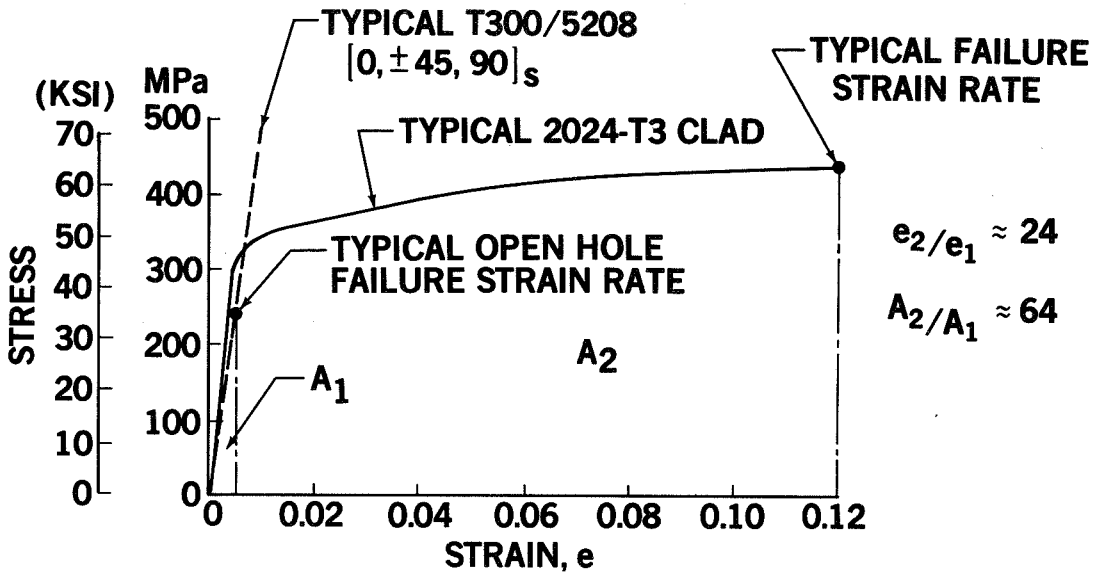

Figure 1.- Stress-strain relationship of graphite/epoxy and aluminum materials.

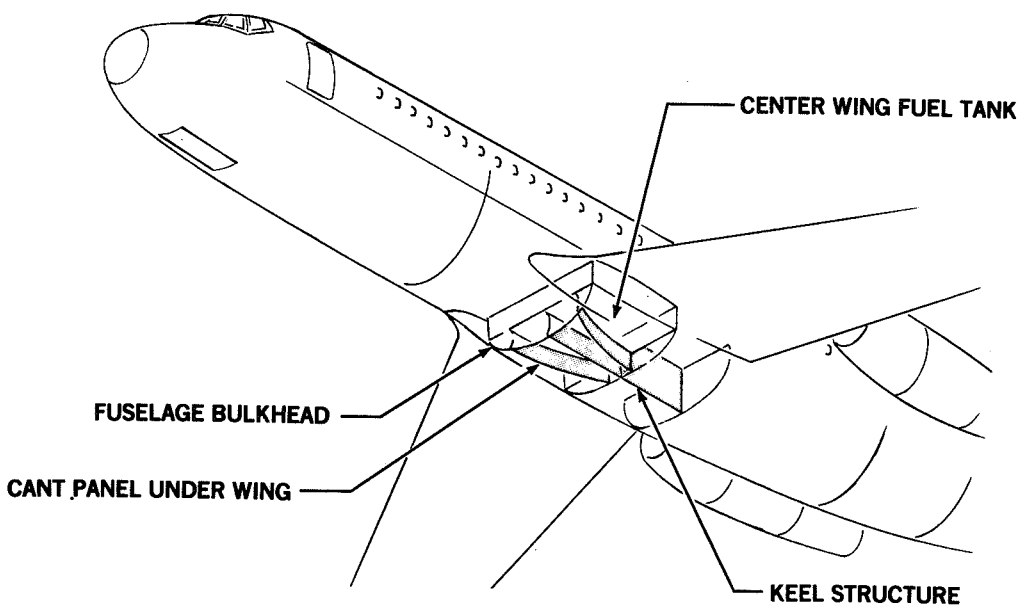

Figure 2.- Protection of center wing fuel tank structure.

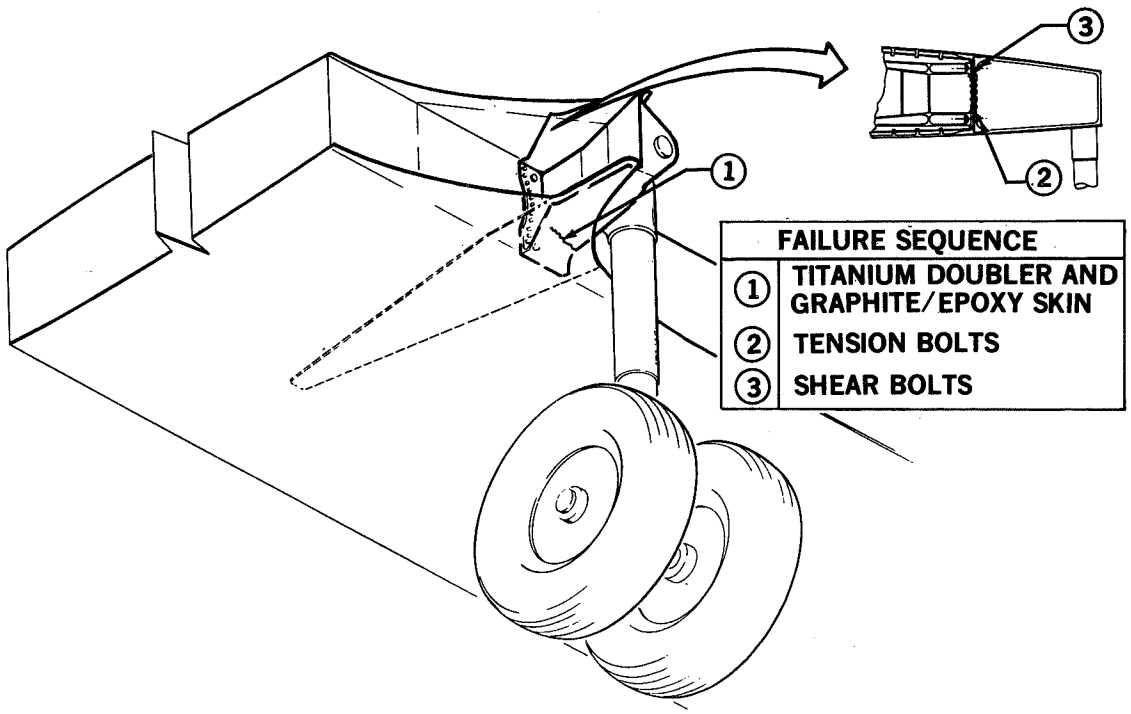

Figure 3.- Main gear breakaway features for structural overload.

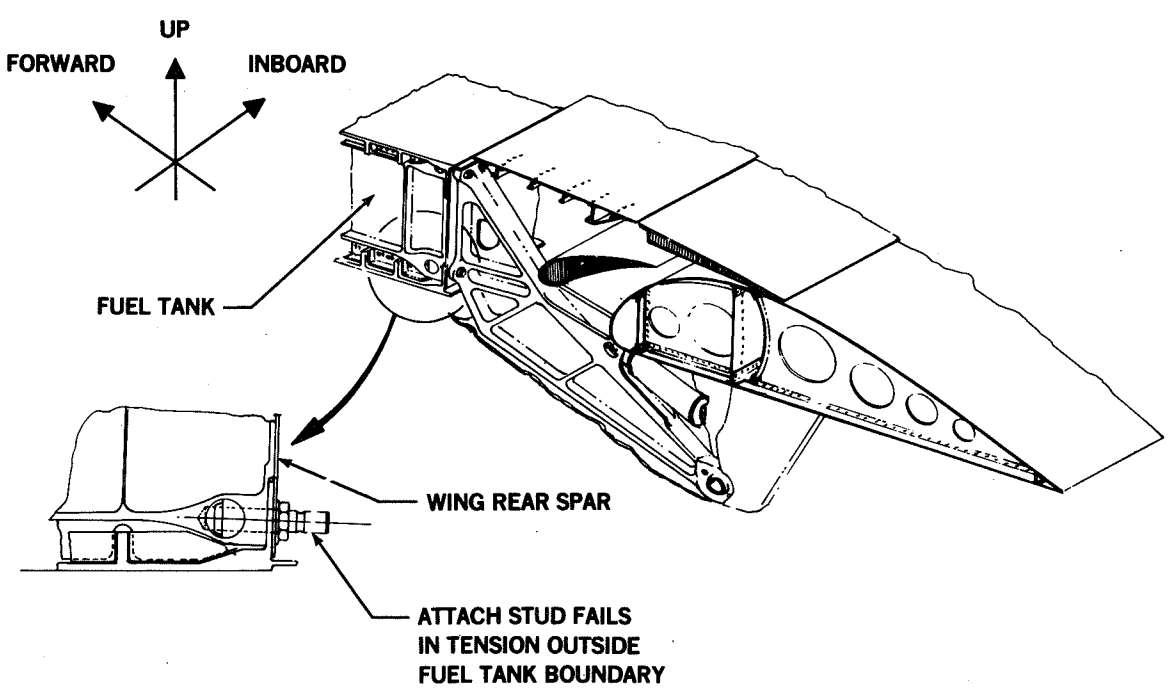

Figure 4.- Flap support structure overload breakaway design.

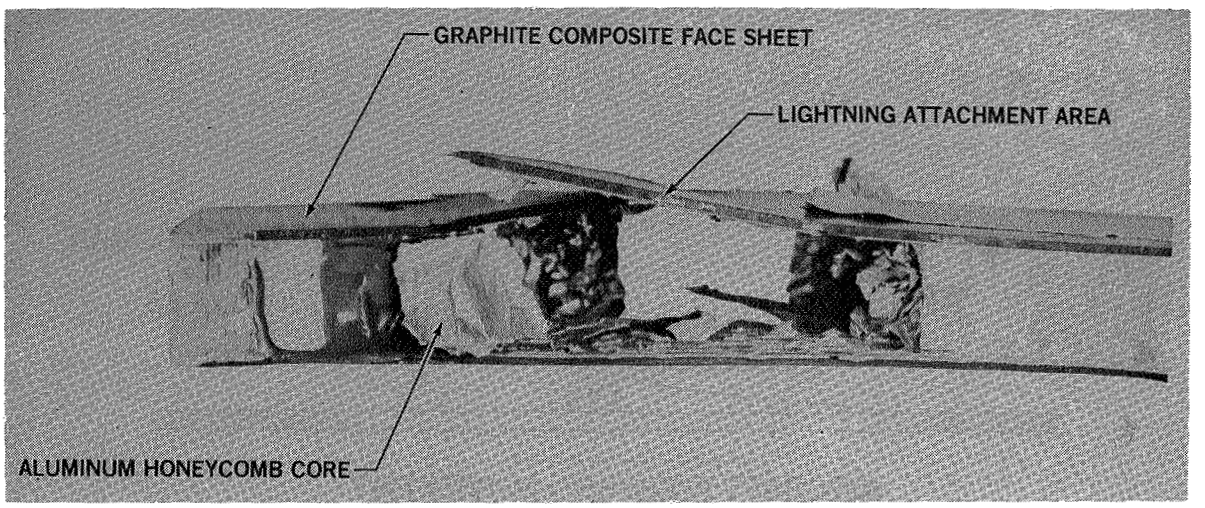

Figure 5.- Lightning strike attachment damage to a sandwich graphite composite panel with aluminum honeycomb core.

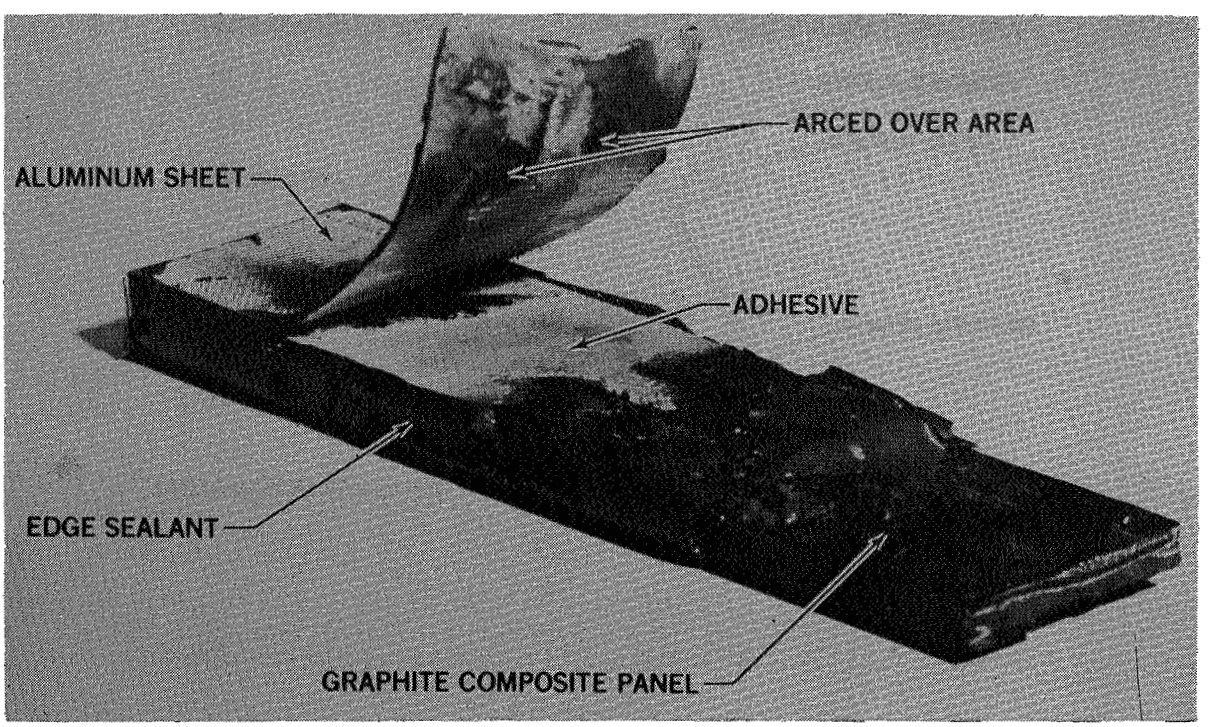

Figure 6.- Metal-to-composite joint damaged after lightning test.

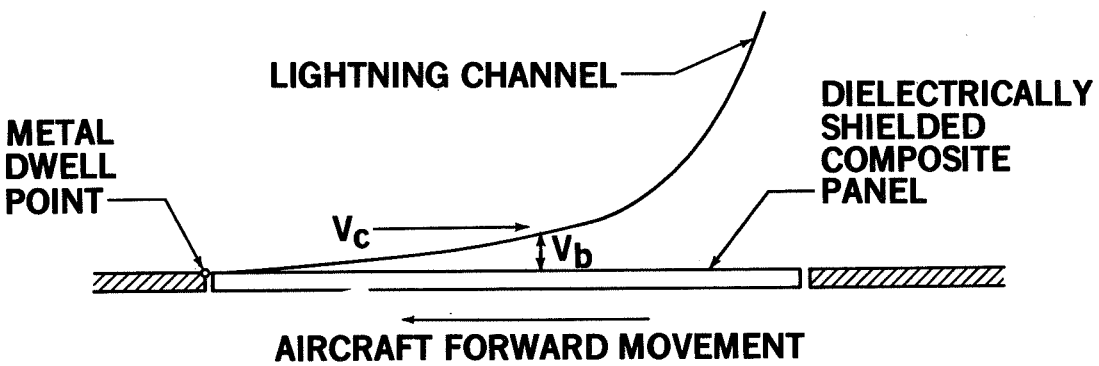

Figure 7.- Swept-stroke attachment criteria.

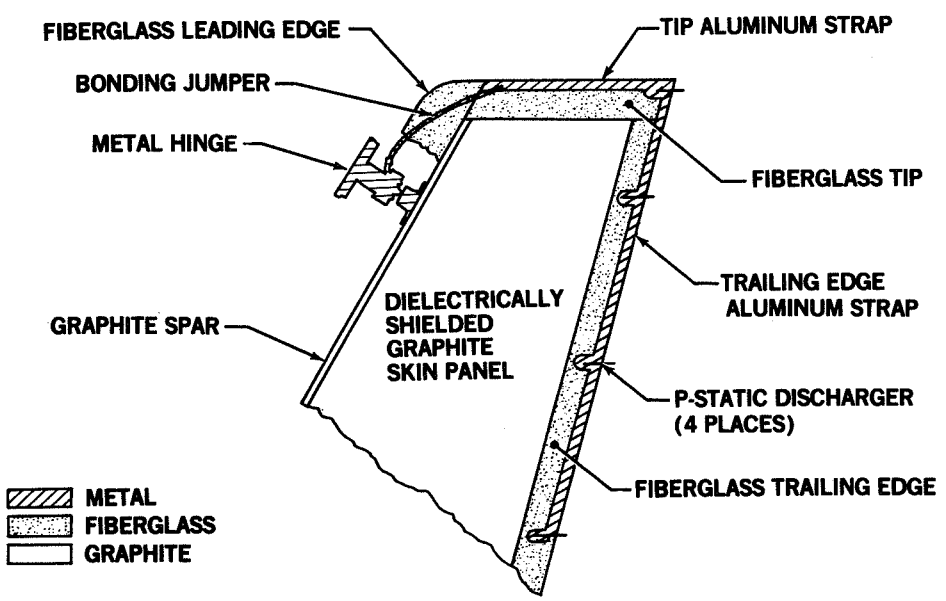

Figure 8.- DC-10 composite rudder lightning protection.

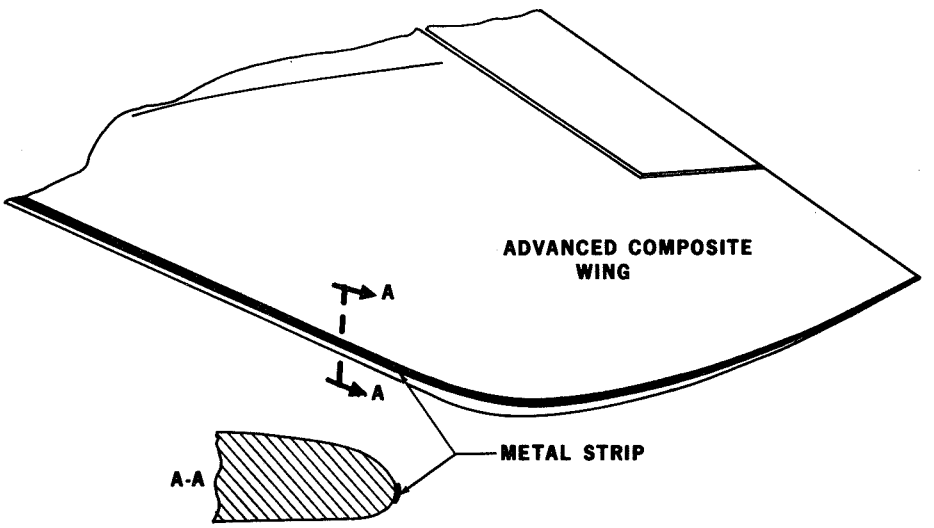

Figure 9.- Lightning strip protection system.

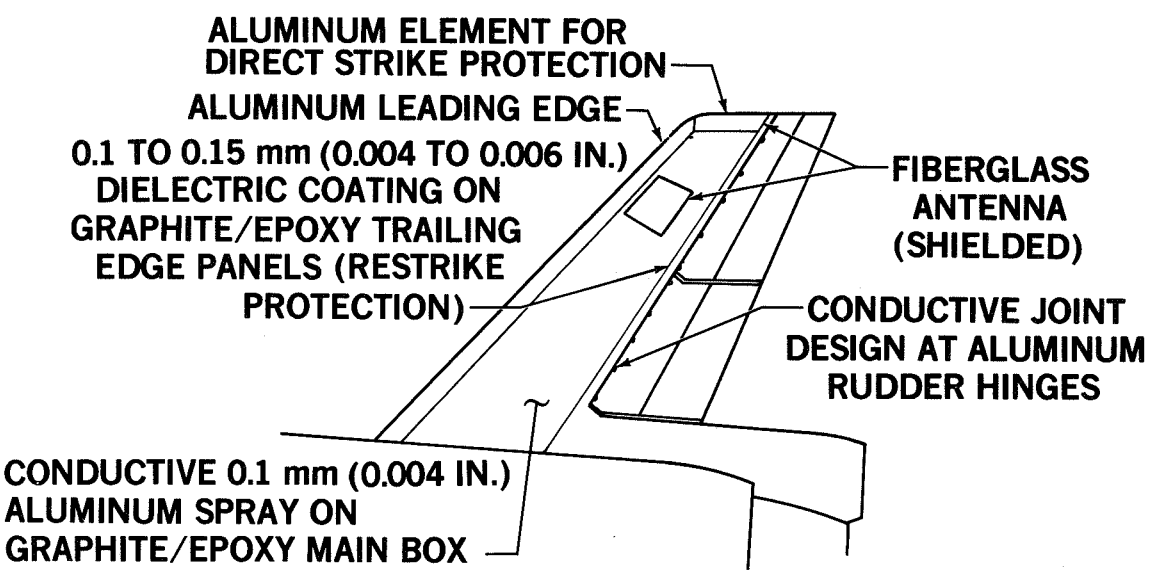

Figure 10.- DC-10 composite vertical stabilizer.

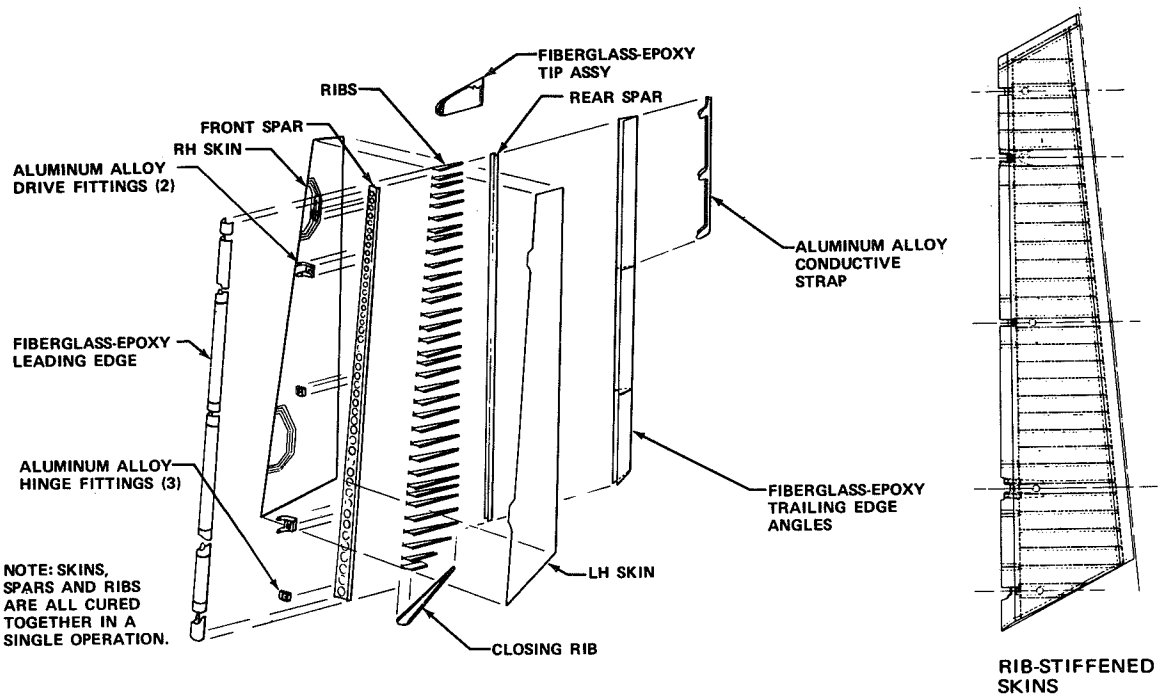

Figure 11.- Rib-stiffened graphite/epoxy rudder.

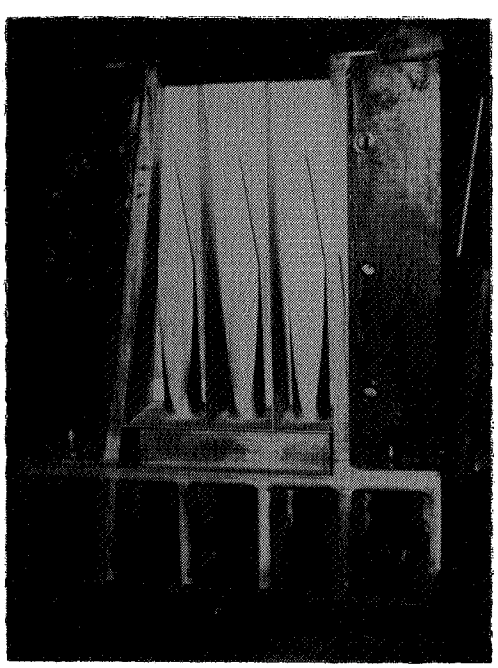

PROBLEMS	SOLUTION
EXCESSIVE PRESSURE	REDUCED RUBBER VOLUME
RUBBER MANDRELS SHRUNK	REMADE RUBBER MANDRELS WITH METAL INCLUSIONS TO STABILIZE DIMENSIONS
POOR FIBER COLLIMATION AND LARGE ACCUMULATIONS OF RESIN	ADDED ELECTRICAL HEATERS WITHIN METAL MANDRELS
RUBBER MANDRELS STUCK	ADDED TEFLON TAPE AT FAYING SURFACES

Figure 12.- Trapped rubber process development.

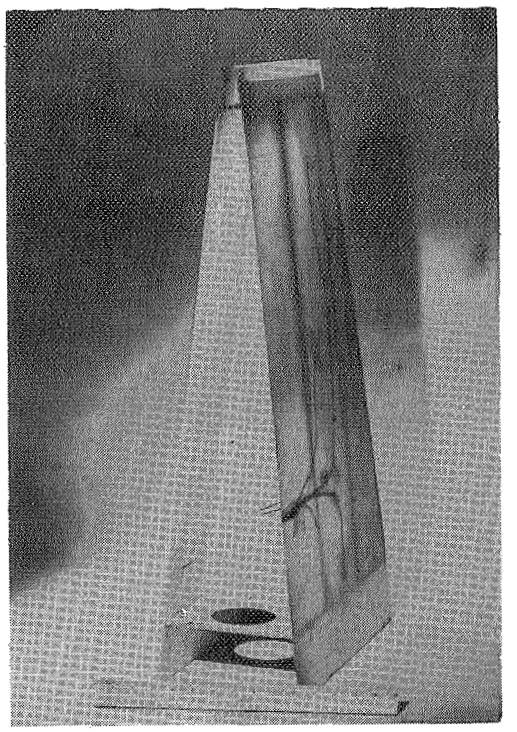

Figure 13.- Fiberglass subcomponent.

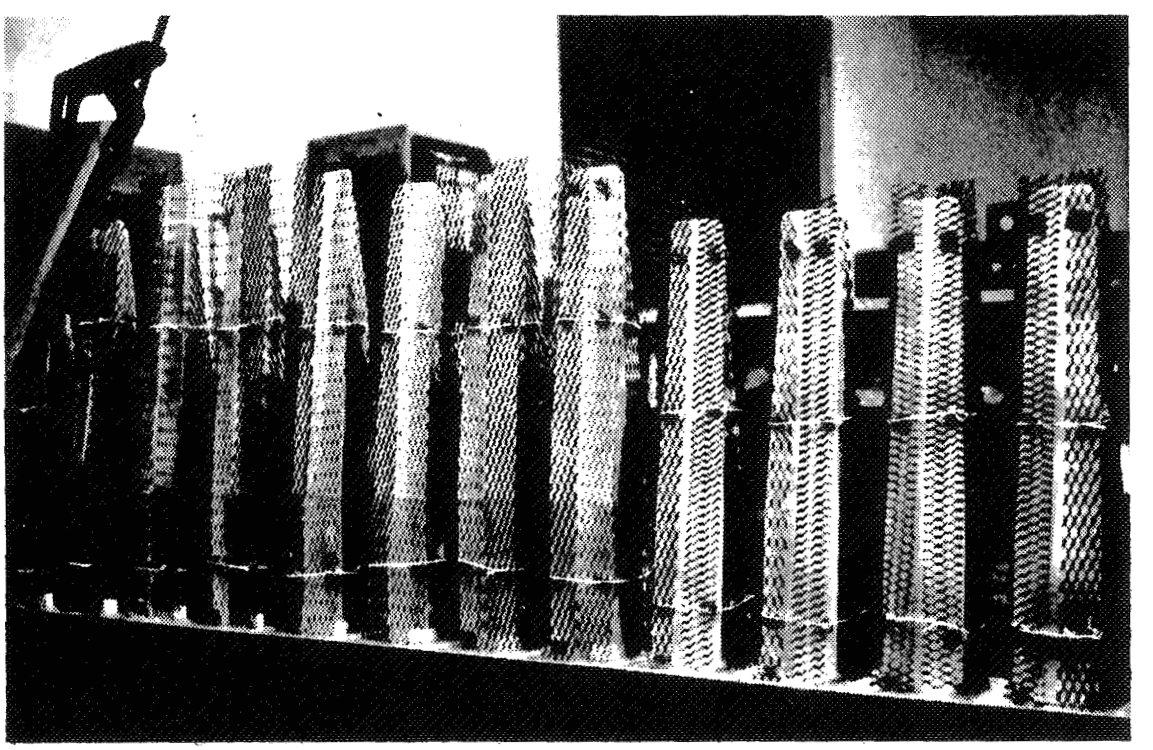

Figure 14.- Wire screen reinforcing.

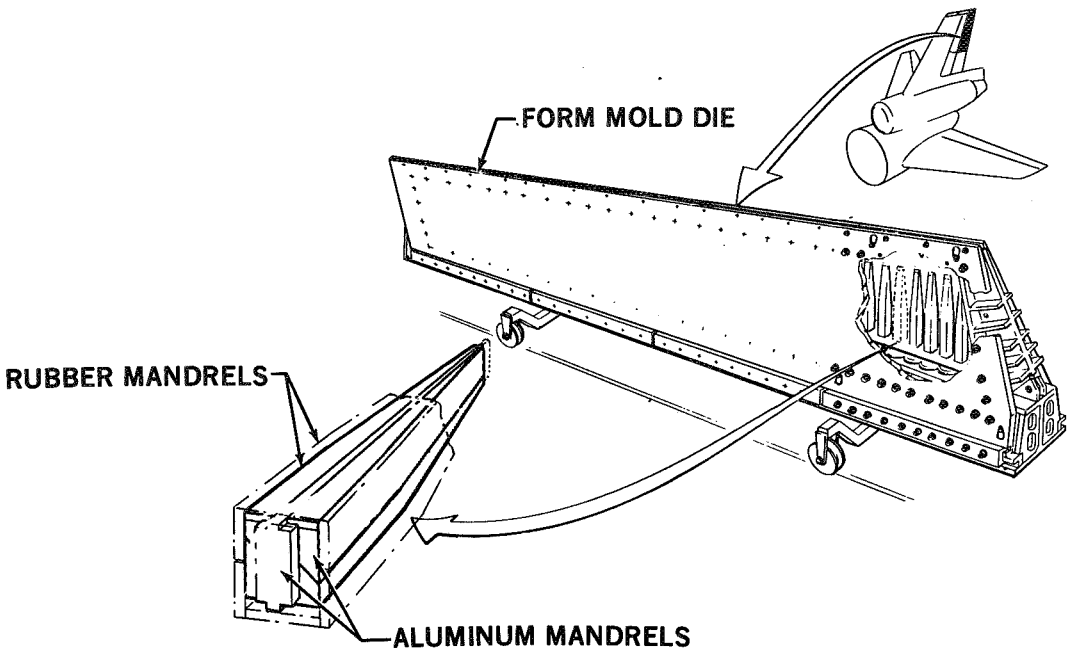

Figure 15.- Composite molding die, upper aft rudder.

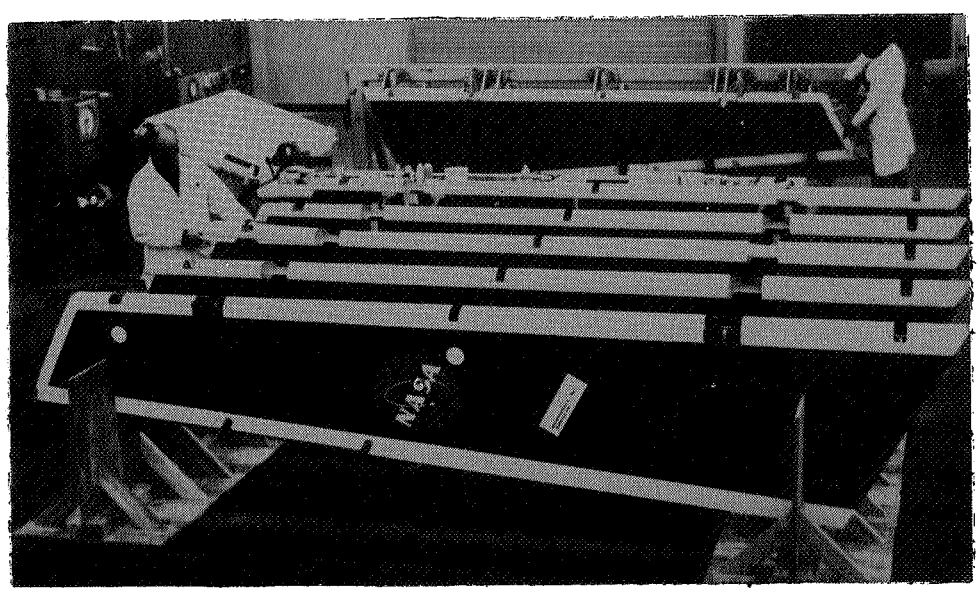

- HIGH TIME AIRCRAFT 6,955 HOURS
- TOTAL FLIGHT SERVICE 30,840 HOURS (THROUGH JANUARY 1978)

Figure 16.- Rudder flight service.

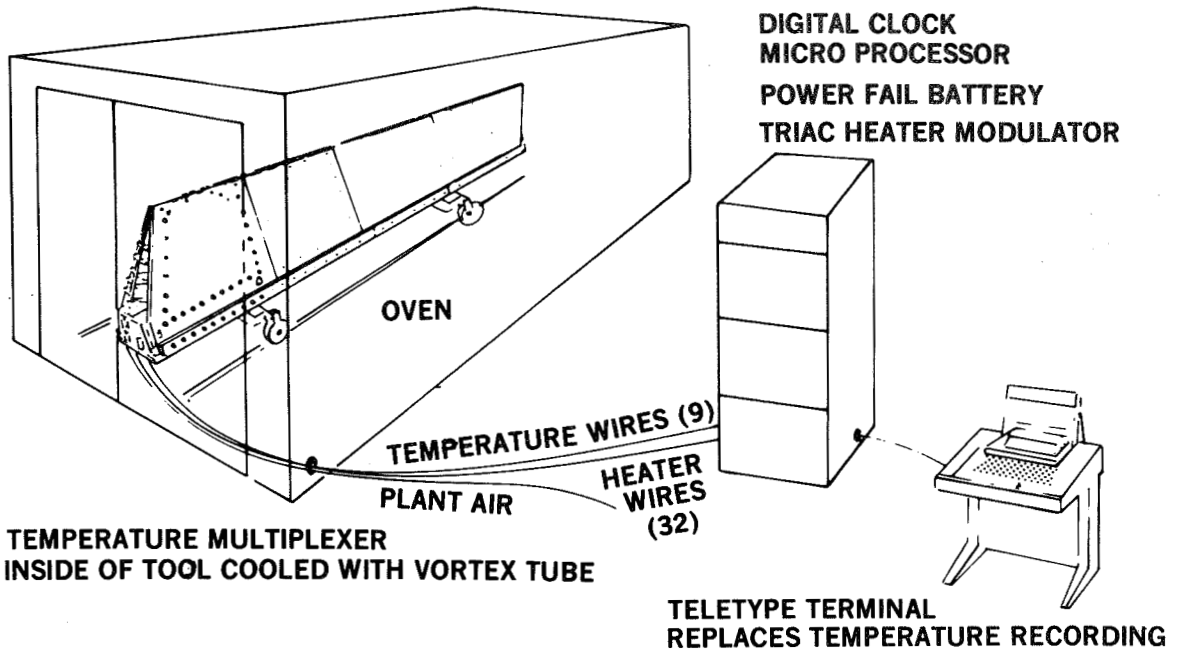

Figure 17.- Thermal temperature control system.

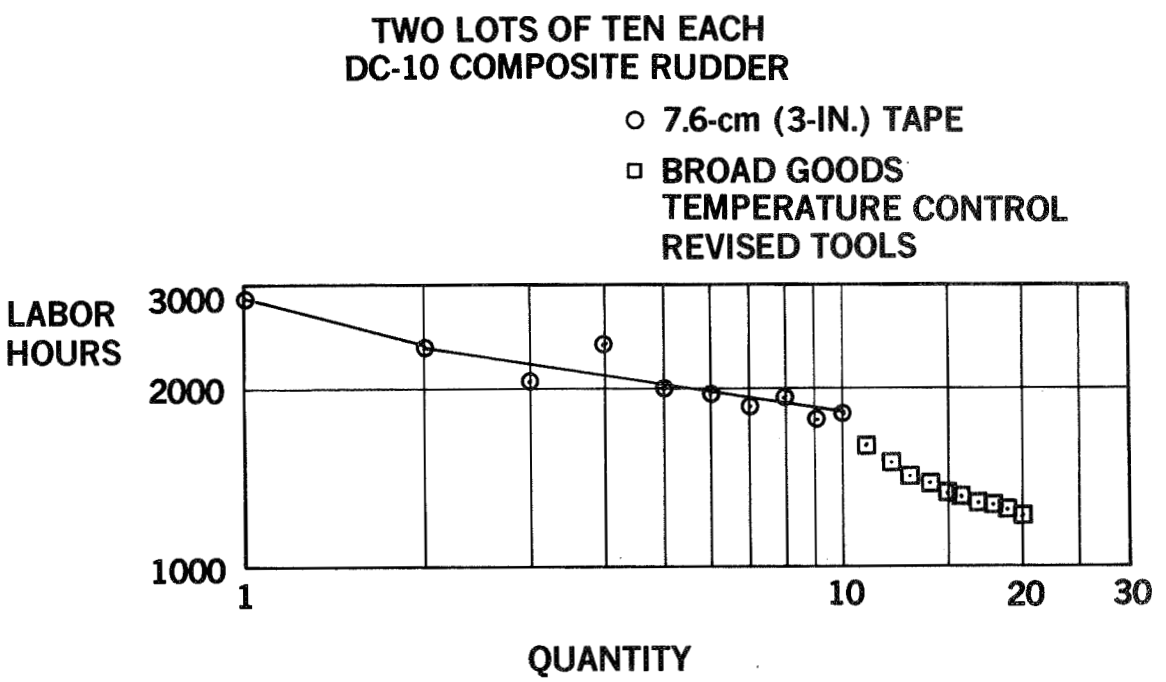

Figure 18.- Comparison of total recurring labor.

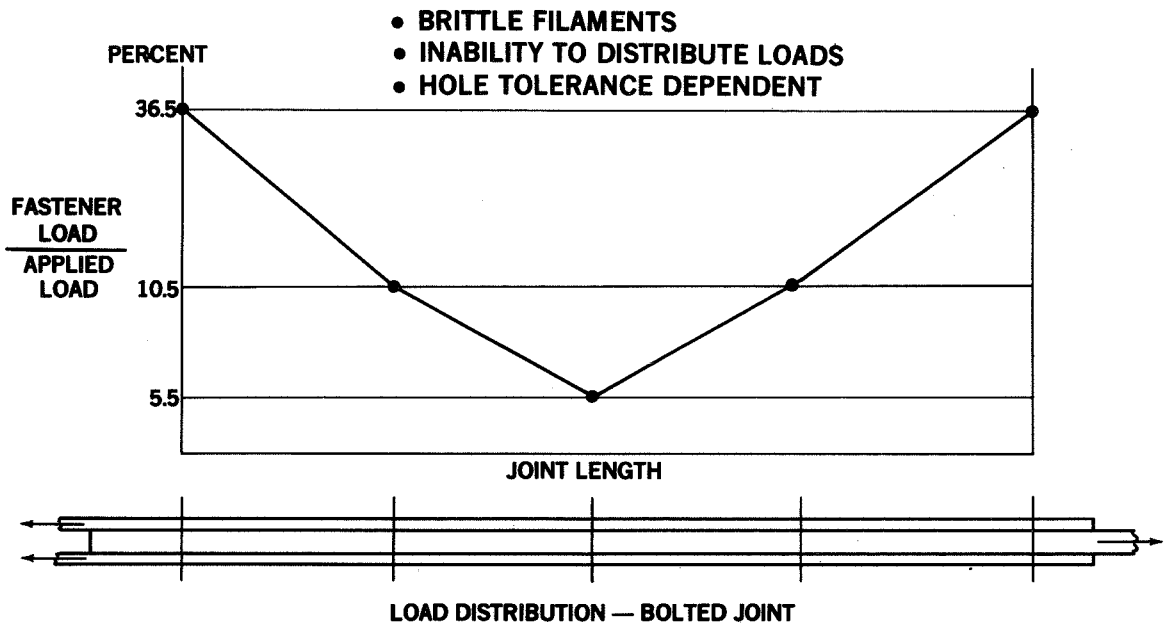

Figure 19.- Major load transfer.

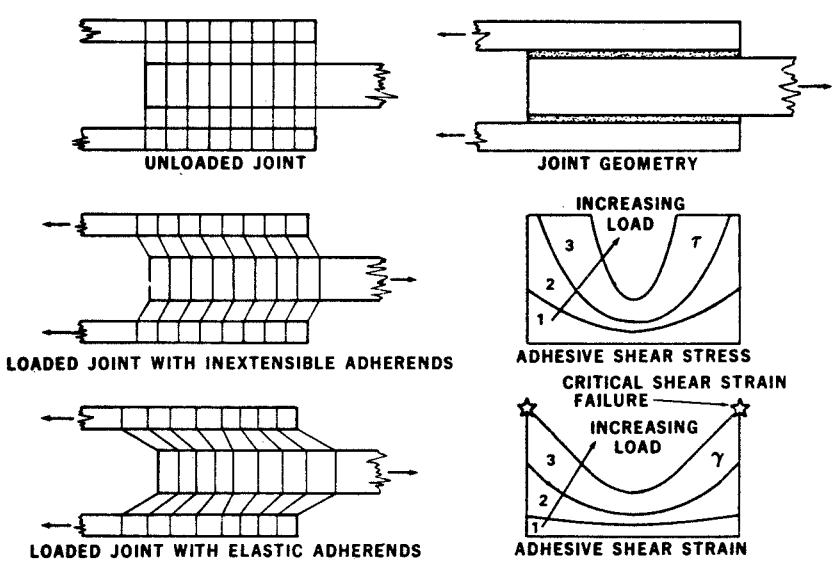

Figure 20.- Shearing of adhesive in balanced double-lap joints.

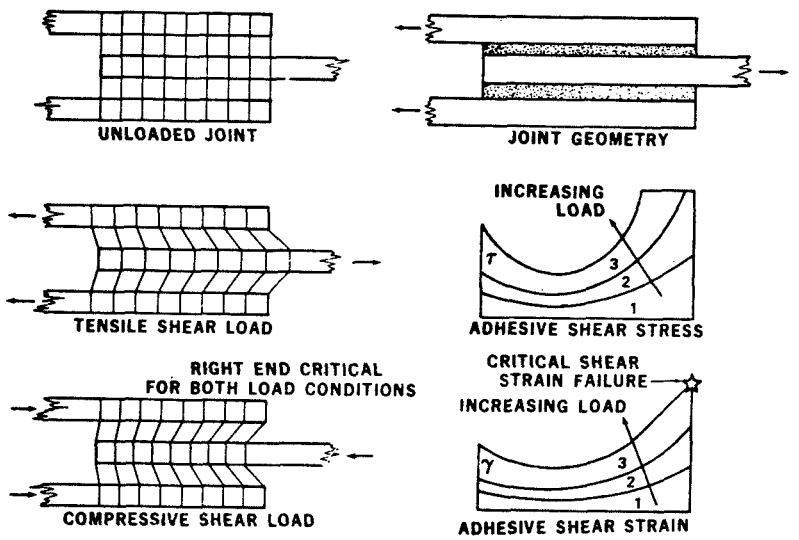

Figure 21.- Stiffness imbalance on adhesive shear.

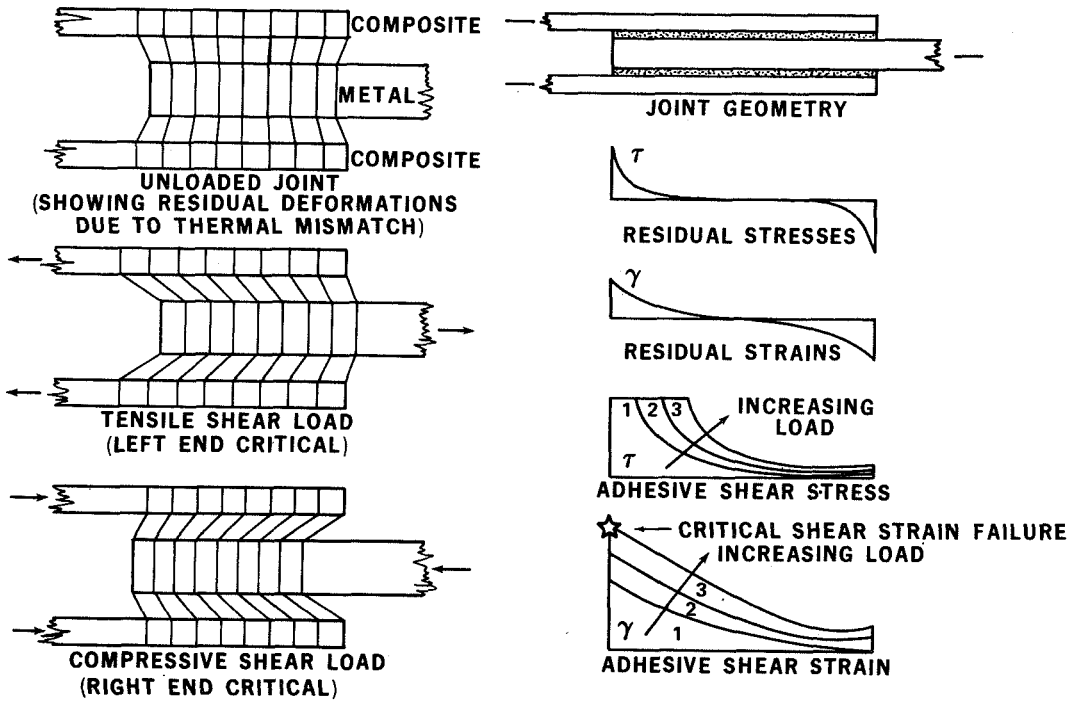

Figure 22.- Effect of adherend thermal mismatch on adhesive shear.

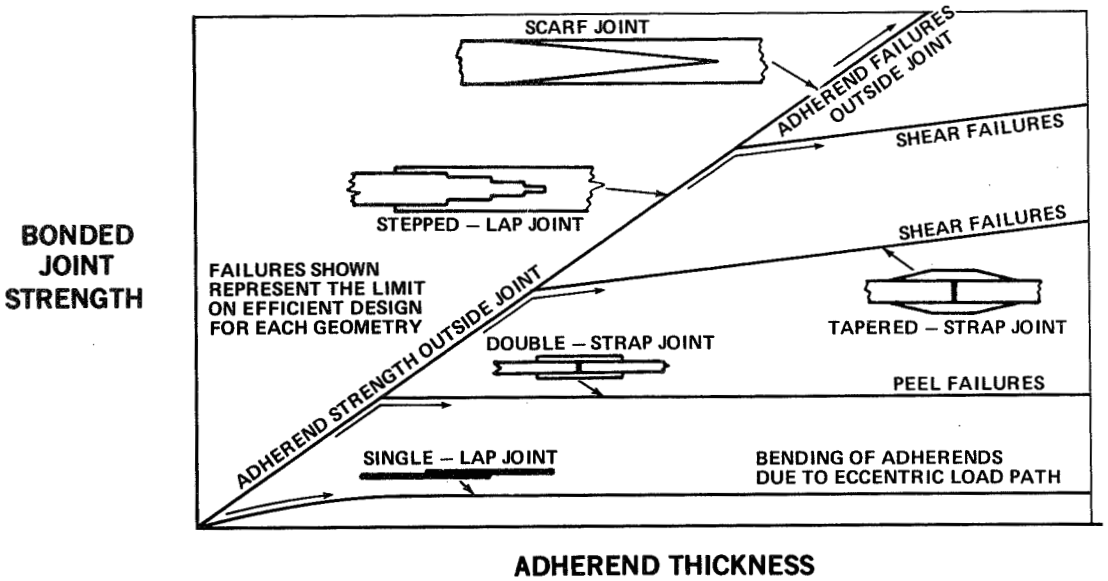

Figure 23.- Relative uses of different bonded joint types.

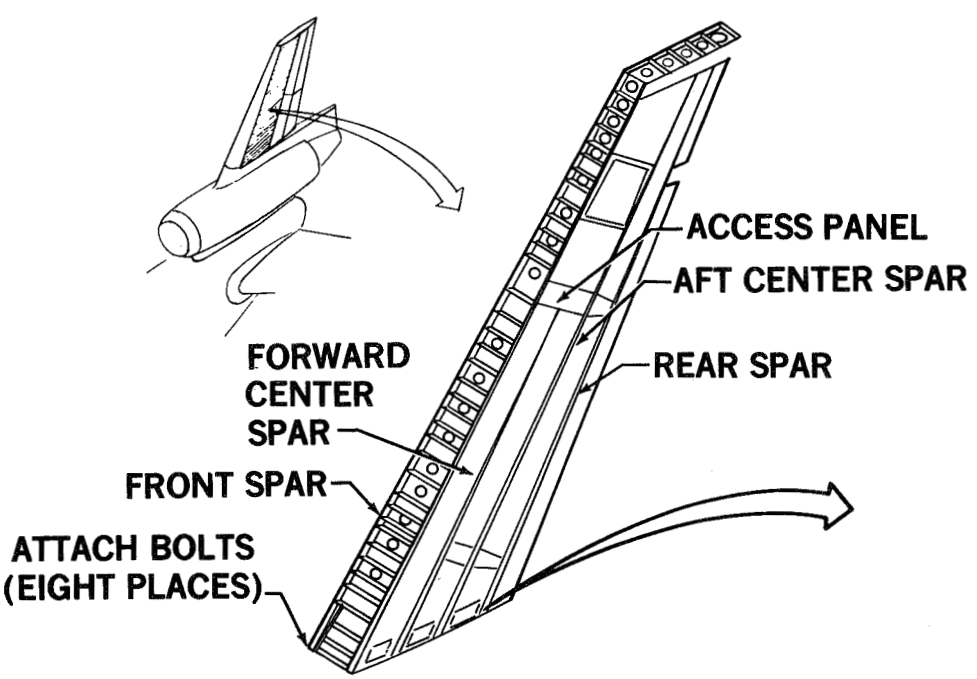

Figure 24.- DC-10 vertical stabilizer box structure.

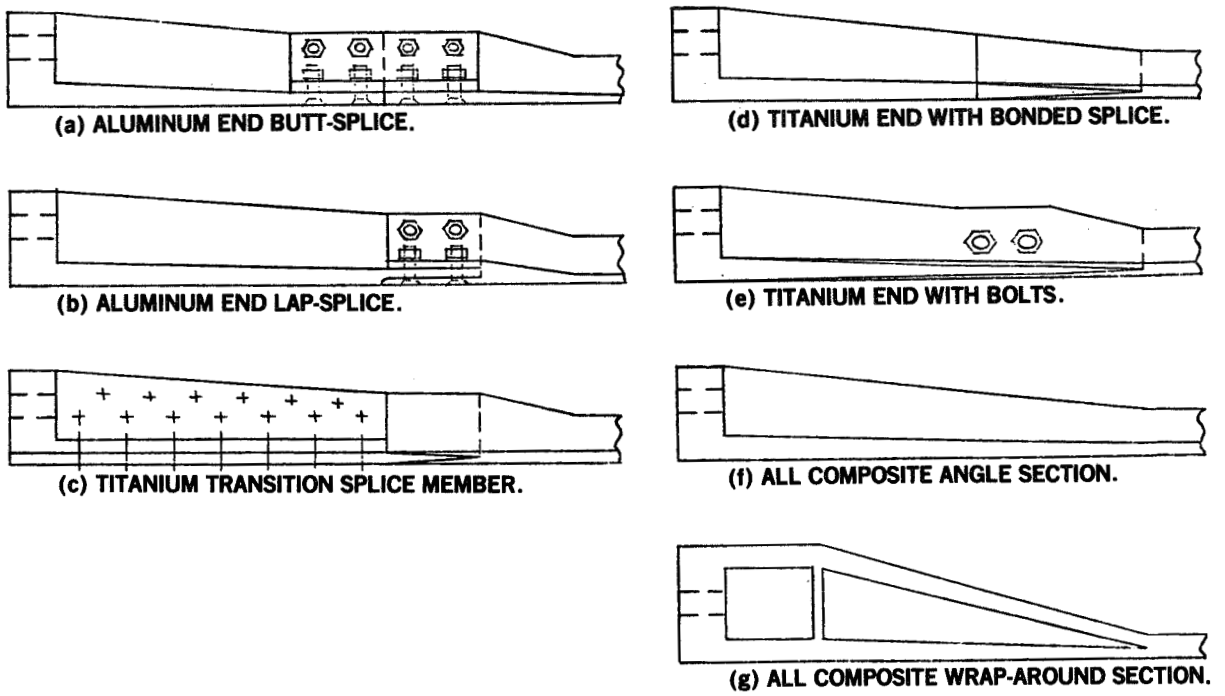

Figure 25.- Spar cap attach fitting concepts.

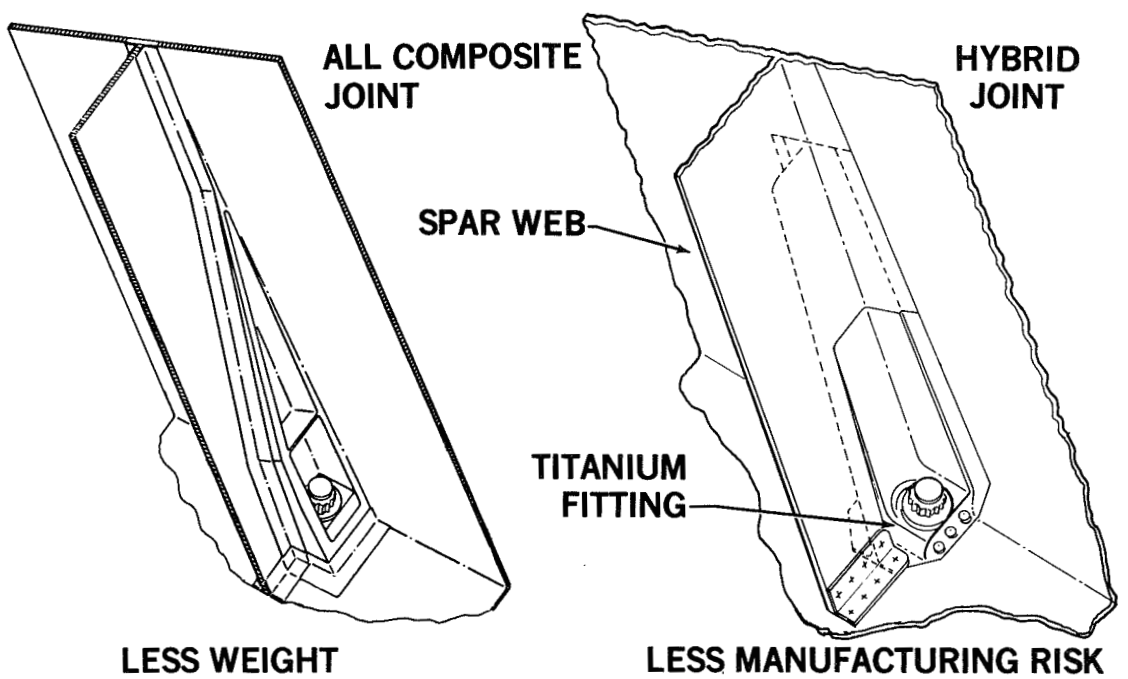

Figure 26.- DC-10 vertical stabilizer lower joint candidate design concepts.

```
#HHAALLFF
#OLD SCARF
#RUN

SCARF       09:03     JUL 01,'77


 ***ELASTIC-PLASTIC ANALYSIS OF SCARF JOINT***

INPUT DATA---ADHESIVE PROPERTIES---
   G-SHEAR MODULUS
   T-ADHESIVE THICKNESS
   GAMMAE-ELASTIC SHEAR STRAIN
   GAMMAP-PLASTIC SHEAR STRAIN
   TAUP-PLASTIC (MAX) SHEAR STRESS
?60000,.005,.1,2.0,6000

INPUT DATA---PROPERTIES FOR ADHEREND 1---
   E1-MODULUS OF ELASTICITY
   T1-THICKNESS
   ALPHA1-COEFFICIENT OF THERMAL EXPANSION
?16.0E+6,.265,4.3E-6

INPUT DATA---PROPERTIES FOR ADHEREND 2---
   E2-MODULUS OF ELASTICITY
   T2-THICKNESS
   ALPHA2-COEFFICIENT OF THERMAL EXPANSION
?16.9E+6,.234,0.0

INPUT DATA---OVERLAP LENGTH & TEMP DIFFERENTIAL
   L-OVERLAP LENGTH
   DELT-TEMPERATURE DIFFERENTIAL
?10.225,-140

     ADHEREND STIFFNESS RATIO          = .9327
     PLASTIC TO ELASTIC STRAIN RATIO =20.00
     THERMAL MISMATCH COEFFICIENT      =  .555
     NON-DIMENSIONALIZED OVERLAP       =24.762


TENSION CASE

     AVG STRESS / MAX STRESS       = 1.00000
     TRANSITION   POINT            = 33.221
     MAXIMUM LOAD   MX (#/IN)      = 61359.0
     SOFT END CRITICAL


COMPRESSION CASE

     AVG STRESS / MAX STRESS       =  .98374
     TRANSITION   POINT            = 17.386.
     MAXIMUM LOAD   MX (#/IN)      = 60352.2
     SOFT END CRITICAL
```

Figure 27.- Sample analysis printout for scarf joint.

ADVANCED STRUCTURAL SIZING METHODOLOGY

W. Jefferson Stroud and Jaroslaw Sobieszczanski-Sobieski

NASA Langley Research Center

INTRODUCTION

Aircraft having unusual and unprecedented configurations may be considered for future CTOL applications in order to meet requirements of energy efficiency, military performance, and economic viability. (See, for example, ref. 1.) In addition, new and emerging technologies such as composite structures, active controls, and laminar-flow control may find application on future aircraft with either conventional or unconventional configurations. This situation presents a challenge to perform the structural design of these future aircraft with little or no historical data base and at a reasonable cost.

A rapidly developing technology that can help engineers meet this design challenge is mathematical modeling and computerized (or automated) structural sizing. The problems and potential of this approach were outlined 5 yr ago in reference 2. Since that time, numerous advances have made computerized structural sizing even more attractive.

The purpose of this paper is to describe Langley Research Center activities aimed at developing useful computerized structural sizing technology. Four areas are considered: overall vehicle design, structural subassembly design, thermal structures, and stiffened panels. In each case, sample results are presented. Details and analytical foundations are found in the references.

COMPUTERIZED STRUCTURAL SIZING METHODOLOGY

For over a decade, Langley Research Center has performed inhouse research and sponsored grants and contracts in the area of computerized structural sizing. That work is now concentrated in the following four research areas:

(1) Overall vehicle - sizing work in which technology is being developed to consider the integrated effect of several disciplines - such as structures, materials, aerodynamics, propulsion, and active controls - early in the design process

(2) Structural subassembly - smaller scale sizing work which concentrates on structural sizing methodology for finite-element structural models

(3) Thermal structures - high-speed aircraft may have special design problems associated with high temperatures, and special sizing techniques are needed to handle these problems

(4) Stiffened panels - Langley has a strong analytical and experimental program aimed at the design of efficient stiffened composite panels. This report considers only a portion of the analytical stiffened panel work

Overall Vehicle Structural Sizing

Desired output.- The output of our current overall vehicle sizing codes is the static and dynamic aeroelastic characteristics of aircraft with and without active controls. We can also obtain structural mass, stiffness distribution, structural layout, and dimensions of key structural members. The goal, however, is more ambitious; we want to obtain propulsion, performance, and economic output.

Level of structural detail.- A typical finite-element model of a low-aspect-ratio supersonic aircraft used in our studies is shown in figure 1. The model shows the level of structural detail being considered. In this example, emphasis is placed on fairly detailed modeling of the wing. The fuselage and tail are modeled more simply to give adequate stiffness and dynamic characteristics.

Structural sizing approach.- The present sizing approach, together with an improved approach denoted "goal," is outlined in figure 2. In the present approach, the airframe geometry (wing planform, wing depth distribution, etc.) is assumed to be given and fixed. Because the procedure includes a static aeroelastic capability (i.e., the pressure distribution depends upon the deflected shape of the wing), iteration is often required to obtain the aerodynamic loading. That iteration is indicated by the circle with arrows connecting the block labeled "Aerodynamic Loads Analysis" with the block labeled "Structural Finite-Element Analysis." The structural elements are also sized for minimum mass. Sizing is indicated by the circle with arrows connecting the block labeled "Structural Finite-Element Analysis" with the block labeled "Sizing of Structural Elements." This sizing affects the stiffness distribution which, in turn, affects the pressure distribution. The sizing is, therefore, a multiloop iterative scheme which results in a strength-sized airframe. Then, if flutter is a problem, the structure can be stiffened with additional material, or an active control system can be employed. The final product is an airframe sized to meet strength and flutter design requirements.

The present approach is sequential. The wing is first sized for strength. During the strength sizing, wing panels are sized for minimum mass on a panel-by-panel basis. That is, no attempt is made to favorably influence the aerodynamic loading or the resulting internal load distributions. After the wing is sized for strength, additional material (or an active control system) is added to prevent flutter. To reduce computer resources, flutter sizing is carried out on a simplified finite-element model rather than on the refined model (fig. 1) used in the strength sizing procedure. A spline function technique is used to transfer sizing data from one model to another. Both the strength and flutter sizing procedures are based on nonlinear mathematical programming, which is a general purpose mathematical search technique. A complete discussion

of the sizing approach, together with example applications, is presented in references 3 and 4.

In contrast with the present sequential approach, the goal is a simultaneous approach in which values of all sizing variables (dimensions of structural members, size and location of active control systems, etc.) are determined based on their effect on all the design requirements (strength, flutter, etc.). In such an approach, all sizing variables and all design requirements are considered simultaneously. The goal approach takes advantage of the interaction between the active control system, structural member size, aerodynamic loading, and wing load paths. Finally, airframe geometry is defined by variables that could be adjusted during the structural sizing process. The goal approach would provide a design that is superior to the one obtained by using the present approach.

Framework of overall vehicle sizing system.- Although the goal in the overall vehicle sizing procedure has not yet been reached, the framework for a large multidisciplinary sizing system called Integrated Synergistic Synthesis System (ISSYS) has been developed and made operational. That framework is depicted in figure 3. One key point about this system is that instead of developing an executive system to link the users to the data base (represented in fig. 3 by the entire large box below the two large arrows), we are using the Control Data Corporation computer operating system (denoted NOS) which is resident on the Control Data computers at Langley. Any modern standard time-share operating system can serve as the executive system.

Users issue commands called tasks, which are represented by the left-hand column of the data base. For example, a user may want to calculate the stresses in a supersonic flight condition. He "punches" Loads and Structural Analysis. From the computer programs represented by the center column of the data base, the computer picks out the appropriate programs - a supersonic aerodynamic program and a structural analysis program. From the right-hand column of the data base, the computer gets the configuration data for the vehicle selected. The problem is worked, and the results are returned to the user.

The integration of a system of engineering programs on NOS is described in reference 5. Information on the computational capabilities of the ISSYS program are given in reference 6. The overall sizing activity is discussed in references 3, 7, and 8.

Example application.- An example of results that can be obtained with ISSYS is shown in figure 4. These results are for the wing of a low-aspect-ratio supersonic aircraft similar to that shown in figure 1. In this example, only the face sheets of the honeycomb core sandwich panels on the wing surface are being sized. The dimensions of the core, webs, and spar caps remain constant. All titanium wings and combinations of titanium and graphite-polyimide are considered.

The bar at the far left in figure 4 indicates the wing mass for an all-titanium design. The strength design is about 6000 kg; the flutter fix increases

the mass to about 6600 kg. The second bar from the left indicates the wing mass for a wing with graphite-polyimide face sheets on the honeycomb core sandwich panels. The remainder of the wing is titanium. The metal-composite strength design is about 4800 kg. Although the flutter fix is larger for the metal-composite design than for the all-metal design, the total mass (5700 kg) of the metal-composite design is about 14 percent less than that of the all-metal design. The remaining two bars show the effect of changing wing area.

Although only wing structure is represented in figure 4, the full structural model shown in figure 1 is used in the analyses. The full model is particularly important for a valid flutter analysis.

Computer resources are also shown in figure 4. Considering the level of structural detail, we feel that the work is being done in a reasonable time and at a very reasonable cost.

Structural Subassembly Sizing

In the overall vehicle sizing activity which was discussed in the previous section, the goal of considering all the various design requirements simultaneously has not yet been met, and improvements are needed in the sizing approach. In the second area, structural subassembly sizing, all of the newest structural sizing technology is incorporated. The problems, however, are smaller - on the order of one-half to one-tenth the size of the overall vehicle sizing problem. In the overall vehicle work, a system of computer programs is used. In the structural subassembly work, a single stand-alone computer program is generally used.

Approach.- As in the overall vehicle work, the structural subassembly sizing work is based on finite-element structural models. A simplified sketch of a finite-element model of a wing structure is shown in figure 5. Many types of inequality constraints have been considered. Deflection and twist constraints, for example, mean that under the design load the deflection and twist of the wing tip must be less than some specified value.

Because the structural subassembly sizing work uses rigorous sizing approaches, numerous constraints, and complex finite-element models, we have developed new techniques to improve computational efficiency. Some of these techniques are listed in figure 5. Approximate analyses are updated periodically to insure a correct solution. Constraint deletion simply means ignoring unimportant constraints. Design variable linking refers to reducing the number of independent sizing variables involved in the computations. Finally, we have made substantial improvements to the basic math programming search techniques that are used in all the subassembly sizing work. Techniques for improving computational efficiency and studies exploring the introduction of various constraints are presented in references 9 to 22.

Example application.- A high-aspect-ratio subsonic wing box made of graphite-epoxy (fig. 6) is sized for minimum mass and subject to design constraints on material strength, deflection and twist of the wing tip, and

buckling of the wing cover panels. The sizing variables are the thickness of wing cover panels, the thickness of spar webs, and the areas of spar caps. The wing box, shown in figure 6, is divided into seven spanwise segments. Two types of sizing variable distributions are considered - (1) a coarse distribution in which the sizing variables are uniform within a spanwise segment and (2) a refined distribution in which the sizing variables have a chordwise variation within the spanwise segment. In the first case, the wing box has only a spanwise variation in the sizing variables. In the second case, the wing box has a chordwise as well as a spanwise variation in the sizing variables. In this exercise, the sizing variable distribution, not the finite-element model, is being refined between case 1 and case 2.

Results are presented in figures 7 and 8. The final chordwise variations in the wing cover skin in segment 4 (fig. 6) are shown in figure 7 for both the coarse and refined distributions. In each sketch, LE and TE stand for leading and trailing edges, respectively, of the wing box. Because a composite material is being used for the wing skins, it is possible to vary the proportions at the different orientations. As expected, in the refined sizing variable distribution case, the 0° filaments, which are spanwise, are concentrated at the trailing edge of this sweptback wing box.

The effect on mass is shown in figure 8. Again, as would be expected, a chordwise variation in material can save weight - in this case, about 15 percent. The computer resources are reasonable.

This example is taken from reference 9. From the point of view of sizing methodology, the studies in reference 9 mark the first time wing panel buckling has been treated properly for an entire wing structure. The procedure takes advantage of the capability to favorably influence load paths.

Thermal Structures

The third structural sizing activity involves thermal structures. This work is aimed at developing the special techniques that might be needed for sizing high-speed aircraft and space vehicles for which temperatures and thermal stresses could become important design considerations. Research in this area is described in references 23 to 28.

Problem characteristics.- The general thermal design problem characterized in figure 9 may involve both thermal and mechanical loads that vary with time so that both steady-state and time-dependent analyses may be required. The temperatures and stresses must be controlled simultaneously. The goal is to trade the mass of the thermal control system, such as insulation, against structural mass to obtain a low-mass total system.

Example.- An example of a steady-state thermal sizing problem is presented in figure 10. The example demonstrates the value of a simple, recently developed sizing procedure denoted thermal fully stressed design (TFSD). It is very similar to fully stressed design (FSD) with stress ratio sizing. In the case of bar elements, sizing formulas for FSD and TFSD are given by the following equations:

(For FSD) $$A_{i+1} = \left(\frac{\sigma_{Mi} + \sigma_{Ti}}{\sigma_a}\right) A_i$$

(For TFSD) $$A_{i+1} = \left(\frac{\sigma_{Mi}}{\sigma_a - \sigma_{Ti}}\right) A_i$$

in which A is the area of the bar element, i is the iteration number, σ_M is the stress due to mechanical loads, σ_T is the stress due to thermal loads, and σ_a is the allowable stress. The same basic approach is used to obtain the sizing formula for membrane elements. The procedure is explained in detail in reference 23.

The sketch at the left in figure 10 gives the results of convergence studies carried out using FSD and TFSD. The sketch shows the trend in the number of cycles required for convergence of each sizing procedure as a function of the temperature, or thermal stress, of the structure. Both procedures diverge for very high thermal stresses. Experience with several thermal sizing problems indicates that in the temperature range where thermal stresses are moderate, TFSD converges two to four times as fast as regular fully stressed design (refs. 23 to 25). These convergence studies were made with fairly simple models such as the one at the right in figure 10. It is believed, however, that the approach is applicable to more complex models.

It is known that FSD provides minimum-mass designs for structures that are statically determinate.[1] Satisfactory results are usually obtained for structures that are nearly statically determinate and for structures whose sizing variables have only a small effect on internal load distribution. According to reference 25, FSD and TFSD converge to the same design. Because of superior convergence characteristics for thermally stressed structures, TFSD is recommended over FSD in thermal design problems. But there are structural sizing problems for which the final designs provided by both FSD and TFSD are not the minimum-mass designs. For these types of problems, rigorous methods such as mathematical programming and rigorous optimality criteria must be employed. These rigorous methods are also being studied in our thermal sizing activities (ref. 23).

Stiffened Panels

The fourth and final area of sizing activity is stiffened panels. As was stated earlier in this paper, Langley has a strong analytical and experimental program aimed at the design of efficient stiffened composite panels. This research program has produced numerous technical reports (refs. 29 to 40)

[1] It is of interest to recall that thermal stresses do not exist for statically determinate structures.

dealing with both analytical and experimental aspects of the program. (Reference 40 is included because it is closely related to the work at Langley.) The present report focuses on the latest stiffened panel sizing code developed under this research program. The code, denoted PASCO (Panel Analysis and Sizing COde), will be available through COSMIC.

Description and capabilities.- Some of the important capabilities of the code are indicated in figure 11. The panel may be loaded by any combination of in-plane loadings (tension, compression, and shear) and lateral pressure. The code includes a rigorous buckling analysis that can account for complex buckling modes of arbitrary panel configurations. The panel cross section is assumed to be an assembly of plate elements, with each plate element consisting of a balanced symmetric laminate of any number of layers. The code can also be used to size metal panels. Stresses caused by a bow-type initial imperfection or lateral pressure are accounted for by using a beam-column approach. A more complete discussion of the code is presented in reference 29.

Examples.- The examples considered in this paper are for blade-stiffened panels having the configuration shown in figure 12. The sizing variables are the element widths B_i and the lamina thicknesses T_j. In this example, 0° filaments are placed in the center and $\pm 45^\circ$ filaments are placed on either side.

The first results, which are presented in figure 13, are for aluminum blade-stiffened panels and graphite-epoxy blade-stiffened panels. The data are presented in the form of a structural efficiency diagram in which the mass index $\frac{W/A}{L}$ (weight per unit area divided by the panel length) is plotted as a function of the loading index N_x/L (longitudinal loading divided by the panel length). Both scales are logarithmic. In a typical aircraft wing structure, the lightly loaded panels near the tip might have a loading index on the order of 700 kPa. The heavily loaded panels at the root might have a loading index of 5000 kPa. In this example, the only constraint considered is buckling. According to figure 13, the aluminum panels weigh about twice as much as graphite-epoxy panels.

But would these panels of figure 13 carry the design load? The answer is that they probably would not. These data are for perfect panels, but real panels are not perfect. There are geometric imperfections that can greatly reduce the buckling load. There are also other design requirements that must be taken into account in order for the design to be practical. The sizing code can account for several of these practical design requirements, including an overall bow-type imperfection.

A panel with an initial bow is shown in figure 14. The magnitude of the eccentricity at the center is denoted e. The bow can be positive or negative. The quantity e/L is an important nondimensional parameter that is useful in scaling designs.

The first-order effect of the bow is assumed to be the additional stresses produced by bending. These additional stresses affect the local buckling load and the loading at which material strength considerations become important. At

the center of the panel, the bending moment is largest and is given by

$$M = \frac{N_x e}{1 - \frac{N_x}{N_{x_E}}}$$

in which N_x is the applied axial load per unit width and N_{x_E} is the Euler buckling load for the panel.

The effect of a bow on the buckling load of a panel designed for zero bow is shown in figure 15. For a panel of length 76 cm (30 in.), a bow of only 0.25 cm (0.1 in.) causes a reduction in the buckling load of about 35 percent. In general, this imperfection curve is not symmetric.

The increase in panel mass caused by accounting for practical design considerations such as an overall bow is shown in figure 16. This structural efficiency diagram is for graphite-epoxy blade-stiffened panels only. As shown in the legend, the solid lines are for buckling only. The dashed curves have an additional requirement that the strains not exceed ± 0.004. Imposing a limitation of 0.004 is an attempt to account for the possible presence of cracks, flaws, delaminations, and impact damage. Some evidence suggests that 0.004 may be too large a number.

The lowest curve in figure 16 is for buckling of perfect panels. It is the same as the graphite-epoxy curve in figure 13. The next higher curve is for buckling of panels with an initial bow of $e/L = \pm 0.003$. The positive and negative sign means that these panels carry the load whether the bow is positive or negative. The curve with long dashes that merges with the solid line shows the effect of adding the strain limitation to the buckling requirement.

The highest curve, which is made up of short dashes, shows the effect of adding shear and extensional stiffness requirements that are typical of aircraft wing panels. In other words, these panels account for stiffness, buckling, overall bow-type imperfections, and have an allowable strain requirement. All of these factors influence the curve. Run times are reasonable, on the order of 2 to 5 min.

CONCLUDING REMARKS

In summary, there are aircraft structural design challenges caused by new and unusual aircraft configurations, new materials, and new technologies such as active controls. In this paper, it is suggested that computerized sizing techniques could help meet some of these design challenges.

There are basically four areas of structural sizing research underway at Langley Research Center. With respect to overall vehicle work, a prototype

version of the structural sizing system has been made operational. With respect to subassembly work, the most advanced sizing techniques have been incorporated in our stand-alone computer programs. In thermal structures, the time-dependent thermal effects problem is now being attacked. And, finally, an advanced stiffened panel sizing code has been developed and will be made available through COSMIC.

REFERENCES

1. Nagel, A. L.: Studies of Advanced Transport Aircraft. CTOL Transport Technology - 1978, NASA CP-2036, Pt. II, 1978, pp. 951-982.

2. Heldenfels, Richard R.: Automating the Design Process: Progress, Problems, Prospects, Potential. AIAA Paper No. 73-410, Mar. 1973.

3. Sobieszczanski, Jaroslaw; McCullers, L. Arnold; Ricketts, Rodney H.; Santoro, Nick J.; Beskenis, Sharon D.; and Kurtze, William L.: Structural Design Studies of a Supersonic Cruise Arrow Wing Configuration. Proceedings of the SCAR Conference - Part 2, NASA CP-001, [1977], pp. 659-683.

4. Ricketts, Rodney H.; and Sobieszczanski, Jaroslaw: Simplified and Refined Structural Modeling for Economical Flutter Analysis and Design. Volume B - Dynamics, Structural Dynamics, AIAA/ASME 18th Structures, Structural Dynamics & Materials Conference, Mar. 1977, pp. 117-126.

5. Sobieszczanski, Jaroslaw: Building a Computer-Aided Design Capability Using a Standard Time Share Operating System. Integrated Design and Analysis of Aerospace Structures, R. F. Hartung, ed., American Soc. Mech. Eng., 1975, pp. 93-112.

6. Giles, Gary L.: Computer-Aided Methods for Analysis and Synthesis of Supersonic Cruise Aircraft Structures. Proceedings of the SCAR Conference - Part 2, NASA CP-001, [1977], pp. 637-657.

7. Sobieszczanski, Jaroslaw: Sizing of Complex Structure by the Integration of Several Different Optimal Design Algorithms. Paper presented at the AGARD Lecture Series No. 70 on Structural Optimization (Hampton, Virginia), Oct. 1974.

8. Giles, Gary L.; and McCullers, L. A.: Simultaneous Calculation of Aircraft Design Loads and Structural Member Sizes. AIAA Paper No. 75-965, Aug. 1975.

9. Starnes, James H., Jr.; and Haftka, Raphael T.: Preliminary Design of Composite Wings for Buckling, Strength and Displacement Constraints. A Collection of Technical Papers - AIAA/ASME 19th Structures, Structural Dynamics and Materials Conference, Apr. 1978, pp. 1-13. (Available as AIAA Paper No. 78-466.)

10. Schmit, L. A., Jr.; and Farshi, B.: Some Approximation Concepts for Structural Synthesis. AIAA J., vol. 12, no. 5, May 1974, pp. 692-699.

11. Schmit, Lucien A., Jr.; and Miura, Hirokazu: Approximation Concepts for Efficient Structural Synthesis. NASA CR-2552, 1976.

12. Haftka, Raphael T.: Automated Procedure for Design of Wing Structures to Satisfy Strength and Flutter Requirements. NASA TN D-7264, 1973.

13. Haftka, Raphael T.; and Starnes, James H., Jr.: WIDOWAC (Wing Design Optimization With Aeroelastic Constraints): Program Manual. NASA TM X-3071, 1974.

14. Schmit, L. A.; and Miura, H.: A New Structural Analysis/Synthesis Capability - ACCESS 1. AIAA J., vol. 14, no. 5, May 1976, pp. 661-671.

15. Schmit, L. A.; and Miura, H.: An Advanced Structural Analysis/Synthesis Capability - ACCESS 2. Int. J. Num. Methods Eng., vol. 12, no. 2, 1978, pp. 353-377.

16. Haftka, Raphael T.: Parametric Constraints With Application to Optimization for Flutter Using a Continuous Flutter Constraint. AIAA J., vo. 13, no. 4, Apr. 1975, pp. 471-475.

17. Haftka, Raphael T.; and Starnes, James H., Jr.: Applications of a Quadratic Extended Interior Penalty Function for Structural Optimization. AIAA J., vol. 14, no. 6, June 1976, pp. 718-724.

18. Miura, Hirokazu; and Schmit, Lucien A., Jr.: ACCESS-1: Approximation Concepts Code for Efficient Structural Synthesis - Program Documentation and User's Guide. NASA CR-144905, 1976.

19. Haftka, Raphael T.; and Yates, E. Carson, Jr.: Repetitive Flutter Calculations in Structural Design. J. Aircr., vol. 13, no. 7, July 1976, pp. 454-461.

20. Haftka, Raphael T.; Starnes, James H., Jr.; Barton, Furman W.; and Dixon, Sidney C.: Comparison of Two Types of Structural Optimization Procedures for Flutter Requirements. AIAA J., vol. 13, no. 10, Oct. 1975, pp. 1333-1339.

21. Stroud, W. Jefferson: Automated Structural Design With Aeroelastic Constraints: A Review and Assessment of the State of the Art. Structural Optimization Symposium, L. A. Schmit, Jr., ed., AMD-Vol. 7, American Soc. Mech. Eng., c. 1974, pp. 77-118.

22. Haftka, Raphael T.: Optimization of Flexible Wing Structures Subject to Strength and Induced Drag Constraints. AIAA J., vol. 15, no. 8, Aug. 1977, pp. 1101-1106.

23. Adelman, Howard M.; Sawyer, Patricia L.; and Shore, Charles P.: Development of Methodology for Optimum Design of Structures at Elevated Temperatures. A Collection of Technical Papers - AIAA/ASME 19th Structures, Structural Dynamics and Materials Conference, Apr. 1978, pp. 23-36. (Available as AIAA Paper No. 78-468.)

24. Adelman, Howard M.; Walsh, Joanne L.; and Narayanaswami, R.: An Improved Method for Optimum Design of Mechanically and Thermally Loaded Structures. NASA TN D-7965, 1975.

25. Adelman, Howard M.; and Narayanaswami, R.: Resizing Procedure for Structures Under Combined Mechanical and Thermal Loading. AIAA J., vol. 14, no. 10, Oct. 1976, pp. 1484-1486.

26. Rao, G. Venkateswara; Shore, Charles P.; and Narayanaswami, R.: An Optimality Criterion for Sizing Members of Heated Structures With Temperature Constraints. NASA TN D-8525, 1977.

27. Adelman, Howard M.; and Sawyer, Patricia L.: Inclusion of Explicit Thermal Requirements in Optimum Structural Design. NASA TM X-74017, 1977.

28. Adelman, Howard M.; and Narayanaswami, R.: Resizing Procedure for Optimum Design of Structures Under Combined Mechanical and Thermal Loading. NASA TM X-72816, 1976.

29. Anderson, Melvin S.; and Stroud, W. Jefferson: A General Panel Sizing Computer Code and Its Application to Composite Structural Panels. A Collection of Technical Papers - AIAA/ASME 19th Structures, Structural Dynamics and Materials Conference, Apr. 1978, pp. 14-22. (Available as AIAA Paper No. 78-467.)

30. Stroud, W. Jefferson; Anderson, Melvin S.; and Hennessy, Katherine W.: Effect of Bow-Type Initial Imperfection on the Buckling Load and Mass of Graphite-Epoxy Blade-Stiffened Panels. NASA TM-74063, 1977.

31. Stroud, W. Jefferson; Agranoff, Nancy; and Anderson, Melvin S.: Minimum-Mass Design of Filamentary Composite Panels Under Combined Loads: Design Procedure Based on a Rigorous Buckling Analysis. NASA TN D-8417, 1977.

32. Anderson, Melvin S.; Hennessy, Katherine W.; and Heard, Walter L., Jr.: Addendum to Users Guide to VIPASA (Vibration and Instability of Plate Assemblies Including Shear and Anisotropy). NASA TM X-73914, 1976.

33. Stroud, W. Jefferson; and Agranoff, Nancy: Minimum-Mass Design of Filamentary Composite Panels Under Combined Loads: Design Procedure Based on Simplified Buckling Equations. NASA TN D-8257, 1976.

34. Rhodes, Marvin D.; Williams, Jerry G.; and Starnes, James H., Jr.: Effect of Impact Damage on the Compression Strength of Filamentary-Composite Hat-Stiffened Panels. Presented at the 23rd SAMPE National Symposium and Exhibition (Anaheim, Calif.), May 2-4, 1978.

35. Rhodes, Marvin D.; Williams, Jerry G.; and Starnes, James H., Jr.: Effect of Low-Velocity Impact Damage on the Compressive Strength of Graphite-Epoxy Hat-Stiffened Panels. NASA TN D-8411, 1977.

36. Mikulas, Martin M., Jr.; Bush, Harold G.; and Rhodes, Marvin D.: Current Langley Research Center Studies on Buckling and Low-Velocity Impact of Composite Panels. Third Conference on Fibrous Composites in Flight Vehicle Design, Part II, NASA TM X-3377, 1976, pp. 633-663.

37. Williams, Jerry G.; and Stein, Manuel: Buckling Behavior and Structural Efficiency of Open-Section Stiffened Composite Compression Panels. AIAA J., vol. 14, no. 11, Nov. 1976, pp. 1618-1626.

38. Williams, Jerry G.; and Mikulas, Martin M., Jr.: Analytical and Experimental Study of Structurally Efficient Composite Hat-Stiffened Panels Loaded in Axial Compression. NASA TM X-72813, 1976. (Also available as AIAA Paper No. 75-754.)

39. Agarwal, Banarsi; and Davis, Randall C.: Minimum-Weight Designs for Hat-Stiffened Composite Panels Under Uniaxial Compression. NASA TN D-7779, 1974.

40. Purdy, D. M.; and Dietz, C. G.: Optimum Design of Composite Primary Structure Aircraft Components. ICAS Paper No. 76-07, Oct. 1976.

DESIRED OUTPUT

- STATIC AND DYNAMIC AEROELASTIC CHARACTERISTICS WITH AND WITHOUT ACTIVE CONTROLS
- STRUCTURAL MASS AND STIFFNESS DISTRIBUTION
- STRUCTURAL LAYOUT AND DIMENSIONS OF KEY STRUCTURAL MEMBERS

TYPICAL FINITE-ELEMENT MODEL

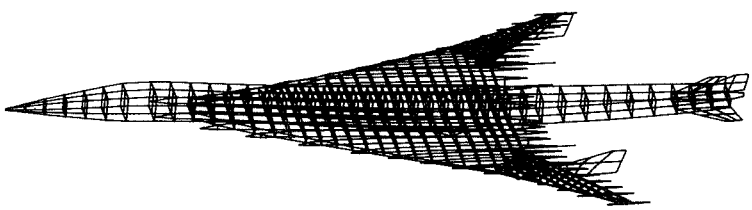

750 GRID POINTS, 2400 ELEMENTS, 720 SIZING VARIABLES

Figure 1.- Overall vehicle structural sizing.

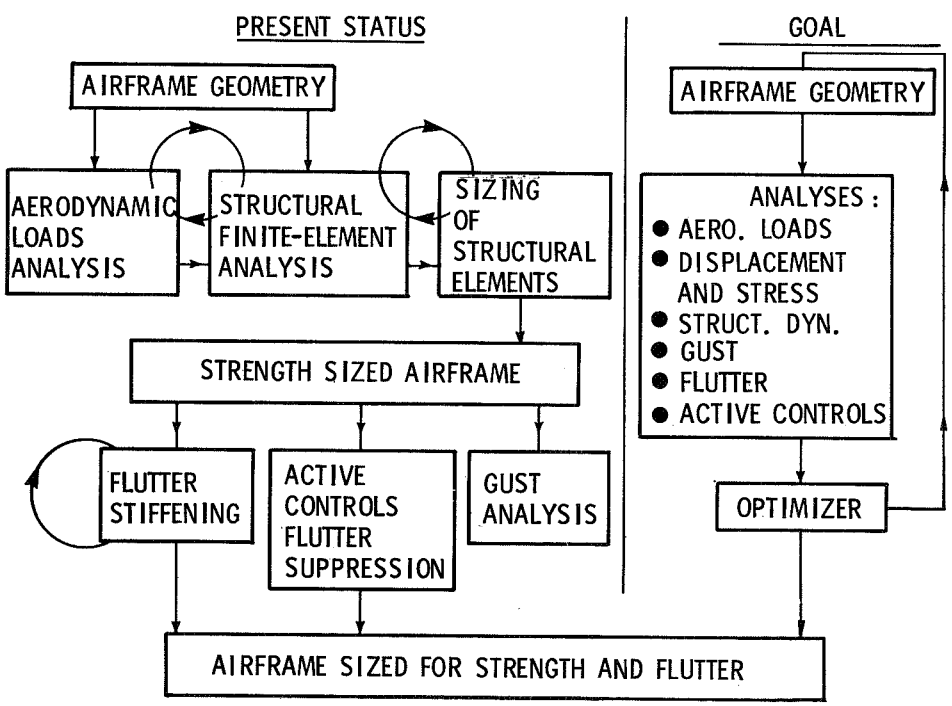

Figure 2.- Airframe structural sizing approach.

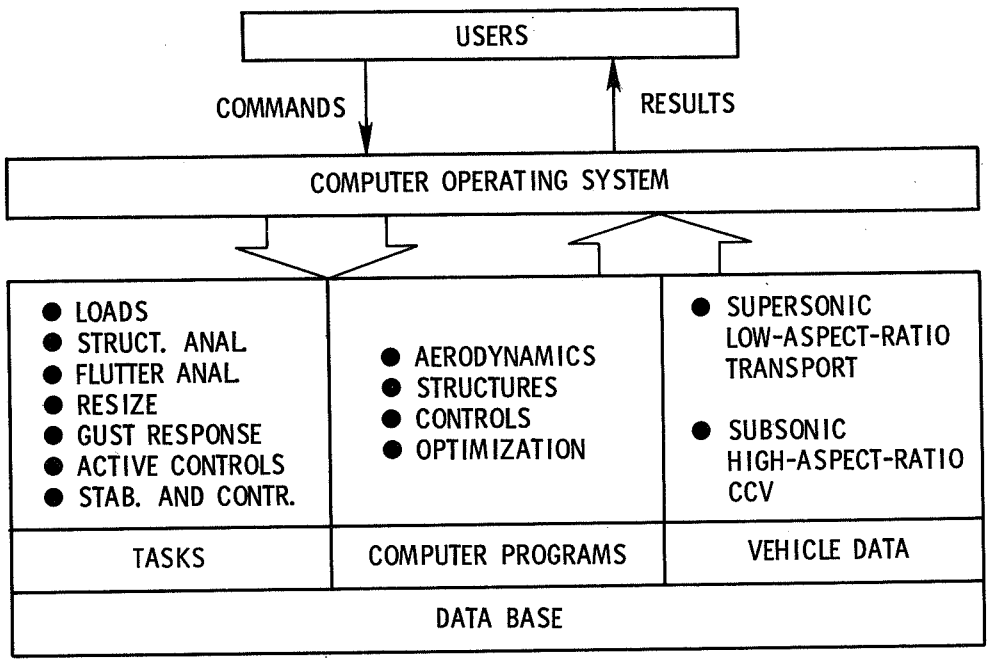

Figure 3.- Integrated multidisciplinary sizing system.

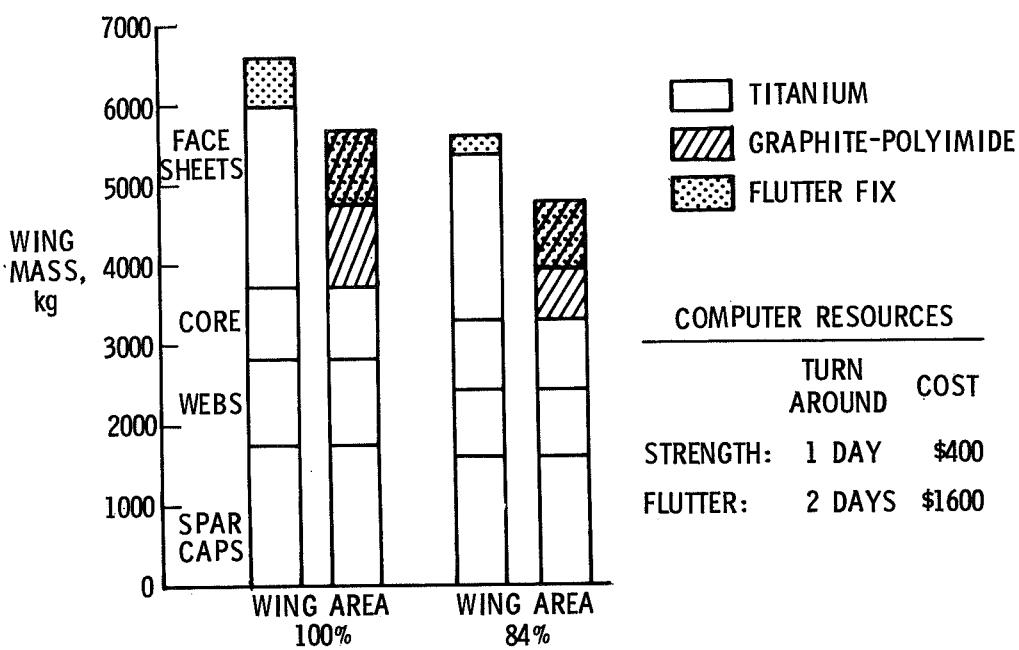

Figure 4.- Mass of optimally sized low-aspect-ratio wings.

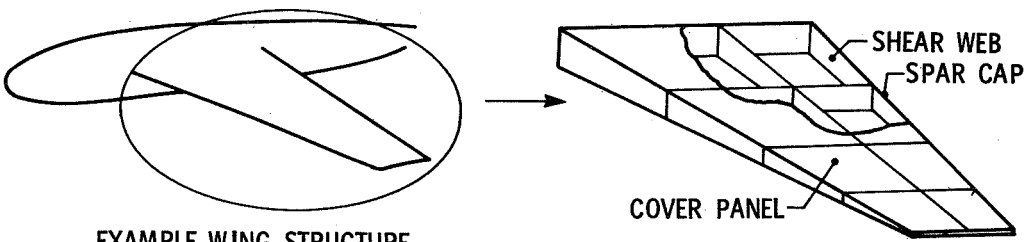

EXAMPLE WING STRUCTURE

SIMPLIFIED SKETCH OF FINITE-ELEMENT MODEL

- CONSTRAINTS CONSIDERED

MATERIAL STRENGTH	BUCKLING
DEFLECTION	NATURAL FREQUENCY
TWIST	FLUTTER
THERMAL STRESS	DRAG

- ADVANCES IN TECHNIQUE

APPROXIMATE ANALYSIS	DESIGN VARIABLE LINKING
CONSTRAINT DELETION	IMPROVED SEARCH TECHNIQUES

Figure 5.-Structural subassembly sizing.

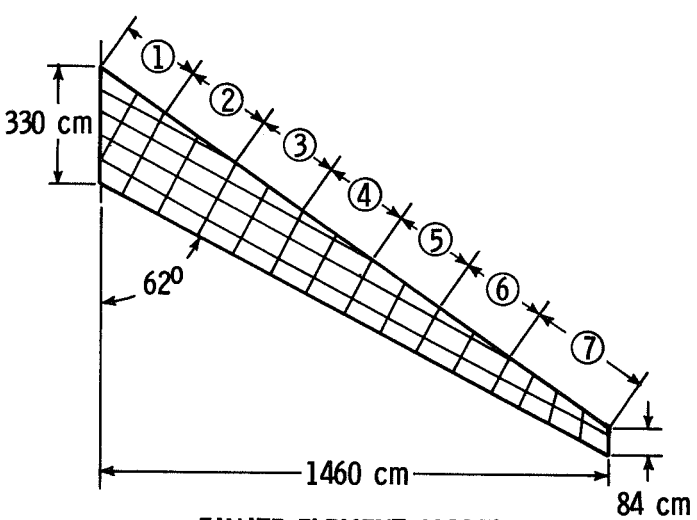

FINITE-ELEMENT MODEL

Figure 6.- Application of subassembly sizing for a graphite-epoxy wing structure with material strength, displacement, and buckling constraints.

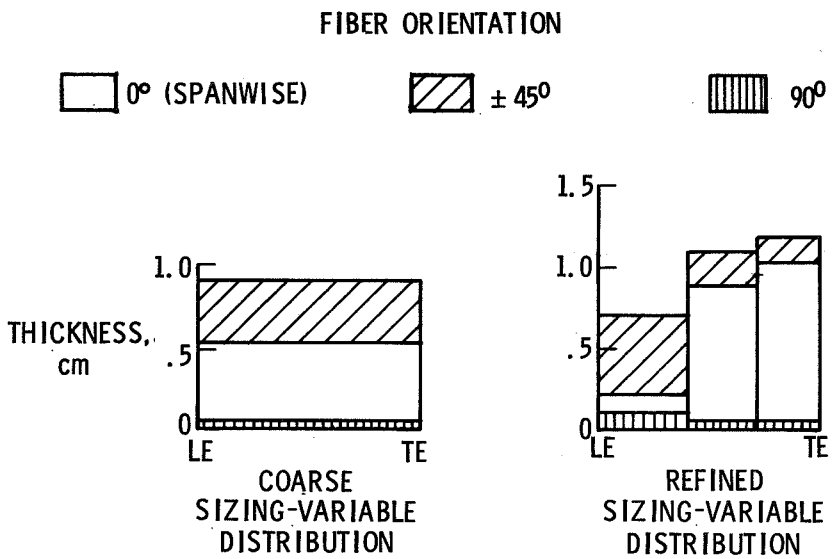

Figure 7.- Cover skin thickness distribution at 40 percent of semispan.

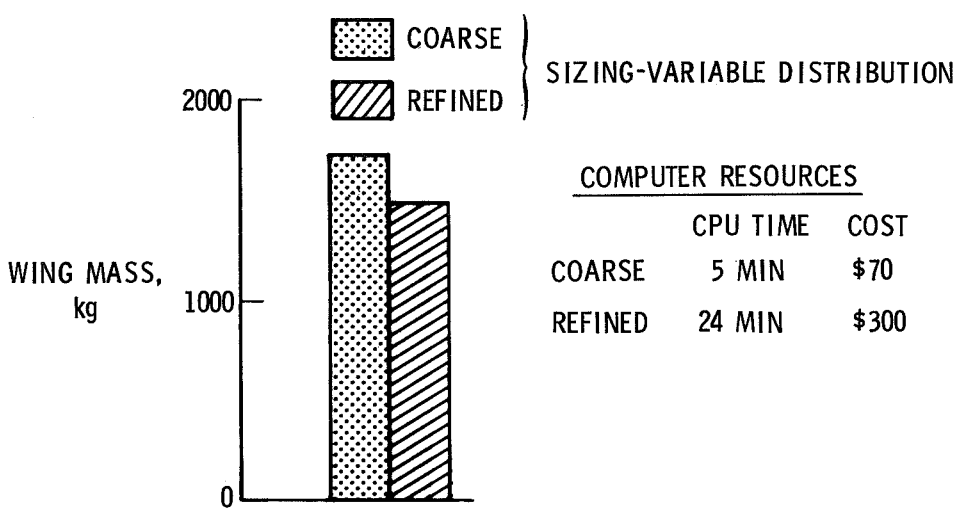

Figure 8.- Mass of optimally sized high-aspect-ratio wing.

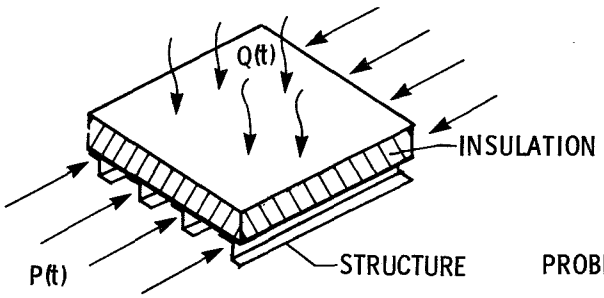

DESIGN PROBLEM

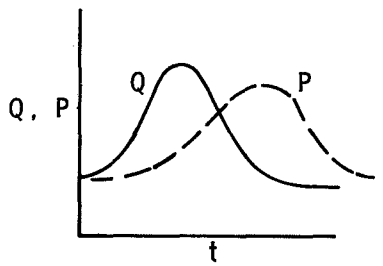

TIME-DEPENDENT THERMAL (Q) AND MECHANICAL (P) LOADS

PROBLEM CHARACTERISTICS

- REQUIRES STEADY-STATE AND TIME-DEPENDENT ANALYSES FOR TEMPERATURES, STRESSES, DISPLACEMENTS, ETC.
- TEMPERATURES AND STRESSES MUST BE CONTROLLED SIMULTANEOUSLY
- TRADE THERMAL CONTROL MASS AGAINST STRUCTURAL MASS TO OBTAIN LOW-MASS TOTAL SYSTEM

Figure 9.- Sizing thermal structures.

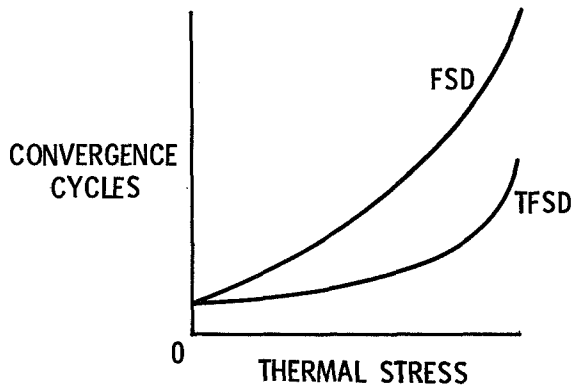

EFFECT OF THERMAL STRESS LEVEL ON CONVERGENCE

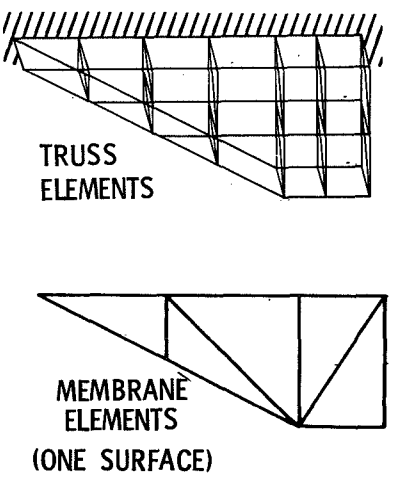

FINITE-ELEMENT MODEL

Figure 10.- Example using thermal fully stressed design procedure for a low-aspect-ratio wing with fixed applied loads and temperatures.

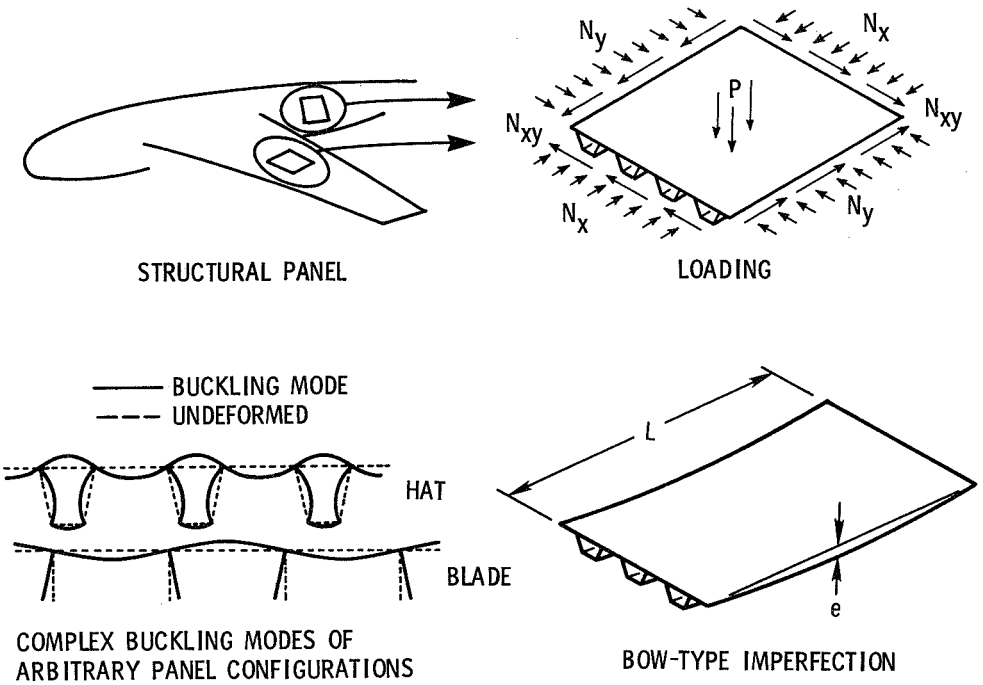

Figure 11.- Stiffened panel design code - PASCO. (N_x and N_y are the longitudinal and transverse in-plane loadings, respectively, N_{xy} is the shear landing, and P is the pressure loading.)

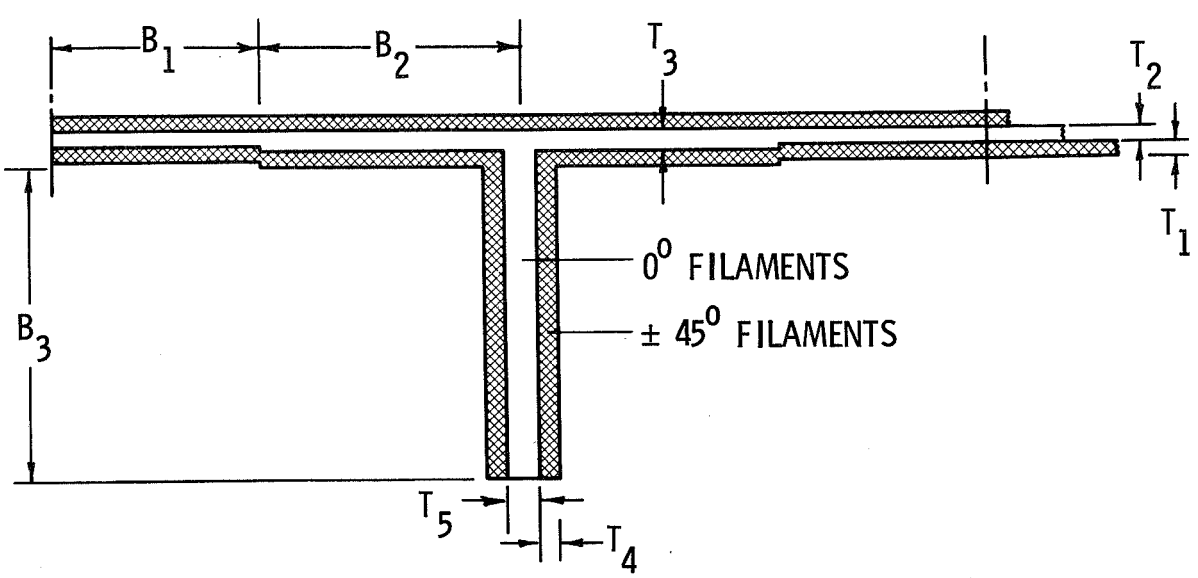

Figure 12.- Sizing variables for composite blade-stiffened panel.

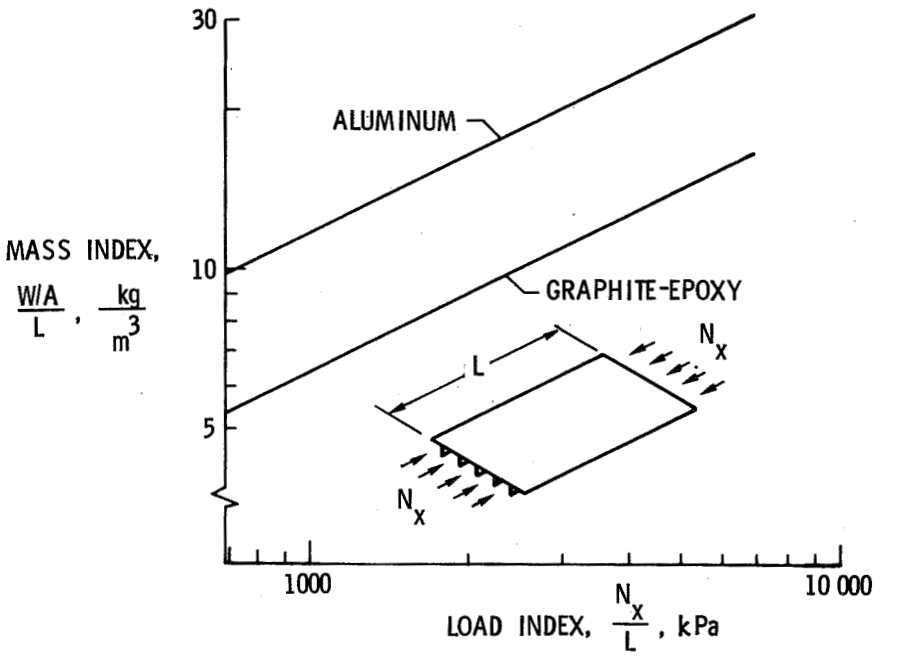

Figure 13.- Structural efficiency of blade-stiffened panels (only buckling considered).

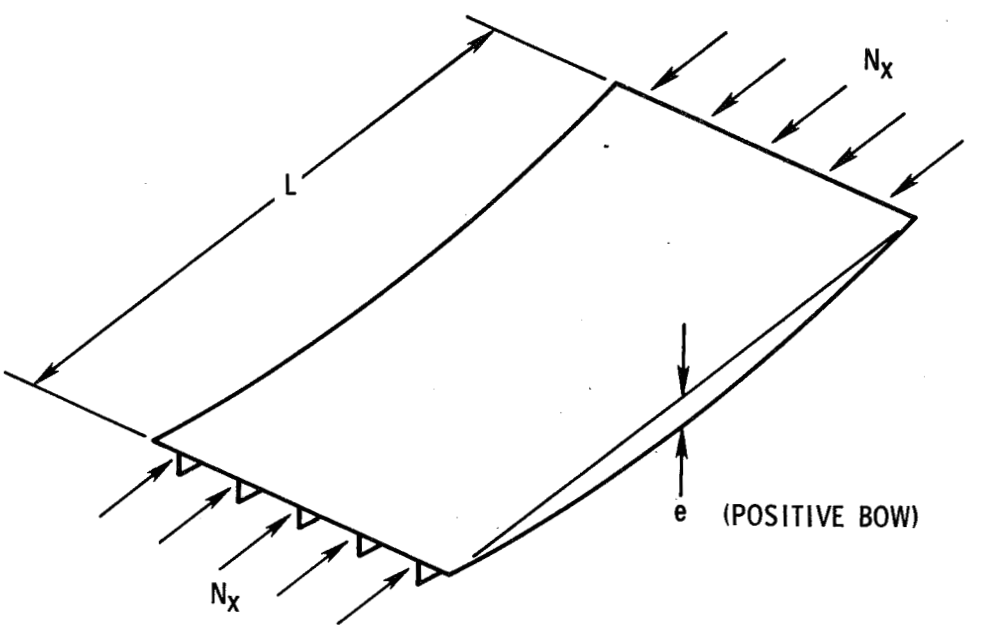

Figure 14.- Panel with initial bow.

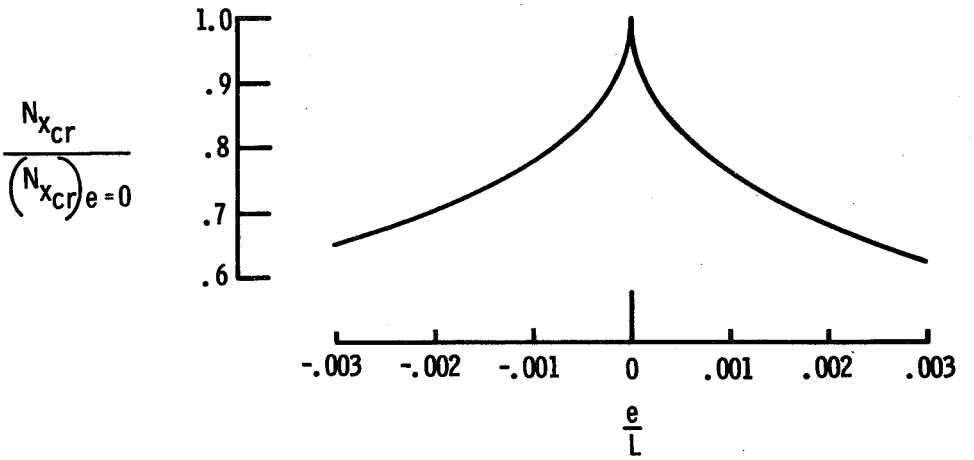

Figure 15.- Effect of bow on buckling load. (Ratio of buckling load $N_{x_{cr}}$ for panel with a bow to buckling load of panel without a bow $(N_{x_{cr}})_{e=0}$ as a function of size of bow e/L for graphite-epoxy, blade-stiffened panel designed for zero bow.)

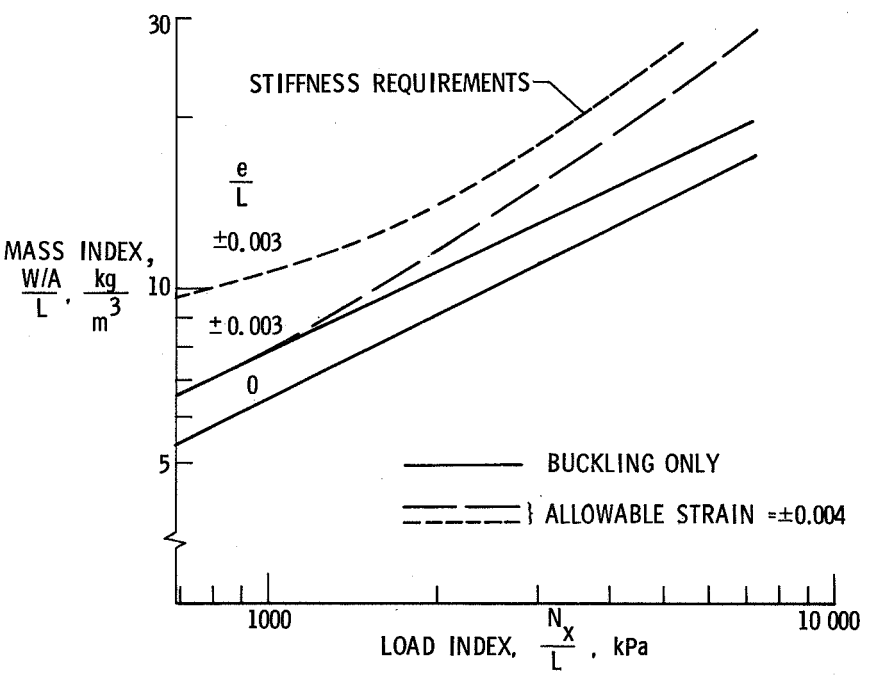

Figure 16.- Structural efficiency of graphite-epoxy, blade-stiffened panels.

TRANSITION FROM GLASS TO GRAPHITE IN MANUFACTURE OF COMPOSITE AIRCRAFT STRUCTURE

Harvey E. Buffum and Vere S. Thompson

The Boeing Commercial Airplane Company

SUMMARY

The Boeing Company has over 650,000 square meters (approx. 7,000,000 square feet) of structural fiberglass composites in commercial aircraft service. This provides a stepping stone for graphite composite structure. Similar design approaches, materials, tooling criteria, manufacturing methods and quality assurance techniques must be emphasized for both fiberglass and graphite composites. Further development is required to make graphite composites more cost-effective, to assure structural integrity and to establish design criteria, methods and data.

INTRODUCTION

This paper describes the transition from fiberglass-reinforced plastic composites to graphite-reinforced plastic composites. The Boeing Company structural fiberglass design and manufacturing background are summarized initially. The paper describes how this experience provides a technology base for moving into graphite composite secondary structure and then to composite primary structure. The paper incorporates the early results of NASA composite contracts to illustrate the transition from glass to graphite composite. The technical requirements that must be fulfilled in the transition from glass to graphite composite structure are also included.

STRUCTURAL FIBERGLASS TECHNOLOGY

Figure 1 illustrates the growth of composite parts on Boeing commercial aircraft and the major structural composite applications by model. (It should be noted that the term "structural fiberglass composite" is being used to distinguish those applications which are a structural part of the airframe from composites used for interior decorative linings, electronic boxes, ducts and other miscellaneous items.) There are over 650,000 square meters (approx. 7,000,000 square feet) of structural fiberglass composite parts currently flying on Boeing commercial jet aircraft.

The use of structural fiberglass parts started with only 18 square meters (approx. 200 square feet) on the Model 707 and has grown to over 930 square meters (approx. 10,000 square feet) on the 747. Applications have increased from the radome and small closure fairings on the Model 707 to wing leading and trailing edge panels, flaps, fairings and control surfaces on the Model 747 (Figure 2). The lower surface wing to body fairing, flap track fairing, wing flap and wing leading edge applications on the Model 747 are shown in Figure 3.

The use of structural fiberglass composites for applications other than radomes did not come easily. A weight saving could readily be shown for most proposed applications, but service experience was required to demonstrate the acceptability of structured fiberglass components. The manufacturing cost advantage was questioned and only after a side-by-side comparison to metal assemblies in the production environment (Figure 4) were decisions made to use composite construction in place of metal. Although initial fabrication costs are important, maintenance and repair costs are significant and should not be overlooked.

Using composites in place of metal required a different design approach. Substituting composite detail parts for the same configurations in metal was not cost effective. A close tie between design and manufacturing capability became essential to effective use of composites; and, as the designer found more applications, manufacturing methods were developed to provide the capability to produce them. Parallel and closely coordinated development programs between engineering and manufacturing organizations were essential to cost effective production. New applications for structural fiberglass components were usually preceded by cost trade studies, fabrication of feasibility hardware and establishment of production methods.

Construction

Sandwich structures were used initially on the Model 727-100. Figure 5 shows the typical construction of composite sandwich parts made from fiberglass/epoxy materials. The sandwich construction shown in this figure reflects that which has been in use since 1962. It should be noted that no separate adhesive layer is used in joining the surface layers to the honeycomb core, and the moisture barrier film is laid up and cured as an integral part of the component.

A wide variety of configurations are being produced with varying contour, size and thickness, depending on application. Some parts are solid laminate construction rather than sandwich. Areas with high localized loading are met using titanium inserts. Other requirements such as antenna ground planes, lightning strike protection are satisfied by bonding of aluminum foil on inner surface, aluminum flame spray on outer surfaces and special finishing.

Materials

Figure 6 illustrates the development of fiberglass material systems. Early parts were made by tailoring the glass fabric to the required configuration and pouring the liquid resin onto the fabric, spreading and sweeping the resin to impregnate the fabric, vacuum bagging the part and tool, and curing in an oven or autoclave. This wet layup method is very labor intensive.

The development of pre-impregnated fiberglass/epoxy materials ("prepregs") was a major step forward. Prepregs provide a relatively uniform amount of resin to the glass fabric and with proper processing yield consistent part properties. The prepreg materials used through the early 1960's required a 177°C (350°F) cure, some "bleeding" to remove excess resin and voids and a separate adhesive layer for joining to honeycomb core. Essentially, the processing requirements were the same as those required for today's graphite composite systems. Development efforts over the years have evolved a prepreg system which Boeing uses for most of its composite parts. This system cures at 120°C (250°F), does not require "bleeding" and does not require a separate adhesive layer for joining to honeycomb core. These advantages result in lower material costs, less labor, reduced flow time and reduced energy requirements.

Unidirectional material forms have been used very sparingly for airplane structural parts at Boeing. This is due in part to the much higher layup costs of unidirectional tapes as compared to woven fabrics.

Initial honeycomb core materials used by Boeing were polyester and nylon-phenolic for radomes. Later, heat resistant phenolic (HRP) core was used. The latest Boeing commercial applications use Nomex core due to a 16 kilograms per cubic meter (1 pound per cubic foot) weight savings compared to HRP core. The HRP core is still being used on earlier models. Polyimide core is used in special areas for temperature applications over approximately 190°C (375°F).

Production Flow

The production flow (Figure 7) for fabricating structure fiberglass parts involves prepreg and core preparation, parts layup on laminating molds, autoclave cure, trim and exterior surface finishing. The prepreg is received in rolls, then "kits" are prepared of the skin, doubler, and filler plies. Kitting is the cutting and storing together of prepreg patterns for a specific part until the production schedule requires that part. Steps required for preparing honeycomb core details include slicing, forming, splicing, machining and potting.

Skin, doubler, filler ply details are oriented on a laminating mold according to the drawing, along with the honeycomb core detail. This is done by hand. With the appropriate design mechanization of the layup process is possible. However, high part quantities and an adequate production rate are needed to justify development and acquisition of suitable equipment.

Autoclaves are the principal curing method. The flexibility of the autoclave is most compatible with the production part mix and curing schedule. After cure, the parts are trimmed to size and painted.

Due to the use of an integrally-applied, bondable, moisture-barrier film applied to the part interior surface prior to cure, the finishing of composite parts is limited to the exterior (mold) surface. Part finishing is accomplished by application of the following: (1) pinhole filler, (2) surfacer, (3) conductive coating, (4) epoxy primer, and (5) enamel.

TRANSITION TO GRAPHITE COMPOSITE SECONDARY STRUCTURE

The transition to graphite composite secondary aircraft structure such as wing control surfaces, wing trailing and leading edge, vertical fin and stabilizer control surfaces and doors is based on our structural fiberglass composite technology base. Similar design approaches emphasizing sandwich construction, materials, tooling criteria, manufacturing methods and quality assurance techniques must be utilized.

The Model 727 Elevator design being developed as part of the NASA-ACEE program (Figure 8) consists of honeycomb sandwich skin panels (Figure 9), honeycomb sandwich ribs, and laminate spars. Woven fabrics, minimum thickness unidirectional tape, "no bleed" prepreg materials and Nomex core are employed to provide a minimum cost and weight structure. The manufacturing approach involves hand lamination, autoclave cure, mechanical assembly and in-process inspection. These design and manufacturing approaches are similar to those used for the Model 747 structural fiberglass components. Except for the single layer of unidirectional tape as the outer ply, the skin panel designs are essentially the same for the Model 727 graphite composite elevator and the Model 747 structural fiberglass rudder and elevator.

The Boeing structural fiberglass technology provides a stepping stone for producing graphite composite components. However, the design evolution work involving new application of different materials, forms and resin systems has necessitated a coordinated engineering/manufacturing development effort during the design of the NASA-ACEE components.

Areas of concern involved the substructure design and the comparative cost of different material forms including the finishing cost and weight impact. To resolve these concerns, feasibility hardware was fabricated to support the preliminary design of the graphite/epoxy elevator. An elevator rib design/manufacturing trade study (Figure 10) showed that a sine-wave laminate rib weighed the same as a sandwich rib, but the sine-wave rib was 2.5 times more costly than a sandwich rib. Based on this study, a sandwich construction was selected for the graphite composite elevator.

Other studies confirmed that woven fabric sandwich structure was most cost effective and provided fewer manufacturing problems than 2-ply preplied tape, 4-ply preplied tape, or 30.5-centimeter (approx. 12-inch) wide unidirectional tape. The relative cost was 1.00 for woven fabric, and 1.25, 1.10, and 1.39 for the tapes, respectively.

When these panels were finished, it was found that the woven fabric panel required 2.9 times longer to prepare the surface to meet aerodynamic requirements than the tape panels; and, the surface filler material caused a panel weight increase of approximately 21.6 grams per square meter (approx. 0.07 ounces per square foot). To minimize finishing time and reduce weight, the elevator skin panel design was changed to replace the outer ply of woven fabric with one ply of unidirectional tape (Figure 11). To prevent distortion, the fabric ply against the core was changed to tape. As noted in Figure 11, these changes did not affect the panel warpage or core collapse characteristics and resulted in only a 1 percent increase in the total fabrication cost. The use of fabric on the drill exit side has been found to minimize fiber breakout.

Additional work is required to make graphite composites secondary structure more cost effective. Important needs include improved material systems, kitting methods to reduce material wastage, hole preparation/fasteners techniques and nondestructive inspection methods.

A cost savings of over $76.70 per square meter (approx. $7.15 per square foot) (Figure 12) can be achieved by developing a controlled-flow, self-adhesive epoxy resin system for graphite composite sandwich construction (Figure 12). This savings would be realized by replacing the current "bleed" resin system. The controlled-flow, self-adhesive resin system would be similar to the present structural fiberglass resin system that has been used since 1965.

The Boeing NASA-ACEE contracts are using a "no-bleed" resin variation of the current "bleed" systems. This has resulted in cost savings of $39 per square meter (approx. $3.60 per square foot). A further cost savings of $38 per square meter ($3.50 per square foot) and a weight savings of 0.58 kilograms per square meter (approx. 0.12

pounds per square foot) can be realized by developing a controlled-flow, self-adhesive, epoxy resin system for sandwich panel fabrication.

The development of titanium rivets and blind fasteners is required for graphite composite secondary structure. These fasteners would replace nut plates and high torque bolts. They would be used for fastening the trailing edge of control surfaces, assembling front spar to rib, and attaching the last skin panel to the rib/spar substructure. A time savings of up to 1-1/2 minutes per fastener can be achieved by implementing titanium rivets and blind fasteners.

TRANSITION TO GRAPHITE COMPOSITE PRIMARY STRUCTURE

The transition to graphite composite primary aircraft structure such as vertical fin, stabilizer, or wing in-spar boxes will be built from our secondary graphite composite technology foundation. As shown by the Model 737 Graphite Composite Stabilizer design (Figure 13) and a wing box structural concept (Figure 14), the design will be skin-stringer rather than sandwich construction. Due to the higher load, more unidirectional or preplied tape will be required, especially on the outer skin plies.

Many of the design and manufacturing approaches that were developed for structural fiberglass or graphite composite secondary structure will be employed to build primary graphite composite structures. However, cost, loads and added structural integrity will require the establishment of new methods. Based on current fabrication cost data, the cost of producing large primary graphite structure such as a wing box is projected at over 6-1/2 hours per kilogram (approx. 3 hours per pound) at airplane 200. This cost must be reduced to less than 2.2 hours per kilogram (1 hour per pound) to be competitive with aluminum primary structure at airplane 200. The required 50 to 70 percent reduction in production cost will necessitate additional development work to improve materials and processing methods, mechanize detail fabrication and assembly operations and improve quality assurance methods.

Major materials and material processing related cost drivers that should be worked include development of structurally acceptable graphite pitch fibers, 160,000 end tow graphite and thicker graphite fiber. These developments would reduce the cost of graphite prepreg from its current level of about $110 per kilogram (approx. $50 per pound) to approximately $22 per kilogram (approx. $10 per pound). Also, improved lower flow, less brittle, no-bleed resin systems are required to produce primary graphite structure. Mechanized kitting equipment using water jet or mechanical cutting should be developed to reduce the cost of preparing the materials for detail fabrication.

Detail fabrication is the most productive area for reducing the cost of manufacturing graphite primary structure. Approximately 39 percent of the cost is incurred during detail fabrication. Mechanized fabrication methods such as pultrusion, compression/elastomeric/ injection molding, machine layup and filament winding must be developed to achieve the 50 to 70 percent reduction in manufacturing cost.

The Boeing pultrusion process (Figure 15) involves the pulling of graphite prepreg through a shaped ceramic die while effecting a continuous cure of the composite material simultaneously with its compaction during the passage through the die. Microwave energy is used for the curing of the material. A feed system is used to handle and feed composite prepreg tapes into the microwave curing chamber containing the ceramic die. The pultrusion process is employed to fabricate substructural shape such as angles, "T's," "Z's," tapered and curved members, and hat sections and sandwich panel stock. A 50 to 80 percent reduction in fabrication labor and tooling cost can be achieved by using pultruded substructural shapes and panel stock.

Elastomeric, compression and injection molding techniques would be used to manufacture clip brackets, fittings and other similar components, while a mechanized layup machine would be used to produce broadgoods and to laminate outer skin plies of structures having large platform areas. For these applications, the machine would lay preplied tape or woven fabric directly onto a laminating mold. Molding of subcomponents and mechanized layup of outer skin plies or broadgoods would result in a projected labor savings of 50 to 60 percent compared to current hand lamination and processing methods.

Filament winding has proven to be an excellent method of fabricating shapes of rotation. Graphite primary structure such as spars, ribs, landing gear beams, wing panels and eventually fuselage sections can be produced by filament winding. A trade study showed that the relative cost of filament winding wing spars would be 0.7 compared to 1.0 for hand lamination and autoclave cure.

To further reduce production cost, mechanized methods should be developed for trimming, drilling, assembling and inspecting graphite primary structure. Automated assembly equipment, similar to the numerical control metal spar machine shown in Figure 16, should be implemented to eliminate the present labor intensive drilling and fastening methods. Also, adaptive and in-line process control techniques (Figure 17) should be used to reduce inspection costs and assure structural integrity.

Figure 18 illustrates how the detail fabrication assembly and inspection methods described previously would be used to produce graphite wing structure. A comparative cost analysis indicated that the use of these methods would result in a projected fabrication cost of less than 2.2 hours per kilogram (1 hour per pound) at airplane 200.

CONCLUDING REMARKS

Structural fiberglass composites provide an excellent stepping stone to graphite composites. The structural fiberglass approaches for design to cost, manufacturing/engineering interface, materials, tooling, production and inspection are a technology base for moving into graphite secondary and primary aircraft structure. The cost and service experience of producing and flying over 650,000 square meters (approx. 7,000,000 square feet) of structured fiberglass in commercial operations further expands this technology base for graphite composites.

Metal technology does not provide a stepping stone for moving into graphite composites. Cost data, design and manufacturing approaches, service experiences are not applicable.

Improved material systems, mechanized fabrication and assembly and adaptive and in-line inspection methods must be developed for graphite composites to become more cost effective. Cost effectiveness will be one of the primary considerations to the implementation of graphite composites on commercial aircraft.

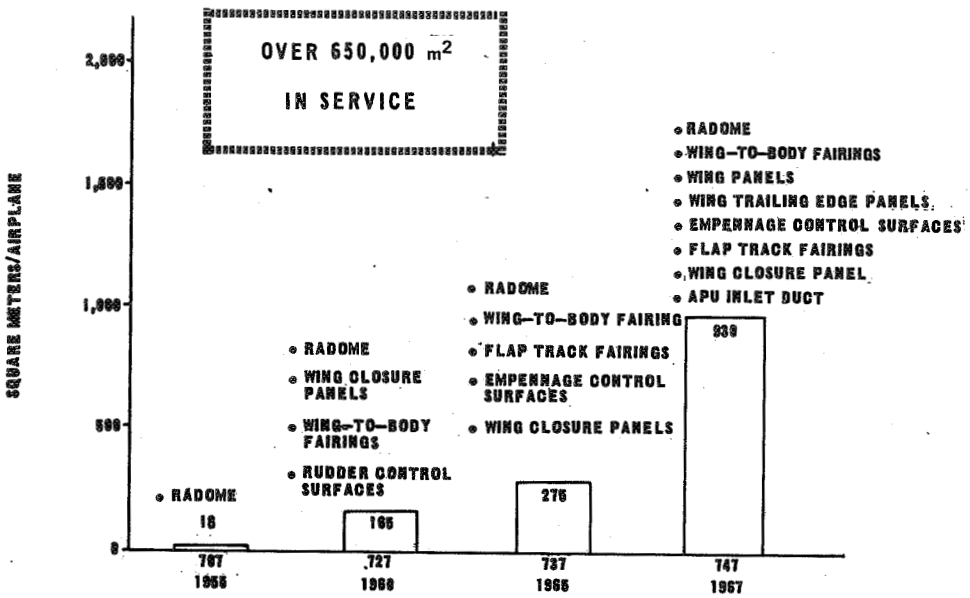

Figure 1.- Commercial structural fiberglass growth.

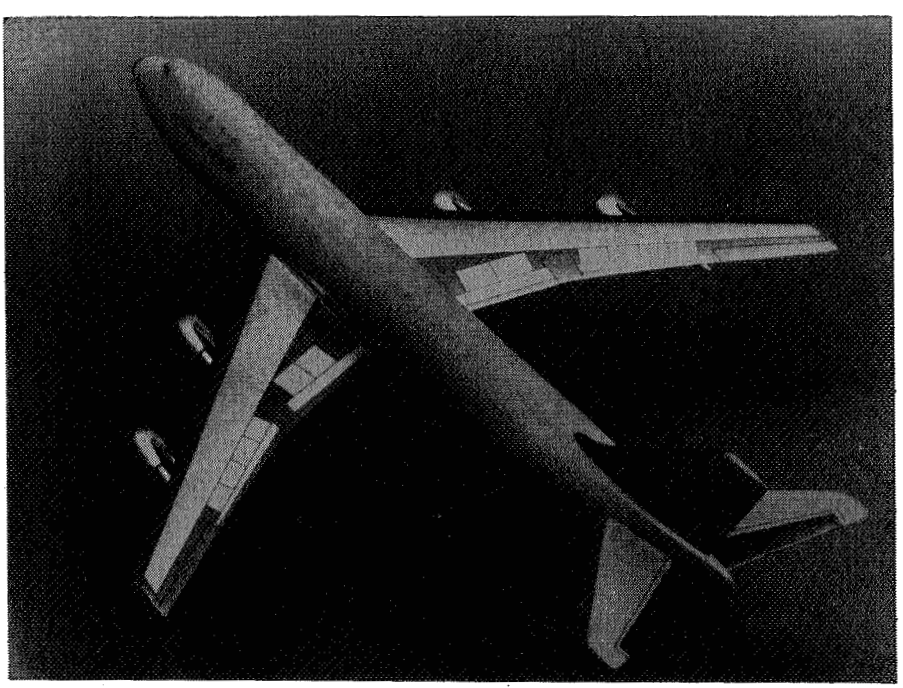

Figure 2.- Applications of model 747.

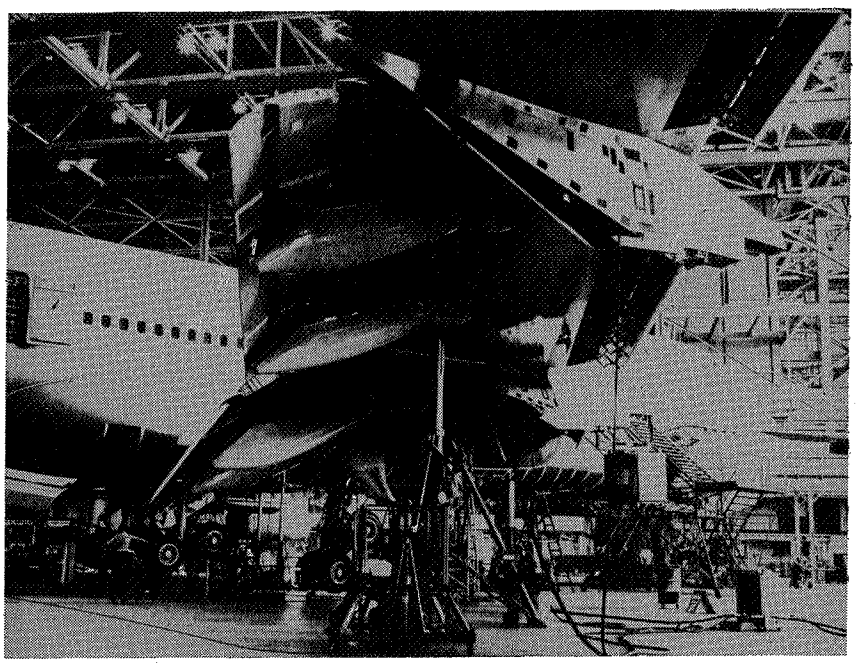

Figure 3.- Lower surface of model 747.

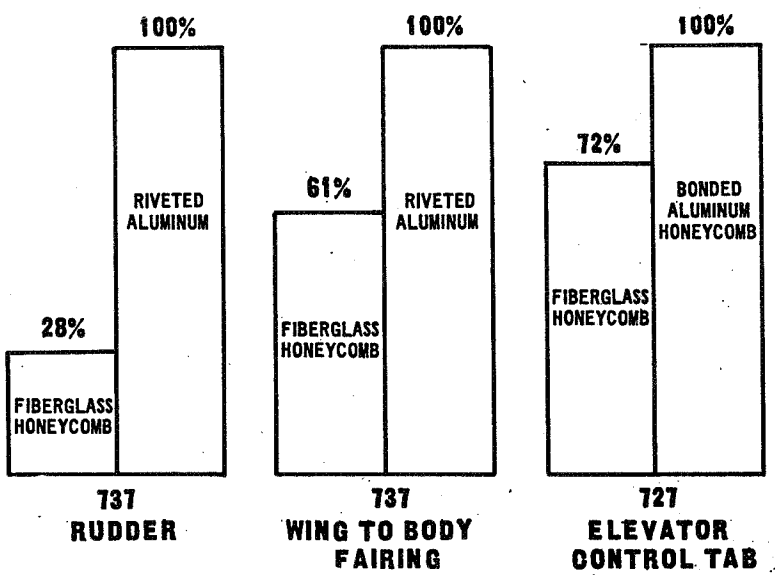

Figure 4.- Cost comparisons.

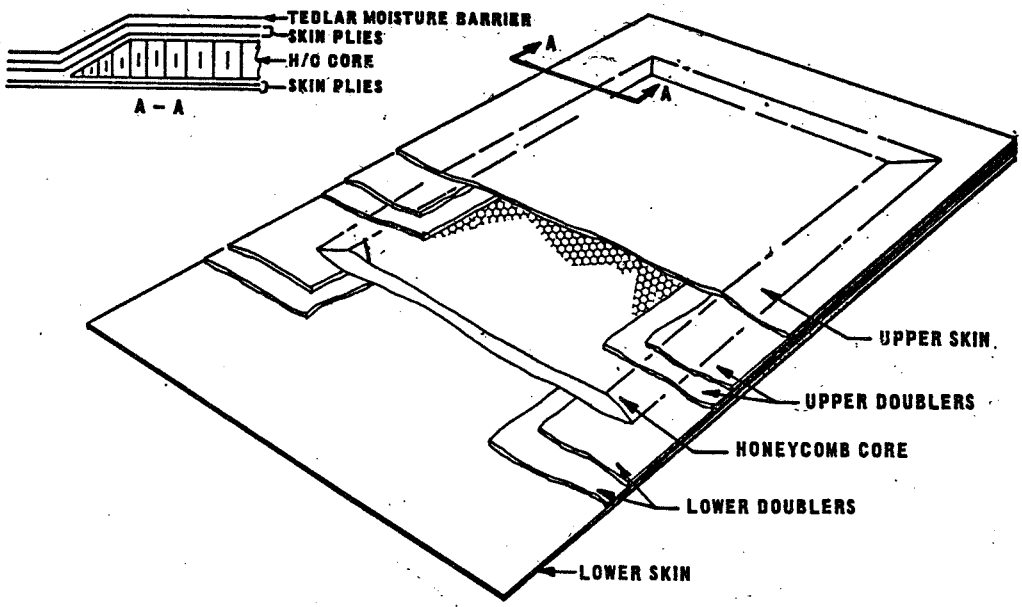

Figure 5.- Typical construction structural fiberglass.

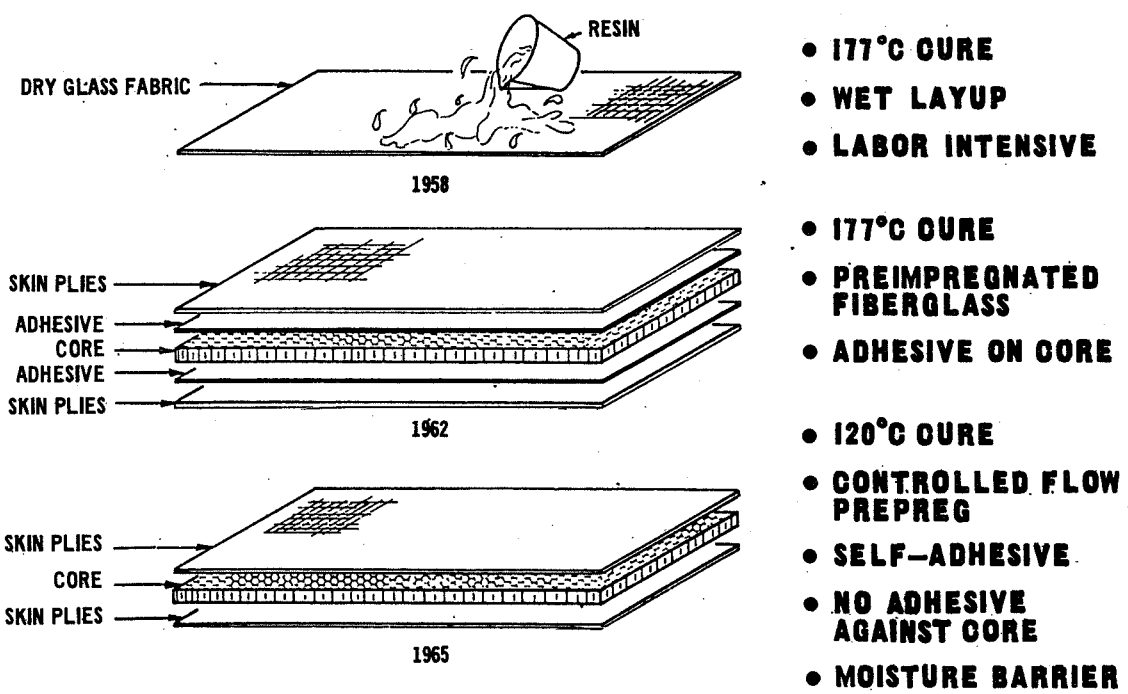

Figure 6.- Fiberglass material development.

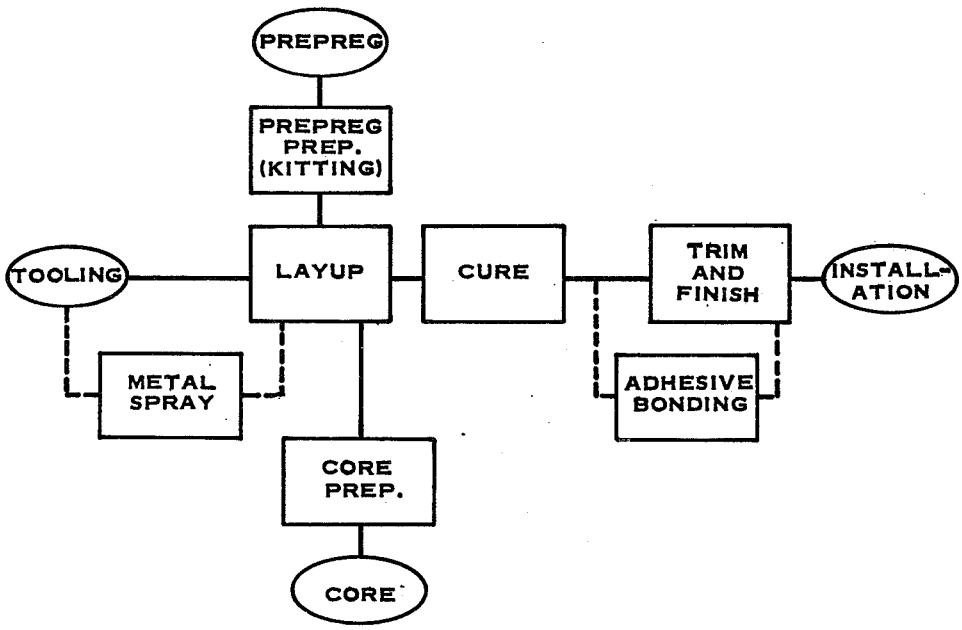

Figure 7.- Production flow.

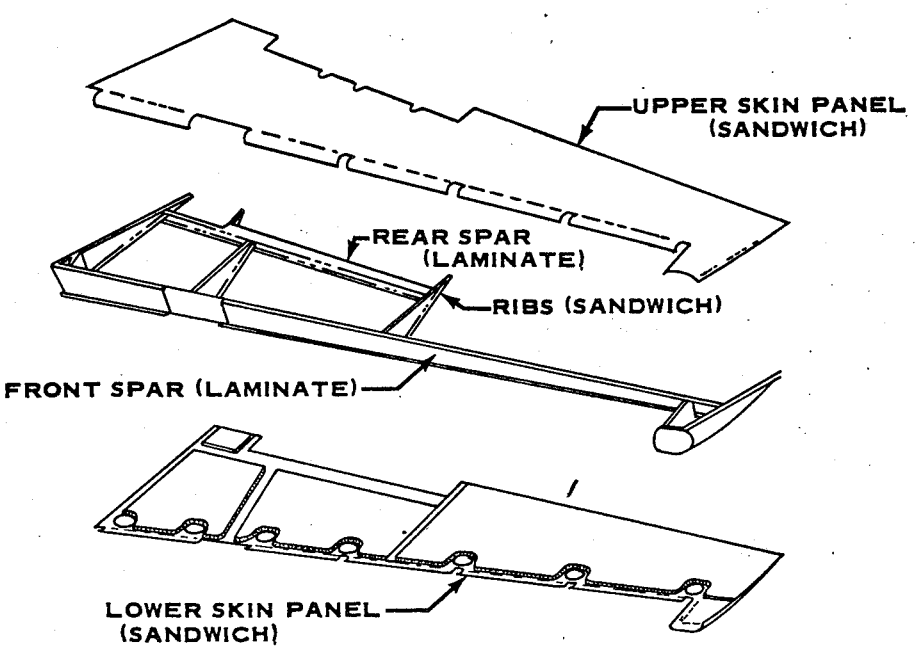

Figure 8.- Model 727 graphite composite elevator.

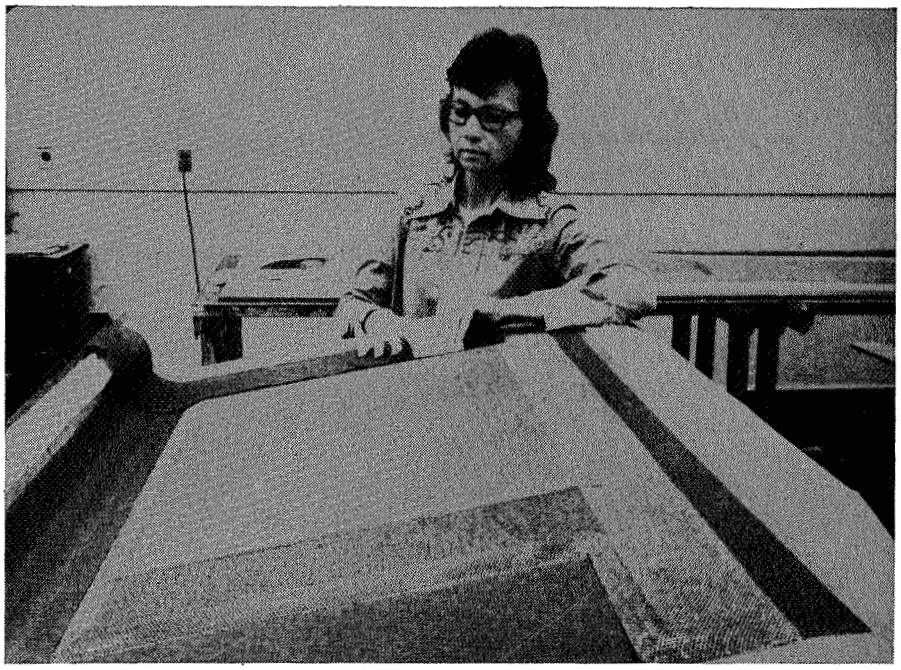

Figure 9.- Elevator skin panel section.

[redacted]

FIGURE 10

RIB DESIGN TRADE STUDY

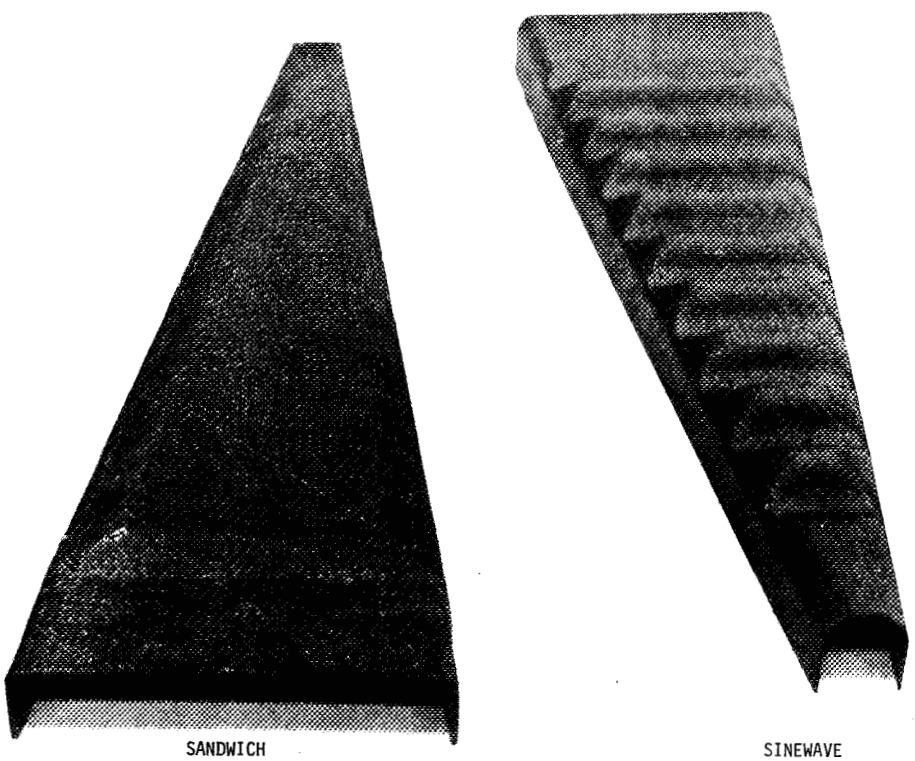

Figure 10.- Rib design trade study.

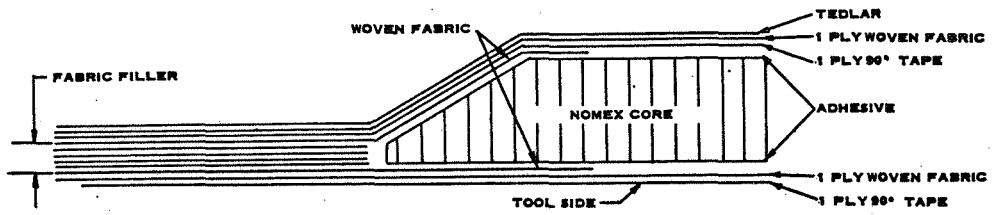

- NO CORE COLLAPSE OR WARPAGE
- RELATIVE COST INCLUDING FINISHING
  - ALL FABRIC 1.00
  - COMBINATION 1.01
  - ALL TAPE 1.35
- SLIGHT DRILLING BREAKOUT – ENTRANCE (TAPE) SIDE
- NO DRILLING BREAKOUT – EXIT (FABRIC) SIDE

Figure 11.- Graphite composite 727 elevator skin panel configuration.

		COST SAVINGS (DOLLARS)	WEIGHT SAVINGS (KILOGRAMS)
• BLEEDER ELIMINATION		$38.77/m^2$	
• NO ADHESIVE		$38.02/m^2$	0.58 kg/m^2
	SUB TOTAL	$76.79/m^2$	0.58 kg/m^2
• 120°C vs 177°C CURE			
• UTILITY SAVINGS		$0.43/m^2$	
• ADDITIONAL IMPACTS			
• MAINTENANCE		+	
• TOOL LIFE			
• SCHEDULE			
	TOTAL	$77.22/m^2$ +	0.58 kg/m2

REFERENCES: INDUSTRIAL ENGINEERING COST STUDIES

Figure 12.- Improved prepregs.

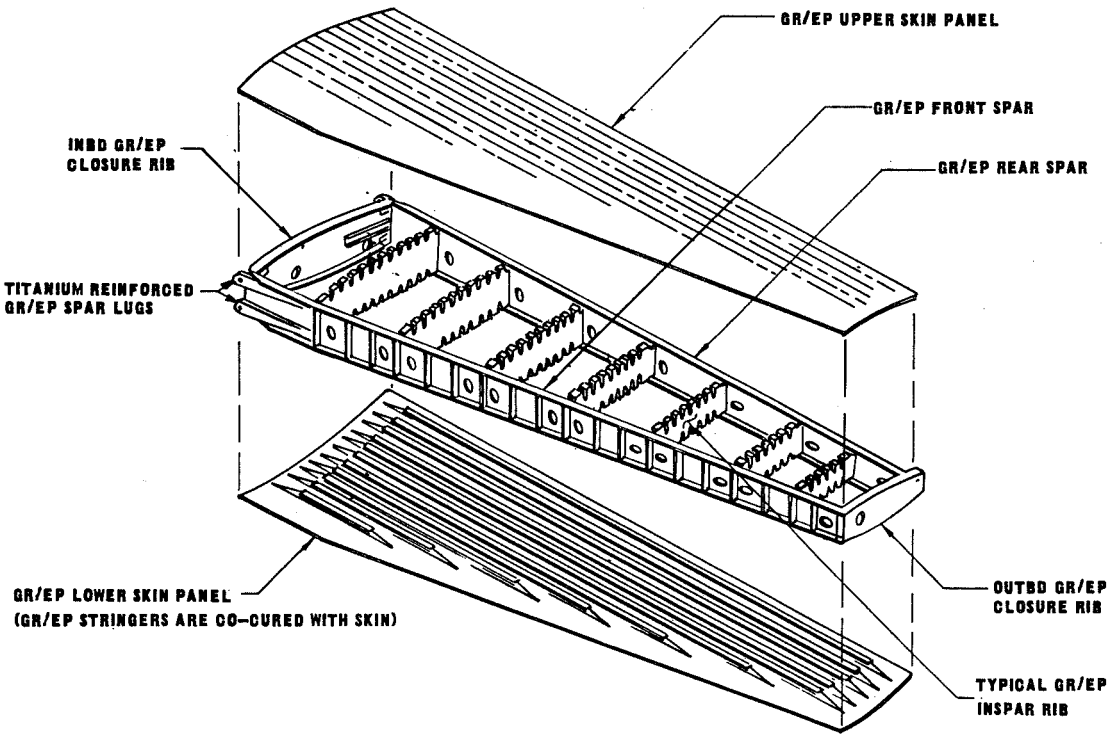

Figure 13.- Model 737 graphite composite stabilizer concept.

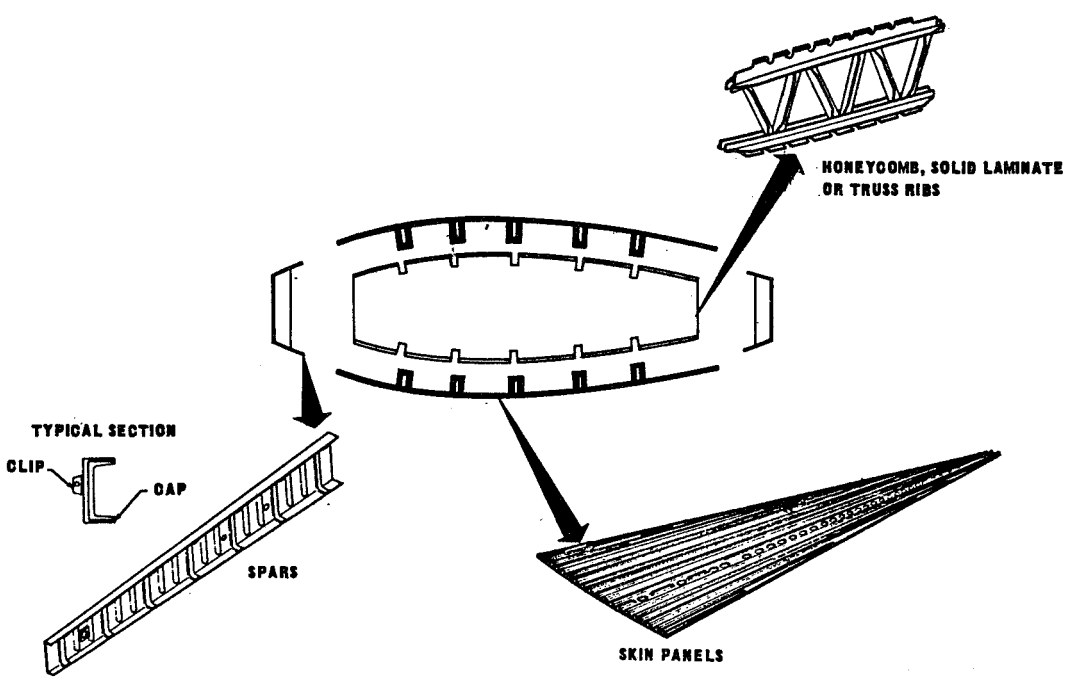

Figure 14.- Graphite composite wing concept.

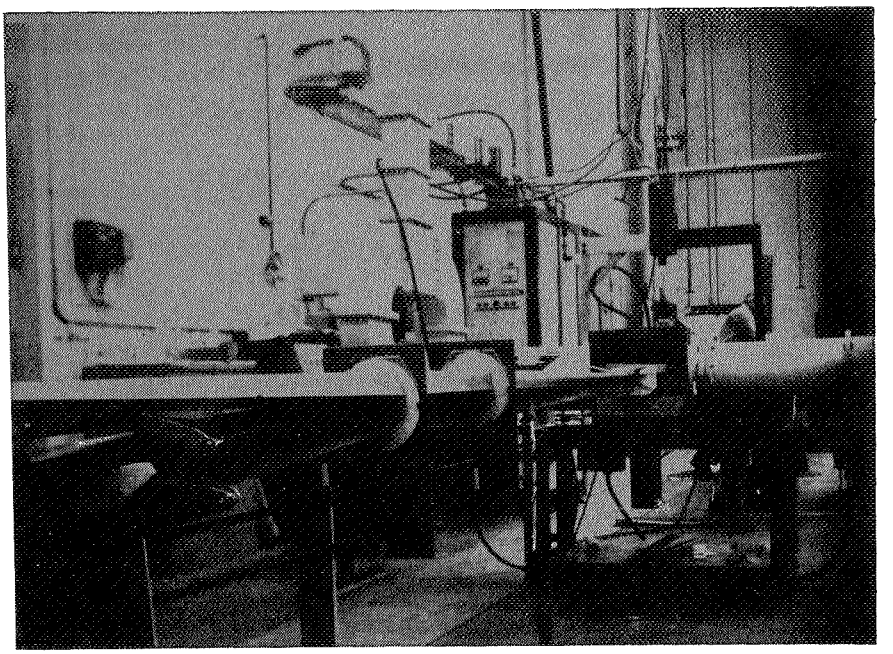

Figure 15.- Boeing pultrusion unit.

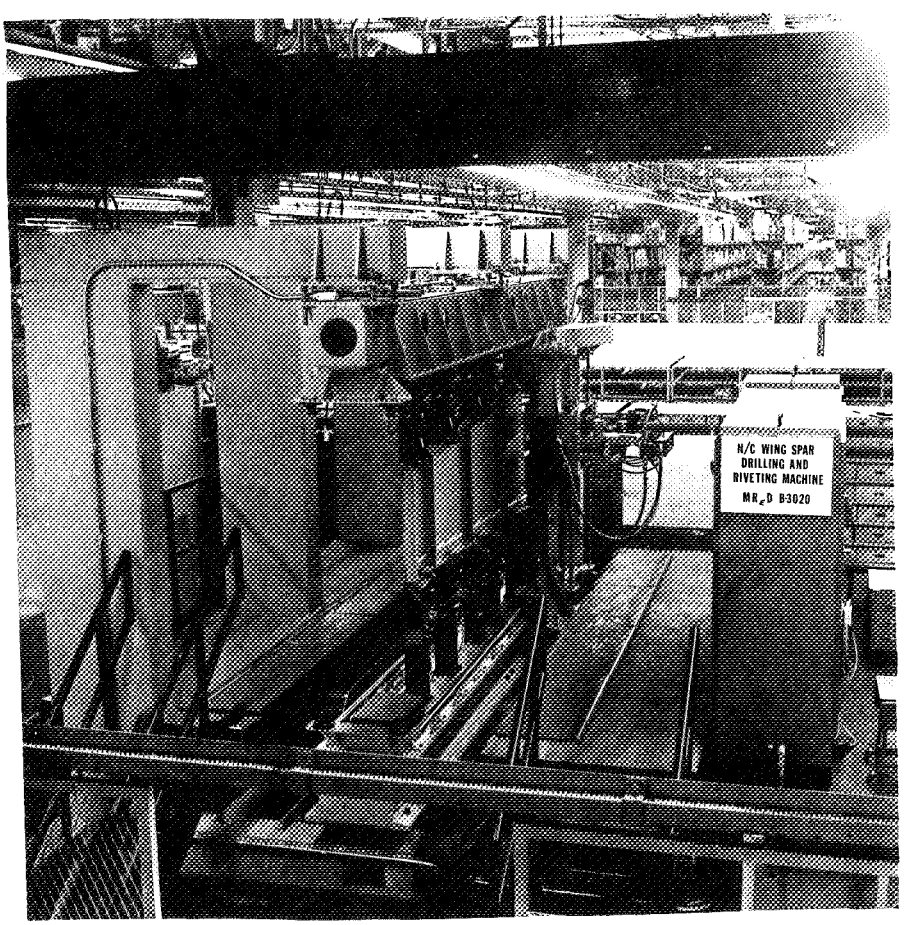

Figure 16.- Metal spar assembly machine.

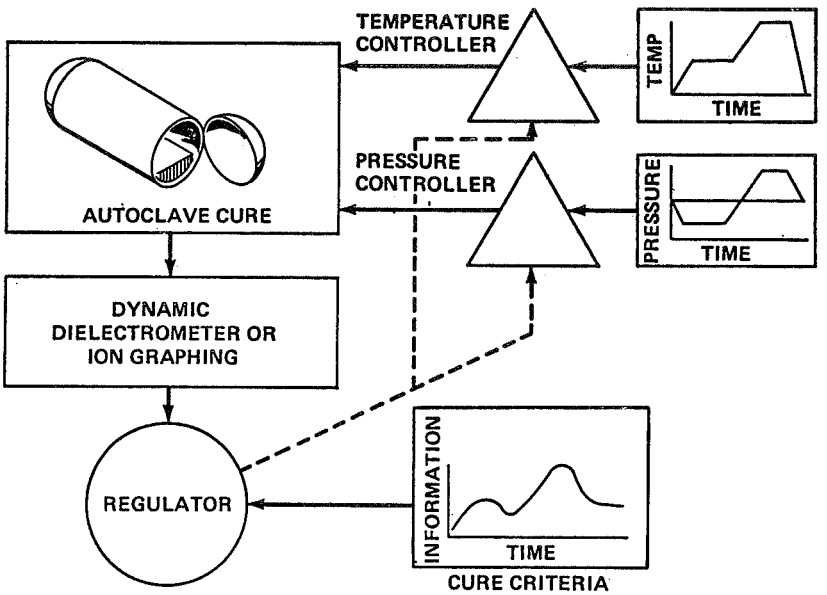

Figure 17.- Adaptive cure process control.

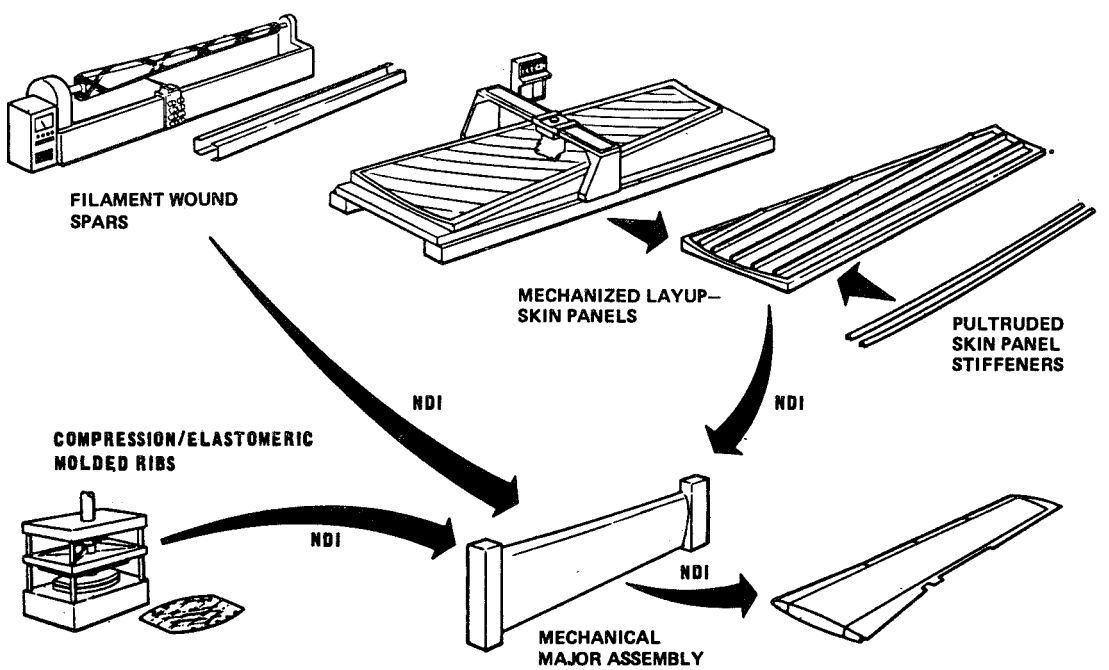

Figure 18.- Production manufacturing concepts.

LAMINAR FLOW CONTROL OVERVIEW

Ralph J. Muraca
NASA Langley Research Center

During the past few years there have been a number of significant developments in laminar flow control (LFC) technology. Although some of the technology developments are generic in nature and will benefit other applications, the major thrusts of these activities are for application to future CTOL long-range transport aircraft. The resurgence of interest in LFC stems from the fact that of all the emerging technologies which will lead to more efficient, economically superior, future aircraft, none has the potential for greater benefit than LFC. A recent study indicates that the application of LFC to the wing and tail surfaces of a long-range transport would provide a 28% reduction in fuel consumption and an 8% reduction in direct operating cost (DOC) from those of a comparable advanced technology turbulent-flow transport (fig. 1) at current fuel prices and even greater DOC reductions at higher fuel prices.

The feasibility of achieving laminar flow through surface suction has been demonstrated many times under controlled conditions. The most memorable program, conducted in the mid-1960's, was the U.S. Air Force X-21 Project in which a B-66 aircraft was refitted with an LFC wing (fig. 2). Although problems were encountered early in the program, they were eventually solved and the aircraft was ultimately able to consistently achieve laminar flow over large regions of the wing surface (fig. 3). This program also demonstrated that once a satisfactorily smooth and wave-free surface was obtained, it was possible to maintain and even repair (fig. 4) the wing surface without deteriorating the LFC system performance. Unfortunately, due to pressures on the Department of Defense budgets in this time period, this program was terminated before operational experience in noncontrolled environments was obtained.

Encouraged by the results of the X-21 program and LFC's potentially large benefits, NASA included LFC as one of the technologies to be advanced as part of the Aircraft Energy Efficiency (ACEE) program. The objective of the ACEE/LFC Project is to demonstrate that LFC can be economically applied to long-range transports in the 1990 time period. Technology advances in aerodynamics, materials, manufacturing, propulsion, etc., since the X-21 program as well as those anticipated to be available in this time period will be evaluated as part of this demonstration. An essential ingredient of the technology validation is the development of accurate life cycle cost data and operational experience. Most of the technology to be reported in this group of papers is directly supported by the ACEE/LFC program; consequently, it is focused to help achieve the stated LFC program goals. The LFC program is planned in three phases. Phase I consists of technology development and system studies; Phase II consists of technology demonstration and system development; and Phase III consists of technology validation through systems demonstration. The major elements of the Phase I program are shown in figure 5. They are

Airfoil development and test

Development and improvement of design methods

Evaluation of leading-edge contamination

LFC system definition and concept evaluation

Airfoil Development and Test:

As shown in figure 1 an LFC aircraft can provide significant improvement over a comparable turbulent-flow transport aircraft. This implies that it can take advantage of technology gains in other areas. One of these areas is supercritical airfoil development. Supercritical airfoils offer the promise of large performance improvement over conventional airfoils. For a given drag-divergence Mach number M_{DD}, the advantage appears as either higher section lift coefficient c_l or increased thickness-chord ratio t/c as shown in figure 6. Obviously, it is essential that a supercritical airfoil which lends itself to laminarization be developed. Using newly developed airfoil transonic-flow methods, it is possible to define candidate airfoils having the desired LFC characteristics with a high degree of confidence, thereby minimizing the amount of development testing. The process, which led to the definition of an airfoil shape for the subscale LFC swept airfoil experiment, will be discussed in the paper by Allison and Dagenhart. The primary difference between the pressure distribution on these airfoils and turbulent-flow supercritical airfoils is that at the design condition the upper surface supercritical flow decelerates isentropically without the generation of a shock, thereby avoiding the need to laminarize the boundary layer through the rapid pressure rise associated with a shock.

Development and Improvement of Design Methods:

The methods used during the X-21 program for stability analysis and determination of suction requirements were empirical in nature. During the ensuing years, progress has been made in the development of computing techniques which allow a direct calculation of the growth of disturbances in the boundary layer. These advances provide the opportunity for greater insight into the mechanism of transition and the effect of suction on this mechanism. Furthermore, they will reduce the uncertainty associated with the design of suction systems and allow the determination of optimized suction requirements. This could lead to significant improvements in airplane efficiency by reducing the size of the system components. Minimizing the degree of oversuction has further benefits such as reducing the equivalent suction drag, reducing the laminar skin friction, and reducing the sensitivity to surface roughness. The paper by Srokowski will outline a recently developed method for determining the growth of disturbances in an incompressible boundary layer, assuming the flow is parallel and ignoring nonlinear effects. In addition, he will discuss the effect some of these assumptions will have on disturbance growth and suction rates.

Leading-Edge Contamination:

It has long been known that maintaining the smoothness of the leading-edge region of an airfoil is essential for laminar flow. For flight conditions representative of commercial transport cruise conditions, the allowable height of a roughness particle which can be tolerated is of the order of 1 mm. This height is significantly smaller than insect excrescence found on current aircraft. Consequently, some means of eliminating or reducing insect excrescence must be found if one expects to develop an economically viable LFC transport. The controlling parameter is Reynolds number based upon the roughness dimension and local flow quantities. Previous experiments indicate that for values of roughness Reynolds number less than about 200, a laminar boundary layer can be maintained. This can be achieved by either keeping the roughness particle heights below a given value or by flying at very high altitudes. Since aircraft configurations envisioned for the 1990 time period will not be able to fly most efficiently at these higher altitudes (fig. 7), some methods must be developed for restricting excrescence size to allowable levels. The paper by Peterson and Fisher describes recent efforts to evaluate both passive and active approaches to this problem.

LFC System Definition and Concept Evaluation:

In addition to addressing specific issues, the LFC program has also attempted to identify potential market opportunities and possible configurations for the 1990 time period. The reduction in drag which results from laminarizing the boundary layer on an airplane can be translated into range capability which allows many new city pairs to be economically served. For configurations envisioned for the 1990 time period, design ranges over 5000 n. mi. appear to be achievable providing key technical problems can be resolved. As indicated previously, one of these deals with the emergence of supercritical airfoils. Another requires the efficient integration of structural and airflow requirements to minimize the parasitic weight associated with LFC systems. However, candidate approaches cannot ignore the operational requirements such as inspection, maintenance, and repairs; consequently, many trade-offs are possible. The advent of developments in both metallic and nonmetallic materials must be considered for any future aircraft; however, regardless of which of these approaches appears most attractive, the unique LFC requirements associated with smoothness and waviness almost dictate that new techniques for fabrication of aerodynamic surfaces must be developed. These trade-offs will be discussed in three papers which have resulted from contractual efforts by Boeing Commercial Airplane Company (BCAC), Douglas Aircraft Company (DAC), and Lockheed-Georgia Company (GELAC), along with some interesting approaches to the solution of specific design problems associated with the LFC system. The work breakdown structure for these contracts is as follows:

Evaluation of laminar flow control system concepts for subsonic commercial transport aircraft

Mission definition baseline configuration

Concept evaluation

Aerodynamics

Structures and materials

Suction system

Auxiliary system

Leading-edge cleaning/protection

Configuration selection and assessment

Recommended subsystem development

The baseline configurations selected by the three companies along with the design mission are shown in figure 8. Detailed information on the aircraft configurations will be provided in three papers by Gratzer, Sturgeon, and Pearce. Sturgeon will discuss the results to date of the GELAC efforts to define a practical design for an LFC transport and also the results of environmental and structural testing of a composite wing design in which the suction ducting is an integral part of the load-carrying structure. Gratzer will discuss the results to date of the BCAC efforts. Boeing has also chosen as a baseline approach an integral structural concept using bonded aluminum honeycomb with a slotted aluminum or plastic strip used to remove the boundary-layer air. He will also discuss the results from a series of wind-tunnel tests on a full-scale swept airfoil with suction. Pearce will focus his presentation on the development of porous composite panels which would be used on the Douglas concept. Douglas has chosen as a baseline structural concept a "glove" approach. That is, the outer surface panel is used solely for boundary-layer air removal and does not carry significant structural loads. He will present data from the aerodynamic and structural tests which have been performed to date on the baseline panel concept.

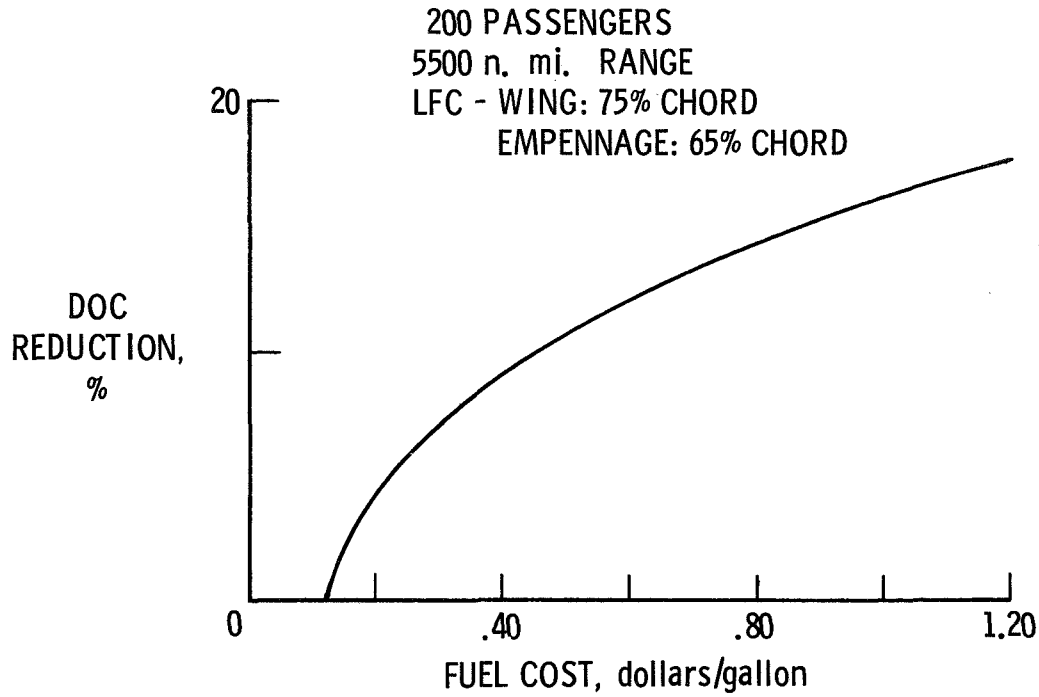

Figure 1.- Economic advantage of an LFC transport over a comparable turbulent-flow transport. (1 gallon = 3.8 liters.)

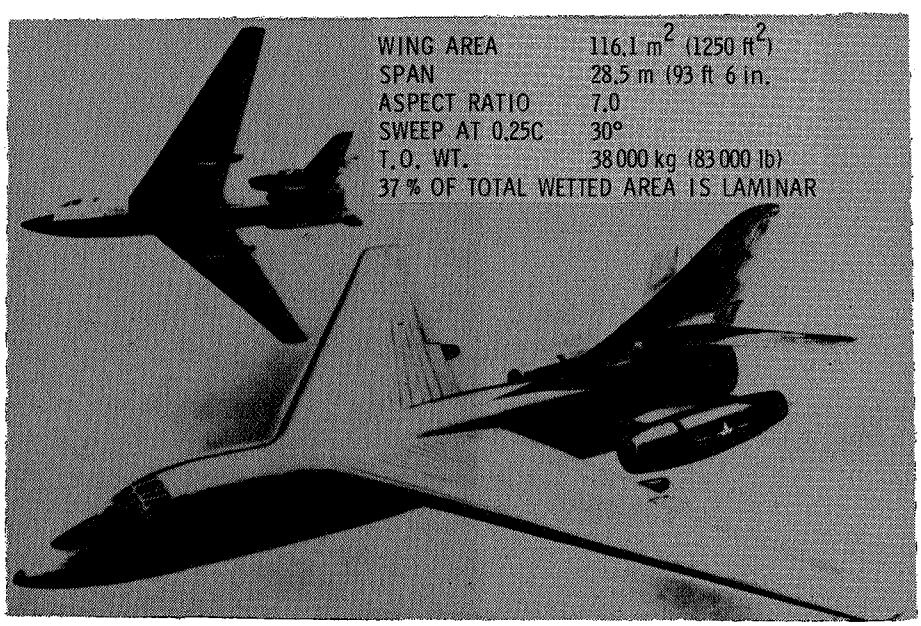

Figure 2.- U.S. Air Force X-21A aircraft.

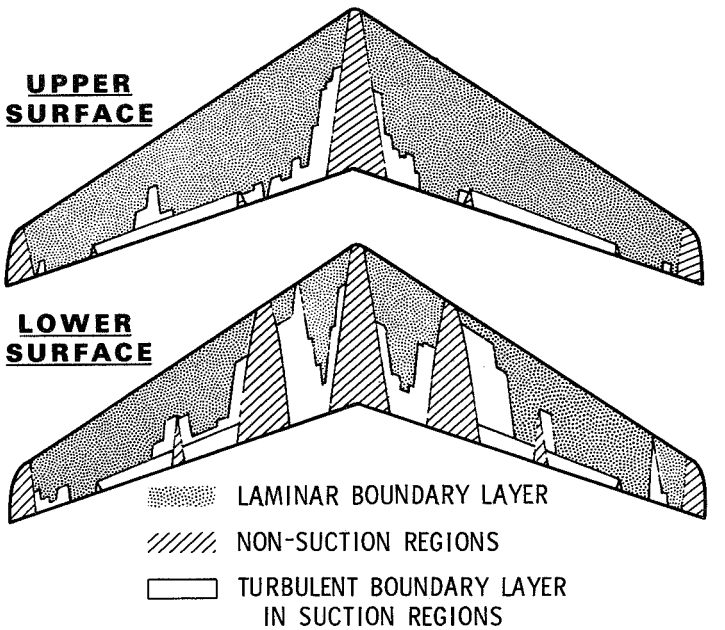

Figure 3.- Typical degree of laminarization achieved on the X-21 wing upper and lower surfaces.

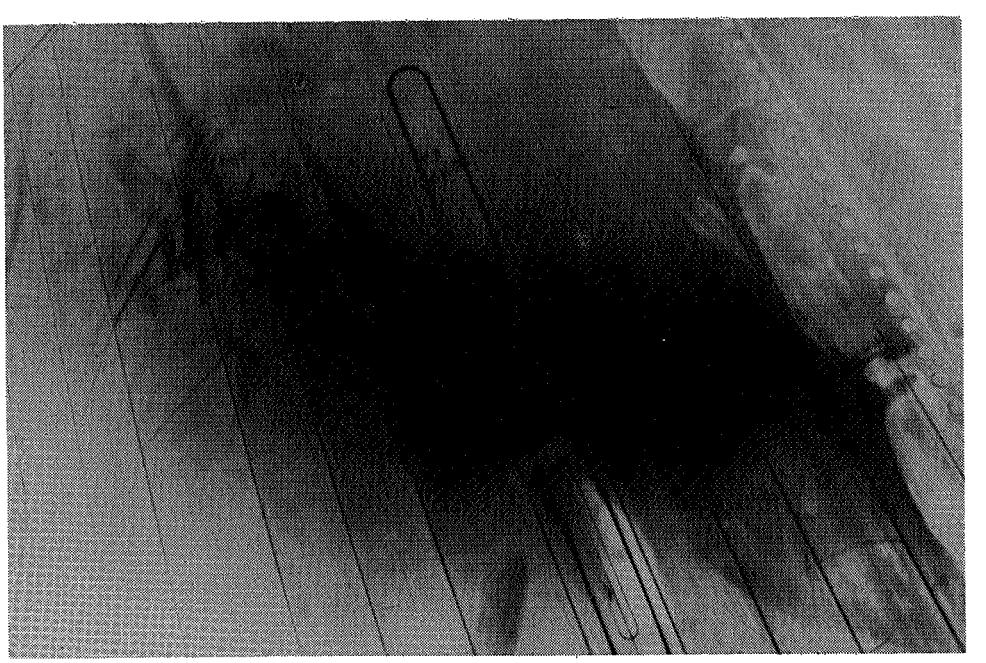

Figure 4.- X-21A wing showing repairability of LFC surface.

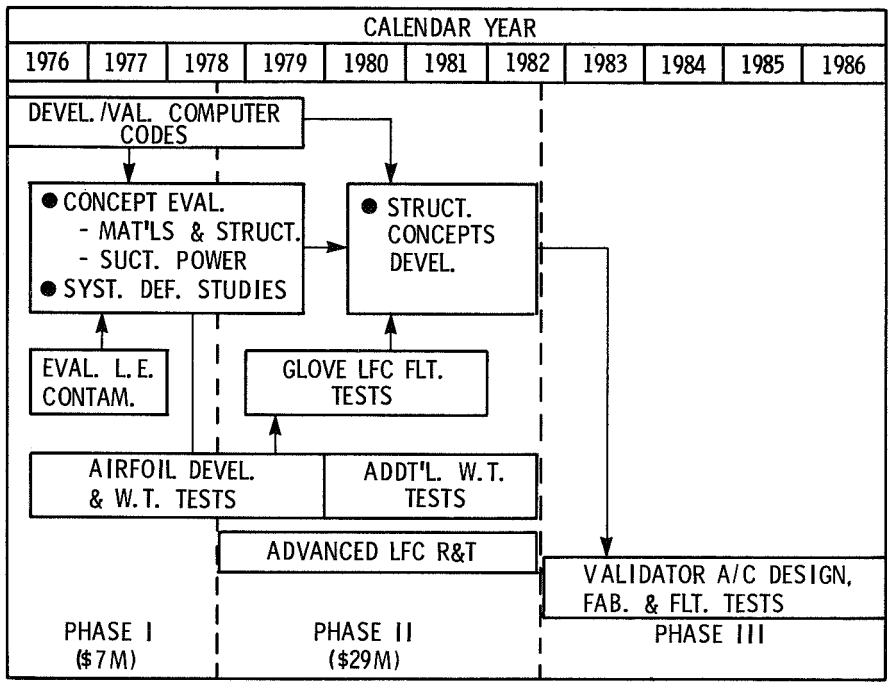

Figure 5.- Laminar flow control program plan.

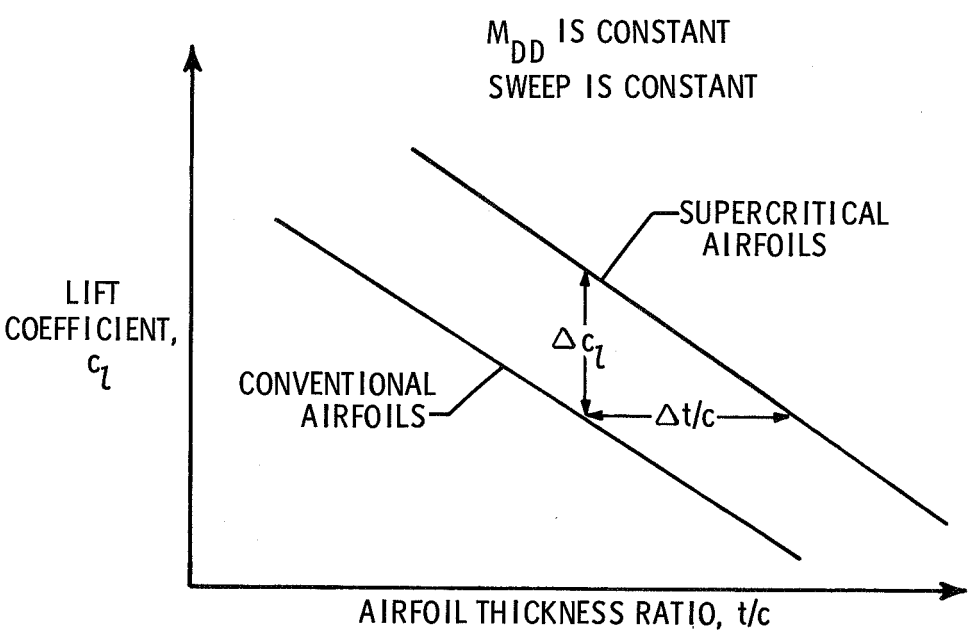

Figure 6.- Performance advantage of current supercritical airfoils.

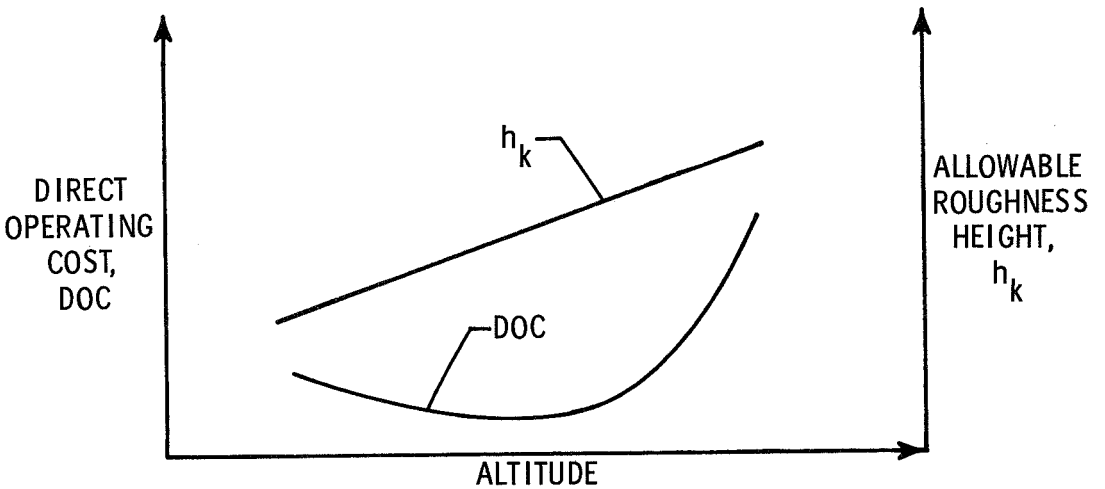

Figure 7.- Effect of altitude on aircraft direct operating cost and allowable roughness height h_k.

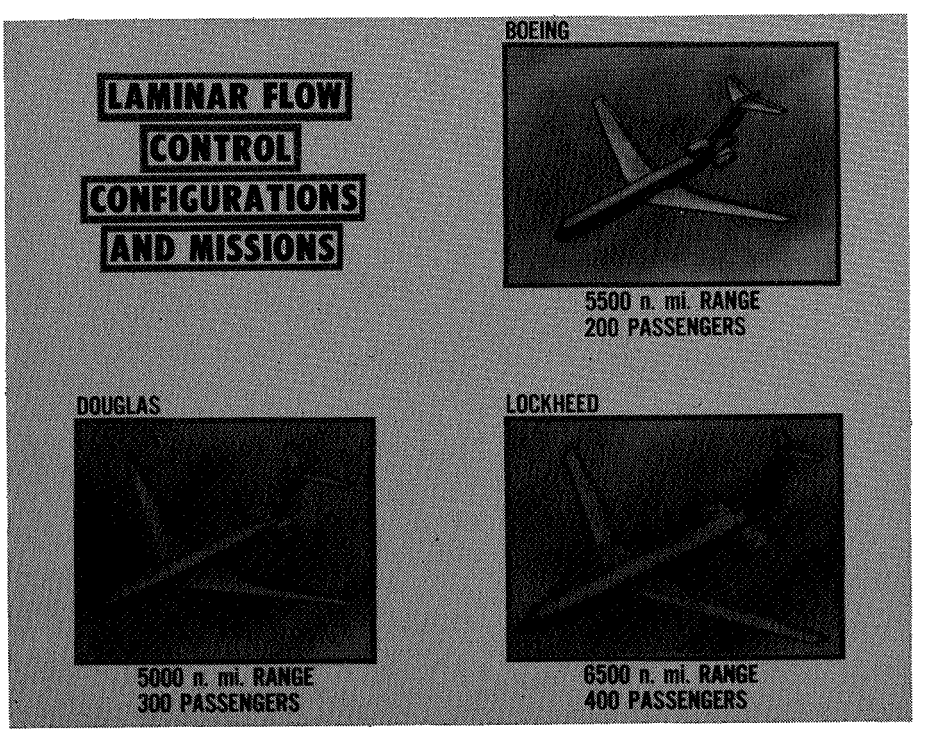

Figure 8.- Selected LFC missions and baseline aircraft configurations.

FLIGHT INVESTIGATION OF INSECT CONTAMINATION AND ITS ALLEVIATION

John B. Peterson, Jr.
NASA Langley Research Center

David F. Fisher
NASA Dryden Flight Research Center

SUMMARY

An investigation of leading-edge contamination by insects was conducted at Dryden Flight Research Center with a JetStar airplane instrumented to detect transition on the outboard leading-edge flap and equipped with a system to spray the leading edge in flight. The results of airline-type flights with the JetStar indicated that insects can contaminate the leading edge during take-off and climbout at large airports in the United States. The results also showed that the insects collected on the leading edges at 180 knots did not erode at cruise conditions for a laminar flow control airplane and caused premature transition of the laminar boundary layer. None of the superslick and hydrophobic surfaces tested showed any significant advantages in alleviating the insect contamination problem. While there may be other solutions to the insect contamination problem, the results of these tests with a spray system showed that a continuous water spray while encountering the insects is effective in preventing insect contamination of the leading edges.

INTRODUCTION

One of the concerns of the designers of a laminar flow control airplane is the possibility that insect remains gathered on the leading edges of the wing during take-off will cause premature transition of the laminar boundary layer during cruise flight. If this occurs, a significant increase in drag could result, possibly negating the fuel savings that laminar flow control can achieve.

Previous insect tests made with a Handley Page "Victor" jet in England (ref. 1) showed that insect remains on the leading edges of the wing were eroded to only one-half their height after a high altitude cruise flight. This erosion of insect remains leads to the possibility that laminar flow might be maintained at the low unit Reynolds numbers obtainable at very high cruising altitudes. Also, experience with an F-94 laminar flow control glove wing indicated that insect contamination was not a problem in flight tests at Edwards Air Force Base at altitudes above 6000 m (20 000 ft). (See ref. 2.) However, the insect population at Edwards Air Force Base is probably much less than in most other areas of the United States.

An examination of the leading edges of jet airplanes based at Langley Research Center before the present flight investigation indicated that insect remains high enough to cause transition at altitudes above 12 000 m (40 000 ft) were present. Whether these insects were picked up during take-off and remained on leading edges during cruise or whether they were only picked up during landing could not be determined, however.

SYMBOLS

C_L	airplane lift coefficient
c	wing chord
h	altitude
k	roughness height
M	Mach number
R_k	roughness Reynolds number, $\frac{u_k k}{\upsilon}$
s	surface distance from the leading edge
u_k	velocity at top of roughness in laminar boundary layer
x	distance from leading edge along chord
Λ	leading-edge sweep
υ	kinematic viscosity
DFRC	Dryden Flight Research Center
L.E.	leading edge
LFC	laminar flow control

DISCUSSION

In order to investigate the insect contamination problem, a flight experiment was conducted using a JetStar airplane at Dryden Flight Research Center. Four aspects of the problem were investigated: (1) investigate the extent of the insect problem at large airports, (2) if the insects were found to be a problem, determine whether insects would erode during cruise flight to a height below that which causes transition, (3) test the ability of new surfaces like superslick and hydrophobic surfaces to alleviate the problem of insect

contamination, and (4) test a leading-edge spray system to determine how well it would protect the leading edge.

A photograph of the JetStar airplane used in the experiments is shown in figure 1. A view of the left outboard leading-edge flap instrumented for this experiment is shown in figure 2. The instrumented flap covered 230 cm of the leading edge spanwise. Figure 3 shows a close-up photograph of the instrumentation used on the flap. The pitot probes shown in figure 3 were spaced every 5 cm spanwise along the flap.

A cross-section drawing of the leading-edge flap showing the instrumentation and spray system is shown in figure 4. The boundary-layer pitot tubes shown 0.13 cm above the surface were located at the outer edge of the laminar boundary layer on the leading edge so that the thicker turbulent boundary layer would cause a reduction in the pitot pressure measured by these tubes, if transition occurred ahead of the pitot tubes. This reduction in pressure from the reference pitot pressure obtained from the reference probe at 5 cm above the surface was calibrated by test flights with known transition locations so that the location of transition on the insect contamination flights could be determined. The spray nozzle, shown under the leading edge, sprayed the mixture out in front of the leading edge where the airstream blew it back onto the leading edge during take-off and flight. These nozzles were designed especially for these tests to protect the upper surfaces of the leading edge only and would not be satisfactory for an actual laminar flow control airplane since the spray nozzles themselves would cause transition on the lower surfaces. Two spray tubes at different angles were used since the spray was blown back at different angles at the various angles of attack encountered during the take-off run and during flight.

A plan view drawing of the JetStar's outboard wing section indicating the test surfaces is shown in figure 5. Each of the five test areas was 46 cm wide. The first two test areas inboard were superslick Teflon surfaces. The next two were hydrophobic coatings. The first of the hydrophobic coatings is used on the airplane windshields to shed rain and the second is used on radomes to shed rain. The fifth surface was a standard reference surface of aluminum alloy. Also, shown are the boundary-layer pitot tubes on the upper surface and spray nozzles under the leading edge.

The effect of three-dimensional-type roughness on the boundary layer on the leading-edge flap of a JetStar at cruise conditions ($M = 0.70$, $h = 11\ 600$ m (38 000 ft) and $C_L = 0.3$) is shown in figure 6. The curves shown in this figure are based on the criteria for roughness height to cause transition given in reference 3. Roughness heights above the crosshatched area will cause transition and those below the crosshatched area will not cause transition. In the crosshatched area, the shape of the roughness particle determines whether it will cause transition. As shown in figure 6, roughness heights above about 0.023 cm will cause transition on the JetStar leading edge and heights below about 0.008 cm will not cause transition.

In order to determine if insects high enough to cause transition would accumulate on the leading edges of airplanes that take-off at large

airports, the JetStar was flown on 15 airline-type take-offs at the locations shown in figure 7. These flights consisted of a normal take-off and climbout without spraying the leading edge. After reaching a cruise altitude of 11 600 m (38 000 ft), the pitot-tube pressures were recorded at Mach 0.70 and a C_L of 0.3. After landing, the leading-edge test areas were inspected and the location of any insects on the leading edges were recorded and their heights measured with a microscope. Insects were found on all but two of the 15 airline-type flights. The number of insects found ranged from 3 to 17.

A plot of the test results from three of the airline-type flights is shown in figures 8, 9, and 10. These airline-type flights were made from Los Angeles, Scramento, and San Francisco in November 1977 and all the landings for inspection of the leading edge after the high altitude cruise were made at DRFC. The figures show an outline of the test areas on the leading-edge flap and the location of insects found on the leading edge are indicated by circles. The area of the circles indicates the measured height of the insect as shown by the keys in the figures. Active pitot tubes are indicated along the top line of the flap outline and transition measured at cruise conditions indicated by a crosshatched area ahead of a pitot tube. The distance ahead of the pitot tubes that transition occurred as determined from the measured pitot pressures is represented by the length of the crosshatched area ahead of the pitot tube, but the area of the crosshatched region does not indicate the actual area of turbulent flow, which is generally wedged shaped and may be either larger or smaller than the crosshatched area shown. The exact shape of the area of turbulent flow could not be determined from pitot-tube data since they were spaced too far apart.

As shown in figures 8 and 9, transition was caused by insect remains on the leading edge ahead of one of the pitot tubes on each of these flights. Apparently, then, some means of protecting the leading edges must be used if transition caused by insect remains is to be avoided.

A close-up photograph of an insect splatter before and after a 15-min cruise at 11 600 m (38 000 ft) and M = 0.75 is shown in figure 11. The insect was picked up on the Teflon tape surface during low passes over agricultural fields near DFRC at 180 knots. It was located at $s/c \approx 0.015$ and its measured height both before and after the high altitude cruise was 0.018 cm. Both the measured heights and the closeup photographs in figure 11 indicated that no erosion of the insect remains took place during the high altitude cruise. As stated in the introduction, tests with a Handley Page "Victor" jet in England (ref. 1) indicated that insect remains were eroded to about one-half their height after a high altitude cruise. Apparently, the reason for this difference was because the insects were blown against the leading edges of the "Victor" jet at about 50 knots and the wings, legs, and antenna were still intact after impact. The height of the insects was probably reduced when the wings, legs, and antenna were eroded by the high altitude cruise. During the JetStar tests, the insects were impacted at 180 knots and erosion of the wings, legs, and antenna took place immediately and no further erosion took place at cruise conditions.

In order to give the JetStar leading-edge spray system a severe test, the JetStar was flown at low altitudes over agriculture fields near DFRC in an area with a high density of flying insects. The photograph in figure 12 shows the density of insect splatters on the leading edge of the JetStar after a typical series of low passes.

Two of the types of insects found over the fields near DFRC are shown in figure 13. The photograph on the left shows an aphid whose body diameter is about 0.8 mm and the photograph on the right shows a checkered beetle whose body diameter is about 2.3 mm. These insects were collected in a net from a light plane during low passes over the same agriculture field used in the JetStar experiments.

After the low passes with the JetStar were completed, it was landed at Dryden Flight Research Center and the leading edges were examined to determine the location and size of any insect remains on the leading edge. The JetStar was then flown to an altitude of 11 600 m (38 000 ft) and the pitot-tube pressure data were taken at $M = 0.70$ and $C_L = 0.3$. Five types of low pass flights were made with the JetStar to test the spray system:

(1) No spray
(2) Water-detergent spray after all low passes
(3) Large droplet water-detergent spray after each low pass
(4) Continuous water spray during low passes
(5) Intermittent water-detergent spray during low passes

The first test was a calibration flight without spray to determine how many insect splatters were encountered during the low passes. As shown in figure 14, many insect splatters accumulated on the leading edge and transition occurred in front of many of the pitot tubes during the high altitude portion of this flight.

Next the spray system was used in an attempt to wash the insects off the leading edges. A photograph of the spray pattern from the spray tubes under the leading edge is shown in figure 15. The body shown in the foreground is the wing-mounted auxiliary fuel tank. The JetStar was in level flight at an altitude of 900 m (3000 ft) and a speed of 180 knots when this photograph was taken. Shown in figure 16 are the results of spraying the leading edge with a water-detergent mixture (0.3 percent liquid detergent) for about 2 min at a rate of 58 kg/min/m^2 of frontal area after all low passes were completed. As can be seen, the spray mixture was not able to wash the insect remains off the leading edge after impact and transition occurred ahead of many of the pitot tubes during the high altitude portion of this flight.

A large droplet water-detergent spray was tried next and the results are shown in figure 17. The spray rate was increased to 205 kg/min/m^2 for about 5 sec after each low pass over the agriculture fields. This larger spray rate was obtained by increasing the diameter of the spray nozzles and blocking off some of them so that only the areas indicated in figure 17 were sprayed. The large doplet spray eliminated some of the insects and reduced the height of the remaining insects in the sprayed areas. Although none of the remaining insects were high enough to cause transition, it is not known whether this

kind of spray would erode larger insects below the critical height. No high altitude portion of this flight was flown.

The results of a continuous water spray is shown in figure 18. Water was sprayed at 24 kg/min/m^2 continuously while encountering the insects during the low passes. No insects were found in the sprayed areas and the boundary layer was laminar ahead of all the pitot tubes during the high altitude portion of the flight. These results show that a continuous water spray was effective in protecting the leading edge from insect contamination. Although the spray system was not optimized for these tests, the analysis of reference 4 showed that the weight penalty of a spray system should be less than 1 percent of the gross weight of an LFC airplane.

In an attempt to use less spray, an intermittent spray during the low passes was tried next. A water-detergent mixture at 29 kg/min/m^2 was sprayed alternately "on" for 2 sec and "off" for 3 sec while encountering insects. The results shown in figure 19 indicate that an intermittent water-detergent spray was unsuccessful since many insect remains were found on the leading edge. No high altitude portion of this flight was flown

CONCLUDING REMARKS

An investigation of the insect contamination problem was conducted at Dryden Flight Research Center with a JetStar airplane instrumented to detect transition on the outboard leading-edge flap and equipped with a system to spray the leading edge in flight. The results of airline-type flights with the JetStar indicated that insects can contaminate the leading edge during take-off and climbout at large airports in the United States. The results also showed that the insects collected on the leading edges at 180 knots did not erode at cruise conditions for a laminar flow control (LFC) airplane and caused premature transition of the laminar boundary layer. None of the super-slick and hydrophobic surfaces tested showed any significant advantages in alleviating the insect contamination problem. The Teflon surfaces, however, were easier to clean after the test flights than either the hydrophobic or aluminum surfaces. Very light pressure while wiping the leading edge with a damp cloth was sufficient to clean the insect remains off the Teflon surface.

While there may be other solutions to the insect contamination problem, the results of these tests with a spray system showed that a continuous water spray while encountering the insects is effective in preventing insect contamination of the leading edges. Although the spray system was not optimized for these tests, an analysis has shown that the weight penalty of a spray system should be less than 1 percent of the gross weight of an LFC airplane

REFERENCES

1. Lachmann, G. V.: Aspects of Insect Contamination in Relation to Laminar Flow Aircraft. C.P. NO. 484, British A.R.C., 1960.

2. Pfenninger, W.; and Groth, E.: Low Drag Boundary Layer Suction Experiments in Flight on a Wing Glove of an F-94A Airplane With Suction Through a Large Number of Fine Slots. Boundary Layer and Flow Control, Volume 2, G. V. Lachmann, ed., Pergamon Press, Inc., 1961, pp. 981-999.

3. Von Doenhoff, Albert E.; and Braslow, Albert L.: The Effect of Distributed Surface Roughness on Laminar Flow. Boundary Layer and Flow Control, Volume 2, G. V. Lachmann, ed., Pergamon Press, Inc., 1961, pp. 657-681.

4. Sturgeon, R. F.; Bennett, J. A.; Etchberger, F. R.; Ferrill, R. S.; and Meade, L. E.: Study of the Application of Advanced Technologies to Laminar-Flow Control Systems for Subsonic Transports. Volume II: Analyses. NASA CR-144949, 1976.

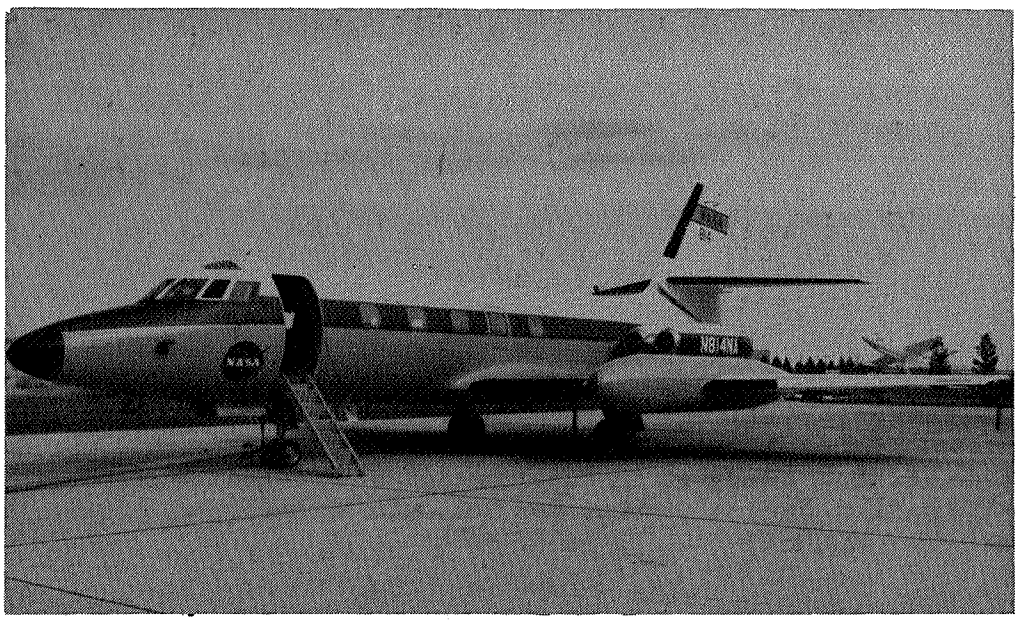

Figure 1.- JetStar at DFRC used in LFC insect contamination study.

Figure 2.- Outboard leading-edge flap of JetStar instrumented for LFC insect contamination study.

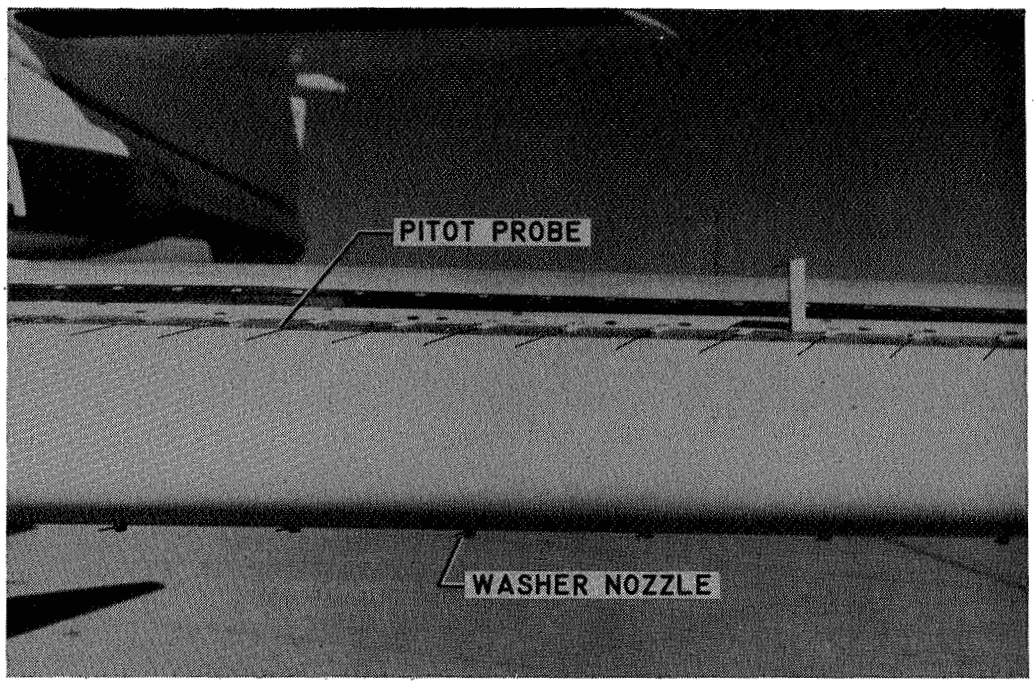

Figure 3.- Leading-edge-flap instrumentation and washer nozzles.

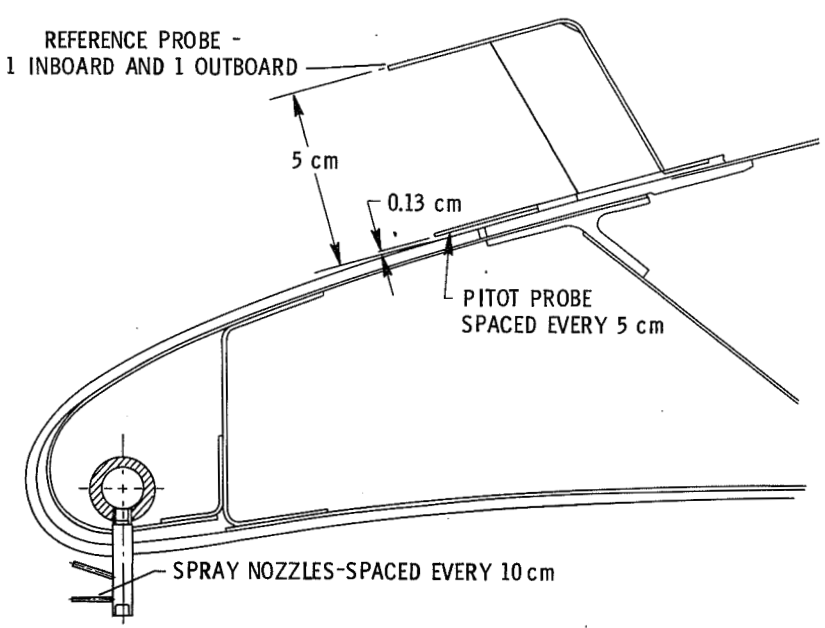

Figure 4.- Cross-section drawing of instrumented leading-edge flap.

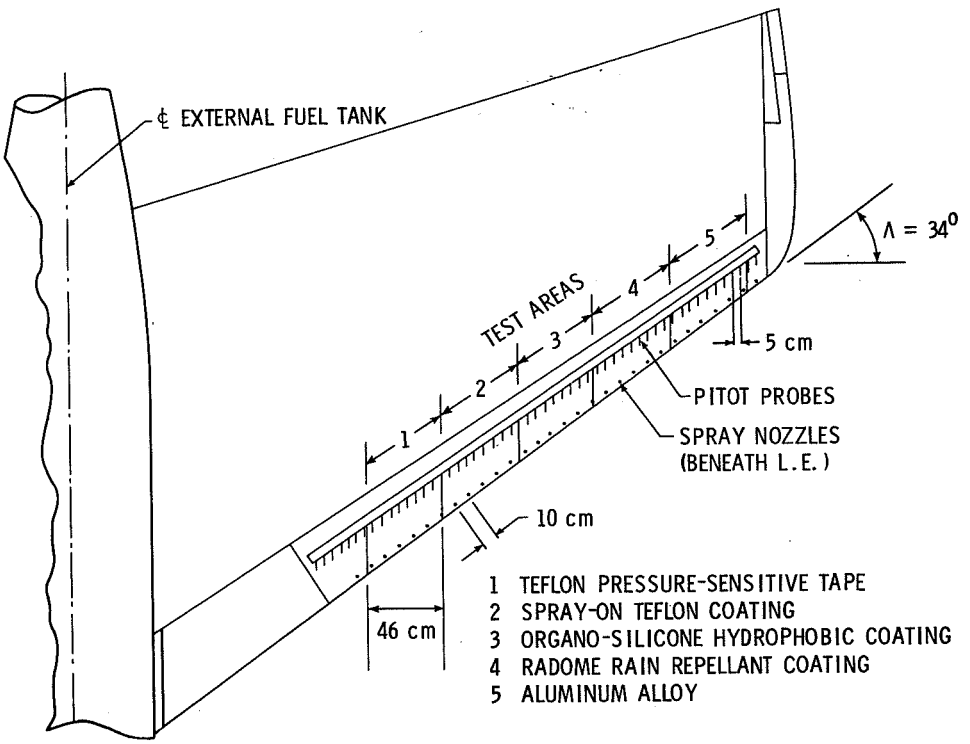

Figure 5.- Plan-view drawing of JetStar outboard wing area.

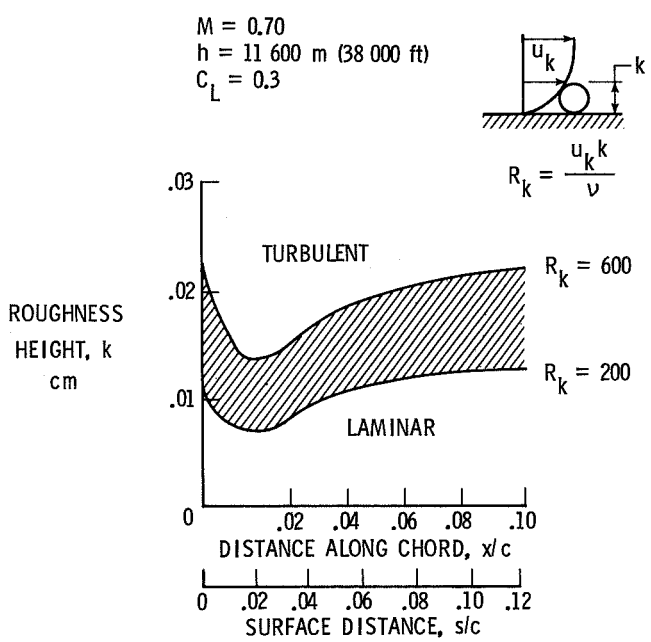

Figure 6.- Effect of three-dimensional roughness on JetStar leading-edge flap.

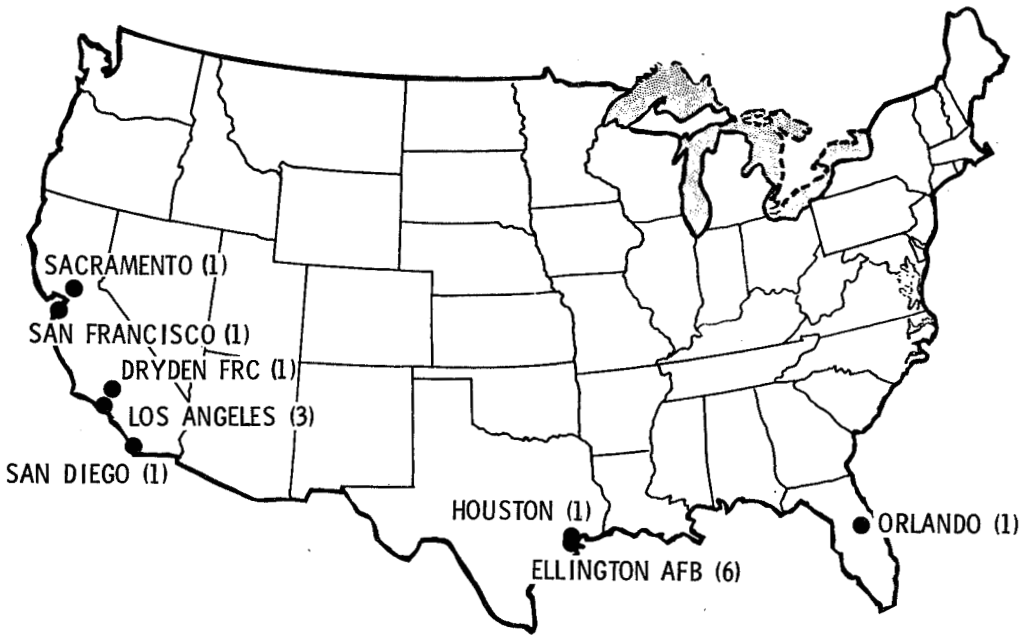

Figure 7.- Location of airline-type flights.

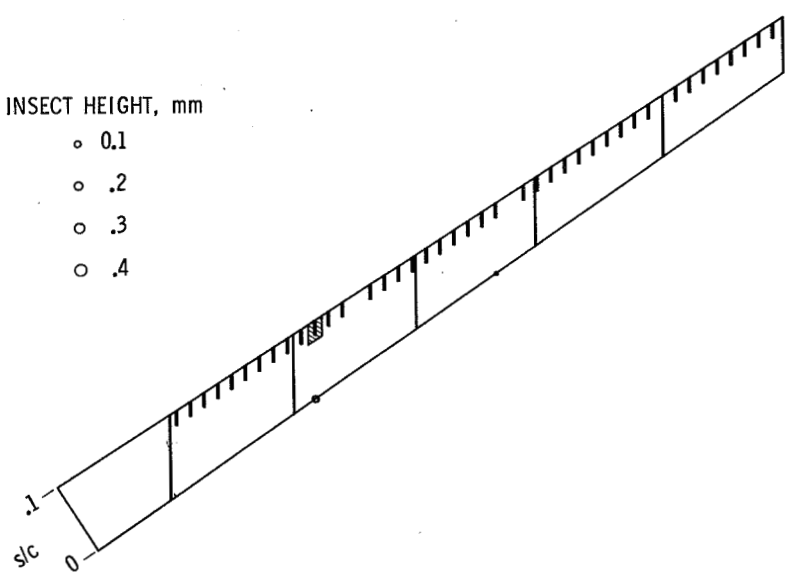

Figure 8.- Diagram of JetStar leading-edge flap showing results of airline-type take-off from Los Angeles International Airport.

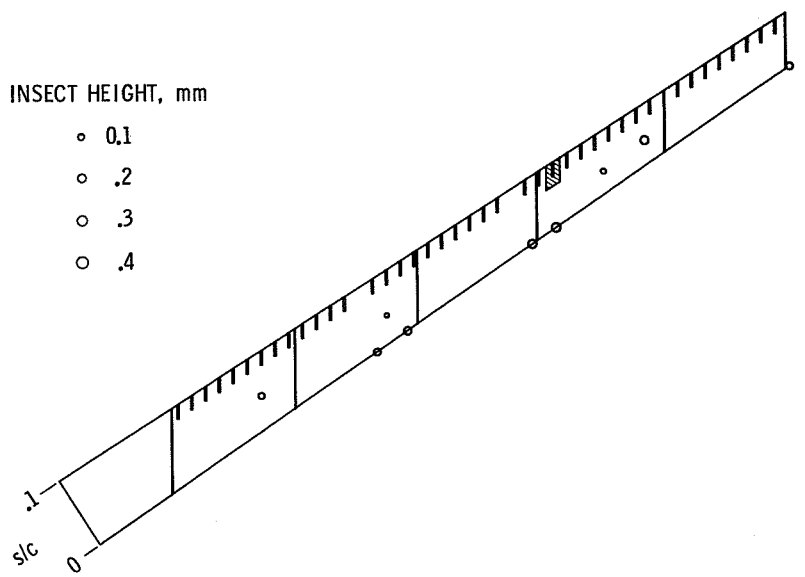

Figure 9.- Diagram of JetStar leading-edge flap showing results of airline-type take-off from Sacramento Metropolitan Airport.

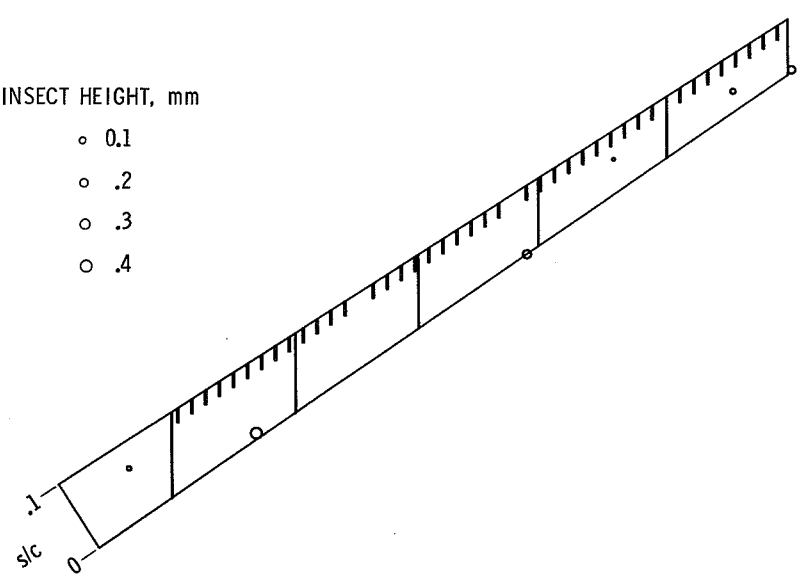

Figure 10.- Diagram of JetStat leading-edge flap showing results of airline-type take-off from San Francisco International Airport.

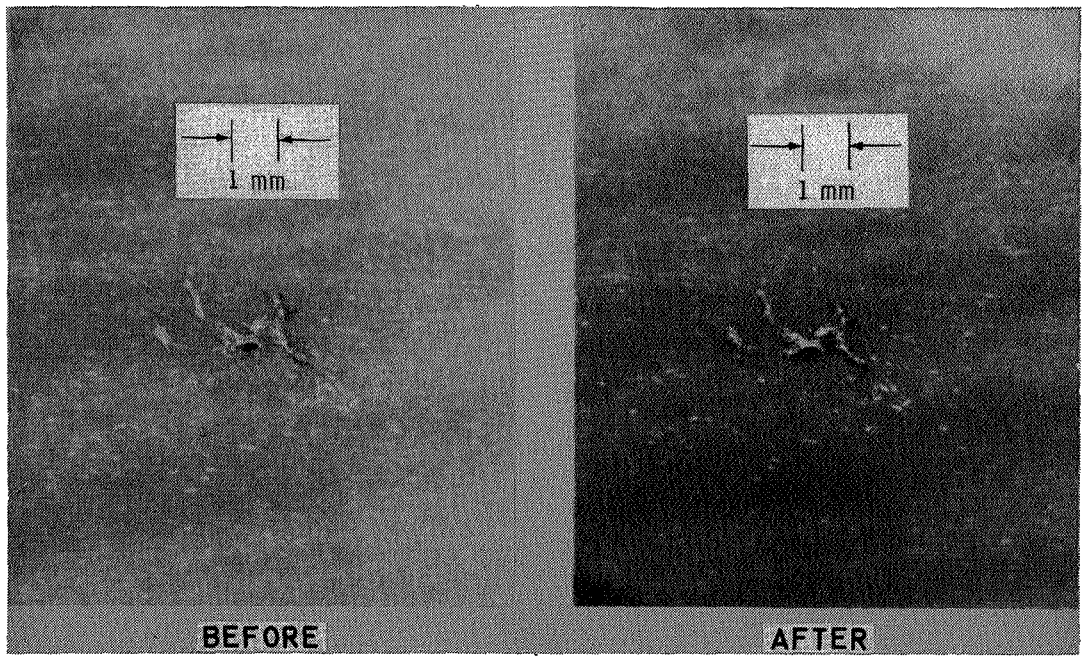

Figure 11.- Erosion of insect splatter by a 15-min cruise at M = 0.75 and h = 11 600 m (38 000 ft).

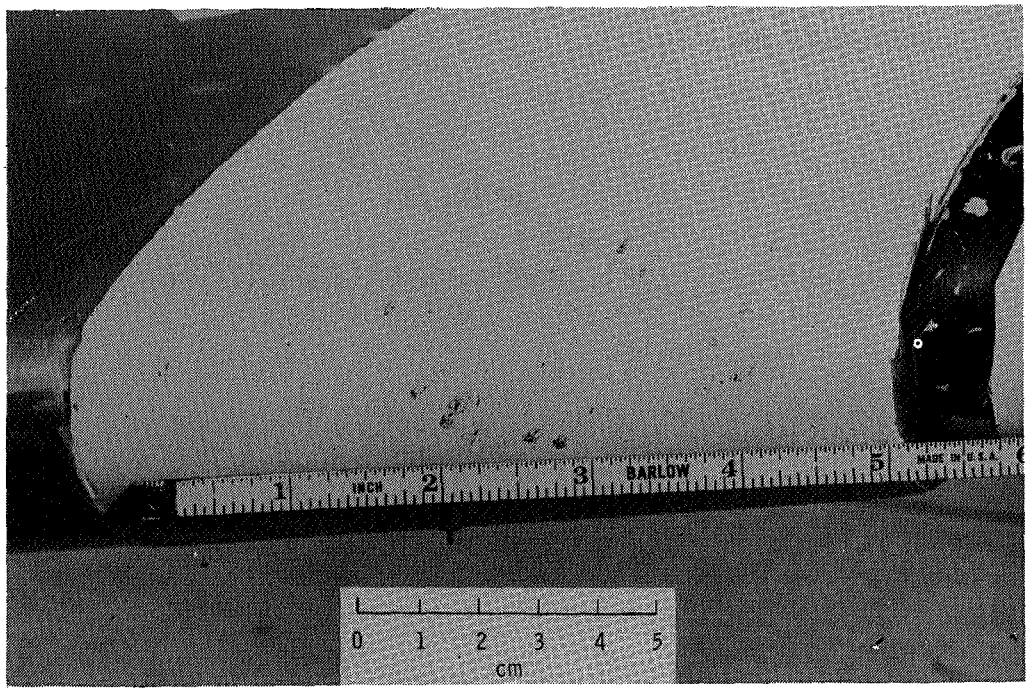

Figure 12.- Insect splatters on leading edge of JetStar after low passes over agriculture fields.

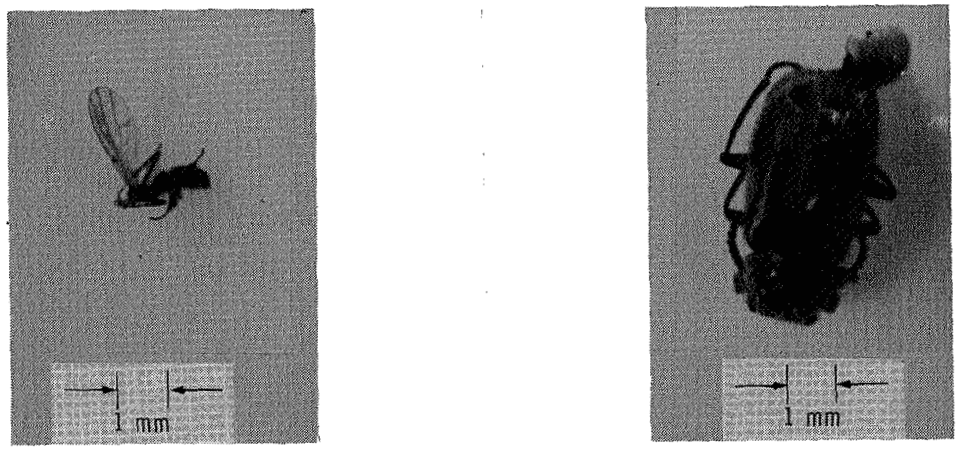

Aphid

Checkered beetle

Figure 13.- Typical insects found over agriculture fields near DFRC.

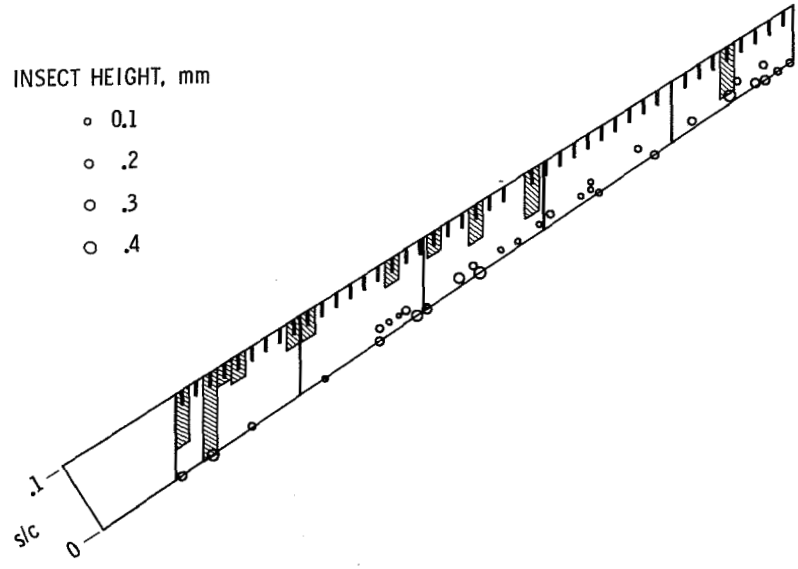

Figure 14.- Diagram of JetStar leading-edge flap showing results of low passes over agriculture fields without leading-edge spray.

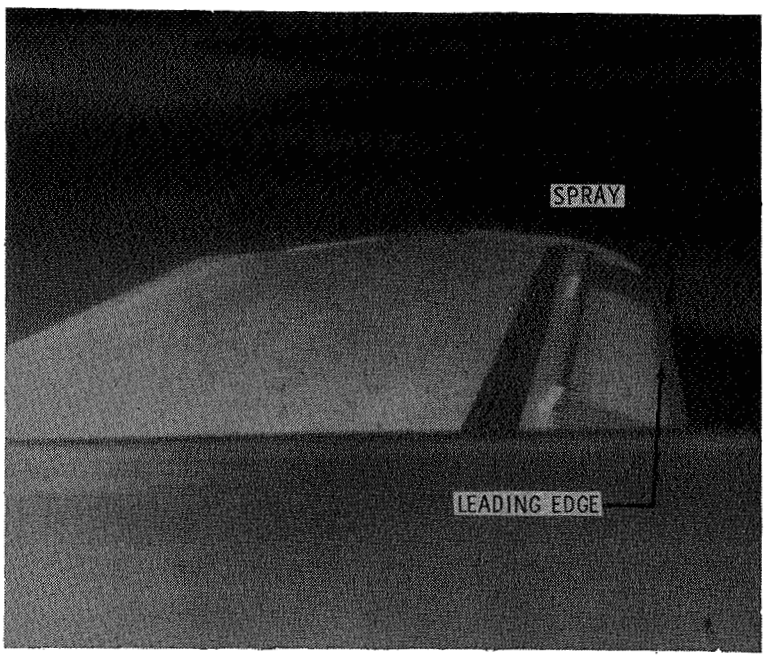

Figure 15.- Spray pattern from spray tubes under the leading edge.

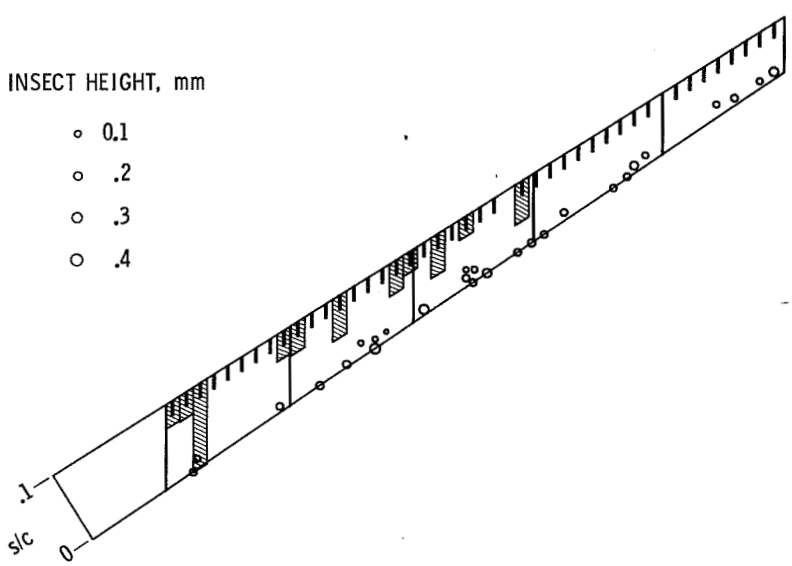

Figure 16.- Diagram of JetStar leading-edge flap showing results of water-detergent mixture spray after all low passes were completed.

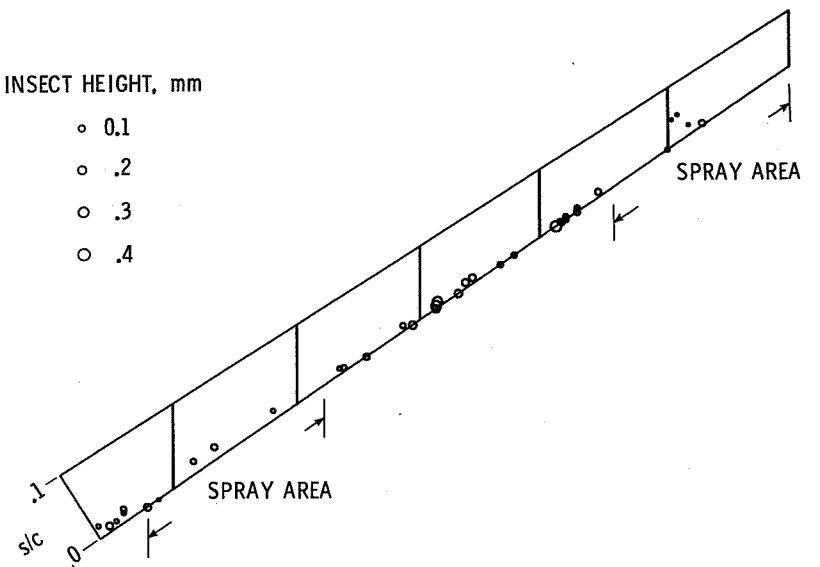

Figure 17.- Diagram of JetStar leading-edge flap showing results of large droplet water-detergent spray after all low passes were completed.

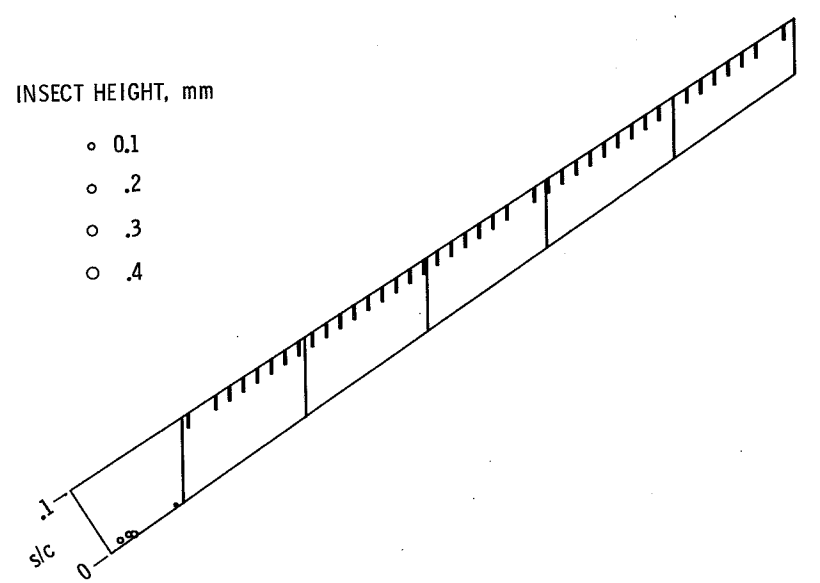

Figure 18.- Diagram of JetStar leading-edge flap showing results of continuous water spray during low passes.

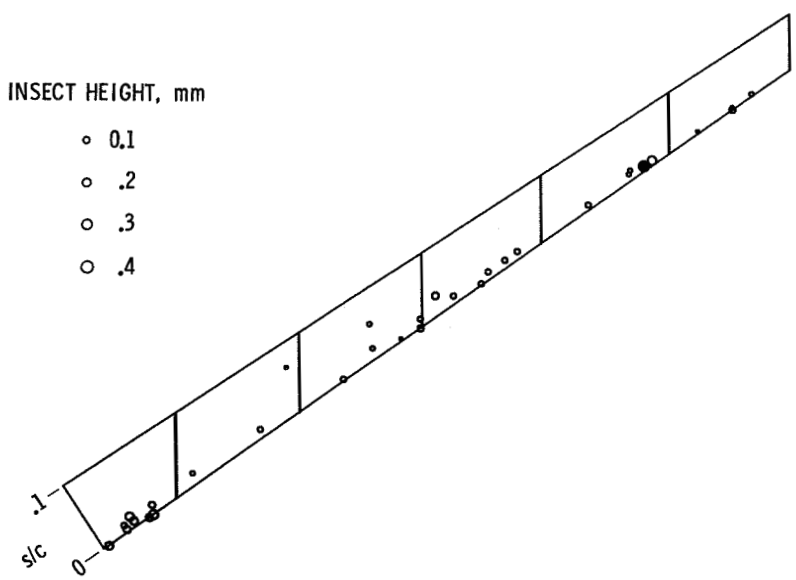

Figure 19.- Diagram of JetStar leading-edge flap showing results of intermittent water-detergent spray during low passes.

DEVELOPMENT OF ADVANCED STABILITY THEORY SUCTION PREDICTION TECHNIQUES FOR LAMINAR FLOW CONTROL

Andrew J. Srokowski
NASA Langley Research Center

SUMMARY

The problem of obtaining accurate estimates of suction requirements on swept laminar flow control wings is discussed. A fast accurate computer code developed to predict suction requirements by integrating disturbance amplification rates is described. Assumptions and approximations used in the present computer code are examined in light of flow conditions on the swept wing which may limit their validity.

INTRODUCTION

The development of viable laminar flow control technology requires consideration of aerodynamics, structures, and maintainability. Advancements in aerodynamics and structures since the X-21 project of the early/middle sixties together with the projected world fuel supply/price situation have resulted in new efforts to develop laminar flow control (LFC) technology for subsonic CTOL transports (ref. 1). Both the aerodynamic and structural considerations in the design of an LFC transport are impacted by the gross amount and detailed distribution of the suction air flow required for laminar flow. The problem of predicting required suction flow rates on swept LFC wings has received little attention in the past 10 years. In this time span, new powerful computers and numerical techniques have evolved which permit the development of practical suction prediction methods using advanced boundary-layer stability theories. (See refs. 2 to 4.) The more sophisticated theories account better for the real-life physics of the boundary-layer stability/transition problem (ref. 5), and thus, allow a higher confidence level in the predicted suction rates for wing configurations and pressure distributions which may be considerably different from those for which experimental data are currently available.

This paper includes (1) a brief look at the physics of the transition problem; (2) a short review of prior methods for determining suction flow rates on swept LFC wings; (3) a general description of the present updated method and computer code and finally (4) other effects not accounted for in the present method, their relative importance, and regions of the swept wing for which they may have to be considered in future suction prediction techniques.

SYMBOLS

c wing chord taken parallel to free-stream direction

C_p pressure coefficient, $\dfrac{p - p_\infty}{0.5\rho_\infty U_\infty{}^2}$

L length scale

N natural logarithm of the ratio of a boundary-layer disturbance amplitude to its amplitude at neutral stability.

n crossflow boundary-layer velocity component (perpendicular to local potential velocity)

p static pressure

R local length scale Reynolds number, $\dfrac{\rho_e U_e L}{\mu_e}$

r radial distance to chord line in conical wing approximation

R_n crossflow Reynolds number, $\dfrac{\rho_e n_{max} \delta_{0.1n_{max}}}{\mu_e}$, where $\delta_{0.1n_{max}}$ is the height at which the crossflow velocity attains 10% of its maximum value (point furthest from the surface)

R_t tangential or streamwise Reynolds number, $\dfrac{\rho_e t_e \theta}{\mu_e}$

s surface distance

t streamwise or tangential boundary-layer velocity component (parallel to local potential velocity)

u_o component of boundary-layer velocity in direction normal to radial boundary-layer coordinate

U total velocity

v component of boundary-layer velocity normal to surface

V_G group velocity

w_o component of boundary-layer velocity along radial boundary-layer coordinate

x distance in chord direction

y	distance normal to surface
α	nondimensional wavenumber in u_0 direction (see figs. 4 and 5), $\frac{2\pi L}{\lambda_{u_0}}$
β	nondimensional wavenumber in w_0 direction, $\frac{2\pi L}{\lambda_{w_0}}$
δ	boundary-layer thickness
θ	boundary-layer momentum thickness of t profile
μ	viscosity
ρ	density
χ	crossflow Reynolds number, $\frac{\rho_e n_{max} \delta}{\mu_e}$
ψ	angle of line that is normal to the disturbance wavefront, $\tan^{-1}(\beta/\alpha)$; also perturbation stream function (eq. (5) and (6))
ω	nondimensional complex frequency

Subscripts

e	local potential flow
i	imaginary part
max	maximum
min	minimum
r	real part
W	wall
∞	free stream

PHYSICS OF THE STABILITY/TRANSITION PROBLEM

A simple visualization of the flow development on a flat plate would include sequentially an initial laminar linear region, a laminar nonlinear region, a transitional nonlinear region, and finally, turbulent flow. The relative length of the pre-turbulent regions depends to a significant extent on a multitude of factors such as surface roughness, free-stream noise and vorticity, and pressure gradient. Any of these factors, if strong enough, may cause some of the preturbulent region to be shortened or bypassed. A detailed discussion of such phenomena may be found in the literature (refs. 5 and 6).

For a laminar boundary layer exposed to relatively weak external disturbances, small disturbances undergo linear amplification. In two-dimensional incompressible flow, the disturbance waves which are amplified the most are those moving in the direction of the external flow (two-dimensional waves). They are due to viscous instability of the boundary layer (refs. 7 and 8).

The situation on a swept wing is complicated by the presence of boundary-layer crossflow. (See refs. 9 and 10.) Figure 1 indicates that near the leading and trailing edges of a swept wing, the slow moving fluid elements in the boundary layer close to the surface are more strongly deflected by the pressure gradients than fluid elements nearer to the edge of the boundary layer. Figure 2 illustrates the resulting boundary-layer profiles. The crossflow profile has an inflection point which is strongly destabilizing (inflexional instability). Thus, on a swept wing there are normally two types of instabilities: the viscous or Tollmien-Schlichting instability and the inflexional or crossflow instability. Figure 3 illustrates the stabilizing effect of suction on these profiles. This effect results from a thinning and alteration of the boundary-layer profile, and also, in the case of the crossflow instability, stronger damping when the inflexion point is brought nearer to the surface. If suction is strong enough, complete stabilization will result with all boundary-layer disturbances being damped. However, this condition would mean excessive suction rates with corresponding system penalties. (See ref. 11.) A more efficient design is to use suction rates and distributions which would allow disturbance growth to the point of incipient transition. The points that have been discussed so far are not new and have been known for the past 10 to 20 years. What is new is the methodology being developed to compute the amount and distribution of suction that will allow disturbances on a swept wing to grow to the point of incipient transition. This will be discussed after a brief review of some previous methods for swept LFC wings.

PREVIOUS METHODS

The method of direct integration of disturbance amplification rates obtained from linear/parallel stability theory computations has been recently used extensively for problems involving axisymmetric bodies in water (ref. 12). However, for the three-dimensional swept-wing problem, local methods have traditionally been used (ref. 13). By local is meant that at selected points along the chord, a flow quantity is examined, and flow stability evaluated solely from an experimental correlation involving that local quantity. One such method is known as the χ method (ref. 14).

In figure 2 there is a maximum crossflow velocity inside the viscous boundary layer. This velocity together with the boundary-layer thickness can be used to form a Reynolds number called the crossflow Reynolds number or χ. For a given experimental airfoil pressure distribution, χ can be calculated along the chord, and the value of χ obtained which corresponds to the physical transition location. A correlation is then obtained between allowable χ values and the extent of laminar flow. The idea is to apply suction to keep χ below a certain critical value so that laminar flow is not lost due to crossflow instability. The problem with this method is that the local crossflow Reynolds

number does not contain any information at all about the disturbance amplification history of the boundary layer which is vital to reliable transition predictions (ref. 5). Wing configurations and pressure distributions significantly different from those used in the correlation may have different levels of χ at transition.

Another local method is known as the X-21 method and was used to determine X-21 suction rates and distributions (ref. 15). This method incorporates stability calculations, but in a local sense. What is done is that the streamwise and crossflow boundary-layer profiles on a swept wing are first normalized in an appropriate fashion and neutral stability curves are then obtained from linear, parallel stability theory. Neutral stability means that condition where boundary-layer disturbances are neither amplified nor damped. The so-called crossflow and streamwise minimum critical Reynolds number ($R_{n,min}$ and $R_{t,min}$, respectively) obtained from neutral stability curves are then related to the second derivative of the appropriate velocity profile (streamwise or crossflow).

The relations that were obtained are (from ref. 15):

$$\text{Crossflow} \quad R_{n,min} = 60 - 0.7 \left(\frac{\partial^2 (n/n_{max})}{- \partial \left(y/\delta_{0.1n,max} \right)^2} \right) \tag{1}$$

$$\text{Streamwise} \quad (R_{t,min})^{1/3} = 6 - 127 \left(\frac{\partial^2 (t/t_e)}{\partial (y/\theta)^2} \right) \tag{2}$$

where n and t are the crossflow and streamwise velocities, respectively, (see fig. 2), y is distance normal to the surface, θ is the streamwise momentum thickness, and $\delta_{0.1n_{max}}$ is the distance above the surface where the crossflow velocity is 10 percent of its maximum value. These relations are valid only for the class of boundary-layer profiles for which they were derived. Additionally, they only track neutral stability.

For the X-21 suction predictions, it was necessary to obtain an idea of the margin by which computed neutral stability Reynolds numbers might be exceeded. This was done by comparison with experiment and it was found that the crossflow Reynolds numbers could be exceeded by about 80 percent and the streamwise criterion by 200.

This comparison results in the following criteria:

$$R_{n,max} = 1.8 \, R_{n,min} \tag{3}$$

$$R_{t,max} = R_{t,min} + 200 \tag{4}$$

Numerous examples of the use of these criteria may be found in the literature (refs. 15 to 18).

The obvious advantage of local methods such as these is that they are easy to apply and do not consume large amounts of computer time. The obvious disadvantage is, of course, the confidence level of these methods. They do not account in any way for the disturbance growth history, which is a necessary part of a rational transition prediction method. Thus, it may be dangerous to rely exclusively on such methods for wing configurations and pressure distributions which depart significantly from those used in their calibration.

The ideal advanced method should account for as much of the physics as possible, should not require an inordinate amount of computer time, and finally, should be user oriented with relative ease of operation. The method to be described in the following section was developed with these goals in mind.

PRESENT METHOD

Description

The present method is designed to compute the incompressible stability characteristics of laminar compressible boundary layers on swept, tapered wings with suction. The boundary-layer profiles are computed by program MAIN (ref. 19). Program MAIN is laminar, compressible, with adiabatic wall and wall suction boundary conditions. Taper effects are incorporated by assuming that the wing can be represented as part of a semi-infinite conical surface. The assumption of conical similarity then allows the results of a computation at one spanwise position to be simply scaled to obtain boundary-layer profiles at any other spanwise station. Boundary-layer computations are made along an arc of constant radius (r). Wing geometry and surface pressures are specified along a chordline parallel to the free stream which intersects the arc of constant radius at the leading edge. Figure 4 indicates these relationships.

The results of program MAIN are input into stability program SALLY, which performs incompressible, linear, and parallel stability computations. SALLY solves the Orr-Sommerfeld equation:

$$\left(\frac{d^2}{dy^2} - \alpha^2 - \beta^2\right)^2 \psi = iR\left\{(\alpha u_0 + \beta w_0 - \omega) \cdot \left[\frac{d^2}{dy^2} - \alpha^2 - \beta^2\right]\psi - \left(\alpha \frac{\partial^2 u_0}{\partial y^2} + \beta \frac{\partial^2 w_0}{\partial y^2}\right)\psi\right\} \tag{5}$$

where the quantity ψ is the perturbation stream function with boundary conditions

$$\psi(0) = \frac{\partial \psi}{\partial y}(0) = 0 \quad (\psi(\infty) \text{Bounded}) \tag{6}$$

α, β are the wave number components of the disturbance, ω is the complex disturbance frequency, u_o and w_o are mean flow velocity components, and R is the Reynolds number. (See fig. 4.)

A spectral technique involving Chebyshev polynominals is used to obtain solutions to this equation. This solution technique has the advantages of high accuracy combined with computational speed and efficiency. Details of the solution procedure are available in reference 2.

SALLY obtains at each chordwise computational station for given wavenumber components α, β, the frequency of the disturbance ω_r, the disturbance amplification rate ω_i, and the group velocity vector V_G where ω_r and ω_i are the real and imaginary parts of ω in equation (5). This information is used to determine the integrated disturbance amplitude ratio in the following manner. First, the frequency of the disturbance that is to be followed is specified, and SALLY proceeds from station to station along the chord until an instability of the required frequency is detected. An iteration is then performed to obtain the wave of maximum amplification at that frequency. This amplification rate is then integrated to the next station (see fig. 5) along the surface distance determined by the direction of the group velocity vector. In addition to determining the direction of integration, the group velocity is used to convert temporal amplification rates obtained from the stability solution to the spatial amplification rates that are actually integrated. Thus, at each station, the amplitude ratio of the disturbance is available. The logarithm of this ratio gives the so-called "N-factor" of the disturbance. A detailed discussion of the present mehtod may be found in reference 20.

Figure 6 illustrates schematically how disturbance growth information can be used to determine suction rates. Assume that an airfoil (without suction) is placed in a wind tunnel, and surface pressures and transition location are determined. The surface pressures and wing geometry are used by program MAIN to compute the boundary-layer profiles which are input to the SALLY stability code. SALLY computes integrated disturbance growth along the chord, and the growth "N factor" at the transition location is determined. If suction is now applied to the surface of the wing so that it is below the disturbance growth factor corresponding to transition, then laminar flow should be maintained. Thus, the first task is to determine allowable disturbance growth factors. This is done by calibration with experiment.

Calibration

Since transition is affected by factors such as free-stream noise and turbulence, calibration of a transition prediction method should involve data

in a low disturbance environment. For this reason data obtained in the Ames 12-foot tunnel was used (refs. 21 and 22). This question will be discussed only briefly here, and the reader is referred to reference 20 for more detail. Figure 7 illustrates the calibration process. Results are shown for two separate experimental investigations in the Ames 12-foot tunnel. One investigation involved an unsucked two-dimensional wing section at various sweeps and Reynolds numbers; the other was a two-dimensional 30° swept wing with suction through spanwise slots. The procedure then is to obtain boundary-layer profiles with program MAIN for the test Mach number and pressure distribution. These profiles are input to SALLY and the disturbance growth N-factor corresponding to the experimentally observed transition location is obtained. Figure 7 gives an example of such a calibration for stationary crossflow disturbances. The curves marked 40B and 40C do not have a transition location because transition occurred forward of the first measuring station at 20 percent chord. Note that the N-factors for the other curves at transition fall in a band $9.5 \lessapprox N \lessapprox 11$. This then gives an indication of allowable crossflow disturbance growth for laminar flow over the front part of the wing. It turns out that three separate calibrations need to be carried out: (1) front part of wing crossflow; (2) mid-chord Tollmien-Schlichting (streamwise disturbances); and (3) rear part of wing crossflow. This aspect will not be addressed here, and the reader is again referred to reference 20. Reference 22 indicates that suction was adjusted on the wing of that experiment so that laminar flow would be maintained along the entire chord with minimum suction flow rates. Note that maximum growth factors obtained for the suction case S2 fall within the range of N factors at transition.

Sample Application

Figure 8 shows the pressure distribution over the upper and lower surface of an LFC applicable supercritical wing section for a design shockless condition. Note the large supercritical region on the upper surface and the very small region of supercritical flow along the lower surface. Figure 9 shows two suction distributions for the upper surface of the airfoil of figure 8. Note the higher suction rates at the front and rear for control of the crossflow, and the relatively low mid-chord suction for control of streamwise Tollmien-Schlichting disturbances. The solid suction curve corresponds to a suction level that allows the highest possible disturbance growth without exceeding established growth limits. This suction distribution should maintain laminar flow to 100 percent of the chord. Figure 10 shows the corresponding crossflow growth factors; solid and dashed curves of figure 10 corresponding to those of figure 9. The dashed curve represents a slightly lower suction level with the result that the solid curve limit is exceeded by about 84 percent chord. This indicates that full-chord laminar flow cannot be maintained with the lower suction level.

Status

The SALLY stability code is operational with

(a) Typical run times: 3 minutes on Control Data CDC 6600 for one spanwise station

(b) 160,000 octal words of storage

Improvements forthcoming are

(a) 40 percent decrease in memory requirements

(b) 45 percent decrease in run times.

OTHER EFFECTS

The assumptions contained in SALLY are that (1) it is incompressible, (2) it is linear, (3) it is parallel, and (4) it has no wall curvature terms. These assumptions are now considered and the flow situations on the wing for which they may have limited validity are examined.

Compressibility

From figure 8 it can be seen that a significant portion of the upper surface is in a region of locally supercritical flow. Although the profiles used by SALLY are generated by a compressible boundary-layer program, SALLY itself solves the incompressible stability equations. So the question is, how much of an error is incurred by using incompressible stability for wings with significant supercritical regions. Figure 11 gives a comparison between compressible and incompressible growth rates for Tollmien-Schlichting (streamwise) disturbances in the upper surface supercritical region of the wing of figure 8. Calculations performed by L. Mack of Jet Propulsion Laboratory (unpublished) indicate that compressibility decreases the local disturbance growth rates and, in addition, it changes the bandwidth of unstable frequencies. Incompressible calculations in supercritical regions would therefore tend to be conservative (and would estimate higher suction rates). It turns out that the crossflow disturbances are dominant in the lower Mach number regions of the flow and calculations for the upper surface of the configuration of figure 8 indicate about a 10 percent decrease in growth rates due to compressibility. Since most of the suction is needed to control crossflow (see fig. 9), it is seen that compressibility effects will not significantly change the total required suction flow, but may be important in determining the details of the suction distribution. Also, because of the low local pressure levels in the supercritical region, the compressibility effects may have a sizeable favorable influence upon the pumping power.

Nonparallel Effects

The assumption of parallel flow in the equations used in SALLY may be violated to some extent. For example, figure 12 shows that in the region in the near vicinity of the slot, streamlines diverge, and the flow is obviously not parallel. How important this effect is has not yet been established. Figure 13 gives an example of the type of calculation (obtained from A. Nayfeh of Virginia Polytechnic Institute and State University) that can only be done accurately by including nonparallel effects. A flat plate, six units long, is placed in a stream of Mach number 0.8, and the integrated growth of a disturbance of nondimensional frequency 1×10^{-5} is determined for a number of suction conditions on the plate. All growth factor levels shown are at the end of the plate. If a given total suction is distributed evenly along the plate, a growth factor of slightly over 4.5 is obtained. If the total suction amount is kept fixed but now distributed only over the first half of the plate, the growth factor goes up to almost 8. Further concentration of the suction results in growth factors which start to approach those obtained with no suction (level indicated by top bar). Increasing suction concentration results in increasing severity of nonparallel flow in the region where suction terminates. A series of alternate suction no-suction strips approximates the real life case of suction through spanwise slots. Also, however, if many fine slots are used, the nonparallel and "solid surface" effects, as shown on figure 13, are probably not very severe, since continuous suction would be approached. When such nonparallel calculations are performed, they may reveal that certain critical slot spacings will result in a resonance phenomenon greatly increasing the normal amplification rates of particular frequencies of streamwise Tollmien-Schlichting disturbances.

Nonlinear Effects

Use of linearized stability equations assumes that growth rates of any wave can be calculated independently of the growth of any other wave. In certain situations, this may not hold. Figure 14 illustrates three situations where nonlinear effects may be important. First, waves may grow to amplitudes where streamwise and crossflow type disturbances begin to interact with each other. Second, although wings will ideally be designed for shockless conditions, off-design shocks will occur and may result in sufficiently rapid mean flow changes to cause nonlinear effects to become important. A third possibility is that the suction slots themselves may induce disturbances sufficient to make nonlinear effects important.

Wall Curvature Effects

It is known that in regions of concave curvature, such as on the lower surface of the wing of figure 8, a centrifugal instability known as Taylor-Goertler instability will occur (ref. 23). These are vortex type instabilities and are due solely to centrifugal effects. New computational stability codes are being developed which will have the capability of computing Taylor-Goertler instabilities quickly and accurately.

CONCLUDING REMARKS

An advanced three-dimensional boundary-layer stability code has been developed to optimize LFC suction requirements. A new version 45 percent faster and requiring 40 percent less computer storage will soon be available. Compressibility effects have been found to be important in the sense that they will impact the details of the suction distribution. The importance of non-parallel, nonlinear, and Taylor-Goertler effects is being investigated.

REFERENCES

1. Sturgeon, R. F.; Bennett, J. A.; Etchberger, F. R.; Ferrill, R. S.; and Mead, L. E.: Study of the Application of Advanced Technologies to Laminar-Flow Control Systems for Subsonic Transports. Volume I: Summary. NASA CR 144975, 1976.

2. Benney, David J.; and Orszag, Steven A.: Stability Analysis for Laminar Flow Control - Part 1. NASA CR-2910, 1977.

3. Saric, William S.; and Nayfeh, Ali Hasan: Nonparallel Stability of Boundary Layers With Pressure Gradients and Suction. Laminar-Turbulent Transition, AGARD-CP-224, May 1977.

4. Hocking, L. M.: Non-Linear Instability of the Asymptotic Suction Velocity Profile. Quart. J. Mech. & Appl. Math., vol. XXVIII, pt. 3, Aug. 1975, pp. 341-353.

5. Reshotko, Eli: Stability Theory as a Guide to the Evaluation of Transition Data. AIAA J., vol. 7, no. 6, June 1969, pp. 1086-1091.

6. Morkovin, Mark V.: Critical Evaluation of Transition From Laminar to Turbulent Shear Layers With Emphasis on Hypersonically Traveling Bodies. AFFDL-TR-88-149, U.S. Air Force, Mar. 1969. (Available from DDC as AD 686 178.)

7. Mack, L. M.: Boundary Layer Stability Theory. 900-277 Rev. A (Contract No. NAS 7-100) Jet Propulsion Lab., California Inst. Technol., Nov. 1969.

8. Betchov, R.; and Criminale, William O., Jr.: Stability of Parallel Flows. Academic Press, Inc., 1967.

9. Pfenninger, W.: Flow Problems of Swept Low-Drag Suction Wings of Practical Construction at High Reynolds Numbers. Ann. N.Y. Acad. Sci., vol. 154, art. 2, Nov. 22, 1968, pp. 672-703.

10. Schlichting, Hermann (J. Kestin, trans.): Boundary-Layer Theory. Sixth ed., McGraw-Hill Book Co., Inc., c.1968.

11. Pfenninger, W.: Some General Considerations of Losses in Boundary Layer Suction Ducting Systems. Rep. BLC-29, Northrop Corp., Feb. 1954.

12. Scotti, R. S.; and Corbett, K. T.: Laminar Body Analysis Heat Plus Suction Stabilized. ONR-CR289-013-1F, U.S. Navy, Dec. 1976. (Available from NTIS as AD-A040396.)

13. Hirschel, E. H.: Theoretical Investigation of Transition Phenomena in the Boundary Layer on an Infinite Swept Wing. DGLR Paper No. 72-124, Symposium on Aerodynamics of Airfoils in Transonic Flow, Oct. 1972.

14. Owen, P. R.; and Randall, D. G.: Boundary Layer Transition on a Sweptback Wing: Tech. Mem. Aero 277, British R.A.E., May 1952.

15. LFC Aircraft Design Data Laminar Flow Control Demonstration Program. Final Report. NOR-67-136 (AF 33/657-13930), Northrop Corp., June 1967. (Available from DDC as AD-819317.)

16. Summary of Laminar Boundary Layer Control Research. Vol. II, ASD-TDR-63-554, U.S. Air Force, Mar. 1964. (Available from DDC as AD 60586.)

17. Gross, L. W.: An Analysis of the Boundary Layer Development on a 30° Swept Laminar Suction Wing. Rep. BLC-134 (NAI-61-244), Northrop Corp., 1962.

18. Pfenninger, W.: USAF and Navy Sponsored Northrop LFC Research Between 1949 and 1967 and Design Considerations of Large Global Range High Subsonic Speed LFC Transport Airplanes. Presented at the AGARD/VKI Special Course on "Concepts for Drag Reduction." (Rhode-St-Genese, Belgium), Mar. 28-Apr. 1, 1977.

19. Kaups, Kalle; and Cebeci, Tuncer: Compressible Laminar Boundary Layers With Suction on Swept and Tapered Wings. J. Aircraft, vol. 14, no. 7, July 1977, pp. 661-667.

20. Srokowski, A. J.; and Orszag, S. A.: Mass Flow Requirements for LFC Wing Design. AIAA Paper No. 77-1222, Aug. 1977.

21. Boltz, Frederick W.; Kenyon, George C.; and Allen, Clyde Q.: Effects of Sweep Angle on the Boundary-Layer Stability Characteristics of an Untapered Wing at Low Speeds. NASA TN D-338, 1960.

22. Gault, Donald E.: An Experimental Investigation of Boundary-Layer Control for Drag Reduction of a Swept-Wing Section at Low Speed and High Reynolds Numbers. NASA TN D-320, 1960.

23. Tobak, M.: On Local Goertler Instability. ZAMP, vol. 22, 1977, pp. 130-143.

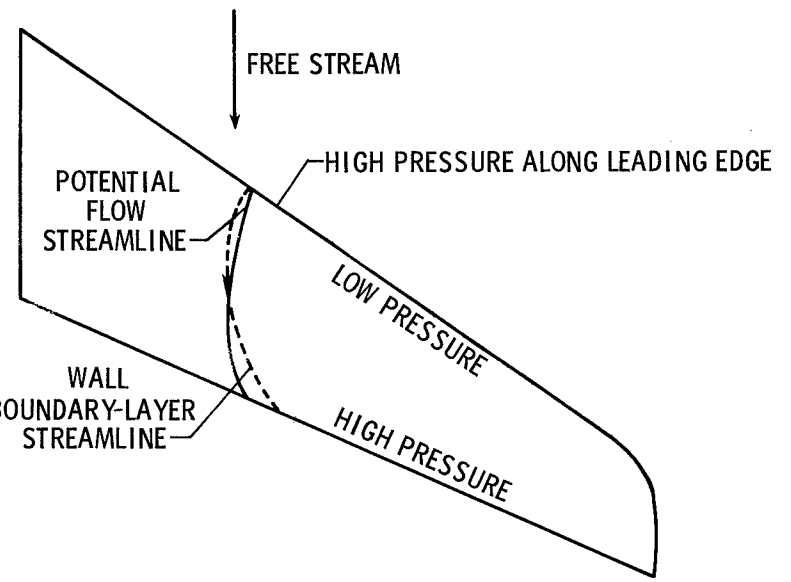

Figure 1.- Flow conditions on typical sweptback wing.

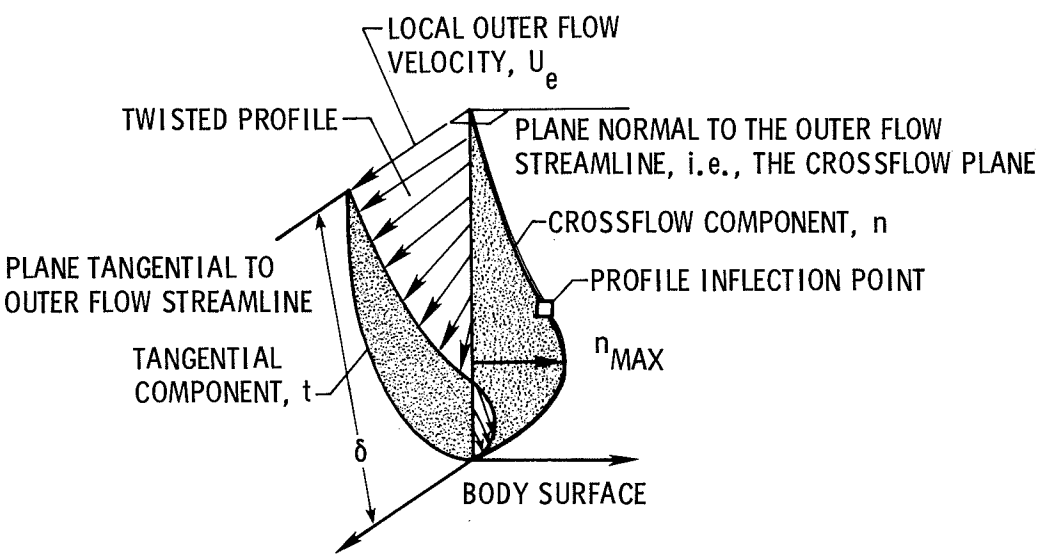

Figure 2.- Swept-wing boundary-layer profiles.

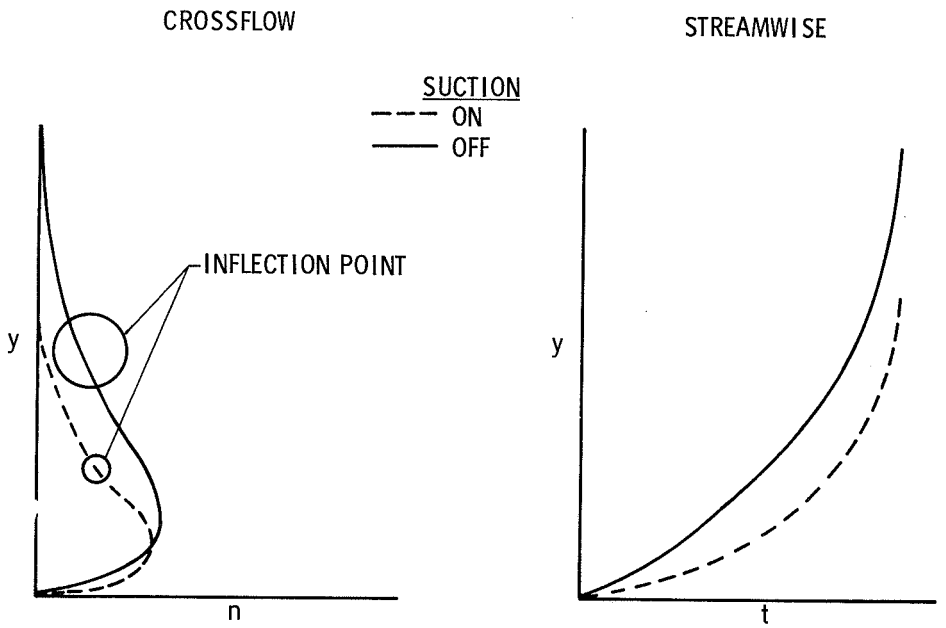

Figure 3.- Effects of suction on streamwise and crossflow boundary-layer profiles.

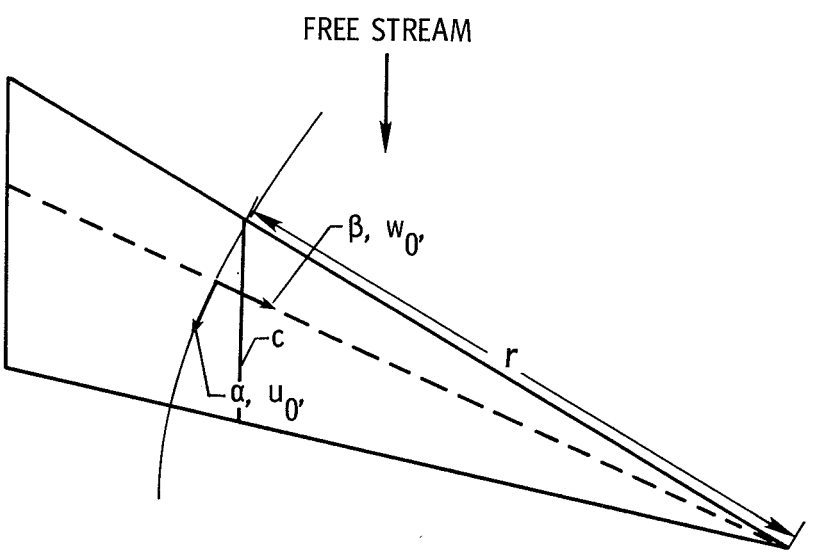

Figure 4.- Coordinates for wing boundary-layer solutions.

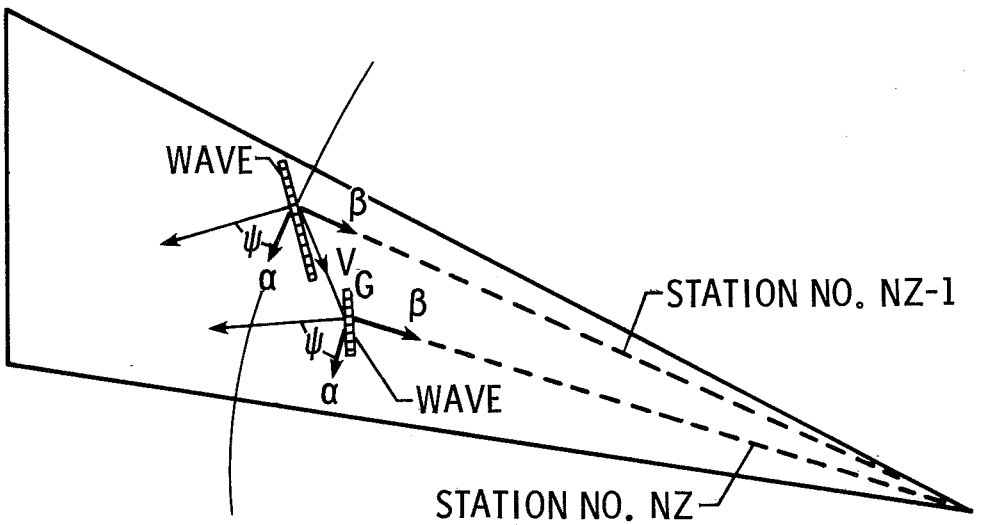

Figure 5.- Schematic of stability code integration path.

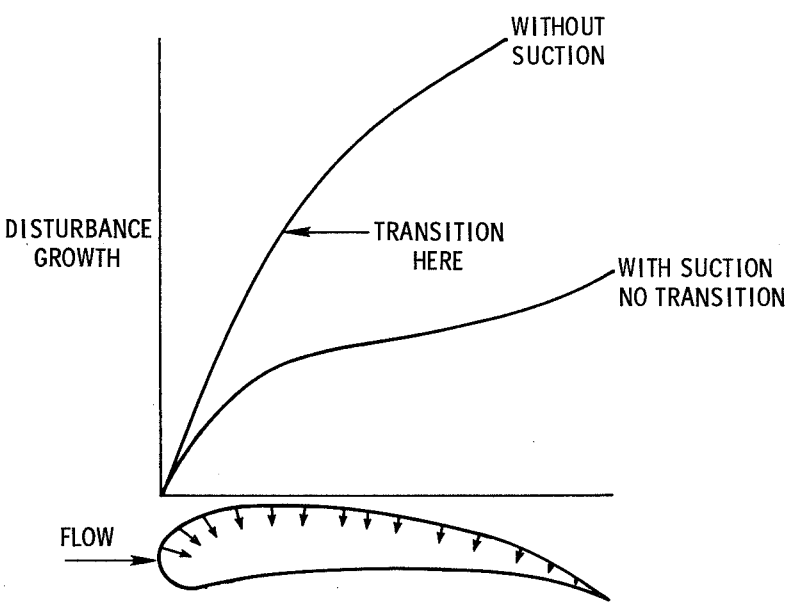

Figure 6.- Illustration of effect of suction on disturbance growth.

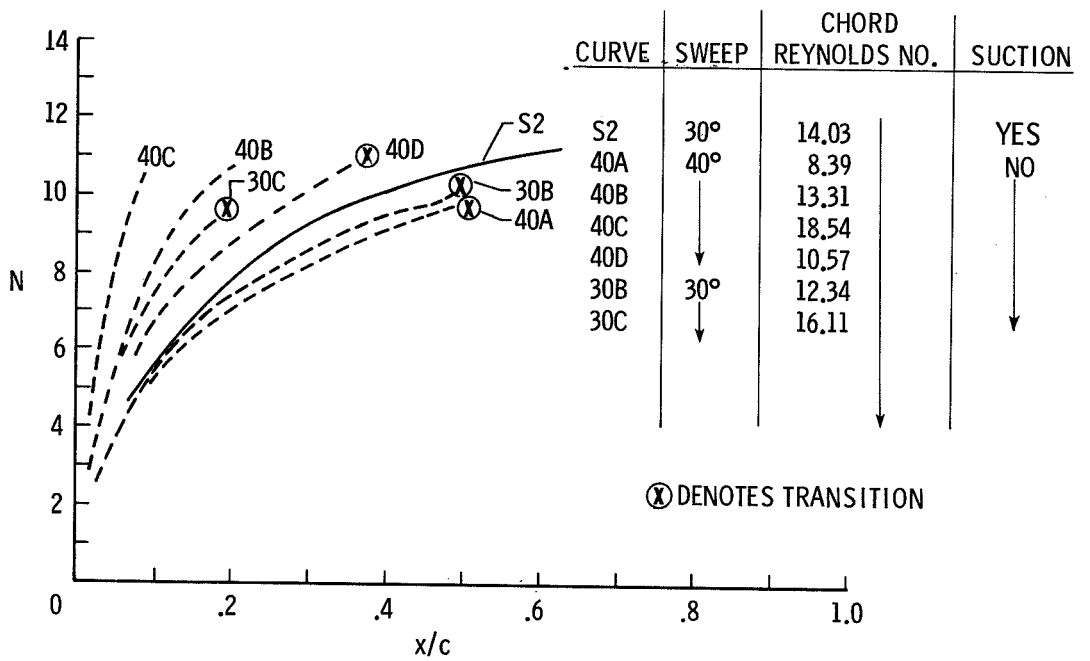

Figure 7.- Integrated "N factors" for stationary crossflow disturbances. (Front part of wing.)

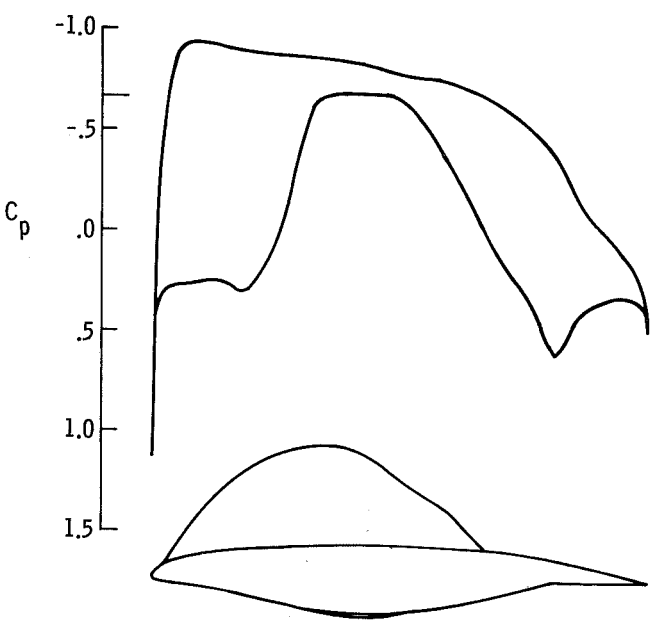

Figure 8.- Laminar flow control applicable supercritical wing section.

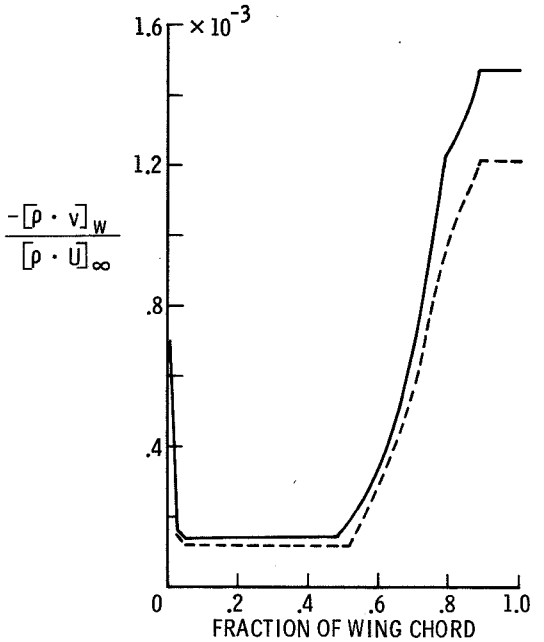

Figure 9.- Suction distributions on upper surface of wing of figure 8.

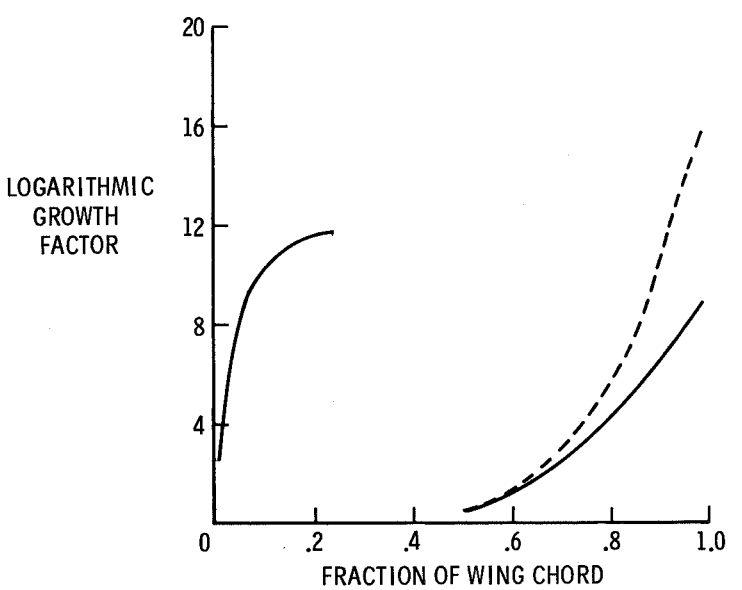

Figure 10. Integrated disturbance growth for upper surface crossflow corresponding to suction distributions of figure 9.

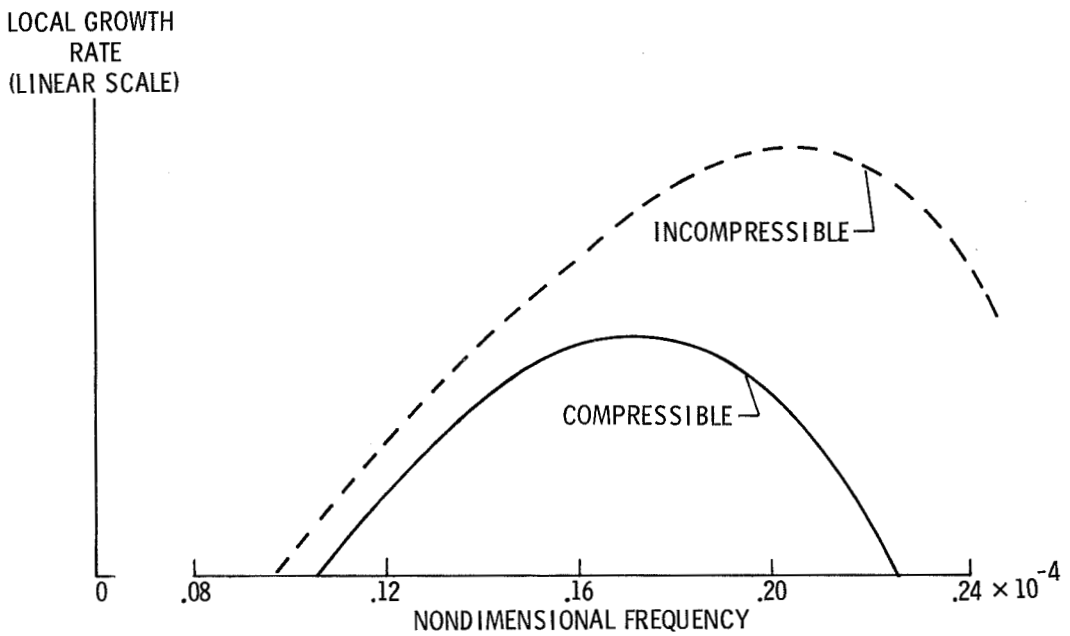

Figure 11.- Effect of compressibility on streamwise (Tollmien-Schlichting) growth rates and frequencies in upper surface supercritical region.

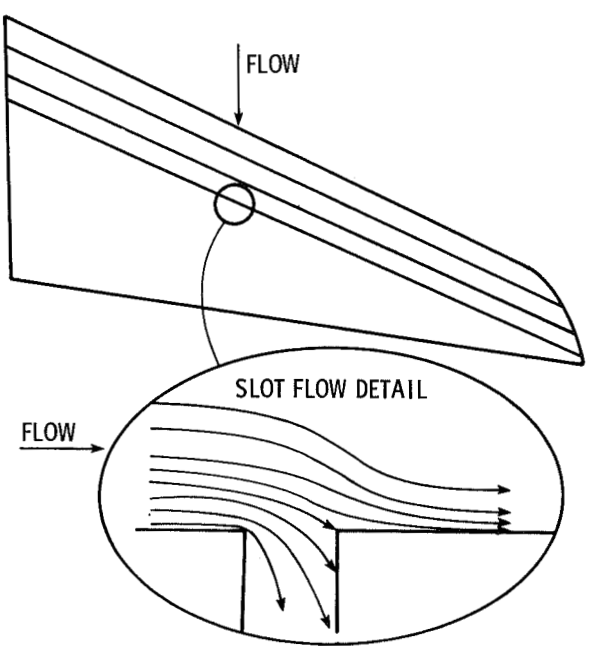

Figure 12.- Nonparallel flow near a slot.

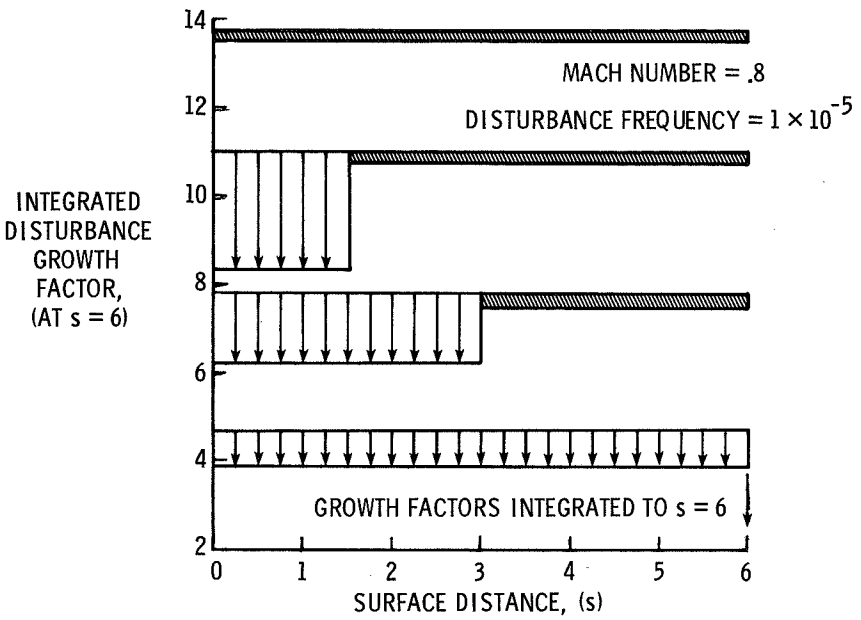

Figure 13.- Example of nonparallel disturbance growth calculation over a flat plate. Total suction fixed; distribution varied.

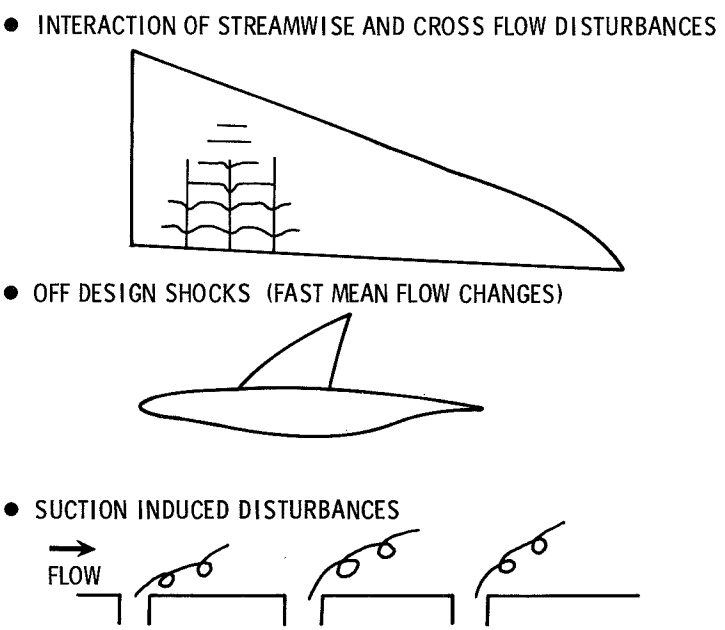

Figure 14.- Illustration of conditions for which nonlinear effects may be important.

DESIGN OF A LAMINAR-FLOW-CONTROL SUPERCRITICAL AIRFOIL FOR A SWEPT WING

Dennis O. Allison and John R. Dagenhart

NASA Langley Research Center

SUMMARY

An airfoil was analytically designed and analyzed for a combination of supercritical flow and laminar flow control (LFC) by boundary-layer suction. A shockless inverse method was used to design an airfoil and an analysis method was used in lower-surface redesign work. The laminar-flow pressure distributions were computed without a boundary layer under the assumption that the laminar boundary layer would be kept thin by suction. Inviscid calculations showed that this 13.5-percent-thick airfoil has shockless flows for conditions at and below the design normal Mach number of 0.73 and the design section lift coefficient of 0.60, and that the maximum local normal Mach number is 1.12 at the design point. The laminar-boundary-layer instabilities can be controlled with suction but the undercut leading edge of the airfoil provides a low-velocity constant-pressure-coefficient region which is conducive to laminar flow without suction. Since the boundary layer can become turbulent due to intermittent adverse environmental conditions or suction failure, the lift can drop significantly. The airfoil was designed to be capable of lift recovery with no suction by the deflection of a small trailing-edge flap. The airfoil is not necessarily one of optimal performance because of the conservative constraints that were imposed on the design problem. However, it should provide a tool for experimental investigation of some fundamental problems relating to combined supercritical flow and laminar flow control.

INTRODUCTION

Laminar-flow-control work in the past has been done with conventional airfoils. Since then, efficient turbulent supercritical-type airfoils have been developed and they give large performance benefits when applied to turbulent aircraft. The current task was to design a laminar-flow-control (LFC) airfoil which maintains the advantages of a supercritical type of airfoil. The airfoil was analytically designed according to the concepts of Dr. Werner Pfenninger and Percy Bobbitt of Langley Research Center. The objective was to combine the advantages of supercritical-type airfoils and laminar flow control by suction for application to swept wings.

Four airfoil-design goals were established to carry out this objective. The first goal involves a set of two-dimensional target values as follows: a thickness-to-chord ratio of 0.13 or greater; a design normal Mach number of about 0.75; and a design section lift coefficient of about 0.60. The performance of a supercritical type of airfoil can be judged by the combination of these three parameters. The target values correspond to a good

turbulent supercritical airfoil. The first goal is to achieve a laminar airfoil which does not sacrifice any of these values. The second goal is to have shockless supercritical flow at and below the design Mach number and lift condition and to have a maximum local normal Mach number of about 1.15 at the design condition. A turbulent supercritical airfoil would have nearly shockless supercritical flow for Mach numbers and lift coefficients at and below the design condition. For laminar flow control a shockless configuration is desirable to minimize the suction requirement, which would be higher if laminarization through a shock wave were required. A maximum local normal Mach number of about 1.15 is high enough to allow good airfoil performance but low enough to minimize the tendency to form off-design shock waves. The third goal is to maintain a laminar boundary layer using suction. The fourth goal is for the airfoil to be capable of lift recovery in the unlikely event of suction failure.

To achieve these goals the airfoil was designed and analyzed by a process that is described in four steps. First, a laminar airfoil was designed for shockless supercritical flow over the upper surface. Next, the lower surface was redesigned for certain laminar-flow-control characteristics and a greater thickness-to-chord ratio. The third step was to analyze the airfoil for off-design shock formation with laminar flow control. The last step was to analyze the airfoil for lift loss and recovery with no LFC suction. The last two steps were, of course, performed iteratively with the first two.

SYMBOLS

The word "normal" refers to a direction normal to the leading edge of an untapered swept wing. The quantities described as normal were either input to or computed by a two-dimensional method.

C_p	normal pressure coefficient
$C_{p,sonic}$	sonic value of C_p
C_Q	suction coefficient, $\frac{\text{velocity into wall x density at wall}}{\text{free-stream velocity x free-stream density}}$
c_l	normal section lift coefficient
c_m	normal pitching-moment about the quarter-chord point
$M_{\ell,max}$	maximum local normal Mach number
M_n	normal component of free-stream Mach number
R	normal Reynolds number based on chord
t/c	normal thickness-to-chord ratio
x/c	nondimensional distance along airfoil chord

y/c	nondimensional normal distance perpendicular to airfoil chord
α	normal angle of attack
δ	normal flap deflection angle
Λ	sweep angle of untapered wing

Subscripts:

l.s.sep.	lower surface boundary layer separation
u.s.sep.	upper surface boundary layer separation

AIRFOIL DESIGN

Many steps were required in the airfoil design process but only two are described in this paper. Airfoil shapes and inviscid pressure distributions are shown in figure 1 for the two steps that are described. The airfoil was designed with no boundary layer assuming that the laminar boundary layer would be kept thin by suction. All the pressure distributions in this paper have a dashed line across them at the sonic value of the pressure coefficient. Pressure coefficients above the dashed line (more negative than $C_{p,sonic}$) correspond to local supersonic flow.

Shockless Supercritical Design

The airfoil in figure 1(a) is the most desirable of several airfoils designed using an early version (ref. 1) of the Bauer-Garabedian-Korn shockless inverse design method. (Ref. 2 contains updates to that version.) That method required many abstract parameters as inputs and produced the airfoil coordinates plus the pressure distribution.

The desirable part of this initial design is the upper surface which has a shockless region of supersonic flow covering about two-thirds of the chord length with a maximum local Mach number $M_{\ell,max}$ of 1.15. The pressure coefficient passes smoothly through the sonic value; in other words, there is no shock wave. Also the small slope in the pressure distribution at the sonic value means that the airfoil will be slow to form shock waves for nearby off-design Mach numbers and lift coefficients. Successive computer runs were made to maximize the combination of the design Mach number, lift, and thickness. The design Mach number M_n of 0.73 and the design lift coefficient c_l of 0.60 were considered acceptable but a thickness-to-chord ratio t/c higher than 0.126 was desired. This airfoil was designated SSC-73-06-126, which denotes shockless supercritical with design conditions of $M_n = 0.73$ and $c_l = 0.60$ with $t/c = 0.126$.

Laminar-Flow-Control Redesign

The airfoil in figure 1(b) is the result of redesigning the lower surface while maintaining the shockless supercritical characteristic of the upper surface. The redesign work was done using the Bauer-Garabedian-Korn-Jameson analysis method (ref. 2) which requires the airfoil coordinates as input and produces the pressure distribution. (Ref. 3 contains updates to the analysis method.) The maximum local Mach number $M_{\ell,max}$ for the redesigned airfoil is 1.12. This airfoil is designated LFC-73-06-135, which denotes laminar flow control with design conditions of $M_n = 0.73$ and $c_l = 0.60$ with $t/c = 0.135$. Coordinates for airfoil LFC-73-06-135 are given in table I.

Lower surface redesign.- The airfoil in figure 1(b) has a different type of lower surface, which might be desirable for certain laminar-flow-control features, and a higher thickness-to-chord ratio. The leading edge of the airfoil is undercut so that it produces a low-velocity region of near-constant pressure coefficient which is conducive to laminar flow without suction. This might allow a leading-edge device to be installed in the lower surface since no suction would be required in this region and the low velocities might permit laminar flow over local surface discontinuities which could arise from the leading-edge device. Another benefit is that the small leading-edge radius alleviates the spanwise leading-edge contamination problem. Also, the magnitude of the pitching moment is slightly lower for the redesigned airfoil (reduced from $c_m = -0.12$ to $c_m = -0.10$). The center of the airfoil was thickened until a very small region of supersonic flow developed, while the front and rear were thinned so as to maintain the design section lift coefficient c_l of 0.60. As a result, the area inside the airfoil remained about the same. This unusual shape for the lower surface was designed with careful consideration of the laminar-boundary-layer instabilities.

Laminar-boundary-layer instabilities.- Three types of laminar-boundary-layer instabilities were considered as indicated in figure 2. The Tollmien-Schlichting instability predominates in the region of small adverse pressure gradient, which covers about one-half of the upper surface. The cross-flow instability is due to wing sweep and predominates in the four steep-pressure-gradient regions of the upper and lower surfaces. The Tollmien-Schlichting and cross-flow disturbance growths were computed by the method described in reference 4. The Taylor-Goertler instability is due to centrifugal effects in the concave regions of the lower surface, and the disturbance growth was computed by the method of Smith (ref. 5).

To maintain a laminar boundary layer the growth of boundary-layer disturbances must be kept within acceptable limits. The airfoil had to be redesigned to control the cross-flow and Taylor-Goertler instabilities. This was done by an iterative process of successively changing the airfoil shape and recomputing the disturbance growths. Another iterative process was required between an assumed suction distribution and the cross-flow instability growth for each airfoil shape. Also, each time the airfoil was reshaped the coordinates had to be adjusted to maintain fairness of the surface.

Contrary to what might be expected, the cross-flow disturbance growth depends more on the time spent in the steep gradient than on the steepness of the gradient. Therefore, it was controlled by confining each steep gradient to a short distance along the chord. That is why the four gradients indicated by the label "cross-flow" in figure 2 are so steep. Similarly, the Taylor-Goertler disturbance growth depends more on the time spent in a concave curvature region than on the magnitude of the curvature. Control was effected by confining each concave curvature to a short distance along the chord. As a result the two concave curvature regions of the lower surface have high curvatures and two dips (labeled Taylor-Goertler) appear in the pressure distribution in figure 2.

LFC suction distribution.- Current plans are to investigate a swept model of an airfoil similar to LFC-73-06-135 with suction in the Ames 12-foot pressure wind tunnel. Such an investigation will require a very complicated wind-tunnel wall liner (design procedure discussed by Newman and Anderson in ref. 6). Figure 3 shows a suction distribution suitable for maintaining laminar flow over airfoil LFC-73-06-135 under a set of proposed test conditions. The two-dimensional Mach number, lift coefficient, and Reynolds number are: $M_n = 0.73$, $c_l = 0.60$, and $R = 10 \times 10^6$. A sweep angle Λ of 35° was chosen to produce cross flows equivalent to those of a full-scale aircraft at cruise altitude with a lower sweep. The suction coefficient C_Q is plotted against non-dimensional distance along the chord. The suction shown is sufficient to keep the laminar-boundary-layer disturbance growths within acceptable bounds according to the criteria set forth in references 4 and 5. Since growth is a cumulative quantity, a different suction distribution could be used to limit the growths to the same bounds.

The suction distribution in figure 3 will be discussed in terms of the pressure distribution in figure 2. A low level of suction is shown over about one-half of the upper surface where the Tollmien-Schlichting instability predominates and the adverse pressure gradient is small. Higher suction levels are shown in the front and rear of the upper surface where the cross-flow instability predominates and the pressure gradients are steep. Only a narrow spike is used in the front since the steep gradient is confined to a short distance along the chord. In the rear the suction coefficient builds up to a higher level since the steep pressure gradient is spread over a larger distance along the chord. On the lower surface, it is desirable to have no suction in the leading-edge region to improve the feasibility of a leading-edge device; no suction is required there since the steep pressure gradient is confined to a very short distance along the chord and the following gradient is nearly zero. Significant levels of suction are shown over most of the lower surface where there are two steep pressure gradients and the cross-flow instability predominates. The level could be lowered in the center of the lower surface but it would be coupled with increased levels elsewhere. No suction is shown in the trailing-edge region of the lower surface since the pressure gradient suddenly reverses itself at $x/c = 0.81$ and sets up a counter cross flow which works against the previous cross flow. No additional suction is required for the Taylor-Goertler instability since it is controlled by airfoil shaping as explained earlier rather than by suction.

AIRFOIL ANALYSIS

Airfoil analysis was performed to study shock-wave formation at off-design conditions with laminar flow control and to study lift loss and recovery with suction failure. A large number of calculations were made using the analysis method of reference 2, and a few samples were selected for discussion in the following paragraphs.

Off-Design Shock Formation With LFC

Effects of off-design Mach numbers, off-design lift coefficients and deflections of a small trailing-edge flap are illustrated by the inviscid pressure distributions for airfoil LFC-73-06-135 which are shown in figures 4 to 6. Shock-wave formation at off-design conditions was studied using laminar-flow pressure distributions which were computed with no boundary layer assuming that the laminar boundary layer would be kept thin by suction.

Off-design Mach numbers.- Figure 4 shows laminar-flow pressure distributions for off-design Mach numbers at the design lift coefficient c_l of 0.60. The design pressure distribution is shown at the lower left for reference. The only shock wave which appears in this figure is for $M_n = 0.75$, which is above the design value of $M_n = 0.73$. For a poorly designed upper surface, a double shock wave could form near the rear of the supersonic zone for a Mach number just below the design value, and it would move forward for lower Mach numbers. No such shock waves appear for the lower Mach number of 0.70. The airfoil does not have off-design shock-wave formation for Mach numbers below the design point.

Off-design lift coefficients.- Figure 5 shows laminar-flow pressure distributions for off-design lift coefficients at the design Mach number M_n of 0.73. The design pressure distribution is again shown at the lower left for reference. The only shock wave which appears in this figure is for $c_l = 0.70$, which is above the design value of $c_l = 0.60$. It should be noted that for a poorly designed upper surface, a double shock wave often forms near the rear of the supersonic zone for a lift coefficient just below the design value, and moves forward as the lift coefficient is decreased. No shock wave appears for the lower lift coefficient of 0.50. The airfoil does not have off-design shock-wave formation for lift coefficients below the design point until the lift coefficient reaches about 0.30. For lift coefficients of 0.30 and lower a shock wave forms on the lower surface for a Mach number of 0.73.

Small trailing-edge flap.- The lift coefficient was controlled in figure 5 by angle-of-attack variations from -0.8° to 0.5°, but it can be controlled by deflections of a small trailing-edge flap. Figure 6 shows laminar flow pressure distributions with the angle of attack held at its design value of $\alpha = 0.1^\circ$ for -3.4° to 1.6° deflections of a 5-percent-chord trailing-edge flap to produce the four lift coefficients shown in figure 5. The pressure distributions in figure 6 show no shock-wave formation until the lift

coefficient is raised above the design value. For the lift coefficient c_l of 0.70 an indication of only a weak shock wave appears. This shows that the lift coefficient can be controlled by deflecting a small trailing-edge flap without spoiling the shockless nature of the topside pressures at lift coefficients below design.

Lift Behavior With Suction Failure

The loss and recovery of lift in the unlikely event of suction failure is illustrated for airfoil LFC-73-06-135 in figures 7 and 8. Suction failure was simulated by computing pressure distributions with a turbulent boundary layer for a wind-tunnel Reynolds number R of 10×10^6 starting at x/c = 0.02 on both the upper and lower surfaces of the airfoil. It is possible to have a turbulent boundary layer with suction but these calculations are for the worst case of a turbulent boundary layer with no LFC suction.

Lift loss.- The calculations in figure 7 are for lift loss at the design Mach number and with the angle of attack held at its design value of 0.1°. The inviscid design pressure distribution simulating LFC suction is shown in figure 7(a) for reference. The pressure distribution with a turbulent boundary layer simulating suction failure is shown in figure 7(b) where $c_l = 0.28$. For a flight Reynolds number R of 40×10^6 a slightly higher lift coefficient c_l of 0.32 is predicted.

The boundary-layer separation predictions (fig. 7(b)) are x/c = 0.95 for the upper surface and x/c = 0.75 for the lower surface. The analysis method is conservative in that it tends to predict separation earlier than it would actually occur. The separated region on the upper surface would probably cover less than 5 percent of chord. On the lower surface, separation would probably occur behind x/c = 0.75 but the analysis method cannot predict reattachment. However, the favorable pressure gradient which starts at about x/c = 0.82 is conducive to reattachment and the flow will probably reattach on the lower surface well before reaching the trailing edge. The prediction of $c_l = 0.28$ may not be accurate since the reattachment point is uncertain, but the lift coefficient is not very sensitive to lower surface changes. Therefore, it is believed that about one-half of the design lift coefficient may be lost due to suction failure.

Lift recovery.- Two ways were considered by which the lift might be recovered with no suction. The results in figure 8 were calculated with a turbulent boundary layer for the design Mach number and the same wind-tunnel Reynolds number as in figure 7. The lift coefficient is restored to 0.60 in figure 8(a) by angle of attack and in figure 8(b) by the deflection of a 5-percent-chord trailing-edge flap. When the lift is recovered by a 1.8° angle of attack (fig. 8(a)), a shock wave forms and the upper-surface separation point moves forward to x/c = 0.91, both of which cause additional drag. Also, the lift calculation may not be valid when the upper-surface separation point moves forward from x/c = 0.95. When the lift is recovered by an 8° deflection of a 5-percent-chord trailing-edge flap (fig. 8(b)) no shock wave

forms and the pressure distribution is similar to the design pressure distribution (fig. 7(a)). For the flap-deflection case (fig. 8(b)), the upper-surface separation remained confined to the last 5 percent of chord. On the lower surface, separation would probably occur behind $x/c = 0.76$ and would probably reattach before $x/c = 0.95$ where the flap is located. It is believed that the airfoil is capable of lift recovery but an experimental investigation is needed to determine what deflection angle is required to recover the lift coefficient of 0.60.

CONCLUDING REMARKS

Airfoil LFC-73-06-135 has been analytically designed and analyzed for combined supercritical flow and laminar flow control and achieves the four goals which were mentioned in the Introduction. This airfoil has a thickness-to-chord ratio of 0.135 which is a little higher than the target value, a design normal Mach number of 0.73 which is a little lower than the target value, and a design section lift coefficient of 0.60 which is equal to the target value. It has shockless supercritical flow for Mach number and lift conditions at and below the design values and the maximum local normal Mach number at the design condition is 1.12. It has laminar-boundary-layer instabilities which can be controlled by suction. In the unlikely event of suction failure, it is capable of lift recovery by the deflection of a small trailing-edge flap.

Because of the conservative constraints that were imposed on the design problem, airfoil LFC-73-06-135 does not have as high a design lift coefficient or Mach number as possible. This airfoil, however, with its maximum local Mach number being higher than for previously tested subsonic airfoils with laminar flow control and with its undercut leading edge, provides a tool for investigating some fundamental problems such as that of maintaining laminar flow through a region of significant supercritical flow. Current plans are for experimental validation of an airfoil similar to LFC-73-06-135 in the Ames 12-foot pressure wind tunnel using a swept model with a small trailing-edge flap.

REFERENCES

1. Bauer, F.; Garabedian, P.; and Korn, D.: A Theory of Supercritical Wing Sections, With Computer Programs and Examples. Volume 66 of Lecture Notes in Economics and Mathematical Systems, Springer-Verlag, 1972.

2. Bauer, Frances; Garabedian, Paul; Korn, David; and Jameson, Antony: Supercritical Wing Sections II. Volume 108 of Lecture Notes in Economics and Mathematical Systems, Springer-Verlag, 1975.

3. Bauer, Frances; Garabedian, Paul; and Korn, David: Supercritical Wing Sections III. Volume 150 of Lecture Notes in Economics and Mathematical Systems, Springer-Verlag, 1977.

4. Srokowski, Andrew J.; and Orszag, Steven A.: Mass Flow Requirements for LFC Wing Design. [Paper] 77-1222, American Inst. of Aeronaut. & Astronaut., Aug. 1977.

5. Smith, A. M. O.: On the Growth of Taylor-Görtler Vortices Along Highly Concave Walls. Quart. Appl. Math., vol. XIII, no. 3, Oct. 1955, pp. 233-262.

6. Newman, Perry A.; and Anderson, E. Clay: Analytical Design of a Contoured Wind-Tunnel Liner for Supercritical Testing. Advanced Technology Airfoil Research, Volume I, CP-2045, 1978.

TABLE I.- COORDINATES FOR AIRFOIL LFC-73-06-135

Upper surface		Lower surface	
x/c	y/c	x/c	y/c
0.00000	0.01200	0.00000	0.01200
.00071	.01593	.00091	.00923
.00183	.01873	.00274	.00758
.00348	.02156	.00556	.00606
.00576	.02441	.00930	.00456
.00865	.02725	.01388	.00309
.01217	.03006	.01933	.00167
.01633	.03282	.02562	.00030
.02112	.03553	.03276	-.00104
.02655	.03815	.04076	-.00237
.03263	.04068	.04959	-.00370
.03937	.04310	.05925	-.00507
.04678	.04541	.06971	-.00647
.05486	.04761	.08095	-.00793
.06361	.04970	.09265	-.00942
.07304	.05171	.10537	-.01105
.08312	.05364	.11880	-.01276
.09384	.05549	.13290	-.01456
.10518	.05727	.14763	-.01645
.11711	.05897	.16293	-.01840
.12962	.06059	.17874	-.02070
.14268	.06214	.19497	-.02360
.15628	.06362	.21151	-.02718
.17038	.06501	.22822	-.03119
.18497	.06632	.24495	-.03537
.20002	.06754	.26150	-.03954
.21552	.06867	.27823	-.04377
.23142	.06972	.29409	-.04748
.24772	.07067	.30978	-.05062
.26438	.07153	.32552	-.05318
.28138	.07230	.34148	-.05521
.29870	.07297	.35767	-.05682
.31629	.07353	.37410	-.05808
.33414	.07400	.39072	-.05903
.35223	.07437	.40753	-.05970
.37051	.07463	.42446	-.06009
.38897	.07479	.44150	-.06022
.40757	.07484	.45860	-.06008
.42628	.07478	.47574	-.05965
.44508	.07461	.49289	-.05892

Upper surface		Lower surface	
x/c	y/c	x/c	y/c
0.46394	0.07434	0.51005	-0.05787
.48283	.07395	.52720	-.05648
.50172	.07345	.54435	-.05474
.52058	.07283	.56150	-.05264
.53938	.07210	.57868	-.05017
.55809	.07125	.59590	-.04735
.57669	.07028	.61318	-.04419
.59515	.06919	.63053	-.04073
.61345	.06797	.64796	-.03698
.63155	.06664	.66500	-.03308
.64943	.06517	.68000	-.02946
.66708	.06358	.70000	-.02450
.68447	.06186	.72000	-.01954
.70158	.06001	.74000	-.01458
.71839	.05803	.76000	-.00962
.73487	.05593	.78000	-.00466
.75103	.05371	.79000	-.00218
.76683	.05136	.80000	.00020
.78227	.04889	.80750	.00165
.79733	.04631	.81500	.00255
.81201	.04361	.82250	.00297
.82630	.04080	.83000	.00307
.84000	.03791	.83500	.00303
.85000	.03570	.84000	.00299
.86000	.03349	.85000	.00290
.87000	.03128	.86000	.00281
.88000	.02907	.87000	.00272
.89000	.02686	.88000	.00263
.90000	.02465	.89000	.00254
.91000	.02244	.90000	.00245
.92000	.02023	.91000	.00236
.93000	.01802	.92000	.00227
.94000	.01581	.93000	.00218
.95000	.01360	.94000	.00209
.96000	.01139	.95000	.00200
.97000	.00918	.96000	.00191
.98000	.00697	.97000	.00182
.99000	.00476	.98000	.00173
1.00000	.00255	.99000	.00164
		1.00000	.00155

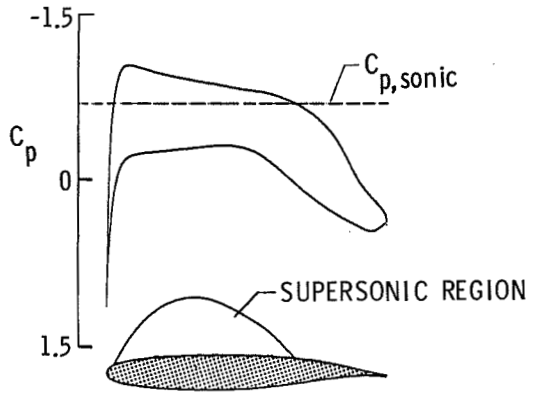

(a) Shockless supercritical design. Airfoil SSC-73-06-126; t/c = 0.126; $M_{\ell,max}$ = 1.15.

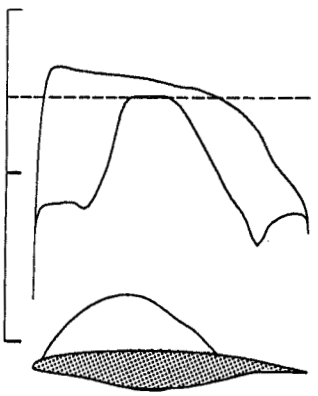

(b) Laminar-flow-control redesign. Airfoil LFC-73-06-135; t/c = 0.135; $M_{\ell,max}$ = 1.12.

Figure 1.- Airfoils and inviscid pressure distributions for two steps in design process with M_n = 0.73 and c_l = 0.60.

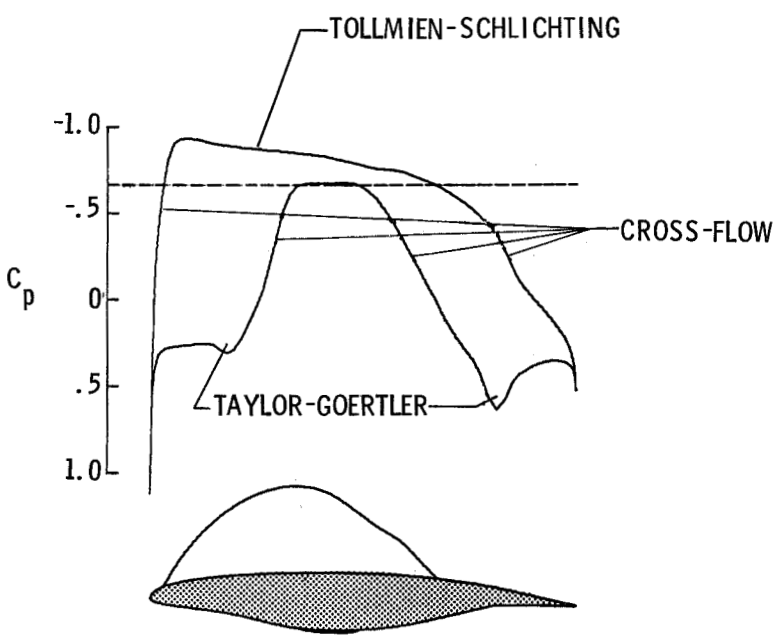

Figure 2.- Laminar-boundary-layer instabilities for airfoil LFC-73-06-135 with M_n = 0.73 and c_l = 0.60.

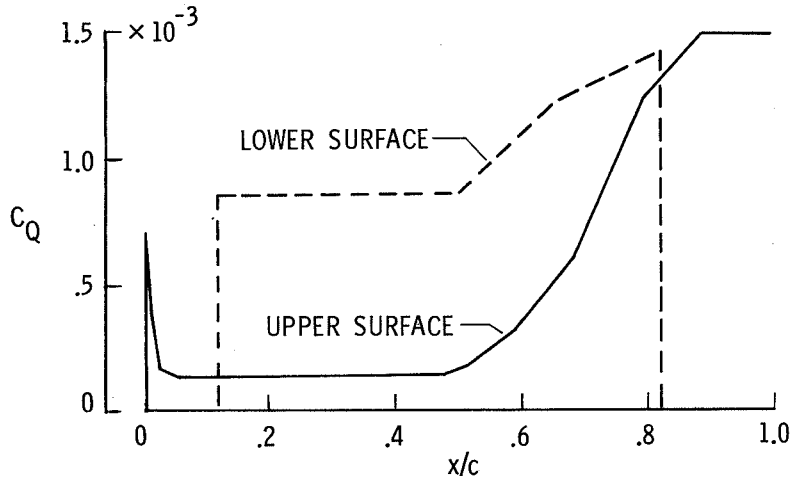

Figure 3.- Laminar-flow-control suction distribution for airfoil LFC-73-06-135 with M_n = 0.73, c_l = 0.60, R = 10 × 10^6, and $\Lambda = 35^o$.

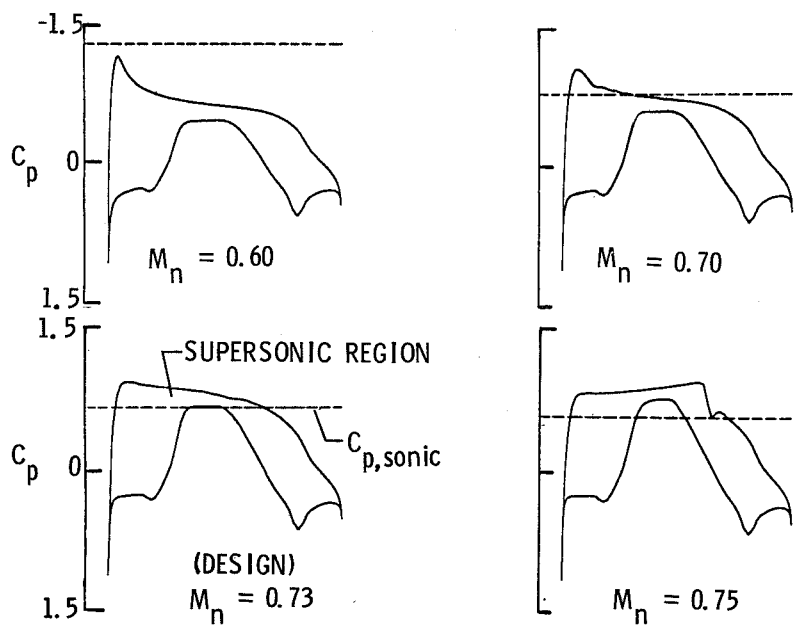

Figure 4.- Inviscid pressure distributions for off-design Mach numbers at design lift coefficient c_l of 0.60 for airfoil LFC-73-06-135.

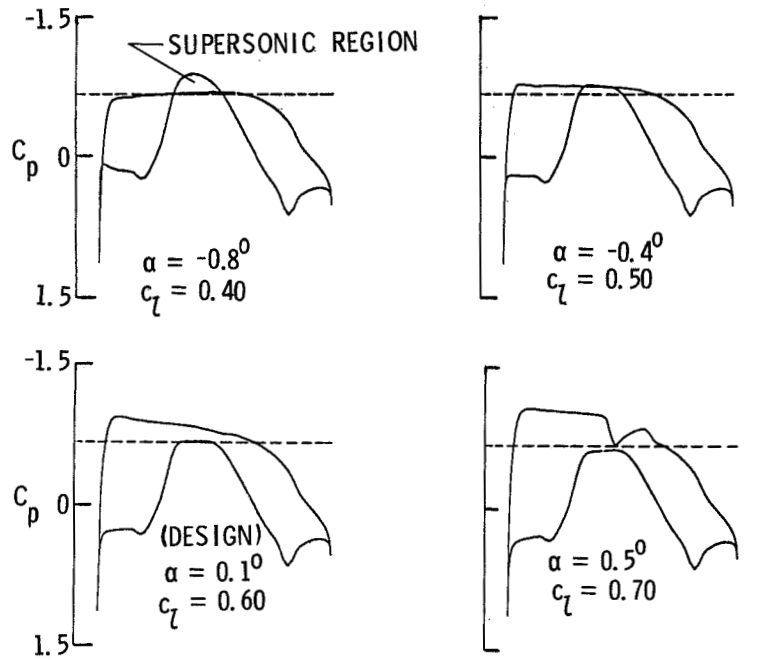

Figure 5.- Inviscid pressure distributions for off-design lift coefficients at design Mach number M_n of 0.73 for airfoil LFC-73-06-135.

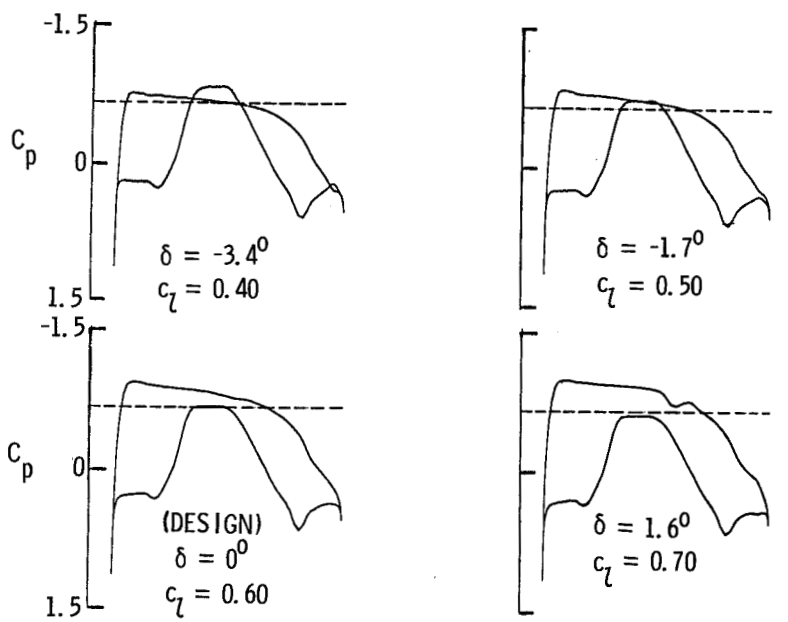

Figure 6.- Inviscid pressure distributions for deflections of a 5-percent-chord trailing-edge flap at design conditions of $M_n = 0.73$ and $\alpha = 0.1^o$ for airfoil LFC-73-06-135.

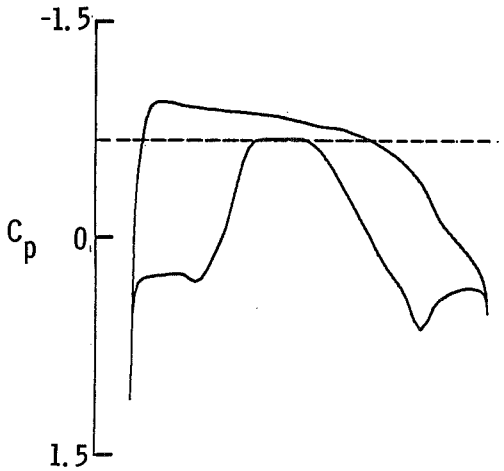

(a) Inviscid design pressure distribution simulating LFC suction for $c_l = 0.60$.

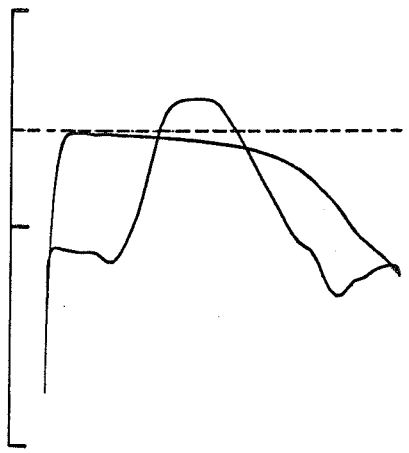

(b) Pressure distribution with turbulent boundary layer for $R = 10 \times 10^6$ simulating no LFC suction with $c_l = 0.28$, $(x/c)_{u.s.sep.} = 0.95$, and $(x/c)_{l.s.sep.} = 0.75$.

Figure 7.- Pressure distributions which show lift loss due to suction failure at design conditions of $M_n = 0.73$ and $\alpha = 0.1^o$.

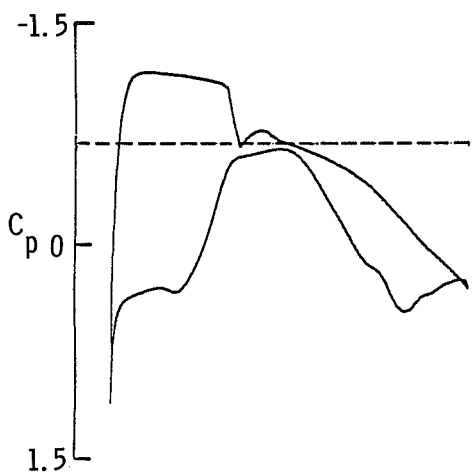

(a) Lift recovery by angle of attack for $\alpha = 1.8^o$ and $\delta = 0^o$ with $(x/c)_{u.s.sep.} = 0.91$ and $(x/c)_{l.s.sep.} = 0.75$.

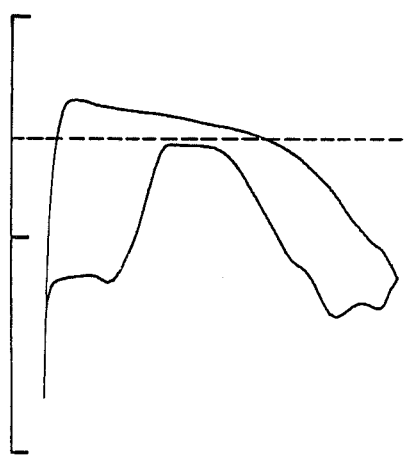

(b) Lift recovery by 5-percent-chord trailing-edge flap for $\alpha = 0.1^o$ and $\delta = 8.0^o$ with $(x/c)_{u.s.sep.} = 0.95$ and $(x/c)_{l.s.sep.} = 0.76$.

Figure 8.- Pressure distributions with turbulent boundary layer for $R = 10 \times 10^6$ which show lift recovery with suction failure at design conditions of $M_n = 0.73$ and $c_l = 0.60$.

APPLICATION OF LAMINAR FLOW CONTROL TECHNOLOGY TO LONG-RANGE TRANSPORT DESIGN

L. B. Gratzer and D. George-Falvy
Boeing Commercial Airplane Company

SUMMARY

Recent implementation of new initiatives to develop Laminar Flow Control (LFC) technology is due largely to the urgency of the energy problem and the realization that successful application to long-range transport aircraft can produce substantial improvements in fuel economy and airline economics. While the techniques of LFC are primarily aerodynamic, the impact on airplane structural concepts and systems is significant and requires a new approach to design integration of the airplane. Based on some 18 months of effort under the NASA LFC program and independent work by Boeing, some critical areas of LFC technology and the potential impact on airplane design are discussed and the corresponding benefits are shown in terms of performance and fuel economy.

Thus, recent advances in laminar boundary layer development and stability analysis techniques are shown to provide a more definitive basis for suction requirements and wing suction surface design. Equally important is the improved physical understanding of disturbance phenomena and the identification of means to cope with real disturbances such as surface imperfections, noise, erosion, ice crystals and other sources. Validation of theory and realistic simulation of disturbances and off-design conditions by wind tunnel testing under appropriate, controlled conditions at full-scale Reynolds numbers are also discussed. The favorable results of an initial series of tests on a partially laminarized wing are presented. Modern developments in the aerodynamic design of airfoils and wings are shown to be compatible with LFC requirements and indeed, to provide a more favorable combination with LFC than could be expected with older aerodynamic design concepts.

As expected, the necessity for slots or porous aerodynamic surfaces and the requirements for surface smoothness and structural integrity pose special and difficult problems for the designer. These imperatives force consideration of structural alternatives involving advanced alloys or composites in combinations now made possible by advanced materials processing and manufacturing techniques. Representative structural arrangements involving the use of advanced materials are presented and the results of their evaluation discussed. The incorporation of active controls concepts in the basic airplane design is shown to provide a means of offsetting weight penalties which would normally result from design requirements peculiar to long-range LFC airplanes.

An outstanding example of systems requirements imposed on the airplane because of LFC is the addition of suction compressor and drive units. The design implications of the choice of units and their location on the airplane

are discussed in relation to performance and reliability. Certain problems associated with operation of LFC airplanes require unusual technological innovation and imaginative design solutions to permit practical operation and economic airline use. The accumulation of insects at low altitudes and the need to cope with various environmental situations are but two areas of concern where possible solutions are presented.

Finally, the manner in which the various design choices are influenced by the state of LFC technology will be displayed. Alternatives for basic airplane arrangement will be shown to depend significantly on answers to crucial questions which are at present unresolved. It will be concluded that the potential for successful application of LFC technology to long-range transport aircraft is only beginning to be understood. Possible directions for and means of future implementation of research and hardware development are outlined.

SYMBOLS

Values are given in both SI and U.S. Customary Units. The measurements and calculations were made in U.S. Customary Units.

A_π	suction unit frontal area, m^2 (ft^2)
c	local wing chord, m (ft)
C_D	drag coefficient
C_L	lift coefficient
C_p	pressure coefficient
C'_Q	slot suction coefficient
h	height of wave on structural surface mm (in.)
L/D	lift drag/ratio
$\dot{m}$	mass flow rate, kg/s (slug/sec)
M	Mach number
q	dynamic pressure, kPa (lb/ft^2)
R	Reynolds number
R/ft	Unit Reynolds number
$R_{\theta_{a.l.}}$	Reynolds number based on θ at the leading edge attachment line
s	distance along airfoil surface, m (ft)

Δs	distance between adjacent slots, m (ft)
S	wing area, m^2 (ft^2)
t	wing thickness, m (ft)
U	freestream velocity, m/s (ft/sec)
U_e	velocity at edge of boundary layer, m/s (ft/sec)
V_{app}	airplane approach speed, m/s (kt)
ΔV	root mean square disturbance velocity, m/s (ft/sec)
w_s	suction slot width, mm (in)
x	distance along chord, m (ft)
δ	boundary layer limit thickness, mm (in)
θ	boundary layer momentum thickness, mm (in)
η	spanwise position (fraction of semi-span)
λ	wave length of structural surface wave, cm (in)
ν	kinematic viscosity, m^2/s (ft^2/sec)
ψ	disturbance wave angle, degrees
ρ	mass density, kg/m^3 ($slug/ft^3$)

Subscripts:

c	chord
cr	critical
L	laminar
REF	reference value
s	slot
T	turbulent
TR	transition
∞	free stream

INTRODUCTION

A resurgence of interest in laminar flow control (LFC) technology is due largely to the urgency of the energy problem and the realization that successful application to long-range transport aircraft can produce substantial gains in fuel efficiency and airplane economics. Significantly, LFC has been identified as one of the few remaining possibilities for achieving the gains noted above and this has resulted in the implementation of a major research effort by the NASA. As part of the Aircraft Energy Efficiency program (ACEE) outlined in reference 1, it involves participation by both industry and the NASA with the ultimate objectives of creating a demonstrator LFC aircraft to establish the economic and operational feasibility of such aircraft in airline service.

The USAF/Northrop X-21 airplane program in the early 1960's (ref. 2) was a major effort to demonstrate the feasibility of LFC on large subsonic aircraft. While substantial success in maintaining laminar flow was achieved, significant design compromises and the lack of overall reliability in a variety of flight conditions left many technical questions unanswered and provided serious concern about the eventual adaptability of LFC to practical operation. From the current vantage point, the need for further research and development is obvious and validates the NASA approach in the ongoing LFC program.

While the techniques of LFC are primarily aerodynamic, the impact on airplane structural arrangements and systems is substantial and requires a new approach to design integration of the airplane. Based on some 18 months of effort under the NASA LFC program as well as independent work by Boeing, this paper will discuss progress in some of the critical areas of LFC technology and show the potential impact on airplane design and the corresponding benefits in terms of performance and fuel economy. Figure 1 illustrates an LFC transport configuration that has evolved from the effort referred to above (ref. 3). It represents a fairly conservative application of LFC technology to a long-range (10 180 km (5500 n. mi.))transport design sized for 201 passengers with cruise operation at Mach .8 and 12,800 m (42 000 ft) altitude. The layout is conventional for a trijet and was chosen to avoid adverse interaction with laminar flow on the wing due either to engine noise or aerodynamic interference between the nacelles and the wing. The wing is laminarized to 80% chord on the upper surface and 70% chord on the lower surface since high suction requirements in the trailing edge areas tend to make further laminarization of marginal benefit. This is compatible with area requirements for ailerons, spoilers and flaps which are less complex and occupy less space than is normal for turbulent airplanes. This characteristic and the elimination of leading edge devices is acceptable because of design requirements peculiar to long-range LFC airplanes. A more aggressive approach involving the use of LFC in appropriate areas of the empennage can be expected in future designs. In any case, the above airplane should be recognized as the basis for the development of the LFC technology applications which will be discussed in this paper.

WING DESIGN FOR LAMINAR FLOW

The central problem in the successful application of laminar flow control is the development of a wing design which permits the maintenance of laminar flow while making efficient accommodation for the structural arrangements and systems necessary to provide LFC. This must be accomplished for a range of flight and environmental conditions corresponding to practical operation in today's airline systems.

Since the fundamental aim is to provide laminar flow over as much of the wing surface as possible, aerodynamic considerations demand first priority. The maintenance of laminar flow at high Reynolds numbers has long been recognized as a laminar boundary layer stability problem requiring increasing amounts of suction on wing surfaces, as Reynolds number increases, to limit the growth of disturbances in the boundary layer. These disturbances can arise from a variety of sources and, if not avoided where possible, or sufficiently controlled, will cause transition to turbulent flow. Thus, it is important to develop a complete understanding of the dynamics of the laminar boundary layer and the methods for its analysis under a variety of conditions encompassing those to be expected in actual operation. This is also essential for the intelligent pursuit of practical design solutions. These solutions must include provisions for wing surface openings of appropriate size and distribution and the internal ducting needed to carry the suction airflow to the suction pump. The suction pump itself must have an efficient driver and the entire unit located to minimize aerodynamic interference and weight. Special considerations include use of a device (e.g., fence or notch) at the wing root to avoid contamination of the wing leading edge flow by the turbulent boundary layer from the fuselage.

Boundary layer analysis methods have undergone considerable development since the X-21 application and figure 2 is intended to show this progression. The classic methods (X-21 period) involved the approaches indicated for the problems of boundary layer development prediction, turbulent boundary layer contamination and laminar boundary layer stability.

Boundary layer development analysis was generally limited to the infinite yawed wing case with approximate means of accounting for compressibility. Even this approach was laborious since computerized methods were usually not available. Analysis of the leading edge area was handled as a special situation which was later recognized to require limiting the attachment line Reynolds number ($R_{\theta_{a.l.}}$) to values less than 100 to 200 for swept, tapered wings. The current approach to development analysis is based on the swept tapered-wing model with full accounting for compressibility and relies heavily on the use of modern computer techniques. The attachment line boundary layer can now be used as the starting point for the stability analysis although the $R_{\theta_{a.l.}}$ criteria may still be invoked under some circumstances; e.g., where turbulent boundary layer contamination from the fuselage is involved. Future developments are likely to involve only minor improvements (e.g., automation,

special cases) since today's methods are essentially complete.

Contamination of the laminar boundary layer at the wing leading edge due to convection of turbulence from the fuselage is a practical problem which has been handled by ad hoc solutions and is not presently susceptible to analysis. The interplay between the various measures indicated in figure 2 is incompletely understood and requires experiment to establish the most favorable configuration for a given application. Also, the turbulent flow at the wing root intersection causes a significant area to be not laminarizeable with current techniques. Further innovation is required to evolve approaches to maintain laminar flow in intersections, particularly if LFC on the fuselage becomes an objective.

Classic methods to analyze laminar boundary layer stability involve the separate treatment of the crossflow and the tangential flow. For the crossflow the streamwise vortices ($\psi \doteq -90^{o}$) are considered the most unstable mode while the Tollmien-Schlichting mode ($\psi = 0^{o}$) is assumed to be critical for the tangential flow. Although this approach has appeared reasonably successful in estimating amplification levels to establish suction requirements, the tenuous connection between predicted amplification and boundary layer disturbance levels has been unsatisfactory and remains so today.

Recently developed methodology has a number of advantages over the classic approach including the implementation of computing techniques to greatly reduce the labor involved in analysis. Moreover, the unified treatment of the compressible three-dimensional boundary layer avoids the artificial separation into the crossflow and tangential flow modes by introducing the disturbance wave angle as a separate variable along with frequency. It also introduces the influence of compressibility on a systematic basis. The calculation of allowable disturbance amplitude ratio and the relationship to the ambient disturbance levels has progressed little beyond that of the classic analysis. The allowable amplification ratio is generally believed to be in the range e^{9} to e^{12} although this implies several assumptions which cannot be verified. A major assumption seems to be that the "normal environment" for laminar flow involves a certain initial level of disturbance which, when amplified to some threshold value, will produce transition. Specification of the allowable amplification ratio implies that the ratio of initial disturbance level to the threshold level is known. This is a dubious proposition in view of the fact that different types of disturbances may exist in the environment or be produced in the course of flow over the surface, each having its own peculiar modal and energy transfer characteristics.

Thus, we are led to hope that the future will see the development of better methods of coping with disturbance growth analysis. New methods are needed to analyze the local effects of flow through slots or porous surfaces including disturbances generated in this process which may persist downstream. Ultimately, a complete three-dimensional analysis involving all possible modes including sound may be required to establish a valid theoretical basis for predicting suction requirements and defining system geometry.

From the previous discussion it will be apparent that the disturbance environment and the control of amplified disturbances in the boundary layer is a major hurdle in the successful design and operation of an LFC airplane. There are many external disturbance sources and the chart of figure 3 illustrates typical allowable levels for those sources of significance. The areas of major design impact are also shown. The allowable engine noise is based on a recent analysis and depends on the criteria assumed for transition and, to a lesser degree, on the portion of the wing surface involved. Surface imperfections can have various manifestations and the ranges shown generally apply for single elements, or elements widely separated on the wing surface. While the values given are representative, they will vary somewhat depending on the unit Reynolds number and the local state of the boundary layer. For closely spaced elements, the allowable levels are obviously much less but remain undefined. It should also be recognized that the values given above are subject to considerable revision depending on the precise configuration of roughness elements, and the presence of other disturbances of any type.

The presence of ice crystals is widespread throughout the upper atmosphere and can substantially influence the choice of cruise altitude even on a daily basis. This is illustrated by the data of figure 4, taken from reference 4, which show the effects of ice particles on LFC degradation at 12 100 m (40 000 ft) altitude and Mach .8. The threshold for significant loss of LFC depends on both particle diameter and concentration as shown and becomes higher as altitude increases. Based on data measured over Kwajalein Atoll throughout the late summer months (ref. 5), it is apparent that, near the equator, the ice particle distribution is such that some loss of LFC could be expected a substantial fraction of time. Fortunately, at higher latitudes, available evidence indicates that the critical particle distributions occur at lower altitudes and tend to diminish rapidly above the tropopause. Thus, an LFC airplane capable of cruise above 12 200 m (40 000 ft) could operate reliably over most of the major airline routes. However, long-range routes involving penetration of the lower latitudes would apparently need additional aids such as weather monitoring, particle sensors, etc., to permit economic operation. Additional data are needed to provide a clear understanding of the operational requirements associated with ice particles and the design requirements for cruise altitude capability.

The presence of atmospheric turbulence is known to have some effect on laminar flow but these effects are difficult to measure and are generally judged from the X-21 experience to be unimportant. This is because the normal atmospheric turbulence spectrum contains very low levels of turbulence in the frequency range critical to laminar boundary layers.

Returning now to the question of engine noise, its potential impact on airplane design can be illustrated by reference to a study (ref. 6) based on noise data taken in flight on a 747 airplane. For conditions appropriate to the LFC airplane of figure 1, the spectrum of the noise incident on the wing lower surface was analyzed to establish the contributions of its significant components, i.e., jet, turbomachinery, boundary layer, etc. Based on the appropriate incident noise levels, the disturbance levels in the boundary layer were estimated using calculated amplification factors for the critical

frequency range. Transition was estimated to occur when the disturbance level exceeded a certain value in terms of $\Delta V/U$. This approach was validated using the results of wind tunnel tests with several types of noise spectra incident on laminar flow surfaces. Analyses were accomplished for several cases involving different engine and acoustic lining combinations. The results are given in figure 5 which shows the potential loss of laminar area on the wing lower surface for two values of transition criteria $(\Delta V/U)_{TR}$ to indicate the sensitivity of the results to the criteria. It is apparent that the 1985 engine having a high bypass ratio (BPR = 7.5) and with LFC lining to reduce internal noise in the critical frequency range will not cause significant loss of laminar area even on the basis of a conservative transition criteria. Moreover, the current engine with LFC lining would, on the basis of a more reasonable criteria, produce essentially no loss in laminar flow. The incident noise range given in figure 3 corresponds to the limits for the above cases. Based on the above results, wing-mounted engines for LFC airplanes could be considered feasible provided that aerodynamic interference between nacelle, strut and wing is not excessive. The inherent advantages of wing-mounted engines in terms of weight and balance provide incentive to further explore this design alternative.

The development of advanced high-speed airfoils for modern wing design has continued to receive attention in relation to their potential for increasing wing thickness, and thereby reducing wing weight, with no reduction in speed. For a number of reasons, the impact of advanced airfoils is even more favorable for LFC airplanes. The following are of principal importance:

1. The increased volume available with greater thickness provides critical accessibility and the space to accommodate internal ducting for suction airflow collection and removal.

2. With laminar flow surfaces, no significant drag penalty due to thickness occurs as in the turbulent wing case.

3. Tailoring the wing pressure distribution to achieve straight isobars with relatively flat chordwise distributions is more easily achieved. This is highly important for LFC wings since proper suction inflow distributions must be achieved with minimum flow losses.

Wing geometry and pressure distribution are shown in figure 6 for the reference airplane (fig. 1) for representative flight conditions. The airfoils at 28% semi-span (η = .28) and beyond are designed with the pressure recovery starting at about 70% chord providing a nearly constant pressure over the major portion of the wing. A slight recovery occurs just behind the leading edge peak to suppress the remaining boundary layer crossflow. The leading edge radius is sufficiently small to maintain $R_{\theta_{a.l.}}$ below 100 for the 25° swept wing. Inboard of η = .28, the airfoils deviate progressively from the basic section shape to that shown at the wing root (η = .11). This shape is fairly characteristic and provides an upper surface pressure distribution

compatible with other areas on the wing. To provide flow conditions limiting $R_{\theta_{a.l.}}$ to 100 in this area, the leading edge radius is held within limits by somewhat flattening the leading edge contour on the lower surface to produce the pressure distribution shown. The wing can be expected to operate over a substantial range of lift coefficient with relatively minor adjustments in suction flow, particularly if slight adjustments in wing flap angle are made. The loss of laminar flow in unusual situations can be expected to produce no adverse flight or performance characteristics beyond those associated with the increased drag due to turbulent flow.

For a laminar flow wing design, a fundamental requirement is the determination of the suction distribution to maintain laminar flow under the appropriate range of operating conditions. This will include variations in chordwise and spanwise pressure distributions, Reynolds number, Mach number, disturbance environment, etc. Thus, as shown in figure 7, the characteristic slot orientation is generally spanwise and along isobars insofar as possible. The suction distribution on both upper and lower surfaces is shown on the right for three spanwise locations. This is given in terms of C_Q' which is based on the mass inflow and average spacing corresponding to each slot. Thus, on upper surface, the spacing is quite small in the leadingeedge area, reflecting the high suction requirement for the unstable boundary layer crossflow situation there. Slot endings at certain spanwise locations are selected to maintain a reasonable slot Reynolds number ($R_s = Uw_s/\nu$) distribution and adhere to proven slot width (w_s) criteria. Avoidance of significant disturbances from the slot ends is extremely important. Over the main portion of the wing box the slot spacing is characteristically wider, corresponding to lower suction requirements in the area where the Tollmien-Schlichting mode is critical. In the pressure recovery area, the combination of adverse pressure gradient and crossflow again raises the suction requirement necessitating smaller slot spacing back to the 80% chord position. Laminarization beyond this point was not used because of high local suction requirements which result in high equivalent suction drag and excessive suction unit size. Thus, the incremental performance gain is very small for laminarization beyond 80% chord. The extreme difficulty of providing suction in areas occupied by ailerons, spoilers and flaps is also a major inhibiting factor.

On the lower surface, the gain due to laminarization is relatively smaller so the suction is terminated at the rear spar position (70% chord). The suction distribution requirements are similar to those of the upper surface, but the quantity is somewhat higher. The slot spacing variation is also similar but the actual number of slots is larger. The above characteristics are due to the longer chordwise extent of both the leading edge crossflow and the trailing edge pressure recovery areas. It will be noted that the slots do not extend spanwise into areas where the turbulent contamination from the wing/body intersection and the wing tip are propagated.

LFC WIND TUNNEL TESTING

From the preceding discussion it should be apparent that wind tunnel tests will be vital to the successful development of LFC wings and the system elements which serve essentially aerodynamic functions. Furthermore, the need is urgent to conduct these tests under realistic conditions, specifically including both unit Reynolds numbers and chord Reynolds numbers, because of the overriding importance and sensitivity of these parameters in relation to boundary layer stability and the effects of disturbances. Because of the latter, the test environment should be one of low ambient disturbance levels--especially the stream turbulence and noise. The effects of Mach number, while significant, are generally not large and can readily be estimated for correlation between low-speed test results and expected flight performance. Some uncertainty currently exists as to the importance of local Mach number effects on slot inflow stability and possible induced downstream disturbances. Although the mechanism is poorly understood, it is not anticipated that the above effects will be of major importance. Several means of minimizing the impact have been considered in suction surface design such as using closely spaced slots or dual-slot arrangements. On the basis of the above considerations, the Boeing Company, in support of LFC design studies done under NASA contract, decided to develop an experimental facility (ref. 7) to permit investigation of the problems associated with laminar flow control by boundary layer suction on large subsonic transport aircraft. The low-speed Boeing Research Wind Tunnel (BRWT) was chosen as the basic facility for the LFC wing model testing since measurements have indicated the turbulence and noise levels were within acceptable limits; i.e., $(\Delta V/U) \doteq .0015$. The 1.53m (5 ft) by 2.44m (8 ft) test section will accommodate a large model permitting near full-scale test Reynolds number (up to $R_c = 25 \times 10^6$). The 2.44m (8 ft) span, 6.1m (20 ft) chord model dimensions were chosen to represent a typical section of a 30° swept wing. The LFC wing test arrangement is shown in figure 8 as installed in the BRWT between floor and ceiling. The airfoil section was designed to provide, in the presence of the tunnel walls, an upper surface pressure distribution typical of the mid-span portion of an LFC transport wing at cruise conditions ($M = .80$, $C_L = .5$). The leading edge was shaped to provide a value of $R_{\theta_{a.l.}}$ approaching 100 at the above condition. Although the general pressure level on the model lower surface corresponded to that of the airplane, the independent selection of leading edge radius (shape) produced nonrepresentative pressure variations near the leading edge. These can, however, be appropriately controlled by selecting a different incidence angle when the lower surface flow is of primary interest. The installation also included fairings on the tunnel floor and ceiling to prevent significant spanwise pressure gradients on the model. A three-segment trailing edge flap was also used to provide flexibility in pressure distribution adjustments.

For the initial phase of the test program, only the first 30% of the upper surface and the first 15% of the lower surface had provisions for LFC. Although these areas are the most critical, the suction area will ultimately be extended to the flap hinge line (80% chord). The suction surface is divided

into four sectors each served by a separate plenum chamber. Each plenum has a separate metering and measuring apparatus and the distribution of the suction flow between individual slots is controlled by slide-valves running the length of each slot. Pumping power is provided by an ejector driven by high pressure air. Two views of the physical installation are provided by the photographs of figure 9. The characteristics of the model described above are evident including the suction slots near the wing leading edge (downstream view).

Validation of the test apparatus has been accomplished in two steps. First, the model was tested with an alternate forward section which had no suction slots but incorporated an ample number of surface static pressure taps. The main objectives were to verify that the desired pressure distributions could be achieved by appropriate settings of the model incidence and flap deflection, and to determine the extent of natural laminar flow and general boundary layer development on the test surfaces. A detailed investigation of the leading edge flow pattern by means of several flow visualization techniques clearly indicated the nature of the transition phenomena on the leading edge. Figure 10 is a photograph of the wing leading edge on which the flow pattern is made visible by painting the surface with a lampblack and kerosene mixture. After long exposure to the flow, the coating is thinly distributed downstream revealing the random wedge distribution pattern which tends to remain stable with time. Although it is apparent that disturbances originate at the apex of each wedge, later inspection generally showed no discernible surface imperfections or accumulation of particles at these locations. The progressive appearance of wedges as the flow velocity is increased indicates the sensitivity to unit Reynolds number and the onset of unstable boundary layer flow conditions in the region of intense crossflow. Boundary layer measurements in the areas of wedge accumulations indicated early transition to turbulent flow, whereas in wedge-free areas the flow remained laminar. Based upon the infrequent appearance of disturbances forward of $s/c = .01$, the first suction slots were provided near this location ($s/c = .013$) on both upper and lower surfaces, thus avoiding the complex vertical slots originally contemplated for the attachment line area.

Having accomplished the first objectives, testing of the suction model followed. The initial aim was to demonstrate that the suction system would function properly and was capable of maintaining laminar flow reliably over the areas where suction was applied. Additional objectives were to establish the suction distribution for maximum efficiency, explore the sensitivity to oversuction and the effects of shutting off certain slots. A further goal was to evaluate several experimental techniques for detecting transition and monitoring LFC system effectiveness. Typical test conditions are given in figure 11 which shows the airfoil pressure distribution and suction flow in individual slots corresponding to an efficient suction level and distribution required to maintain laminar flow to 30% chord. The corresponding slot Reynolds numbers, R_s, are shown on the right-hand scale of the lower plot indicating general adherence to the criteria $R_s \leq 100$. No difficulty was experienced with operation of the first slot beyond $R_s = 150$ and, indeed,

operation at suction levels 50% higher than normal exhibited no critical characteristics.

Typical results of boundary layer surveys are presented in figure 12 which shows profiles at the same location just downstream of the last suction slot. Without suction the characteristic turbulent boundary layer profile appears, as would be expected, and the thickness, δ_T agrees well with predicted growth. With suction applied, the flow remains laminar although the profile shape is fuller than the characteristic Blasius shape as would be expected just downstream of a suction slot. The profile in this case is only about 80% as thick as could be expected from normal laminar boundary layer growth, reflecting the application of suction ahead of the measuring point. Although an ultimate objective is to compare the suction requirements with theory, considerable analytical development along the lines suggested in figure 2 will be required before valid comparisons can be made. This is because the presence of noise and turbulence in the wind tunnel, for example, introduces disturbances in the laminar boundary layer which can only be roughly accounted for. The best to be expected for the immediate future is to compare calculated disturbance amplification ratios corresponding to observed positions of transition in these wind tunnel tests for a variety of test conditions. These comparisons can also be assessed in relation to data from other sources. If a history of correspondence in amplification ratio can be shown to exist, a certain confidence in the validity of this criteria may be established for known types and levels of the disturbance environment. Regardless, an assessment of the test results and the general experience to date leads to the conclusion that the objectives outlined above have been achieved. Although much experience and considerable data has been accumulated in connection with the X-21 program and related activities, much remains to be accomplished; particularly the investigation of the myriad questions associated with design choices which must be made in the development of efficient and practical LFC systems. The Boeing facility will be useful for such work and will, hopefully, contribute substantially to the advancement of LFC technology.

STRUCTURAL CONCEPTS FOR LFC

The previous discussion has emphasized the characteristics of LFC wings which are unusual and stem primarily from the fundamental requirement to establish and maintain laminar flow throughout a reasonable flight envelope. As expected, the necessity for maintaining suction through slots or porous aerodynamic surfaces and the requirements for surface smoothness while maintaining structural integrity pose special and difficult problems for the designer. These imperatives force consideration of structural arrangements involving advanced alloys or composites in combinations now made possible by the use of advanced materials processing and manufacturing techniques. The familiar requirements for achieving acceptable reliability, repairability and maintainability characteristics remain as demanding as in today's structures, while more elusive in the design process due to the added complexity of structures and systems. The search for satisfactory solutions involves the

consideration of a large number of alternative concepts and arrangements which must be carefully evaluated in relation to the design requirements and objectives. Of fundamental and, in some cases, overriding importance is the weight impact of the various candidate designs under consideration. No design can be expected to be ultimately successful which does not closely approach the unit weight level of the best of today's wing structures. Thus, attention to selecting concepts which minimize parasitic weight features must be emphasized at the outset. During the extensive design activity phase of the current contract, many alternatives have been considered and subjected to critical review based on the criteria discussed above. Promising candidates continue to be evaluated and quantitatively compared to a contemporary baseline structure of aluminum skin-stringer design.

One of the more promising concepts is illustrated in figure 13 which shows a typical wing cross section and details of the wing box structure. The laminated aluminum honeycomb design is a sandwich arrangement which features laminated inner and outer skins built up of aluminum sheet sections. These overlap sufficiently to provide required fail-safe characteristics. The skin bonding operations are done in a bonding assembly jig contoured to required surface tolerances. During the bonding cycle, pressure is maintained sufficient to insure proper wing shape and smoothness. The intermittent honeycomb core is placed with appropriate gaps to form the spanwise duct edges so that, with the assembly and bonding of the inner and outer skins and the core, a complete sandwich is formed incorporating spanwise ducts of the required cross-sectional areas. This second stage operation, which includes bonding of the rib chords and spar chords to the inner skin, is carried out in the same bonding assembly jig used in the skin manufacture. Assembly of the upper and lower sandwich panels to form the complete wing box is done by attaching the rib and spar webs to their respective chords with mechanical fasteners.

The suction air is removed through continuous spanwise slots. In this case, the slot is formed by bonding two strips into a machined recess in the outer skin. The stepped recess also provides a plenum area below the slot to diffuse the flow before it passes through appropriately spaced bleed holes into the tributary ducts. The bleed holes are drilled and cold-worked to avoid fatigue penalties which can be significant, particularly for the wing lower surface. Section A-A shows a better view of these ducts which serve to meter the flow through the nozzles into the main spanwise duct which carries the flow to the suction unit. An evaluation of the wing weight potential of this LFC concept shows it to be only about 6% heavier than the conventional riveted skin-stringer aluminum wing of a turbulent airplane.

The suction slot arrangement is shown in figure 14 for both the upper and lower wing surfaces. The slots have the same orientation as the spanwise ducts located directly below them and each slot is served by a single spanwise duct. For slots ending at various spanwise positions, the ducts will also end at corresponding locations. It will be apparent that with this particular concept, the structural arrangement is closely tied to the slot arrangement. Since this poses some difficulties, other concepts are being explored to provide some independence between structural elements, slots and associated ducting.

A variation of the arrangement shown is one involving the use of essentially constant slot spacing at least over major portions of the wing box. If the front spar is used as the base position, this allows considerable reduction in total slot length and avoids the spanwise termination of slots in the laminar areas. In the pressure recovery areas, spanwise tapering of the slot spacing can again be used to accommodate suction requirements as a function of spanwise position. The use of suction opening designs which avoid rigid adherence to current slot Reynolds number criteria can also be used to permit a slot configuration which is more adaptable to the efficient arrangement of structural elements.

For each suction position, the geometry of the flow passages should ideally match the local inflow requirement. However, it is generally possible to select a suction surface configuration such that a small number of standard slot widths can be used to accommodate the various local needs. Also, a large number of possibilities exist for the design of the opening itself. Figures 15(a) and 15(b) present a number of candidates each having its own set of advantages. The first option (integral slot) is basic and has been used on the X-21 airplane, other flight hardware and wind tunnel models. In the laminated structural design of figure 13, the cavity would be machined and the bleed holes drilled and cold-worked before bonding of the outer ply. The slot sawing is the final operation and may represent the most critical part of the process. Because of the inherent disadvantages (i.e., manufacturing, maintenance, etc.) of the integral slot, various types of inserts have been devised to facilitate the manufacture, installation, maintenance, repair and replacement of suction surface openings. Concepts 2 and 3 are simple slotted inserts which function in the same way as Concept 1. Concept 4 consists of an insert assembly which contains not only the slot but the plenum cavity. This avoids some of the difficulties of manufacture and tolerance control of Concepts 2 and 3 but will tend to produce higher flow losses. However, it has the further advantage that the suction flow can be metered as a function of position on the wing, thus avoiding the use of tributary ducts and allowing more flexibility in the geometry of the main bleed holes. Concept 5 is another attempt at simplifying manufacture and installation through the use of an aluminum foam base which can be depressed on installation to minimize joint discontinuities. Concept 6 is a simple strip containing an appropriate perforation pattern which can be readily manufactured using the Steigerwald electron-beam drilling process. Fatigue sensitivity is a disadvantage unless an appropriate material can be found. These and other variations are all adaptable to the basic structural arrangement shown in figure 13. A final choice will depend on many factors which can be appropriately balanced only after complete evaluation and testing to determine structural and functional suitability in the realistic operating environment.

Reference has previously been made to studies of a number of structural alternatives based on promising combinations of innovative arrangements and advanced materials made possible by new processes or manufacturing techniques. The arrangement shown in figure 13 is one such based on the extensive use of bonding and improved aluminum alloys to reduce weight and meet the smoothness requirements for laminar flow surfaces. This concept has been chosen (ref. 8) as the most likely candidate for application in the relatively near term since

it involves the use of familiar materials and processes and would probably not involve long-term, extensive development programs. Other promising concepts which have undergone considerable design development and evaluation are shown in figure 16. The first concept, using graphite fibers with an epoxy matrix, is characteristic of several evolving from the work being carried on today under the NASA-sponsored composites activity in the ACEE program. This particular arrangement incorporates a thin titanium outer skin to provide a smooth, durable surface and protection against lightning strike. Evaluation of this concept has shown it to be generally compatible with LFC requirements and to have outstanding weight reduction potential; i.e., about 14% lighter than conventional structure. However, on the basis of current and foreseeable development activity, it is considered to be applicable only in the longer term

The bonded aluminum skin-stringer arrangement shown next permits efficient distribution of material throughout most of the wing and avoids the use of elements tending to be parasitic (e.g., honeycomb). It has the added advantage that bonding provides better fatigue resistance in comparison to conventional riveted skin-stringer arrangements, but the question of shear-tie effectiveness remains a cause for concern and further study. It is potentially competitive from a weight standpoint with conventional structure and thus continues to be an attractive structural alternative.

The third concept (fig. 16(b)) contemplates the use of titanium throughout and fabrication by means of the simultaneous superplastic forming and diffusion bonding process (SPF/DB) which is currently undergoing development for higher temperature applications. This was considered to be a candidate for LFC structures because of its apparent adaptability to forming of intricate assemblies involving many parts where significant production economies might be realized. However, an evaluation of variations on this approach have not been competitive from a weight standpoint. The recognized long-term nature of the development cycle and the facility expense involved for production have served to discourage further effort in this direction.

The fourth concept is very similar in arrangement to the laminated aluminum honeycomb design and contemplates using a suitable chemical bonding process for assembly which would require development for production application. This approach has not proven competitive with the aluminum concept primarily because the structural elements tend to be somewhat less stable and, therefore, heavier.

The last two concepts (fig. 16(c)) are characterized as riveted skin-stringer types because the basic underlying structure uses aluminum with conventional structural shapes and assembly processes. For the fifth concept, the fiberglass outer skin panel(s) can be configured more or less independently of the main structure and are applied after the latter is built. This final phase is accomplished by bonding spacer strips to the stiffener flanges and machining to contour. Bonding of the outer fiberglass skin containing slots (or suitable inserts) is done last. Although this approach involves parasitic elements and less efficient use of structural material, the manufacturing

advantages appear significant and further design development may lower the overall weight into the range of interest. This possibility will become more attractive if the costs of other, more exotic approaches prove to be unacceptable.

The sixth concept shown contemplates the use of so-called "snap-in" strips to close out the space between structural elements and provide a continuous outer surface. The use of a resilient material for the strip or a slightly deformable insert design of standard sectional shape is essential for this concept. The strip also incorporates the suction opening, the sub-surface plenum and bleed hole pattern which carries the suction airflow into the inter-stiffener spaces which form the spanwise ducts. Of the various concepts discussed above, the first four have been evaluated and their relative potential for application has been discussed above. The last two concepts and options derived from them are still in various stages of development and evaluation.

ADVANCED TECHNOLOGY IMPACT

The above discussion highlights structural concept development in which favorable combinations involving different materials and types of construction have been sought. The application has been to the wing structure where it is difficult to assess the separate impact of each new technology element. While it is recognized that these developments can benefit the turbulent airplane as well as the laminar airplane, the overall effect is significantly greater for the latter since design studies continue to point toward higher wing area and span for LFC airplanes. The use of advanced materials and construction techniques is thus more important to reduce wing weight in this case. The chart of figure 17, however, avoids the above type of comparison and instead provides a simple statement of impact on the weights of major LFC airplane components. A definitive comparison of the relative impact for laminar versus turbulent airplanes is left for the time when final designs of each aircraft, both performing the same mission, are available. It is apparent from figure 17 that extensive application of graphite/epoxy composites to the airplane exhibits the greatest potential for weight saving. However, it must be recognized that these gains are applicable in the longer term than are those for improved alloys and bonded construction. However, application of composites to trailing surfaces is considered appropriate in the near term.

To complete the assessment of various elements of advanced technology that could be applicable to an LFC transport airplane in the 1990 time period, figure 18 summarizes the gains appropriate to each element. Of major significance, of course, is laminar flow control itself which provides a 26% gain in lift to drag ratio with wing LFC only. The weight impact, which applies mainly to wing and systems, continues to be assessed and remains to be determined (TBD). As previously pointed out, advances in airfoil design are of somewhat greater significance for an LFC airplane and result in substantial weight improvements without the corresponding drag penalties associated with

increased thickness for the turbulent airplane. Reduced roughness provides a significant L/D gain which arises because of the inherent smoothness of the LFC wing and also the smoothness associated with bonded construction on the fuselage and empennage.

The projected incorporation of active controls provides significant improvements in both weight and drag, primarily through reduction in horizontal tail size and trim drag. Load alleviation impact will tend to vary with airplane configuration but recent analyses support a conservative 8% reduction in weight of the wing box. This again tends to be higher for the LFC airplane because of the basic tendency toward higher aspect ratio and lower wing loading than for the turbulent airplane. The use of a flutter suppression system (FSS) may be appropriate depending on the airplane configuration and the wing weight penalty associated with providing normal flutter margins. A small penalty is preferable to the added complexity of a FSS. However, if the performance benefits of high wing aspect ratio become sufficiently important, the use of a FSS should be considered.

An advanced turbofan may be a reasonable possibility in the 1990 time period provided that continuing studies (e.g., the EEE program) continue to support substantial performance and weight gains such as those shown. Such gains would have to be achieved with high confidence that unfavorable maintenance trends with current high bypass ratio engines could be avoided. Results of current LFC airplane studies tend to show significant fuel savings for bypass ratios up to 7.5 with small effects on direct operating costs (DOC).

LFC SYSTEMS

The suction system is a prominent example of systems requirements imposed on the airplane because of LFC which impacts many areas of the airplane design as well as its performance and reliability. Studies directed toward the evaluation of various alternatives for suction system elements and compressor/drive components have been completed and a system selection made for the baseline airplane as reported in reference 9. The chart of figure 19 displays the important options for both the suction compressor and the power source together with the related choice of unit location on the airplane. The two-pressure level compressor arrangement appears to provide the best compromise between the need for high system efficiency and the desire to avoid undue complexity. The two levels generally correspond to those for the upper and lower wing surfaces with appropriate allowance for inflow and duct losses which are characteristically about $.05q_\infty$ and $.15q_\infty$, respectively. Trade studies to determine the appropriate exhaust velocity levels for both the suction compressor and the drive unit are the subject of current study.

The drive type selection involves a number of possibilities which have to be evaluated on a consistent basis. This has been done for all the options shown in the first category under "drive-type" (except electrical and hydraulic) for systems located in the aft-body area close to the main engines and

below floor level. Suction air in this case was ducted from the wing root through an unpressurized area below floor level back to the suction units as described in reference 3. In this location the turboshaft engine drive rated consistently high in all areas including performance, except in comparison with the direct mechanical coupling where its fuel consumption was only about .5% higher. The turboshaft engine was also the logical choice for the wing-mounted location because of distance from the main engines. In a case where the empennage is also laminarized, the use of an APU which would normally be provided for the airplane, is considered to be appropriately sized and would be located in the aft-body area.

Based on studies carried out to assess the relative advantages of the various options above, the suction unit installation on the wing appears most desirable and the location at the root was selected on the basis of arrangement convenience and least interference with laminar flow areas. The main features of this installation are shown in figure 20. Although this location appears attractive, the configuration details are important to the overall performance. Of major significance is the effect of the suction unit on drag. The wind tunnel data of figure 21 show this impact for a representative simulation of the suction unit fairing. It is apparent that a significant increase in drag and reduction in critical Mach number occurs in the cruise C_L range. The oil flow picture shows the disturbed area which tends to go beyond the normal turbulent wedge from the wing/body intersection. Such effects are unacceptable and highlight the need for further tailoring of the installation or perhaps reconsideration of the initial choice of location.

As shown previously, one of the major factors affecting the maintenance of laminar flow is the disturbance environment in which the airplane must operate. The leading edge roughness associated with the residues of insects encountered at low altitudes is recognized as a major operational problem. Thus substantial effort has been devoted to developing solutions which are reliable and do not adversely affect other operational characteristics or the economics of the airplane. Many solutions have been proposed which, for one reason or another, are impractical or difficult to implement. Past approaches include:

- "Superslick" films
- Hydrophobic sprays
- Sublimation coatings
- Mechanical scrapers
- Deflectors
- Fly-away covers
- Washing systems
- Liquid films

Of these, the last technique appears to have some promise based on recent NASA tests on a Jetstar aircraft at Dryden FRC. Figure 22 illustrates a variation of this concept in which the liquid (H_2O + anti-freeze) is continuously ejected during takeoff or landing to prevent adherence of impinging insects to the surfaces. An obvious disadvantage is the requirement for system maintenance and continuous liquid supply.

Two other candidates are also shown which appear to have potential. The cryogenic frost system operates on the principle of expanding a cryogen (LN_2) into a mixing chamber to provide cold air (about -15°C) for distribution along the leading edge. The cold metal would, except in a dry atmosphere, cause the formation of frost in a relatively short time prior to takeoff. During the takeoff and climb, adherence of impinging insects would be inhibited by the frost. With shutdown of the system, the airstream would quickly melt the frost leaving a clean surface for laminar flow. However, this type of system would not be effective during landing approach so that ground preparation for following flights would frequently involve manual cleaning of the leading edges.

The third concept uses high pressure bleed air to provide two-dimensional jets directed forward into the airstream. At flight speeds, the jets are turned back onto the leading edge to avoid significant adverse aerodynamic effects while acting as a shield to prevent the impingement of insects on the leading edge. Although the principles involved in the approaches shown are obvious, considerable development and testing under simulated operating conditions is required to establish feasibility and determine the appropriate system parameters and characteristics.

Additional features of the cryogenic frost system are shown in figure 23, which illustrates the combination of the frost system and the anti-icing system which share a common distribution duct having a spanwise series of holes to direct the flow toward the wing leading edge. In the frosting mode of operation, the return flow through the auxiliary spar mixes with the primary flow of N_2 in proportions controlled by the characteristics of the ejector nozzle to yield the proper leading edge temperature. The pressure bleed valve is used to maintain the appropriate pressure in the wing cavity. For the anti-icing mode, engine bleed air is mixed with the return flow in a similar manner to provide a controlled temperature as required.

In addition to the leading edge insect protection and anti-icing systems described above, the LFC suction air must be conveniently routed to the suction unit. Since the suction rates in the leading edge area tend to be high, with correspondingly smaller slot spacing, it has been found desirable to provide plenum type ducts for both upper and lower surfaces in this area, since individual ducts serving each slot would tend to physically interfere. Figure 24 shows a workable arrangement for the portion ahead of the front spar which can be used with many of the structural concepts previously discussed. Honeycomb sandwich panels are used for both upper and lower surfaces and the divider separating the plenum ducts. The nose portion ahead of the auxiliary spar contains no slots and is made of titanium to minimize erosion problems and susceptibility to other damage. The distribution duct in this area serves the

function described above for the frost/anti-icing system with the nose cavity providing the return path. No return flow crosses the auxiliary spar in this case.

AIRPLANE DESIGN REQUIREMENTS AND ALTERNATIVES

Airplane design requirements appropriate to long-range LFC transports were discussed briefly in connection with the presentation of the configuration shown in figure 1. Based on operational requirements studies to date, cruise altitude and climb capability under turbulent flow conditions emerge as controlling factors in the design which largely determine wing loading and thrust loading. Because of this, the takeoff distance and approach speed requirements no longer tend to dominate as in the case of the turbulent airplane. The way in which these factors interact will be illustrated in relation to the important configuration parameters such as wing loading, aspect ratio, sweep, etc., in the following discussion. Before doing this, however, it should be pointed out that the baseline airplane is the product of a design cycle involving a number of preliminary trade studies such as required to determine extent of laminarization, high lift system configuration, engine location, empennage configuration and other features. Thus, for example, laminar area on the wing has been defined to extend to 80% chord on the upper surface and 70% chord on the lower surface. This relationship works out to be appropriate because high suction requirements in the trailing edge area lead to only marginal net benefits for laminarization beyond the points chosen. This turns out to be compatible with smaller chord flaps and spoilers than normally found useful, because low speed requirements are no longer critical.

For a laminar airplane, the choice of wing sweep turns out to be strongly influenced by considerations which relate directly to the maintenance of laminar flow in the critical leading edge area. Reducing sweep is beneficial from this standpoint since it reduces the requirement for suction quantity and allows the placement of the first slot further downstream where there is less susceptibility to erosion and other incidental damage. On the other hand, increasing sweep allows greater wing thickness, reduced weight and better accessibility. A final selection of wing sweep will have to be based on a balanced compromise and supported by extensive analyses and wind tunnel tests still to be accomplished.

Returning to a consideration of the primary factors governing airplane configuration, it is appropriate to choose an example illustrating some fundamental relationships when wing sweep and aspect ratio are fixed. Although the 15° swept wing configuration was selected for illustration, trade studies show that very similar trends exist for the 25° swept wing (baseline) which has somewhat better levels of performance and DOC. Thus, the principal effects of cruise altitude on performance and direct operating costs (DOC) are shown in figure 25. Here it is apparent that increasing altitude substantially increases gross weight because engine size and wing area must increase to permit flight at higher altitudes. At some value of wing loading, there is a

minimum gross weight for each altitude which occurs at progressively lower wing loadings as altitude increases. Corresponding relationships are evident for block fuel as a function of altitude. When the effects on DOC are examined, it is apparent that DOC variations more closely parallel those for gross weight as is usually the case when payload is held constant. Since the effects of altitude on DOC are significant, it is important to consider carefully the factors which tend to dictate high cruise altitude. Since the prevalence of ice crystals is of major concern, there currently appears to be no reasonable basis to relax the requirement for cruise above 12 200 m (40 000 ft). Nevertheless, it is necessary to continually seek ways of alleviating this requirement. The acquisition of further data in global areas of the major airline routes may provide better guidance toward the final resolution of this question.

With a provisional selection of wing sweep, a choice of wing aspect ratio in combination with wing loading must be made and expansion of studies like that discussed above to include other aspect ratios is required. Recently completed analyses show the significant relationships when plotted in the form given in figure 26. This is constructed by selecting points from the relative DOC curves for each altitude to correspond to a .5% increase in DOC from the minimum value. Since there are two such points for each curve, the one with the lowest value of wing loading is selected. This results in less block fuel in all cases providing a hedge against possible rises in relative fuel costs. The upper plot shows that the DOC is nearly independent of aspect ratio but sensitive to increasing altitude as seen previously. Also, higher altitudes correspond to lower wing loadings as do lower aspect ratios.

On the other hand, as shown in the lower half of figure 26, block fuel levels are generally sensitive to aspect ratio changes, decreasing significantly with increase in aspect ratio. Thus, with a given requirement for cruise altitude (e.g., 12 800 m (42 000 ft)) the choice would tend to hinge on the potential for fuel saving which favors higher aspect ratio. Studies of this type are usually based on strength-designed wings and considerations such as flutter penalties are initially set aside, unless the selection tends to move in directions where such factors would significantly modify the conclusions. More complete analysis usually tends to show that higher aspect ratio wings (i.e., beyond 10) particularly without wing-mounted engines, are increasingly sensitive to flutter. While the acceptance of small flutter weight penalties may permit a somewhat higher aspect ratio (and performance gains), the need for a flutter suppression system as much higher aspect ratios are approached is increasingly likely. Thus, a conservative choice would be aspect ratio 10 corresponding to a wing loading of about 4.3 kPa (95 psf) for a cruise altitude of 12 800 m (42 200 ft). This selection would have the added advantage that smaller chord and simpler flaps could be used and thus reduce weight, cost, and complexity. This is possible because the approach speed requirement is not critical in the range of interest and permits the use of less effective but simpler high-lift systems. While the above conclusions tend to appear definitive, it should be recognized that results are sensitive to requirements and the state of LFC technology development at any given time. Consequently, conclusions may change somewhat, hopefully in the direction of improving DOC and fuel usage.

CONCLUDING REMARKS

Significant results of the NASA-sponsored LFC technology development effort continue to show progress and to indicate the potential for airplane operating cost reductions and substantial fuel savings. Airplane design work actively supports this development by following closely or anticipating technology advances and solutions to critical problems.

Recent advances in laminar boundary layer development and stability theory provide important new aids for the aerodynamic design of LFC wings. There is, however, a need for further validation and automation of methods to facilitate design decisions. New methods are needed to analyze the local effects of flow through suction surfaces including disturbances generated in this process. Ultimately, a complete three-dimensional analysis involving all possible modes including sound, may be necessary to provide a valid theoretical basis for predicting suction requirements in the presence of disturbances present in the flight environment.

The continuing development of advanced high-speed airfoils for modern wing design is important to provide increasing wing thickness and reduced weight with no reduction in speed. The impact of such development is even more favorable for LFC airplanes since their requirements for wing volume and controlled pressure distributions are more demanding than for turbulent airplanes.

Wind tunnel testing is an essential supporting activity which is needed to provide basic data leading to design decisions which result in airplane performance improvements. The implementation of a wind tunnel test program by Boeing and the achievement of initial test objectives represents a first step toward filling these needs and will hopefully contribute to the advancement of LFC technology.

The search for satisfactory solutions to the structural and systems problems imposed by the requirements for maintaining laminar flow has involved the consideration of a large number of alternate concepts and arrangements. This has resulted in the development of at least six major structural approaches involving the use of advanced structural arrangements and materials. These have been subjected to critical evaluation and review resulting in the preliminary selection of the laminated aluminum honeycomb concept for application in the near-term. The use of graphite/epoxy composites in wing structure has been shown to be compatible with LFC requirements and to provide outstanding weight reduction potential. However, on the basis of current and foreseeable development activity, it is considered to be applicable only in the longer term.

The major additional systems requirements due to LFC are associated with the wing suction distribution and ducting systems and the suction compressor and drive. The important options for the various elements of these systems including their location on the airplane have been evaluated and the overall

arrangement selected. The suction units, each consisting of a 2-pressure level compressor with turboshaft engine drive, are located at the trailing end of each wing/body intersection.

In the category of special systems, that required to provide protection against the accumulation of insects at the wing leading edge is of critical importance. Several promising candidates for such a system have been identified and assessed for technical feasibility. These involve the use of 1) a liquid film (H_2O + anti-freeze), 2) a cryogen (LN_2) expanded into the leading edge cavity to produce frost on the leading edge, and 3) an air shield using high velocity jets. These must be subjected to further analysis and testing under simulated operational conditions.

Airplane design requirements, notably cruise altitude and turbulent climb capability, have been shown to have a major influence on the geometric definition of the long-range LFC transport to provide near-optimum performance and economics. In particular, configurations tend toward lower wing loadings and thrust loadings and somewhat higher aspect ratios than for turbulent aircraft. The wing sweep will tend toward a value which is close to optimum (25° sweep at Mach .8) without compromising reliability in the airline operational environment.

It is recognized that the work under existing Phase I contracts represents only a start toward full-scale system design and that further work is required in technology development and testing of advanced structural and systems concepts. The LFC program should continue to focus on hardware design and development leading to construction of a validator airplane. This is essential to provide the practical experience needed to determine the operational and economic feasibility of introducing LFC transport aircraft onto commercial airline routes in the foreseeable future.

REFERENCES

1. Klineberg, J. M.: Technology for Aircraft Energy Efficiency. ASCE International Air Transportation Conference, Apr. 4-6, 1977.

2. Goethert, B., et al: Toward Long-Range Aircraft with Laminar Flow Control (Series of articles on the X-21 and the state of the art on laminar flow control). Astronautics and Aeronautics, July 1966.

3. BCAC Preliminary Design Department: Evaluation of Laminar Flow Control System Concepts for Subsonic Commercial Transport Aircraft, Interim Report on Research and Development (Contract NAS1-14630), June 1977.

4. Pfenninger, W.: Flow Problems of Swept Low-Drag Suction Wings of Practical Construction at High Reynolds Numbers. Annals New York Acadmey of Sciences, vol. 154, art. 2, Nov. 1968.

5. Barnes, Jr., A. A. and Metcalf, J. I.: ALCOR High Altitude Weather Scans. AFCRL/A.N.T. Report No. 1. AFCRL-TR-75-0645, Air Force Cambridge Research Laboratories, Dec. 31, 1975.

6. Bohn, A. J. and Mangiarotty, R. A.: Study of Noise Effects on Laminar Flow Control due to Engine Placement on Wings of LFC Aircraft. Boeing Document D6-44651, Jan. 1978.

7. George-Falvy, D.: Initial Tests on a 20-ft Chord, 30° Swept Wing Section with Laminar Flow Control over 30% of the Chord. Boeing Document D6-46302, Feb. 1978.

8. BCAC Preliminary Design Department: Structural Concept Evaluation and Selection for Laminar Flow Wing, Boeing Document D6-46301, Oct. 1977.

9. Lambert, W. R.: Suction Pump and Propulsion System Trade Studies for LFC Baseline Airplane. Boeing Document D6-46304, Oct. 1977.

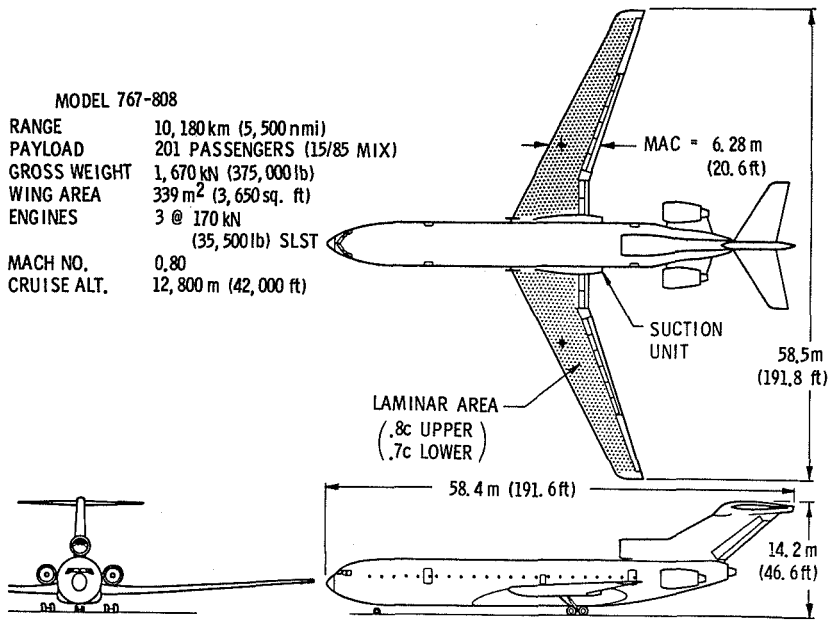

Figure 1.- LFC transport configuration.

	CLASSIC METHODS	CURRENT APPROACH	FUTURE
BOUNDARY LAYER DEVELOPMENT	INFINITE YAWED WING ($R_{\theta_{a.i.}}$ < 100 TO 200)	• TAPERED WING/COMPR. FLOW (COMPUTERIZED METHODS) • ATTACHMENT LINE BOUNDARY LAYER STARTING POINT FOR STABILITY ANALYSIS	POSSIBLE MINOR IMPROVEMENTS
TURBULENT BOUNDARY LAYER CONTAMINATION	• REDUCE SWEEP OR L.E. RADIUS • USE FENCE, BUMP OR NOTCH	SAME	?
BOUNDARY LAYER STABILITY	•CROSS FLOW AMPLIFICATION ($\psi \doteq -90^0$) •TANGENTIAL FLOW AMPLIFICATION (TOLLMIEN-SCHLICHTING, $\psi = 0^0$) •ESTABLISH SUCTION DISTRIBUTION (AREA SUCTION MODEL)	• BOUNDARY LAYER AMPLIFICATION (WAVE ANGLE ψ, FREQUENCY) • ALLOWABLE AMPLITUDE RATIO BASED ON ESTIMATED INITIAL DISTURBANCE LEVELS (NORMAL RANGE: e^9 TO e^{12}) • DEFINE SUCTION DISTRIBUTION (AREA SUCTION MODEL)	INCLUDE: - EFFECTS OF DISCRETE SLOTS, PERF. STRIPS, ETC. - DISTURBANCE GROWTH ANALYSIS - COMPLETE MODAL ANALYSIS INCLUDING NON-LINEAR EFFECTS

Figure 2.- Progress in boundary layer methodology.

DISTURBANCE	ALLOWABLE LEVEL AT 12,200 m (40,000 ft), MACH NO. 0.80	DESIGN IMPACT
NOISE	100 dB TO 110 dB	• ENGINE LOCATION* • NOISE TREATMENT
SURFACE IMPERFECTIONS:		
- STEPS	.2mm (DOWN)/.4mm (UP)	• STRUCTURAL DESIGN
- GAPS	2.5mm (ALONG)/5mm (ACROSS)	• MANUF. TOLERANCES
- ROUGHNESS (EROSION)	1.5mm	• MAINTENANCE
- WAVES (h/λ)	.0008 TO .0010	
INSECT RESIDUES	1.5mm TO 3mm	• L.E. CLEANING/PROTECTION SYSTEM
ICE CRYSTALS	30 μm DIA. 10^5/SEC m^2 PART. FLUX	• CRUISE ALTITUDE
ATMOSPHERIC TURBULENCE	NOT CRITICAL	

* BASIC NOISE LEVELS ON WING SURFACE: 120 dB (ENGINES ON WING)
100 dB (ENGINES ON AFT-BODY)

Figure 3.- Impact of disturbances on design.

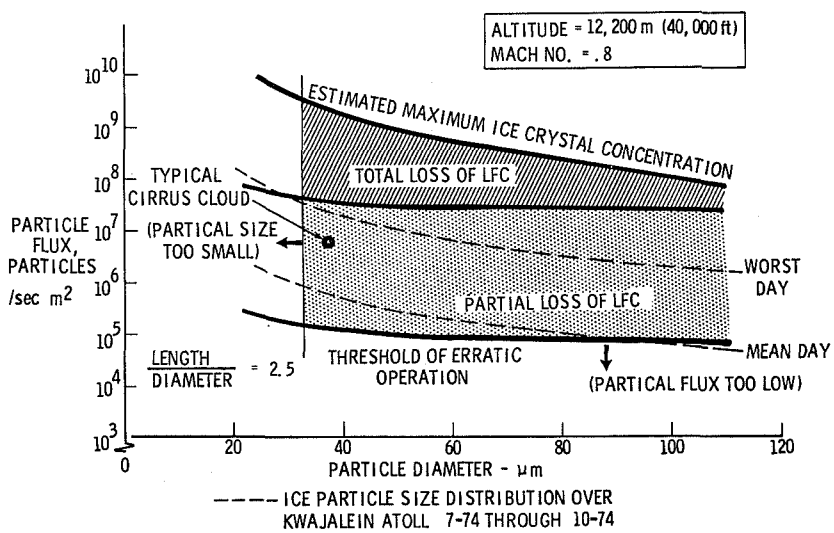

Figure 4.- Estimated effects of atmospheric ice particles on LFC.

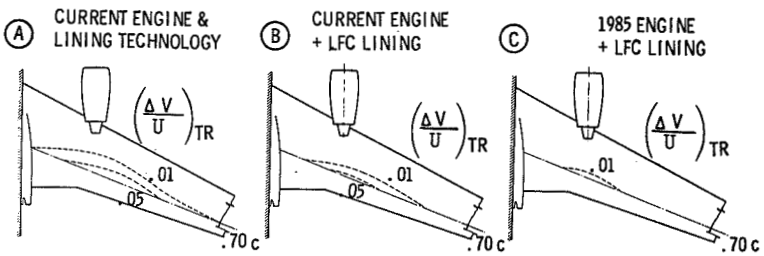

$\left(\frac{\Delta V}{U}\right)_{TR}$	POTENTIAL LOSS OF LAMINAR AREA (LOWER SURFACE)*		
	Ⓐ	Ⓑ	Ⓒ
.01	20%	8%	2.5%
.05	7%	1.5%	0

* NORMAL SUCTION LEVELS

Figure 5.- Engine noise effects on laminarization.

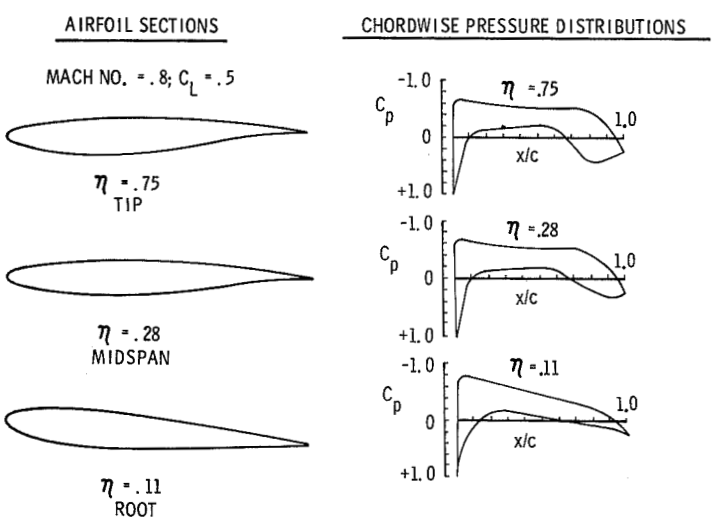

Figure 6.- Wing sections and pressure distributions.

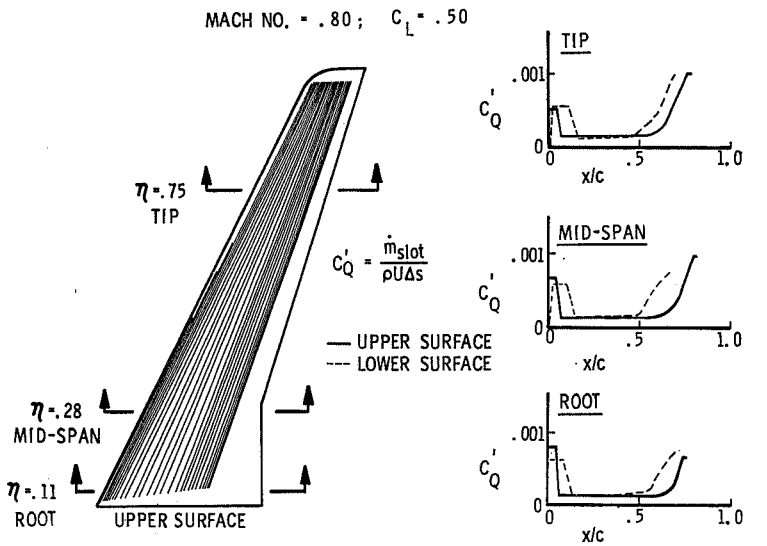

Figure 7.- Wing suction distribution.

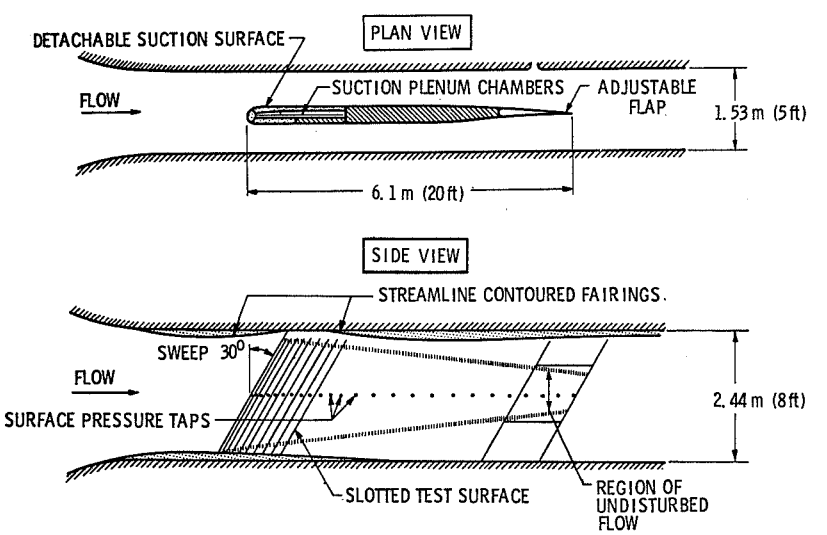

Figure 8.- LFC wing test arrangement.

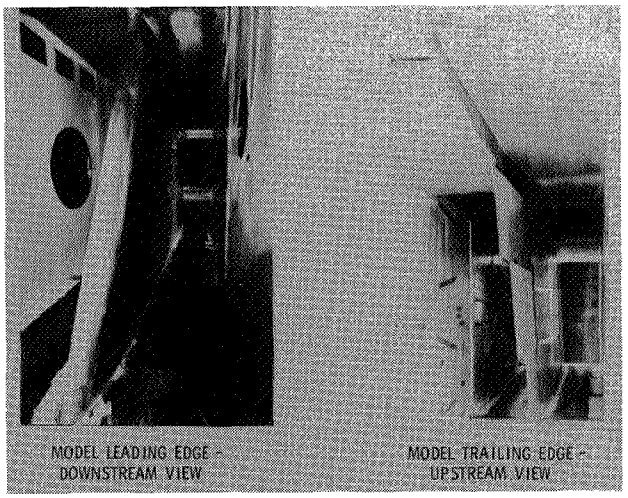

Figure 9.- LFC wing section installation Boeing research wind tunnel.

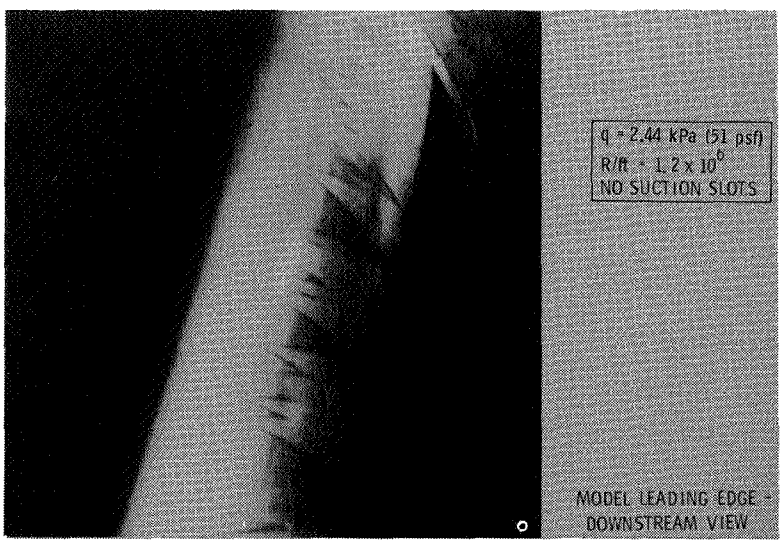

Figure 10.- Leading edge transition pattern.

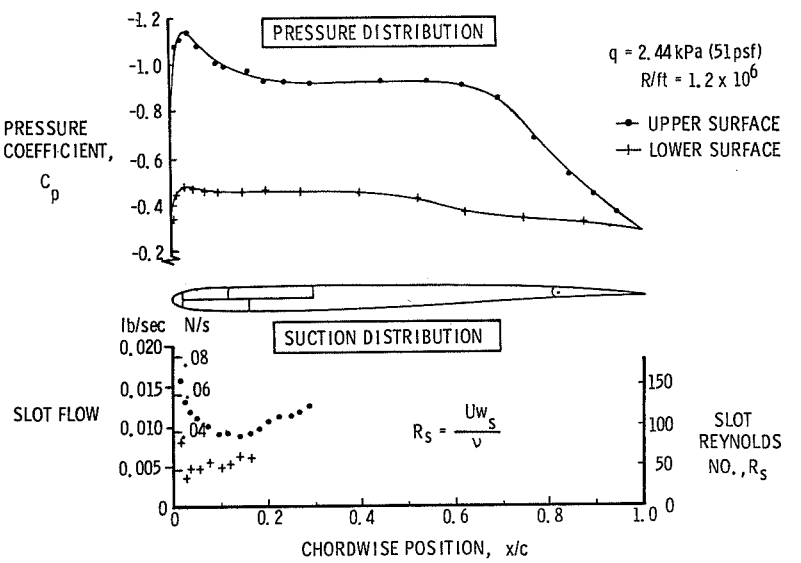

Figure 11.- LFC model test conditions.

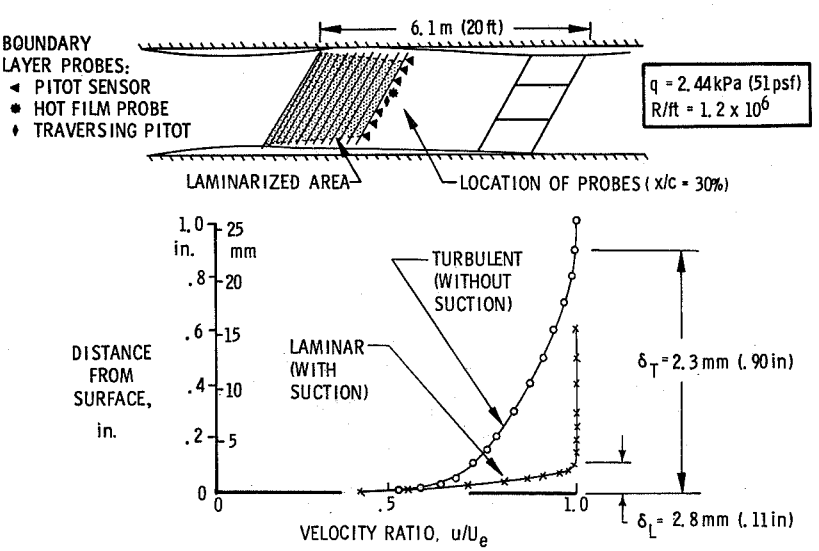

Figure 12.- Boundary layer survey results.

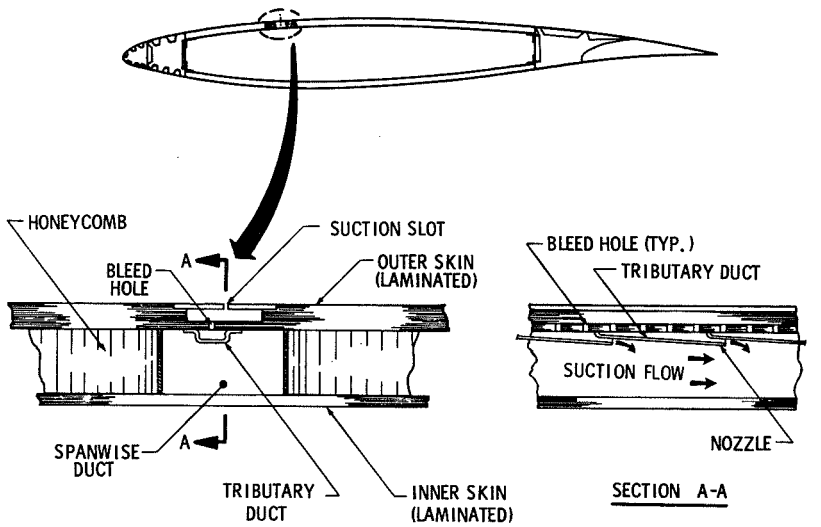

Figure 13.- Typical LFC wing section laminated aluminum honeycomb design.

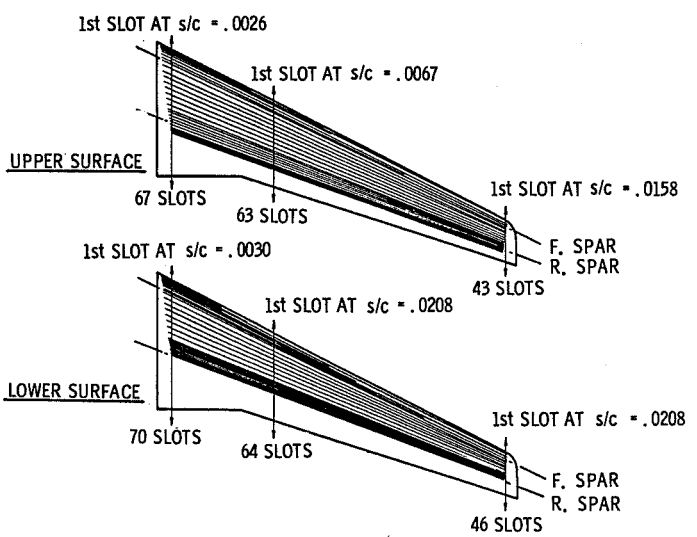

Figure 14.- Suction slot arrangement.

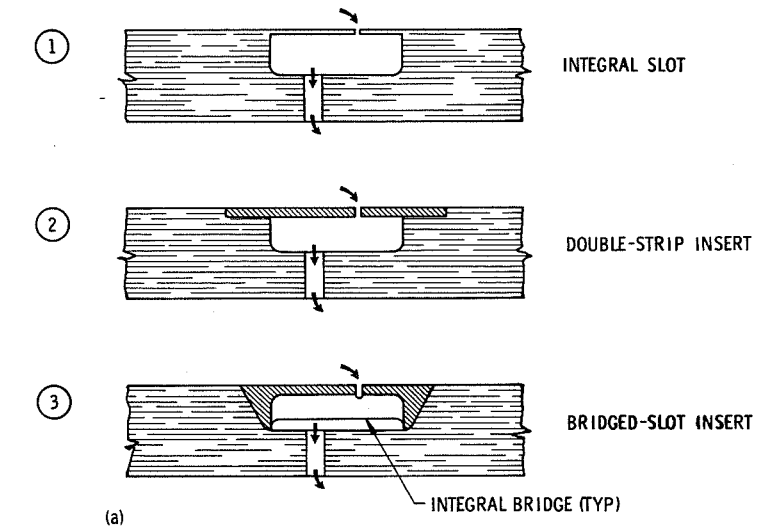

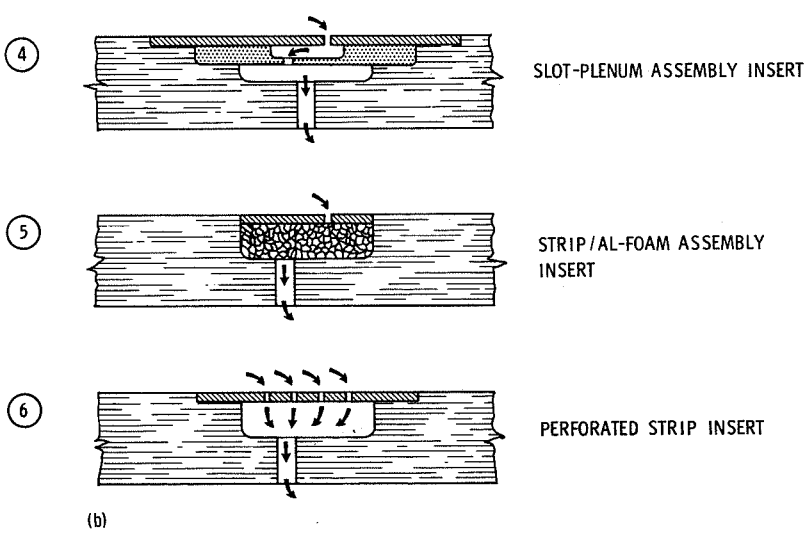

Figure 15.- Suction opening options.

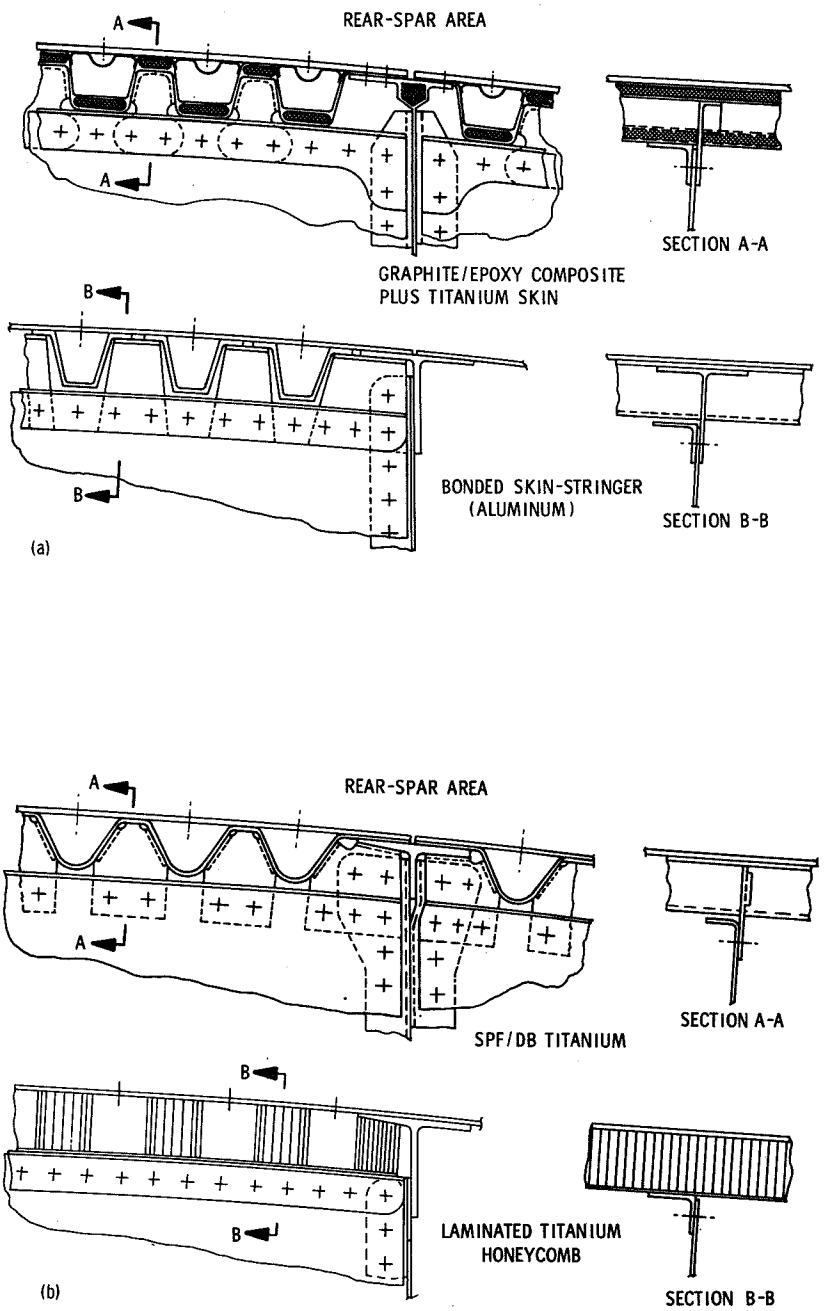

Figure 16.- Alternative structural concepts.

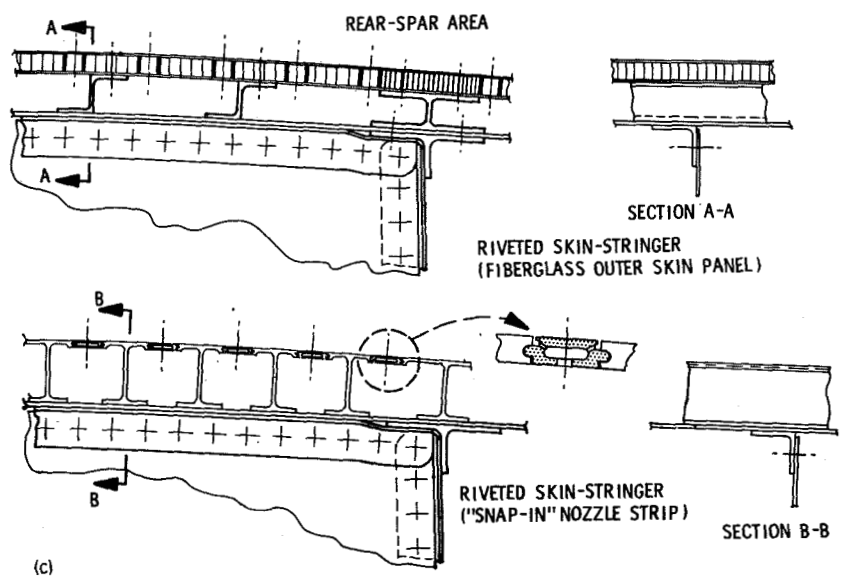

Figure 16.- Concluded.

REFERENCE: EXISTING LEVELS

	△ COMPONENT WEIGHT
ADVANCED STRUCTURES/MATERIALS	
- IMPROVED ALUMINUM ALLOYS	-7% WING BOX -4% FUSELAGE -4% EMPENNAGE
- BONDED CONSTRUCTION	-6% WING BOX -5% FUSELAGE -5% EMPENNAGE
- GRAPHITE/EPOXY COMPOSITES	-25% TRAILING EDGE SURFACES -27% WING BOX* -15% FUSELAGE * -15% EMPENNAGE *
- CARBON BRAKES	-10% LANDING GEAR

*APPLICABLE IF COMPOSITES USED IN PLACE OF IMPROVED ALLOYS AND BONDED CONSTRUCTION

Figure 17.- Advanced technology impact.

REFERENCE: EXISTING LEVELS

	△ COMP. WEIGHT	△(L/D)	△SFC
AERODYNAMICS			
- LAMINAR FLOW CONTROL	TBD	26% (41%)*	2.3% (3%)*
- ADVANCED AIRFOIL SECTION	- 14% WING BOX - 8% EMPENNAGE		
- REDUCED ROUGHNESS		2% (5%)*	
ACTIVE CONTROLS			
- REDUCED LONGITUDINAL STABILITY	- 20% HORIZ. TAIL	3%	
- LOAD ALLEVIATION	- 8% WING BOX		
PROPULSION			
- ADVANCED TURBOFAN (BPR = 7.5)	- 13% ENGINE		-14%

* APPLICABLE FOR LAMINARIZED WING AND EMPENNAGE

Figure 18.- Advanced technology impact.

SUCTION COMPRESSOR	DRIVE TYPE	UNIT LOCATION
• SINGLE PRESSURE LEVEL • MULTI-PRESSURE LEVEL • EXHAUST VELOCITY LEVEL	• MAIN ENGINE: - BLEED AIR/TURBINE - MECHANICAL COUPLING - ELECTRICAL - HYDRAULIC • BLEED/BURN/TURBINE • TURBOSHAFT ENGINE	• AFT-BODY - SINGLE UNIT - MULTI-UNIT
	TURBOSHAFT ENGINE	• WING - MULTI-UNIT
APU	APU	AFT-BODY * (EMPENNAGE LFC)

* ASSUMES WING-MOUNTED UNITS FOR WING SUCTION

Figure 19.- Suction unit arrangement options.

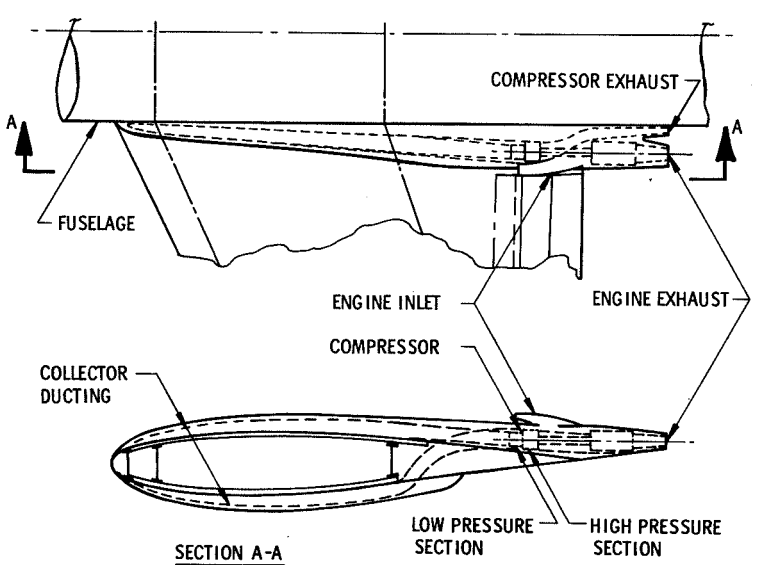

Figure 20.- Suction unit installation at wing root.

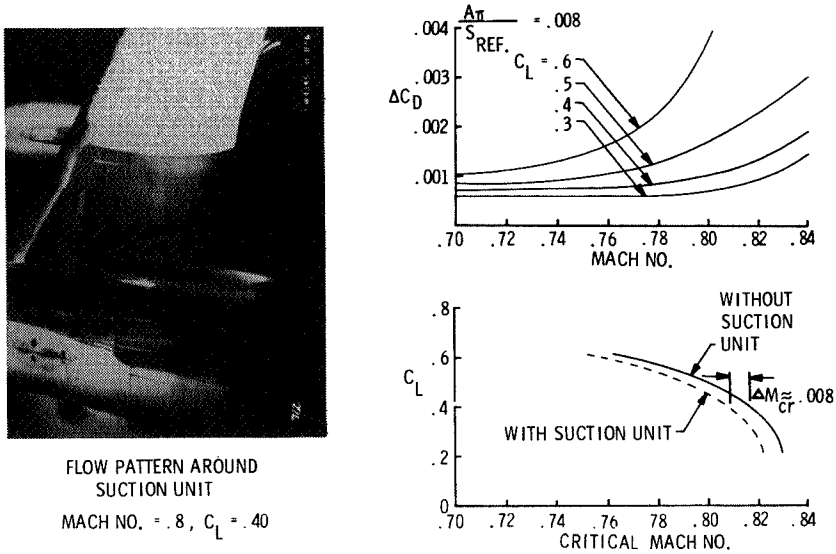

Figure 21.- Suction unit effect on drag.

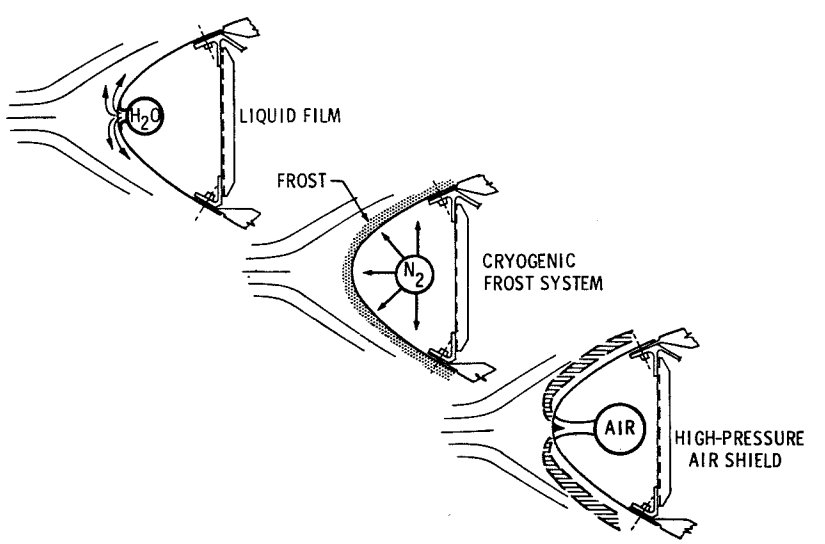

Figure 22.- Leading edge region cleaning concepts.

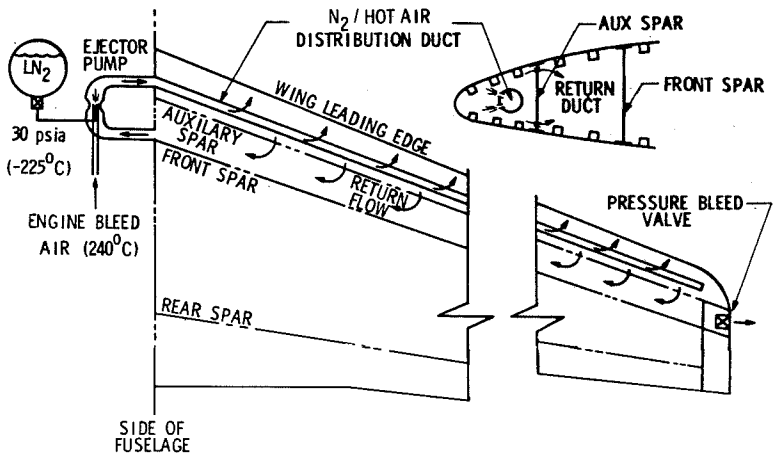

Figure 23.- Leading edge frost/anti-icing system.

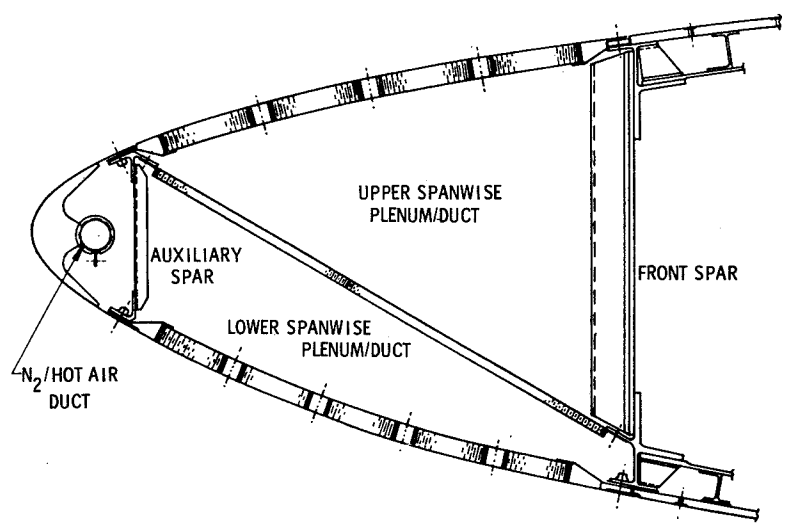

Figure 24.- Leading edge systems arrangement.

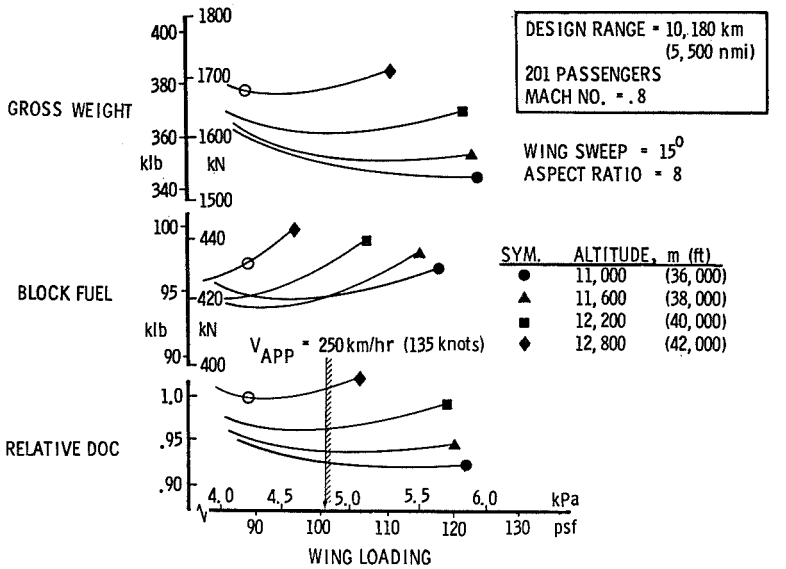

Figure 25.- Cruise altitude effects on performance and economics.

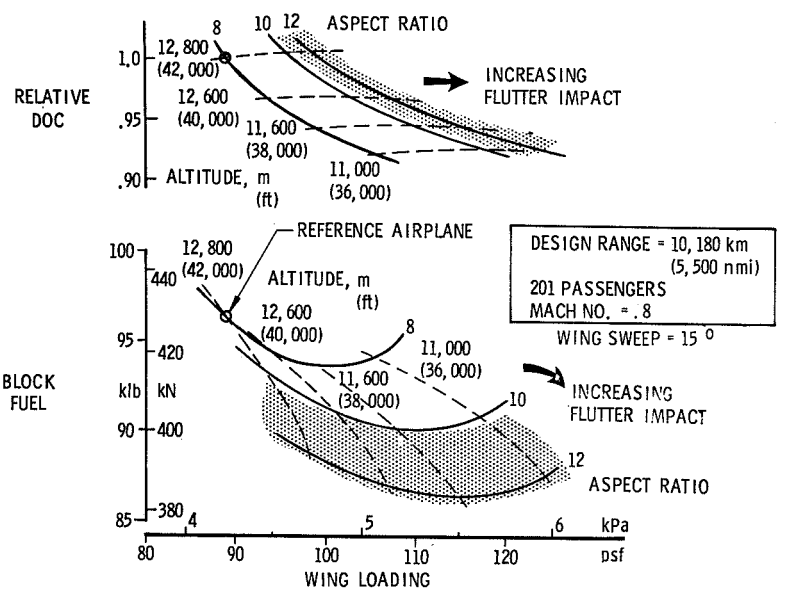

Figure 26.- Wing aspect ratio effects on doc and block fuel.

TOWARD A LAMINAR-FLOW-CONTROL TRANSPORT FOR THE 1990'S*

R. F. Sturgeon
Lockheed-Georgia Company

SUMMARY

Analyses were conducted to define a practical design for an advanced technology Laminar-Flow-Control (LFC) transport for initial passenger operation in the early 1990's. Included in these analyses was the definition of mission requirements, appropriate design criteria, and level of technology for the study aircraft. The characteristics of the selected configuration were established, aircraft and LFC subsystems compatible with the mission requirements were defined, and the aircraft was evaluated in terms of fuel efficiency. A wing design integrating the LFC ducting and metering system into advanced composite wing structure was developed, manufacturing procedures for the surface panel design were established, and environmental and structural testing of surface panel components were conducted. Test results revealed a requirement for relatively minor changes in the manufacturing procedures employed, but have shown the general compatibility of both the selected design and the use of composite materials with the requirements of LFC wing surface panels.

INTRODUCTION

Of all advanced technology concepts currently under consideration for application during the next two decades, Laminar-Flow-Control (LFC) offers the greatest potential for improving the efficiency of long-range transport aircraft. In operation, this efficiency improvement may be translated into reduced fuel consumption or improved payload/range performance.

Both the theoretical methods and engineering and design techniques requisite to the application of LFC have been reasonably well-known since the mid-1940's. The validity of this background and the potential of LFC were partially evaluated in the 1960-1966

* This paper is based on studies conducted under Contract NAS1-14631, "Evaluation of Laminar-Flow-Control System Concepts for Subsonic Commercial Transport Aircraft," sponsored by the NASA Langley Research Center, Hampton, Virginia.

period by Northrop as a part of the X-21A LFC Demonstration Program (ref. 1-4). Recent studies, described in reference 5, have evaluated the potential economic advantages of LFC in the projected airline environment. However, a conclusion common to all previous evaluations is that significant advances are required in both the development of basic design criteria and in the operational verification of LFC prior to the incorporation of this technology on a production transport. The current LFC development program, sponsored by the NASA as one element of the Aircraft Energy Efficiency Project, is directed toward the satisfaction of these requirements. The contracted study on which this paper is based is one of several current efforts included in the first phase of the LFC development program.

As a part of the subject contract, an advanced technology LFC transport configuration was developed for a design mission range of 12,038 km (6500 n mi) and a payload of 400 passengers. The resultant configuration, which will be used in subsequent study phases for the evaluation of alternative LFC system concepts, has optimum configuration geometry for the design mission. While all elements of the LFC systems installation have not been optimized at this point in the study, the configuration is representative of a practical advanced technology commercial transport compatible with initial operation in the early 1990's.

The analyses conducted in the process of selecting the aircraft configuration and the pertinent characteristics of the selected aircraft are described. Included as a part of these analyses is a definition of the mission requirements, pertinent design criteria, and the level of technology assumed for the aircraft. The selected aircraft geometry, engine, and operational parameters are outlined, and the characteristics of the study configuration are defined.

In addition to the general discussions devoted to overall aircraft characteristics, the investigations completed in the development of LFC wing structural concepts are described. A wing design integrating the LFC ducting and metering system into advanced composite wing structure, manufacturing procedures for the design concept, and environmental and structural testing of surface panel components are described. A variety of test results are summarized.

SYMBOLS AND ABBREVIATIONS

Values are given in both SI and U. S. Customary Units. The measurements and calculations were made in U. S. Customary Units.

b	slot duct width, mm (in)
C_p	pressure coefficient
d	metering hole diameter, mm (in)

g	acceleration of gravity
h	slot duct depth, mm (in)
H_s	pressure on wing surface at slot entry, N/m^2 (lb/in^2)
M	Mach number
M_D	design dive Mach number
P	absolute pressure, N/m^2 (lb/in^2)
R_N	chord Reynolds number
s	metering hole spacing, mm (in)
V_D	design dive speed, knots
W/S	wing loading, kg/m^2 (lb/ft^2)
x/c	chord location
y	metering hole offset, mm (in)
η	cruise power ratio
Λ	wing sweep, rad (deg)
Λ_{LE}	wing sweep, leading edge
AR	aspect ratio
BPR	bypass ratio
cg	center of gravity
DOC	direct operating cost
EDM	electro-discharge machining
EPNdB	effective perceived noise - dB

FAA	Federal Aviation Administration
FAR	Federal Aviation Regulation
FOD	foreign object damage
LFC	laminar flow control
OWE	operating weight empty
PL	payload
RSS	relaxed static stability
TOGW	takeoff gross weight

SCOPE

The study on which this paper is based has the following primary objectives:

- Evaluation of alternatives in the design of LFC transports for operation in the 1990 time period.
- Definition of requirements for subsystem development in subsequent program phases.

Figure 1 outlines the overall plan developed to achieve the study objectives. Using the projected technology data base and the selected study mission, a baseline configuration was developed. Concurrently, advanced LFC system concepts are being evaluated in the areas of:

- Aerodynamics
- Structures and materials
- Suction systems
- Leading-edge cleaning
- Integration of auxiliary systems

As a part of the structures and materials task, a fabrication and test program for LFC surface elements culminates in the environmental and structural testing of .91 m x 1.52 m (3 ft x 5 ft) LFC surface panels. Upon completion of the concept evaluations and test programs, the optimum LFC system elements will be integrated into the baseline configuration as a part of the configuration selection and assessment task. The development of recommendations for subsequent activities will be based on the results of all study activities.

Although concept evaluations have been conducted in all appropriate technology areas, this paper will be limited to a description of the study baseline aircraft and a summary of progress in the design, fabrication, and testing of LFC surface panel components.

GUIDELINES

Mission Definition

An extensive evaluation of traffic projections and market analyses was conducted to define probable missions for commercial transports entering service in the post-1990 period. The selected mission is illustrated by the payload/range curve of figure 2. With a full passenger payload of 400, the study aircraft has a range of 12,038 km (6500 n mi) plus allowances for diversion to an alternate airport, winds at cruising altitude, track distances which exceed great circle distances, and a manufacturer's tolerance. The resulting still-air range is in excess of 13,890 km (7500 n mi) with full passenger payload. At reduced ranges, the aircraft has the capability of transporting the full passenger payload and 16,873 kg (37,200 lb) of belly cargo. Average stage length was estimated to be 6112 km (3300 n mi).

A cruise speed of M = 0.80 was selected for the study aircraft. Airport performance is compatible with projected international airports, with a FAR field length of 3048 m (10,000 ft) and maximum approach speed of 145 knots.

The market analysis established a minimum production quantity of 300 aircraft to be delivered over a 10-year period.

Reference Technology Levels

The assumed development schedule for the study aircraft is shown in figure 3. For initial passenger operation in 1993, the selected airframe and engine technology levels of 1988 and 1987, respectively, are appropriate. The technology levels illustrated in

figure 4 are consistent with the assumed development schedule for the study aircraft.

Aerodynamics

The level of aerodynamics technology considered in this study includes the use of advanced airfoil sections in the form of a modified supercritical airfoil. Favorable supercritical flow permits design of wings with low sweep and greater thickness. The baseline airfoil pressure distribution shown in figure 5 is a compromise between the high aft-loaded airfoil and the supercritical airfoil.

Flight Controls

Active controls are utilized to reduce wing bending moment on the wing to a level equivalent to a 2.0g symmetric maneuver without active controls. The use of trailing-edge wing active controls results in a wing torsion increase above the wing torsion loads for a 2.5g symmetric maneuver without active controls. The achievement of wing bending moment equivalent to a 2.0g maneuver is a 33% reduction in incremental bending moment. Torsion moment increases approximately 30%.

An active gust load alleviation is used to reduce wing bending due to gust on the inner 50% of the wing to the levels that would be obtained for a 2.0g symmetric maneuver without active controls. Gust loading is critical on this aircraft due to the high lift curve slope produced by the LFC and the high aspect ratio of the wing. A 40% - 50% reduction in incremental gust wing bending moment is required to achieve the desired load level. Wing torsion moment due to gust is low, and the active control system causes only a slight increase in torsion. This 40% - 50% reduction is obtained throughout the flight envelope with suitable wing and horizontal stabilizer trailing-edge control surfaces.

The aircraft is designed to be free from flutter and divergence at speeds up to 1.2 V_D/M_D in accordance with the requirements of paragraph 25.629 of FAR Part 25. Active flutter suppression is used to provide the flutter speed margin above V_D/M_D.

For the aircraft of this study, relaxed static stability (RSS) is employed to provide flexibility of establishing center-of-gravity envelopes. Assumptions for the RSS system employed for study aircraft are summarized below:

Aft cg limit (x/c)	0.51
Yaw acceleration control (rad/sec^2)	0.116
Pitch acceleration control (rad/sec^2)	0.265

In sizing the vertical and horizontal tails of study aircraft, adequate requirements were imposed for engine-out control, pitch acceleration capability, and yaw acceleration capability.

Propulsion

The Pratt & Whitney Aircraft STF-477 study engine was chosen as the basis for the primary propulsion units for the study aircraft. This engine cycle was the end product of Tasks II and III of a P&WA study performed under contract to the NASA Lewis Research Center and reported in reference 6.

The STF-477 twin-spool engine cycle has a fan pressure ratio of 1.7 at a bypass ratio of 8.0. The engine overall pressure ratio is 45 : 1 with a maximum combustor exit temperature of 1427°C (2600°F). The low-pressure spool consists of a one-stage fan and three low-pressure compressor stages. These components include advanced blading aerodynamics and seals for better component efficiency and lower noise while maintaining good component life and performance retention. The low-pressure spool is driven by a five-stage uncooled turbine, incorporating higher loading and advanced aerodynamics and seals. The high-pressure spool incorporates a ten-stage compressor driven by a two-stage highly-loaded turbine, both incorporating technology advances similar to the low-pressure spool. The high-pressure turbine also includes advanced metallurgy, cooling, and coating technologies.

Materials

The selection of materials for the major structural components of the study configurations was based on the results reported in the studies of references 5, 7, and 8. Candidate materials and structural concepts were examined for each element of the structure. Materials and concepts were selected on the basis of the lowest cost per pound of weight saved. Weight technology factors were developed for a constant-size airplane by substituting different materials and structural concepts and computing the weights of structural elements for identical structural requirements. A weight factor of 1.00 was assigned to the conventional aluminum structure, and the ratio of the advanced material and concept to that of aluminum was defined as the weight technology factor. The full benefits of advanced materials were realized by sizing the total airplane, including the power plant and other systems, to take advantage of the lower structural weights.

Table I describes the distribution of advanced materials among the airframe components and lists the corresponding weight technology factors. Utilization of advanced materials for 66% of the airframe weight results in study aircraft which weigh about 67% as much as comparable current transports.

Design Criteria

Recent projections of the IATA Technical Committee indicate that airlines will expect a minimum design life objective of 90,000 flight hours for long-range aircraft entering service in the post-1990 period. The airlines do not expect a crack-free structure for this length of service but do expect an airframe which can be maintained economically. Previous wide-body jet experience indicates that the airlines will expect a service life

warranty contract of approximately one-half of the design life objective. Therefore, a warranty service life of 45,000 flight hours was used to establish the wing ultimate tension cutoff stress level for the baseline airplane. The current wide-body jet warranty life is on the order of 30,000 flight hours.

The study aircraft satisfy the requirements for type certification in the transport category under Federal Aviation Regulations - Part 25, and are capable of operating under pertinent FAA rules.

Based on realistic estimates of achievable progress for the technology readiness date assumed for the study aircraft, the following noise criteria were selected:

- o Takeoff sideline — FAR 36 -10 EPNdB
- o Takeoff flyover — FAR 36 -6 EPNdB
- o Approach flyover — FAR 36 -5 EPNdB

These levels are 2 EPNdB below the standards currently proposed as a part of NPRM 75-37C in reference 9.

The study aircraft are provided with fuel reserves in accordance with the requirements of FAR 121.645. In addition to the fuel reserve allowances specified in this regulation, the LFC study aircraft are designed with adequate reserve fuel to accommodate loss of the LFC system due to weather phenomena during six percent of the mission cruise time.

The basic design criteria for LFC systems developed as a part of the X-21 Program represent the most comprehensive set of guidelines currently available. Therefore, the criteria established by this program and reported in reference 10 form the basis for the definition of LFC systems for the study aircraft.

Elements of the LFC systems developed for study aircraft reflect advances in all technical disciplines which are appropriate for commercial aircraft to be introduced in the early-1990 period.

BASELINE CONFIGURATION SELECTION

Configuration Parameters

A comprehensive analysis was conducted to evaluate the influence of aircraft performance and geometry parameters on the economic efficiency of commercial transport aircraft compatible with the study mission. A conventional wide-body fuselage configuration, sized for 400 passengers and 16,873 kg (37,200 lb) of belly cargo, was used for all analyses. The parametric configurations use two LFC suction units mounted in the fuselage

near the wing root. Power for these suction units is independent of the main propulsion units and suction air is exhausted at free-stream velocity.

The results of the studies reported in reference 5 relative to the use of external fuel tanks, alternate engine locations, extent of laminarization, and various levels of static stability were used in design decisions for the baseline configuration.

The methodology employed in selecting configuration parameters is summarized in figures 6 and 7. A parametric configuration was optimized for each of the twelve cruise-altitude/cruise-M combinations shown in figure 6. The resultant aircraft were evaluated on the basis of direct operating cost. Optimum configuration parameters were developed for each combination using the procedure illustrated in figure 7. The optimization required two phases. In the first phase, wing loading and aspect ratio were varied to establish optimum configuration geometry independent of airport performance constraints. In the second phase, engine bypass ratio, cruise power ratio, and aspect ratio were varied parametrically to optimize airport performance for each configuration geometry.

The results of these analyses are summarized by figure 8, in which DOC is plotted versus cruise Mach number for the several altitudes considered. One additional optimization was also performed for a cruise altitude of 12,802 m (42,000 ft) to furnish more complete data for variation of DOC with altitude. The curves show that, between M=0.75 and M = 0.85, DOC varies less than 0.018 ¢/seat km (0.03 ¢/seat s mi) for the two lowest altitudes. The leading-edge sweep angle of 0.437 rad (25 deg) associated with M = 0.80 is less critical from a leading-edge contamination standpoint than the sweep of 0.551 rad (31.5 deg) associated with M = 0.85. For this reason and others associated with the more severe design problems associated with compressibility effects, a cruise M of 0.80 was selected for the baseline aircraft.

As illustrated by the cross plot for M = 0.80 shown in figure 9, higher altitudes suffer progressively greater DOC penalties. Since the lower unit Reynolds number associated with increasing altitude is beneficial to LFC because of its influence in reducing sensitivity to surface imperfections, an altitude of 12,192 m (40,000 ft) was selected as a reasonable compromise for the cruise altitude of the baseline aircraft.

Configuration Description

The general arrangement of the baseline aircraft selected to satisfy the previously defined mission requirements is illustrated in figure 10. The aircraft is a wide-body configuration designed to carry 402 passengers and baggage over an intercontinental range of 12,038 km (6500 n mi) at M = 0.80 with adequate fuel to account for adverse winds, intermittent LFC disruptions due to atmospheric conditions at cruise altitude, and normal international fuel reserves. A typical cabin arrangement accommodates a 10/90 passenger mix, with 40 in first class and 362 in tourist class cabins. Space allowances are made for galleys, lavatories, closets, cabin crew provisions, as well as rest areas for flight crew as

dictated by FAR Part 121.485 for flights of more than 12 hours duration. Space for LD-3 cargo containers is provided forward of the wing box and aft of the main landing gear bay. A bulk cargo bay is also provided at the rear of the pressurized belly. These cargo bays will accommodate 16,873 kg (37,200 lb) of cargo.

The baseline airplane is a low-wing, T-tail, monoplane with four aft-fuselage mounted propulsion engines. An independently-driven LFC suction unit is located in a fairing under each wing root, as shown in figure 11. Fuel is carried in the wing including the wing center section box. The wing has a moderate sweep of 0.437 rad (25 deg) at the leading edge with an aspect ratio of 11.6. Full-span flaps, including drooped ailerons, provide the required airport performance. Leading-edge high-lift devices are not required. Partial-span spoilers are incorporated as required. Small-chord secondary flaps, incorporated into the main flaps, provide upper surface pressure gradient and shock position control for off-design operation as well as serving as active controls to minimize structural requirements.

LFC suction capability is provided on both wing surfaces from 0 to 75% chord, and on the empennage from 0 to 65% chord. The LFC ducting and metering system is integrated into the aircraft wing structure. A combination anti-icing, anti-contamination system is incorporated in the leading-edge region.

The weights for the different airplane groups were calculated from statistical weight equations based on current transport aircraft. These weights were adjusted in the primary and secondary structural areas by applying the composite and advanced material weight technology factors shown in table I. Other adjustments to the aircraft weight such as LFC engines and ducts were estimated by methods developed specifically for these elements. The surface panel weights were calculated from design layouts. A weight statement for the baseline LFC airplane is presented in table II. Weights of LFC system elements are listed in table III. It will be observed that the total weight of the LFC system is less than 3.6% of the aircraft operating weight.

The relative performance of the study aircraft is illustrated by figure 12. Based on the data of reference 11, figure 12 shows the fuel efficiency of representative current commercial transports as a function of stage length. The corresponding curves for the study aircraft show that, for a full passenger payload, the LFC transport has a fuel efficiency at the design range which is over 2.5 times that of current commercial aircraft. For a combined passenger/cargo payload, the fuel efficiency at shorter stage lengths is about 1.8 times that of current wide-body transports.

LFC Systems

The LFC system includes all portions of the boundary layer suction system, including the suction surface through which a portion of the boundary layer is taken into the airplane, the system for metering the level and distribution of the ingested flow, the ducting

system for collecting the flow, and the pumping units which provide the suction and sufficient compression to discharge the suction flow at velocity equal to or higher than free-stream.

Figure 13 shows a flow map of the LFC suction airflow for the complete aircraft. LFC flow is drawn forward at intervals over the wing through chordwise ducts into leading-edge trunk ducts which carry the flow inboard to the suction pumps. Empennage suction flow is carried from the tail surfaces through trunk ducts located in the fuselage to mix with wing flow prior to entry into the suction pumps.

Figure 14 depicts in some detail the selected LFC surface configuration with suction flow denoted by arrows. Boundary layer air is pulled through spanwise surface slots into spanwise capillaries, then through metering holes into the structural hat stiffeners. Suction flow is carried spanwise until it reaches the chordwise collector duct, which is formed by hollow rib caps located on alternate ribs.

The LFC surface is constructed of graphite/epoxy. Each element is bonded in place with mechanical fasteners used at rib caps to facilitate wing assembly. The entire surface is covered by a sheet of 0.51 mm (.020 in) titanium. This LFC surface is designed to accommodate slot spacings of 5.08 and 7.62 cm (2 and 3 in) or multiples thereof.

Figure 15 provides a cross-sectional view of the wing leading edge and shows the hat-stiffened surface panels with the integrated surface slots and ducting. The removable nose cap is maintained at a constant leading-edge radius in the wing-root region and incorporates a system of chordwise suction slots with sub-surface compartments to control spanwise contamination and the rapidly changing pressure gradients existing over the extreme leading-edge surface region. The anti-icing, anti-contamination system incorporated in the leading-edge region consists of a porous band at the upper and lower limits of stagnation point excursion across the leading-edge dictated by varying angle of attack. Each porous band is approximately 2.54 cm (1 in) wide, fed by a pressure system which sprays the liquid into the airstream on both sides of the stagnation point forming a cloud through which the wing passes.

The slot configuration of the baseline system for the LFC surfaces in the wing-box region is defined by the following:

- Slot spacing — 15.24 cm (6 in)
- Slot width — 0.28 mm (0.011 in) outboard of wing break
0.31 mm (0.012 in) inboard of wing break
- Skin thickness at slot — 0.51 mm (0.020 in) outboard of wing break
1.27 mm (0.050 in) inboard of wing break

Figure 16 presents a schematic of the metering system and illustrates the primary structural composite skin with the slots of the bonded titanium surface centered on the slot

duct. Metering holes penetrate the composite skin and meter the flow from the slot duct into the composite hat-section structural stringers. Significant dimensions include the slot duct width, b, which is limited to 7.6 mm (0.30 in) by the allowable overhang of the 0.51 mm (0.020 in) thick titanium surface skin. The slot duct depth, h, is a selected value but should be held to a low value to minimize structural impact of the slot on the composite skin. The metering hole diameter, d, spacing, s, and offset, y, are selectable dimensions. It is advantageous to maintain a high offset value. Therefore offset is taken to be the maximum possible within the limits of metering hole tangency to the slot duct wall and the diameter of the metering hole.

The following summarizes the metering configuration selected for the wing-box region of the study aircraft:

- Slot duct width, b — 7.6 mm (0.30 in)
- Slot duct depth, h — 2.5 mm (0.10 in)
- Metering hole diameter, d — 2.1 mm (0.083 in)
- Metering hole spacing, s — 12.7 mm (0.50 in)

Figure 17 shows a schematic of the suction ducting system and illustrates the chordwise flow of suction air forward to the trunk ducts and then inboard to the suction pumps. The low-pressure air from the upper wing surface and leading-edge region enters the forward trunk duct, while the high-pressure flow from the lower surface enters the aft duct. A shut-off valve is provided in both trunk ducts to isolate the inboard wing surface, thus permitting continued laminarization of this surface in the event of the failure of a suction pump. Shut-off valves are also provided in the pump inlet ducts to permit isolation of a failed pump and allow in-flight starting of the suction pump with ambient air by means of the ambient vent valves. The pressure in the duct system in-flight is always well below ambient and if this ambient vent arrangement were not provided, the pump would be required to start under load. Cross ducts are provided between the pump inlet ducts. The empennage suction flow is ducted into the low-pressure duct system through a shut-off valve.

The pump consists of a primary element with a boost element provided for the low-pressure flow. Pump discharge is turned through approximately 3.15 rad (180 deg) and discharged through a nozzle in a near axial direction at free-stream velocity. The pump is driven by an independent shaft engine provided with a ram inlet and a near axial discharge at free-stream velocity.

Calculated pressure losses are shown in table IV for the suction systems on the selected configuration. Accumulated pressure losses are shown as a percent of the static pressure acting on the surface of the airfoil. This does not allow for any pressure recovery due to the small velocity heads present in the boundary layer flow removed by the suction system. These accumulated losses are indicated for the entry and exit flow in each component of the ducting system. The pressure loss at the entry to the hat section includes

the losses associated with the slot and metering system. All losses include the accumulated duct, metering and mixing losses to that point in the system.

LFC SURFACE PANEL DEVELOPMENT

The overall plan employed for the development of LFC surfaces is outlined in figure 18. As illustrated by this flow diagram, the plan proceeds from the selection of a design concept through the development of detailed designs, the formulation of manufacturing procedures, and two phases of panel fabrication and testing prior to the ultimate definition of panel design criteria.

Panel Design

Following the conceptual design activities devoted to the identification of candidate concepts, preliminary design investigations were conducted to develop consistent weight and cost factors for comparison during the evaluation. To develop these data, the preliminary design effort included the estimation of loads for a typical LFC aircraft wing, selection of materials, and the sizing of various surface/wing elements. For study purposes, the evaluation was restricted to the portions of the LFC upper and lower surfaces forming the main structural elements between the wing front and rear spars.

In addition to the above, the following were accomplished for each design concept:

- Manufacturing procedures were developed.
- Estimates of manufacturing costs were completed.
- Maintainability and reliability were assessed.
- Procedures for repairing damaged surfaces were developed.
- Compatibility with surface design criteria and other elements of the LFC system was evaluated.

Upon completion of this procedure for each of the candidate concepts, recommended non-structural, structural, and combination concepts were selected. These concepts were subsequently compared to permit selection of a single concept.

During the course of the evaluation, a total of four non-structural concepts, six structural concepts, and three combination concepts, employing elements of both non-structural and structural designs, were evaluated. On the basis of these evaluations, the skin and hat-section stiffener design illustrated in figures 14 and 15 was selected for further development.

Details of the surface concept, including the selection of materials and number and orientation of the 5208/T300 graphite/epoxy plies, are shown in figure 19. The selection of titanium for the face sheet was based on requirements for lightning protection and resistance to erosion and corrosion.

Manufacturing Procedures

The manufacturing procedures evaluated during this phase of the study were directed toward the development of two .91 m x 1.52 m (3 ft x 5 ft) LFC surface panels to be employed in subscale testing. To permit fabrication of the selected LFC surface design, manufacturing development was required to economically produce acceptable slots in titanium and fabricate basic hat-stiffened wing-box structure from graphite/epoxy composite material in sections thicker than had previously been fabricated. A variety of slotting procedures and graphite/epoxy structure fabrication and assembly procedures were evaluated in the selection of manufacturing procedures providing a high-quality, dimensionally accurate LFC wing panel structure. Following is a brief discussion of the investigations conducted.

Surface Slotting

The following criteria were established for slots in the titanium LFC surface:

- A slot width range of 0.076 mm to 0.228 mm (0.003 to 0.009 in).
- A slot width tolerance of $\pm$ 10%.
- The slot entrance equal to or thinner than the slot exit to minimize slot contamination.
- Sharp slot edges to facilitate control of air flow through the slots.

Table V summarizes the results of investigations conducted in the evaluation of candidate slotting procedures. Of the eight procedures evaluated, including both pre-assembly and post-assembly techniques, the electro-discharge machining (EDM) process was judged to be most compatible with requirements for the slotting of titanium in a production environment. However, initial results obtained with the laser are sufficiently promising that this procedure should be the subject of further investigation.

The EDM procedure results in a slot which is somewhat wider on the side of the sheet from which the cutting is accomplished. Consequently, due to the requirement that the slot entrance be equal to or smaller than the slot exit on the wing surface, it is necessary to slot the titanium skin prior to assembly. To facilitate handling of the skin during the slotting and bonding process, 1.27 mm (0.050 in) connecting tangs were left in the slots at 15.24 cm (6 in) intervals. After bonding, the tangs were removed with a jeweler's saw.

A photograph illustrating the EDM procedure is shown in figure 20.

Structural Skin

A major problem in the development of thick sections of 5208 graphite/epoxy was the ply thickness distribution through the skin. Bleeding from one side yielded plies against the bleeder which were too thin and plies away from the bleeder which were too thick. A 20-ply stack which was pre-bled yielded uniform ply thickness. Thus, pre-bleed was selected as the preferred process for thick 5208 graphite/epoxy sections.

Slot ducts were formed by aluminum strips tack riveted to the skin tool with 16-ply graphite/epoxy between the aluminum strips. An aluminum foil backing sheet was used to prevent splintering during drilling of the metering holes. Figure 21 illustrates the completed structural skin.

Hat-Section Stiffeners

The hat-section stiffeners were produced in a female mold. A 0.61 m (24 in) long prototype tool was made from aluminum, and an attempt was made to let the vacuum bag mold the inside of the part. While the part was generally acceptable, there were wrinkles caused by bag folds. Cracking also occurred in the 20-ply 0° stacks in the hat crown. The four-ply (+45/-45/-45/+45) modules were pre-bled prior to forming into the mold. Pre-bled modules were found to be much easier to form since they were well compacted.

A rubber plug was made to mold the center of the hat and was used on additional prototype runs. Cracking of the 0° plies in the crown was not resolved. One try placed a ply of graphite fabric in the center of each of the 20-ply 0° stacks but failed to alleviate the cracking. Some changes to the cure cycle were also made, but neither helped the cracking problem or completely eliminated voids. Crack-free structural components were achieved by reducing the number of 0° plies in the crown to ten. Completed hat-section stiffeners are shown in the photograph of figure 22.

Panel Assembly

In the bonding of the hat-section stiffeners to the structural skin, the web flange stiffness of the hat sections was found to be adequate to withstand light autoclave pressure. Therefore, a verification bond run with the adhesive encapsulated in 0.013 mm (0.0005 in) Teflon was conducted at 68.94 kN/m^2 and 137.88 kN/m^2 (10 psi and 20 psi) autoclave pressure. After the adhesive cured, the hat was stripped from the skin and a replica of the bond line was removed from between the Teflon. Both cure pressures produced a good bond with adhesive thickness from 0.051 mm to 0.152 mm (.002 in to .006 in).

In bonding the titanium skin to the structural skin, the initial attempt used a 121°C (250°F) curing adhesive, American Cyanamid FM 73. A demonstration panel was made by bonding a strip of slotted titanium to a part of the first 96-ply panel. Warpage of 1.01 mm (.040 in) in 0.61 m (24 in) was experienced, which precluded using an elevated temperature bonding procedure for attaching the titanium skin to the surface panel. A room-

temperature curing adhesive was selected which had been used previously for bonding titanium doublers to aluminum structure on aircraft. Both Hysol EA 9309.1 and MIL-S-8802 polysulfide sealant were evaluated as room-temperature curing adhesives. The panel with MIL-S-8802 resulted in non-uniform bond lines and a step at the slot edges; therefore, Hysol EA 9309.1 was selected. This adhesive, made by the Hysol Division of the Dexter Corporation, is a two-component paste and can be used under vacuum pressure applications. A demonstration panel was made and exhibited no warpage.

A photograph of the panel during assembly is presented in figure 23. The completed surface panel is shown in figure 24. Table VI compares LFC surface smoothness criteria and the values achieved on this panel.

Summary of Manufacturing Procedures

The following summarizes the manufacturing procedures employed for fabrication of the first two LFC surface panels:

- The outer skin, inner skin, and hat stiffeners are separately cured and subsequently joined by structural adhesive bonding. During the final bonding cycle, the shear clips are integrally molded in place.
- The titanium face sheet is slotted using the electro-discharge machining process. In this process, 1.27 mm (0.050 in) tangs are left in the slots at 15.24 cm (6 in) intervals to maintain integrity of the sheet and permit handling prior to final assembly.
- The slotted face sheet is bonded to the outer skin with room-temperature curing adhesive and the tangs are removed with a jeweler's saw.

Subsequent testing of surface panel components showed the selected manufacturing procedures to be satisfactory with two exceptions:

- In many cases, slot width tolerances were exceeded in the removal of connecting tangs. Alternatives to the use of hand-held jewelers' saws are being investigated.
- In compression testing of the panel, the titanium skin began buckling and disbonding at approximately 50% of the failure load. The room-temperature curing adhesive used for this bond will be replaced with an adhesive that cures at an elevated temperature. Identification of a suitable adhesive is currently in progress.

Panel Testing

Subscale testing of LFC surface panels was conducted in the following areas:

Environmental

- o Temperature
- o Icing
- o Corrosion
- o Foreign object damage
- o Repairability
- o Lightning

Structural component tests

- o Rib clip tension
- o Rib clip shear
- o Compression

Test specimens were cut from the two .91 m x 1.52 m (3 ft x 5 ft) LFC surface panels described in the preceding section. A photograph of the first surface panel illustrating the allocation of test specimens is presented in figure 25. The sectioning of the second surface panel to acquire the large specimens for the compression tests is illustrated by figure 26. The number and characteristics of test specimens is outlined in table VII. The narrative which follows summarizes pertinent results of selected tests.

Temperature

Thermal testing was conducted to evaluate the effect of temperature changes on the width of slots in the LFC surface panel and to verify handbook values for the thermal coefficient of expansion for the thick composite structural skin. The thermal test panel and instrumentation are illustrated by figure 27. In the temperature range from -51°C (-60°F) to 82°C (180°F), the maximum variation in slot width ranged from $+6.35$ and -6.10×10^{-4} mm ($+25$ and -24×10^{-6} in.). Thus, slot width variations due to temperature changes are considered to be insignificant. An acceptable comparison of measured and handbook values for the coefficient of expansion for the composite structure was obtained.

Icing

Icing tests were conducted to evaluate the effect of entrapped water in the hat-section stiffeners and in the surface ducts and metering holes.

As shown by figure 25, a specimen was cut from the panel for icing tests, and the ends of the hats were closed by clamping aluminum plates with a rubber seal to each end. A stand-pipe was attached to one end and filled with water. The specimen was placed in a low-temperature chamber and frozen at -18°C (0°F). One hat flange separated from the skin. As illustrated by figure 28, failure was within the composite hat flange. The flange separation emphasizes the need to keep water out of the hat sections during low-temperature operation.

For the evaluation of icing in the surface ducts and metering holes, the ducts and holes were filled with water through the skin slots. The specimen was exposed to 15 freeze-thaw cycles. There was no visually detectable damage after the 15 freeze-thaw cycles. Removal of the titanium skin did not reveal any hidden damage. A section was cut through a metering hole, and the specimen was mounted and polished. Microscopic examination up to 200X showed no delamination or cracking.

Corrosion

Tests were conducted to evaluate the effect of environments representative of those encountered in airline operations on the bending strength of the LFC surface panel.

Three 10.16 x 25.40 cm (4 x 10 in) panel specimens were exposed to 30 days of salt fog, 30 days of high humidity, and 30 days of Weather-O-Meter, respectively. In addition, a 0.15 x 0.61 m (6 x 24 in) specimen was exposed to 30 days in the Weather-O-Meter environment. After exposure, the specimens were static tested in a four-point bending test, as illustrated by figure 29. Test results are summarized in table VIII. As shown in table VIII, the maximum reduction in bending strength was 18% for the specimen subjected to the Weather-O-Meter environment.

Foreign Object Damage

The objective of this test was to determine the resistance of an LFC surface panel to foreign object damage.

Using the experimental arrangement shown in figure 30, the LFC surface panel was impacted over the slotted surface duct and over the composite-supported titanium at energy levels of 5.76, 11.52, 23.04, 46.08, and 92.16 m-kg (5, 10, 20, 40, and 80 in-lb). The depth of the maximum indentation at each impact point was measured with a depth micrometer and is reported in table IX. Figure 31 shows the result of a 92.16 m-kg (80 in-lb) impact over a surface duct. Apparent damage over solid laminate supported titanium was minimal. Removal of the titanium skin revealed little visual damage to the composite over the plenum and none over solid laminate.

The data of table IX indicate that none of the impacts in the range tested would create a surface indentation sufficiently deep to cause transition of the laminar boundary layer if the impact occurred over titanium supported by composite. However, depending on chord location, impacts in the range of 11.52 - 23.04 m-kg (10 - 20 in-lb) over a surface plenum would result in an unacceptable surface discontinuity. For purposes of comparison, a 1.27 cm (0.5 in) diameter stone at a relative velocity of 120 K is equivalent to a 57.6 m-kg (50 in-lb) impact energy level.

Repairability

The objective of this investigation was to demonstrate that typical damage to the slotted titanium LFC surface can be repaired by methods usable in-service by fleet operators.

The LFC surface panel specimen which was damaged in the foreign object damage test described in the preceding section was used as the test specimen. Repairs were made to the dents produced by the 23.04 m-kg (20 in-lb) to 92.16 m-kg (80 in-lb) impacts in the titanium over the surface ducts.

Removal of the damaged titanium surface with a hole saw was considered to be partially successful. A pilot hole was drilled in the center of the damaged area and allowed to penetrate the composite for approximately 0.63 cm (0.25 in). Additional control of the cutting tool was accomplished with a guide. Removal of the titanium skin was readily accomplished with the hole saw but it was not possible to stop the cut precisely in the adhesive layer and slight scoring of the composite occurred each time.

The second method attempted was the use of a counterbore, chucked in a low-speed, hand-held, drill motor. A pilot hole and cutting guide were used. The cut was terminated in the adhesive layer with no damage to the composite substrate. No problem was experienced with overheating. However, the edge of the cut in the titanium was not square due to the normal radius on a counterbore. A special counterbore was prepared with a square edge and a grind more suited to titanium cutting. Excellent results were obtained. Control of the cut using the hand-held drill was easily accomplished.

A patch was prepared from EDM-slotted titanium sheet with a connecting tang in the center of the patch, as illustrated by figure 32. Preparation for bonding was by conventional procedures. The composite surface was prepared by light sanding followed by an acetone wash. Both surfaces were lightly coated with Hysol EA 9309 adhesive and the patch was placed in position. Small strips of shim stock were used to align the slots, light pressure was applied, and the adhesive was allowed to cure at room temperature. The connecting tang was removed using a hand-held jeweler's saw.

Step profile measurements were made on several patches to determine smoothness. A typical patch had a total surface variation within a 5.08 cm (2 in) circle of only 0.063 mm (0.0025 in) and a maximum step of 0.038 mm (0.0015 in), which is well within the requirements established in reference 5.

It was demonstrated that a damaged slot can be returned to the original configuration using hand-held tools. While the tests were conducted on a bench, the entire operation could have been conducted either on the upper or lower surface of an aircraft wing. Repairs of this nature could be performed within a time span of four to six hours by using heat lamps to accelerate the adhesive cure.

Lightning

Preliminary tests were performed to ensure that the structural arrangement of the LFC surface panel is resistant to lightning strike. The test specimen shown in figure 25 was tested by NASA personnel in the NASA LRC lightning strike test facility.

Two specimens were tested. One panel was tested for baseline data and the other was subjected to 260 thermal-humidity cycles. Test conditions are outlined in table X.

In all six tests, the titanium face sheet was effective in preventing the current from penetrating the composite. The panel after four lightning strikes is shown in figure 33. The extent of disbonding between the face sheets and composite was examined using ultrasonic techniques. The results of this effort and the physical appearance of the panels suggest the possibility that aerodynamic forces encountered after a lightning strike might cause additional delamination. Indeed, these aerodynamic forces might become more intense due to irregularities in the wing surface caused by the lightning strike and the subsequent loss of local laminar flow.

The LFC panel used for these tests incorporated no underlying metallic structure or wiring. It is important to point out that the introduction of such conductors might alter the extent to which lightning current would tend to enter the composite structure. Such common elements as rivets, rib clips, and wiring bundles could cause intensification and internal arcing. These tests did, however, establish that lightning strikes to wing panels would not cause a catastrophic bond failure.

Compression

The objective of the panel compression test was to obtain design data for a four-element compression panel. The acceptable criterion for the compression panel was a design ultimate load of 6.49 MN/m (37.08 kips/in) without failure.

A 0.61 m x 1.52 m (24 in x 60 in) compression panel was removed from the second LFC wing surface panel shown in figure 26. The specimen ends were potted using Magnabond 69-9 tooling plastic and machined as required for the test configuration. The specimen was instrumented with thirty-four axial strain gauges and seventeen deflection transducers. Aluminum "T" sections, simulating rib caps, were attached to the rib clips.

The compression test of the four-element panel was conducted in a 5.34 MN (1200 kip) Baldwin Universal Testing Machine. The 5.34 MN (1,200,000 lb) load range was used, having an accuracy of plus or minus 0.5 percent of indicated load. All strain gauge and deflection transducer readings were recorded by a B&F Model SY 156 data acquisition system.

The specimen was loaded in .445 MN (100,000 lb) increments. While loading between .890 MN (200,000 lb) and 1.334 MN (300,000 lb), it was noted that the titanium

skin was buckling at the top and the bottom edge of the panel, including areas that had previously been determined to have some disbonding. This was documented by the photograph shown in figure 34. Loading was continued to 2.224 M N(500,000 lb) and buckling of the titanium strips progressed over the length of the panel, as shown in figure 35. The specimen withstood 3.959 M N(890,000 lb), the design ultimate load, when failure occurred by delamination of the hats and skin, as shown in figure 36.

Following is a summary of significant events during the test:

Load		Maximum strain	Equivalent G force	
MN	1000 lb			
.890	200	.0012	.84	Audible noises
1.334	300	.0019	1.26	Titanium skin began buckling
2.224	890	.007*	3.75	Panel failed at 100% ultimate load

* Extrapolated value. No strain data were obtained at failure.

Both the environmental testing and the structural testing conducted in this phase of the study provided results demonstrating the compatibility of the selected LFC surface panel design with the anticipated operational environment for future LFC transports.

CONCLUDING REMARKS

This paper has illustrated some selected aspects of the development of a practical LFC configuration for the 1990's and provided some insight into the development of an efficient LFC wing design. Current study results support the following conclusions:

- The optimum performance and geometry parameters for a commercial transport utilizing LFC are not appreciably different from those for current turbulent transports. The selection of a cruise Mach number of 0.80 and a cruise altitude of 12,192 m (40,000 ft) provides near-minimum DOC and permits reasonably efficient LFC system design.
- The most efficient LFC wing design is one which integrates the LFC ducting and metering system into advanced composite wing structure.
- Although all surface smoothness requirements were not satisfied in all areas of the two LFC surface panels fabricated to date, it appears that additional manufacturing development will permit the fabrication

of graphite/epoxy structural elements with a slotted titanium surface which will be compatible with LFC system requirements.

- Environmental and structural testing have illustrated the requirement for relatively minor changes in panel design and manufacturing procedures. Testing to date has verified the compatibility of the selected panel design and the use of composite materials with the requirements of LFC wing surface panels.

Although they are not described in this paper, parallel efforts are proceeding in the analysis of the laminar boundary layer, optimization of LFC airfoil and wing designs, the evaluation of alternative LFC system elements, and the evaluation of concepts to prevent leading-edge contamination. The results of these activities will contribute to the data base requisite to the ultimate validation of LFC in an operational environment.

REFERENCES

1. Antonatos, P. P.: Laminar Flow Control Concepts. Astronautics and Aeronautics, July, 1966.

2. Whites, R. C., Sudderth, R. W., and Wheldon, W. G.: Flight Test Results of the Laminar Flow Control X-21 Airplane. Astronautics and Aeronautics, July, 1966.

3. Anon.: Division Advisory Group Review - X-21A Program Summary. DAG 65-1-0, Northrop Corporation, Norair Division, 1965.

4. Anon.: Report of Review Group on X-21A Laminar Flow Control Program. USAF Aeronautical Systems Division, November, 1965.

5. Sturgeon, R. F., et al: Study of the Application of Advanced Technologies to Laminar-Flow Control Systems for Subsonic Transports. Vol. II, NASA CR-133949, prepared by the Lockheed-Georgia Company under Contract NAS1-13694, May, 1976.

6. Gray, D. E., et al: Study of Turbofan Engines Designed for Low Energy Consumption. PWA-5318, NASA CR-135002, Pratt & Whitney Aircraft Div. of United Technologies Corp., April, 1976.

7. Lange, R. H., et al: Study of the Application of Advanced Technologies to Long-Range Transport Aircraft. Vol. I, NASA CR-112088, prepared by the Lockheed-Georgia Company under Contract NAS1-10701, May, 1972.

8. Boundary Layer Control Study, Oral Status Report, prepared by the Boeing Company under USAF Contract F33615-76-C-3035, July, 1976.

9. NPRM 75-37C, "Noise Standards, Aircraft Type and Airworthiness Certification. Proposed Alternative Noise Reduction Stages and Acoustical Change Requirements for Subsonic Transport Category Large Airplanes, for Subsonic Turbojet Powered Airplanes and for Single Engine Transport Category Airplanes," Federal Register, Vol. 41 No. 209, Oct. 28, 1976.

10. Staff, LFC Engineering Section: Final Report on LFC Aircraft Design Data, Laminar Flow Control Demonstration Program. NOR 67-136, Northrop Corporation, Norair Division, June, 1976.

11. Shevell, R. S.: Technology, Efficiency, and Future Transport Aircraft. Astronautics and Aeronautics, September, 1975.

TABLE I. - WEIGHT TECHNOLOGY FACTORS

Component	Advanced material weight (%)	Weight technology factor
Wing	85	0.61
Fuselage	71	0.66
Horizontal tail	67	0.74
Vertical tail	67	0.74
Nacelle and pylon	35	0.79
Landing gear	23	0.84
Weighted average	66	0.67

TABLE II. - WEIGHT SUMMARY

	kg	lb
Structure	64,320	141,808
Propulsion system	15,585	34,359
Systems and equipment	30,138	66,441
Weight empty	(110,043)	(242,608)
Operating equipment	14,007	30,880
Operating weight empty	(124,050)	(273,488)
Passenger payload	38,465	84,800
Zero fuel	(162,515)	(358,288)
Fuel	94,654	208,673
Gross	257,169	566,961

TABLE III. - LFC SYSTEM WEIGHTS

	kg	lb
Surfaces		
Wing	2077	4578
Horizontal tail	197	435
Vertical tail	240	528
Suction units	489	1079
Ducting	854	1883
Installation	607	1338
Total	4464	9841

TABLE IV. - REPRESENTATIVE SUCTION SYSTEM PRESSURE LOSS

Suction flow station	Cumulative pressure loss % P/H_s
Wing surface	0
Spanwise hat section duct:	
Entering	1.07
Leaving	1.10
Chordwise ducts:	
Entering	1.85
Leaving	5.00
Trunk duct:	
Tip	8.50
Root	9.00
Pump inlet	10.00

TABLE V. - EVALUATION OF SLOTTING PROCEDURES

	Verified production potential	Comments
Electro-discharge machining	Yes	Further development required to get slot width to 0.076 mm (0.003 in)
Joining machined strips		
Bonding	No	Slot tolerance exceeded 0.025 mm (±.001 in)
Welding	No	Slot tolerance exceeded 0.025 mm (±.001 in)
Electron beam	No	Failed to produce slots consistently
Water jet	No	Too slow in titanium
Laser	To be determined	
Planer	No	Minimum slot width of 0.20 mm (0.008 in)
Saw	No	Too slow in titanium
Chem-milling	No	Failed to provide square corner

TABLE VI. - SURFACE TOLERANCE COMPARISONS

	Tolerance		Measured values			
			No.	No. exceeding	Maximum	
	mm	in			mm	in
Steps	0.152	0.006	60	1	0.161	0.0063
Waves (5.08 cm, 2 in)	0.076	0.003	60	11	0.114	0.0045
Slot width (Nominal 0.152 mm, 0.006 in)	0.015	0.0006	207	37	0.051	0.002

TABLE VII. - TEST SPECIMENS

Type of test	Number of specimens	Dimensions	
		cm	in
Temperature	1	30.5 x 91.4	12 x 36
Icing	1	15.2 x 30.5	6 x 24
Corrosion (4 pt bending)			
Skin	4	10.2 x 25.4	4 x 10
Panel	2	15.2 x 61.0	6 x 24
Foreign object damage and repairability	1	30.5 x 30.5	12 x 12
Lightning (6 strikes)	2	30.5 x 30.5	12 x 12
Rib clip			
Tension	1	15.2 x 30.5	6 x 12
Shear	1	15.2 x 30.5	6 x 12
Compression			
2 elements	1	30.5 x 91.4	12 x 36
4 elements	1	61.0 x 152	24 x 60

TABLE VIII. - TEST SUMMARY - CORROSION/BENDING

Environment	Specimen		Reduction in bending strength - %
	cm	in	
Salt fog	10.2 x 25.4	4 x 10	11
Humidity	10.2 x 25.4	4 x 10	13
Weather-O-Meter	10.2 x 25.4	4 x 10	18
Weather-O-Meter	15.2 x 30.5	6 x 24	7

TABLE IX. - TEST SUMMARY - FOREIGN OBJECT DAMAGE

Impact load		Depth				Ply damage
		Over duct		Over laminate		
m-kg	in-lb	mm	in	mm	in	
5.76	5	0.025	0.001		0	0
11.52	10	0.152	0.006	0.025	0.001	0
23.04	20	0.457	0.018	0.050	0.002	0
46.08	40	0.508	0.020	0.075	0.003	0
92.16	80	0.813	0.032	0.101	0.004	10

TABLE X. - TEST RESULTS - LIGHTNING STRIKE

Test number	High voltage spike kV	Continuing current amp	Continuing current msec	Edges grounded	Burn thru	Disbond
1	25	0	0	All	No	No
2	42.5	0	0	All	No	Some
3	25	500	200	All	Yes	Yes
4	25	500	200	One	Yes	Yes
5	25	500	200	All	Yes	Yes
6	45	0	0	All	No	Yes

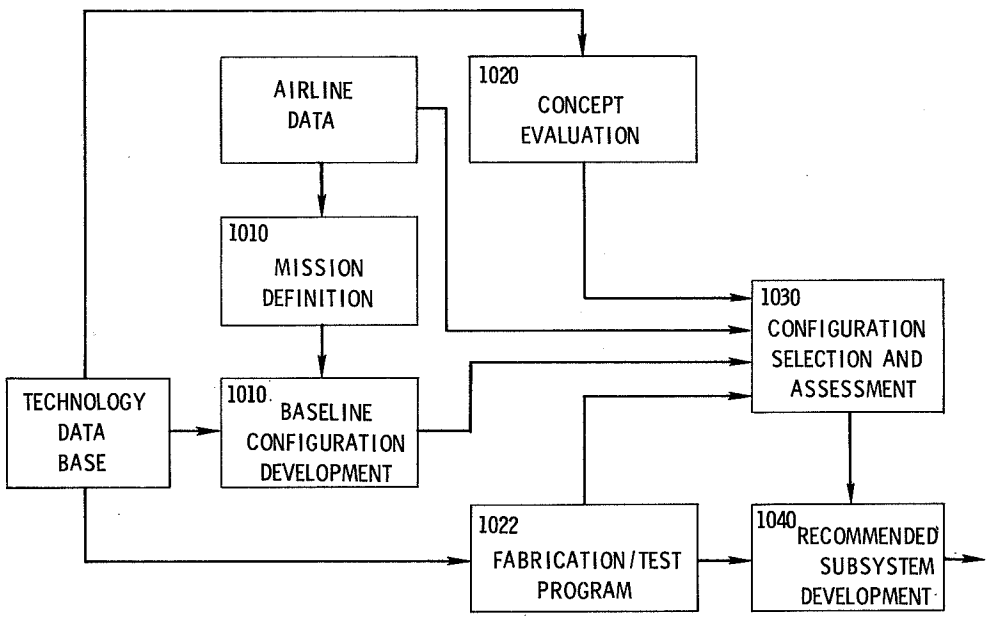

Figure 1.- Study plan.

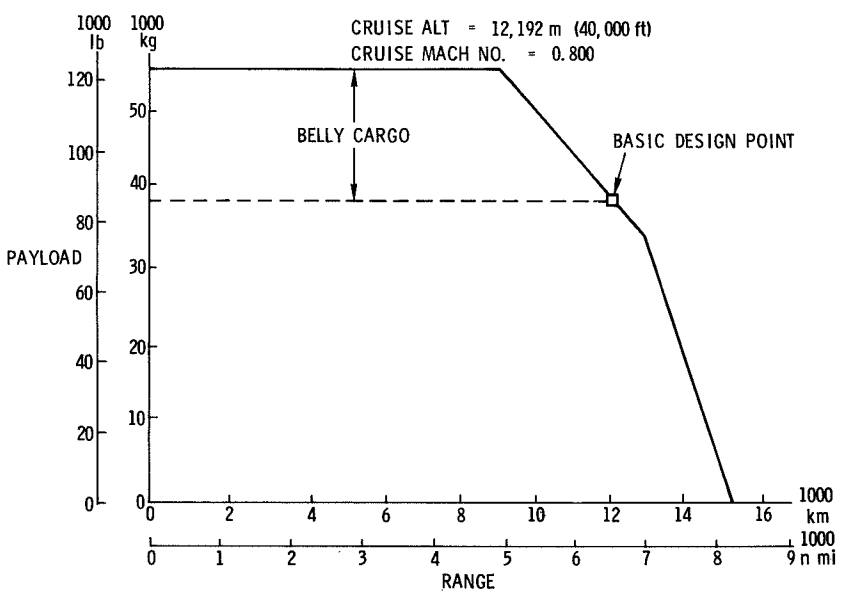

Figure 2.- Payload/range.

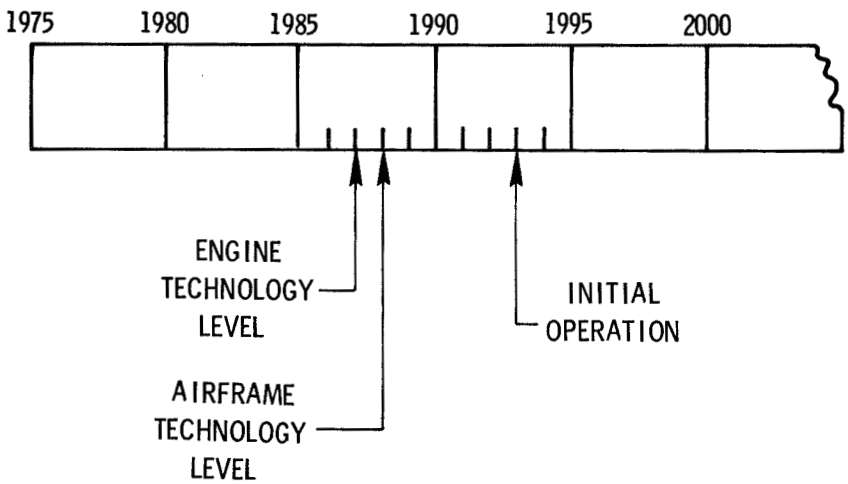

Figure 3.- Development schedule.

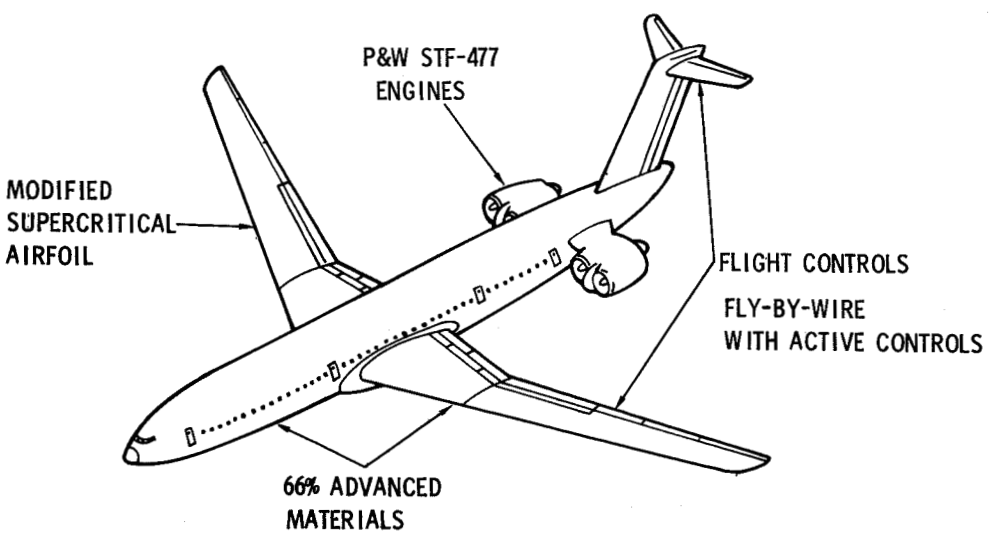

Figure 4.- Reference technology level.

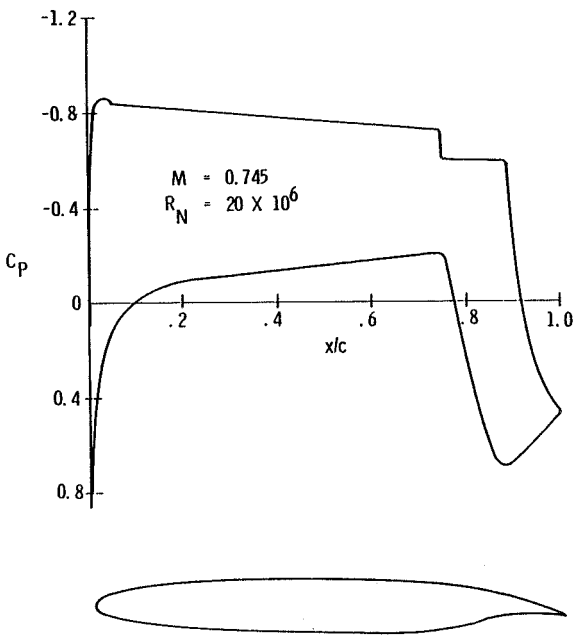

Figure 5.- Airfoil design pressure distribution.

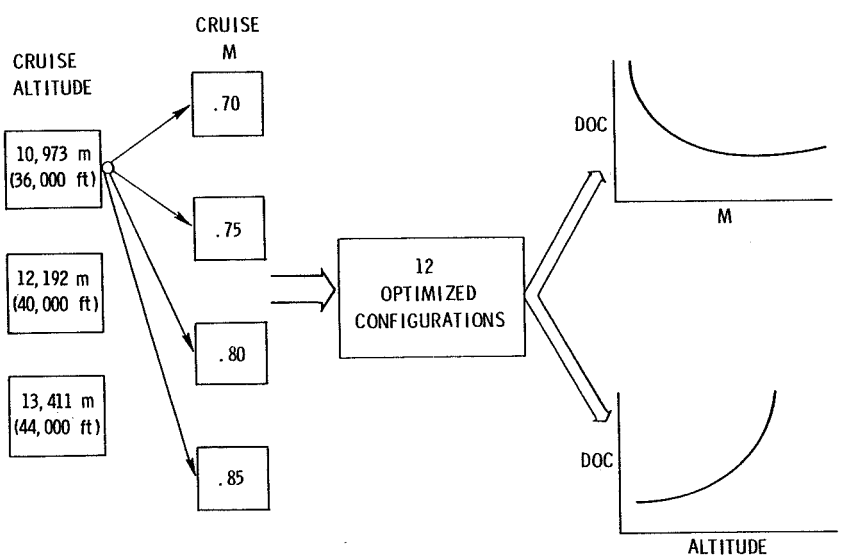

Figure 6.- Parametric configurations.

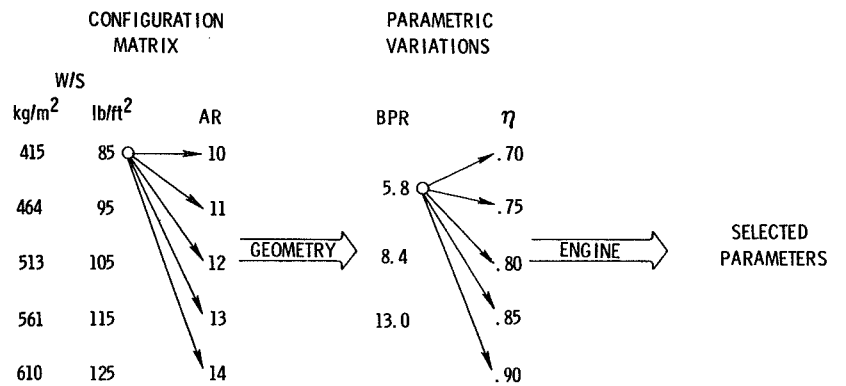

Figure 7.- Parametric procedures.

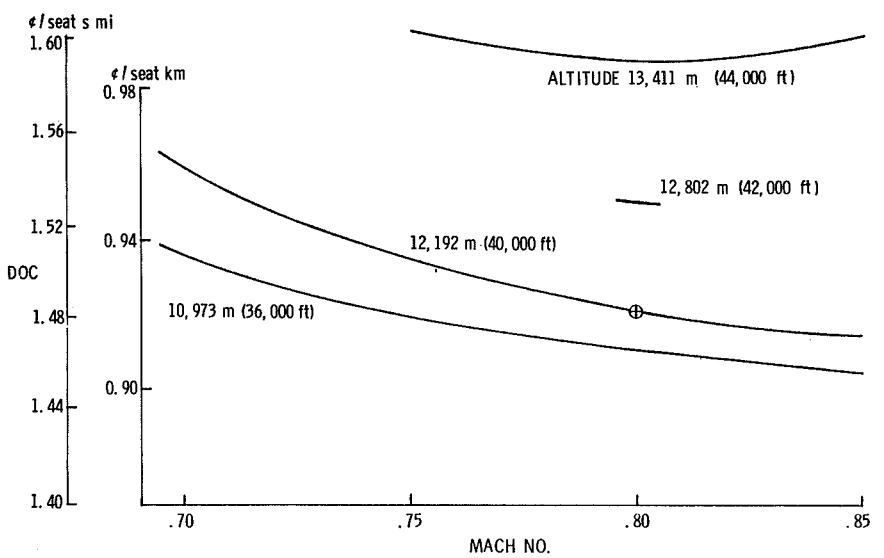

Figure 8.- Variation of DOC with Mach number.

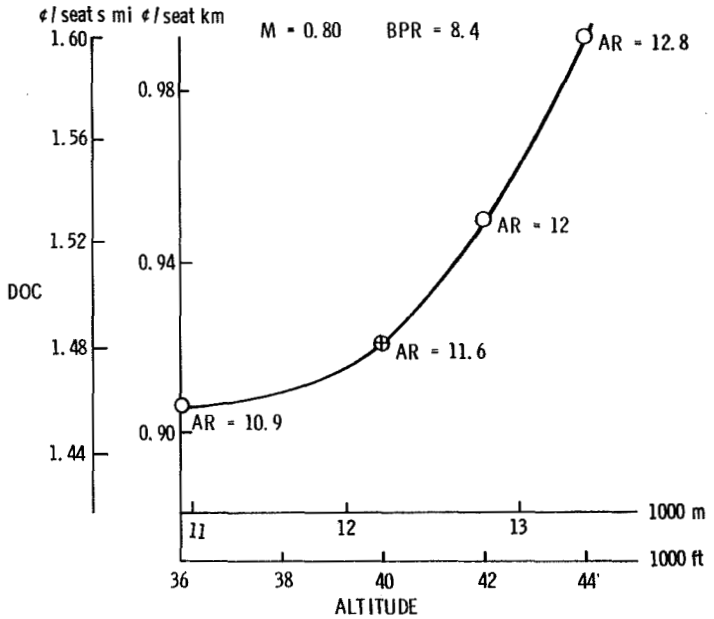

Figure 9.- Variation of DOC with altitude.

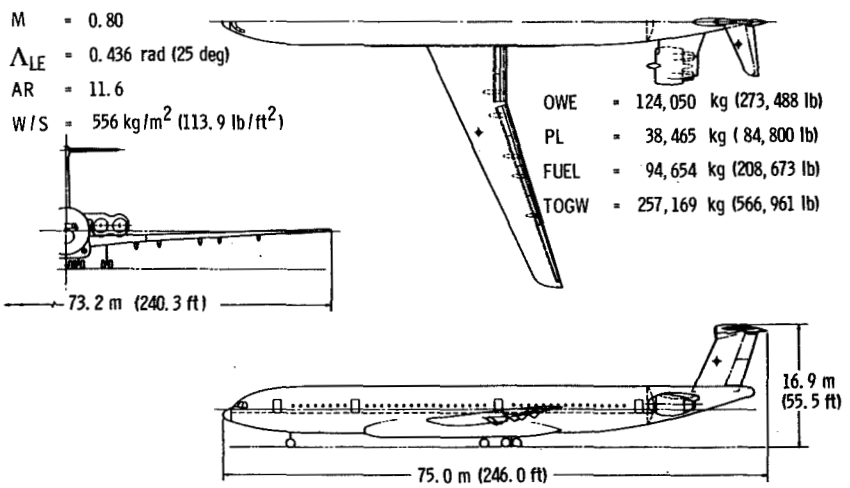

Figure 10.- Baseline aircraft configuration.

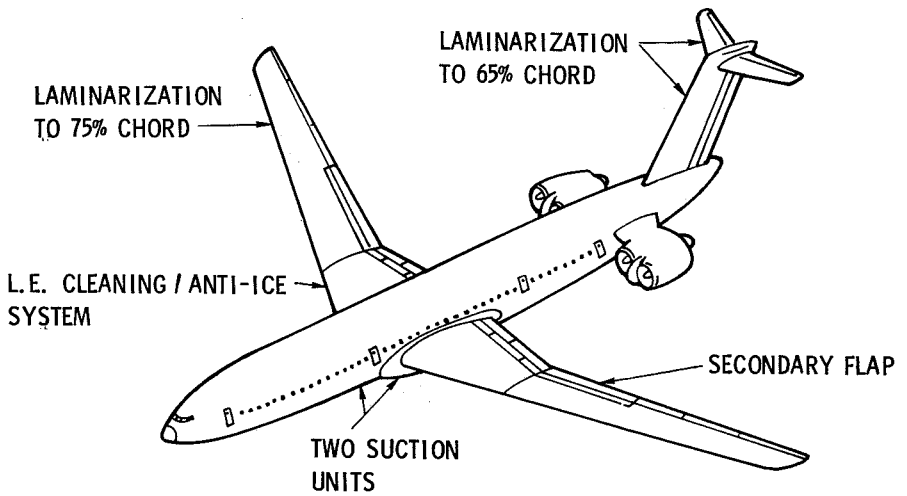

Figure 11.- LFC system configuration.

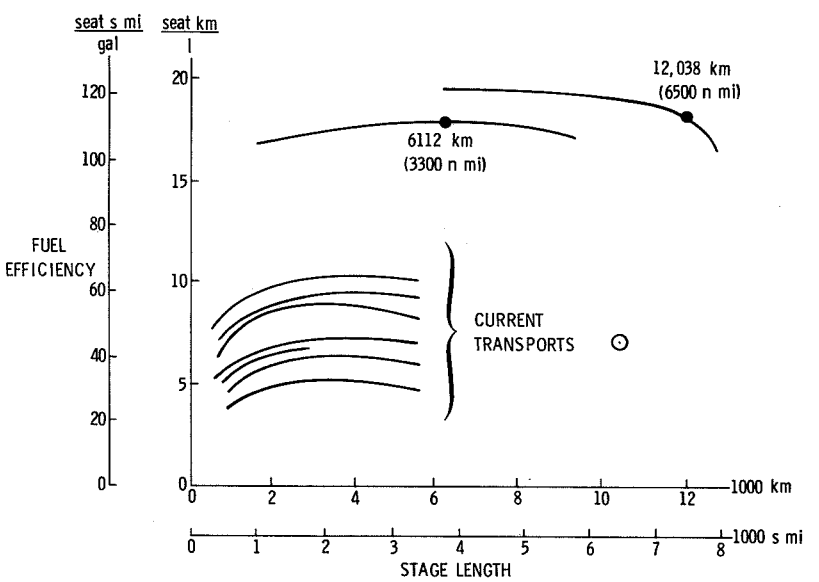

Figure 12.- Fuel efficiency comparison.

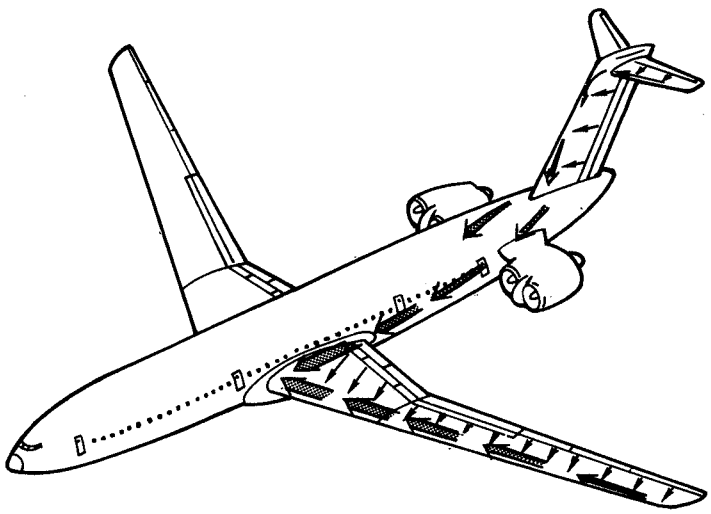

Figure 13.- LFC ducting configuration.

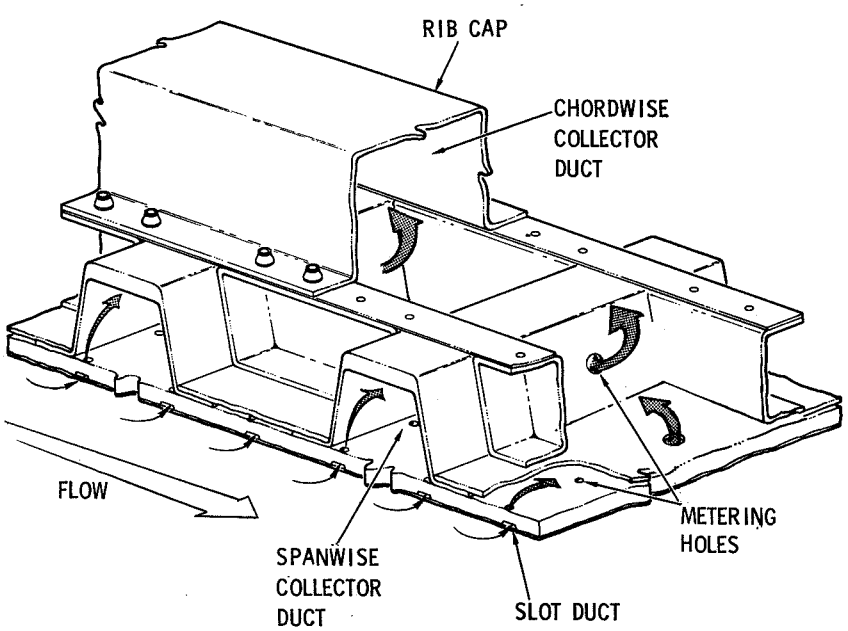

Figure 14.- LFC surface design.

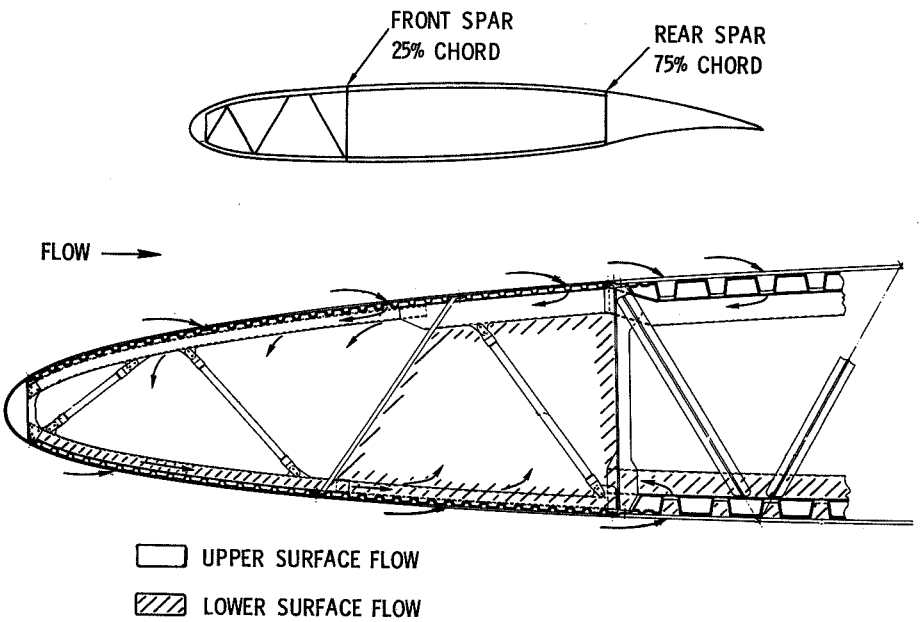

Figure 15.- LFC wing design.

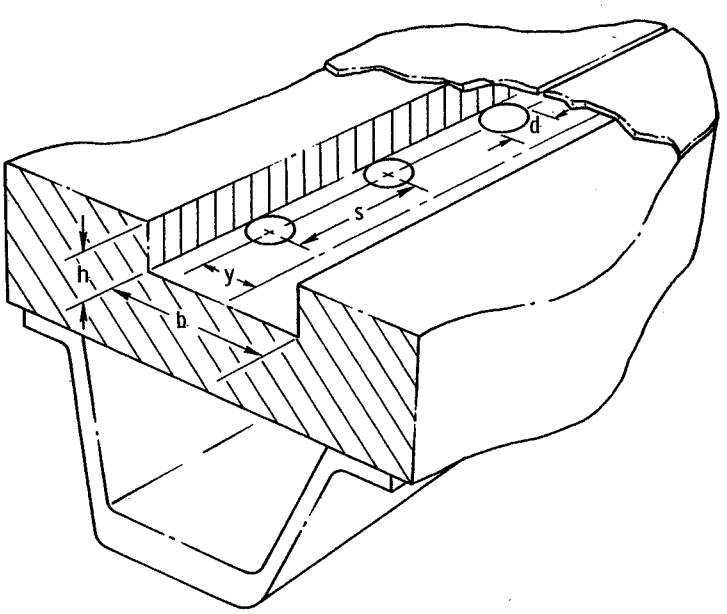

	mm	in.
w	0.28	0.011
h	2.5	0.10
b	7.6	0.30
d	2.0	0.08
s	12.7	0.50
y	2.8	0.11

Figure 16.- Surface metering configuration.

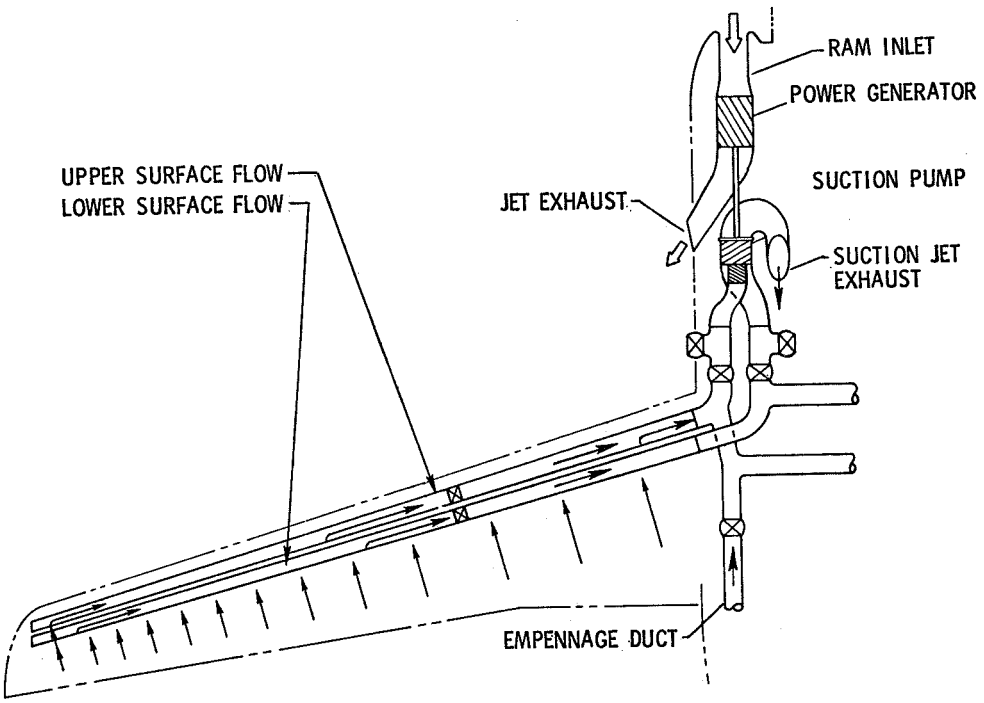

Figure 17.- Suction unit installation.

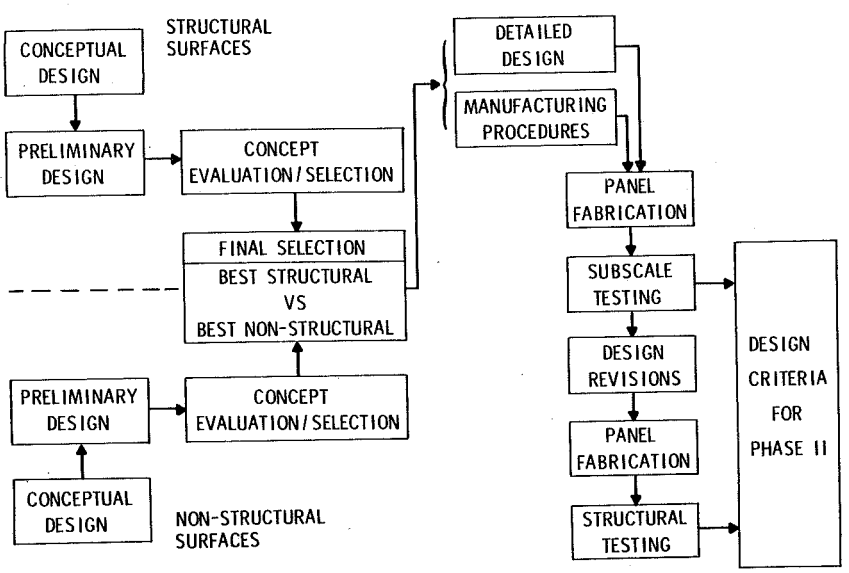

Figure 18.- LFC surface development.

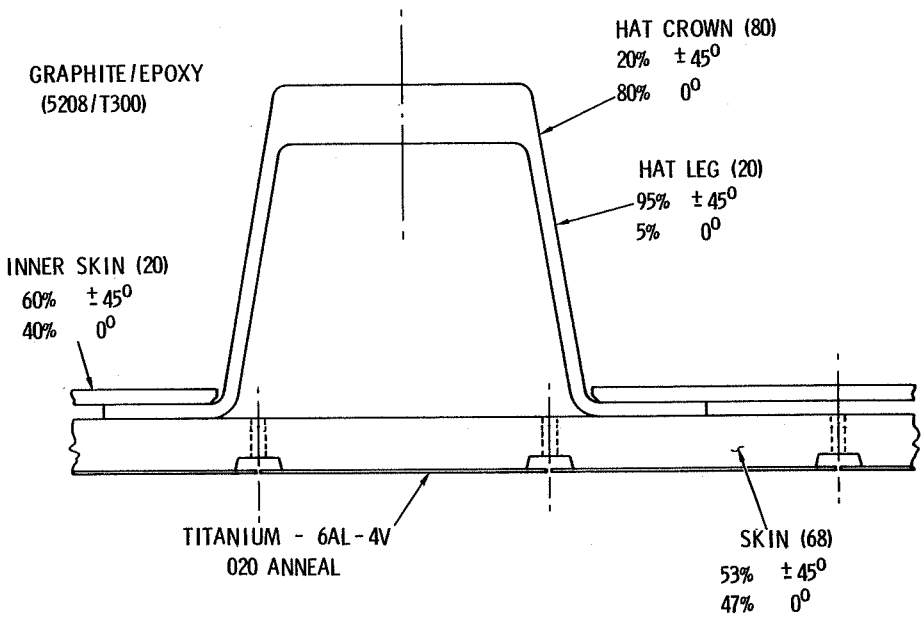

Figure 19.- Surface materials and sizing.

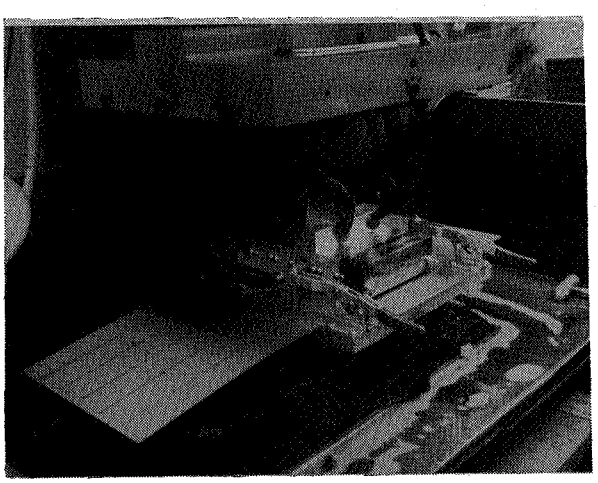

Figure 20.- EDM slotting of titanium.

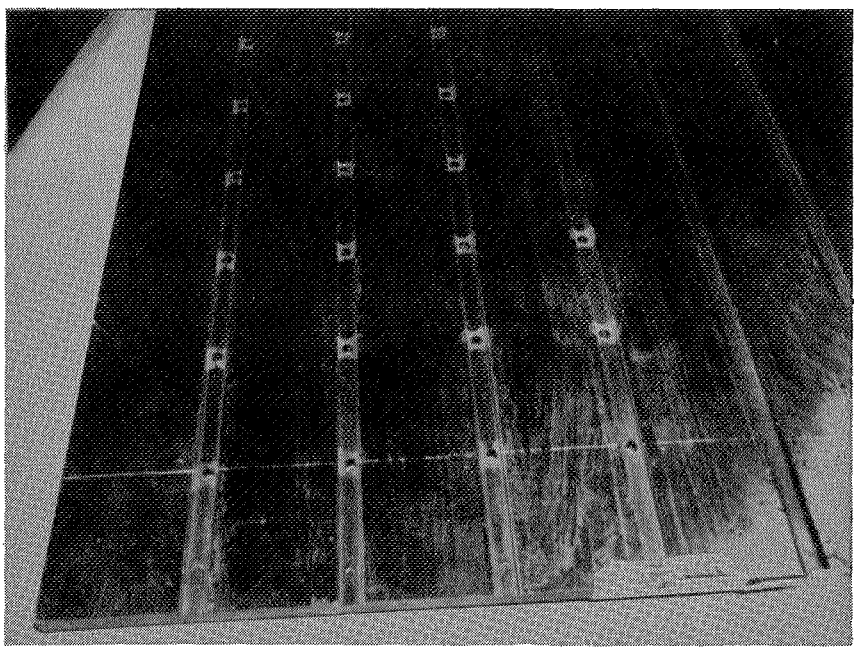

Figure 21.- Structural skin.

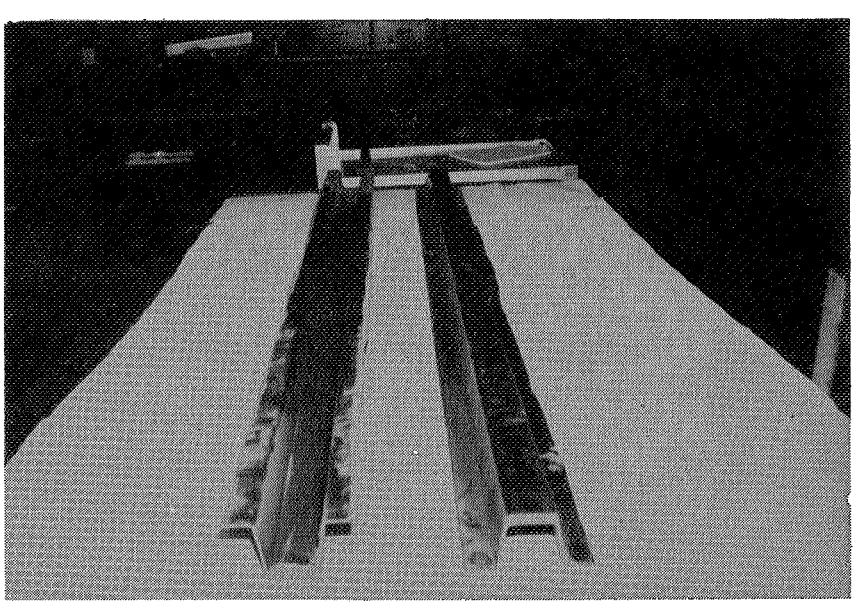

Figure 22.- Hat section stiffeners.

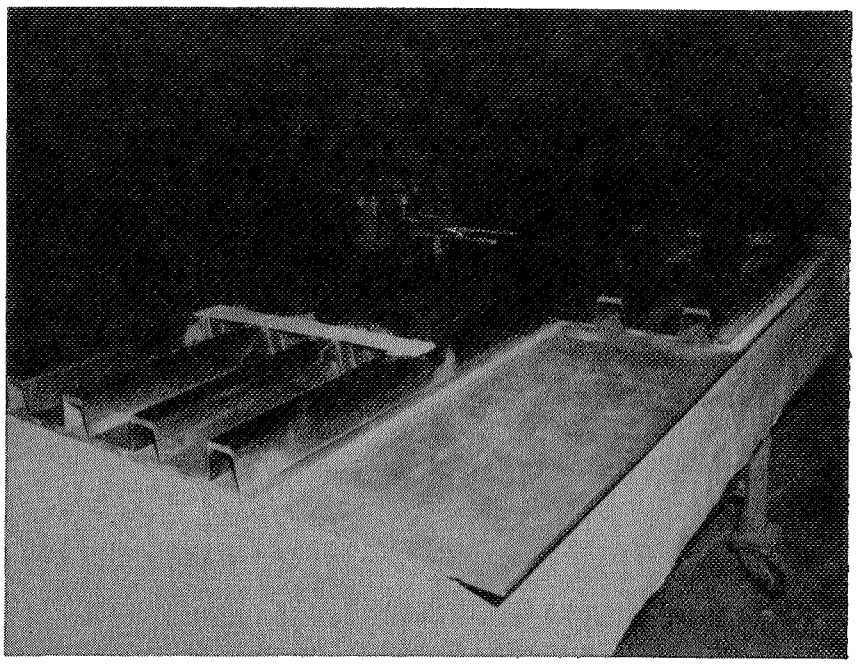

Figure 23.- Panel assembly.

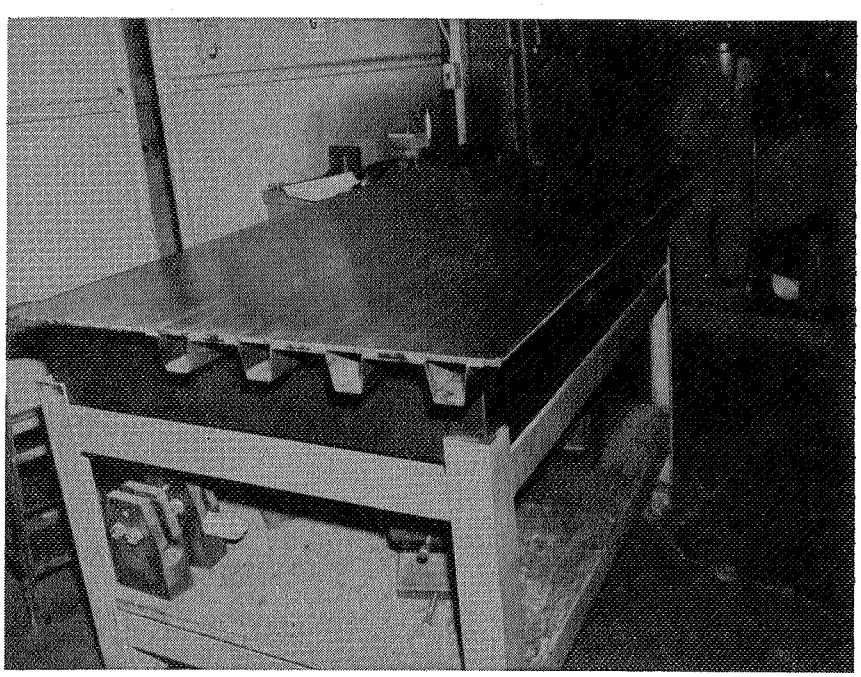

Figure 24.- Complete LFC surface panel.

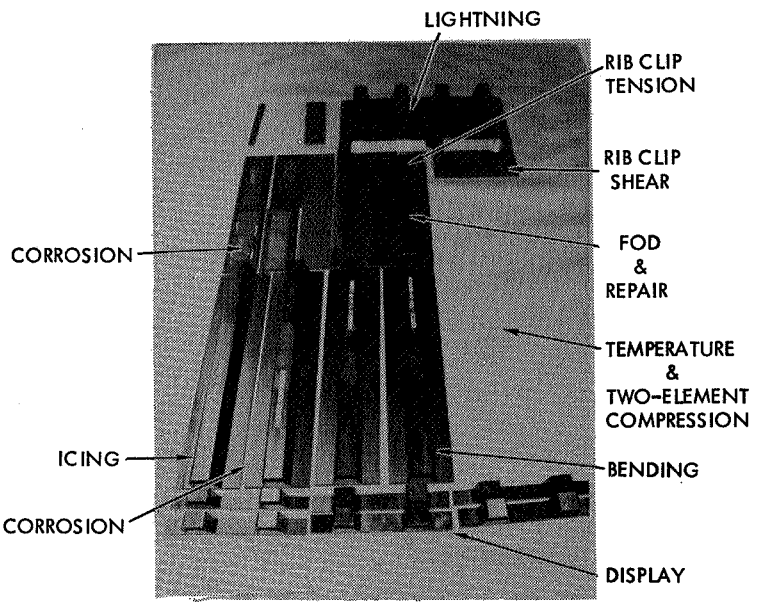

Figure 25.- Test specimens - LFC surface panel No. 1.

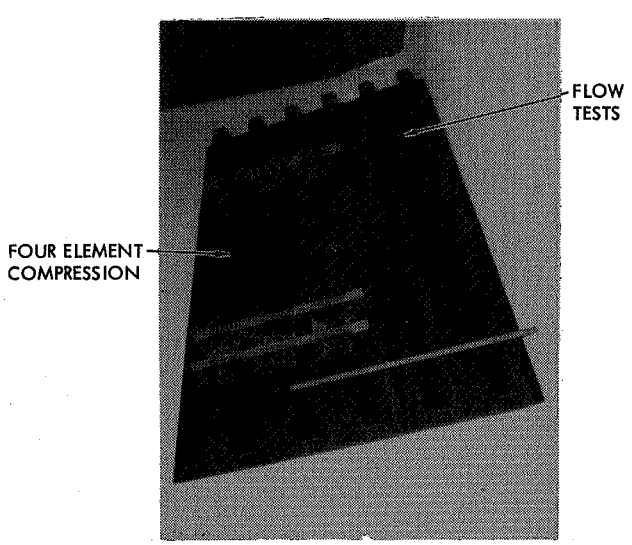

Figure 26.- Test specimens - LFC surface panel No. 2.

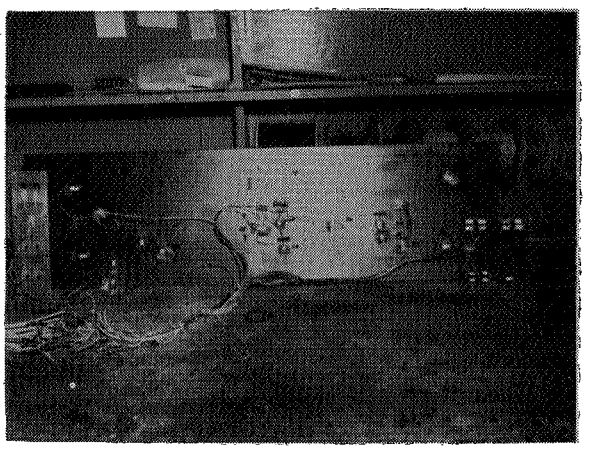

Figure 27.- Temperature test arrangement.

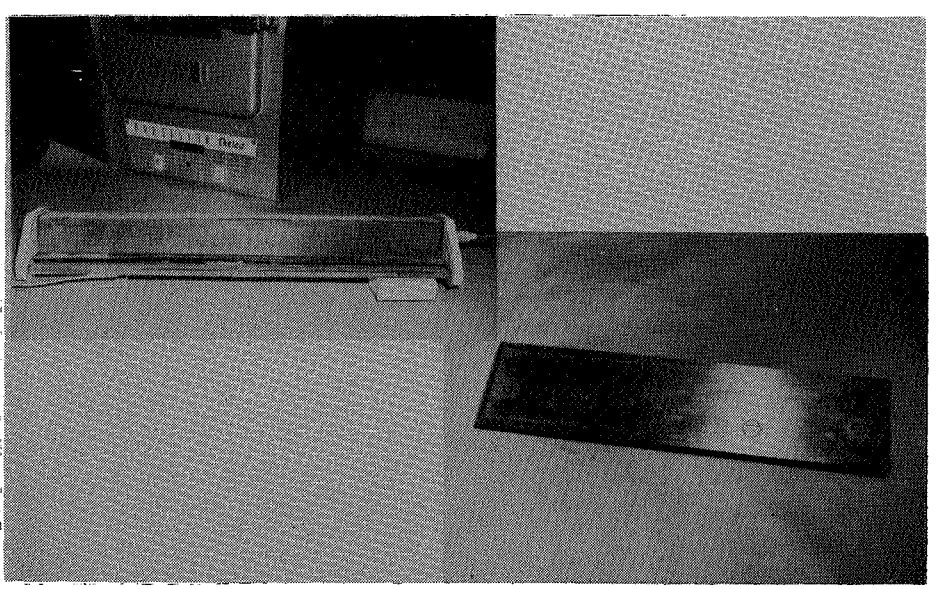

Figure 28.- Icing test specimen.

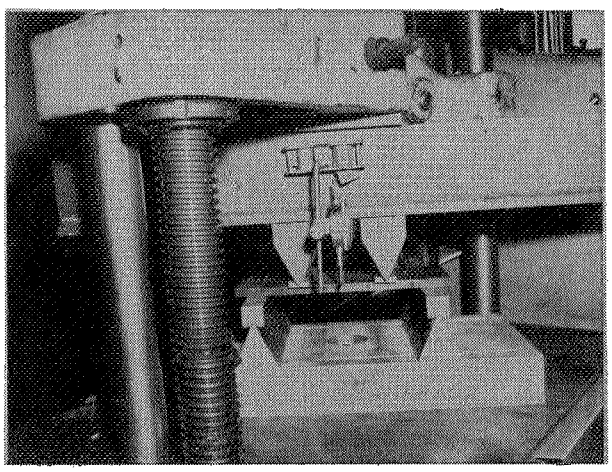

Figure 29.- Corrosion/bending test arrangement.

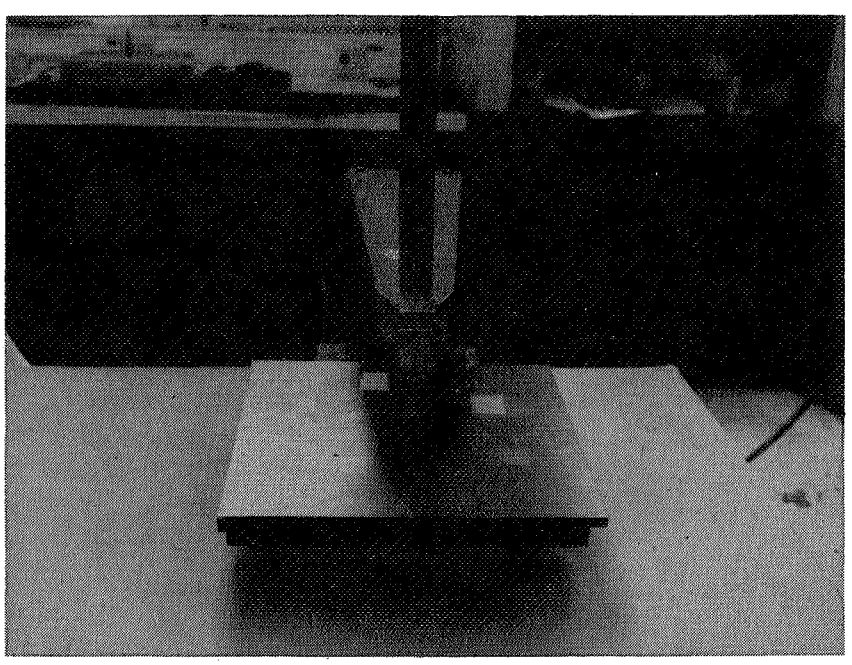

Figure 30.- Impact test arrangement.

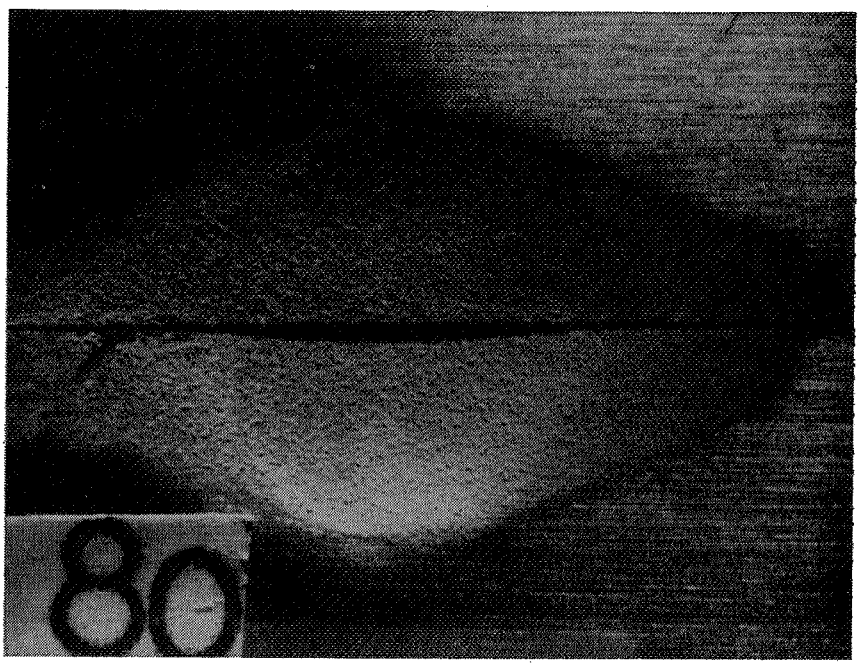

Figure 31.- Impact test specimen.

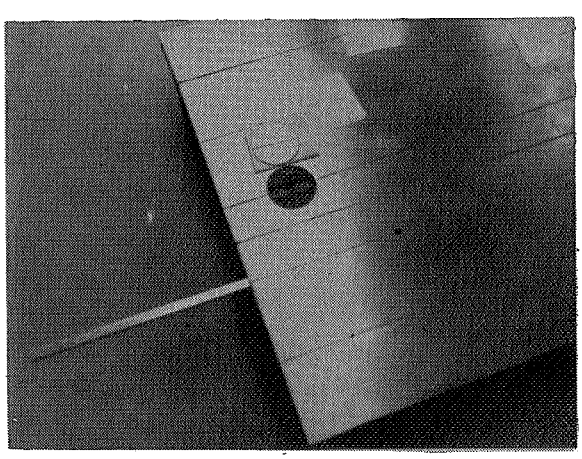

Figure 32.- Repairability test specimen.

Figure 33.- Lightning test specimen.

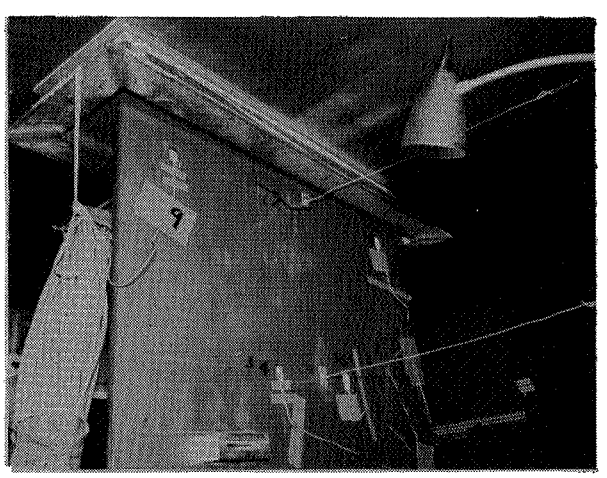

Figure 34.- Compression panel test - 1.334 MN (300,000 lb).

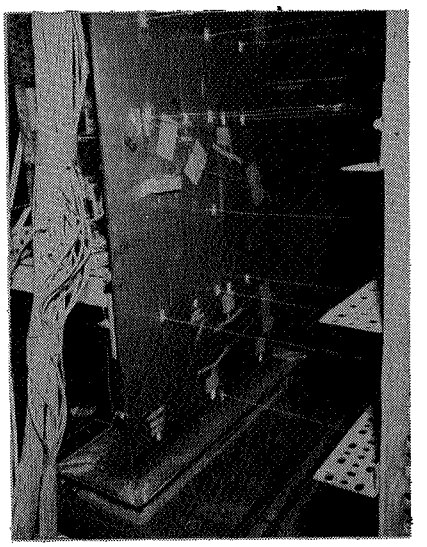

Figure 35.- Compression panel test - 2.224 MN (500,000 lb).

Figure 36.- Compression panel test - failure mode.

APPLICATION OF POROUS MATERIALS FOR LAMINAR FLOW CONTROL

Wilfred E. Pearce
Douglas Aircraft Company

SUMMARY

The use of porous glove suction panels on the wings of commercial transport aircraft to reduce drag by maintaining laminar flow over the wing surface offers some advantages over alternative methods.

Design studies, wind tunnel testing, and materials and process development work done recently at the Douglas Aircraft Company in Long Beach, California, support the porous glove approach to achieving laminar flow control.

Experimental and development work on porous surfaces to achieve laminar flow has, in the past, received far less attention than the slotted surface alternative. However, the encouraging results achieved so far with porous materials warrant increased activity in this field to expand the data base for practical design purposes.

Douglas, supported by NASA, is continuing design and development on the application of porous materials.

INTRODUCTION

It is well known that laminar flow can be maintained by using suction to remove a small fraction of the boundary layer as its thickness increases in the direction of the flow across the surface.

An obvious advantage of using porous surface material to achieve laminar flow control is that suction can be applied gradually at low velocities normal to the surface, thereby minimizing disturbances and discontinuities within the boundary layer. Also, because the direction of flow within the boundary layer relative to the porous material is not significant, no special orientation is necessary.

With a continuous porous surface, suction air must be ducted from beneath the whole laminar flow control (LFC) surface. A suction glove approach is therefore desirable to avoid a need for multiple holes through the primary supporting structure and to provide a substantial barrier between the air ducting system and the integral fuel tank. This is illustrated in figure 1.

Compared with a slotted system, it offers the advantages of avoiding the difficult problem of machining large numbers of continuous spanwise slots, approximately 0.1 mm (0.004 inch) wide, in tough corrosion-resistant material and of maintaining the close slot tolerances necessary during assembly and in flight with associated structural deflections.

A porous surface may also be useful for distributing freezing-point depressant fluid over the wing leading edge and lower surface regions to avoid an accumulation of insects and dirt that could otherwise initiate transition to turbulent flow.

Porous surfaces are not without their own special problems and a number of these are discussed in this paper. However, their potential advantages are sufficient to have encouraged Douglas to investigate

their application for laminar flow control on large commercial transport aircraft. This paper has resulted from that activity.

SYMBOLS

c = wing chord

C_p = pressure coefficient

C_Q = suction coefficient

E_G = Young's modulus for glove panel materials

M_∞ = Mach number

$M_\perp$ = Mach number component normal to sweep

ΔP = pressure drop

R_c = chord Reynolds number

t = airfoil thickness

V = airflow velocity

V_W = average airflow flow velocity through suction surface

V_S = average standard velocity through surface (V_W corrected to sea level conditions)

X_{TR} = transition distance from leading edge

ϵ_{max} = maximum strain

σ_G = stress level in glove panel

Λ = wing sweep angle at 1/4 chord

μ = air viscosity

ρ = air density

POROUS MATERIALS

Based on previous experience (reference 1), four types of fairly smooth porous materials having approximately the right level of porosity were selected for study; Doweave, Fibermetal, Dynapore, and perforated titanium sheet.

The Doweave is woven in three directions from Kevlar fibers. The weave is too open to be used directly as an LFC surface. It was stacked in layers to reduce its porosity and was metallized to increased environmental resistance. The stainless steel Fibermetal is too weak to be self-supporting and was bonded to basic Doweave for added strength. The basic Doweave is shown in figure 2 and the material combinations are shown in figure 3.

Dynapore is a stainless steel woven material that is available in a variety of weaves and gauges. Two grades considered for use as an LFC surface are illustrated in figure 4. Figure 5 shows the 50 x 250 weave photographed at various magnifications using an electron microscope. The flattened surfaces are due to the calendering process which squeezes the woven material to a specified thickness and reduces its porosity. The gaps between the strands can be seen clearly. There are approximately 8700 holes per square centimeter (56,000 holes per square inch) in 80 x 700 and 3900 holes per square centimeter (25,000 per square inch) in 50 x 250 material, as woven.

Figure 6 shows a hole pattern obtained in 0.64 mm (0.025 inch) thick titanium sheet by the electron beam process. The holes are 0.1 mm (0.004 inch) diameter and are spaced 1.0 mm (0.04 inch) apart in both directions. The process is extremely rapid; the hole pattern is preprogrammed and was produced at a rate of about 1200 holes per minute. The rate can be increased up to about 1200 holes per second with thinner sheeting and closer spacing.

Table 1 provides a very rough indication of cost. Some Dynapore weaves are used commercially as filter elements; however, the particular weaves selected were specially produced for Douglas. Perforated titanium and sintered Fibermetal were supplied on an experimental basis only.

No effort was made to project costs on a production basis. However, glove material cost may be put into perspective by considering the $175 per square meter for each LFC surface using a double layer of Dynapore compared with a typical overall wing cost on the order of $6000 per square meter.

SURFACE SMOOTHNESS TESTING

The first step in the selection of porous materials was to test the effective smoothness of alternative surfaces and to determine whether inherent roughness would cause transition. This was investigated on an unswept model with a flat suction surface using the low-turbulence wind tunnel at the Douglas plant in Long Beach.

The model chord was 3.0 meters (10 feet) spanning the 1.37 meter (4.5 foot) tunnel width. It consisted of a flat panel 51 mm (2.25 inch) thick with a sharp wedge section forward and a hinged tapered flap aft. A central pivot allowed variation of the angle of incidence. The porous specimen had a span of approximately 1.2 meters (4 feet) and a chord of 0.3 meter (1 foot). Its leading edge was located approximately 0.6 meter (2 feet) from the leading edge of the model. A plenum chamber beneath the porous specimen was connected to a suction line via a flowmeter and a gate valve to regulate suction. This arrangement is illustrated in figure 7.

The boundary layer was surveyed using a sensor on a hand-held wand. The sensor consisted of a tapered probe with a 1.6 mm (1/16 inch) diameter hemispherical nose covered by a thin platinum film. The film was used as the sensing element of a constant temperature anemometer. The anemometer responded to velocity fluctuation within the boundary layer. The output was amplified

and displayed visually on an oscilloscope and played through a loudspeaker. The audio effect was useful for homing in on the transition region but the visual display was used for more precise location of transition. Typical displays corresponding to various flow conditions are shown in figure 8. Laminar flow is indicated by a low-amplitude oscillation as shown in figure 8A. As the probe is moved downstream, regular peaks may occur as in figure 8B and a constant frequency noise can be heard, sounding rather like a large mosquito. This is caused by the Tollmien-Schlichting small disturbance wave, which has a regular frequency. Further downstream bursts of turbulence can be heard and appear on the oscilloscope as in figure 8C. Further downstream still, the flow becomes completely turbulent as in figure 8D. Transition is judged to have occurred when the turbulent bursts are equal in duration to the intervening laminar conditions. This judgment is noticeably enhanced by the visual display.

SURFACE COMPARISONS

Typical results of transition location are shown in figure 9. The solid symbols identify results obtained with a smooth flat surface at chord Reynolds numbers from 5.2×10^6 to 11.7×10^6. The flat plate transition results are better than those normally expected ($R_{max} = 3 \times 10^6$ from reference 2) due to a favorable pressure gradient obtained upstream of the test specimen. Comparison with the 50 x 250 Dynapore test panel represented by the open symbols in the figure indicates that without suction, there is an initial upstream movement of transition due to inherent surface roughness and the tolerances achieved on the test panel installation. As suction is applied through the surface of the test panel, the transition point moves to a point further downstream than for the flat plate.

Figure 10 compares the transition results obtained at the same Reynolds number with a variety of porous surfaces. Both Dynapore surfaces were more effective than the others at economical low suction flows. The slotted aluminum and the porous titanium panels required much higher suction levels to be as effective. The sintered Fibermetal was less effective than these, and the metallized Doweave was a failure. The 80 x 700 Dynapore surface was clearly the most effective of those tested.

The effect of airflow direction relative to the weave direction for the 50 x 250 Dynapore is shown in figure 11. The surface is less efficient at low suction flows with the airflow at 90 degrees to the weave direction, but even so the coarser Dynapore is still more effective than the alternative surfaces tested.

During tunnel testing with the perforated titanium specimen, it was noticed on two occasions that a particle had become lodged in the surface, causing a turbulent wedge to appear. Laminar flow was restored by rubbing the surface smooth without removing the blockage, thus proving that transition had been caused solely by the protrusion of the particle above the surface. These conditions were not experienced during any of the testing with the Dynapore specimens.

The relative merits of alternative suction surfaces when subjected to cross flow conditions still need to be evaluated using a swept wing wind tunnel model. Flight testing would be necessary to obtain fully representative conditions at high Mach numbers combined with high Reynolds numbers.

Typical pressure distributions for airfoils suitable for laminar flow are shown in figure 12. For a swept wing, suction requirements increase in the regions of steep pressure gradients that occur both near the leading edge and aft of approximately 60 percent chord. This is reflected in the suction flow velocity requirements for the upper and lower surfaces, as shown in figures 13 and 14.

Outflow through the surface must be avoided as it would destroy laminar flow. Suction pressure below the surface must therefore be less than the lowest pressure over any external surface area that is connected to a common plenum or local duct region. This requirement defines the minimum pressure drop allowable through the surface. A typical value is 0.013 of the free-stream dynamic pressure for the upper surface of the glove panel in the main structural box region. For a flight condition of Mach 0.8 at 12,190 meters (40,000 feet) altitude, the minimum pressure drop through the surface would be 110 Pa (2.3 lb/ft^2) with a velocity of 0.03 m/sec (0.1 ft/sec). Most of the flow resistance within the glove panel is supplied by the porous surface material itself, but there is additional resistance in the backing material and flow channels.

SUCTION CHARACTERISTICS

Typical flow rates versus pressure drop for the suction surfaces compared previously are shown in figure 15. It is interesting to note that the Dynapore material retained a straight-line relationship with the pressure drop directly proportional to the velocity as indicated by the 45-degree slope, whereas this relationship varied for the other materials. For the slotted surface, for example, the pressure drop changed from being proportional to V_S toward a V_S^2 relationship at the higher velocities. All of these surfaces were more open than that required, as illustrated.

Since both suction velocity and surface pressure drop requirements increase with increasing external pressure gradients (either positive or negative), the required porosity envelope tends to follow a ΔP versus V_S relationship similar to that of the porous materials themselves. This characteristic should allow a porous surface with a single level of porosity to cover a fairly wide range of external pressure conditions. Methods of varying porosity were next considered, with particular reference to the Dynapore materials that were shown previously to have the most promising surface characteristics.

POROSITY REDUCTION

The effective porosity for perforated or slotted surfaces can be modified by changing hole size and distribution or slot width and spacing, respectively.

The possibilities for reducing porosity on Dynapore woven materials include the following: (1) varying the fiber thickness and weave; (2) increasing the calendering (or squeezing) of the material after weaving; (3) adding metering layers beneath the surface layer, (4) plating the fibers after weaving, and (5) blocking the porosity.

Figure 16 shows the effect of calendering on 50 x 250 and 80 x 700 weaves. For a single layer, considerable squeezing is necessary for either weave to reduce porosity to the useful range indicated. Too much calendering reduces the strength of the individual fibers by introducing severe stress raisers, particularly from the aspect of fatigue. The necking of the fibers is illustrated in figure 17. To retain acceptable strength characteristics, the amount of squeezing is being limited to no more than 40 percent.

The addition of metering layers may not bring about as rapid a reduction in porosity as might be expected. Increasing the number of porous metering plies sandwiched between relatively open Doweave layers was found to result in a diminishing effect. The pressure drop, with as many as five intervening layers, was still well below the desired level and increasing the number of layers further had little effect.

Plating may be used to reduce porosity but with the triangular-shaped pores in Doweave measuring only 0.043 mm by 0.02 mm (0.0017 by 0.0008 inch), the plating process would need to be very carefully controlled.

During early experiments, the bonding adhesive wicked and spread very badly on one specimen of 50 x 250 Dynapore bonded to a honeycomb cell backing; this is shown in figure 18. In effect, the specimen was surfaced with a regular pattern of porous holes with random nonporous areas superimposed. To our surprise, the surface performed satisfactorily in the tunnel. A comparison with the results obtained on an unblocked 50 x 250 panel is shown in figure 19. This encouraging result indicated that porosity could be satisfactorily reduced by intentional blocking. Two possibilities were considered: (1) blanking off large continuous areas to create a porous strip effect, and (2) using a perforated sublayer to obtain a distributed blanking effect. Both methods offer the additional advantage of an opportunity for varying porosity levels within a single panel.

Figure 20 gives the dimensions of a porous strip panel that was tested. The static flow characteristics are shown in figure 21. As indicated, the porosity moved into the desired range and the pressure drop remained directly proportional to the velocity.

The laminar flow performance of the porous strip configuration (figure 22) is better than for the original 50 x 250 panel for low-suction flows. This is probably due to reduced surface roughness as indicated by the increased extent of laminar flow obtained with porous strips compared with the unblocked specimen, with suction off.

Various hole patterns are currently under consideration for the perforated sublayers.

SURFACE IMPACT RESISTANCE

A further consideration with respect to surface sublayers is impact resistance. The Dynapore is woven in a softened condition and is work-hardened to some extent during the calendering process. However, it is still too soft to be used at the outer surface without some reinforcing. A perforated fiberglass sublayer used to partially block the porosity can also be used to provide increased impact resistance.

As an aid to bonding the 80 x 700 Dynapore surface to the fiberglass sublayer and to improve strength accross the perforations, an additional layer of 80 x 80 Dynapore may be interposed between them and diffusion-bonded to the outer surface layer. Penetration of resin into the more open weave results in a stronger bond between the Dynapore and the fiberglass layers. Figure 23 shows an 80 x 80 sublayer diffusion-bonded to an outer 80 x 700 surface.

Test results indicate that by adding the perforated glass laminate under the Dynapore, it should be possible to provide a surface with adequate impact resistance for the main box area. As a repair procedure for any accidental dents that may occur in the surface, local filling, even with the resulting blocking of the porosity, may be satisfactory due to the apparent insensitivity of the laminar flow performance to local blockage. This would not be acceptable, however, if a cratered lip were to occur around a large dent, as was experienced before introducing the reinforcing sublayer. The initial design aim would be for impacts up to 5.65 N-m (50 lb-in.) to be quickly repairable by filling, if necessary.

STRAIN COMPATIBILITY

A major consideration for glove panel design is strain compatibility with the main load-carrying structure because the glove must strain with the structure to avoid surface gaps. Primary structural materials with a high ratio of stiffness to usable strength are therefore advantageous. Figure 24 illustrates this factor for a number of primary structural materials. Of the materials considered, graphite/epoxy composite structure would be the most compatible, aluminum second, and titanium last from this point of view.

In addition to structural loads, differential thermal expansion stresses must be taken into consideration. By subtracting the thermal strain that could be induced in the glove from the total strain available, the strain remaining for structural loads can be obtained.

The combined effect of structural and thermal strain for a number of material combinations is shown in table 2. The table shows that a Dynapore surface supported by a fiberglass sandwich panel should be compatible with all of the primary structural materials considered.

LFC GLOVE PANEL DESIGN

The selected glove panel design is based on the Lockcore* principle. This construction was developed primarily for use as a noise-damping panel for engine air inlets; it is illustrated in figure 25.

Figure 26 shows how the Lockcore principle can be applied to a laminar flow control panel. It provides a porous LFC surface and internal suction flow collector ducts and could have adequate impact resistance, strength, and stiffness. With LFC on, air is sucked from the boundary layer through the diffusion-bonded Dynapore layers and the supporting perforated fiberglass layer. It then passes through the outer porous fiberglass layer of the supporting sandwich panel and flows into channels formed by the fluted stiffeners.

To avoid not having suction for more than a short distance along the flow direction within the boundary layer, all suction flow discontinuities including panel joints may be inclined across the flow direction. The glove panel stiffeners may also be included parallel with the panel joints, as illustrated in figure 27.

GLOVE PANEL AND WING STRUCTURE COMBINED

The LFC suction glove panel is attached to the integral blade stiffeners of the primary wing box structure, as illustrated in figure 28. The figure shows how suction air flowing within the Lockcore panel is transferred to collector channels ending in adjustable nozzles that control the flow into each main spanwise integral duct formed by blade stiffeners on the main load-carrying panel. The flow channels within the Lockcore panel are blocked in line with each main stiffener. This limits the effect of external chordwise pressure variations and allows pressure drop requirements through the surface to be kept small. The integral ducts run closely parallel with the wing isobar pattern: this also helps to reduce pressure drop requirements along the duct. The collection channels and adjustable nozzles are an integral part of the glove panel. The nozzles can therefore be preset on the bench to meet the required flow values and to compensate for any variations in panel porosity. This is a considerable advantage in initial assembly and maintenance.

*Lockcore is a Douglas patent process.

By using removable porous glove panels surrounding the basic wing structure, further advantages arise, which include the following:

1. Choked or damaged panels could be removed and cleaned or replaced without disturbing the primary wing structure.

2. A smooth external surface matching the airfoil profile is not a requirement for the basic structure. Hence, joints, attachments, doublers, and any repairs or modifications of the basic structure may be simplified.

3. The removable glove suction panels do not have to meet the same fatigue life requirements as the primary wing structure.

4. The main structural box, integral ducting, and systems are accessible for inspection, maintenance, and repair, by removing the glove panels, and manholes can be provided in the primary structure to gain access to fuel tanks in the normal manner without conflicting with the suction system.

5. With external blade stiffeners, the main structural box benefits from a smooth interior surface. This simplifies rib design by avoiding stiffener cutouts, and simplifies the diffusion of concentrated loads into the main box shell. Trapped pockets of unusable fuel are also avoided.

CONTAMINATION AVOIDANCE

The remains of any insects impacted on the surface exceeding a height of about 0.1 mm (0.004 inch) are likely to cause transition followed by a wedge of turbulent flow on the surface. One way of avoiding this situation that has been tested on a Jetstar airplane is to ensure coverage of the impact region with a continuous fluid film during the period of exposure to insects.

A porous surface offers the possibility of providing fluid coverage over critical areas by using porous strips for fluid distribution. Fluid flowing back across a smooth surface has a tendency to collect into rivulets. This could leave the surface between the rivulets exposed to contamination. Tunnel testing with fluid flowing back on porous surfaces, however, has shown that once the porous surface is wet, there is no longer a tendency to form rivulets. This suggests that for a porous surface, the high rate of flow necessary to wet the surface could be reduced subsequently to a more economical level.

A difficulty is caused by the movement of the stagnation point around the leading edge during takeoff and climb. Because the fluid could not flow against the airstream, it may be necessary to distribute fluid through the surface over the entire stagnation region to ensure complete coverage.

Testing also showed that a porosity suitable for laminar flow control would result in excessive fluid flow in order to maintain an even distribution. Therefore, either a higher pressure drop through the surface would be needed or the fluid flow would need to be pulsed at intervals. The latter alternative would be more consistent with the requirement for wetting the entire surface initially.

Freezing point depressant (FPD) type fluid would be required for the anticontamination system, and this could also be used for de-icing.

CONCLUDING REMARKS

The results of Douglas studies to date support the use of porous materials to achieve laminar flow. Various porous materials have been considered for application to LFC wing surfaces, and four candidate porous surface materials have been subjected to a series of screening evaluations with the following results:

Laminar flow tests with suction, which account for Tollmien-Schlichting instabilities but not cross-flow instabilities, indicate that all but one of the surfaces tested are sufficiently smooth. Of these, fine mesh Dynapore requires far less suction to substantially extend the region of laminar flow than the other surfaces, including a slotted one.

The LFC performance of the Dynapore surfaces is not affected by locally blocked regions and the overall porosity may be tailored to meet LFC requirements by controlled blockage that can produce porous strips or porous hole patterns.

Dynapore surfaces perform satisfactorily with the weave in either direction relative to the flow, but perform better with the airflow at 90 degrees to the warp.

The impact resistance of a Dynapore surface is inadequate without backup layers that may also be used to moderate porosity.

Tests indicate that the porous surface could be used with fluid systems for the prevention of contamination and icing.

A possible LFC suction glove arrangement has been identified with material combinations compatible with thermal expansion and structural strain.

REFERENCES

1. Development of Technology for the Fabrication of Reliable Laminar Flow Control Panels on Subsonic Transports. NASA CR-145125, October 1976.

2. Schlichting, Hermann: Boundary Layer Theory. McGraw Hill, 1968.

TABLE 1

LFC SURFACE MATERIALS COSTS

MATERIAL	APPROXIMATE COST ($/m^2)	
	SINGLE PLY	FOR EQUAL ΔP
• METALLIZED DOWEAVE[2]	116	231[1]
• SINTERED FIBERMETAL	646[2]	770[1][3]
• DYNAPORE		
50 x 250	113	113
80 x 700	133	133
80 x 700/80 x 80	175	175
• PERFORATED TITANIUM	1884[2]	1884

[1] MULTIPLE LAYERS — BONDING COST EXCLUDED

[2] EXPERIMENTAL QUANTITY

[3] SUPPORTED BY DOWEAVE

TABLE 2

COMPATIBILITY OF MATERIALS (STRUCTURAL PLUS THERMAL STRAINS)

FEASIBLE COMBINATIONS		
	PANEL MATERIAL	STRUCTURE MATERIAL
SINGLE MATERIAL PANELS	316L DYNAPORE KEVLAR/EPOXY GLASS/EPOXY	GRAPHITE BORON ALUMINUM TITANIUM
MULTIMATERIAL PANELS	50 x 250 + KEVLAR	GRAPHITE BORON ALUMINUM
	50 x 250 + GLASS	GRAPHITE BORON ALUMINUM TITANIUM

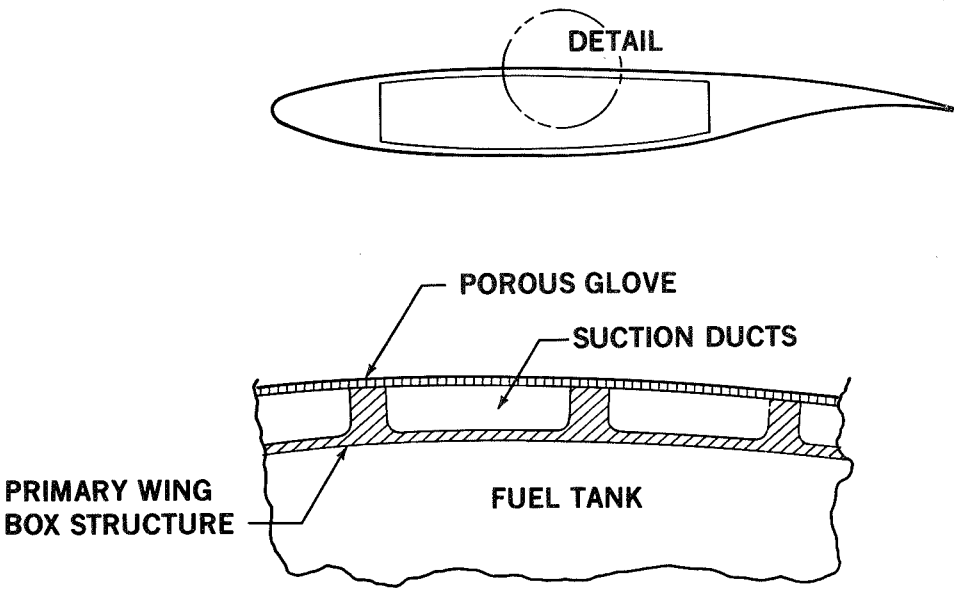

Figure 1.- LFC porous suction glove.

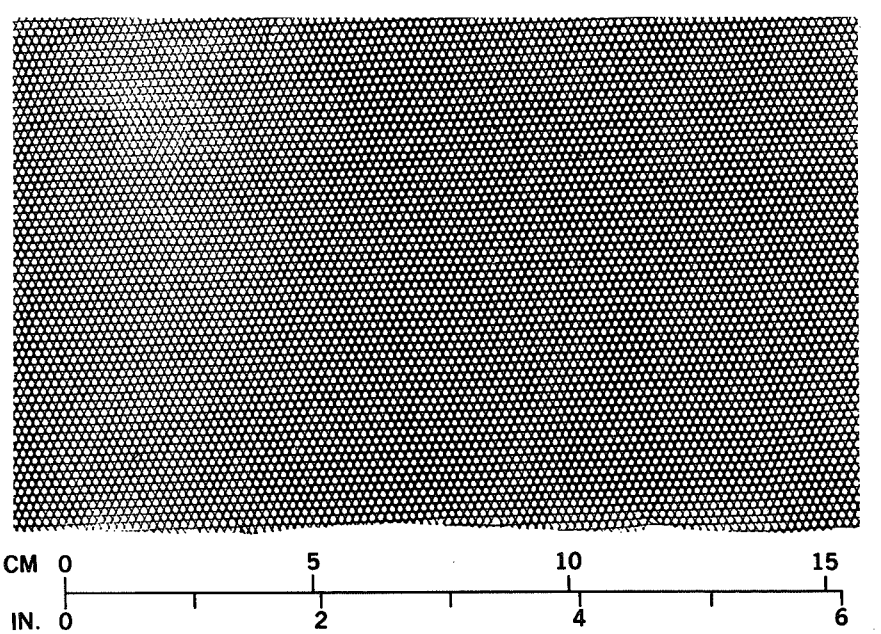

Figure 2.- Basic Doweave.

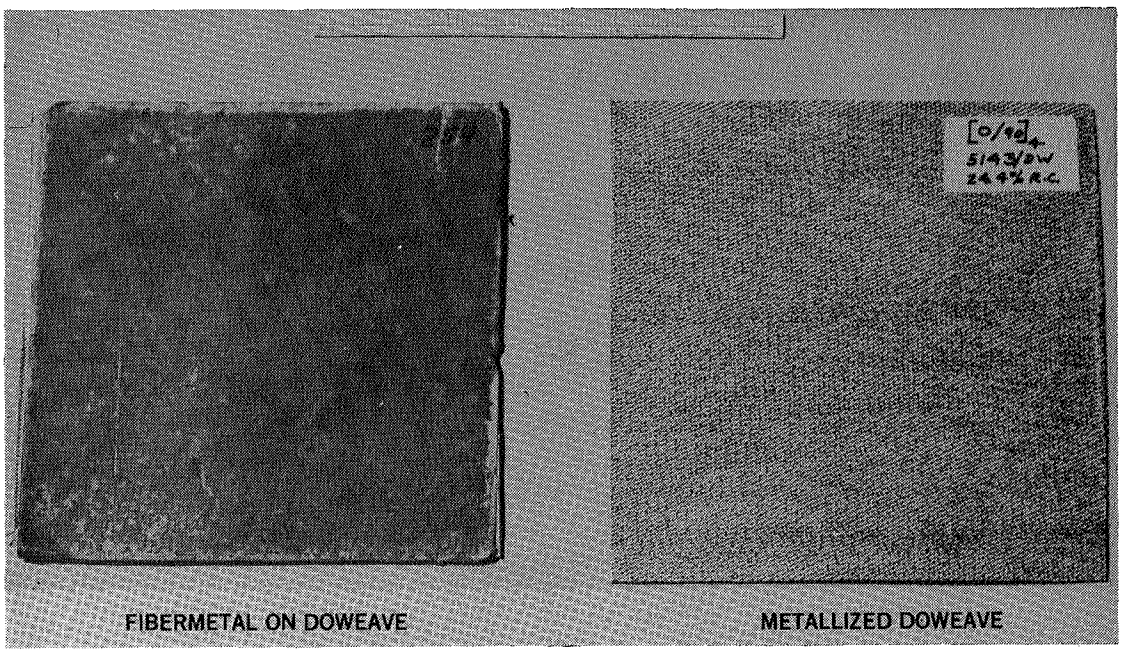

Figure 3.- Porous surface samples.

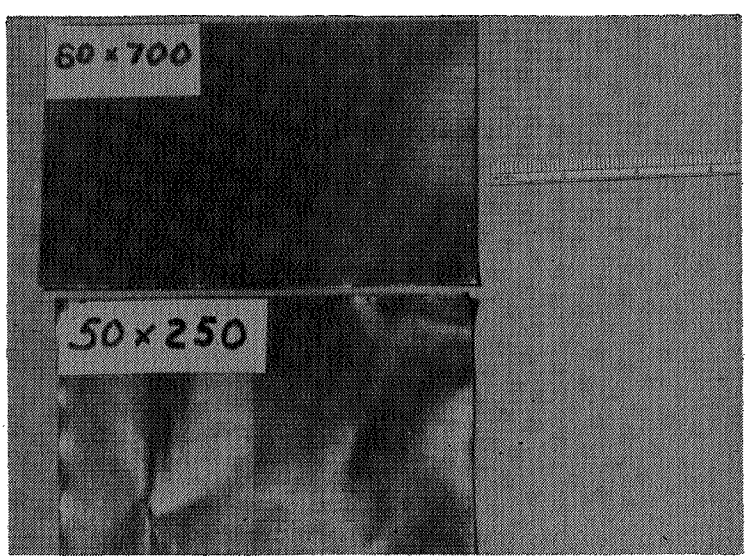

Figure 4.- Dynapore surfaces.

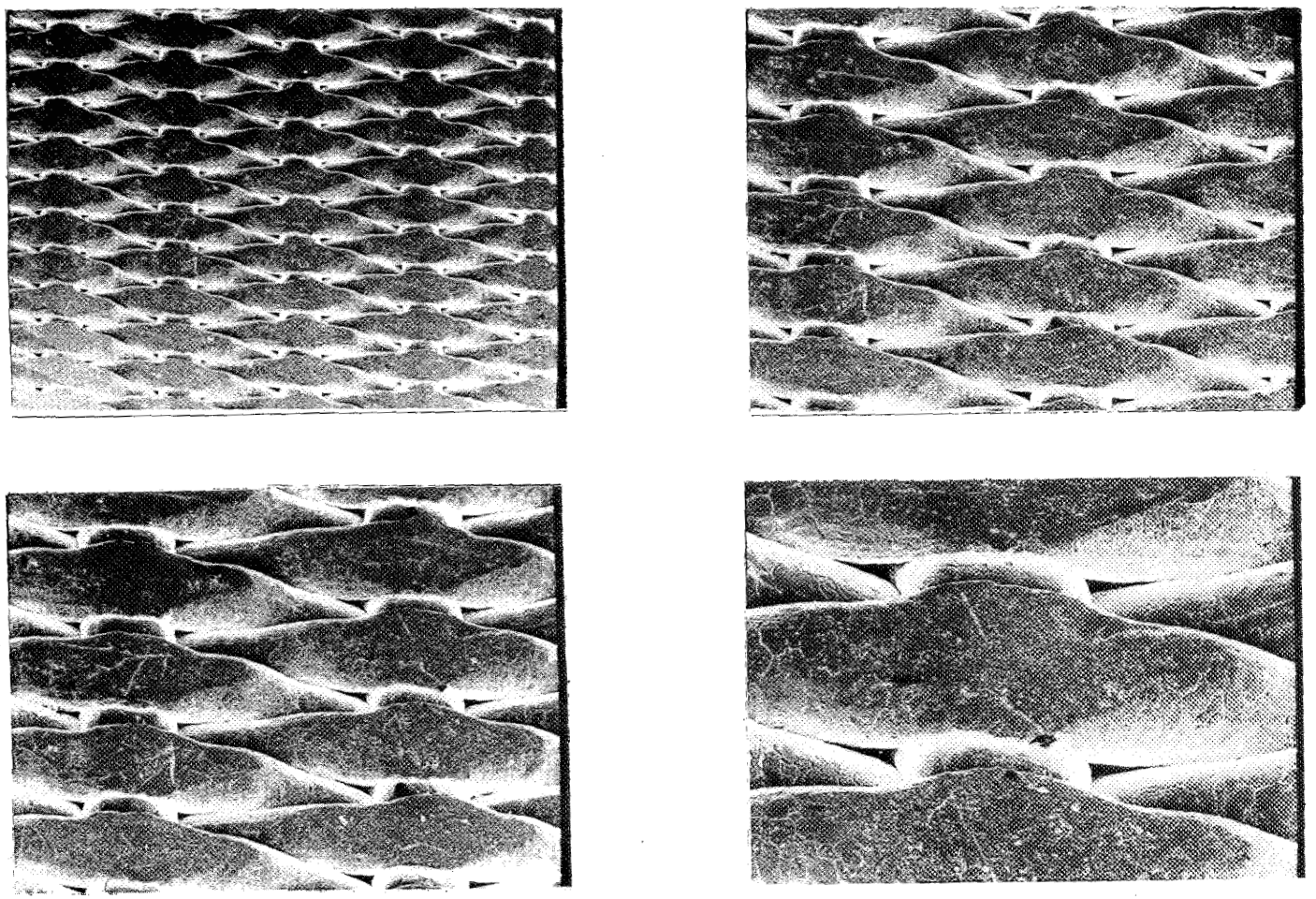

Figure 5.- 50 × 50 Dynapore surface englarged (40× to 200×).

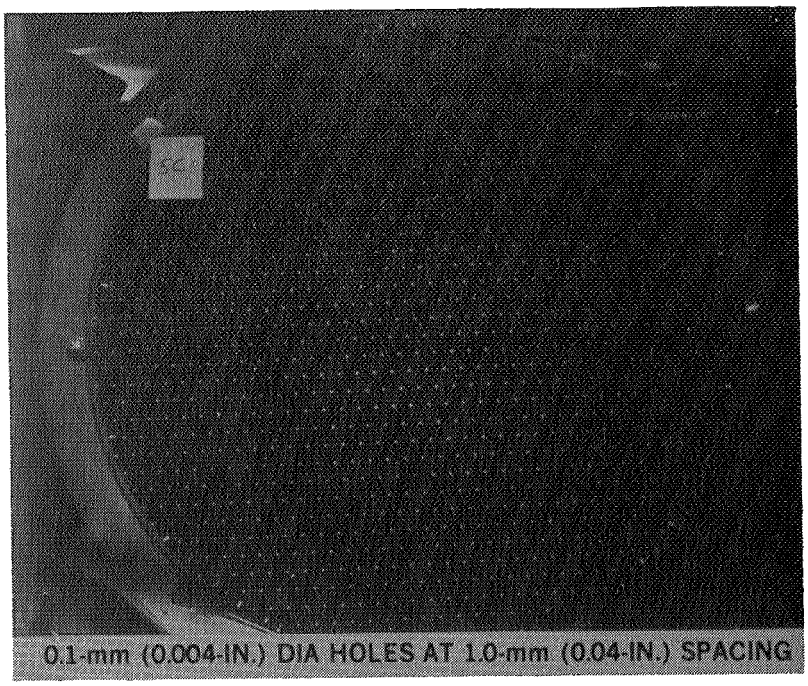

Figure 6.- Electron beam perforations in titanium sheet.

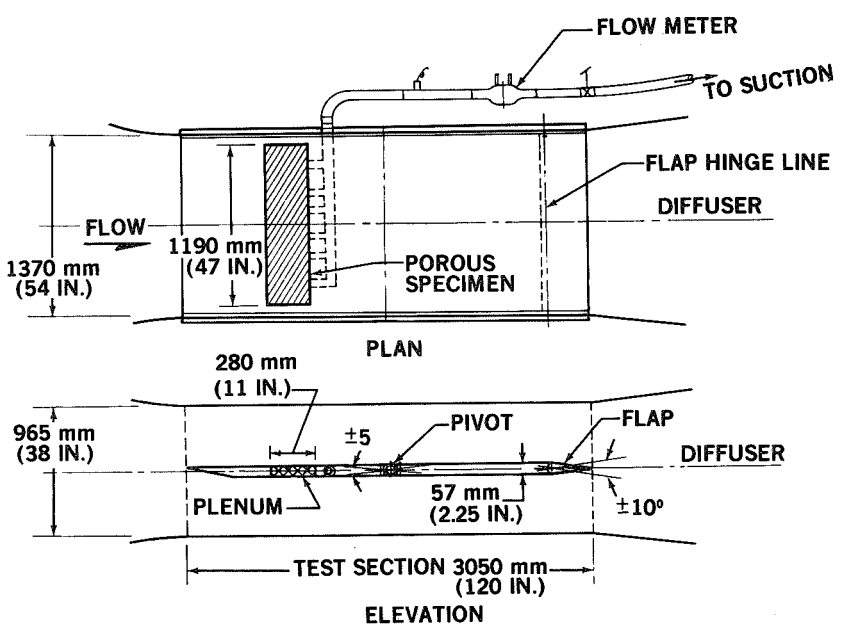

Figure 7.- Wind tunnel model test for laminar flow with porous surface specimens.

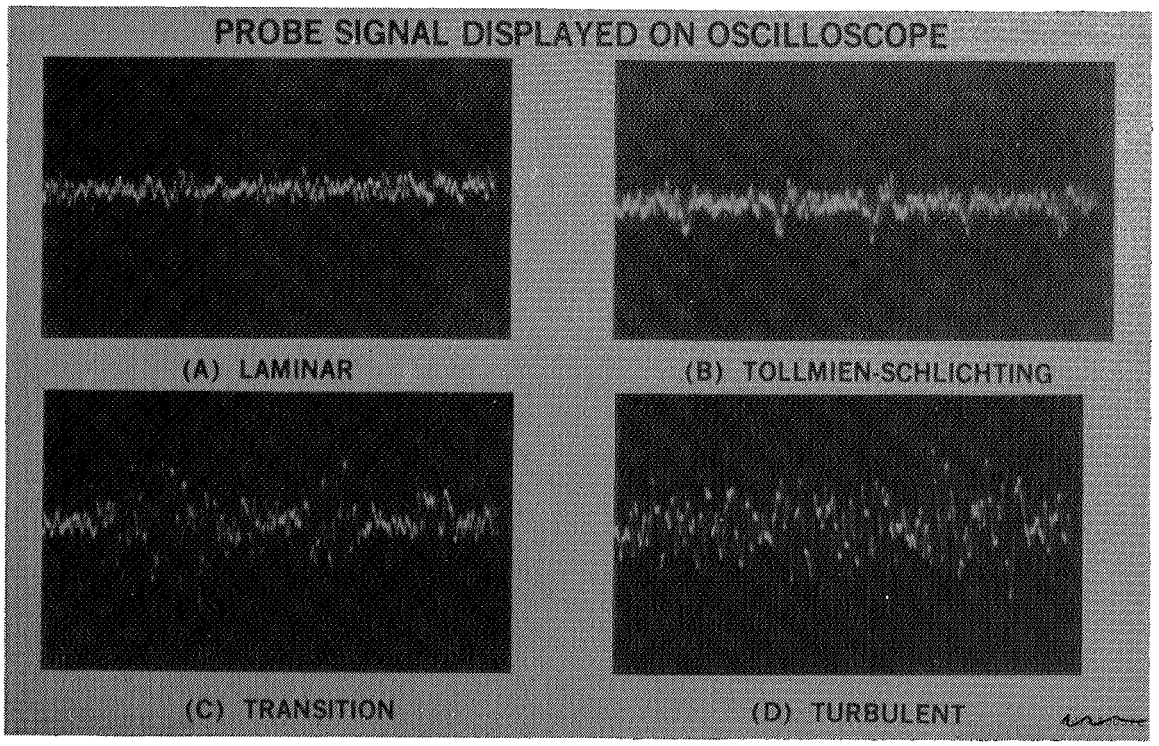

Figure 8.- Boundary-layer signatures.

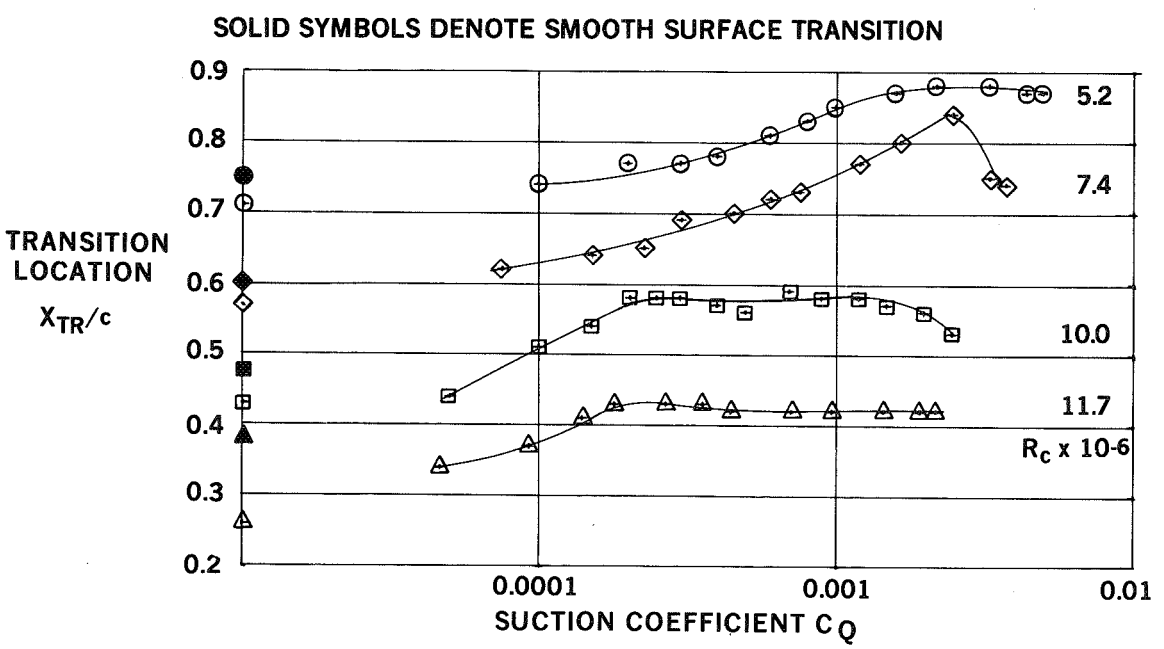

Figure 9.- Typical results — transition location, 50 × 250 Dynapore surface.

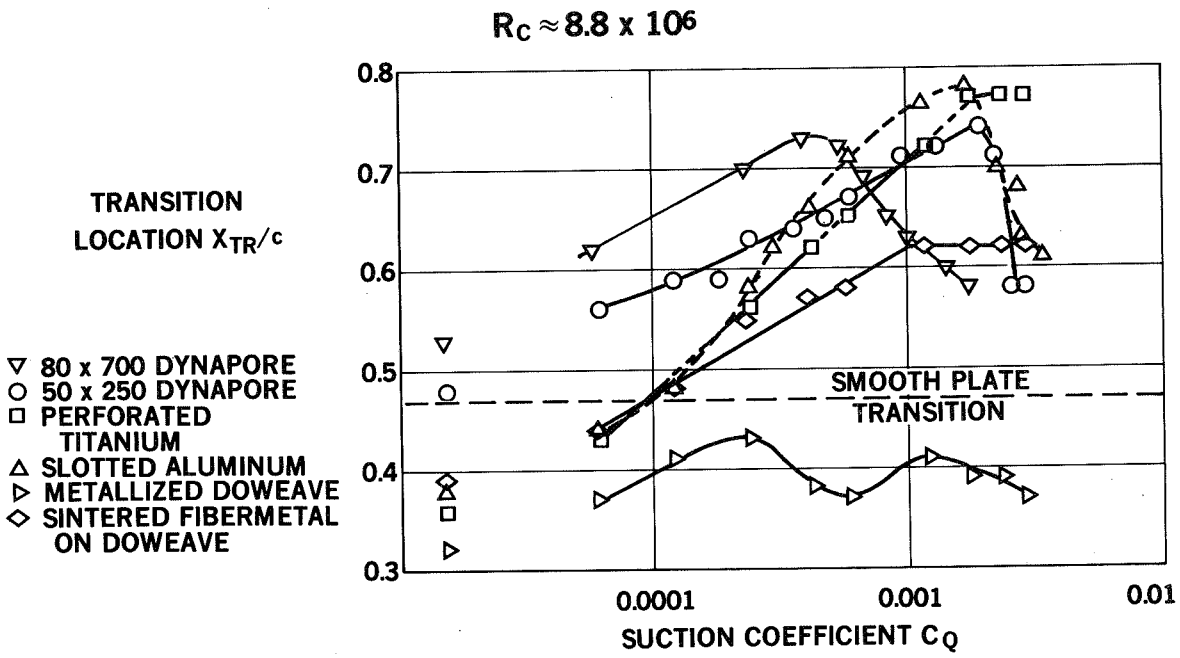

Figure 10.-Comparative effectiveness of laminar flow control surfaces.

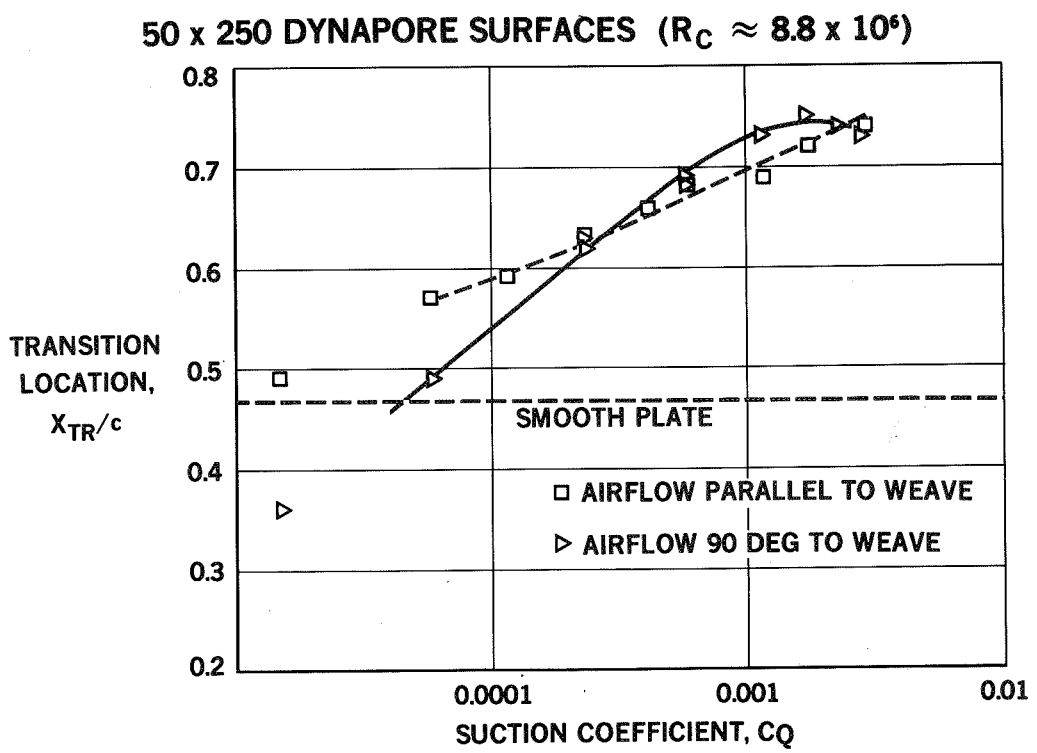

Figure 11.- Effect of airflow direction relative to weave.

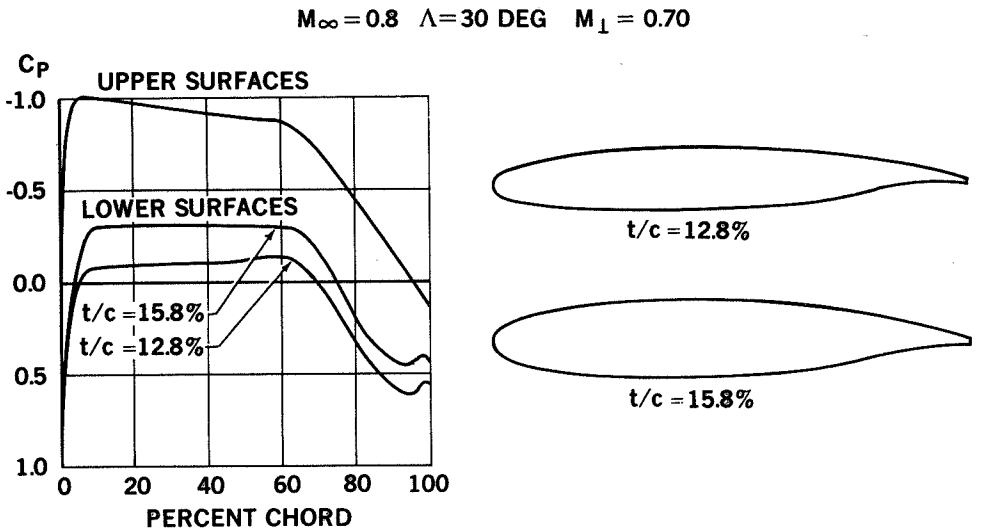

Figure 12.- Typical design pressure distributions and airfoil shapes.

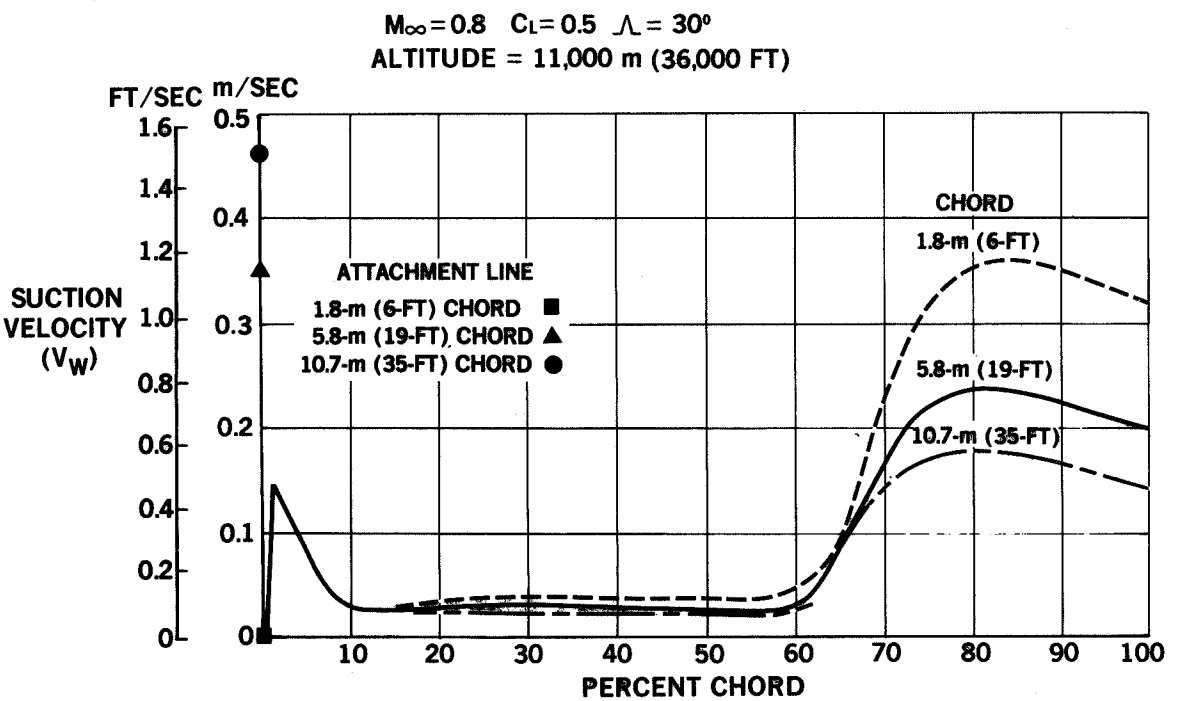

Figure 13.- Typical suction distributions — upper surface.

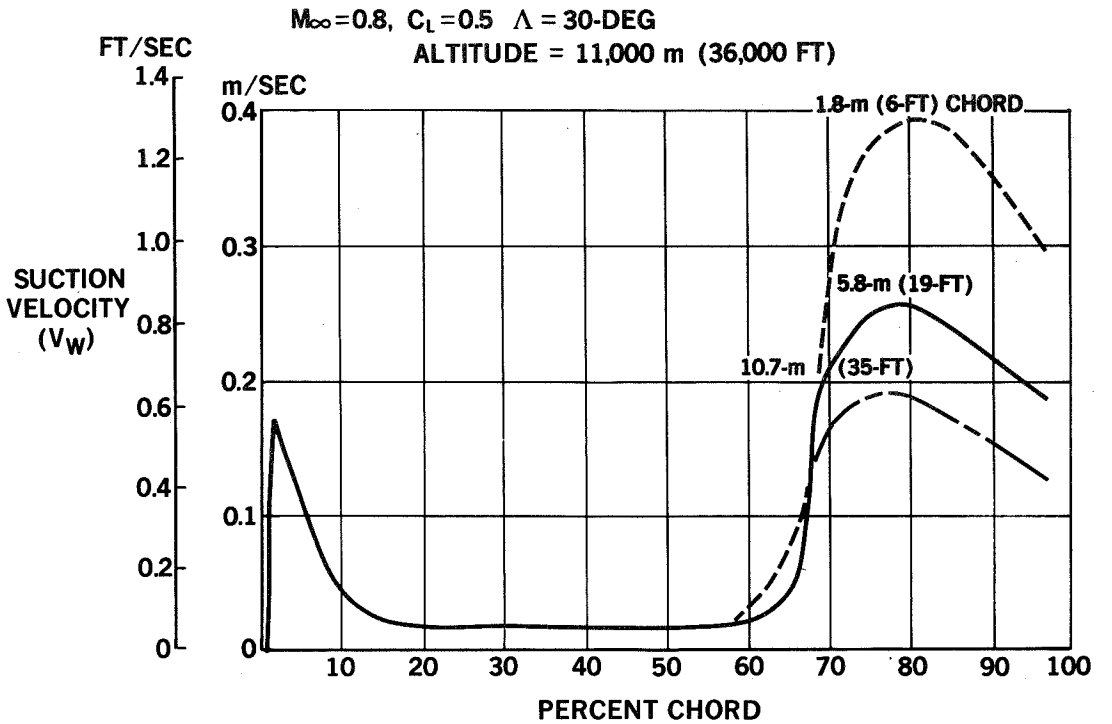

Figure 14.- Typical suction distributions — lower surface.

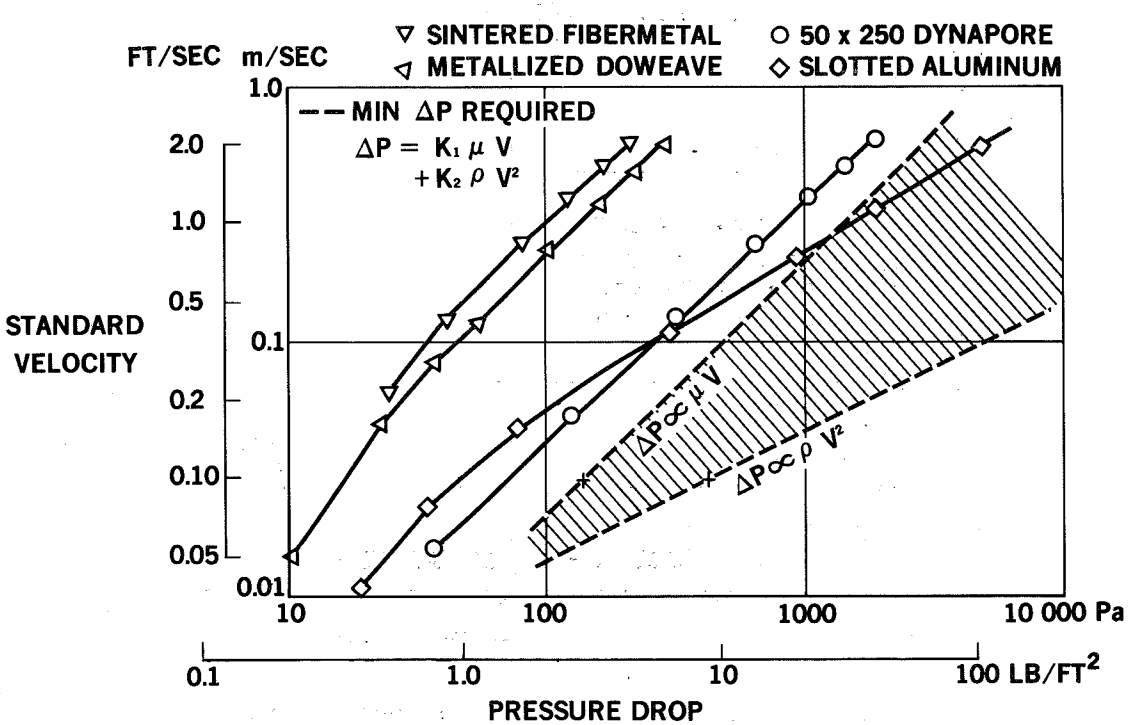

Figure 15.- Comparative static flow characteristics (sea-level test).

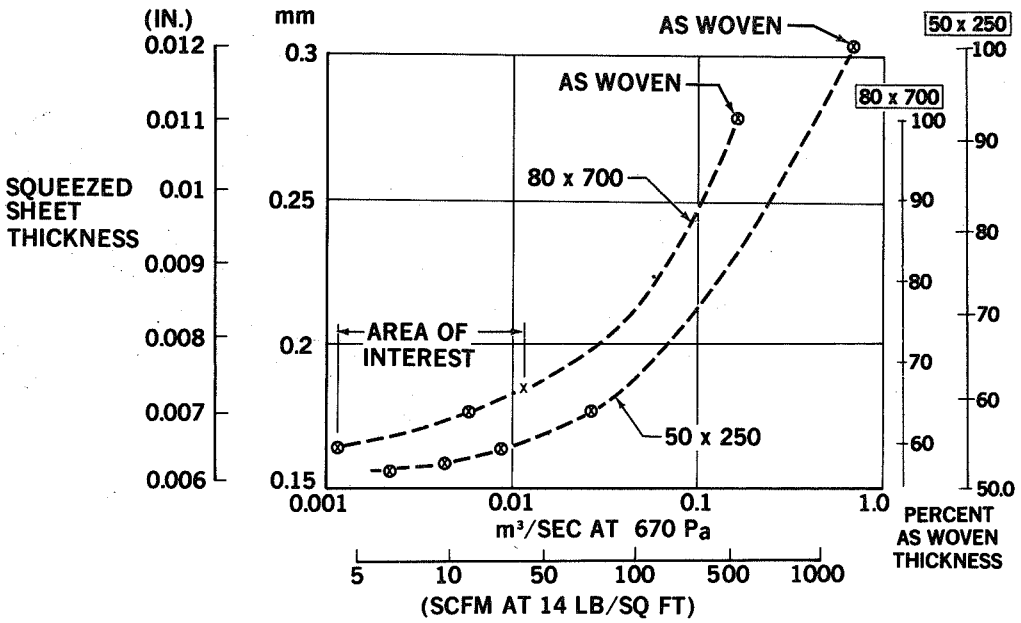

Figure 16.- Effect of calendering on porosity of Dynapore materials.

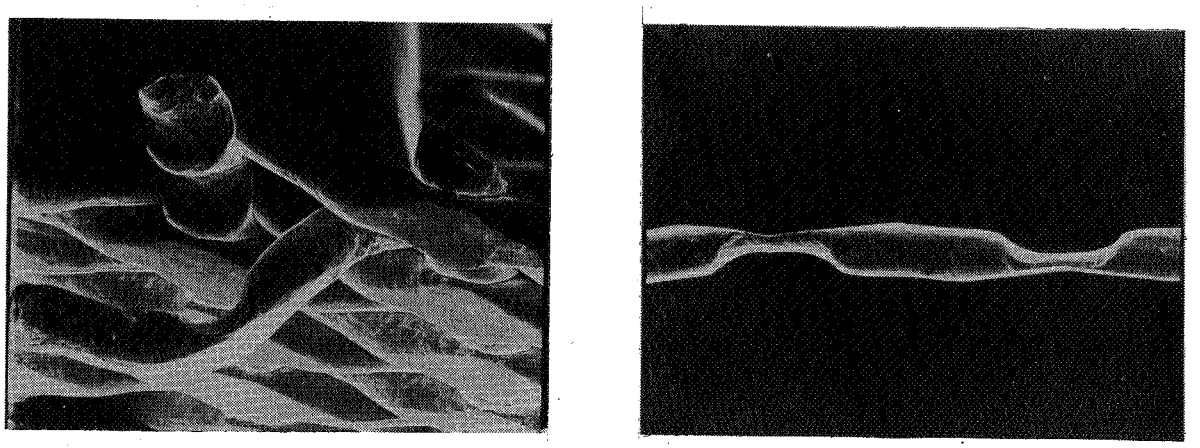

Figure 17.- Effect of oversqueezing Dynapore during calendering process.

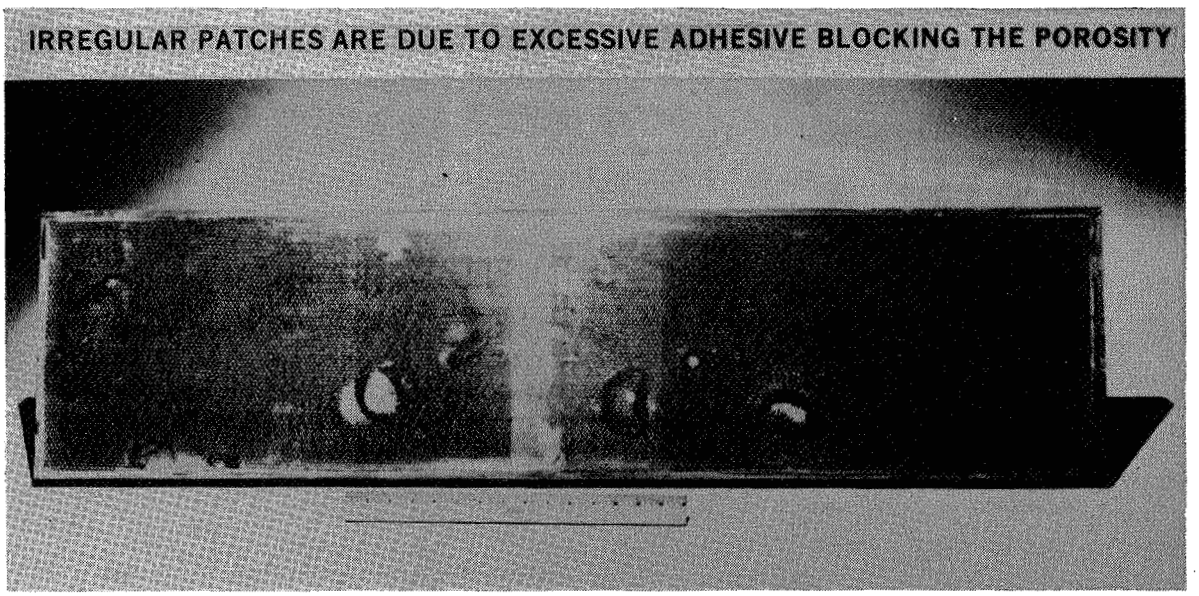

Figure 18.- 50 × 250 Dynapore-honeycomb sandwich — adhesive blocking porosity.

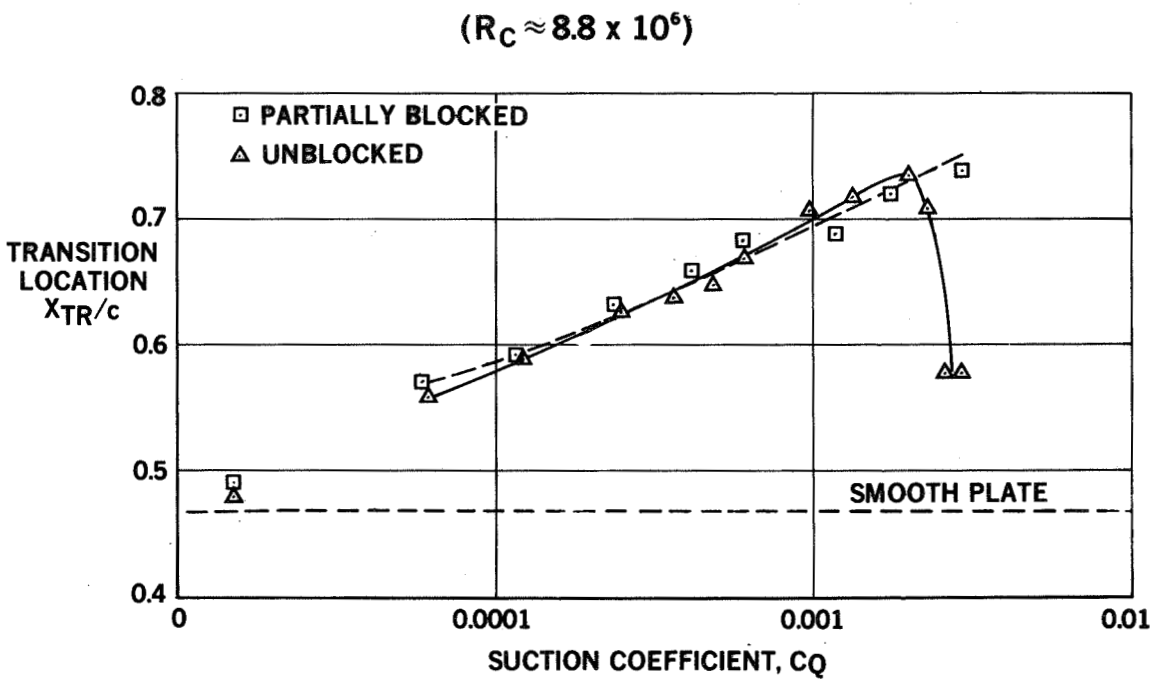

Figure 19.- Porosity blockage effect on 50 × 250 Dynapore surfaces.

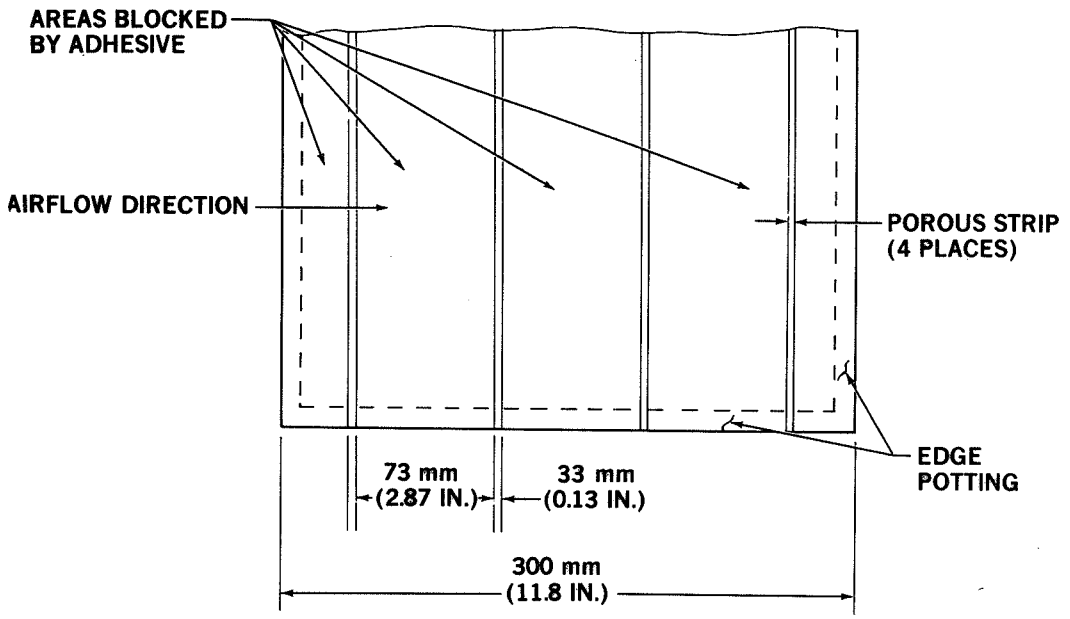

Figure 20.- Porosity strip test panel.

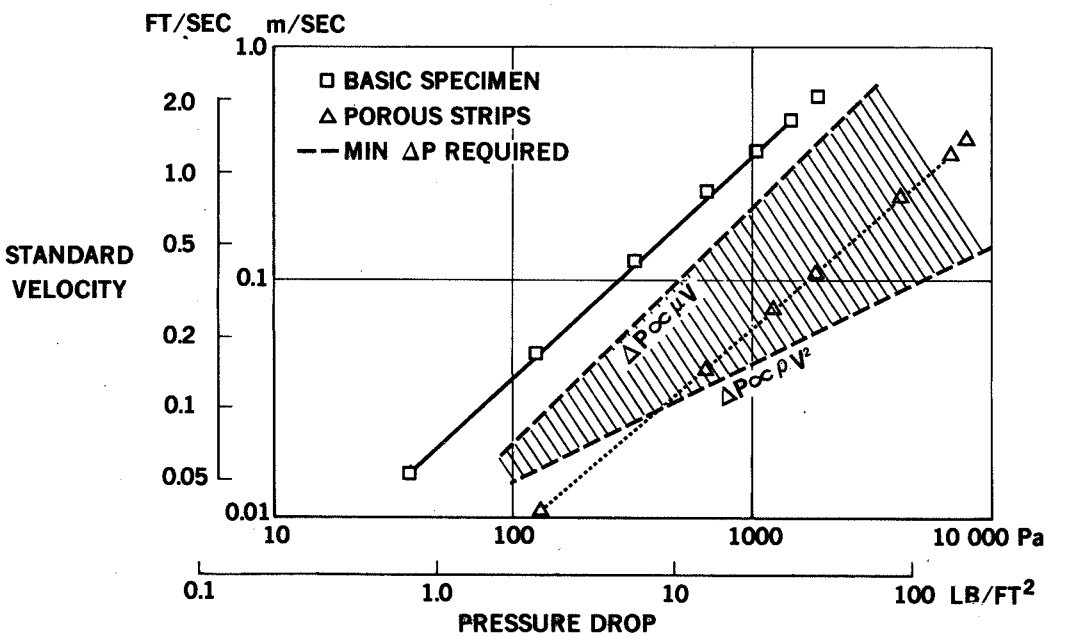

Figure 21.- Porous strip static flow comparison, 50 × 250 Dynapore.

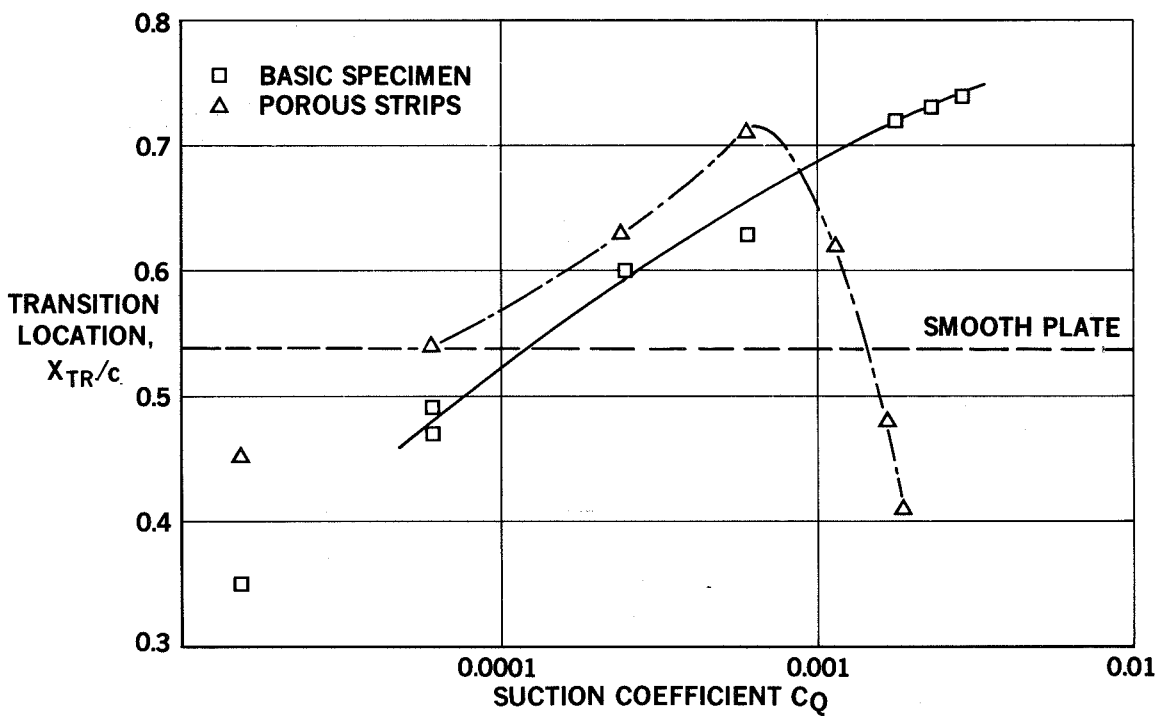

Figure 22.- Porous strip LFC performance comparison, 50 × 250 Dynapore.

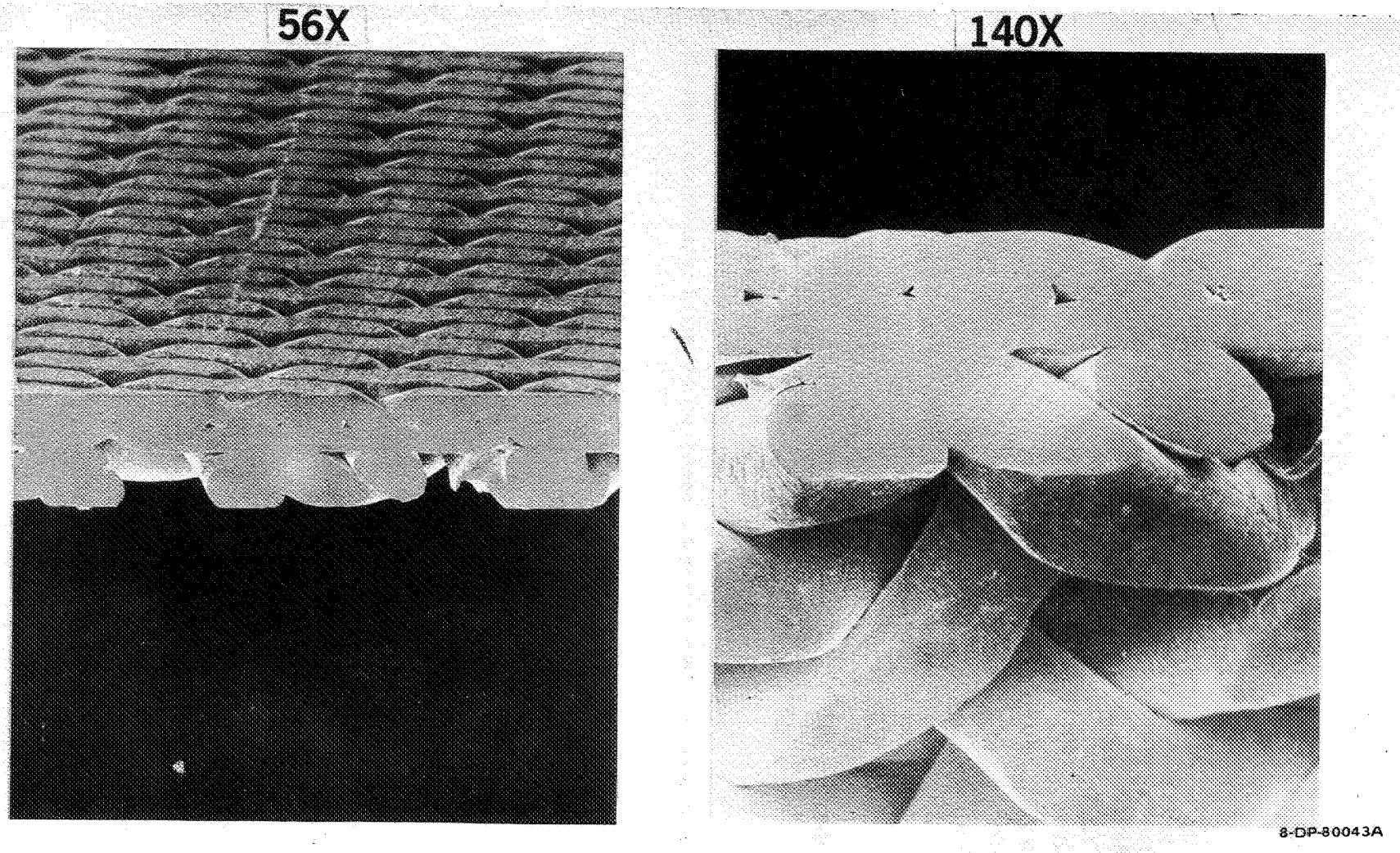

Figure 23.- 80 × 700 Dynapore surface plus diffusion-bonded 80 × 80 sublayer.

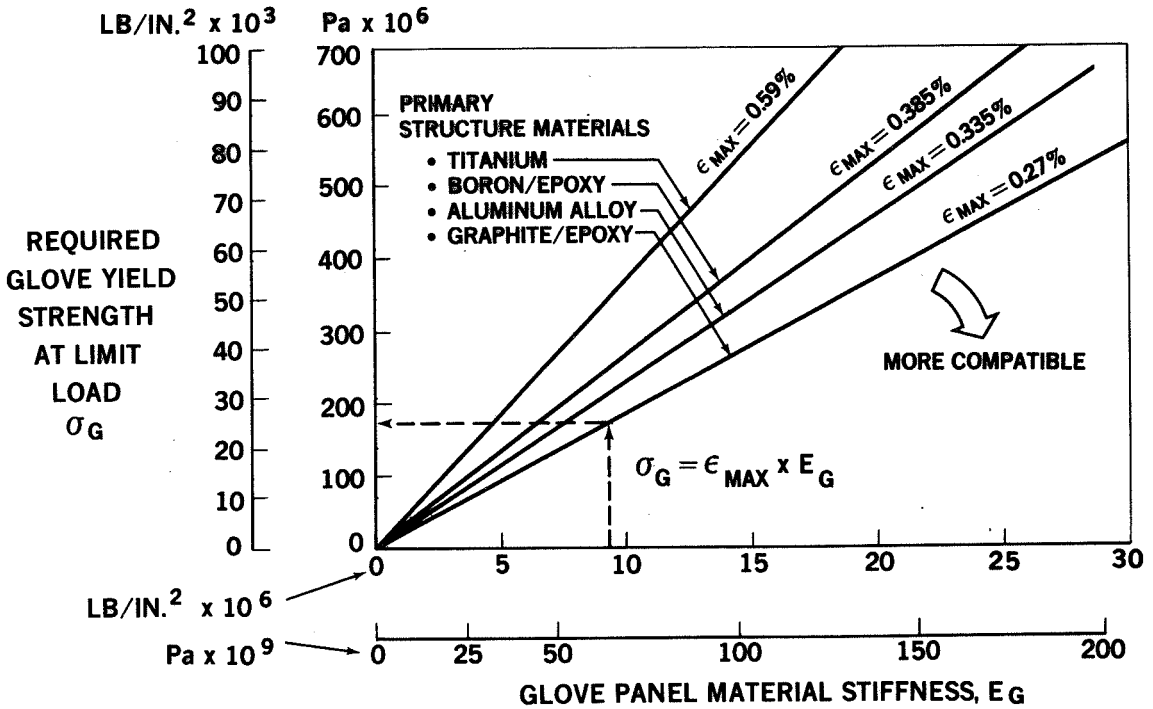

Figure 24.- Glove strength required to match structural strain.

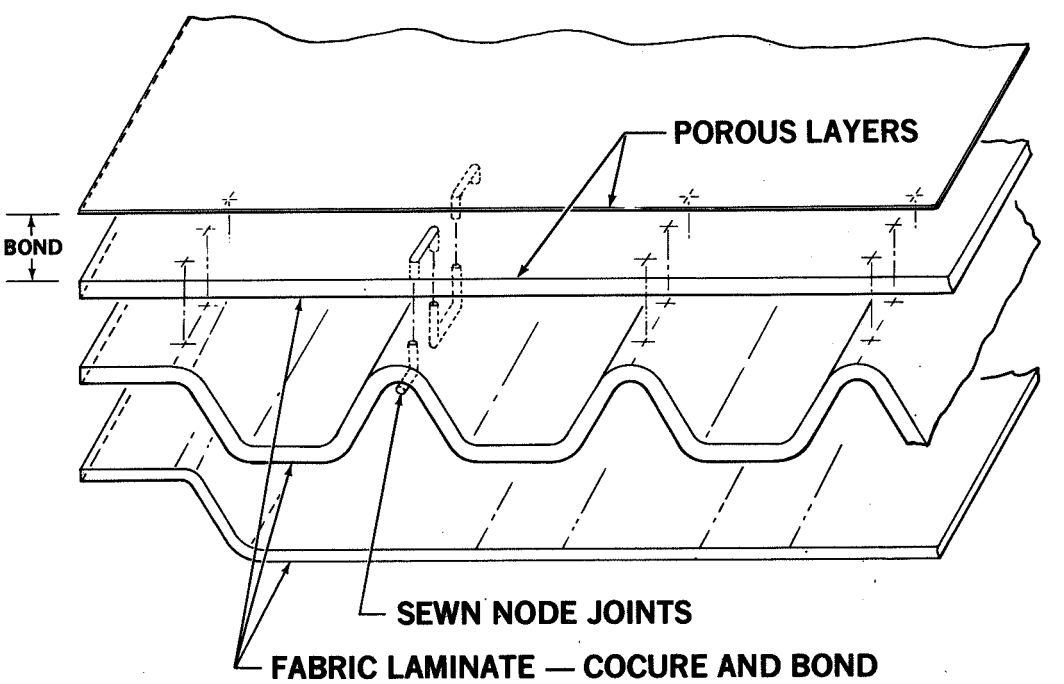

Figure 25.- Typical Lockpore panel construction.

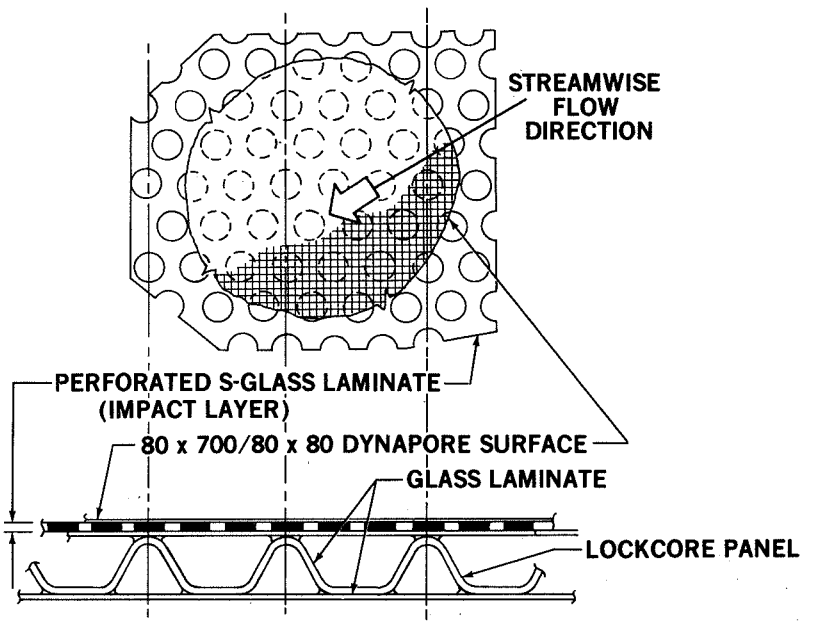

Figure 26.- Glove panel with perforated fiberglass sublayer.

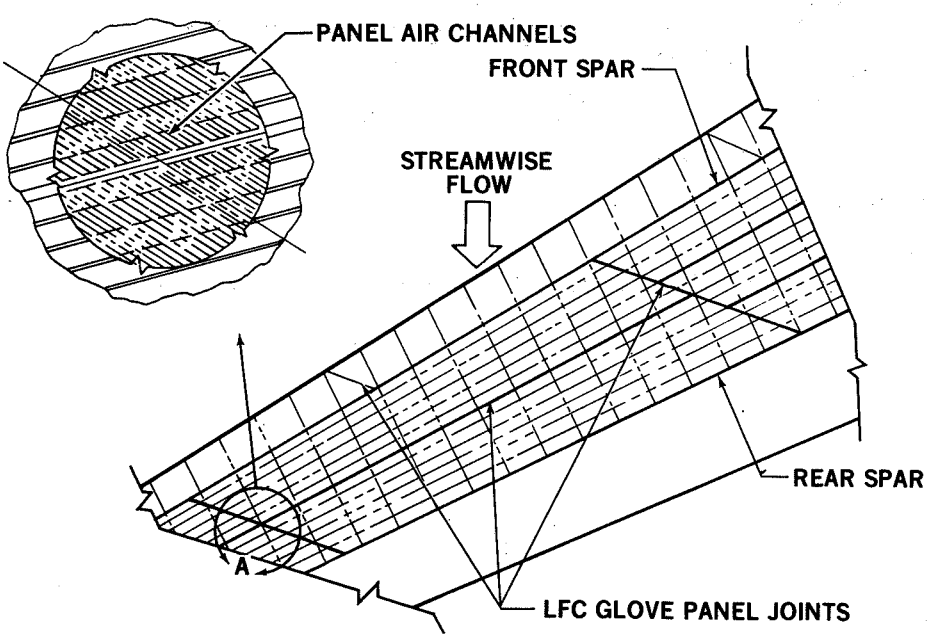

Figure 27.- Typical wing box glove panel arrangement.

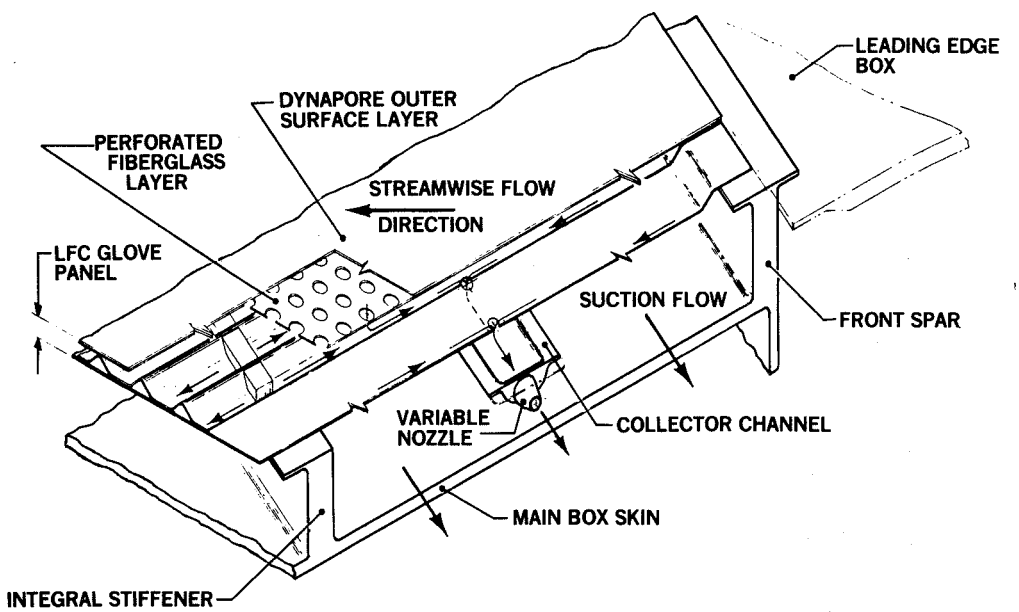

Figure 28.- Gloved wing structural concept.

1. Report No.	2. Government Accession No.	3. Recipient's Catalog No.
NASA CP–2036, Part I		

4. Title and Subtitle	5. Report Date
CTOL Transport Technology – 1978	June 1978
	6. Performing Organization Code
7. Author(s)	8. Performing Organization Report No. L–12178
	10. Work Unit No. 516–50–23–01
9. Performing Organization Name and Address NASA Langley Research Center Hampton, VA 23665	11. Contract or Grant No.
	13. Type of Report and Period Covered Conference Publication
12. Sponsoring Agency Name and Address National Aeronautics and Space Administration Washington, DC 20546	14. Sponsoring Agency Code

15. Supplementary Notes

16. Abstract

The proceedings of the NASA CTOL Transport Technology Conference held at Langley Research Center February 28 – March 3, 1978, are presented in this compilation. New technology generated by NASA in-house and contract efforts, including the ongoing Aircraft Energy Efficiency (ACEE) program, in the various disciplinary areas specifically associated with advanced conventional take-off and landing (CTOL) transport aircraft are presented. The conference was divided into six sessions:

1. A session on propulsion addressed jet engine performance deterioration and improvement; energy efficient engine design and integration; advanced turboprops, engine materials, noise, and emissions; and broad specification fuels.

2. A session on structures and materials addressed structural sizing methodology; environmental effects of composites; and applications of advanced composite materials.

3. A session on laminar flow control addressed insect contamination and alleviation; suction prediction techniques; porous materials; and laminar flow applications.

4. A session on advanced aerodynamics and active controls technology addressed advanced wings, winglets, and nacelles; aerodynamic flow calculation techniques; fault-tolerant computers; and active control applications.

5. A session on operations and safety addressed safety research; wake vortex phenomena; advanced landing-gear research; noise prediction; improved terminal area operations; airline operating costs; and a method for cost/benefit analysis for aeronautical research and technology.

6. A session on advanced systems addressed developments in short-haul and supersonic transport research; coal-derived fuels and aircraft systems; and advanced transport concepts.

17. Key Words (Suggested by Author(s))	18. Distribution Statement
Engines, Turboprops, Noise, Emissions, Fuels, Structures, Composite materials, Laminar flow control, Aerodynamics, Winglets, Active controls, Safety, Wake vortices, Landing gear, Aircraft economics, Aircraft concepts	Distribution – Unlimited Subject Category 01

19. Security Classif. (of this report)	20. Security Classif. (of this page)	21. No. of Pages	22. Price*
Unclassified	Unclassified	531	$15.50

* For sale by the National Technical Information Service, Springfield, Virginia 22161

NASA-Langley, 1978

National Aeronautics and
Space Administration

Washington, D.C.
20546

Official Business
Penalty for Private Use, $

SPECIAL FOURTH CLASS MAIL
BOOK

Postage and Fees Paid
National Aeronautics and
Space Administration
NASA-451

U.S.MAIL

10 1 1U,A, 051278 SC0903DS
DEPT OF THE AIR FORCE
AF WEAPONS LABORATORY
ATTN: TECHNICAL LIBRARY (SUL)
KIRTLAND AFB NM 87117

NASA

POSTMASTER: If Undeliverable (Section 158
Postal Manual) Do Not Return